AIIM

Association for Information and Image Management

1100 Wayne Avenue, Suite 1100
Silver Spring, Maryland 20910
301/587-8202

Centimeter

Inches

MANUFACTURED TO AIIM STANDARDS
BY APPLIED IMAGE, INC.

LBL-33049

Synchrotron Radiation in Transactinium Research

Report of the Workshop

at

Lawrence Berkeley Laboratory

October 1–2, 1992

Organized by:

N.M. Edelstein and A.S. Schlachter

Lawrence Berkeley Laboratory
University of California
Berkeley, California 94720

This work was supported by the Director, Office of Energy Research, Office of Basic Energy Sciences, Materials Sciences Division, of the U.S. Department of Energy under Contract No. DE-AC03-76SF00098

Contents

Contents (continued)

Synchrotron Radiation in Transactinium Research

Workshop

October 1–2, 1992
Lawrence Berkeley Laboratory

This workshop will explore the scientific opportunities that would be made possible by an actinide beamline at the Advanced Light Source (ALS). The ALS is a national facility for scientific research and development, located at the Lawrence Berkeley Laboratory of the University of California. When this facility begins operations in spring 1993, it will generate the world's brightest synchrotron radiation available as an experimental tool in the far ultraviolet and soft x-ray regions of the spectrum. The proposed actinide beamline would deliver synchrotron radiation in the energy range 20–1000 eV for the study of the transactinium elements and their compounds.

The major question in studies of the physical and chemical properties of these elements is the role of the 5f electrons. The ALS offers the high brightness and spectral range necessary to study the electronic properties of the actinides both in the vapor phase and in the solid state. It will be possible to probe the 5f, 6d, 7s, and inner electron shells unambiguously and to explore the unique role of the 5f electrons throughout the series. Such data combined with theoretical calculations will result in a coherent picture of 5f electron systems.

To obtain a registration package, please fill out and return the postage-paid card below.

Advanced Light Source Workshop
Synchrotron Radiation in Transactinium Research

I am interested in attending the workshop on Synchrotron Radiation in Transactinium Research. Please send me a registration package.

Name____
Organization ____________________________________
Mailing Address__________________________________

____

Telephone____________________ Fax____________________

Workshop on Synchrotron Radiation in Transactinium Research
Lawrence Berkeley Laboratory
Bldg. 2 - Room 100B
October 1-2, 1992

Thursday, Oct. 1

8:00-8:30 am	Registration	Bldg. 2, First floor lobby
8:30 am	N. Edelstein, C.B. Harris Lawrence Berkeley Lab.	Introduction and Welcome
8:40 am	A. Schlachter Lawrence Berkeley Lab.	ALS Overview
9:00 am	P. Heimann Lawrence Berkeley Lab.	Characteristics of the U-8 Undulator Beamline at the ALS
9:20 am	M. Krause Oak Ridge National Lab.	Gas Phase Actinide Studies with Synchrotron Radiation
10:00-10:30 am	BREAK	
10:30 am	Y.-K. Kim National Institute of Standards and Technology	Atomic Structure Calculations for Heavy Atoms
11:10 am	P.C. Canfield Los Alamos National Lab.	Flux Growth of Single Crystal Uranium Compounds - Extension to Transuranics
11:50 am	LUNCH	
1:00 pm	G. Kaindl Free Universität Berlin	X-ray Absorption Near-Edge Structure Studies of Actinide Compounds
1:40 pm	E. Tamura Lawrence Livermore National Lab.	The Surface as a New Stage for Studying Actinides: Theoretical Study on Surface Electronic Structure of Uranium
2:20 pm	G.H. Lander European Institute for Transuranium Elements	Experiments at Resonant X-ray Energies with Actinides - Results and Future Prospects
3:00-3:30 pm	BREAK	
3:30 pm	S. Sasaki, H. Ohno, H. Konishi, and K. Kobayashi Japan Atomic Energy Research Institute	Beamline Instruments for Radioactive Materials
4:10 pm	J.G. Tobin, G.D. Waddill, T. Gouder, and C.A. Colmenares Lawrence Livermore National Lab.	The Search for X-Ray Absorption Magnetic Circular Dichroism in Actinide Materials: Preliminary Experiments Using UFe_2 and US
5:00 pm	Bus to reception	

Workshop on Synchrotron Radiation in Transactinium Research
Lawrence Berkeley Laboratory
Bldg. 2 - Room 100B
October 1-2, 1992

Thursday, Oct. 1 (cont.)

5:30 pm	RECEPTION	
7:00 pm	DINNER	
8:45 pm	Bus to Shattuck Hotel	

Friday, Oct. 2

8:00 am	Bus to workshop from Shattuck Hotel	
8:30 am	A. Arko Los Alamos National Lab.	The Laboratory Light Source - A Source of Preliminary Transuranic Data
9:10 am	J. Allen University of Michigan	Electron Spectroscopy Studies of Actinide Systems
9:50-10:20 am	BREAK	
10:20 am	T.H. Gouder and C.A. Colmenares Lawrence Livermore National Lab.	Study of Thin Layers of Actinides, Present Status and Future Use of Synchrotron Radiation
11:00 AM	J. Naegele European Institute for Transuranium Elements	High Resolution Electron Spectrometry on Highly Radioactive Actinides: Consequences for a Future Transactinium Synchrotron Beamline
11:40-1:00 pm	LUNCH	
1:00 pm	B. Cooper West Virginia University	Electronic Structure and Correlated-Electron Theory for Actinide Materials
1:40 pm	M.B. Maple University of California, San Diego	Heavy Fermion and Kondo Phenomena in Actinide Materials
2:20 pm	SUMMARY - P.N. Ross Lawrence Berkeley Lab. and A. Arko Los Alamos National Lab.	
3:00 pm	ALS Tour	
4:00 pm	Bus to Shattuck Hotel	

SYNCHROTRON RADIATION IN TRANSACTINIUM RESEARCH

OCTOBER 1-2, 1992

Jagan Akella
Lawrence Livermore National Lab.
Livermore, CA 94550
(510) 422-7097

James W. Allen
University of Michigan
Randall Laboratory
Ann Arbor, MI 48109-1120
(313) 763-1150

A. Arko
Los Alamos National Laboratory
Los Alamos, NM 87545

Bryan B. Bandong
Nuclear Chemistry Division
Lawrence Livermore National Lab.
7000 East Avenue
Mail Stop L-396
Livermore, CA 94550
(510) 422-6596

Jerome J. Bucher
Lawrence Berkeley Laboratory
1 Cyclotron Road
Berkeley, CA 94720
(510) 486-4484

Paul C. Canfield
Los Alamos National Laboratory
MS K764
Los Alamos, NM 87545
(505) 667-4133

Alison Chaiken
Lawrence Livermore Natl. Lab.
P. O. Box 808
Livermore, CA 94550

Carlos Colmenares
Lawrence Livermore Natl. Lab.
P. O. Box 808
Livermore, CA 94551

Bernard R. Cooper
Department of Physics
West Virginia University
P. O. Box 6315
Morgantown, WV 26506-6315
(304) 293-3423

Larry E. Cox
Los Alamos National Laboratory
NMT-5, MS E506
Los Alamos, NM 87545
(505) 667-2346

Norman M. Edelstein
Lawrence Berkeley Laboratory
1 Cyclotron Road, 70A-1150
Berkeley, CA 94720
(510) 486-5624

Thomas Gouder
Lawrence Livermore Natl. Lab.
P. O. Box 808
Livermore, CA 94551

Charles B. Harris
Lawrence Berkeley Laboratory
1 Cyclotron Road
Berkeley, CA 94720
(510) 486-6382

P. Heimann
Lawrence Berkeley Laboratory
1 Cyclotron Road
Berkeley, CA 94720

Paul Johnson
Lawrence Berkeley Laboratory
1 Cyclotron Road
Berkeley, CA 94720

As of 11/5/92

SYNCHROTRON RADIATION IN TRANSACTINIUM RESEARCH

OCTOBER 1-2, 1992

G. Kaindl
Free Universität Berlin
Arnitnallee 14
Berlin 33, Ger W-1000

Yong-Ki Kim
Natl. Inst. of Standards & Technology
Bldg. 221, Room A267
Gaithersburg, MD 20899

Jeffrey B. Kortright
Ctr. for X-Ray Optics
Lawrence Berkeley Laboratory
1 Cyclotron Road
Berkeley, CA 94720
(510) 486-5960

Manfred O. Krause
Oak Ridge National Laboratory
P. O. Box 2008
Oak Ridge, TN 37831-6201
(615) 574-5019

Gerry H. Lander
Institute for Trans. Elements
Commission of the European Comm.
Joint Research Centre
Postfach 2340
Karlsruhe, Ger D-7500

M. Brian Maple
Univ. of California, San Diego
0319
9500 Gilman Drive
La Jolla, CA 92093-0319
(619) 534-3968

Jochen R. Naegele
Institute for Trans. Elements
Commission of the European Comm.
Joint Research Centre
Postfach 2340
Karlsruhe, Ger D-7500

Heino Nitsche
Lawrence Berkeley Laboratory
1 Cyclotron Rd., Bldg. 70A-1150
Berkeley, CA 94720
(510) 486-6509

Ralph H. Page
Lawrence Livermore National Lab.
P. O. Box 808
Mail Stop L-471
Livermore, CA 94550
(510) 422-2774

Dale Perry
Lawrence Berkeley Laboratory
1 Cyclotron Road, 70A-1150
Berkeley, CA 94720

Marvin L. Poutsma
Oak Ridge National Laboratory
P. O. Box 2008, MS 6182
Oak Ridge, TN 37831-6182
(615) 574-5028

Phil Ross
Lawrence Berkeley Laboratory
1 Cyclotron Road
Berkeley, CA 94720

Shigemi Sasaki
Japan Atomic Energy Res. Inst.
Tokai-mura, Naka-gun
Ibaraki, Jap 319-11
292-82-5442

Fred Schlachter
Lawrence Berkeley Laboratory
1 Cyclotron Road
Berkeley, CA 94720

David K. Shuh
Lawrence Berkeley Laboratory
1 Cyclotron Road, 70A-1150
Berkeley, CA 94720
(510) 486-6937

As of 11/5/92

SYNCHROTRON RADIATION IN TRANSACTINIUM RESEARCH

OCTOBER 1-2, 1992

Herb Silber
(San Jose State University)
Lawrence Berkeley Laboratory
1 Cyclotron Road
Berkeley, CA 94720

Lynda Soderholm
Argonne National Laboratory
9700 S. Cass Avenue
Argonne, IL 60439
(708) 252-4364

B. Ray Stults
Battelle, Pacific Northwest Laboratory
P. O. Box 999
Richland, WA 99352
(509) 375-2687

Joost Sytsma
G. T. Seaborg Institute
c/o Lawrence Berkeley Laboratory
1 Cyclotron Road, 70A-1150
Berkeley, CA 94705
(510) 486-5141

E. Tamura
Lawrence Livermore Natl. Lab.
P. O. Box 808
Livermore, CA 94551

Kim H. Tan
University of Wisconsin
CSRF
3725 Schneider Drive
Stoughton, WI 53589
(608) 877-2200

David H. Templeton
Lawrence Berkeley Laboratory
1 Cyclotron Road
Berkeley, CA 94720
(510) 486-5615

Lieselotte K. Templeton
Lawrence Berkeley Laboratory
1 Cyclotron Road
Berkeley, CA 94720
(510) 486-5615

Louis J. Terminello
3680 Andrews Dri. #303
Pleasanton, CA 94588

James G. Tobin
Lawrence Livermore Natl. Lab.
P. O. Box 808
Livermore, CA 94551
(510) 422-7247

Johannes van Ek
Lawrence Livermore Natl. Lab.
P. O. Box 808
Livermore, CA 94550

G. D. Waddill
Lawrence Livermore Natl. Lab.
P. O. Box 808
Livermore, CA 94551

Executive Summary

Norman M. Edelstein and Alfred S. Schlachter
Lawrence Berkeley Laboratory
Berkeley, CA 94720

Introduction

The Advanced Light Source (ALS), a national synchrotron radiation facility, is nearing completion at the Lawrence Berkeley Laboratory (LBL). Beginning in spring 1993, when it opens its doors to researchers, the ALS will produce the world's brightest light for experiments utilizing the vacuum ultraviolet (VUV) and soft x-ray regions of the spectrum.

For the first time, a synchrotron radiation source will be located at a laboratory that has an ongoing and active program in actinide research—in fact, at the very place where the first transuranium elements were discovered. As a result, the infrastructure is available for the safe handling of actinide materials. A beamline dedicated to research on actinides and other radioactive materials has been proposed for the ALS. Planned as a branchline of ALS Beamline 9.0, it will deliver photons in the energy range 20–300 eV from an 8.0-cm-period undulator (U8) into an isolated enclosure housing the actinide end stations. The U8 photon beam will be characterized by tunability, brightness, high flux, narrow bandwidth, and very small spot size. Photons up to 1000 eV also may be deflected from an adjacent bending-magnet beamline into the actinide end stations.

This proposed actinide facility will have numerous applications that would help solve difficult problems of national concern. Taking advantage of the high photon flux, tunability, and small spot size, researchers can map radioactive elements on surfaces while distinguishing their oxidation states; elucidate elemental diffusion profiles; evaluate radiation damage in activated reactor materials; and investigate and characterize radionuclide materials used in medical applications. Environmental applications include the examination of container materials used for storing nuclear fuel rods, surface-interface investigations of materials (e.g., glasses) used for encapsulating nuclear waste, depth-profiling of such materials for various radionuclides before and after leaching tests, the study of corrosion effects on spent nuclear fuel rod cladding and materials, and the demonstration of surface passivation of actinide materials and their containers for long-term storage. In the area of nonproliferation of nuclear materials, the actinide facility will provide a capability for the trace analysis of the ratios of uranium and plutonium.

Overview

A workshop on "Synchrotron Radiation in Transactinium Research" was held at LBL on October 1–2, 1992. Its purpose was twofold: (1) to evaluate the community interest in the use of synchrotron radiation in the energy range from 20 eV to approximately 1000 eV for the study of the electronic, magnetic, and structural properties of the transactinium elements and their compounds; and (2) to define the scientific opportunities that will be made available by the proposed actinide facility.

An earlier international workshop, "Perspectives on the Use of Synchrotron Radiation in Transuranium Research," was held at Karlsruhe, Germany, in 1985. One major conclusion of this workshop was that the use of synchrotron radiation in transuranium research is highly desirable, in both the VUV and the hard x-ray range, because of important scientific results that would be obtained. Nevertheless, to date, no VUV facility that can utilize radioactive materials has been built at any synchrotron.

At LBL, sixteen invited speakers described the types of basic and applied scientific research that could be conducted at the proposed actinide facility. The topics encompassed a broad range of physics and chemistry. A number of speakers described high-resolution and resonant photoemission experiments on heavy Fermion systems and emphasized that the electronic-structure information obtained from transuranium systems would greatly enhance the understanding of electron correlation effects, not only in the actinides but also in other parts of the Periodic Table. To this end, the theories used to describe these phenomena must also undergo continuing development. The high flux and tunability of the photon beam allow the surface of materials to be investigated and depth profiling measurements to be made. Measurements of this type are important for determining surface structures, interface phenomena, catalytic behavior, and corrosion properties. Surface-structure electronic calculations must be correlated with the experiments. Applications of magnetic circular dichroism (MCD) experiments with synchrotron radiation were also discussed.

Many speakers noted that the characteristics of the photon beams from an ALS actinide beamline—tunability, brightness, narrow bandwith, and very small spot size—are paramount in transuranium research because they allow the use of very small samples, which greatly reduces radioactivity safety concerns. These characteristics also are essential for vapor-phase studies of the actinides because of the inherently small number density in such systems. Vapor-phase measurements traditionally have provided fundamental information, such as the binding energies and ionization probabilities of the outermost electron shells, as well as information on higher-order effects, such as relativistic and quantum-electrodynamic interactions. Again, theoretical advances in these areas must go hand-in-hand with the experimental measurements.

One means of studying actinide materials in the VUV and soft x-ray regions is to build a laboratory laser plasma light source (coupled with a monochromator) that can be placed in an existing facility. Such a project is under way at Los Alamos National Laboratory and will make valuable contributions to the understanding of actinide materials. However, this facility cannot compete with the proposed 8.0-cm-period undulator beamline at the ALS because the brightness of the plasma light source will be at least 100 times less and its resolution will be at least a factor of 10 less with a limited photon range.

The workshop critically addressed the safety aspects of handling actinide materials at a synchrotron dedicated to a large user community. Speakers described their experiments with radioactive materials utilizing in-house, fixed-energy, laboratory x-ray and UV sources. Their experiences led them to conclude that, with careful design, a branchline and end stations used to study radioactive materials are feasible and can be reliably operated with extremely low risk at a synchrotron radiation facility. A feasibility study of an actinide facility at a synchrotron, commissioned by the European Institute for Transuranium Elements, was conducted by Savoia and Perfetti. This study discusses in great detail the proposed safety systems necessary to protect the beamline, monochromator, and storage ring.

Experiments utilizing harder x rays with actinide materials, such as near-edge absorption studies (NEXAFS) and x-ray magnetic scattering investigations, also were described. In this energy range, the actinide samples can be encapsulated to greatly reduce the safety hazards. In addition, the synchrotron ring vacuum is isolated from the sample by a Be window. Details about two beamlines under construction at the Photon Factory in Japan were given—one producing soft x rays in the region 1.6–6 keV and the other producing x rays in the region 6–17 keV. These beamlines will be used to study the properties of materials irradiated with high-energy particle beams, uranium and thorium materials, and radioisotopes used as tracers.

Conclusion

The speakers at the workshop and the discussions that followed the talks indicated the very great interest in the construction of an actinide (radioactive materials) facility at the ALS. The willingness of the workshop participants to become actively involved in the programs at the proposed facility was clearly expressed. There is no doubt that very strong basic and applied scientific research programs relevant to the DOE mission would develop at the proposed facility.

Acknowledgments

We would like to thank the invited speakers, the session chairpersons, and all participants for their contributions. We gratefully acknowledge the support of the LBL conference group, Ms. Mollie Field and her staff; the ALS office, Ms. Jackie McDonald and her staff; and Ms. Gloria Lawler for her editorial and technical assistance before, during, and after the workshop.

ALS Overview

A. S. Schlachter
Advanced Light Source
Lawrence Berkeley Laboratory
Berkeley, CA 94720

The Advanced Light Source (ALS) will begin operations in spring 1993—generating the world's brightest synchrotron radiation in the extreme ultraviolet and soft x-ray regions of the spectrum (<10 eV to ~10 keV). This $99.5 million facility, funded by the U.S. Department of Energy, is available to qualified researchers from industry, universities, and government laboratories.

Light from the ALS possesses special characteristics that make it a research tool of great versatility:

- Very high brightness
- Linear or circular polarization
- Tunability
- Pulsed nature
- High degree of coherence.

Of these, the unique characteristic is the light's high brightness, a measure of its spatial and spectral concentration (see Fig. 1). That is, the light has a high photon flux per unit source area and per unit solid angle into which the source radiates. (Flux is the number of photons delivered per second.)

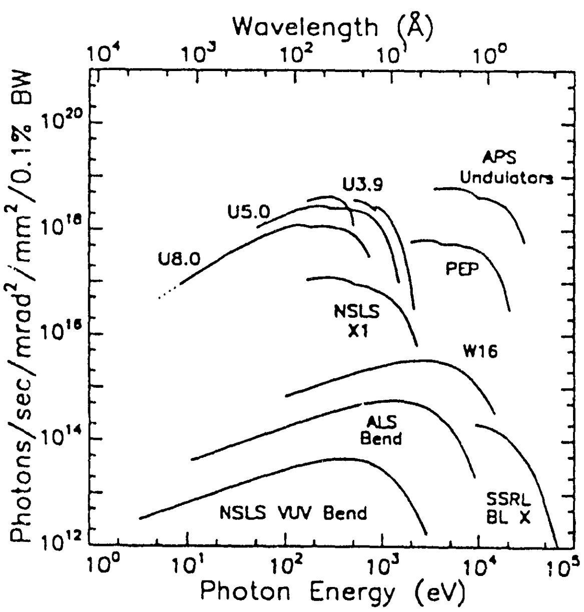

Figure 1. Plots of spectral brightness are shown for three ALS undulators, an ALS wiggler, the ALS bending magnets, undulators planned for the Advanced Photon Source (APS), and representative insertion-device and bending-magnet sources at the National Synchrotron Light Source (NSLS) and Stanford Synchrotron Radiation Center (SSRL and PEP). The discontinuities in the undulator curves represent shifts from the fundamental to the third harmonic or from one harmonic to the next.

As a consequence of high brightness, very high spatial resolution becomes possible because many photons can be focused on an extremely small spot. With help from beamline optics, the ALS is expected to achieve spot sizes as small as 200 Å.

Another effect of high brightness is high spectral resolution. By narrowing the slits of a monochromator, one can select a very narrow range of wavelengths from a beam of synchrotron radiation and still have a sufficient number of photons to use for imaging or measuring the properties of a sample. Many experiments that were previously impractical because of insufficient resolution or long measurement times become feasible using light from the ALS. Figure 2 illustrates the improvement in spectral detail possible with high spectral resolution.

Apart from the issue of spectral resolution, the tunability of light from the ALS is important in itself. From the range available in a beam, one can select specific photon energies, for example, to probe the 5f, 6d, 7s, and inner electron shells of the actinides.

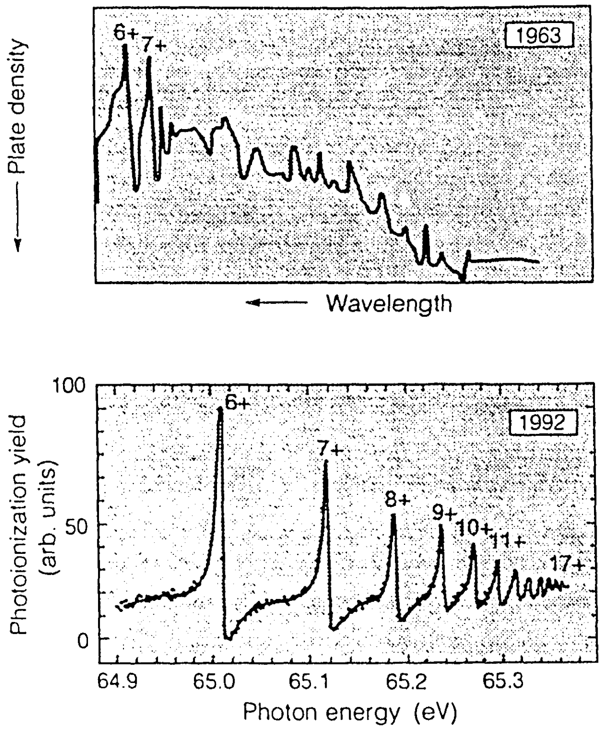

Figure 2. Synchrotron radiation of certain photon energies absorbed by helium atoms leads to the simultaneous excitation of two electrons into a series of distinct quantum states. A 1992 measurement of this phenomenon, made at the Stanford Synchrotron Radiation Laboratory, had the advantage of a tenfold improvement in resolution and considerably higher flux over the original measurement made in 1963. In addition, the more recent experiment measured ionization, whereas the 1963 experiment measured absorption. Work done by T. Reich, Z. Hussain, E. Moler, G. Kaindl, D. A. Shirley, and M. Howells (bottom) and R.P. Madden and K. Codling (top).

Light from the ALS is naturally pulsed because the electrons producing the radiation travel in bunches (see Fig. 3). Standard pulses are 35 ps wide (FWHM) and occur at intervals of 2 ns. This time structure can be varied by injecting one or a few electron bunches into the storage ring. In the few-bunch mode, the ALS delivers pulses at intervals up to 656 ns. The pulsed nature of the light, the high flux, and the ability to vary the interval between pulses make it possible to perform time-resolved studies, for example, on the kinetics of a chemical reaction or the lifetime of excited states of atoms or molecules.

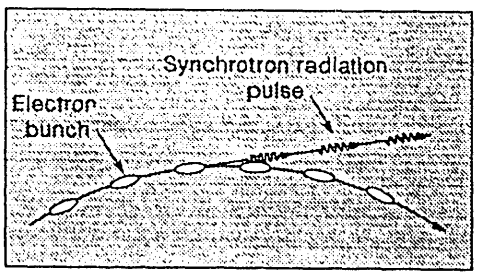

Figure 3. Schematic illustration of the bunched structure of the electron beam circling the ALS storage ring and the corresponding pulsed nature of the synchrotron radiation. Up to 250 electron bunches circle the ring. Each has a duration of about 35 ps. The time interval between bunches, dictated by the rf frequency, is 2 ns.

The ALS storage ring consists of 12 arc sectors alternating with 12 straight sections. The arcs are embedded in a lattice of bending and focusing magnets that force the beam into a curved trajectory and constrain it to a tight ellipse, 40 μm x 200 μm (σ). The three bending magnets in each arc cause the electron orbit to curve and thus generate synchrotron radiation. The straight sections can accommodate insertion devices—undulators and wigglers—that also generate synchrotron radiation, but with enhanced characteristics. Undulators and wigglers consist of two arrays of permanent magnets that create a magnetic field of alternating polarity perpendicular to the electron beam. One array is installed above and the other below the vacuum chamber. The alternating magnetic field causes the beam to curve horizontally from side to side as it passes between the rows of magnets. As the electrons curve back and forth, they emit synchrotron radiation.

Undulators and wigglers differ in the amount of angular deflection their magnets produce. The angle at which a wiggler's magnets deflect the electron beam is large compared with the natural emission angle of synchrotron radiation. As a result, a wiggler produces a continuous spectrum of radiation, similar to that produced by a bending magnet that has the same magnetic field strength—but more intense. The angle at which an undulator's magnets deflect the electron beam is close to the natural emission angle of the radiation. Consequently, the waves of light emitted at each pole in the array reinforce or cancel one another to enhance the emission of certain wavelengths. For this reason, undulator radiation at the enhanced wavelengths is extremely bright—brighter than either bending-magnet or wiggler radiation. Furthermore, because it emerges in a narrow cone (see Fig. 4) and is partially coherent, it is similar to the light from a laser. Also, it is linearly polarized. Circularly polarized radiation can be produced by using specialized undulators or wigglers, or by a bending magnet.

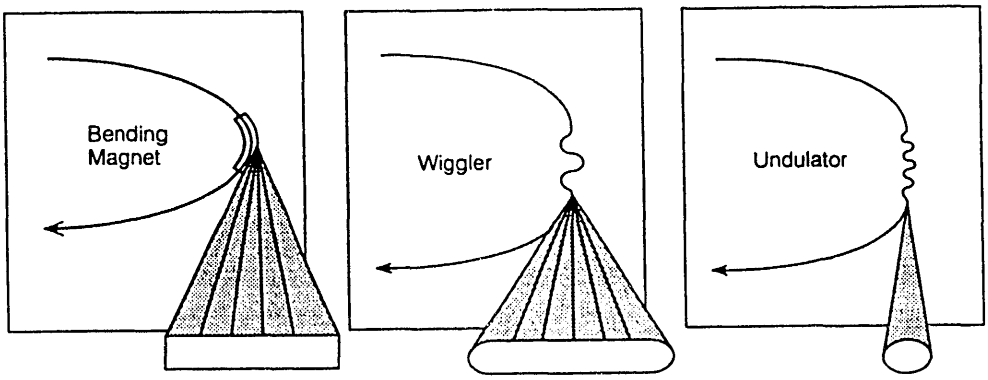

Figure 4. Bending magnets and wigglers generate fan-shaped beams of synchrotron radiation, whereas undulators emit pencil-thin beams.

The ALS will support an extensive research program in the many scientific disciplines that use x-ray and ultraviolet radiation to study and manipulate matter: atomic and molecular physics, chemistry, the life sciences, materials science, and actinide science (see Fig. 5). When the facility begins operations in 1993, five beamlines will deliver photons to experimental stations: three with undulator sources and two with bending-magnet sources. By 1995, an additional five beamlines will be in operation.

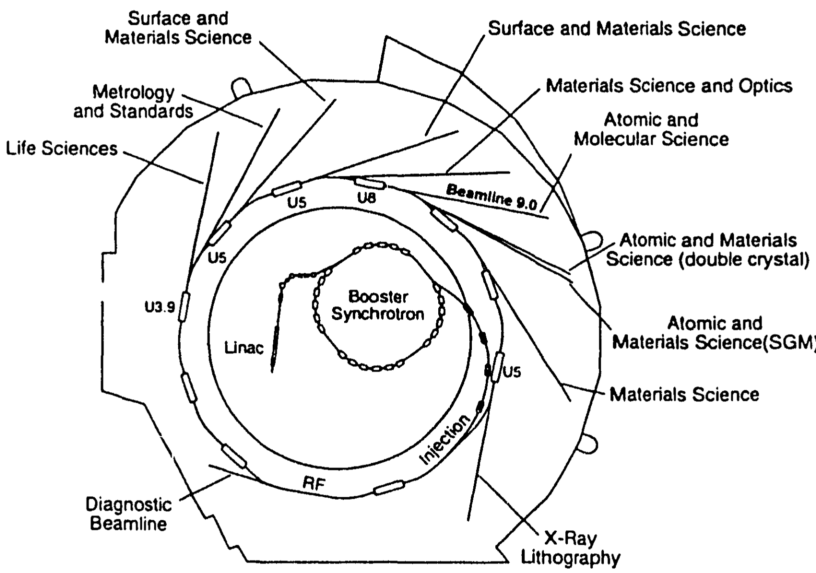

Figure 5. ALS floor plan showing locations of insertion devices and beamlines, and their applications. The proposed actinide program will use Beamline 9.0 .

The initial complement of five beamlines includes Beamline 9.0, which will deliver 20–300-eV photons produced by an 8-cm-period undulator. The proposed actinide program, for which an experimental station dedicated to the study of the transactinium elements and their compounds is planned, will use this undulator and beamline. Preliminary safety system requirements for this station have been considered.

Lawrence Berkeley Laboratory and ALS management have a commitment to making access to the beamlines as convenient as possible. We are developing efficient systems for user registration and training in order to minimize the time it takes users to meet institutional requirements and maximize the time for productive work. Construction of essential laboratory facilities for users is under way, and space has been made available for offices, a library, and a shop dedicated to users. Our goal is to see high-quality research conducted at the ALS, starting on the first day of operations.

THE ADVANCED LIGHT SOURCE

- Third-generation synchrotron light sources are characterized by ultraviolet and x-ray beams of unprecedented brightness.
- High brightness allows high spatial and high spectral resolution, and partially coherent radiation.
- This provides new research opportunities in physics, chemistry, biology, technology, and other fields.
- The U8 undulator and its beamline will provide an exceptional facility for actinide research.

Fred Schlachter
University of California
Lawrence Berkeley Laboratory
Berkeley CA 94720

X-RAYS ARE AN IMPORTANT PROBE OF MATTER

ALS

- Interact with electrons in atoms $\Rightarrow$ element selectivity (e.g., K, L edges)
- Energy appropriate for inner shells of atoms
- Short wavelength $\Rightarrow$ image small objects
- Absorption coefficient appropriate $\Rightarrow$ penetrate matter
- Relatively easy to produce and detect
- Can be polarized (linear, circular)
- Variable (tunable) energy
- Short-pulse time structure

THE ADVANCED LIGHT SOURCE: OVERVIEW

ALS

- National user facility

- Provides <u>UV and soft x-ray beams</u> of unprecedented brightness: (<10eV to ~10 keV)
  - Broadly tunable with narrow spectral features (resolution 10,000) $\epsilon/\Delta\epsilon$
  - Partially coherent (optics, interference)
  - 35 psec time structure (life times, time of flight)
  - Polarized (linear, circular)

- Utilized by researchers from industry, academic, and national laboratory communities:
  - Materials and surface science
  - Atomic and molecular physics
  - Chemistry
  - Life sciences
  - Technology

  overlap with spectral range of lasers

- Construction project began in late 1986

- Begin operations in spring 1993 April 1993

- Construction cost – $99.5 million

The ALS Is Open To All Qualified Users

- Open to all qualified users
- Proposals evaluated by peer review (Program Review Panel)
- No user fees (presently) for research published in open literature and supportive of the broad mission of DOE
- Full cost recovery for proprietary research

The ALS Has Space for 10 Wigglers and Undulators and 36 Bend-Magnet Beamlines

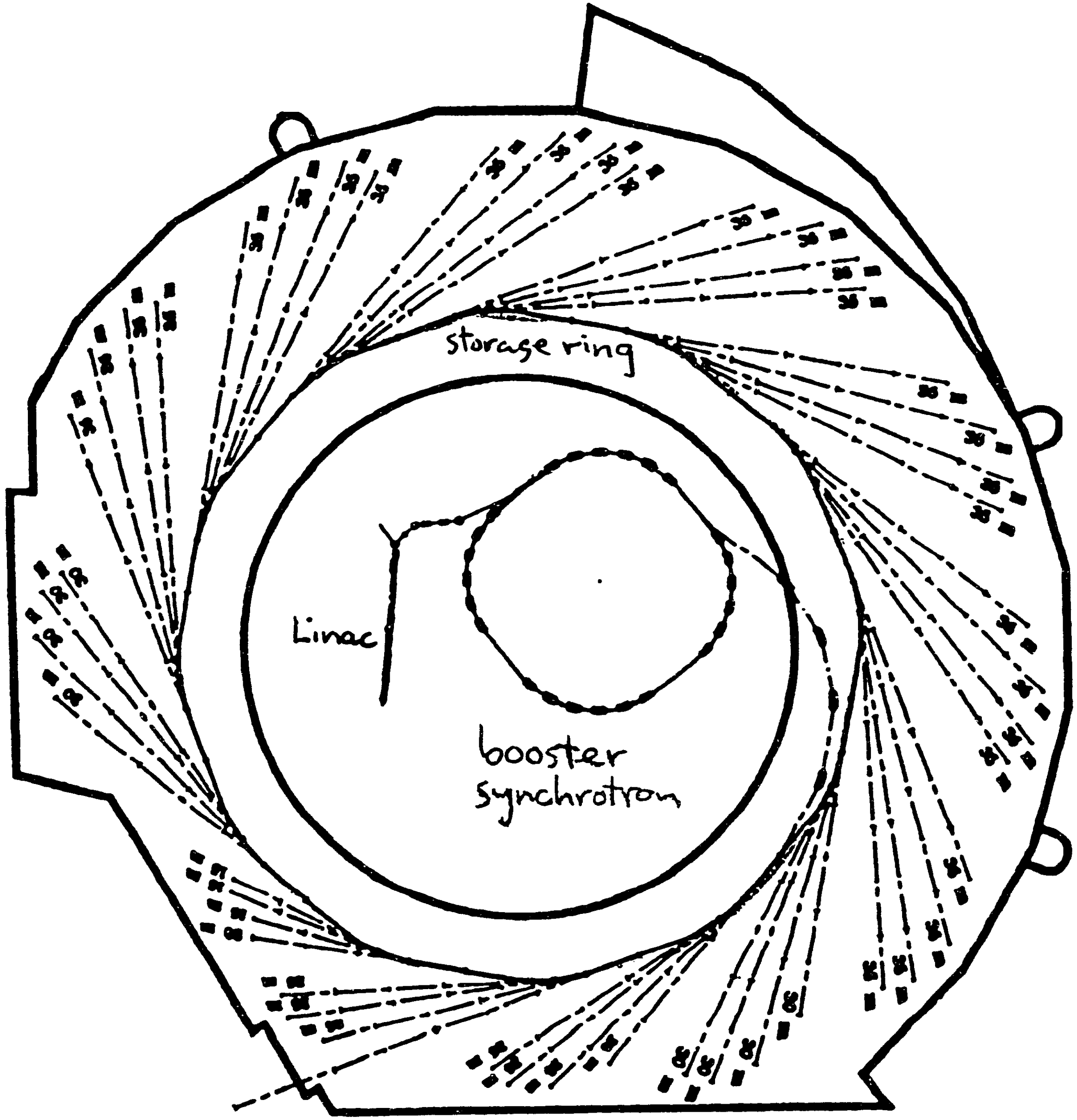

CBB 785-6423

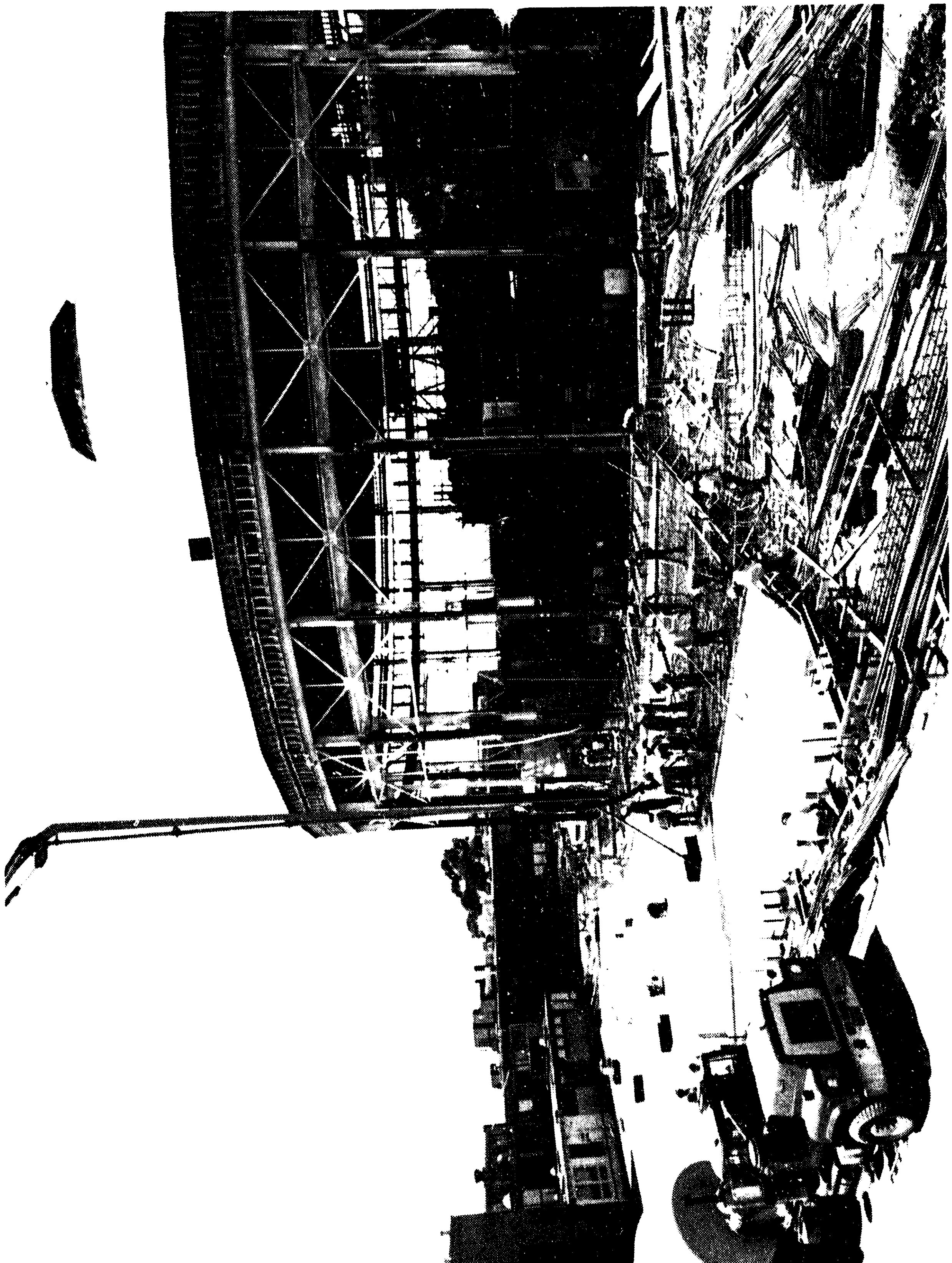

XBC 896-5395

XBC 890-10664

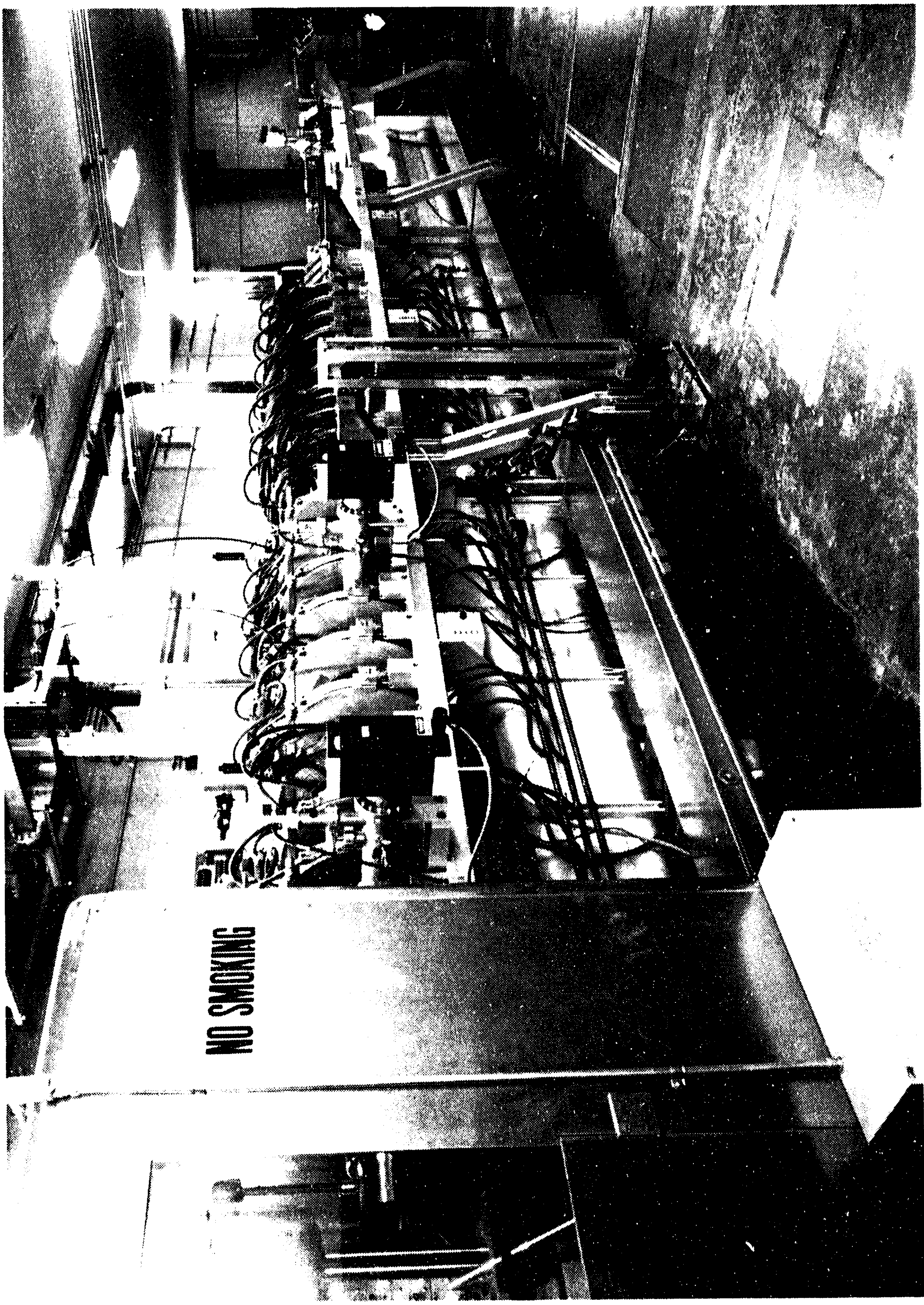

XBC 6010-9512

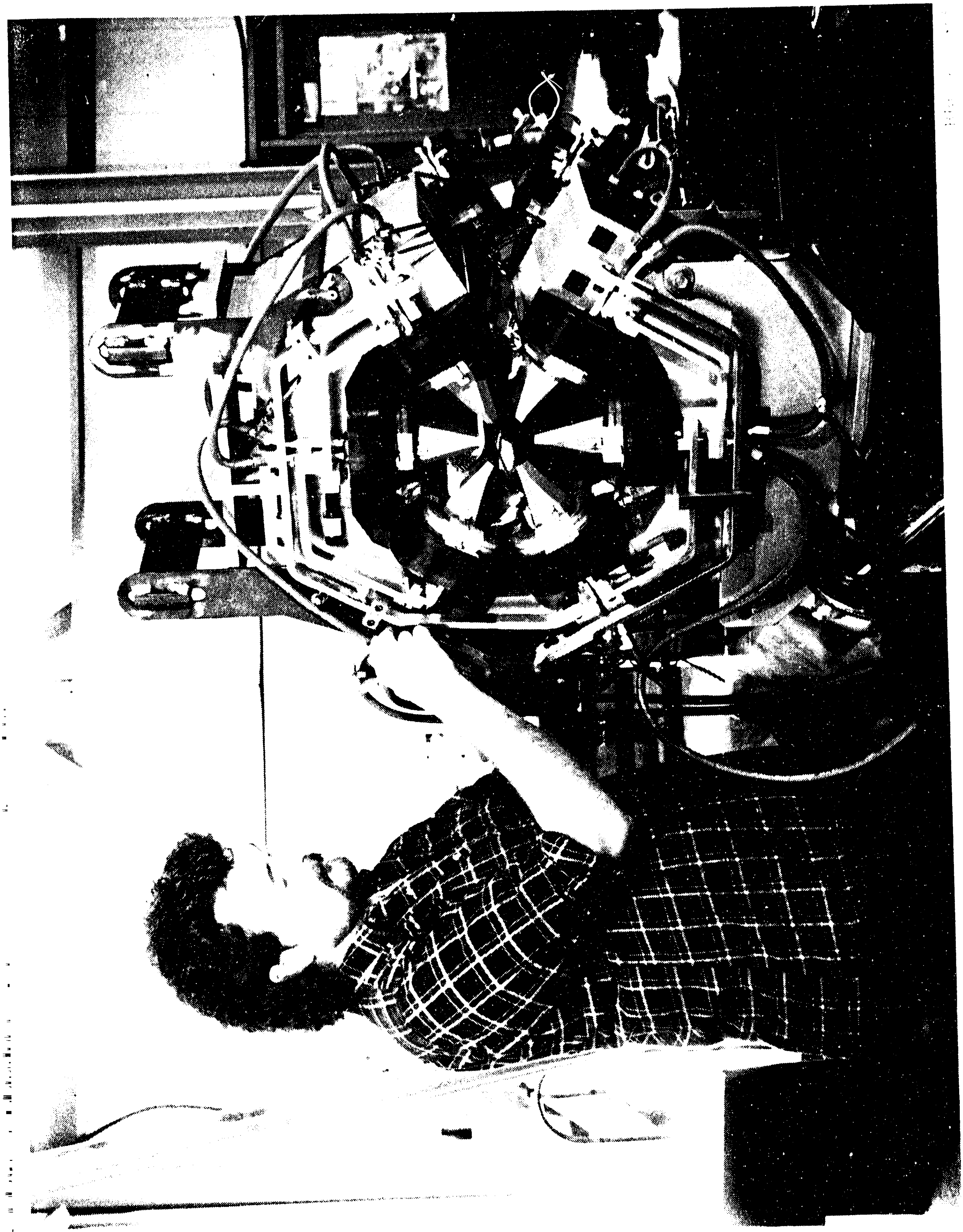

CBB 905-3869

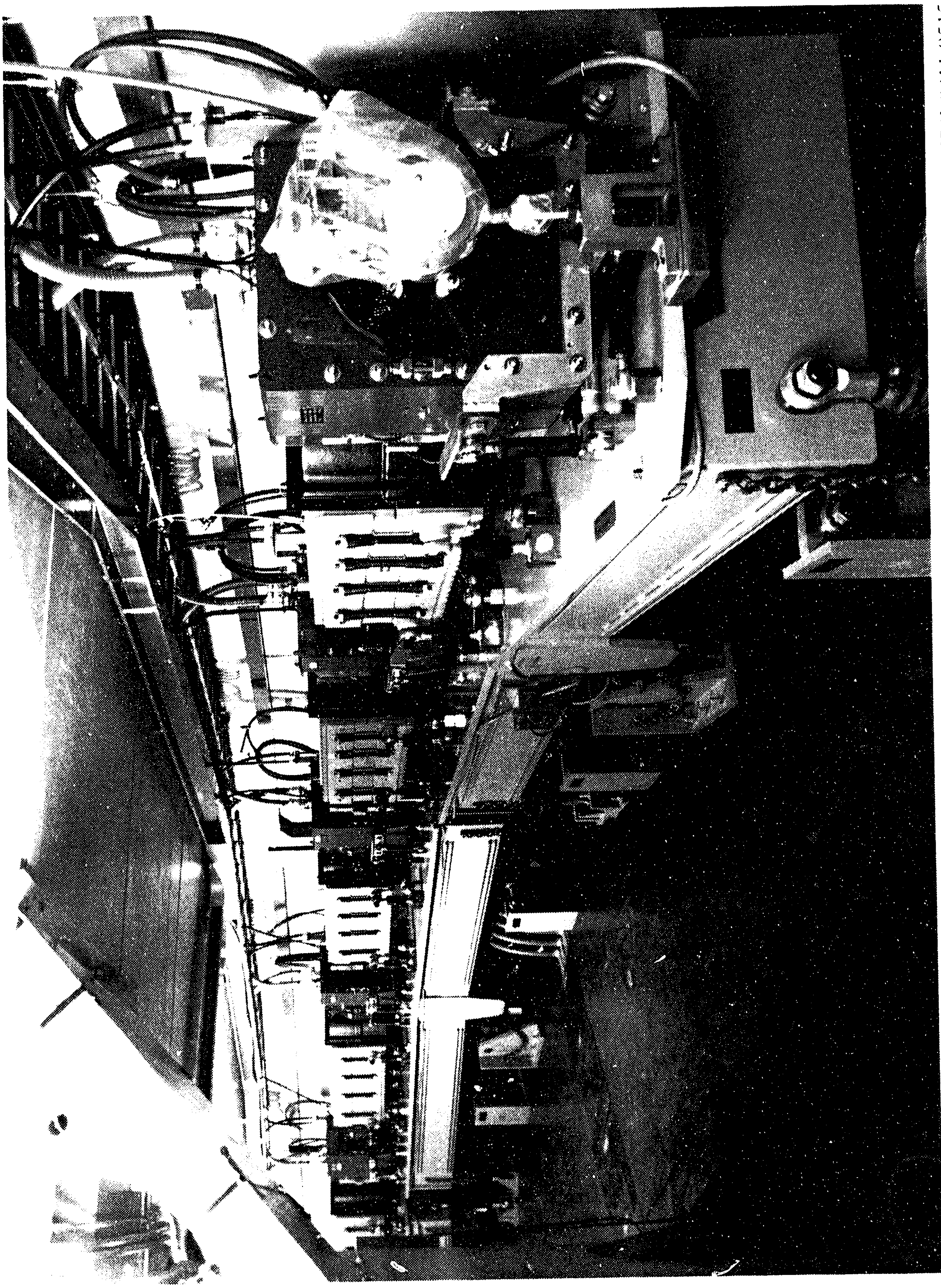

XBC 9011-9515

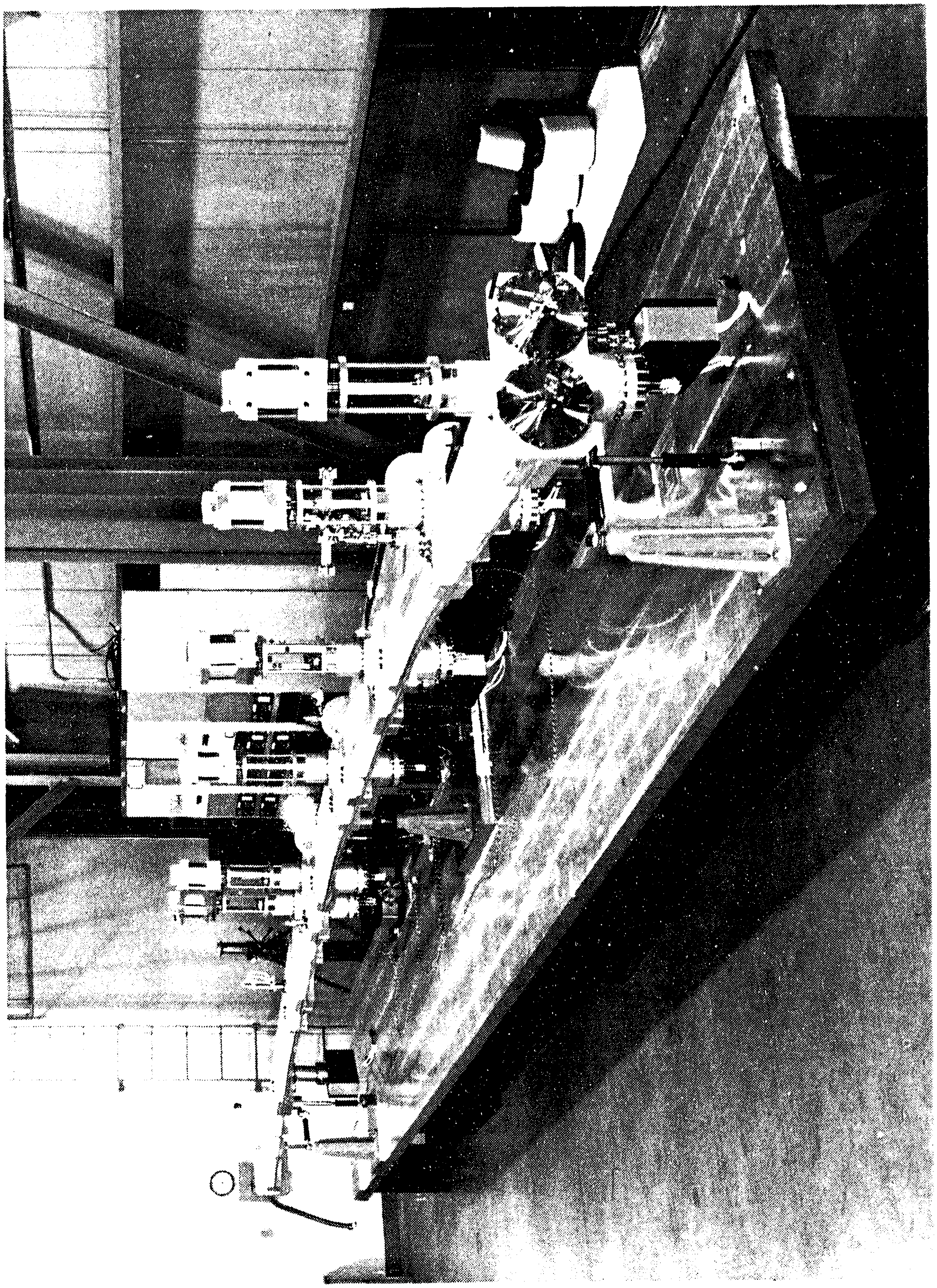

CBB 860-10807

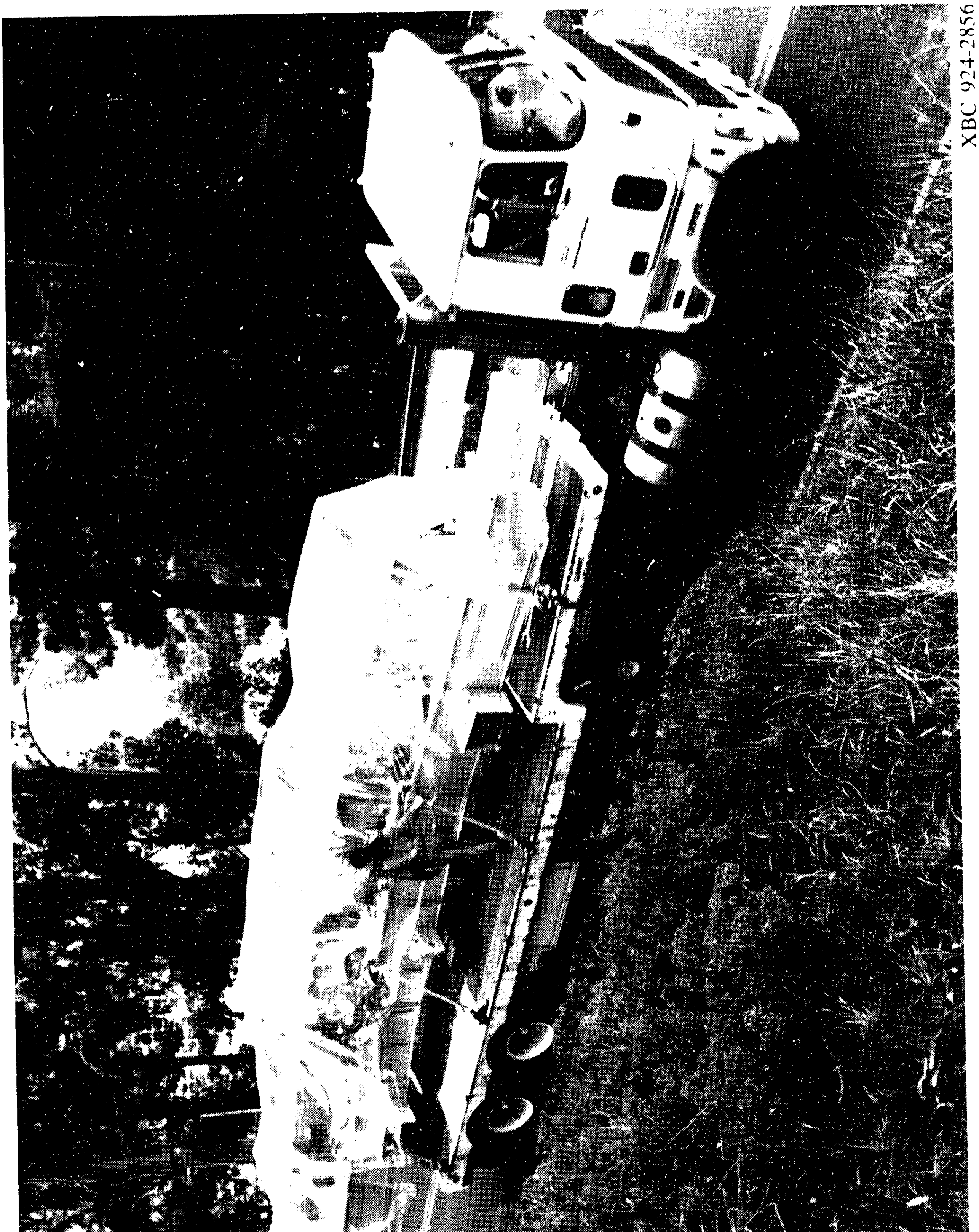

XBC 924-2856

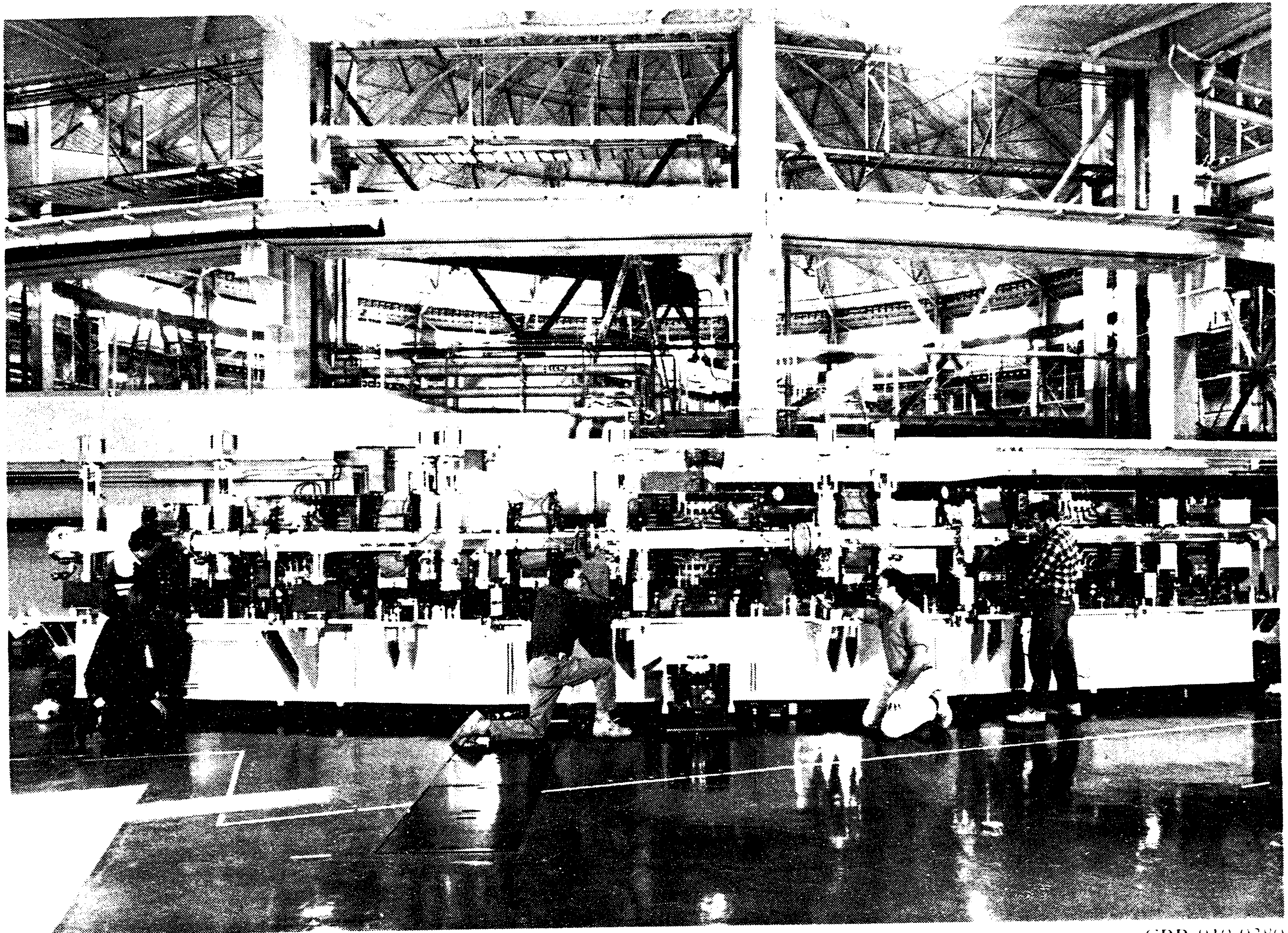

CBB 910-9380

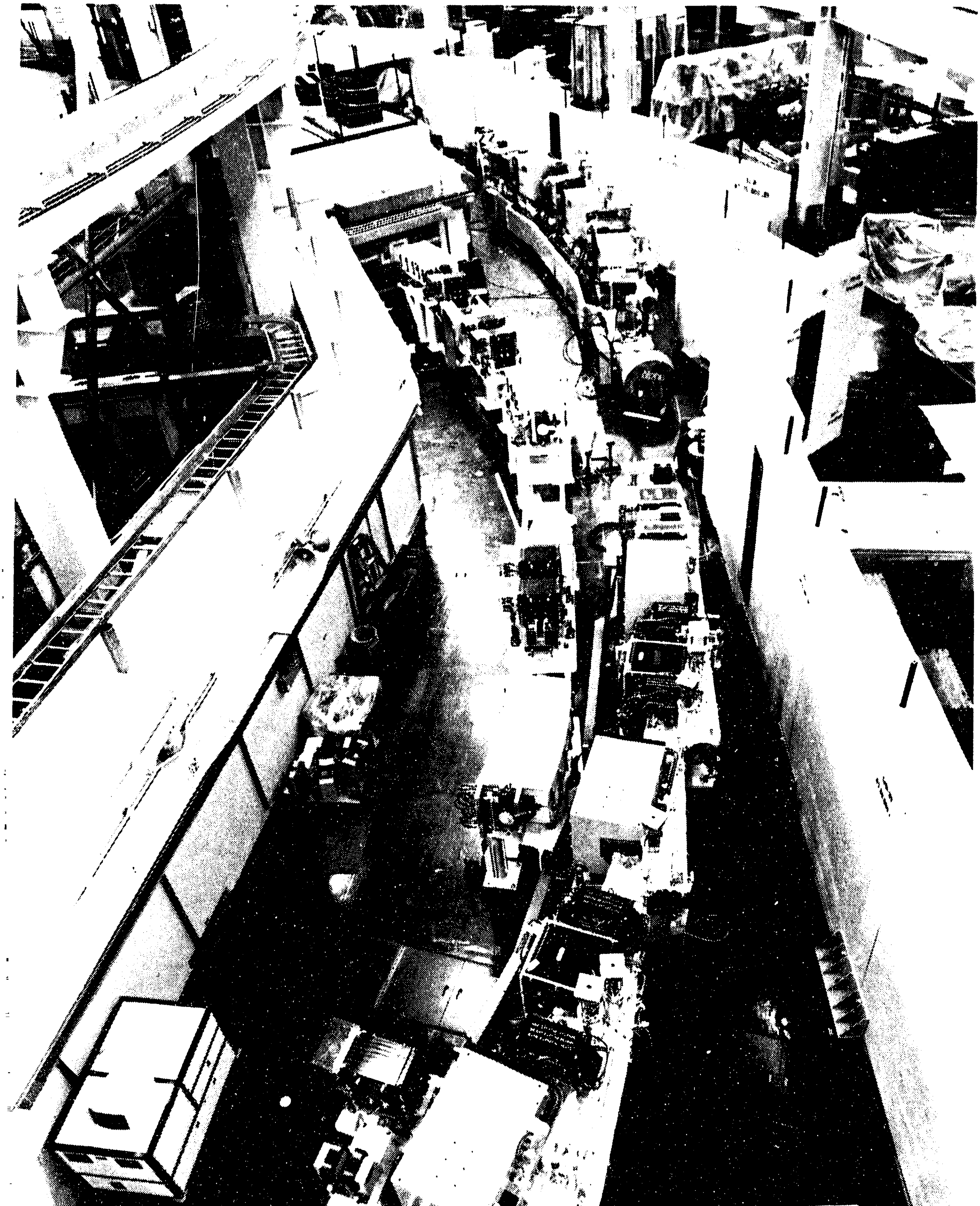

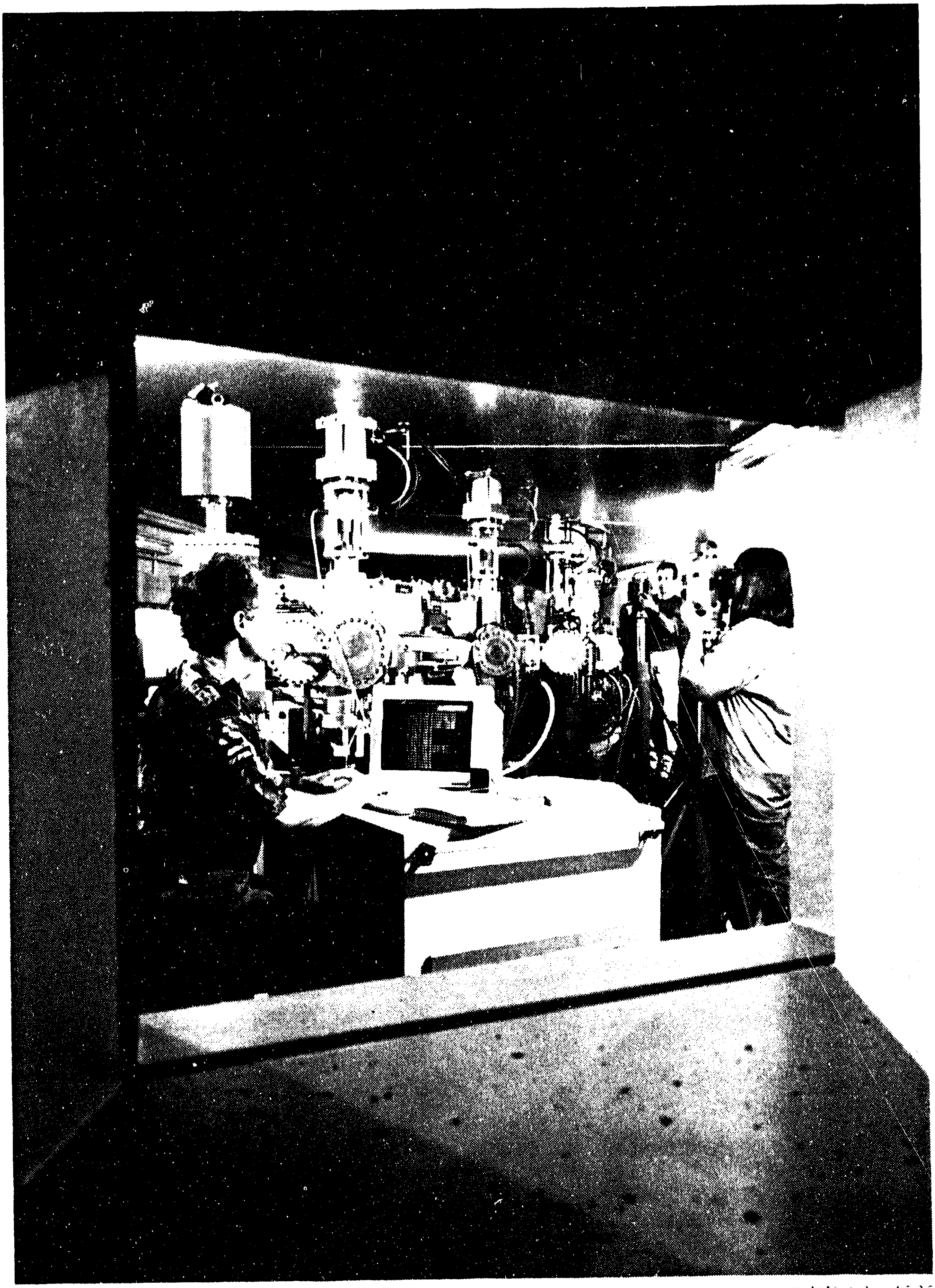

CBB 926-4525

Evolution of Synchrotron Radiation

ALS

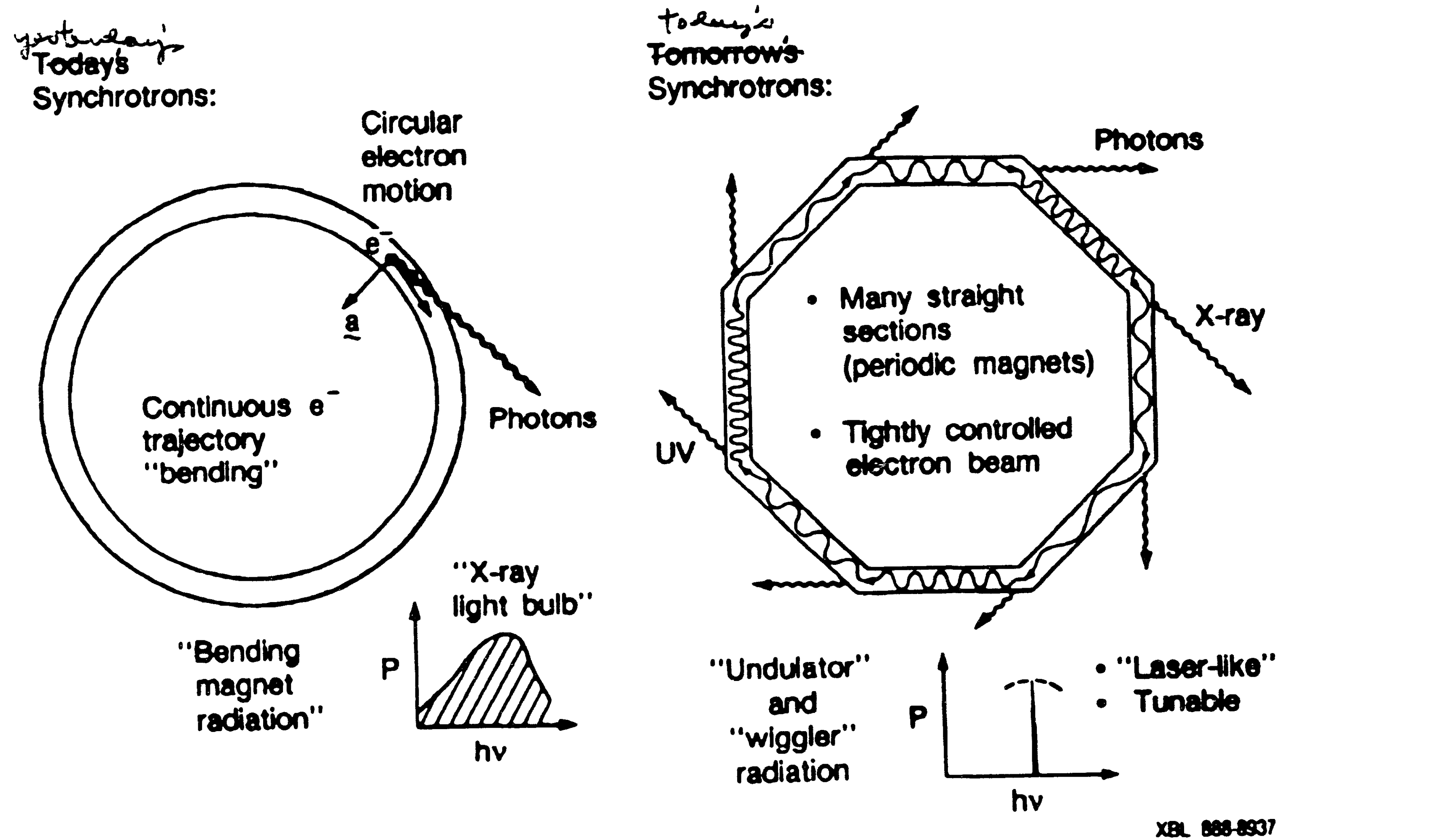

Insertion Devices (Undulators and Wigglers) Dramatically Improve X-Ray Production

ALS

- Periodic magnetic structure
- Usually array of alternating permanent magnets

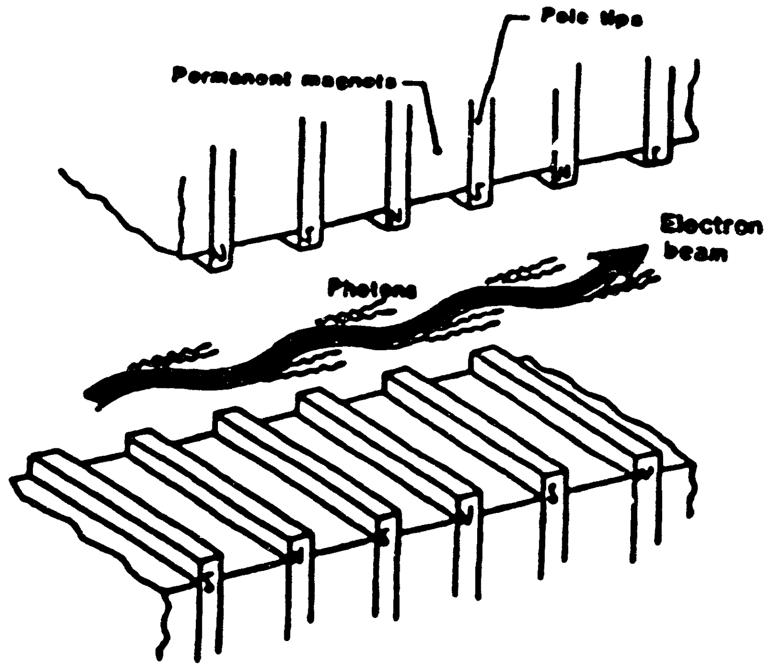

- For N periods: flux and brightness increase by a factor of N (N ~ 100 for ALS undulators)

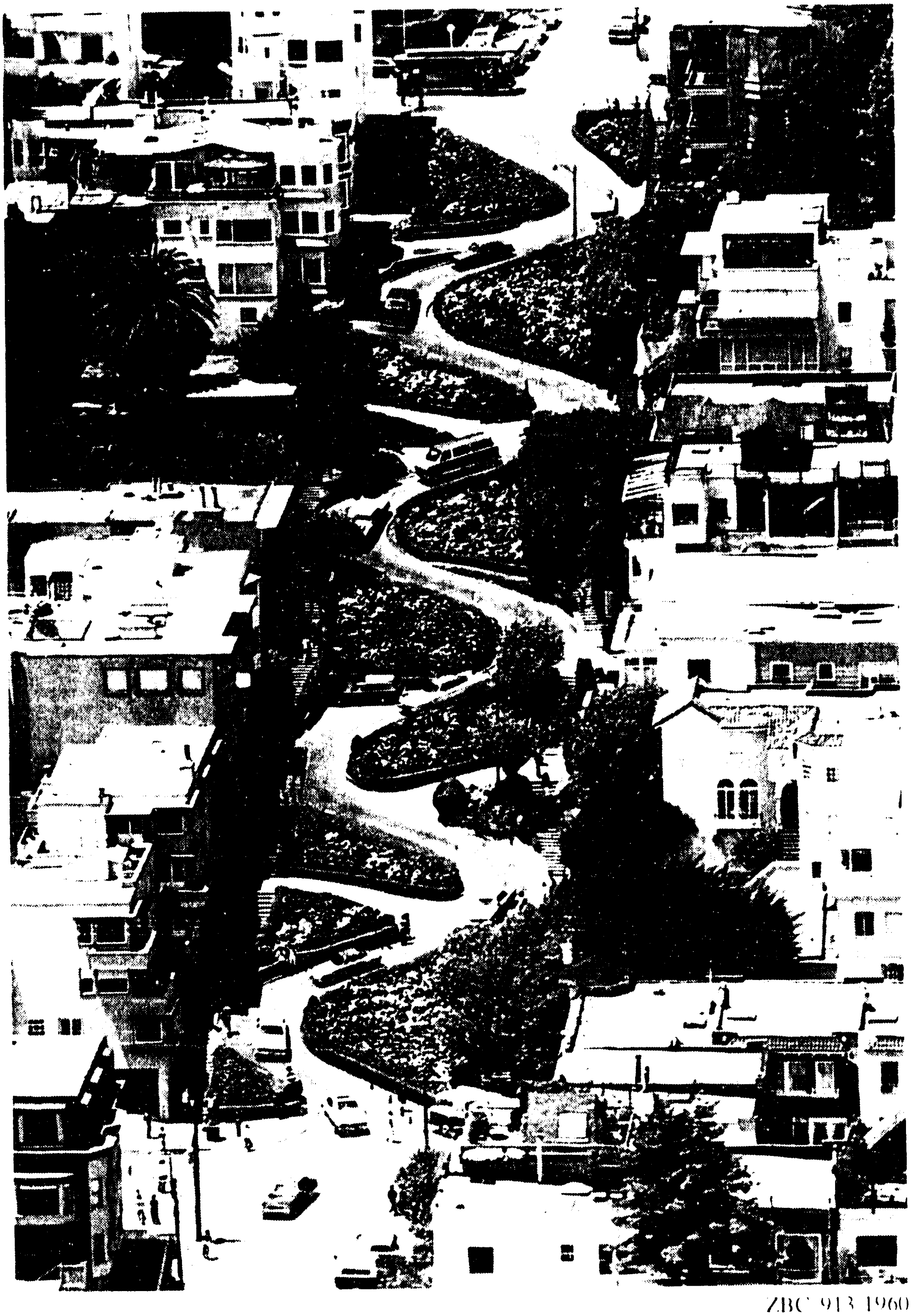

ZBC 913 1960

An Undulator Produces a Very Bright Beam of VUV or X Rays

- Coherent superposition of radiation from electrons bent many times in periodic permanent-magnet structure

- Properties of undulator radiation:

  — High brightness
  — Tunable photon energy
  — Partial coherence
  — High linear polarization
  — Picosecond time structure

An undulator is a tunable soft-x-ray picosecond strobe light with laser-like properties

The ALS Has Both Undulators and Bending Magnets

Bending magnet radiation (sweeping searchlight)

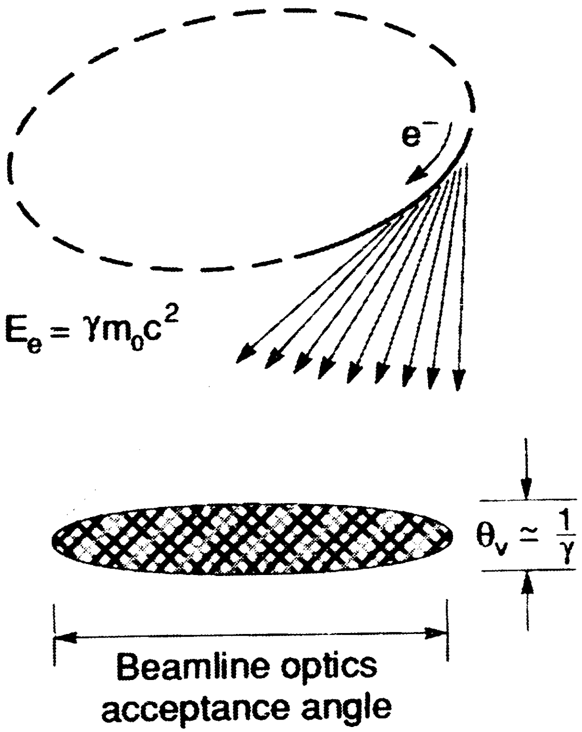

Undulator radiation

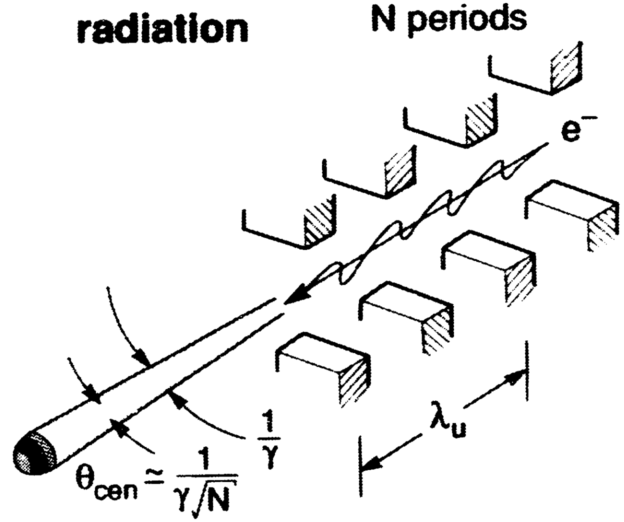

$$\lambda_x = \frac{\lambda_u}{2\gamma^2}\left(1 + \frac{K^2}{2} + \gamma^2\theta^2\right)$$

in the central radiation cone:

$$\frac{\Delta\omega}{\omega} \simeq \frac{1}{N}$$

$$\theta_{cen} \simeq \frac{1}{\gamma\sqrt{N}}$$

XBC 911-370

Angular Divergence of Bending Magnet and Undulator Radiation

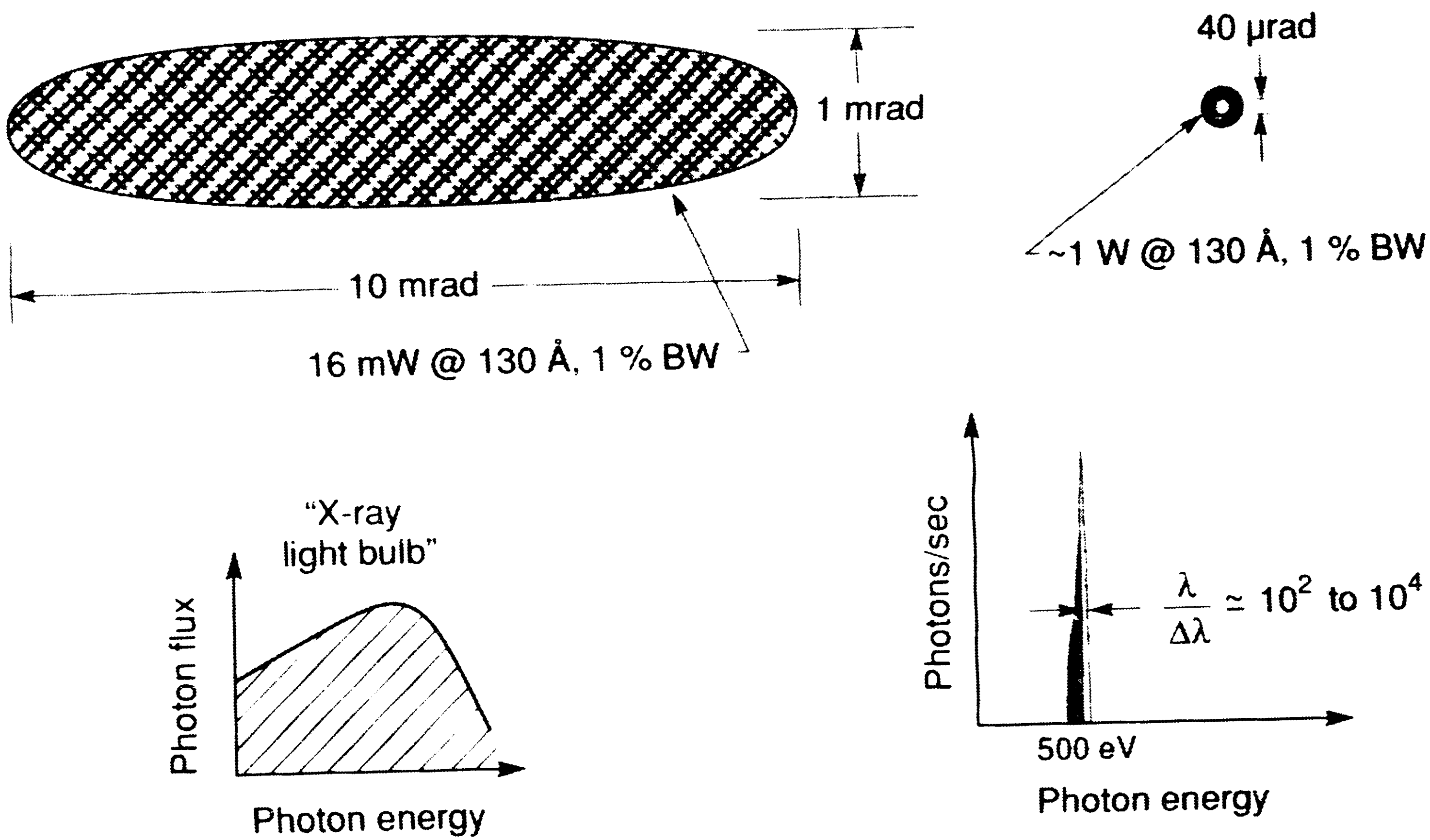

XBC 911-369

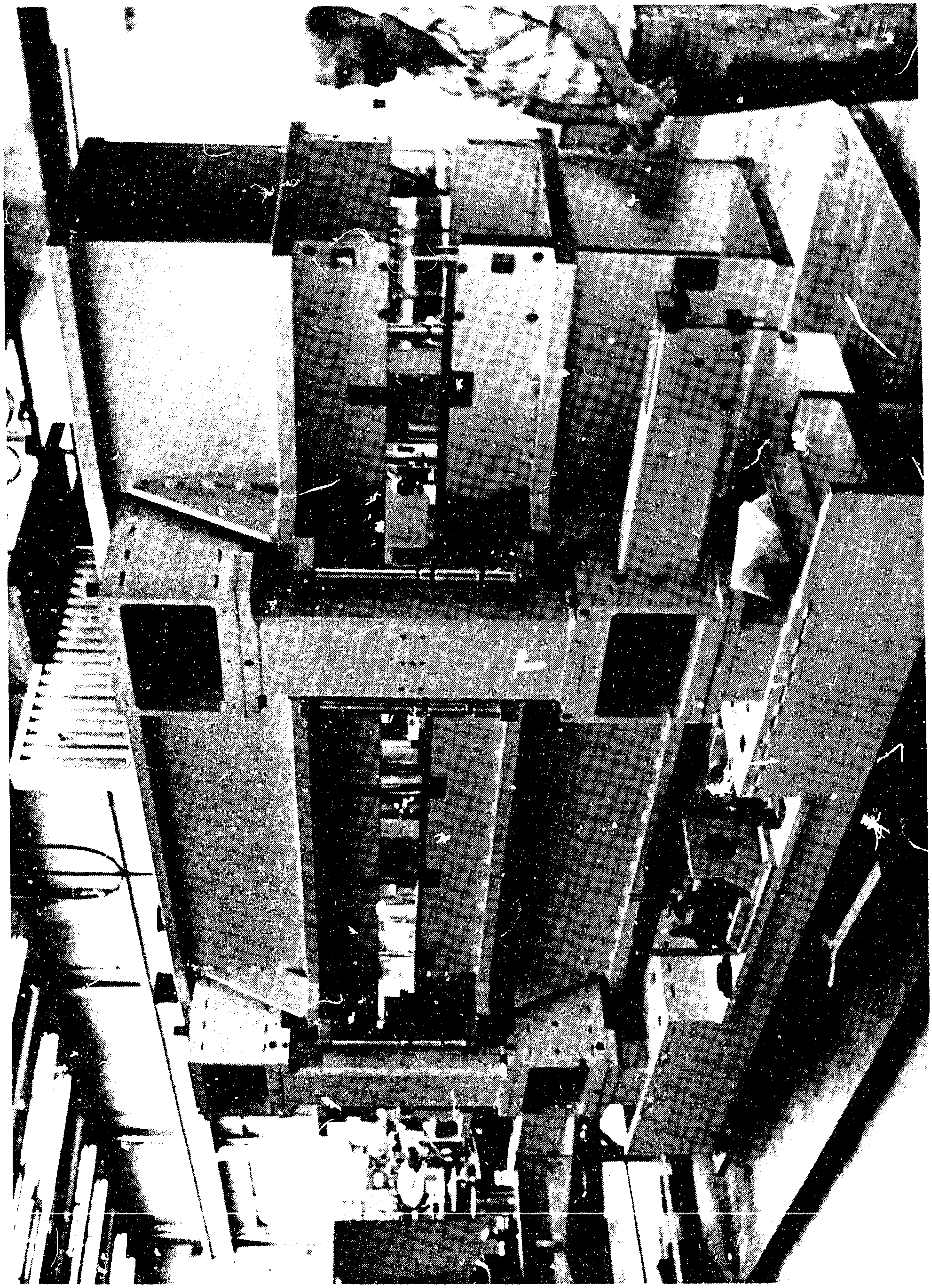

HIGH BRIGHTNESS IS THE MAIN FEATURE OF THE ALS

ALS

- High flux onto a small spot
  microns to 100's of Å
- High resolution $E/\Delta E \approx 10{,}000$
- Ease of focussing ⇒ microscopy
- Element-specific sensitivity
- Partial coherence
- Broad tuning range
  (< 10 eV to > 1 keV)
- Short pulses

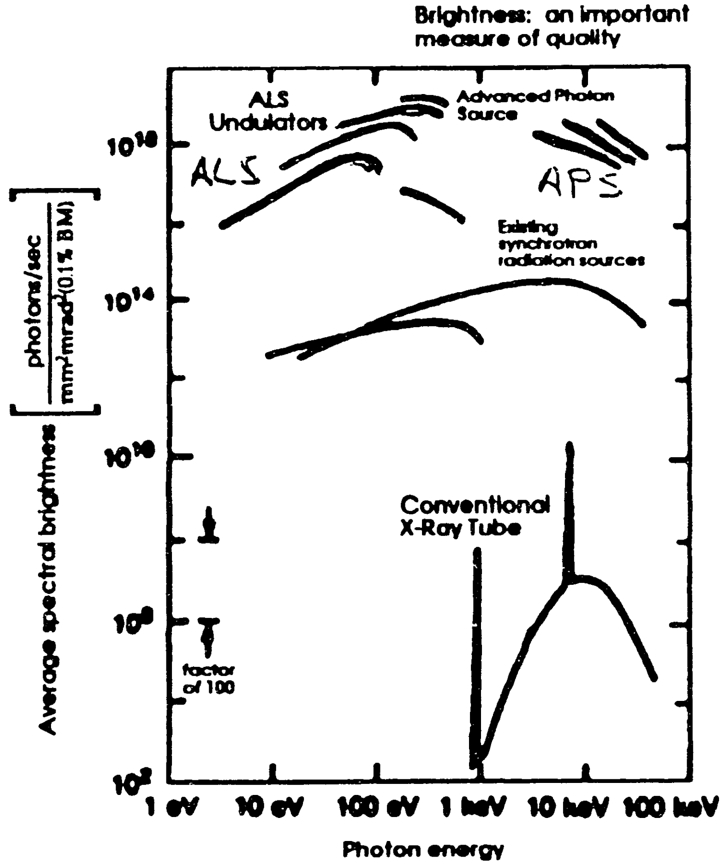

THIRD-GENERATION SYNCHROTRON-RADIATION SOURCES HAVE HIGH BRIGHTNESS

ALS

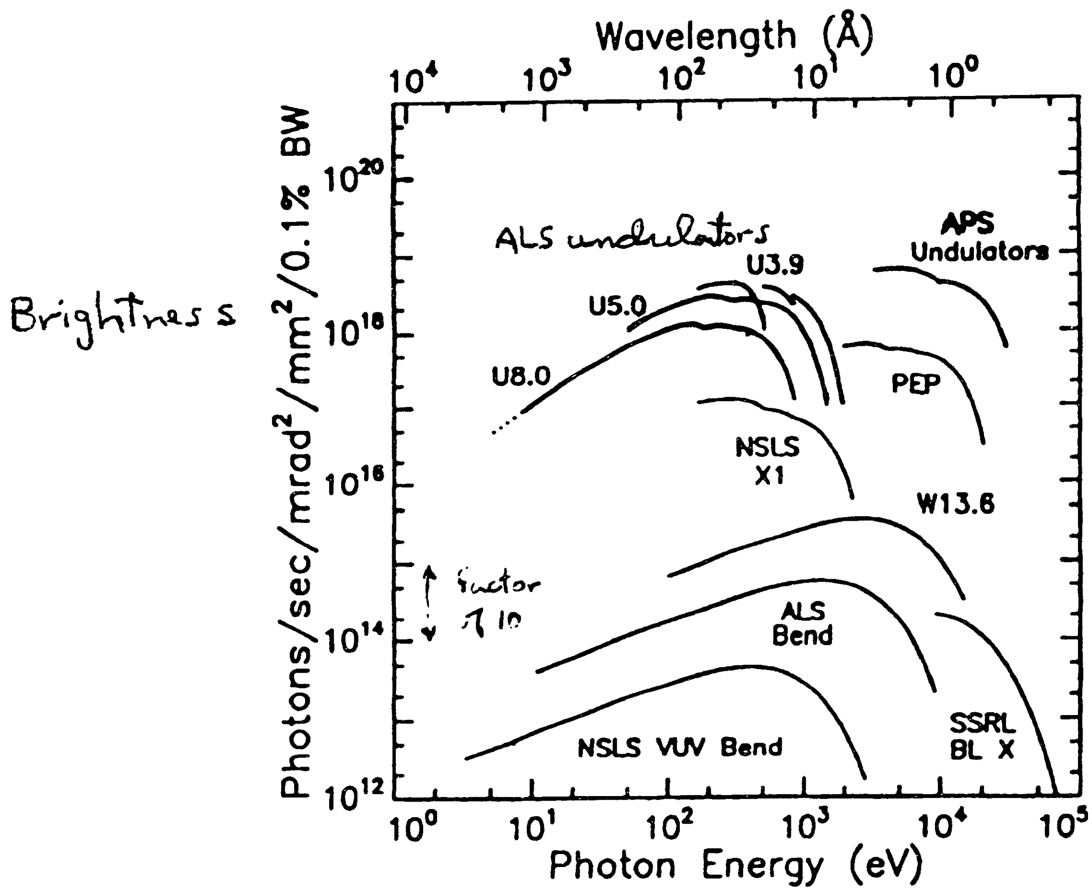

- **ALS undulators produce a beam which is a factor of 10,000 brighter than that from bend magnets**

AN ALS UNDULATOR ALSO PRODUCES HIGH FLUX

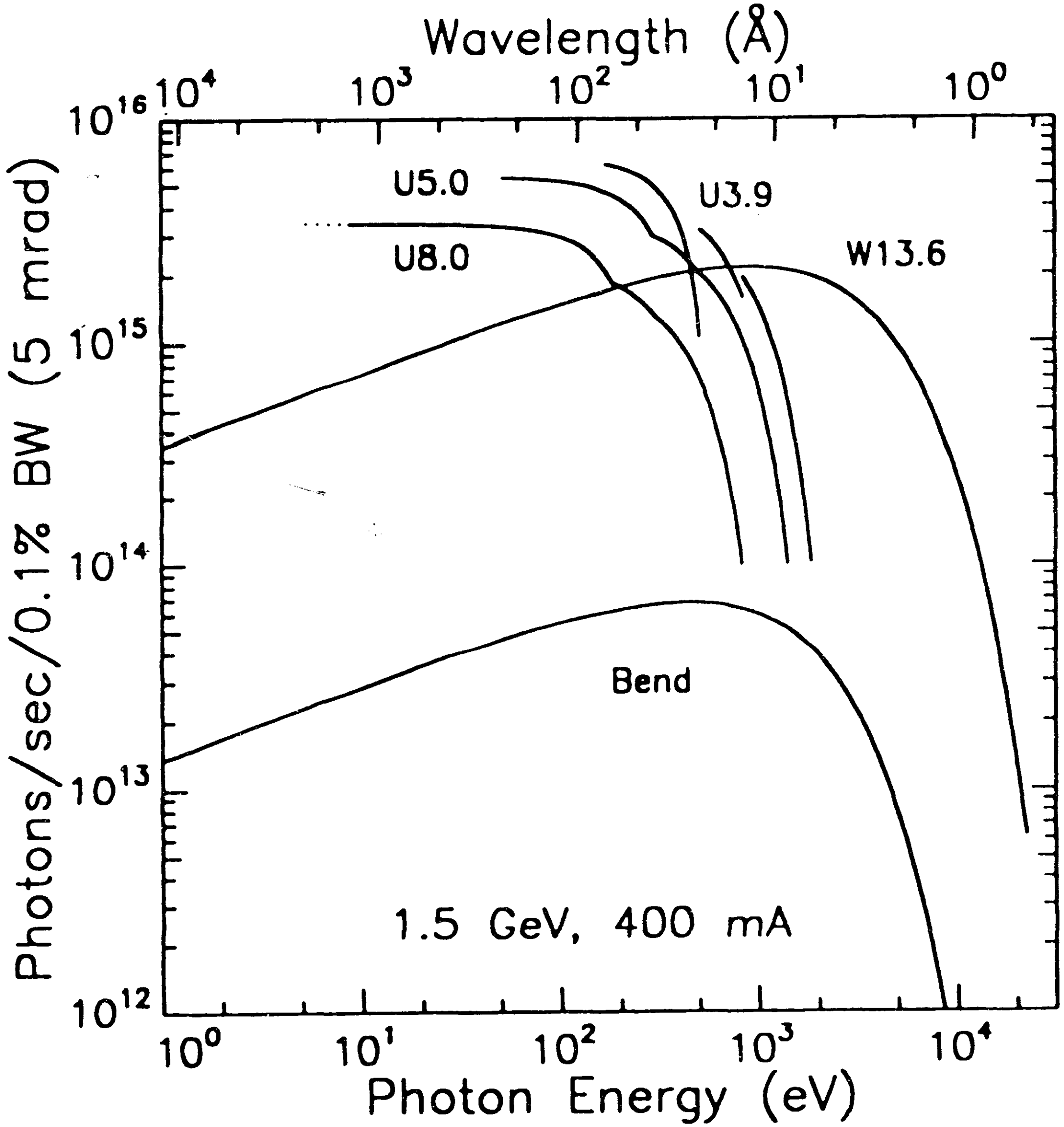

ALS Can Access Core Levels of Essentially All Elements: (200 - 1200 eV)

ALS

PERIODIC TABLE OF THE ELEMENTS

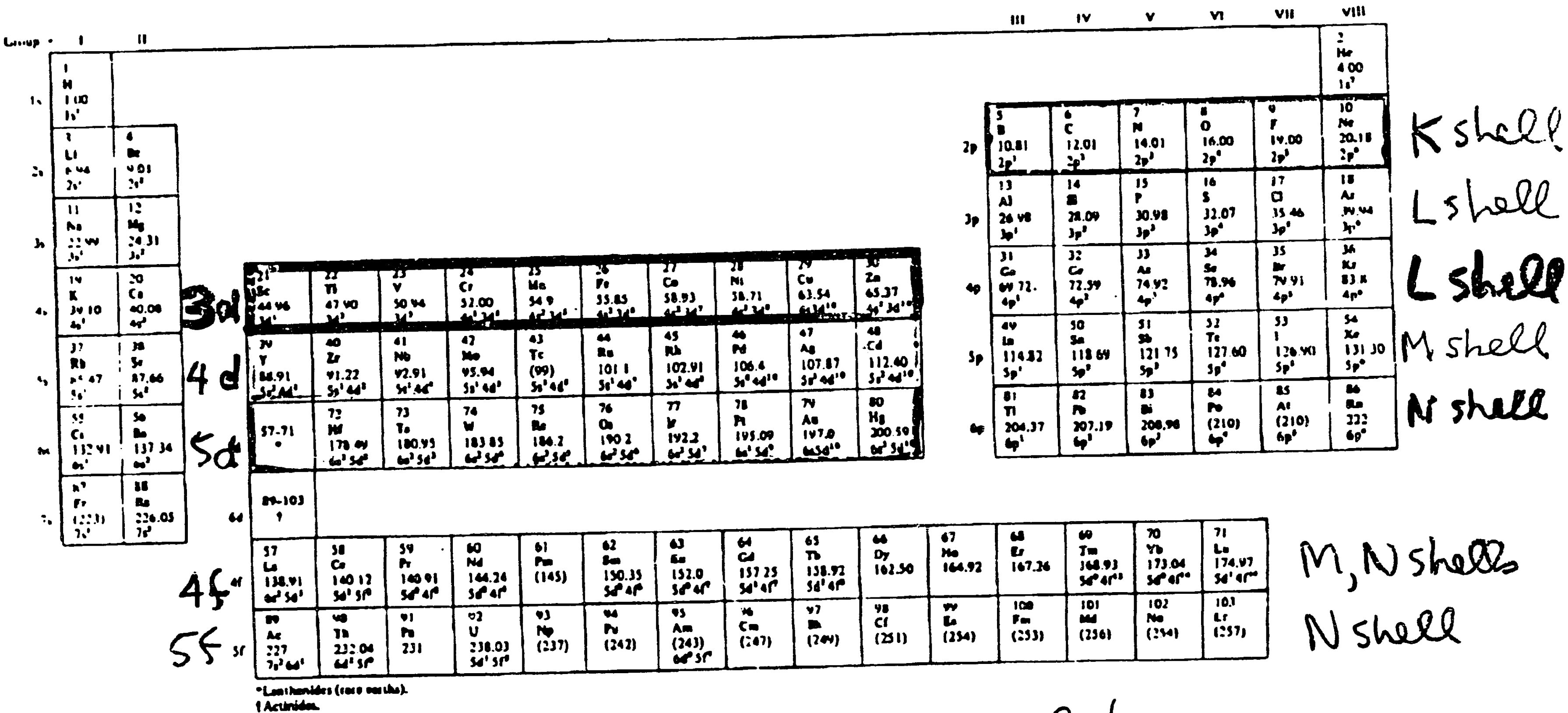

U8 undulator: 20-300eV

MANY LIGHT SOURCES ARE BEING BUILT

ALS

United States

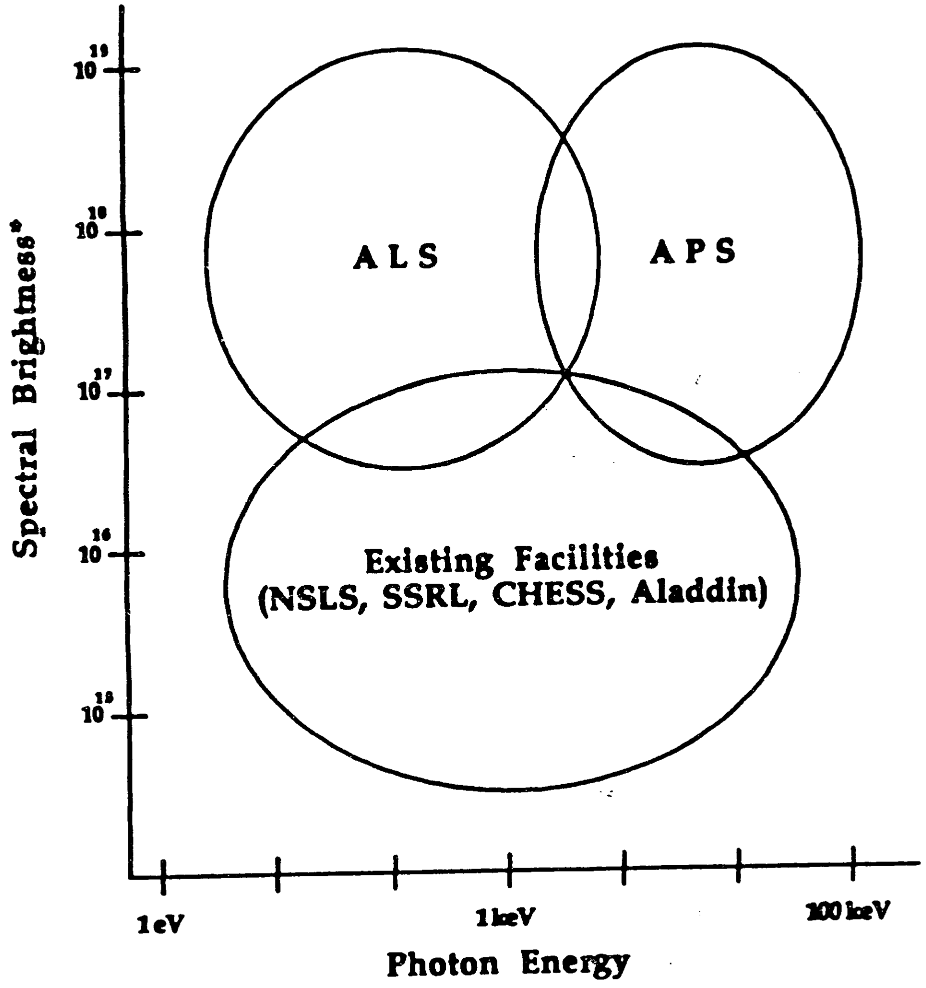

*Photons/mrad^2/mm^2/0.1% BW

Elsewhere

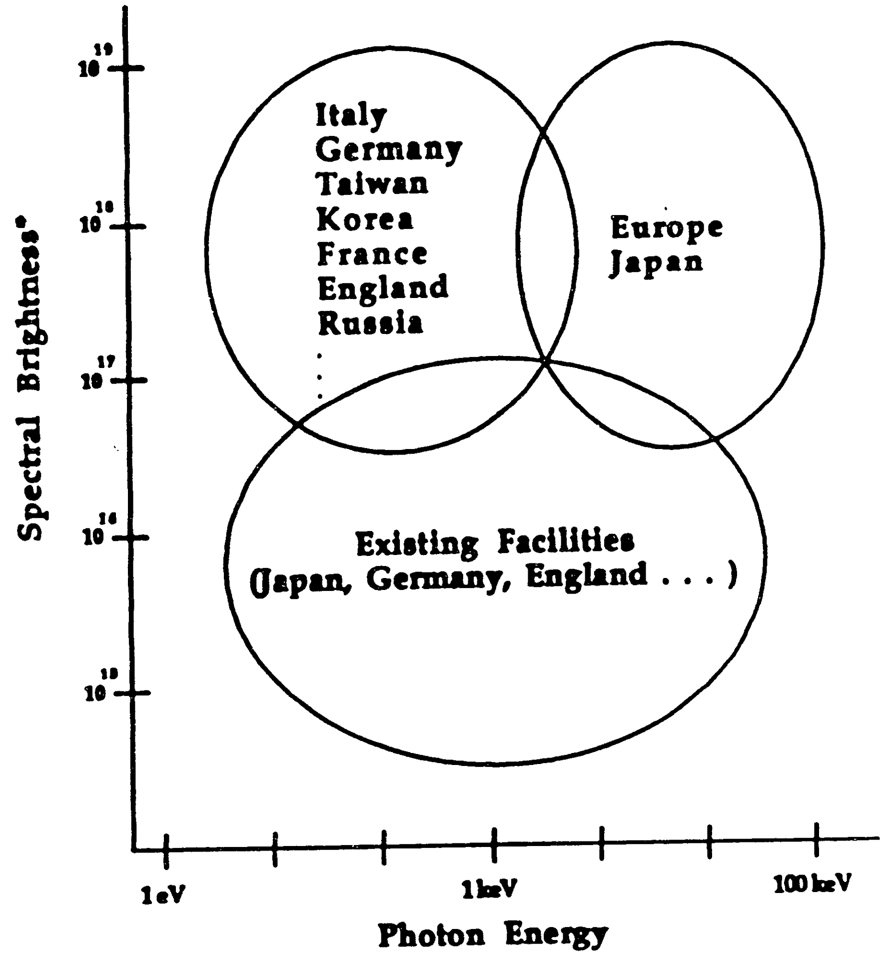

*Photons/mrad^2/mm^2/0.1% BW

JM: SLAC Mtg. (10/24-25/91 Pg. 3
mod FS 2/92

Double Excitation in Atomic Helium

- Use of high resolution: SX-700 monochromator at BESSY
- Auto-ionizing states below threshold of He+(n=2-7)

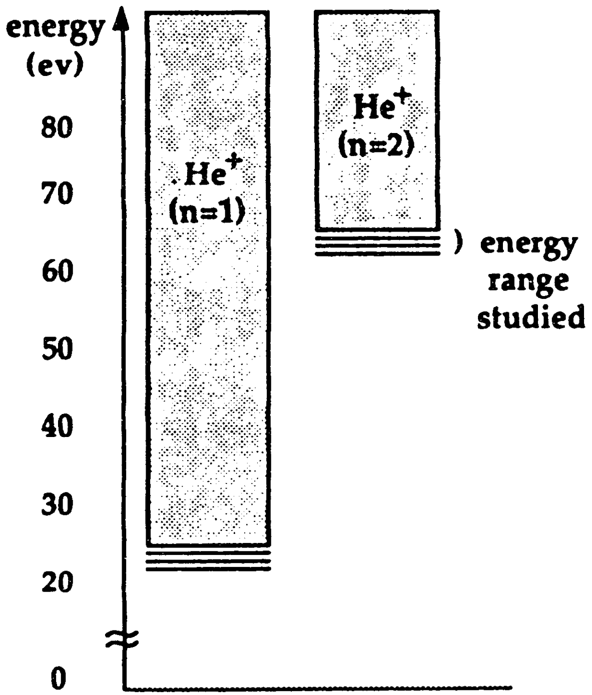

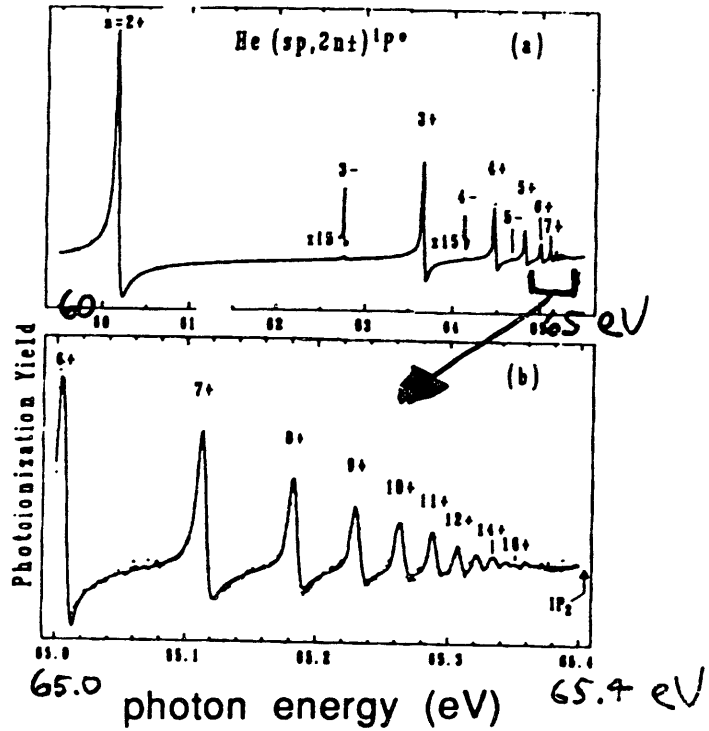

Ref: Domke et al., (September 1990)
BESSY

Phys. Rev. Letters 66, 1306 (1991)

The Short Pulse Length Will Be Useful for Timing Studies

A L S

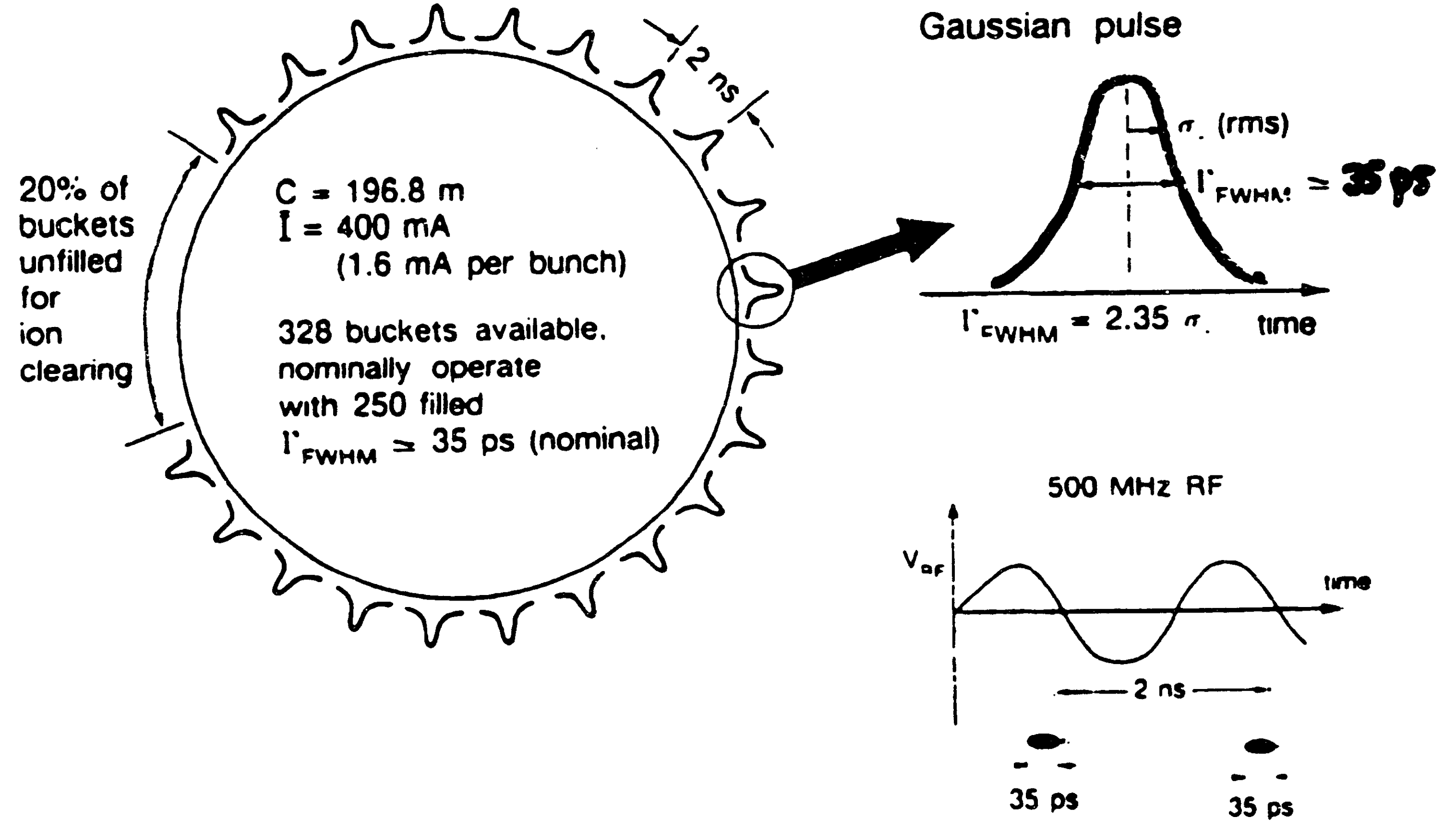

- Pulse length: 35 ps FWHM
- Bunch structure can be selected: single bunch, multiple bunches

Time Structure is Useful for Some Experiments

ALS

- Time structure of storage ring is different from that of laser

  — CW laser
  — Pulsed laser

    -- Low repetition rate
    -- Pulsed length depends on laser (µs to fs)

  — Storage ring (ALS)

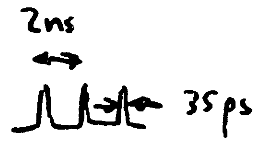

    -- High repetition rate (500 MHz)
    -- 35-ps pulse at 2-ns intervals standard
    -- Variable filling pattern changes pulse spacing (e.g., single bunch with 650 ns between pulses; pseudo-random filling pattern)

- Select physical problems on ps, or longer, time scale

- Can use multiple photons with time delay (pump-probe)

  — Laser synchronized with storage ring
  — Photons from undulator and bend magnet

- Energy per pulse is lower with SR than with laser

  — Laser: high-pulse energy for harmonic generation
  — SR: low-pulse energy; undulator output includes harmonics

The ALS will have ten beamlines in 1994

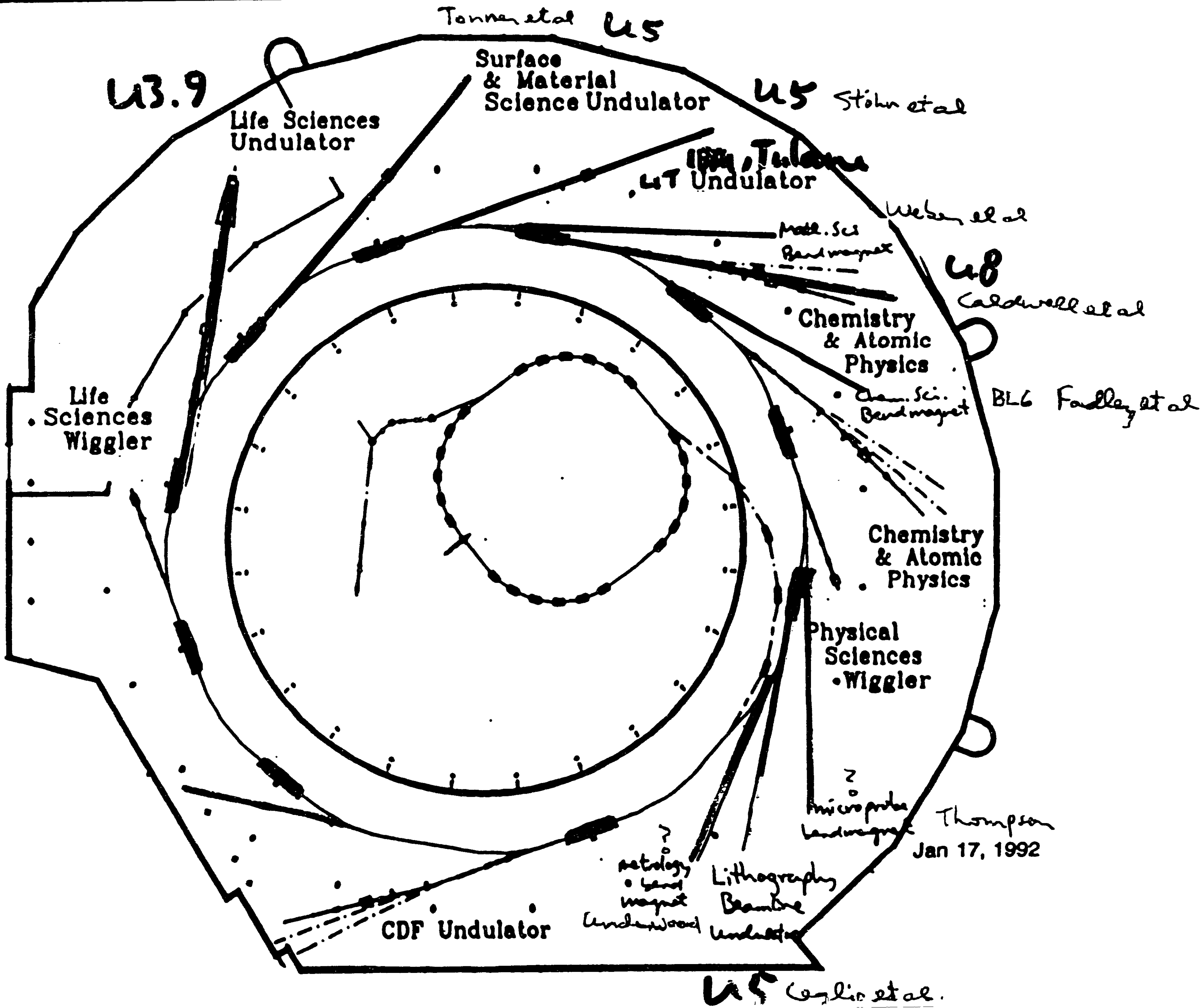

NEW CAPABILITIES, NEW RESEARCH

A L S

Next-Generation VUV Synchrotron-Radiation Facility Optimized for Insertion Devices

• INTENSITY, BRIGHTNESS • COHERENCE • Polarization • SHORT PULSES: 35 ps *(35 trillionths of a second)* • TUNABILITY	⟹	• Biological imaging • Measurements on small or dilute samples • Studies of ultrafast processes • Studies of dynamic processes in biological systems • Bond-selective chemistry • High-spatial-resolution studies • Lithography for chip fabrication

FS: ALSUA Mtg. 8/23/90 Pg. 3

The ALS Provides an Exceptional Opportunity for Important New Research

ALS

- Uniqueness of the Source:
  - Very high brightness/high flux
  - Wide spectral range/tunable
  - High degree of polarization
  - High resolution
  - Partial coherence
- Importance of the Research:
  - Materials: spectroscopy, spectromicroscopy
  - Life Sciences: microscopy, spectroscopy, crystallography
  - Atomic Physics: experiments with tenuous targets
  - Chemistry: reaction dynamics
- Applications to Technology and Industry:
  - Materials characterization
  - Optics development for lithography

ISSUES FOR RESEARCH WITH ACTINIDE MATERIALS

- The approved U8 PRT proposal includes actinide research.
- This beamline will produce bright beams from 20 eV to 300 eV.
- An adjacent bend-magnet beamline will produce higher energy beams.
- Floor space and beam time will be available.
- Preliminary consideration has been given to safety issues.

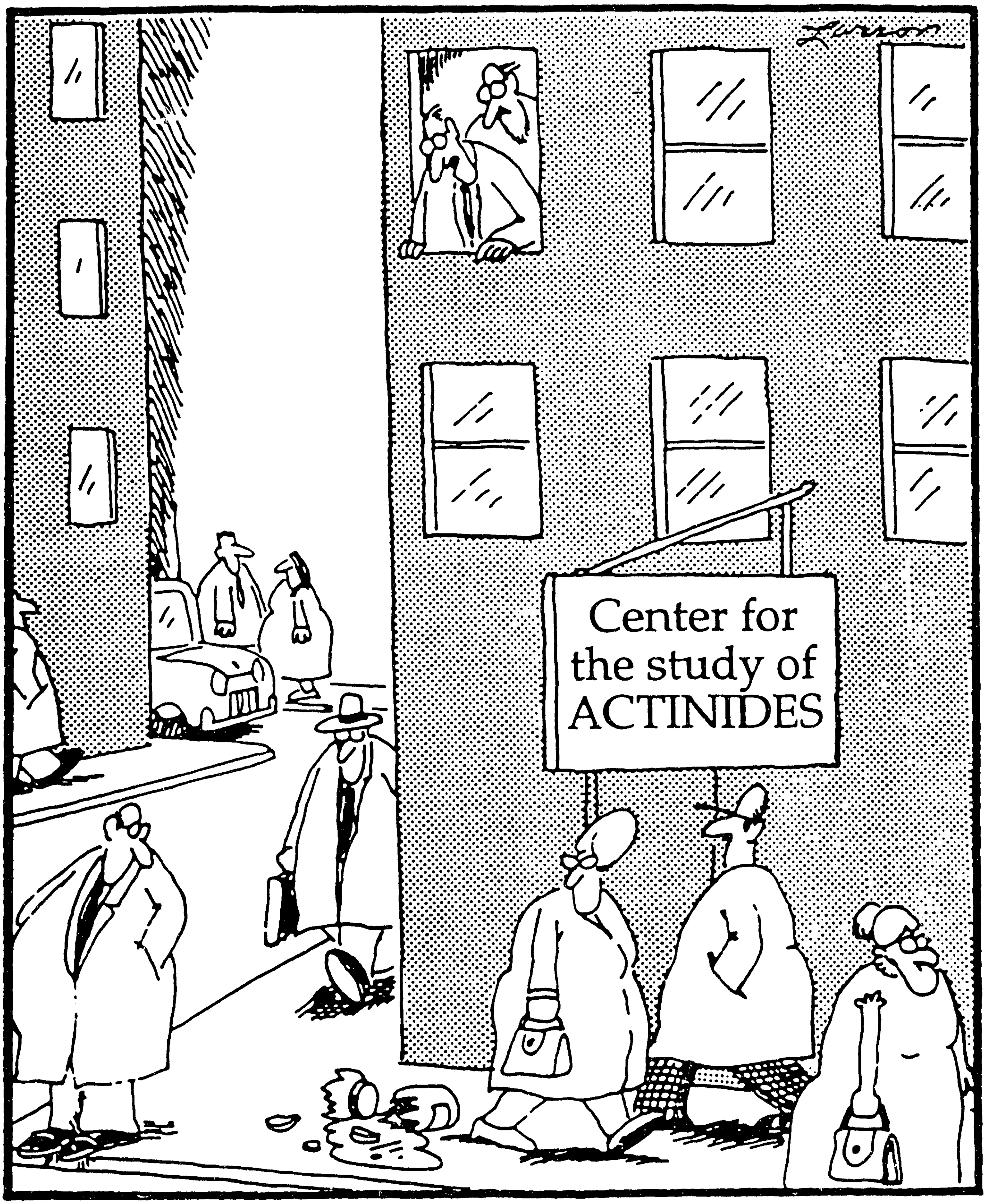

"Uh-oh."

ALS FEATURES

ALS

- High brightness
  - — Focus to small spot
  - — High resolution with high flux
- Fast pulse (35 ps)
- Tunable over wide range (VUX, soft X ray)
- Partial coherence
- Polarization (linear, circular)

XBC 891-1688

THE ADVANCED LIGHT SOURCE U8 BEAM LINE, 20 - 300 EV

P.A. Heimann

Advanced Light Source
Lawrence Berkeley Laboratory
Berkeley, CA 94720

The U8 is a beam line under construction at the Advanced Light Source, which will be completed in the spring, 1993. This beam line will be described along with its performance, emphasizing aspects relating to experiments. The radiation from an 8 cm period undulator is collected by two spherical mirrors. Next, the monochromator consists of an entrance slit, three interchangeable gratings having a 15° deviation angle and a moveable exit slit. At the end, a bendable refocusing mirror and branching mirrors provide a focus in one of several possible experimental chambers. Three horizontal reflections at 5° incidence angle were chosen to deflect the beam toward an actinide hutch in order to have sufficient space. Calculations have been made of both the resolution and output flux over the photon energy range of 20 - 300 eV. The design goal is to achieve high intensity, 10^{12} photons/s, at a high resolving power, E/ΔE, of 10,000. The predicted resolution and photon flux are shown in the figures below. Preliminary plans for harmonic rejection use thin filters, such as Al.

Fig. 1. The calculated resolution, where the solid lines show the slit width limit (10 μm) and the dashed lines show the worst aberration coma.

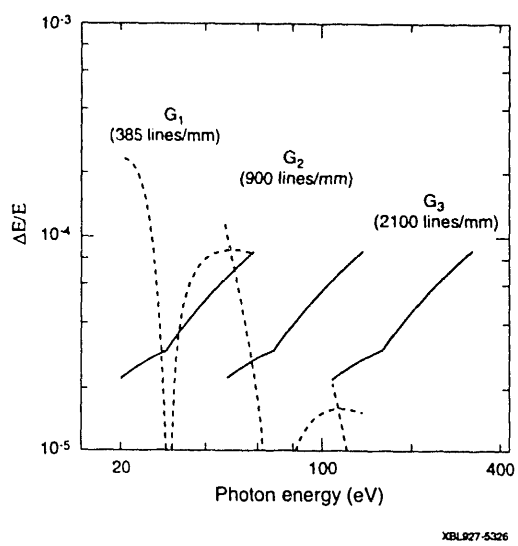

Fig. 2. The calculated photon flux for 10,000 resolving power (slit width limit) and 400 mA. Three gratings span the energy range 20 - 300 eV.

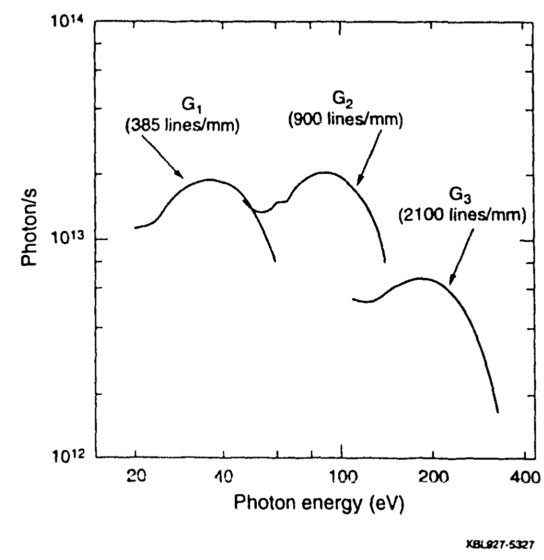

The Advanced Light Source U8 Beam Line, 20 - 300 eV

Philip Heimann
ALS Experimental Systems Group

1. Layout of the Beam Line: 8 cm period Undulator and Spherical Grating Monochromator.

2. Activities in the U8 Construction: Schedule and Show and Tell.

3. Expected Performance: Flux at High Resolution, Resolution, Focus at the Sample, Layout of Space for Experimental Chambers

Layout

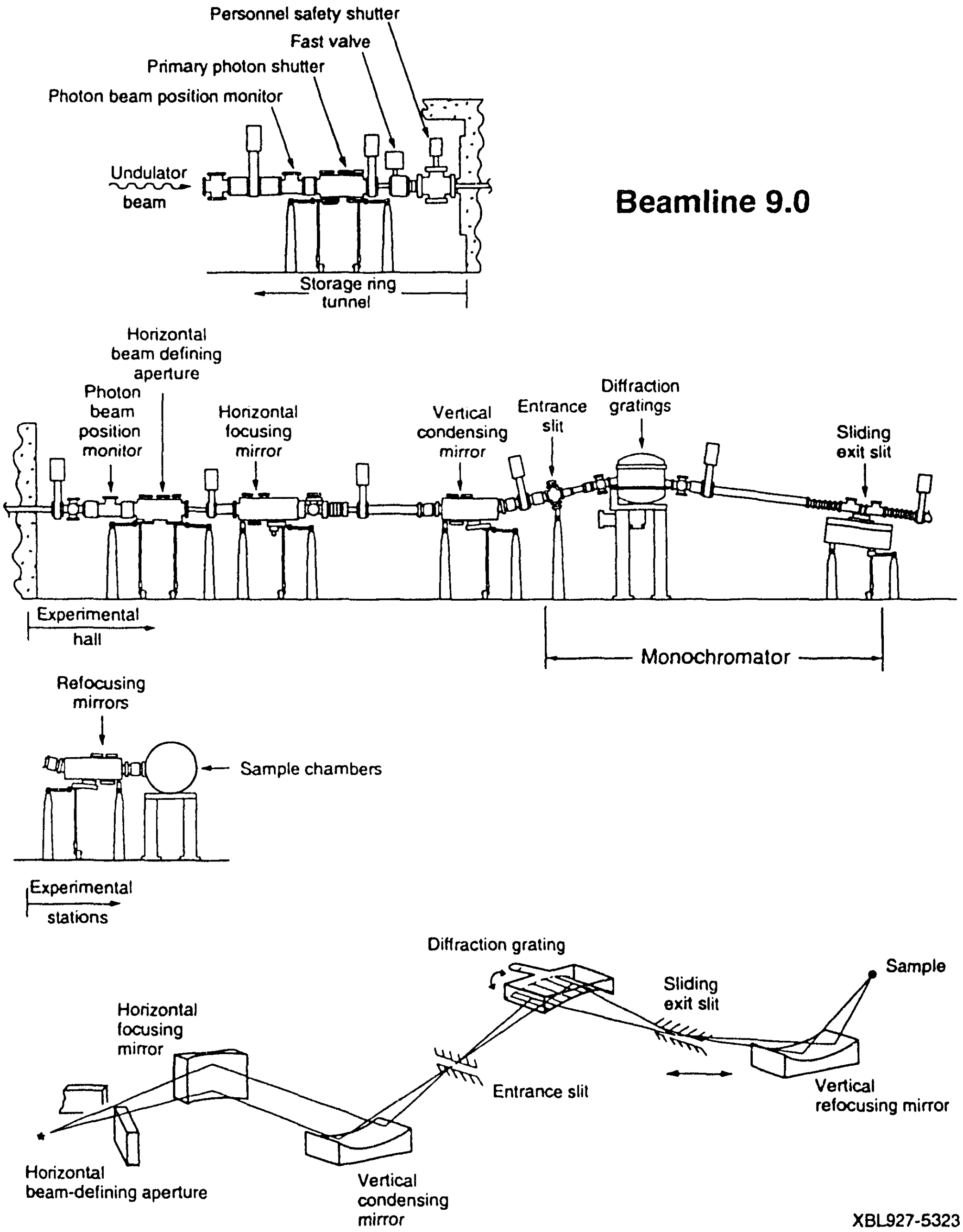
Personnel safety shutter
Fast valve
Primary photon shutter
Photon beam position monitor
Undulator beam
Storage ring tunnel
Beamline 9.0
Horizontal beam defining aperture
Photon beam position monitor
Horizontal focusing mirror
Vertical condensing mirror
Entrance slit
Diffraction gratings
Sliding exit slit
Experimental hall
Monochromator
Refocusing mirrors
Sample chambers
Experimental stations
Diffraction grating
Sliding exit slit
Sample
Horizontal focusing mirror
Entrance slit
Vertical refocusing mirror
Horizontal beam-defining aperture
Vertical condensing mirror
XBL927-5323

U8 Construction Schedule

1. U8 Undulator

1992 September	November	1993 January	March
Support and Drive finished	Undulator Assembled in Bldg. 6	Magnetic Measurements	Ready for Installation
Magnetic Subassemblies Complete	Welding the Vacuum Chamber		

2. U8 Beamline

1992 September	November	1993 January	March	May	July
Photon Shutter Ready to be Installed	Entrance and Exit Slit Design Completed		Install Front End	Install Monochromator	
M1 and M2 Mirrors Polished	Begin Big Assembly of Components			Delivery of Refocus Chambers	

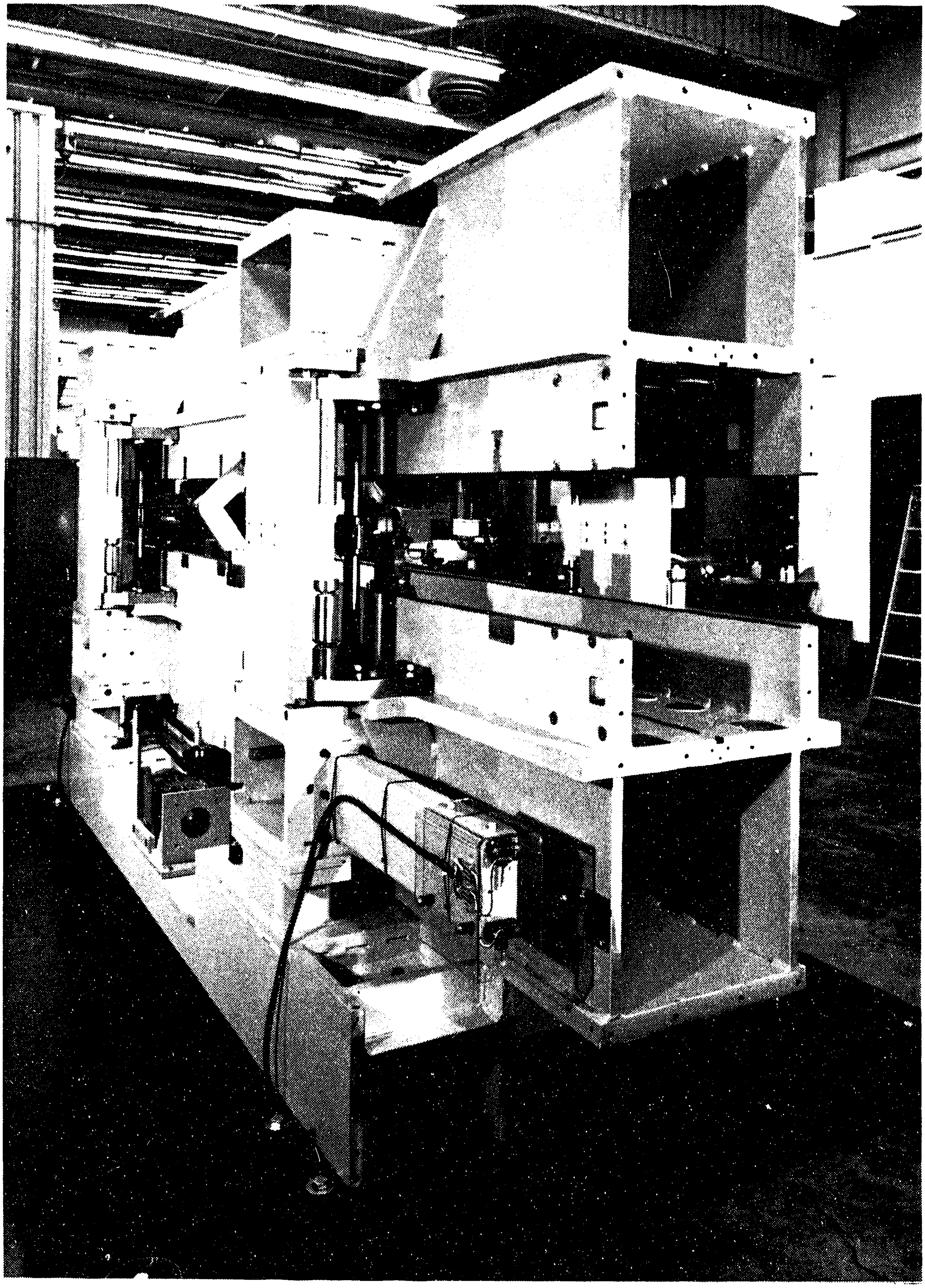

CBB 9110-8205

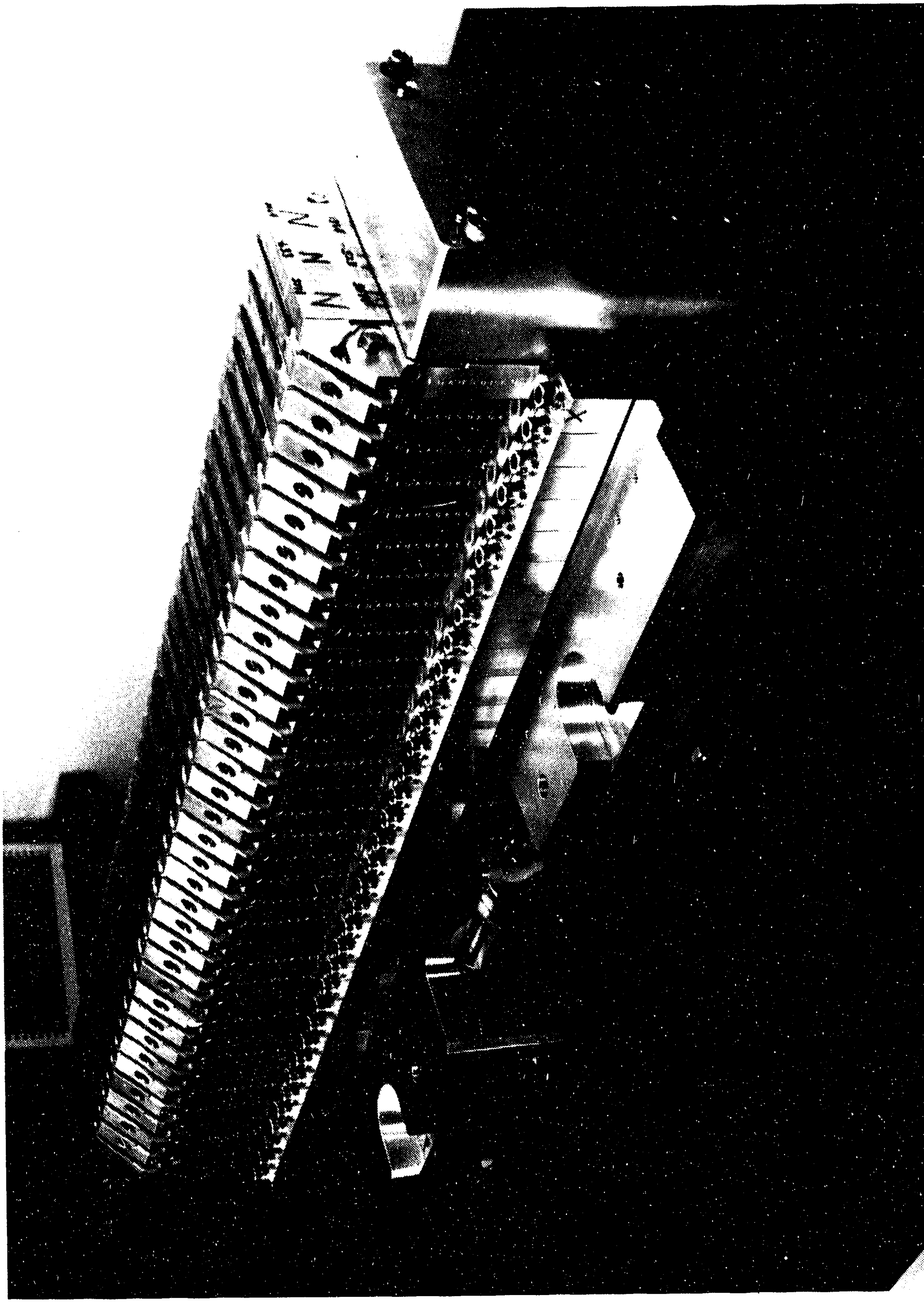

CBB 9110-8213

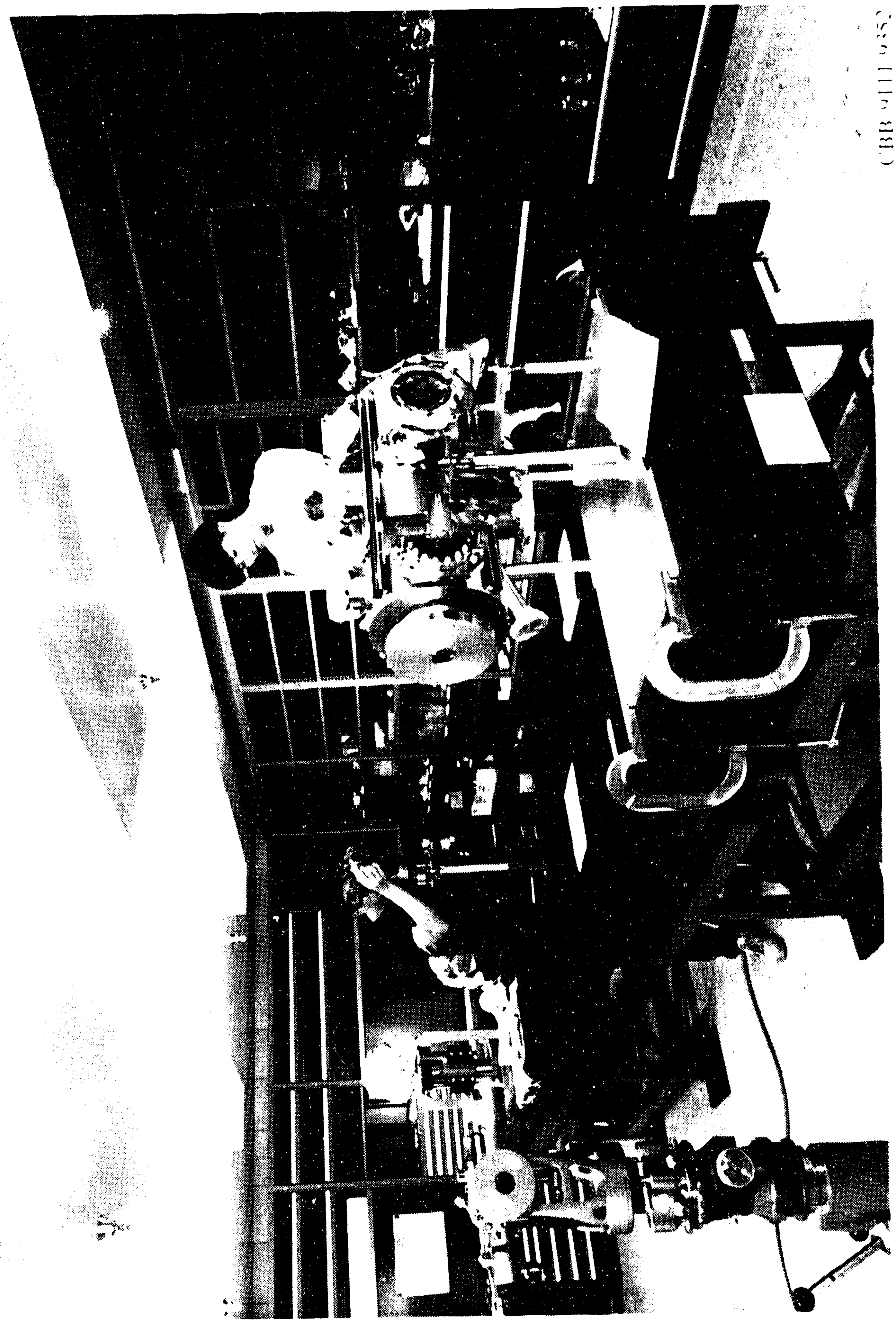

CBB 9111 6352

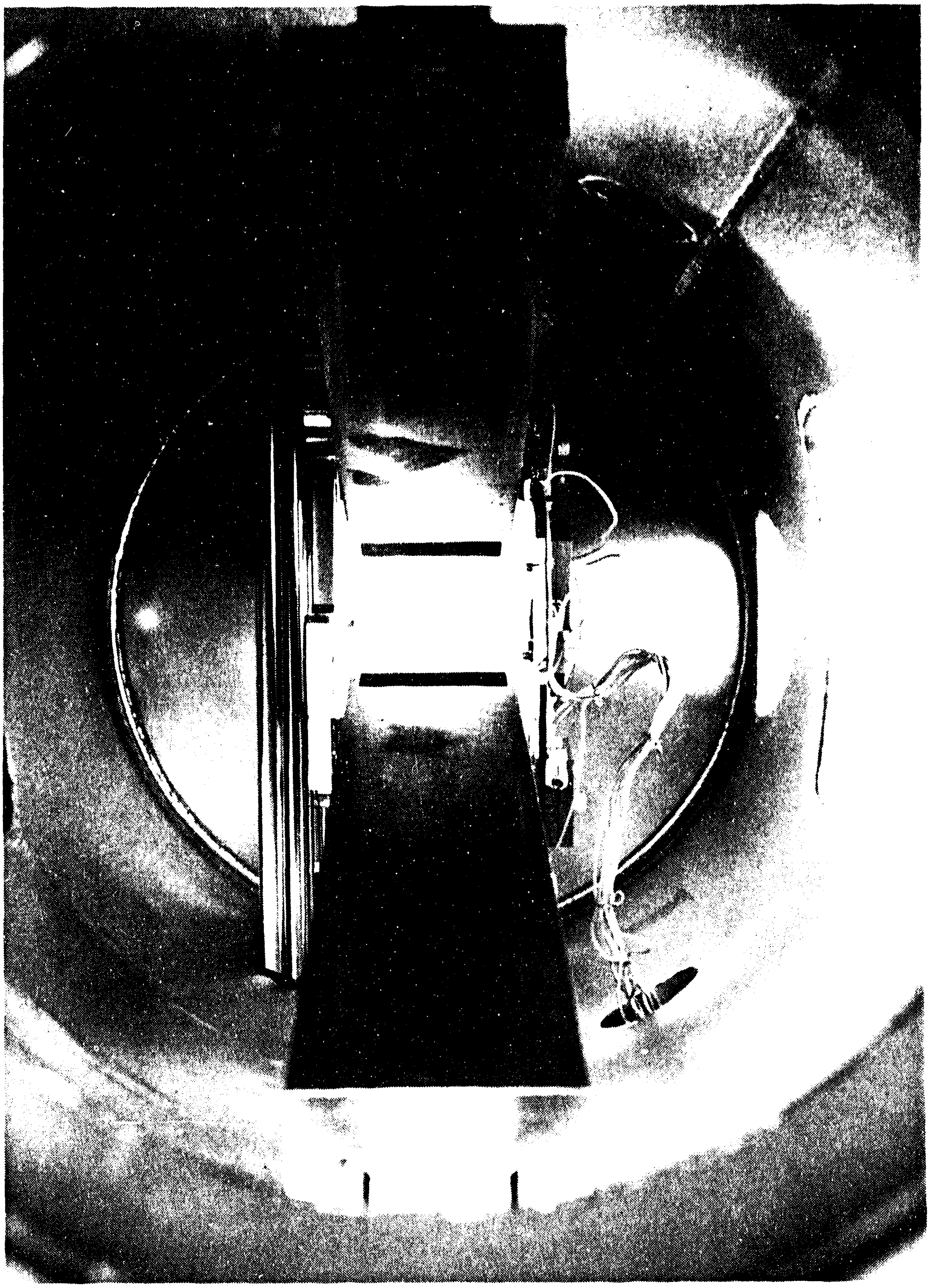

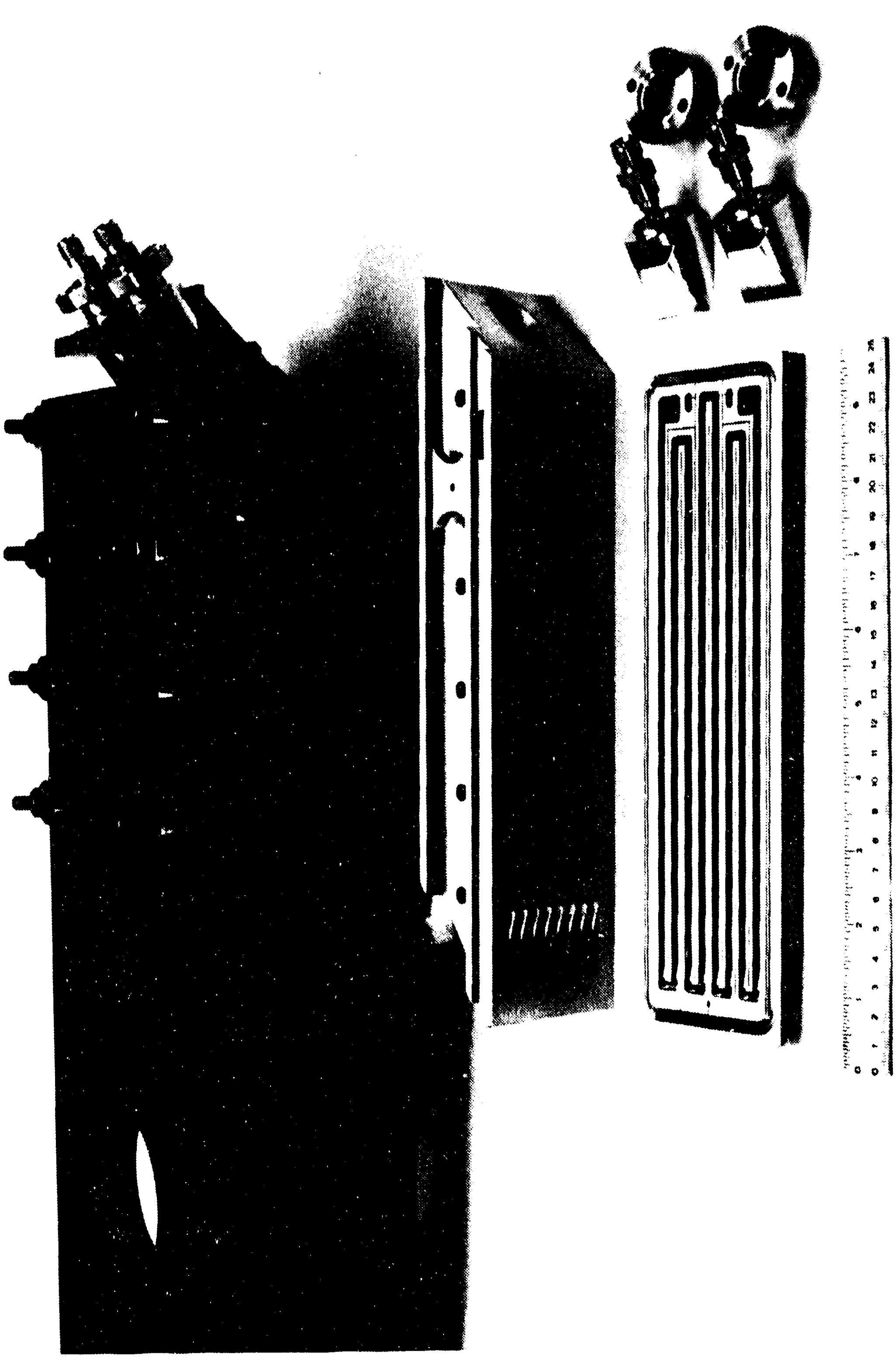

CBB 915-3545

8-cm-Period Undulator

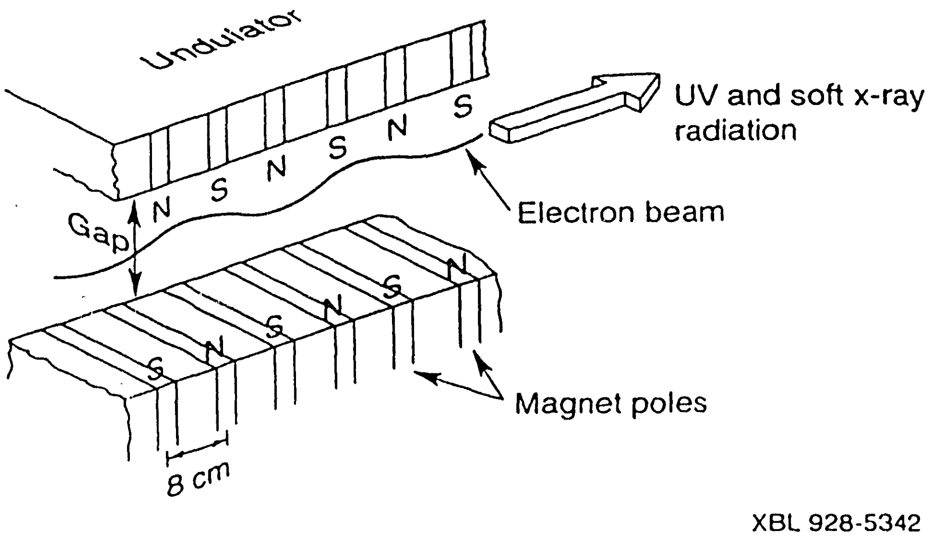

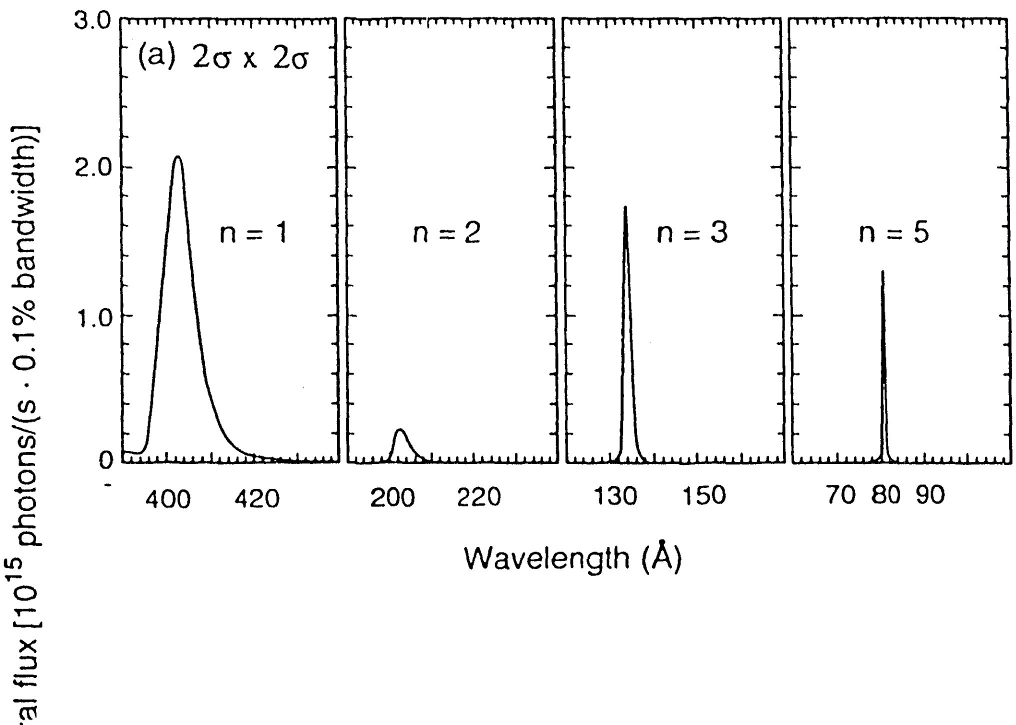

K = 4

Monochromator Resolution

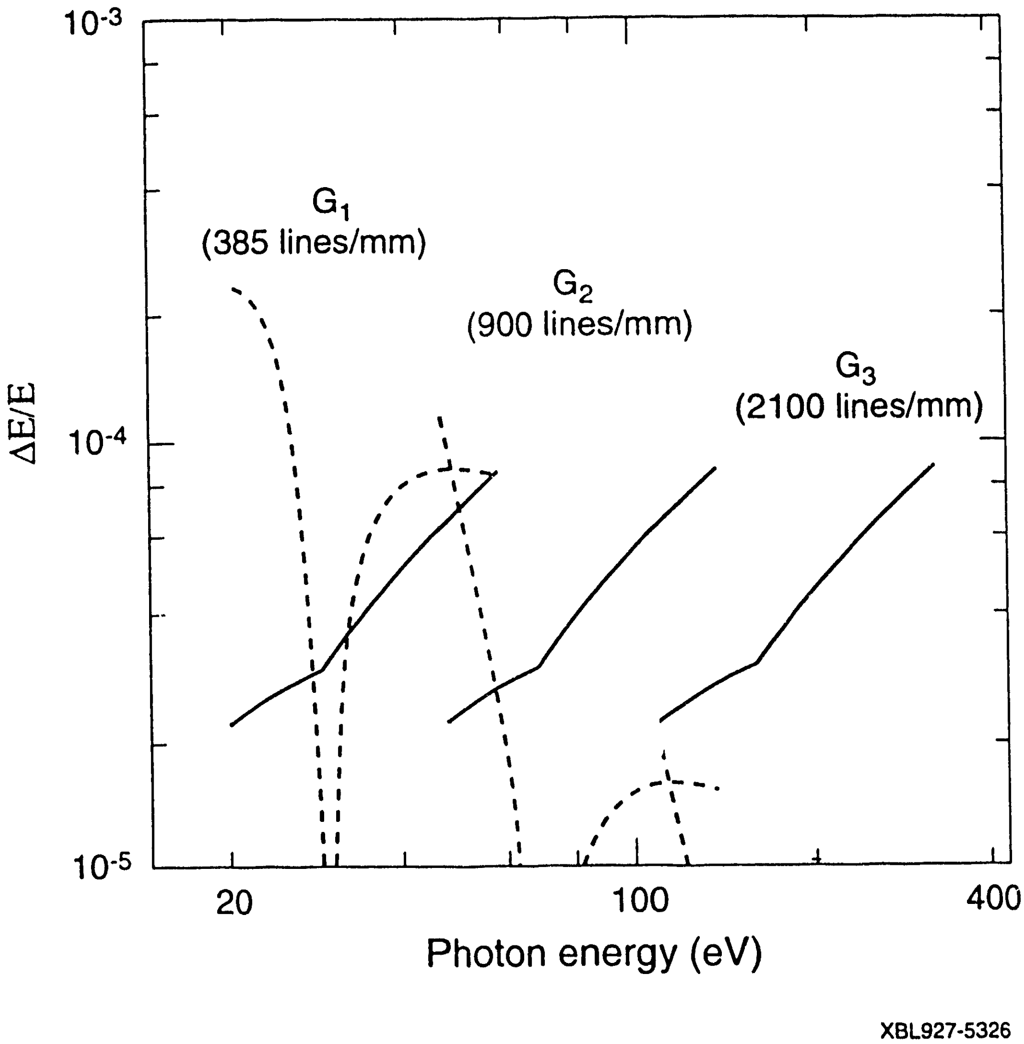

_____ from 10 μm slits

_ _ _ from coma aberration

Comparison

SX-700 II (BESSY): Resolving Power 11,000 at 65 eV, 1991.

X1B (NSLS): Resolving Power 8,000 at 400 eV, 1991.

Resolved Flux

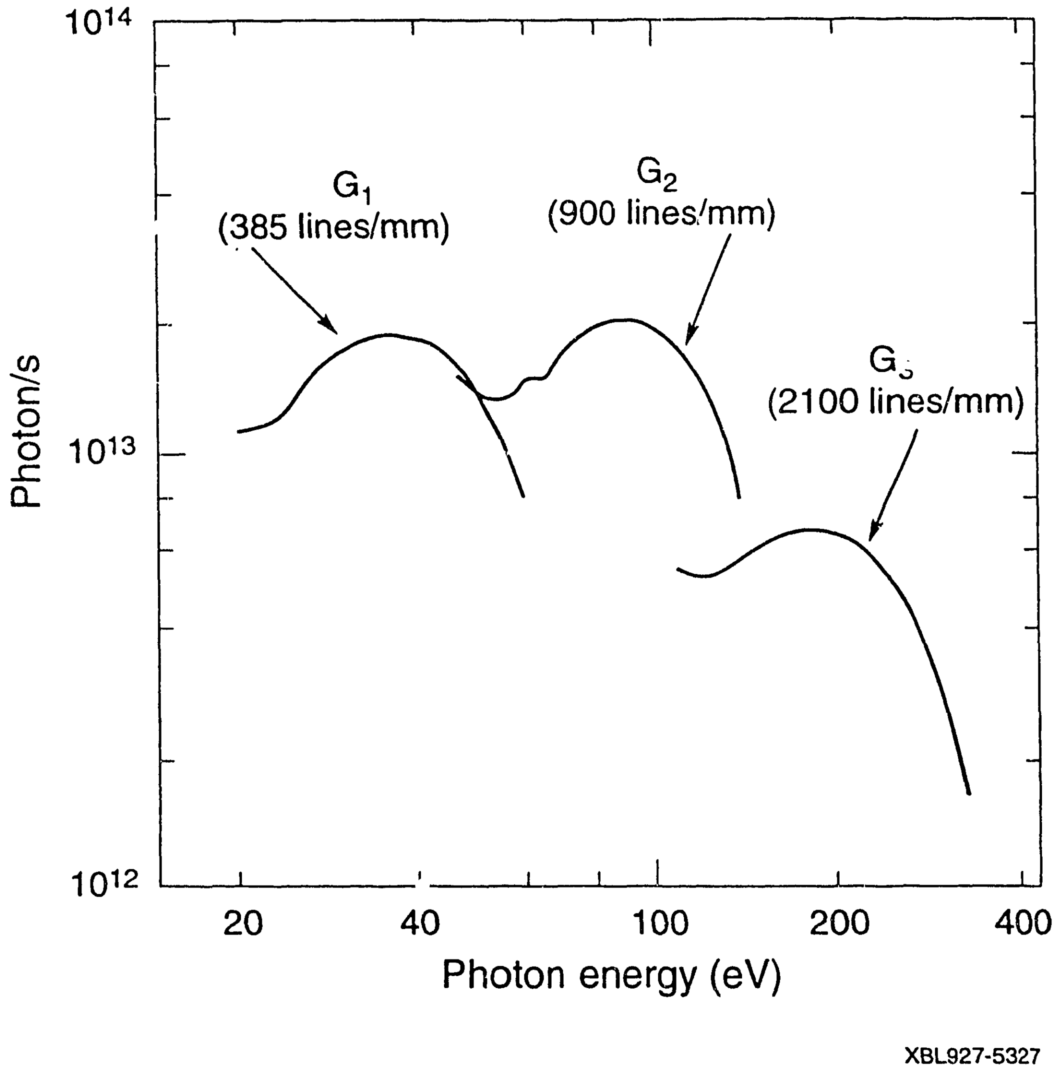

Variable Slit Openings Set for 10,000 Resolving Power

Comparison:

6 m TGM (SRC): 2×10^{11} photon/s at 2,000 RP, 60 eV

Laser Plasma Source (CXRO): 10^9 photon/s at 100 RP, 100 eV

M1 - HORIZONTAL DEFLECTION MIRROR

SGM - SPHERICAL GRATING MONOCHROMATOR

ES - EXIT SLIT

D - DEFLECTION MIRROR

S1, S2 - GAS-PHASE ELECTRON SPECTROMETRY

Full Layout

U8END30
2/4/92

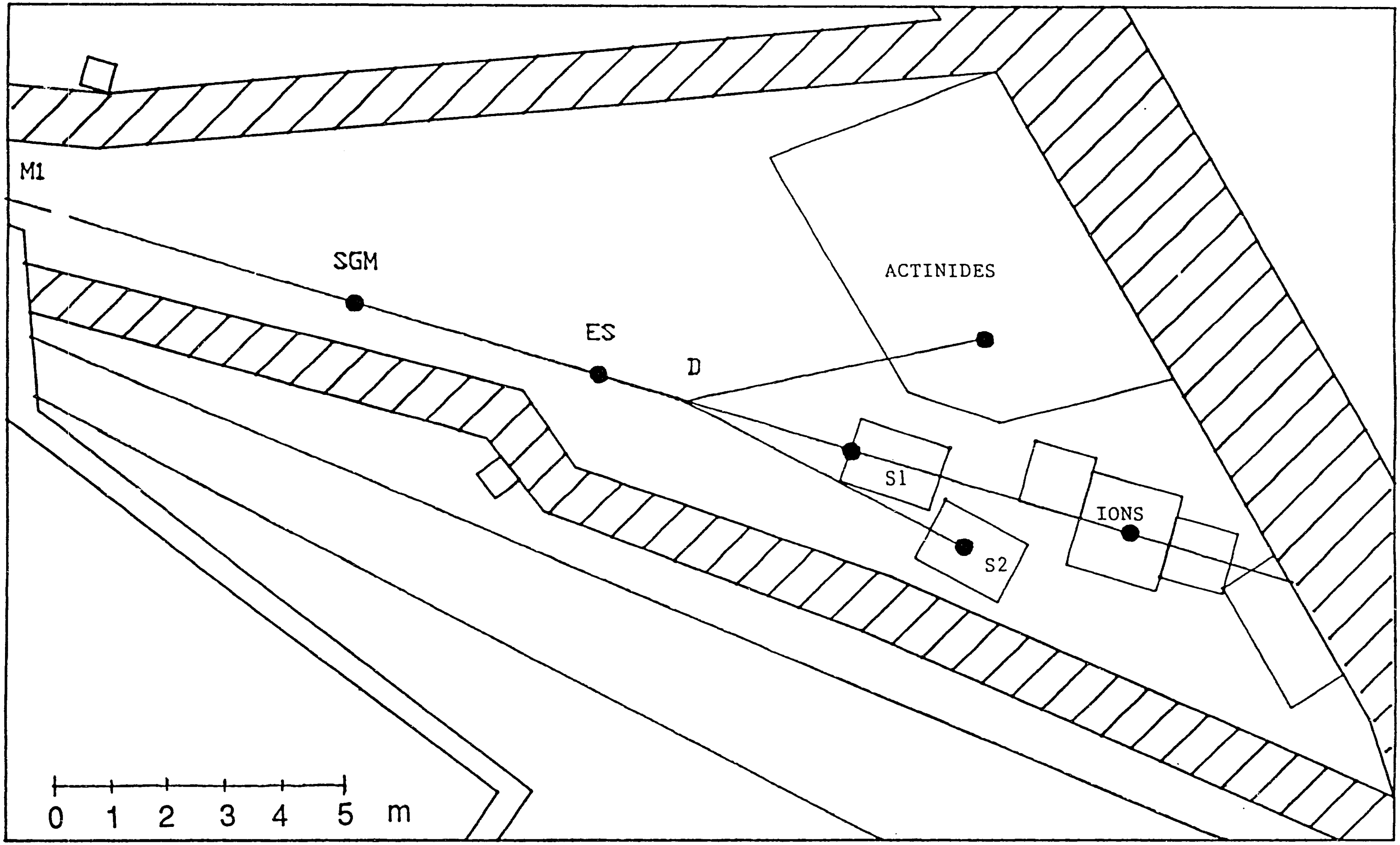

Refocusing and Deflecting Mirrors

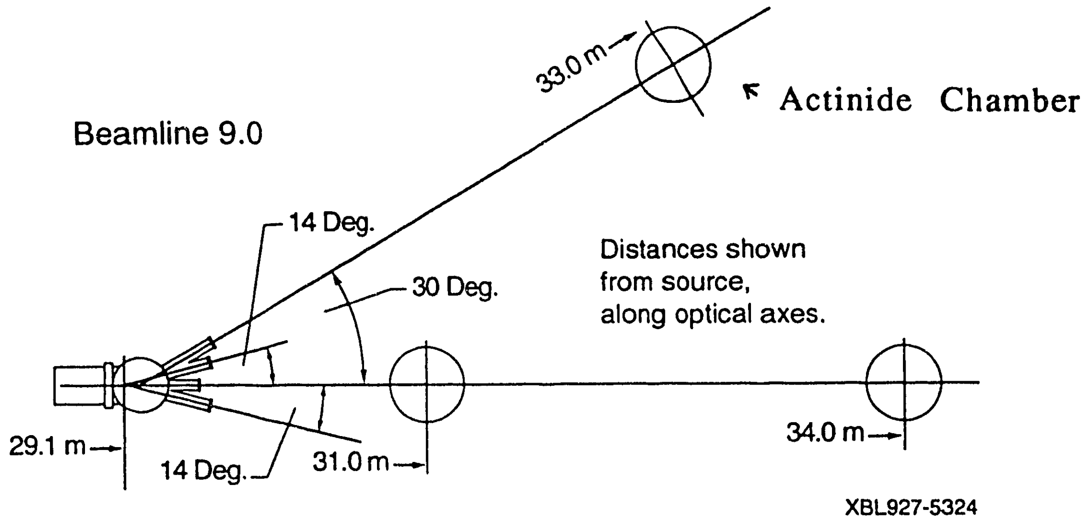

Focus at the Sample: 900 μm (horizontal) x 50 - 500 μm (vertical)

Triple Deflection: 3 x 5° incidence

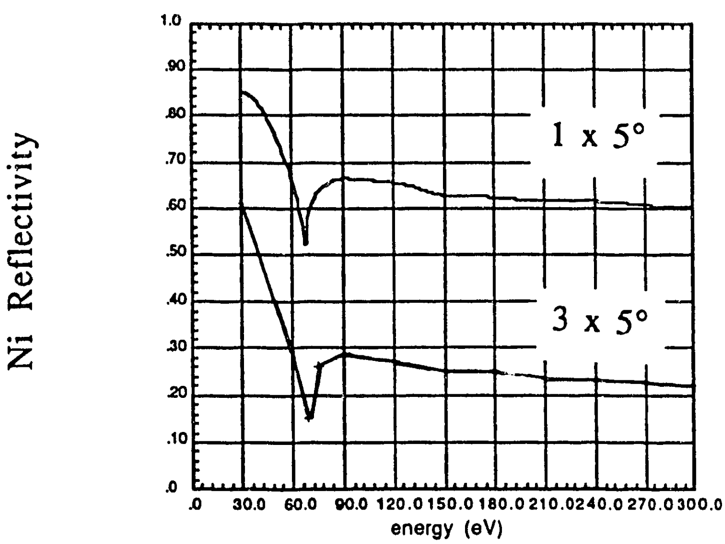

Contributing People

Undulators

Engineers and Designers

Egon Hoyer
John Chin
Dave Humphries
Dave Plate
Paul Pipersky

Technicians

Bill Gath
Darrel Howler
John Worth
Paul Wong
John Jaeger
Jerome Cummings
Ted Keffler
Paul Knopf
Bob Conners

Scientists

Brian Kincaid
Bill Hassenzahl
Steve Marks
Ross Schlueter
Johannes Bahrdt
Klaus Halbach

Undulator Beam Lines

Engineers and Designers

Dick Digennaro
Tom Swain
Don Yee
Bruce Gee
Worley Low
Steve Abbott

Technicians

Tony Catalano
Andy Lunt
Brenda Liu
Dennis Calais
Steve Klingler
Bruce Rude
Frank Zucca
Vladamir Moroz
Jim Rounds
Pete Chavez

Scientists

Tony Warwick
Phil Heimann
Wayne McKinney
Steve Irick
Malcolm Howells
Carl Cork

Summary

1. Description:

    Beamline is an 8 cm period Undulator and a Spherical Grating Monochromator

2. Constuction:

    The Undulator will be ready next March. The Beamline will be completed during the following summer, 1993.

3. Expected Performance:

    The Photon energy range is from 20 - 300 eV.
    The Resolving Power will be 10,000 $\Delta E/E$.
    At high resolution the flux will be 10^{12} photon/s.
    The spot size will be 900 μm x < 500 μm.

GAS-PHASE ACTINIDE STUDIES WITH SYNCHROTRON RADIATION

M. O. Krause

Oak Ridge National Laboratory
Oak Ridge, TN 37831-6201

Gas-phase studies of actinides at ALS will primarily involve atomic metal vapors and molecules of high volatility. Photoelectron spectrometry will be the technique of preference with the photons supplied by the U-8 undulator line in the range from 20 to 300 eV and, additionally, by a bending-magnet line for energies up to 1100 eV. A special spectrometer located in a unique Actinide Station will be used for the measurements.

Photoelectron spectrometry has proven to be a powerful probe of the electronic structure and dynamics of atoms and molecules. Ever since the tunable synchrotron radiation source has been at our disposal, we have gained a much improved understanding of electronic properties for free atoms and molecules through much of the periodic table. However, there has remained an absolute void toward the end of the periodic table: in particular, the nature of the 5f and 6d electrons has not been elucidated for any of the transuranic elements. To illustrate this point, Table 1 presents the knowledge we have at present on such a basic property as the electron binding energy. As exemplified in the case of Am and Cm, no experimental data exist for the 5f and 6d levels, while the theoretical predictions based on a single-particle model are suspect to be considerably off the mark. In fact, the comparison between theory and experiment for the binding energy of the 7s level, the only level energy that was experimentally determined, reveals a discrepancy of about 1 eV, which on a "chemical scale" gives an uncomfortably large uncertainty of more than 20 kcal.

Table 1 Comparison of Theoretical and Experimental Binding Energies (in eV) for Am and Cm

^{95}Am			
Level	Theory Atom	Experiment Atom	 Solid
$4f_{7/2}$	450.8	—	448.5
$6p_{3/2}$	23.3	—	18
$5f_{5/2}$	5.58	—	4.9
$5f_{7/2}$	2.99	—	4.9
7s	4.88	5.99	---
^{96}Cm			
$4f_{7/2}$	480.9	---	472.4
$6p_{3/2}$	26.1	---	18
$6d_{3/2}$	4.97	---	---
$5f_{5/2}$	10.64	---	5.6
$5f_{7/2}$	7.48	---	5.6
7s	5.470	6.02	---

Evidently, we are uncertain about the binding energies of the chemically important 5f and 6d electrons throughout the actinide series, and we face a theory that is inadequate for the outer electronic region of the 5f elements. Interestingly, experimental data exist for the innermost levels, K and L levels, for several actinide elements, and the accord with theory is quite satisfactory at a level of accuracy of 10^{-4} in that instance. Higher-order processes, as for example, the Breit interaction and quantum electrodynamic effects (Lambshift), are sufficiently well understood to lead to this impressive agreement in the innermost region. Although the higher-order processes, which become strong for the heavy elements, exert an effect even in the outer electronic regime, as summarized in Table 2, it is the electron correlation effects that we implicate for causing a strong shift in the binding energies. In viewing Table 2, one notes in particular that the ***relative*** contributions of the various effects (given below the absolute energies as 2(-3) = 2×10^{-3}) remain fairly constant through the shell structure for a particular ℓ value, except in the case of the f electrons. In the latter case, the magnetic and QED effects are more pronounced for the 5f electrons than the 4f electrons according to theory.

Table 2 Various Contributions to the Binding Energy for Am *(From Huang et al (1976))*

Level	E(total) (eV)	Breit (meV)	Vacuum Pol (meV)	Self Energy	Corr
$1s_{1/2}$	124976	-552eV 4(-3)	+103eV 8(-4)	378eV 3(-3)	~1eV 1(-5)
$4f_{5/2}$	465.3	+31 7(-5)	-42 9(-5)	?	?
$5f_{5/2}$	5.58	+72.5 1(-2)	-8.9 2(-3)	?	?
$5f_{7/2}$	2.99	+111 4(-2)	-8.4 3(-3)	?	?
$7s_{1/2}$	4.89	-12.1 2(-3)	+4.1 8(-4)	~15meV 3(-3)	?

With ALS coming on line as a photon source of high brightness, we will be in the unique position to embark for the first studies of the 5f electrons in the isolated atom and, by determining the binding energies, gain an understanding of the presumably strong correlations present in the outer many-electron cortege of the actinides. Americium and curium are suitable first candidates, but other actinides will doubtless be added as experimentation improves and theory advances in interplay with experiment.

Although the fundamental nature of these first studies of atomic level energies cannot be overemphasized, investigations of other electronic properties, and the extension of the work to molecules, will assume great importance and enter into entirely uncharted territory. Utilizing the wide range of the singular photon source, this novel research will include the elucidation of the dynamic properties as contained in the photoionization cross section, the photoelectron angular distribution, the natural level width, and the electron correlation satellites. Studies of volatile molecular species, such as the hexafluorides, amides, cyclopentadienides, etc, will allow us to classify the role of the 5f and 6d electrons, and their hybridization, across the actinide series. Work of this type would be in part complementary to laser-based research and would, in addition, provide access to structure and phenomena occurring at higher energies, as for example, the inner valence levels and autoionization resonances.

Research sponsored by the Division of Chemical Sciences, Office of Basic Energy Sciences, U.S. Department of Energy under contract DE-AC05-85OR21400 with Martin Marietta Energy Systems, Inc.

GAS PHASE ACTINIDE STUDIES WITH SYNCHROTRON RADIATION

Manfred O. Krause
Oak Ridge National Laboratory
Oak Ridge, TN

Electronic Structure and Dynamics
of the Free Atoms and Molecules:
Experimental Opportunities.

Table 1 Comparison of Theoretical and Experimental Binding Energies (in eV) for Am and Cm

^{95}Am			
Level	Theory Atom	Experiment Atom	 Solid
$4f_{7/2}$	450.8	---	448.5
$6p_{3/2}$	23.3	---	18
$5f_{5/2}$	5.58	---	4.9
$5f_{7/2}$	2.99	---	4.9
7s	4.88	5.99	---
^{96}Cm			
$4f_{7/2}$	480.9	---	472.4
$6p_{3/2}$	26.1	---	18
$6d_{3/2}$	4.97	---	---
$5f_{5/2}$	10.64	---	5.6
$5f_{7/2}$	7.48	---	5.6
7s	5.470	6.02	---

<u>Am</u> $5f^7 7s^2$ $({}^8S^0_{7/2})$ spectroscopic notation

Not a "pure" state, but:

$+ 6d^2 + 7p^2 + 7d^2 + 7f^2 + 7g^2 + \ldots +$ higher n

coefficients $c_1, c_2 \text{ --- } c_n$

There are no experimental data!

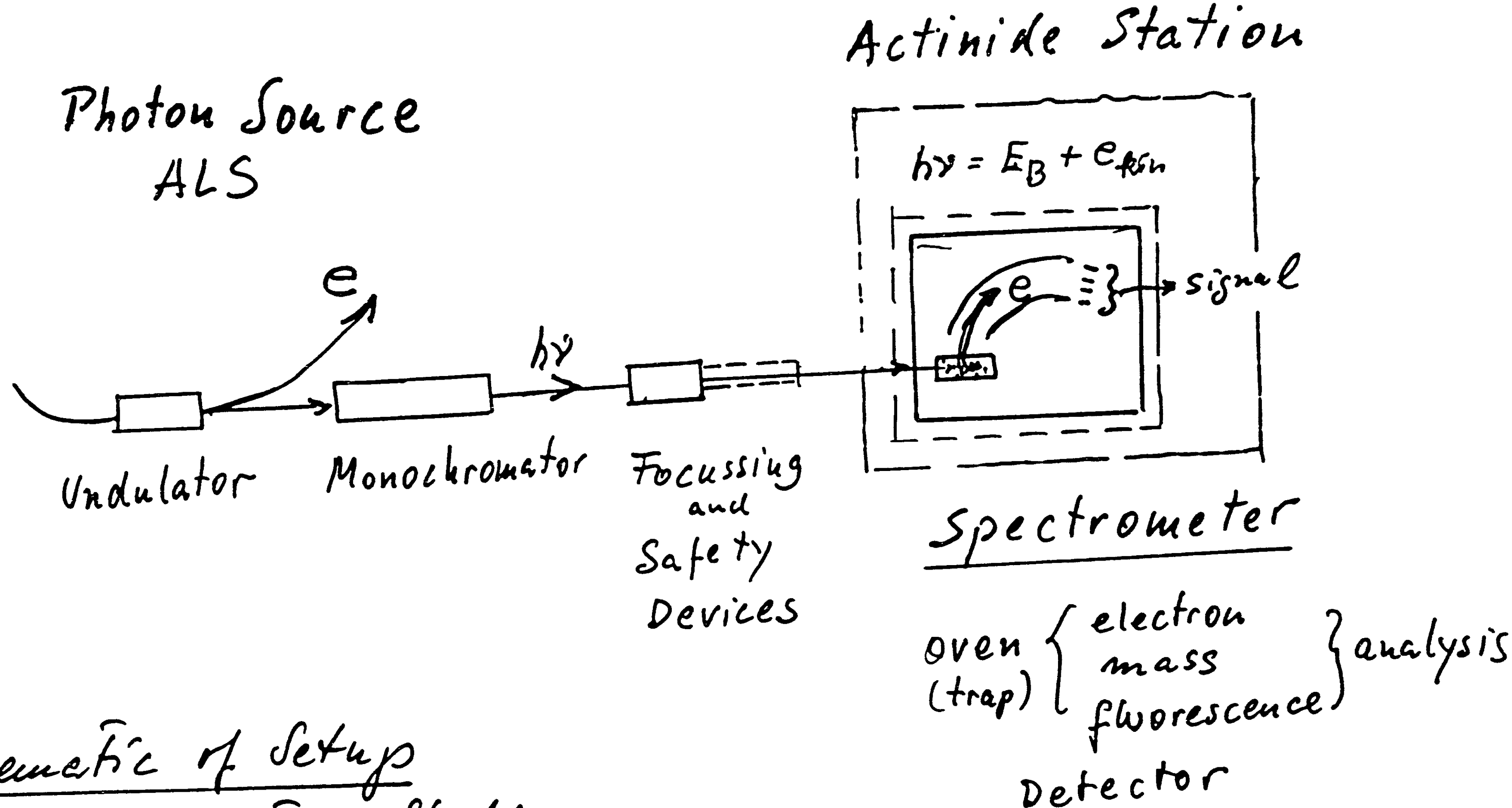

Schematic of Setup for Photoionization Studies of Actinides in the Gas Phase

Experimental Setup

Generic system for Angle Resolved Photoelectron Spectrometry of atoms, molecules, vapors etc

ORNL-DWG 80-9619RA

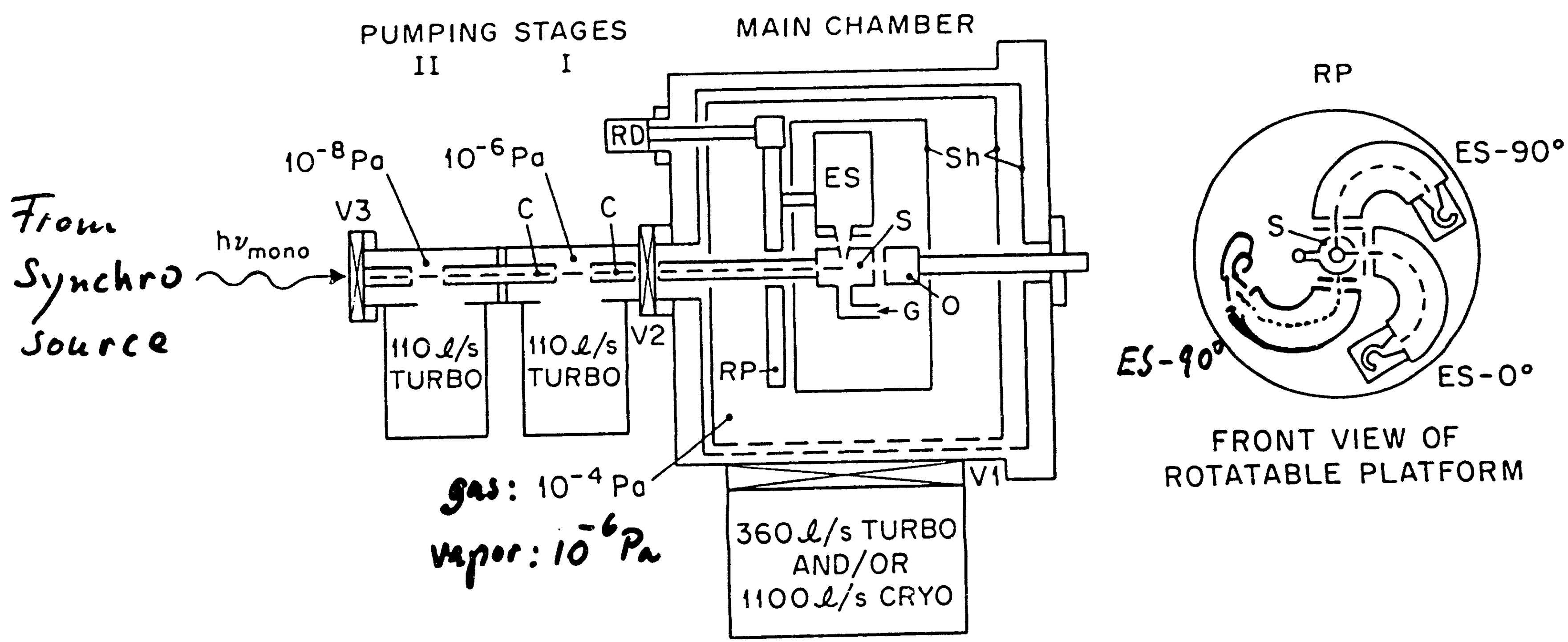

MOK-ORNL

Typical high-efficiency oven for Electron Spectrometry of free species (atoms, molecules) with the use of Synchrotron Radiation.

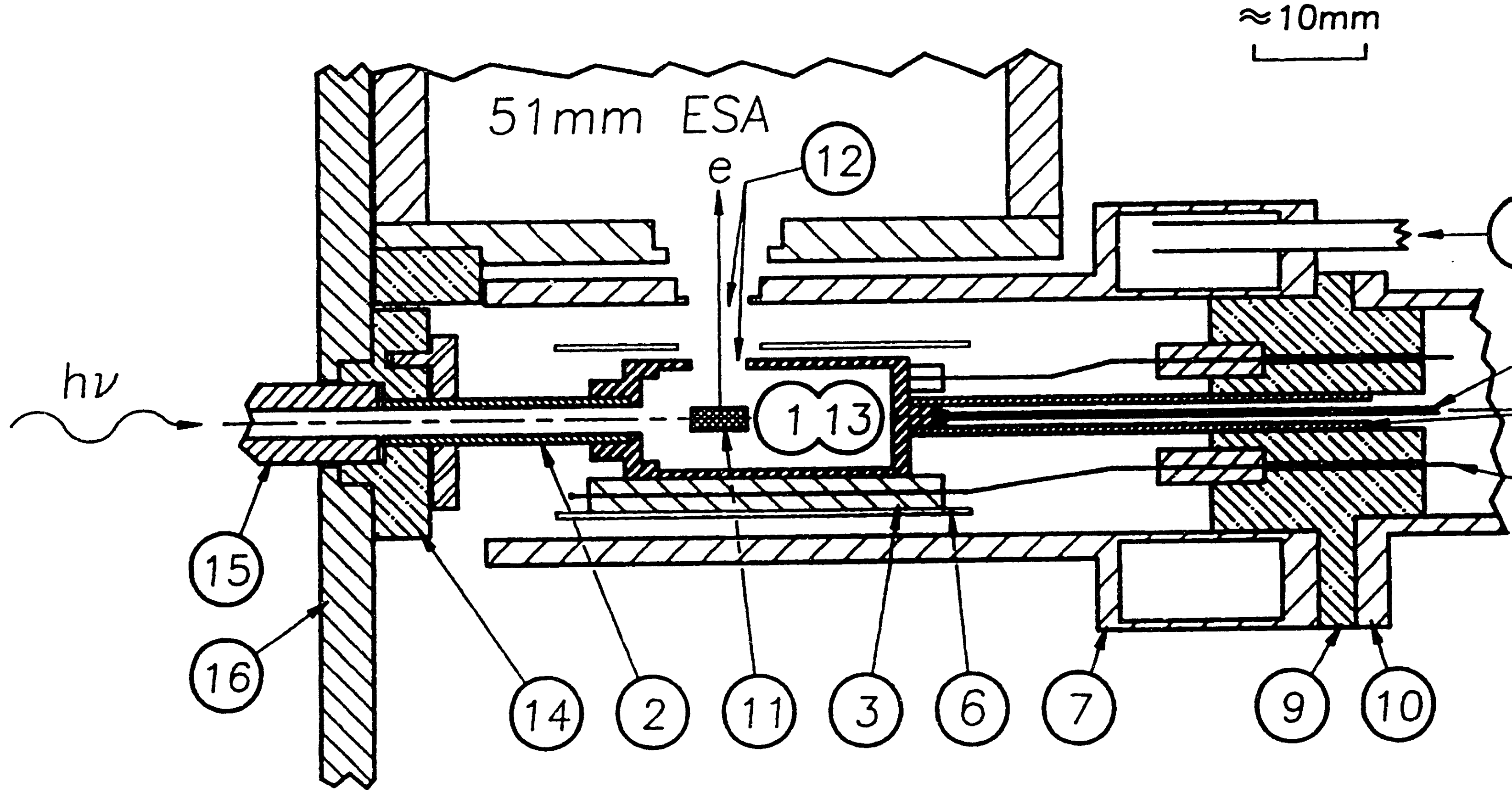

ESSR of Metal Vapors — Internal Oven

ORNL — 80/88

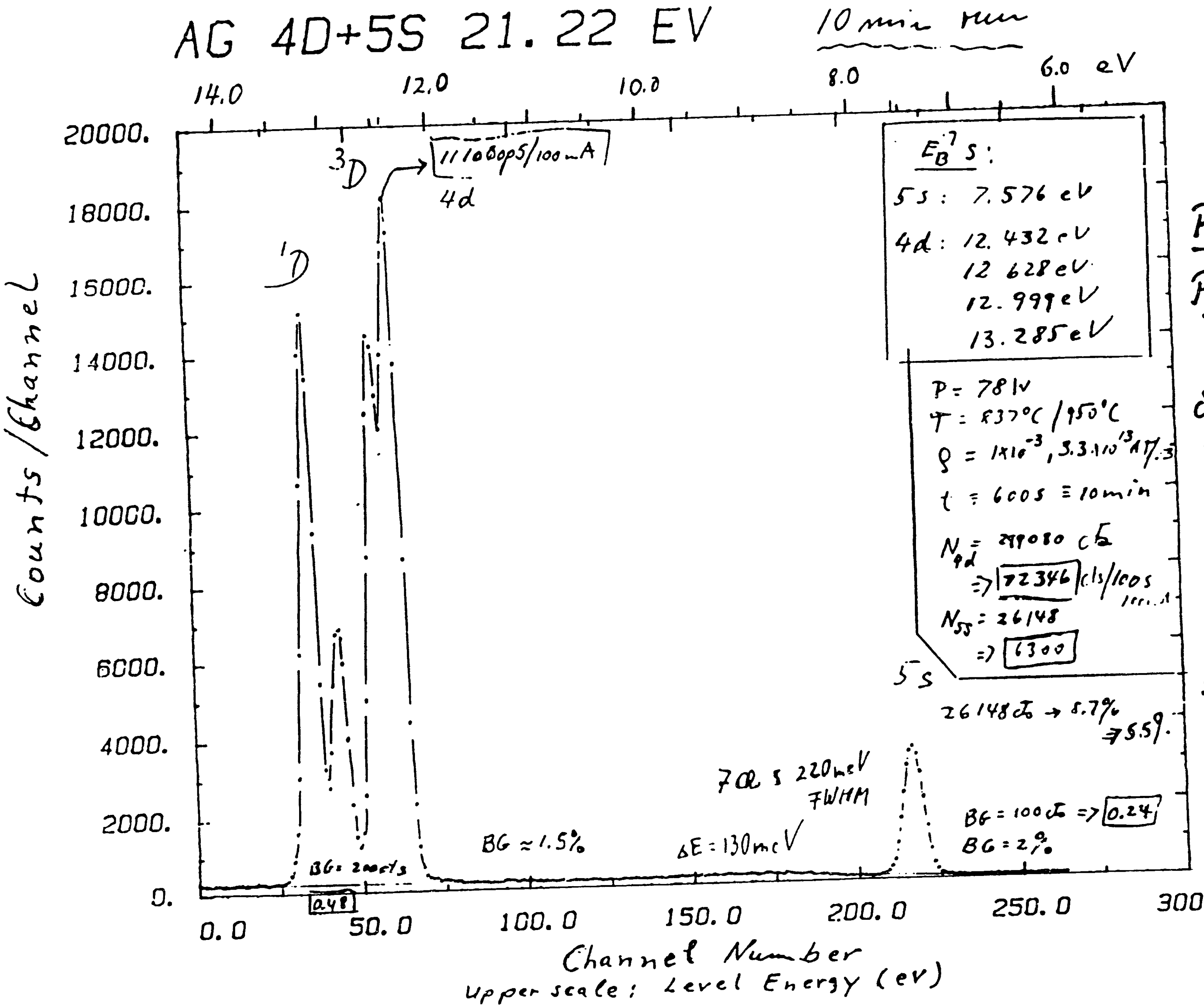

Prototype Photoelectron Spectrum of Ag Atoms

Small sample: 5mg

Synchrotron radiation experiment at SRC, Wisconsin

Composition of Electron Binding Energy

a) Electric Energy
b) Rearrangement energy
c) Breit interaction (magnetic & retardation)
d) Nuclear size effect
e) Lamb shift (selfenergy and vacuum polarization)
f) Electron Correlation / multi-configuration interactions

g) Chemical shifts for molecules

→ Dirac-Fock Multiconfiguration
- includes relativity
- many correlations

- QED effects

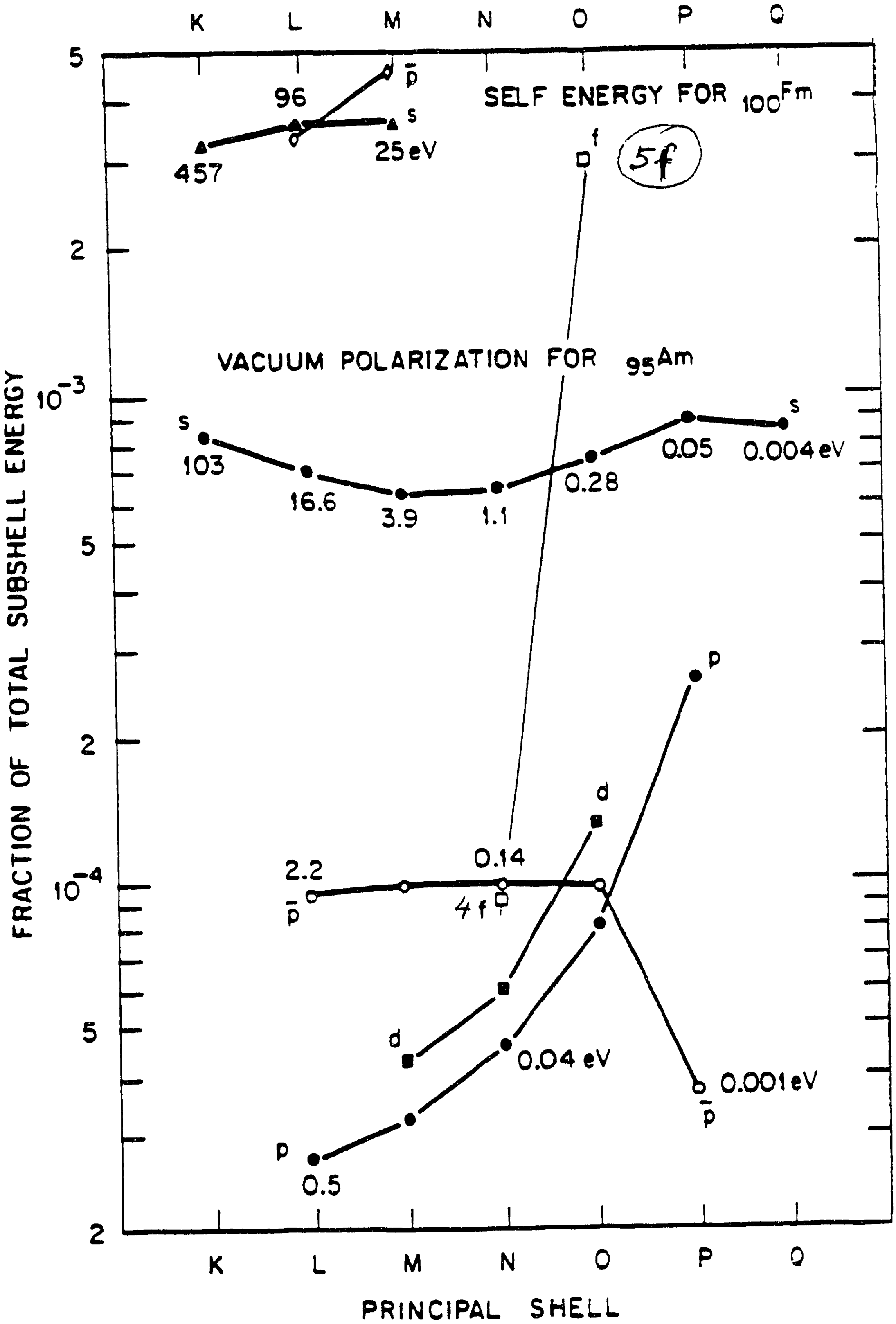

The variation with principal shell of the quantum-electrodynamic contributions to the total energy of a given subshell.

Table 2 Various Contributions to the Binding Energy for Am *(From Huang et al (1976))*

Level	E(total) (eV)	Breit (meV)	Vacuum Pol (meV)	Self Energy	Corr
$1s_{1/2}$	124976	-552eV 4(-3)	+103eV 8(-4)	378eV 3(-3)	~1eV 1(-5)
$4f_{5/2}$	465.3	+31 7(-5)	-42 9(-5)	?	?
$5f_{5/2}$	5.58	+72.5 1(-2)	-8.9 2(-3)	?	?
$5f_{7/2}$	2.99	+111 4(-2)	-8.4 3(-3)	?	?
$7s_{1/2}$	4.89	-12.1 2(-3)	+4.1 8(-4)	~15meV 3(-3)	?

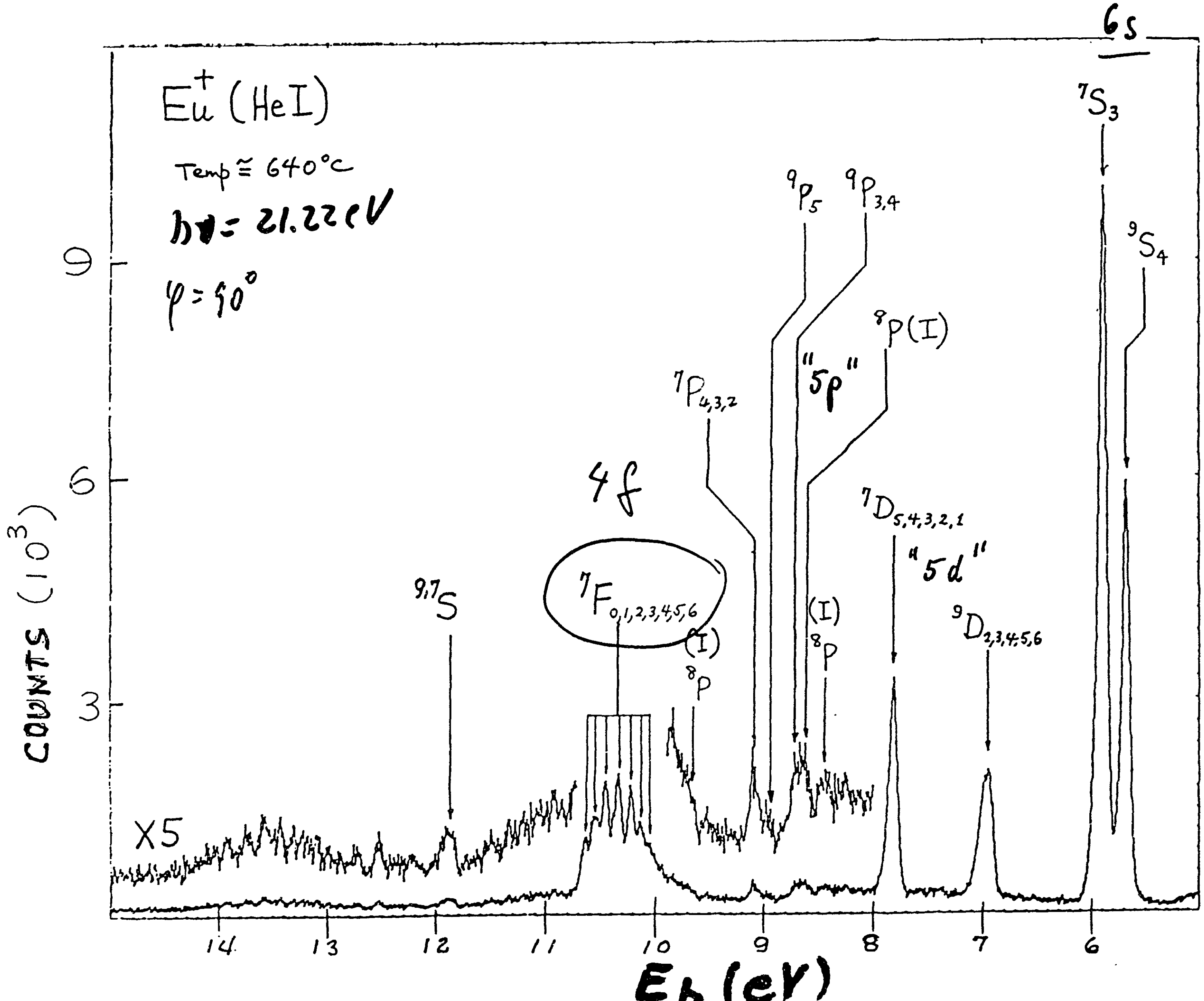

What do the rare gas photoelectron spectra tell us? What might be expected for Am?

BNL

Table 3 Temperatures Required for Photoelectron Spectrometry of the Higher Actinides

Element	T(°C) for ~10^{-3} Torr	Isotope/half-life
Am	900 (solid)	243 7K a
Cm	1400 (liquid)	248 300K a
Bk	1100 (liquid)	249 320 d
Cf	600 (solid)	249 351 a
Es	360 (solid)	253 20 d

Which elements?

- Temperature — U ≈ 1900°C
- Activity — Np ≈ 1700°C
- Availability — Pu ≈ 1400°C
- "treatability"
  (Th $6d^2s^2$; Am $5f^7$; ^{101}Md f^{13})

→ start with Am
then Cm ....

The analytical application and some basic explorations

4f doublet in the An oxydes

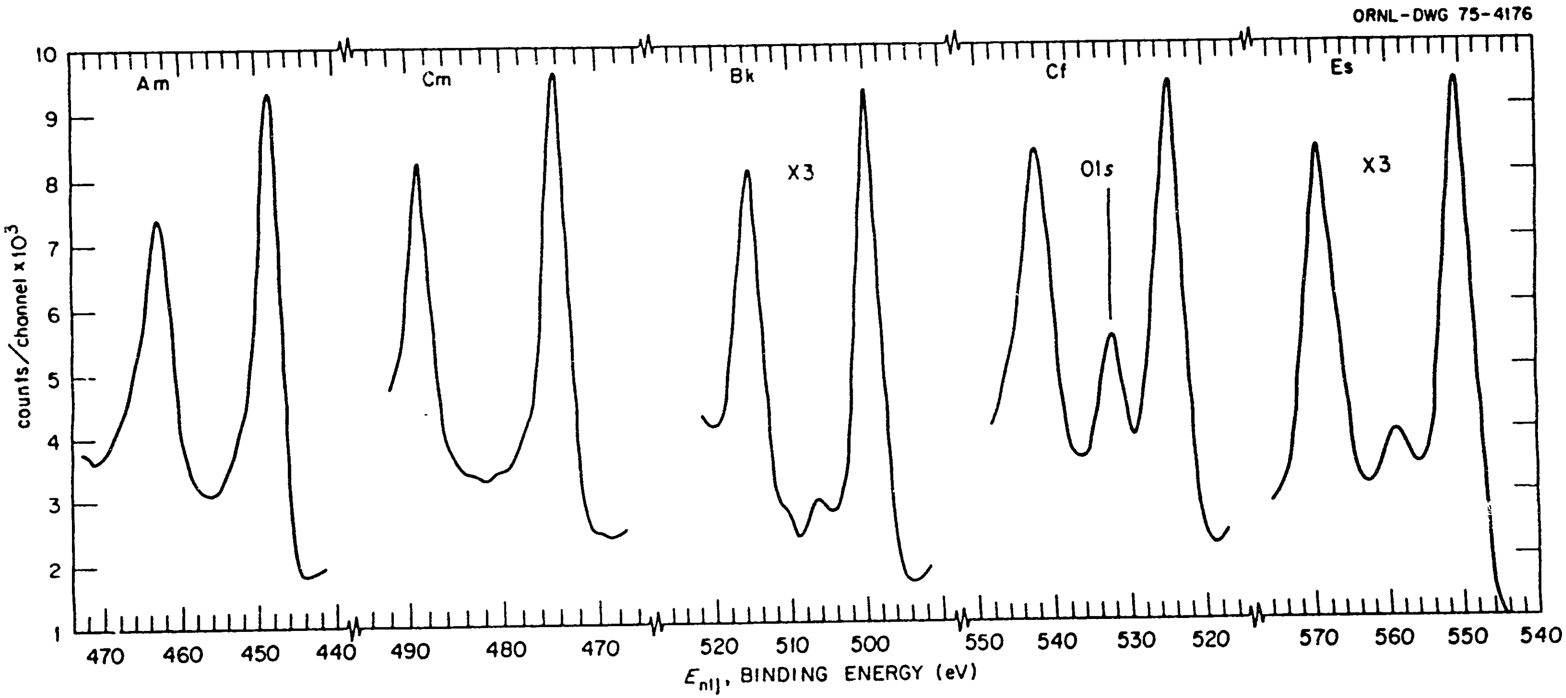

Mok et al 1986

Photoionization Cross Sections

for $Z \gtrsim 95$

below ≈ 1 KeV

	Experimental	Theoretical
σ_{tot}		HS
σ_{4f}		HS Single-Particle
σ_{5f}		
σ_{6d}		
σ_{7s}		

$$\sigma \propto \left| \langle \chi_0^* \right| \sum_\mu \exp(i\vec{k}_\nu \cdot \vec{r}_\mu)\, \varepsilon\, d_\mu \left| \chi_f \rangle \right|^2$$

initial state
neutral atom

final state
ion plus electron

How to locate the electrons (states) of different parentage and symmetries in a valence/conduction band.

VARIATION OF THE PHOTOEMISSION CROSS SECTION WITH PHOTON ENERGY FOR DIFFERENT ELECTRON ORBITALS

— U 6d
— U 5f
— Mn 3d

($\sigma_{s,p} \approx 0$!)

From J. Naegele

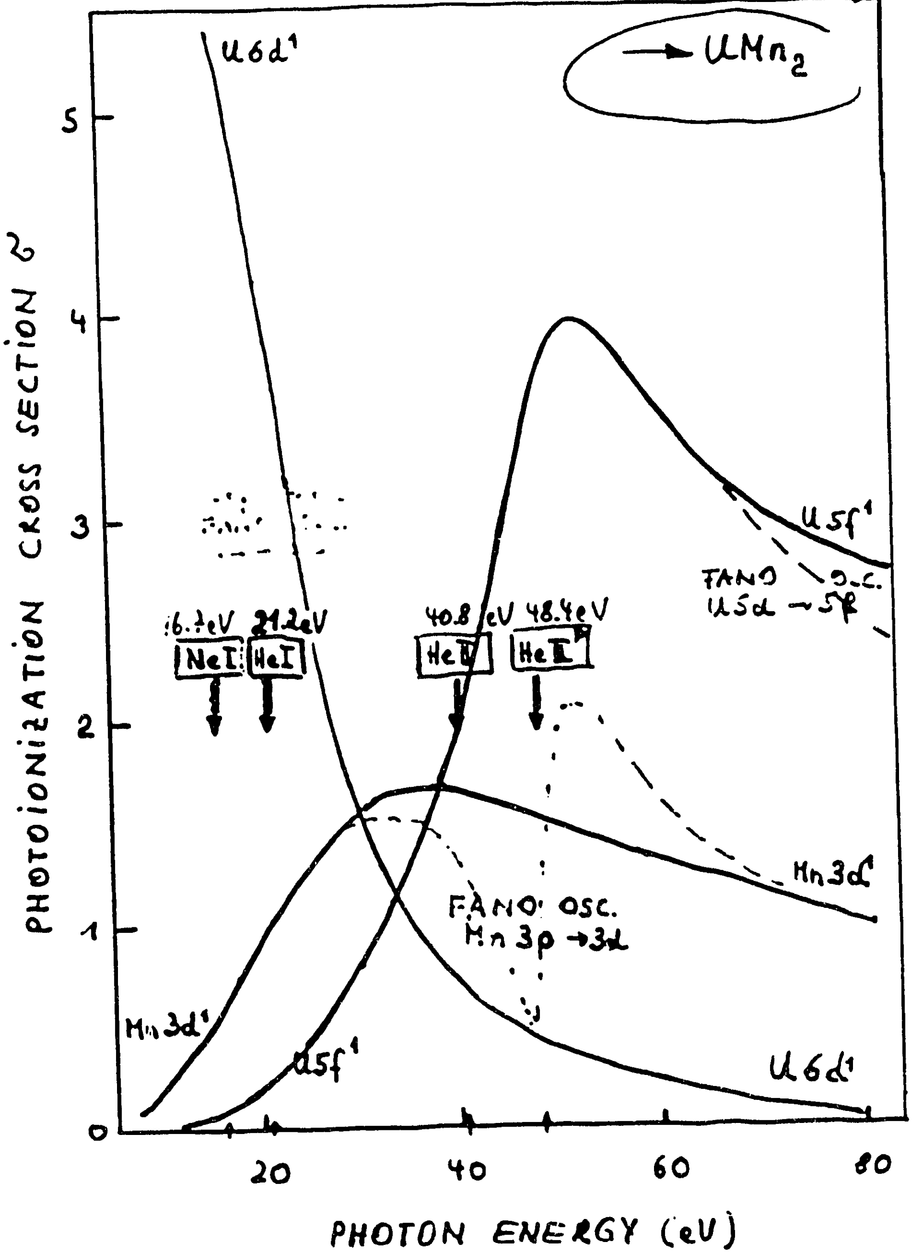

(J.J. Yeh, I. Lindau, 1985) Hertree-Slater Single-Part

First-Order Prediction for 5f Electrons

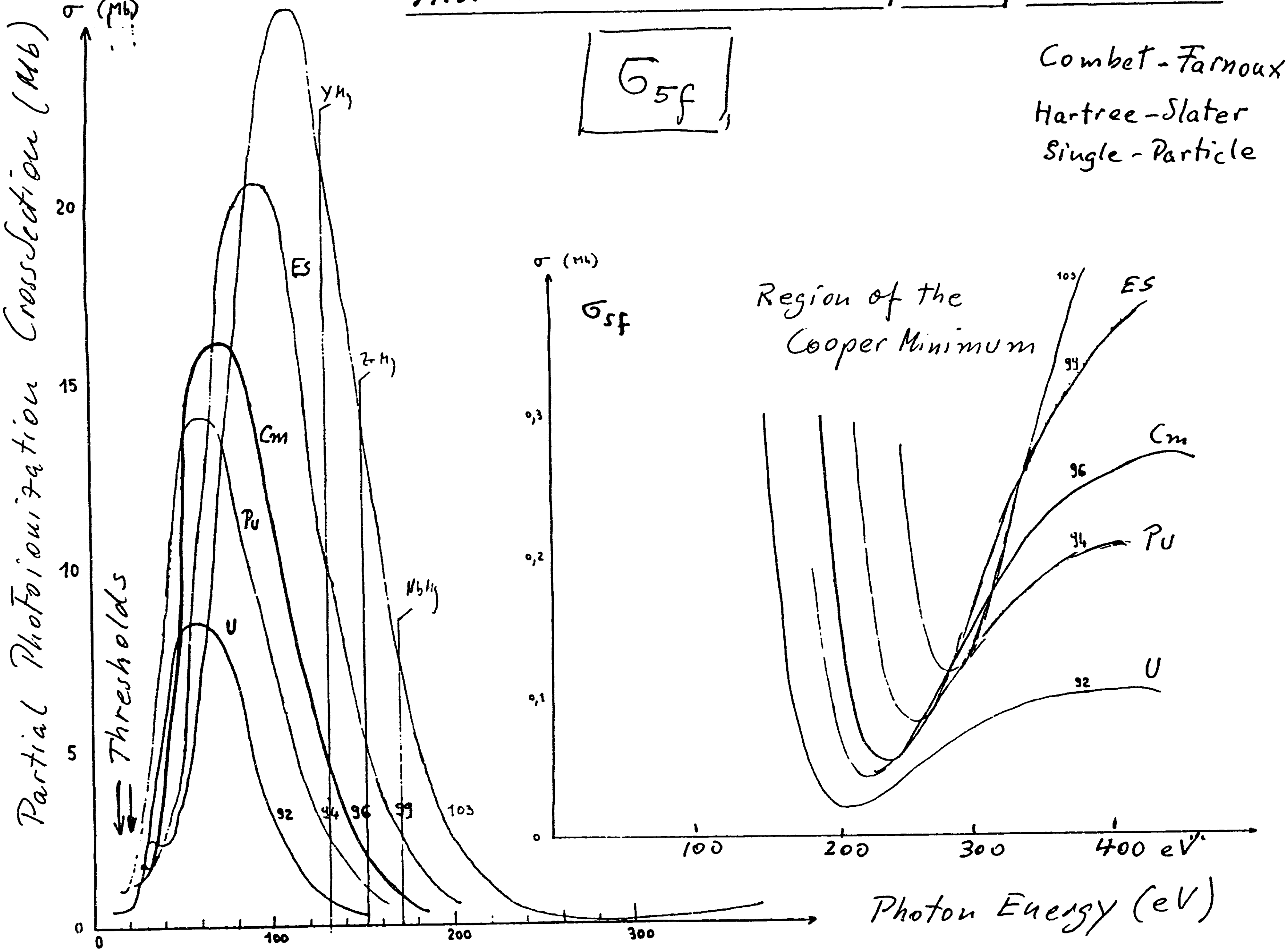

ORNL
1973

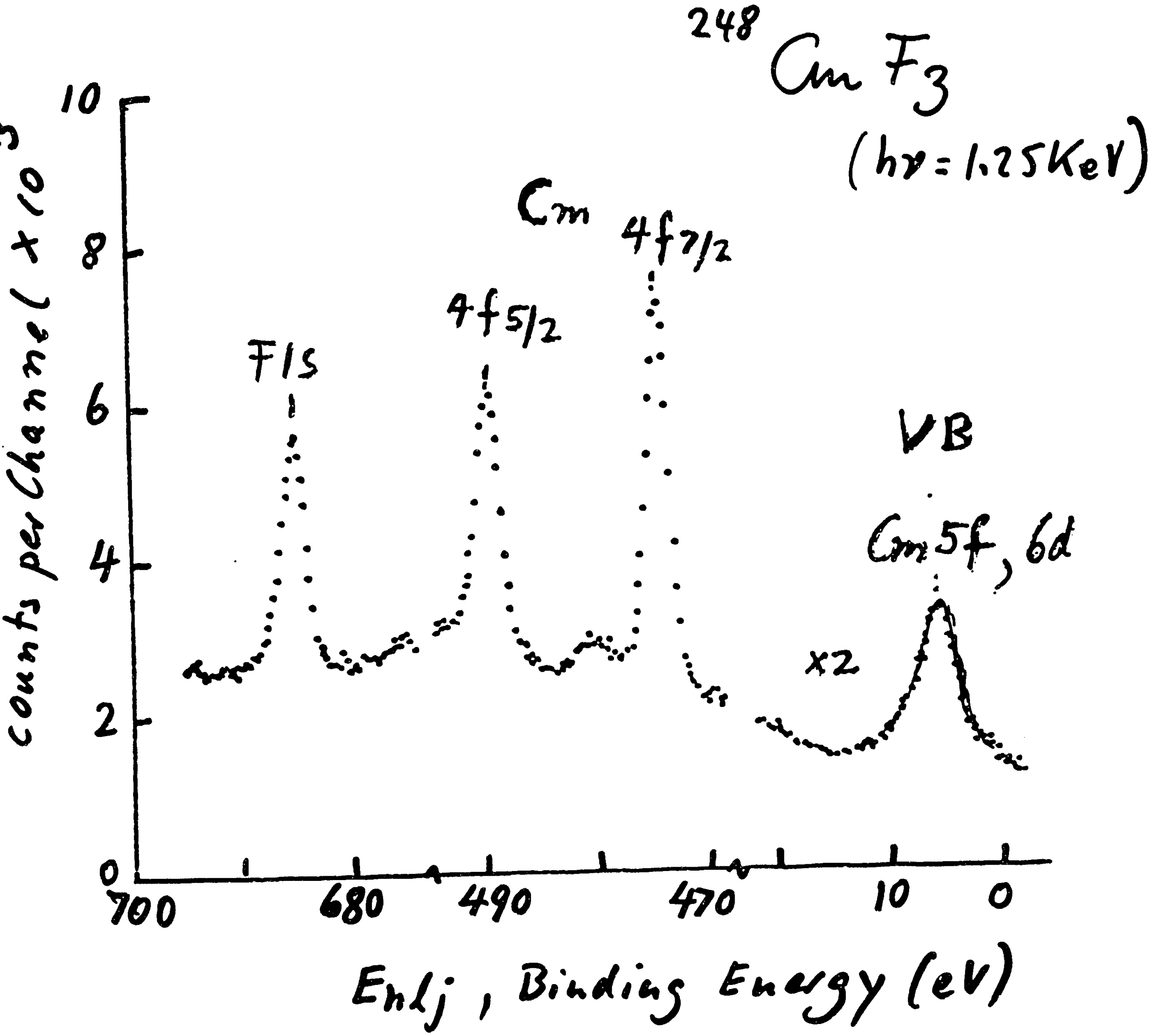

The solid system;
Question: Valence band structure of the free molecule?

Cm atom $5f^7 6d^1 7s^2$

Molecules

Synchro : 15 to 200 eV

- Valence band structure
  - vibrational structure

- Molecular fragmentation
  - bonding, energies
  - compound identification
  - "inner" appearance potentials

Lasers : ion appearance thresholds (multiphoton ionization)
ionization threshold

- high volatility compounds:
  halides (Fluorides)
  (sub) oxides
  cyclopentadienides

- low volatility compounds
  by way of laser ablation

High sensitivity $\approx 10\,\mu g$

Electronic Structure and Dynamics of Free Actinide Atoms and Molecules

- Virtually no experimental data exist, neither for binding energies nor cross sections
- Inadequate theoretical predictions
- ALS Actinide Station as a unique opportunity to determine Electron binding energies of the chemically important 5f, 6d and 7s electrons
- Similarly, photoionization cross sections can be determined at the subshell level.
- Baseline for advanced theoretical models and approximations allowable.
- Baseline for condensed-matter studies, such as locating 5f, 6d, etc states.
- Identification of An-containing compounds as an excellent analytical technique
- Last, but not least, fully elucidate the role of f electrons and explore the uncharted region of the Actinide Elements

— SUMMARY —

ATOMIC STRUCTURE CALCULATIONS FOR HEAVY ATOMS

Yong-Ki Kim

National Institute of Standards and Technology
Gaithersburg, Maryland 20899

Atomic structure calculations for heavy atoms require sophisticated descriptions of both relativistic and electron correlation effects. For heavy atoms (Z > 55), these effects cannot be separated easily. Purely *ab initio* calculations for heavy atoms will be difficult even if the theory is based on a relativistic formalism, such as the Dirac-Fock method, due to a strong coupling between relativistic and correlation effects.

Although relativistic effects alter mostly deep core orbitals, valence orbitals are affected as well because valence orbitals must be orthogonal to core orbitals of the same angular symmetry and see a more screened effective nuclear charge than a nonrelativistic theory would predict. This is known as an indirect relativistic effect. For instance, outer d and f orbitals may expand in orbital size, rather than contract as the hydrogenic Dirac theory predicts, due to the indirect relativistic effect. However, this orbital expansion is a subtle effect of the order of a few percent, and competes with changes due to correlation effects. This is one of the underlying reasons for the theoretical difficulties in predicting the behavior of 5f, 6d, 7s and 7p electrons in actinides.

Relativistic Hartree-Fock theory with options to include correlation orbitals, commonly referred to as the Multiconfiguration Dirac-Fock (MCDF) method, is one of the most powerful and versatile methods to calculate atomic wavefunctions and expectation values. In its most advanced form, it can predict atomic energy levels--including intermediate coupling, correlation and QED corrections--for highly charged ions to a high degree of accuracy, often 0.1% or better, without resorting to any empirical or adjustable parameters.[1] This remarkable performance is often repeated in atoms and ions for which relativistic effects dominate.

However, the MCDF method is ineffective when correlation effects are more important than relativistic effects. Typical examples are neutral carbon (competition among the $2s2p^3$, $2p3d$ and $2p4s$ configurations) and neutral calcium. For this reason, a straightforward application of the MCDF method to actinides, for which correlation and relativistic effects are equally important, is unlikely to succeed in predicting energy levels with high precision unless a large number of correlation orbitals are introduced.

There are, however, some qualitative aspects of the MCDF method that may still provide useful information without an overwhelming amount of computational effort. For instance, even the simplest form of the Dirac-Fock (DF) method, which does not include any correlation orbitals, correctly predicts inversion of fine-structure splittings, such as that between the $4f_{5/2}$ and $4f_{7/2}$ levels of neutral copper. Predictions by the DF method on fine-structure splittings in alkali-like atoms--i.e., one electron outside a closed shell core--have invariably agreed with known experimental results, while predictions of such inversions using nonrelativistic theories required a great deal of sophistication to emulate the core polarization.

A Dirac-Fock calculation without any additional correlation orbital--known as the single-configuration Dirac-Fock (SCDF) calculation--for neutral Fr (Z = 87) indicates that the 6^2D, 7^2D and 5^2F levels are all inverted. The magnitudes of these inversions predicted by the SCDF method may not be reliable, but the fact that they are inverted is almost certainly correct.

Table 1. Dirac-Fock expectation values, $<r>$, of valence orbitals in Fr-like ions (in a.u.).

Orbitals	Fr	Ra^+	Ac^{2+}	Th^{3+}
$5f_{5/2}$	17.951	7.922	1.982	1.543
$5f_{7/2}$	17.946	7.899	2.055	1.578
$6d_{3/2}$	8.172	3.767	2.967	2.575
$6d_{5/2}$	8.095	3.873	3.057	2.651
$7s_{1/2}$	5.923	4.516	3.849	3.420
$7p_{1/2}$	8.108	5.588	4.553	3.940
$7p_{3/2}$	8.763	6.056	4.925	4.255

When a d or f orbital is about to be occupied in a ground-state configuration, their orbital sizes undergo drastic changes as the atomic number increases, as witnessed around Sc (Z = 21) and La (Z = 58). This rapid change in orbital sizes manifests itself in a variety of ways, but most notably as delayed onset of photoabsorption (or ionization) cross sections involving 4f electrons.[2] A similar change in orbital sizes also occurs in actinides. In Table 1, we have listed the expectation value $<r>$ of the valence orbitals of ions in the Fr isoelectronic sequence. For Ac^{2+} (Z = 89), the 5f orbitals (j=5/2 and 7/2) are already inside other valence orbitals, but their energy levels are still not the lowest.

Table 2. Low-lying levels of Ac^{2+} (excitation energies, E_x, in cm^{-1})

Level	E_x (experiment)[3]	E_x (theory)[4]
$7s_{1/2}$	0.	0.
$6d_{3/2}$	801.0	1 163.7
$6d_{5/2}$	4 203.9	3 853.1
$5f_{5/2}$	23 454.5	32 665.3
$5f_{7/2}$	26 080.2	34 610.4
$7p_{1/2}$	29 465.9	28 729.7
$7p_{3/2}$	38 063.0	36 700.6

Unlike alkali atoms with low atomic numbers, the SCDF method utterly fails to correctly predict the energy level ordering among valence electrons of Fr-like ions, as can be seen in the

AIIM

Association for Information and Image Management

1100 Wayne Avenue, Suite 1100
Silver Spring, Maryland 20910
301/587-8202

Centimeter

Inches

MANUFACTURED TO AIIM STANDARDS
BY APPLIED IMAGE, INC.

2 of 5

example of Ac^{2+} in Table 2. This is very discouraging, because this implies that it is necessary to use a large-scale configuration mixing even to predict energy levels of an alkali-like structure. This is a worthwhile challenge to relativistic atomic structure theorists, who now have a wide range of experience in lighter atoms and more powerful computers at their disposal.

Similar theoretical difficulties exist for lanthanides,[2] though relativistic effects are not as strong as those for actinides. One of the lessons we have learned through numerous studies of the lanthanide series is that qualitative predictions concerning cross sections based on wavefunctions of moderate accuracy were very helpful in understanding the behavior of lanthanide atoms in both gas and solid phases.[2] To see if this is also the case for actinides, systematic comparisons between experiment and theory for actinides are desirable. At present, several theoretical options are available, such as relativistic Hartree-Fock theory for continuum orbitals, relativistic random phase approximation, and relativistic many-body perturbation theory to calculate photoionization cross sections using theories that include relativity, .

For example, relativistic Hartree-Fock theory can produce term-dependent continuum wavefunctions, i.e., different continuum wavefunctions for different total J, which significantly affect photoabsorption cross sections above ionization thresholds. As in the case of lanthanide atoms, it may be too optimistic to expect such theoretical methods to produce *quantitatively reliable* data, but they are likely to provide *qualitatively useful* information in interpreting experimental results. Discussions at this workshop will serve to identify topics for fruitful collaboration among theorists and experimentalists.

1. Y.-K. Kim, D.H. Baik, P. Indelicato and J.P. Desclaux, Phys. Rev. A **44**, 148 (1991).
2. Many excellent review articles on the role of the 3d and 4f electrons can be found in *Giant Resonances in Atoms, Molecules, and Solids*, edited by J.P. Connerade, J.M. Esteva and R.C. Karnatak (Plenum Press, New York, 1987).
3. J. Blaise and J.-F. Wyart, *Energy Levels and Atomic Spectra of Actinides* (Tables de Constantes, Paris, 1992).
4. Present work, results from single-configuration Dirac-Fock wavefunctions.

ATOMIC STRUCTURE CALCULATIONS

FOR HEAVY ATOMS

Yong-Ki Kim

Atomic Physics Div., NIST

COWORKERS

- **Theory**

  Mohamed A. Ali (Howard Univ.)

  Dai Hyun Baik (KAERI)

  Jean-Paul Desclaux (CEN Grenoble)

  Paul Indelicato (Univ. Paris, VI)

  Peter Mohr (NIST)

  Andy Weiss (NIST)

- **Experiment**

  Victor Kaufman (NIST)

  William C. Martin (NIST)

  Joseph Reader (NIST)

  Jack Sugar (NIST)

Hydrogenic Energy Levels

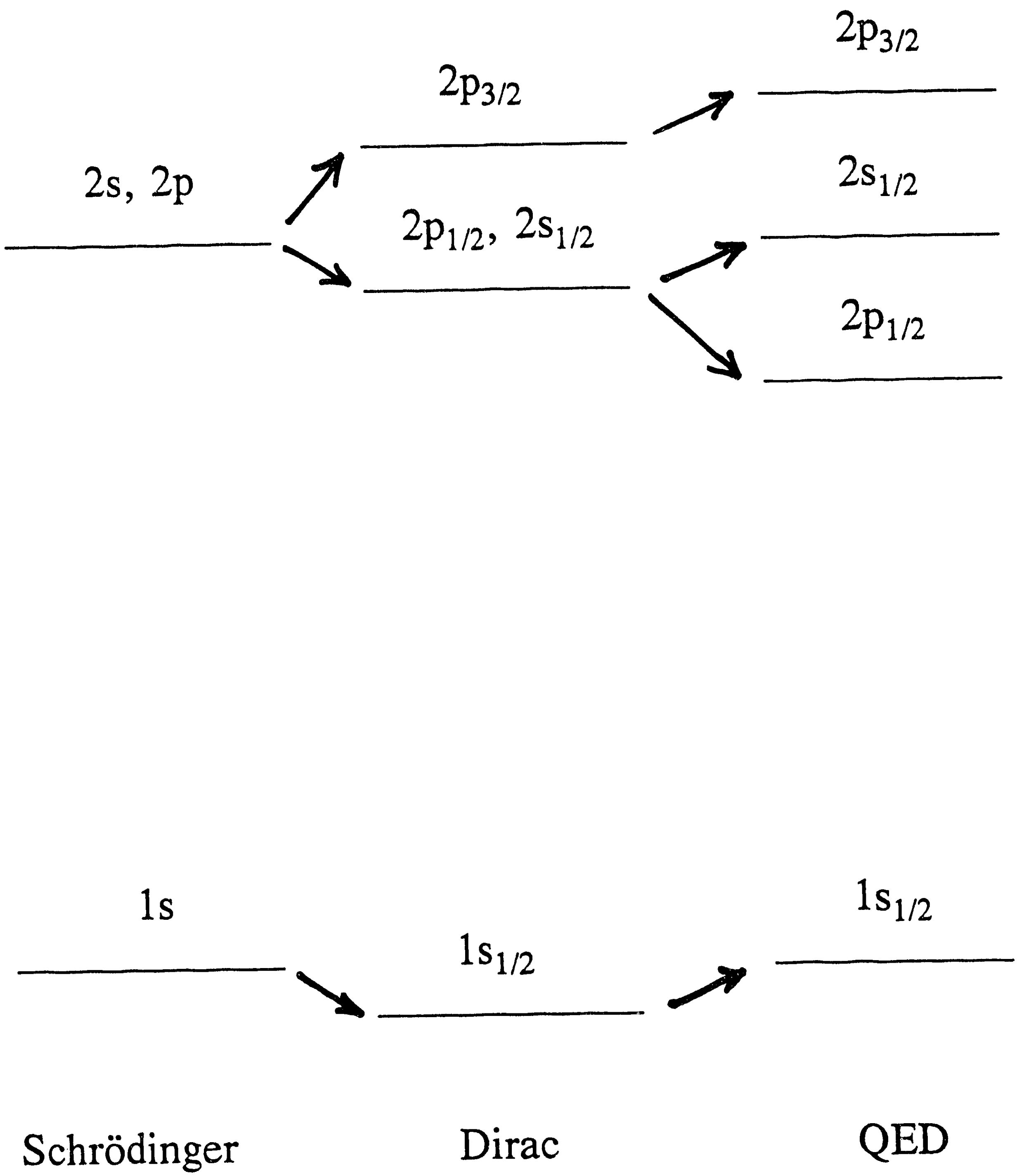

Major Effects on Atomic Energy Levels

	$Z_{eff} \leq 20$	$Z_{eff} \leq 60$	$Z_{eff} > 60$
Correlation	Dominant	Important	Needed
Relativity	Needed	Important	Dominant
QED	Marginal	Needed	Important

$Z_{eff} \sim Z_{Nucl}$ − # OF CORE ELECTRONS

Total Charge Densities for HG

• • • Dots = Nonrelat. and Solid = Relat. ____

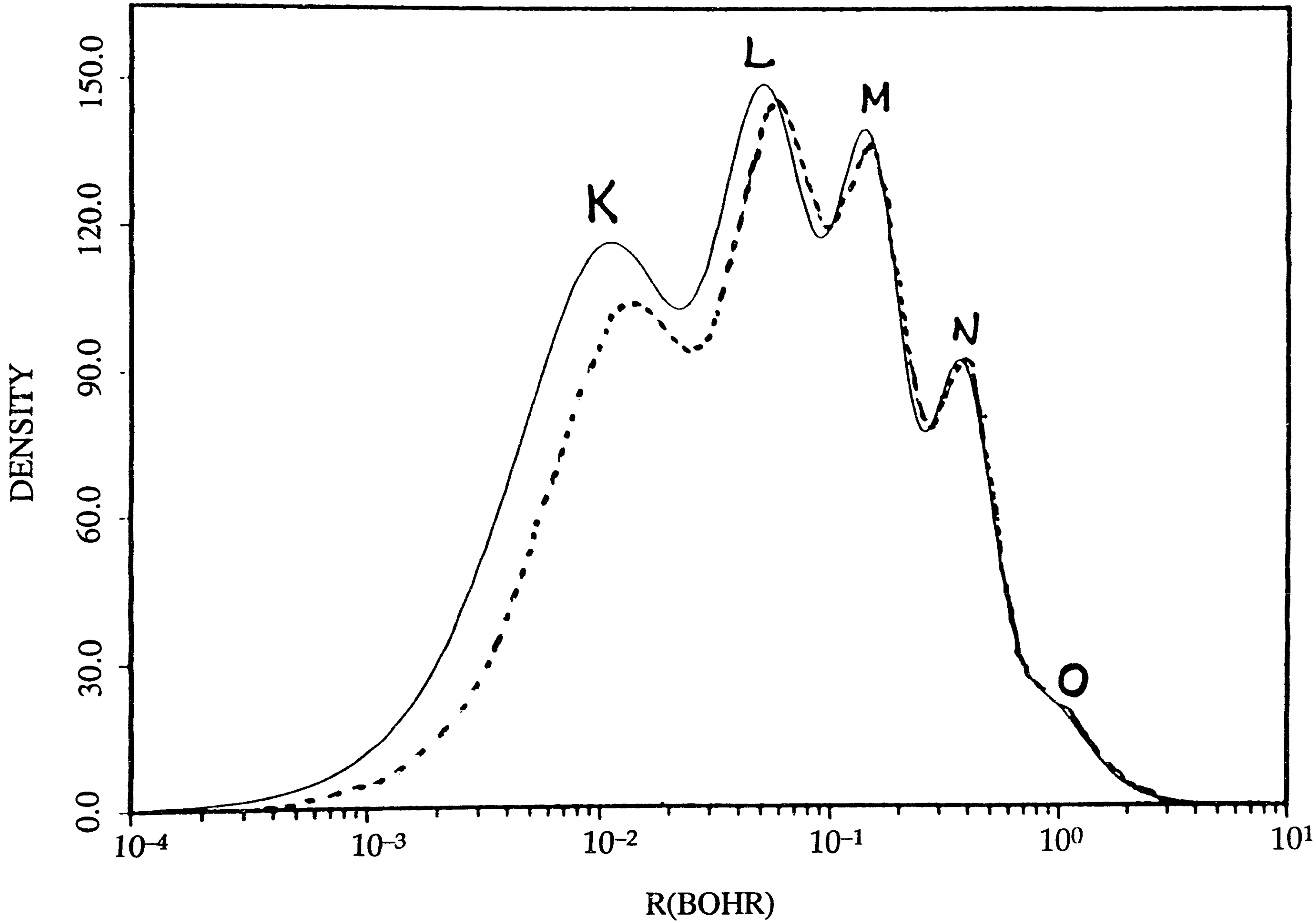

Numerical Example

Mg-Like Ions

Wavelengths for the $3s^2\ ^1S_0 \rightarrow 3s3p\ ^3P_1$ transition

	Mg	Ca^{8+}	Cu^{17+}	Mo^{30+}
Experiment(Å)	4572.5	691.37	345.54	190.47
Hartree-Fock(%)	68.2	88.1	87.2	82.3
Dirac-Fock(%)	68.6	90.3	93.3	95.7
Multiconfig. Dirac-Fock(%)	96.2	99.3	99.7	99.99

Major Computational Methods

A. Multiconfiguration Dirac-Fock (MCDF) Theory

- Extension of nonrelativistic, multiconfiguration Hartree-Fock (MCHF) theory

- Radial functions (large and small components) can be numerical, or expanded in terms of basis functions (STO's, GTO's, splines).

- Radial functions can be derived using:
  - An average-config. potential (CI=config. interaction);
  - A potential optimized for each level (OL=optimized level); or
  - A simplified exchange potential (HS=Herman Skilman)

- Advantages

- General-purpose codes available (Grant, Desclaux)
- Can be applied to configurations with many open shells
- Produces compact wavefunctions for other applications
- Can quickly incorporate major part of correlation

- Disadvantages

- Convergence problems for numerical MCDF solutions
- Dependence on basis functions used
- May be affected by the Brown-Ravenhall *disease*
- Difficult to incorporate core-valence correlation
- "Clean" interface with QED is difficult because MCDF is a nonperturbative theory while the current form of QED is a perturbation theory

B. Relativistic Many-Body Perturbation Theory (RMBPT)

- Extension of nonrelativistic many-body perturbation theory (MBPT)

- As in the MCDF theory, radial functions can be numerical, or expanded in terms of basis functions

- All radial functions must be derived using a common potential (A complete set needed!)

- Usually, unperturbed wave functions are derived from a closed-shell configuration (*i.e.*, single-determinant ground state)

- Some start from a multi-determinant ground state

- **Advantages**

- Provides a clear "physical" picture (Brueckner-Goldstone diagrams) of what's included and what's not
- Can be extended to QED using the same basis functions and similar diagrammatic technique
- Easy to avoid the Brown-Ravenhall disease
- Similar diagrammatic techniques can be developed for other atomic properties

- **Disadvantages**

- Can handle only a limited number of open-shell configurations (closed shell, alkali-like)
- Many orders of perturbation may be needed for neutral and lightly-charged atoms
- Difficult to write a general-purpose code
- Resulting wavefunctions are cumbersome

Major Theoretical Issues for Heavy Atoms

- Correlation and relativity *cannot* be separated

  Relativity affects core orbitals; but

  Valence orbitals must be orthogonal to the core orbitals!

- Competing valence orbitals

  7s, 7p, 6d, and 5f orbitals all compete with each other

  A correlation "nightmare" for theorists

- Hydrogenic ordering only when ionized many times!

- No *ab initio* theory can handle heavy ($Z > 86$) atoms

- Some qualitative aspects of MCDF may still be useful:

- Level inversion

  Magnitude may be bad, but sign is usually right

  Fr ($Z=87$): 6^2D, 7^2D, 5^2F are inverted according to DF

- Orbital size

  Affects f values

- Delayed photoionization peak for 5f orbitals

  Similar to lanthanides (delayed peak for 4f)

  Predictions from MCDF will probably be useful

- BINDING ENERGIES

Table 1. Dirac-Fock expectation values, <r>, of valence orbitals in Fr-like ions (in a.u.).

Orbitals	Fr	Ra^+	Ac^{2+}	Th^{3+}
$5f_{5/2}$	17.951	7.922	1.982	1.543
$5f_{7/2}$	17.946	7.899	2.055	1.578
$6d_{3/2}$	8.172	3.767	2.967	2.575
$6d_{5/2}$	8.095	3.873	3.057	2.651
$7s_{1/2}$	5.923	4.516	3.849	3.420
$7p_{1/2}$	8.108	5.588	4.553	3.940
$7p_{3/2}$	8.763	6.056	4.925	4.255

Table 2. Low-lying levels of Ac^{2+} (excitation energies, E_x, in cm^{-1})

Level	E_x (experiment)	E_x (theory)
$7s_{1/2}$	0.0	0.0
$6d_{3/2}$	801.0	1 163.7
$6d_{5/2}$	4 203.9	3 853.1
$5f_{5/2}$	23 454.5	32 665.3
$5f_{7/2}$	26 080.2	34 610.4
$7p_{1/2}$	29 465.9	28 729.7
$7p_{3/2}$	38 063.0	36 700.6

f values for Au (Z = 79)

	$6^2S \rightarrow 6^2P_{1/2}$	$6^2S \rightarrow 6^2P_{3/2}$
Nonrelat. HF	0.63	1.26
Dirac-Fock	0.39	0.79
MCDF	0.30	0.62
Bates-Damgaad	1.03	1.21
Core polarization	0.16	0.36
Experiments	0.06 – 0.19	0.08 – 0.41

Comparison of X-ray Energies (eV)

U(Z=92)	Theory		Experim.
2S − 1S	93837.1	*	93840.8
$2P_{1/2}$−1S	94653.4		94651.45
$2P_{3/2}$−1S	98435.4		98432.21
3S − 1S	110044.8	*	110050.9
$3P_{1/2}$−1S	110412.6	*	110416.38
$3P_{3/2}$−1S	111292.1	*	111295.80

QED corrections

- Needed to supplement the original Dirac theory
- Self energy
  - Dominant QED correction
  - Exact values known for point nucleus, hydrogenic levels
  - Must be corrected for nuclear size, screening by other bound electrons
  - "Phenomenological methods" available for the screening correction
  - Rigorous QED-based methods being developed
- Vaccum polarization
  - The second most important correction, opposite in sign from the self energy
  - Becomes equally important for very high-Z ions
  - Screening provided by the Uehling potential

- Importance of QED corrections (in eV)

U^{89+}, $2s \rightarrow 2p_{1/2}$ transition

Dirac-Fock, without Breit	286.54
DF, Breit interaction	36.44
Correlation (RMBPT - DF)	-0.73
QED corrections, hydrogenic self energy	-43.96
Screening of the self energy (charge density ratio)	2.38
Screened QED corrections	-41.57
Total, DF + RMBPT	280.68
Experiment (Schweppe et al.)	280.59±0.10
Blundell ("honest" QED theory)	280.83

CONCLUSION

- Much to be done in theory
  - Try basis-set expansion of radial functions to control numerical convergence
  - f-value calculations for valence levels
  - Photoionization cross sections, using term-dependent continuum orbitals

- To assess the reliability of theory, we need experimental data on:
  - Energy levels of simple configurations, *e.g.*, Fr-like ions
  - f values involving valence electrons
  - Photoabsorption cross sections, up to ~ 100 eV above threshold
  - BINDING ENERGIES
- If theory cannot handle Fr-like ions, no hope for others!

FLUX GROWTH OF SINGLE CRYSTAL URANIUM INTERMETALLICS: EXTENSION TO TRANSURANICS.*

P. C. Canfield

Los Alamos National Laboratory
Los Alamos, NM 87545

The importance of single crystal samples for photoelectron spectroscopy can not be over emphasized, specifically in the case of oxygen sensitive f-electron materials. The use of single crystals can allow for the minimization of grain boundary effects, help insure clean surfaces upon cleaving, avoid concern of second phase contamination due to paratectic decompositions, and, of course, allow for angle resolved measurements. In the past, the availability of high quality, adequately sized single crystals has been the limiting step in the use of single crystals, but by using low melting metallic fluxes a wide variety of intermetallic compounds can be grown in single crystal form. In many instances, crystals of roughly 2-4 mm^3 can be grown over 100 hour cooling cycles.

The details of this flux growth method have been reviewed in Fisk and Remeika[1] and Canfield and Fisk[2]. The basics of this method involve the proper choice of flux, dilution of solute in the flux, temperature schedule used for growth and removal of grown crystals from remaining flux at the end of the growth cycle. Each of these steps is non-trivial and can usually only be solved by a combination of experience and trial and error experimentation. For the growth of materials out of binary melts, much of the guess work is removed by reference to one of several collections of binary phase diagrams.

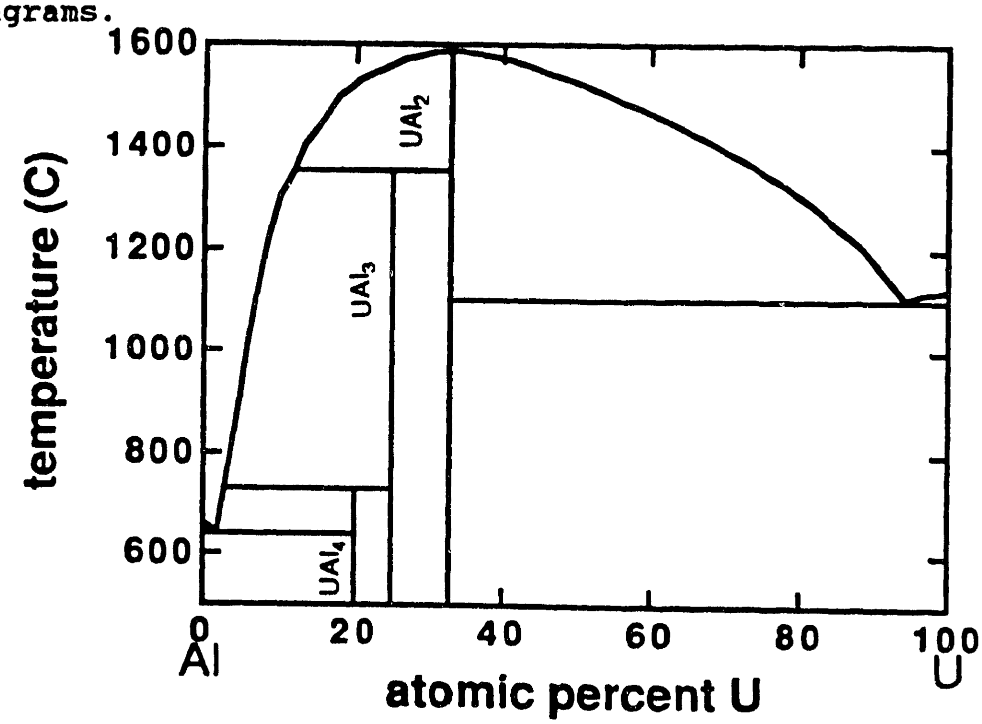

Al-U binary phase diagram from reference 3.

The figure is a reproduction of the salient features of the U-Al binary phase diagram taken from Hansen[3]. The primary features are the liquid-solid line, the three intermediate, line compounds: UAl_4, UAl_3 and UAl_2, and the paratectic decomposition lines of UAl_4 and UAl_3 at 730 C and 1350 C respectively. The two compounds that we will focus on are UAl_3 and UAl_2. These are both members of isostructural families that include Np and Pu analogues, with UAl_3, $NpAl_3$ and $PuAl_3$ having the primitive cubic $AuCu_3$ structure and UAl_2, $NpAl_2$ and $PuAl_2$ having the face-centered cubic Cu_2Mg structure.

Since UAl_3 decomposes paratectically at 1350 C, it can not be grown in a pure form from a stoichiometric melt. If U and Al are mixed in a ratio of 1:3, heated to 1600 C and cooled UAl_2 will initially form, and only below 1350, the UAl_3 paratectic temperature, will UAl_3 form. On the other hand, the growth of UAl_3 can easily be accomplished by growing the material out of excess Al. A starting concentration of 93 atomic percent Al will allow for crystal growth of UAl_3 below 1200 C. The U-Al mixture can be heated to above 1200 C to ensure thorough mixing and then slowly cooled to just above 730 C, the UAl_4 paratectic temperature, and then rapidly cooled. The crystals can then be removed from the excess Al by a NaOH etch, or by a second melting of the remaining Al and removing the molten flux from the crystal via centrifugal force. Since the binary phase diagrams for Np-Al and Pu-Al are similar, this is a likely method for the growth of $NpAl_3$ and $PuAl_3$.

The more difficult growth of the UAl_2 family of materials, as well as the use of this method to grow ternary intermetallics will also be discussed as time allows.

* This work was performed under the auspices of the United States Department of Energy.

1. Z. Fisk, J. P. Remeika, in *Handbook on the Physics and Chemistry of Rare Earths*, edited by K. A. Gschneidner, Jr. and L. Eyring, Vol. 12 (Elsevier Science Publishers B. V., 1989), p. 53.

2. P. C. Canfield, Z. Fisk, Phil. Mag. B 65, p. 1117 (1992).

3. M. Hansen, *Constitution of Binary Alloys*, (McGraw-Hill, 1958), p. 143.

Flux Growth of single crystal Uranium intermetallics: *Extension to Transuranics.*

Los Alamos National Laboratory

Paul C. Canfield

Zach Fisk

Synchrotron Radiation in Transactinium Research Workshop
Lawrence Berkeley Laboratory
October 1-2, 1992

Bulk Materials:

Polycrystalline

Solid state reaction

Arc melt

On-line growth

Single crystal

Δ Flux growth

Δ Chemical transport

$$ Zone refining

$ Czochralski

Intermetallic Single Crystals

-Well defined structures and ligands.

-Can "tune" An-An distance and hybridization.

-The possibility of easy sample cleavage and relatively stable surfaces. (Structure dependent)

-Well defined samples 3mm on a side for average, several day growth. (Highly sample dependent: 1-10mm on a side.)

Sugar and water:

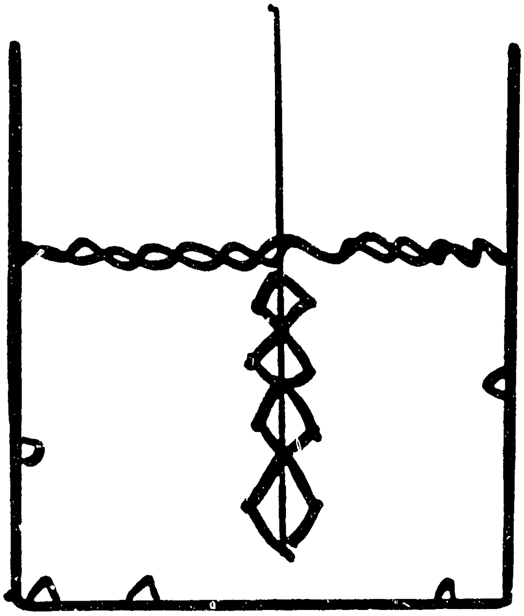

Sugar: xx.xx g
Water:yy.yy g

$$20 \xrightarrow{3\,hr} 90 \xrightarrow{3\,hr} 90 \xrightarrow{48\,hr} 20 \xrightarrow{c} 20$$

Lower melting point:

Sucrose: 185 C
NaCl: 800 C

Easy removal (while flux is still molten).

Possible inclusion and / or incorporation of flux into sample.

Binary Sugar/Water Phase Diagram

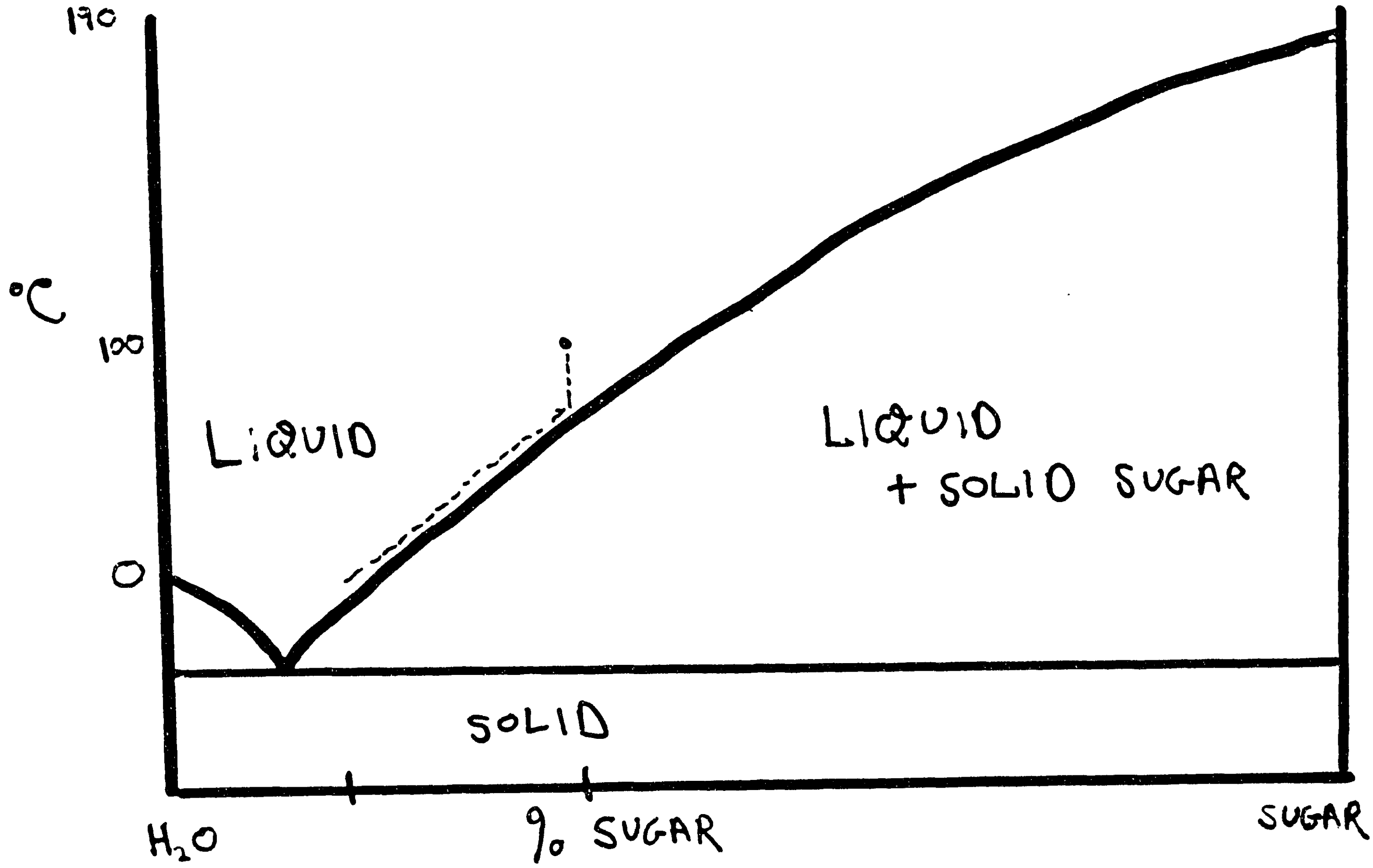

~ 50 % YIELD

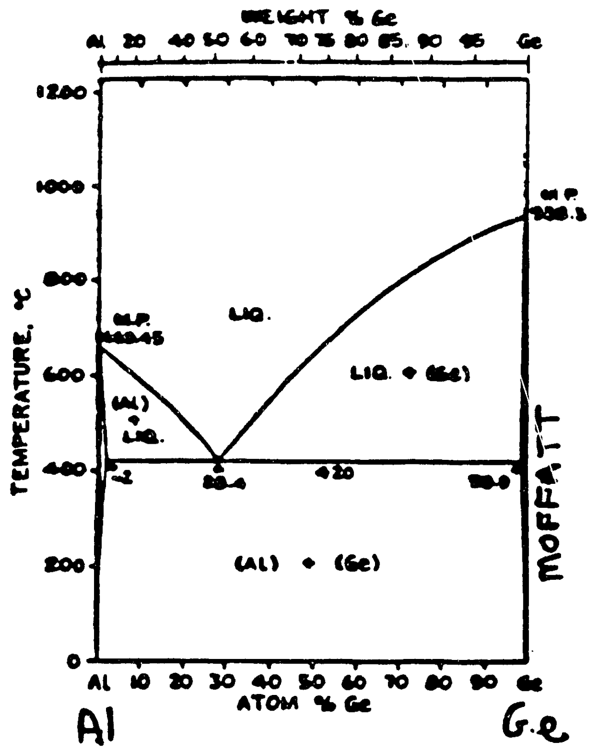

Binary Phase Diagrams.
Several compilations of binary phase diagrams. Data set relatively complete.

Ternary phase diagram data is very incomplete.

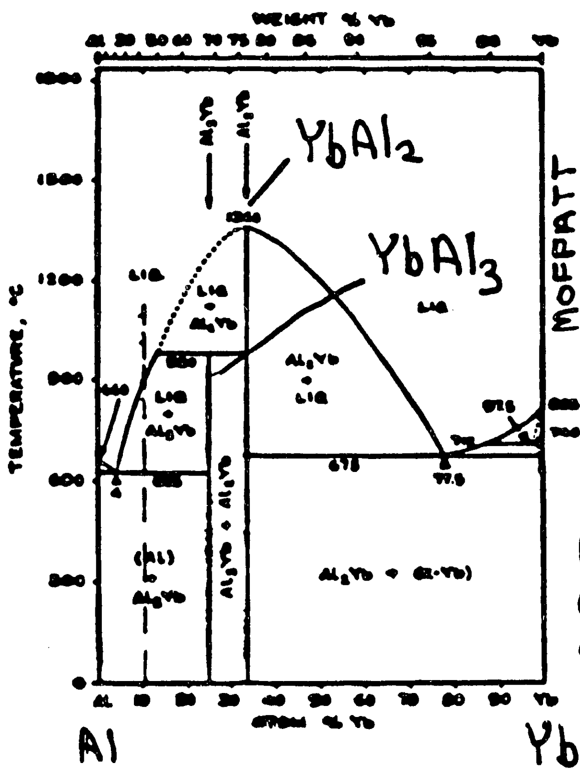

10% Yb IN Al WILL GIVE $YbAl_3$ CRYSTALS + Al ON COOLING

$YbAl_2$ melts congruently, i.e. it can be grown from the pure melt.

$YbAl_3$ melts incongruently, i.e. it can not be grown in a pure form from a stoichiometric melt.

Both $YbAl_2$ and $YbAl_3$ can be grown out of excess Al and $YbAl_2$ can be grown out of excess Yb.

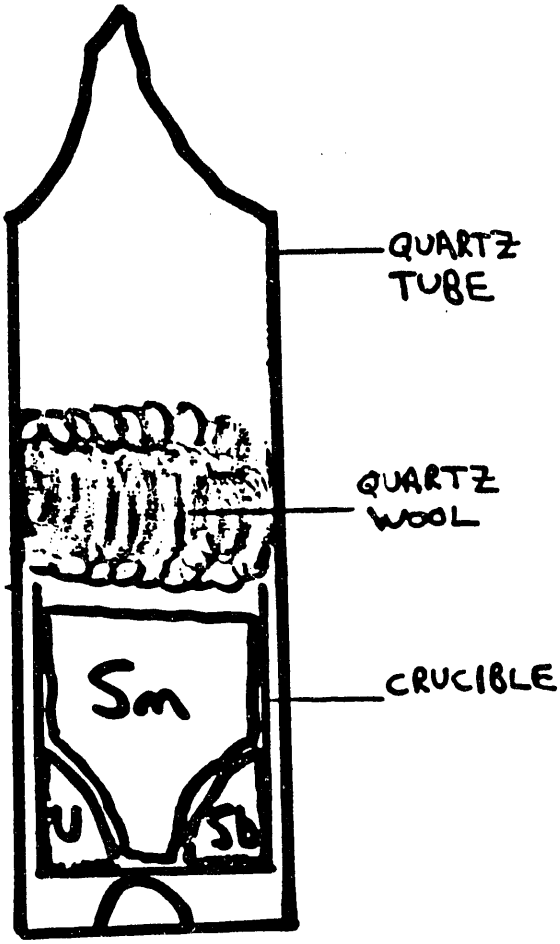

- Idea for Growth
- Check binary phase diagrams
- Pack tube
- Growth cycle
- Remove Flux
- Examine crystals
  i) Is it expected crystal?
  ii) What is it?
- "Linus Pauling"

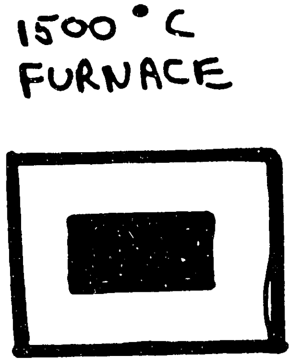

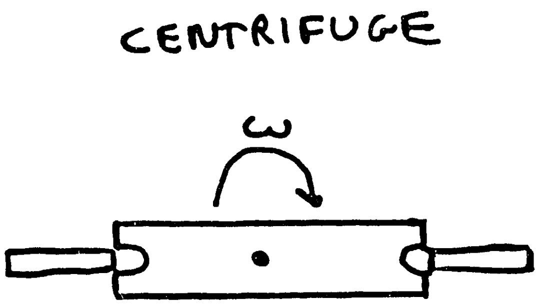

NOTE:

–Very quick. (Over night growths/10 tubes in a furnace)

–Very simple equipment

--Uncommon technique

CeSb: Melts 1800 C.

Ce-Sb

Grow out of excess Sb or Ce only down to 1500 C.

Try to lower growth temperature by use of third element as flux.

Try a variety of low melting fluxes.

Al, Ga, Pb, Sn, In

Sn works!

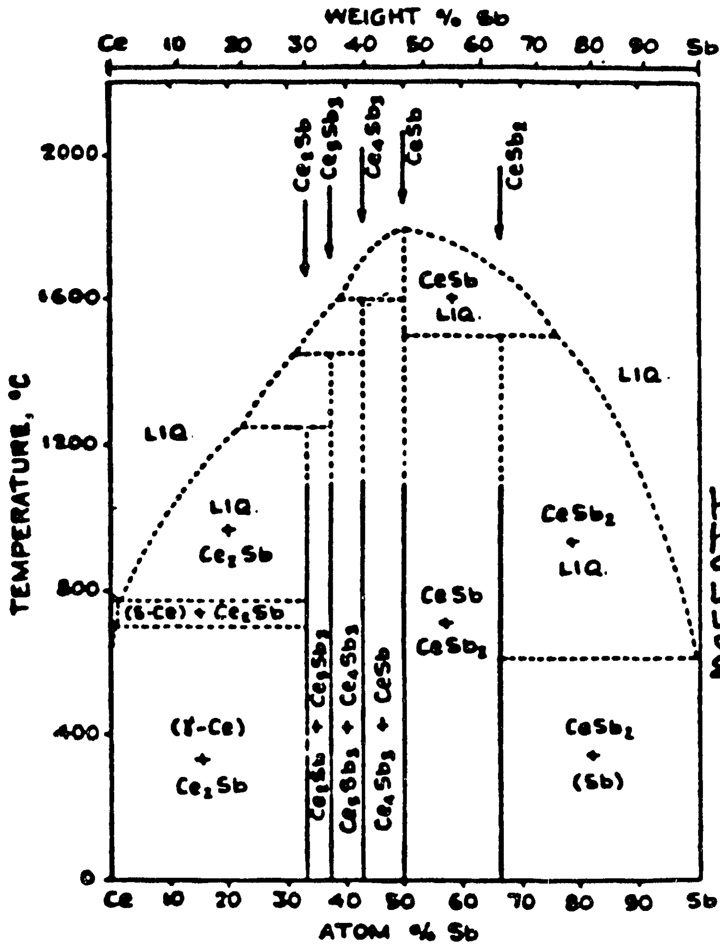

CeSb/Sn : $(CeSb)_{0.05}Sn_{0.95}$

Ce: 0.78 g
Sb: 0.68 g
Sn: 12.00 g

$20 \xrightarrow{4} 1150 \xrightarrow{4} 1150 \xrightarrow{48} 750 \xrightarrow{c} 750$

NOTE:

Sn melts at 250 C, but spin off above 700 C to avoid second phase of $CeSn_3$.

Ce-Sn and Sn-Sb Binaries:

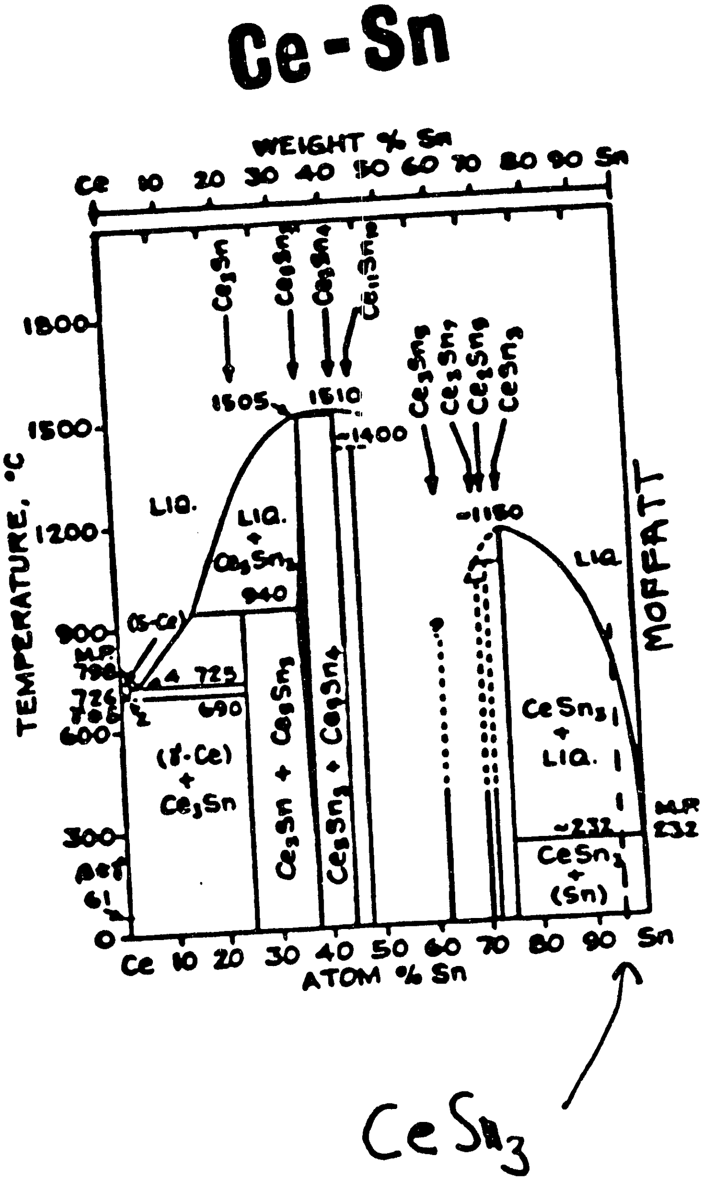

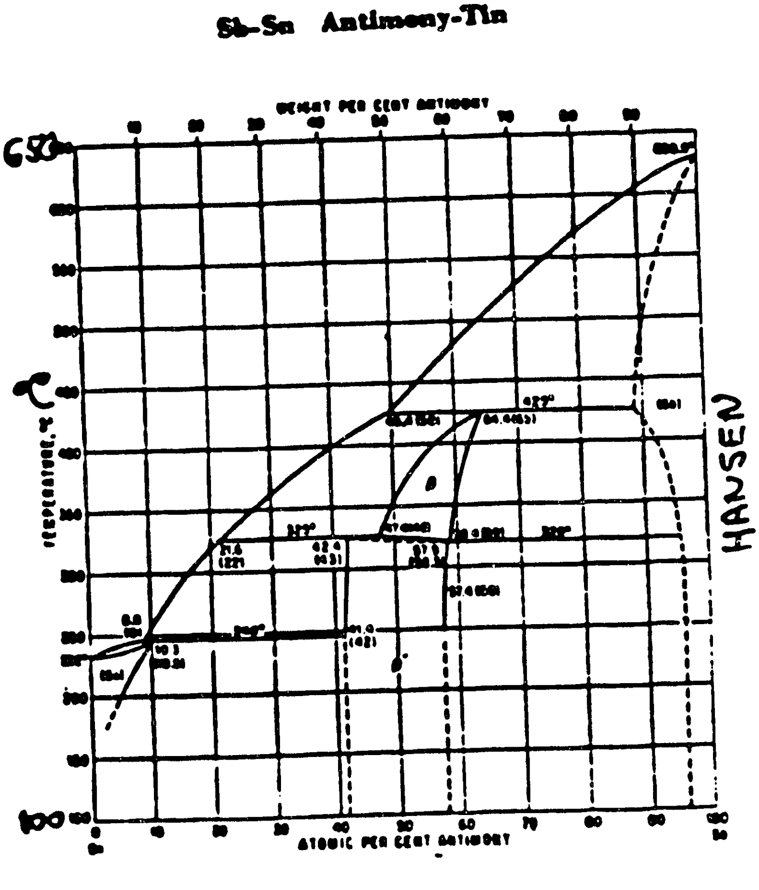

Transactinium Intermetallics:

Grow isostructural compounds and look for systematics across the early actinides.

$AnSn_3$ and similar binaries.

$AnAl_3$ and other Al flux growths

AnSb/Sn and ternary compounds

Glove box requirements.

AnSn3---Cu3Au Structure

Pu-Sn

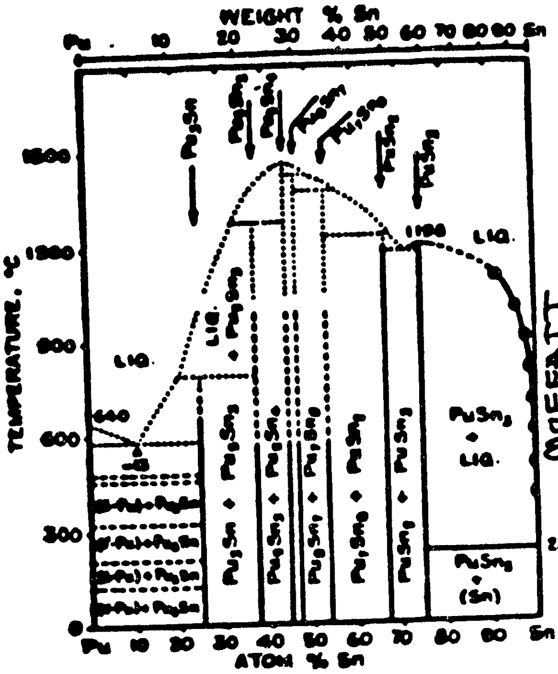

Sn-U

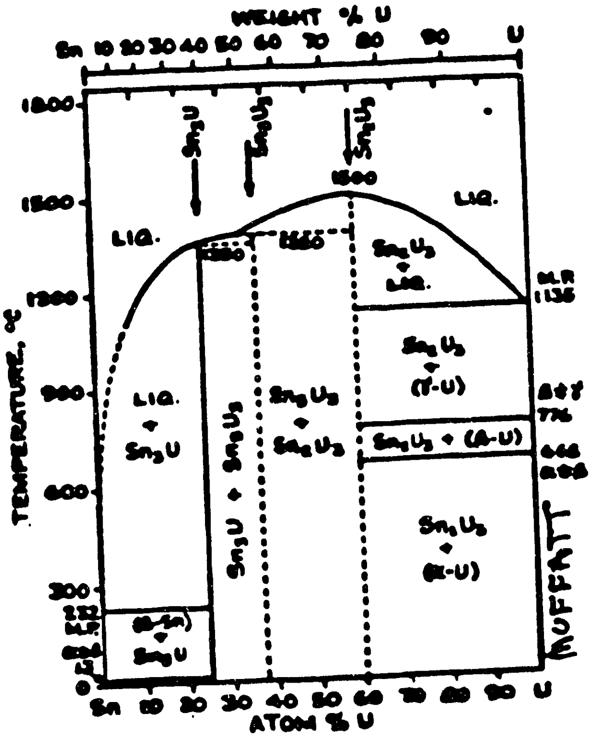

- Low melting flux and grows well.
- Twins along (1,1,1) direction.
- AnPb3 is similar.

AnAl$_3$—Cu$_3$Au Structure

Problem with Al as flux:

Al attacks the quartz tube, causing a loss of protective atmosphere.

Requires a vertical tube (V. T.) furnace and gas handling system. V. T. will become contaminated and can be awkward to use in a glove box.

Advantages of Al as flux:

Easy to etch with NaOH. No spin is required if sample is stable, samples can be handled only at room temperature

Can grow a number of Borides and Berylides out of dilute Al melts.

AnSb/Sn and Ternaries

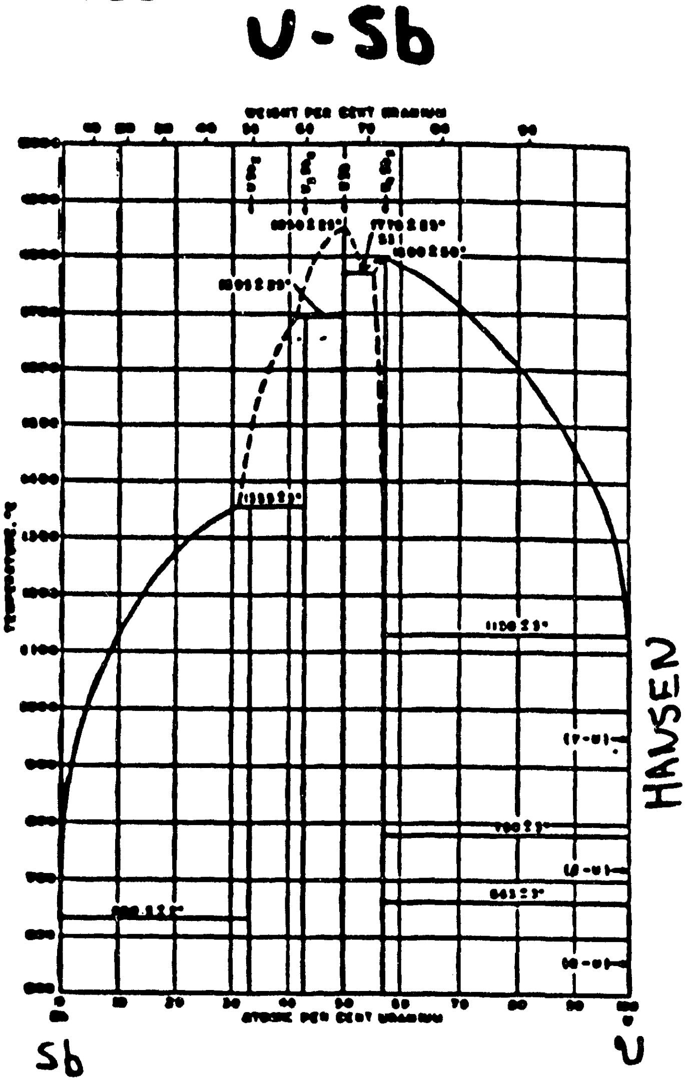

Dilute USb/Sn
Spin off at
750 to avoid
USn_3.

USb MELTS
~1850 °C

IF NOT Sn, THEN TRY
In, Pb, Ga & Al

Sn and In are good for the growth of $ThCr_2Si_2$ compounds.

$AnCu_2Si_2$ $AnNi_2Si_2$

$AnCu_2Ge_2$ $AnNi_2Ge_2$

Known for An=U and Np

Glove box requirements:

A LARGE hot glove box that can accommodate:

Sample preparation space

--balance

--cutting tools

--microscope

Sample growth space

--hydrogen/oxygen torch

--high temperature furnace
(1200 or 1500 C)
(Box or Vertical Tube)

A FAMILY TREE

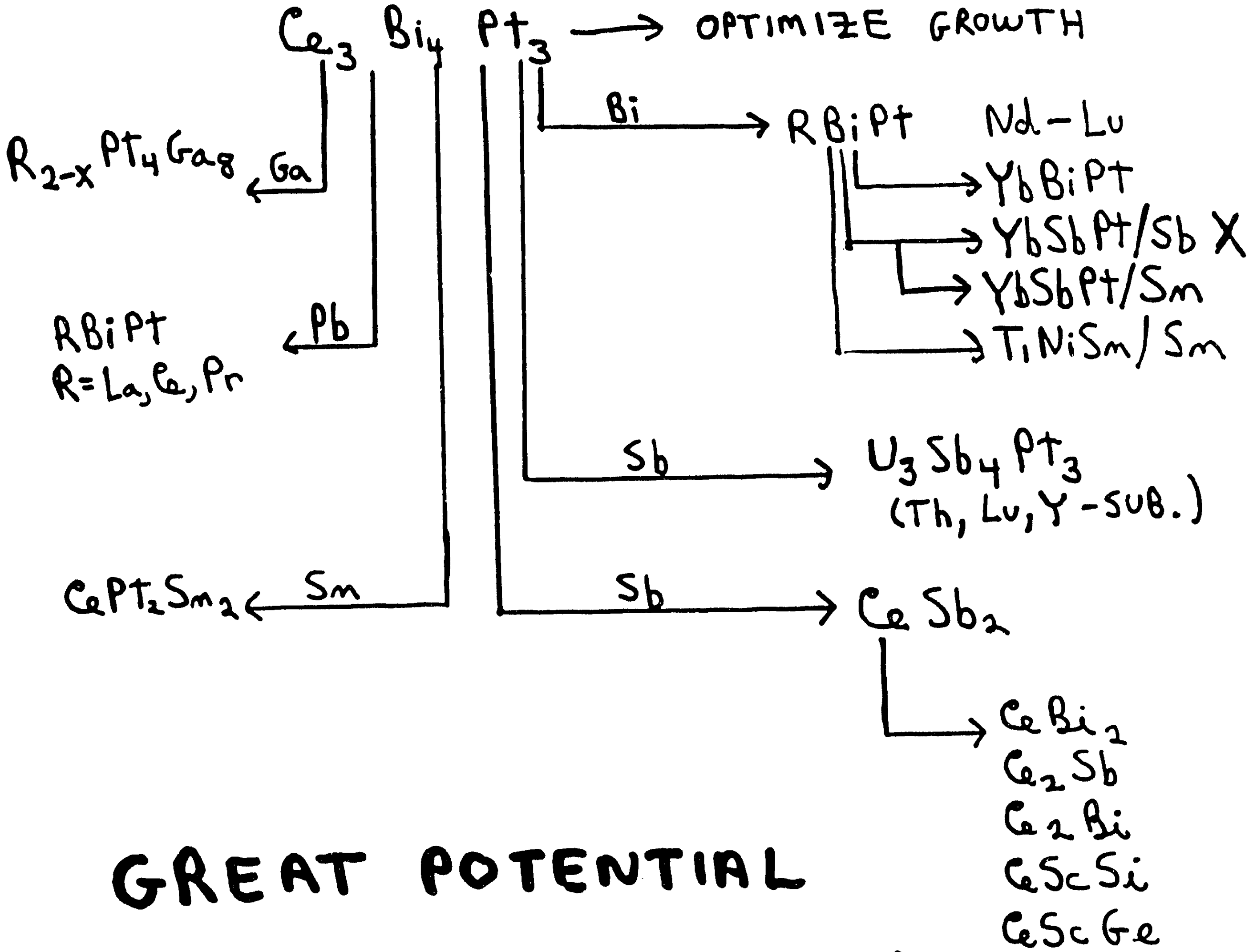

GREAT POTENTIAL FOR THE DISCOVERY OF NEW MATERIALS

Basic Growth Philosophy:
Have a basic agenda(s)

<u>BUT</u>

Keep your eyes open for interesting new phases.

To do this there must be a sorting mechanism to determine what is interesting.

$\rho(T)$

Rough Sorting

$\chi(T)$

C (T)
S(T)
Hall Effect

Second Phase Physical Measurements

X-ray diffraction

Structural Refinements

Elemental Analysis

X-RAY ABSORPTION NEAR-EDGE STRUCTURE STUDIES OF ACTINIDE COMPOUNDS

G. Kaindl

Institut für Experimentalphysik, Freie Universität Berlin,
Arnimallee 14, W-1000 Berlin 33, Germany

The present status in the use of x-ray absorption (XA) with synchrotron radiation in the study of the electronic structure of compounds of the light actinide elements is reviewed. The useful XA thresholds cover the range from the VUV ($O_{IV,V}$), via soft x-rays ($N_{IV,V}$; $M_{II,III}$; $M_{IV,V}$) to the hard x-ray region (L_{I-III}). [1] Due to the lack of an actinide beamline at present synchrotron radiation facilities, most studies of the more radioactive materials (Np, Pu, Am) have been performed at the L thresholds, where due to the hard x-ray energies of ≅ 20 keV, the absorber material can be safely encapsulated.[2-4] In this photon-energy range, the XA method is also readily applicable to high-pressure studies.[5,6] The talk will therefore emphasize work at the L absorption thresholds, but will also try to glance at the perspectives of future work in the soft x-ray region.

In the authors group, L-edge XA studies were performed up to now for a variety of metallic and nonmetallic compounds of Th, U, Np, Pu, and Am using synchrotron radiation from the ROEMO beamlines of HASYLAB at DESY in Hamburg.[1-6] The information on the correlated electronic structure of these materials is contained in those studies in the threshold energies and in the x-ray absorption near-edge structure (XANES). The XANES spectra at the L_{II} and L_{III} thresholds exhibit intense white lines (WL) due to optical excitation of a 2p core electron to unoccupied 6d final states with a high density of states close to E_F. These white lines are found to shift with the valence state of each actinide element [2-4] and often exhibit fine structures due to core-excited final states with different 5f occupancies, which are populated due to the interaction of the localized 5f electrons with the valence states.[3] Figure 1 gives as an example a graphical plot of L_{III}-WL shifts relative to the respective dioxides as reference compounds for a series of chalcogenides and pnictides of U, Np, Pu, and Am.[2,4] The observed chemical shifts are essentially caused by the Coulomb interactions between the 5f electrons with the 2p core hole as well as the excited 6d electron. The magnitude of these shifts is found to increase systematically from U to Np, Pu, and Am, which reflects the increasing localization of the 5f states.

The most extensive study of L_{III}-XANES spectra has been carried out so far for compounds of Np with formal valencies ranging from III to VII.[3] In this case, the L_{III}-WL of Np^{V}, Np^{VI}, and Np^{VII} compounds exhibit fine structures due to different core-ionized many-body final states, which reflect the correlated groundstates of these systems. The weighted mean positions of the L_{III}-XANES WL structures shift to higher energies with decreasing 5f occupancy and, for

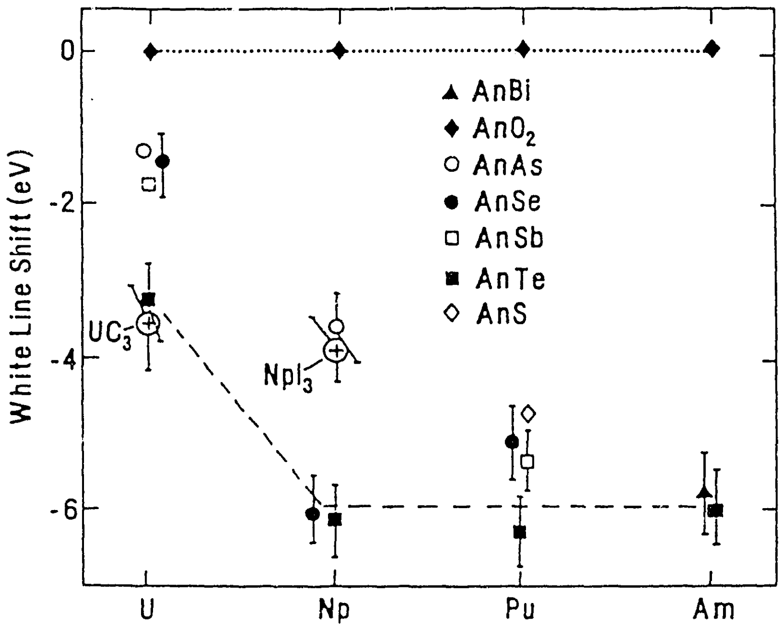

Figure 1. Shifts of the L_{III} white line for compounds of U, Np, Pu, and Am relative to those of the respective dioxides.

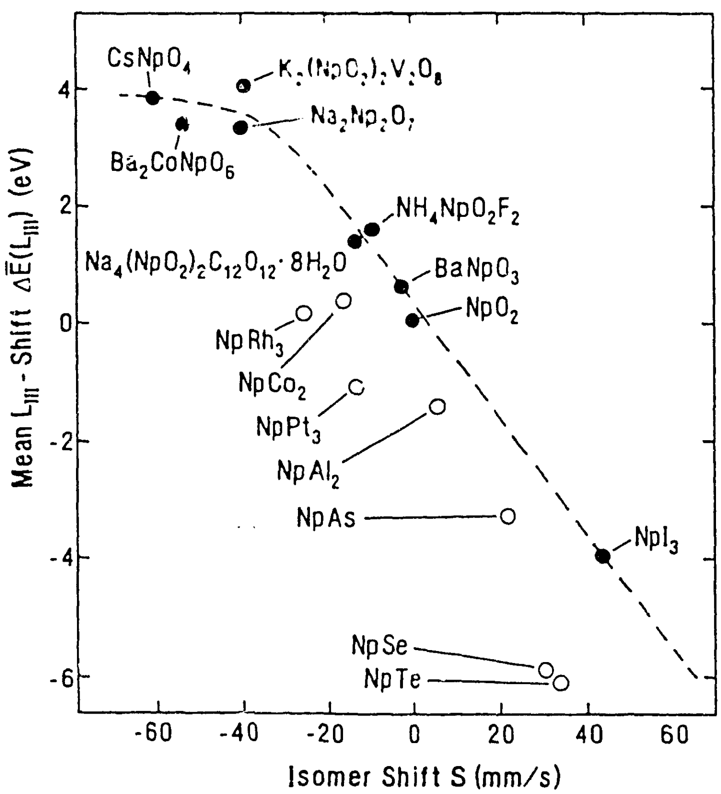

Figure 2. Correlation between mean L_{III} shift, $\Delta E(L_{III})$, and Mössbauer isomer shift, S, for nonmetallic (filled circles) and metallic (open circles) compounds of Np. The dashed curve through the data points for nonmetallic compounds serves as a guide to the eye.

non-metallic compounds, depend monotonically on the respective Mössbauer isomer shifts of the 59-keV nuclear gamma transition of ^{237}Np. This correlation is given in Fig. 2. Systematic deviations from this correlation are observed for metallic Np compounds caused by the contributions of the conduction electrons to the Mössbauer isomer shift, which - due to their itinerant nature - have little influence on the L_{III}-WL energies.

XANES measurements at the L-XA thresholds of actinide elements are also readily applicable to studies of the effects of high external pressure on the electronic structure of actinide compounds. Using a diamond-anvil high-pressure cell, such investigations have only been performed up to now for compounds of Th and U.[5,6] In all cases studied, the L_{III} white lines were found to shift to higher energies with increasing pressure due to increasing 5f delocalization, i.e. decreasing 5f occupancy. In addition, structural phase transitions were found to lead to discontinuities in the pressure derivatives of the WL energies.

This work was supported by the Bundesminister für Forschung und Technologie, project No. 05-5KEAXI-3/TP01.

1. G. Kalkowski, G. Kaindl, W.D. Brewer, and W. Krone, Phys. Rev. B35, 2667 (1987).
2. G. Kalkowski, G. Kaindl, S. Bertram, G. Schmiester, J. Rebizant, J.C. Spirlet, and O. Vogt, Sol. State Commun. 64, 193 (1987).
3. S. Bertram, G. Kaindl, J. Jové, M. Pagès, and J. Gal, Phys. Rev. Lett. 63, 2680 (1989).
4. S. Bertram, G. Kaindl, Z. Hu, J. Rebizant, and J.C. Spirlet, to be published.
5. G. Schmiester, S. Bertram, G. Kaindl, and O. Vogt, in *Theoretical and Experimental Aspects of Valence Fluctuations,* edited by L.C. Gupta and S.K. Malik (Plenum Publ. Corp., 1987) p. 397.
6. S. Bertram, G. Kaindl, G. Schmiester, and O. Vogt, High-Pressure Research 2, 361 (1990).

X-Ray Absorption Near-Edge Structure Studies of Actinide Compounds

G. Kaindl

Institut für Experimentalphysik, F.U. Berlin

Outline

- Introduction to XANES
- Useful XA thresholds in actinides
- L-edge XA in Th, U, Np, Pu, Am ....
- Detailed L_{III}-XA study of Np compounds
- High-Pressure effects
- Summary and outlook

Funded by the Bundesministerium für Forschung und Technologie, FRG

Collaborators and Contributors

S. Bertram † G. Schmiester G. Kalkowski W. Krone G. K.	Freie Universität Berlin
J. Rebizant J.C. Spirlet	European Institute for Transuranium Elements
J. Jové M. Pages	Institut Curie Paris
O. Vogt	ETH Zürich
J. Gal	Ben-Gurion University of the Negev

(A) Introduction to XANES in An compounds

- XANES = X-ray Absorption Near-Edge Structure

monitors unoccupied electronic structure
+ effects due to correlated nature of 5f states.

- Why is electronic structure of An compounds interesting?

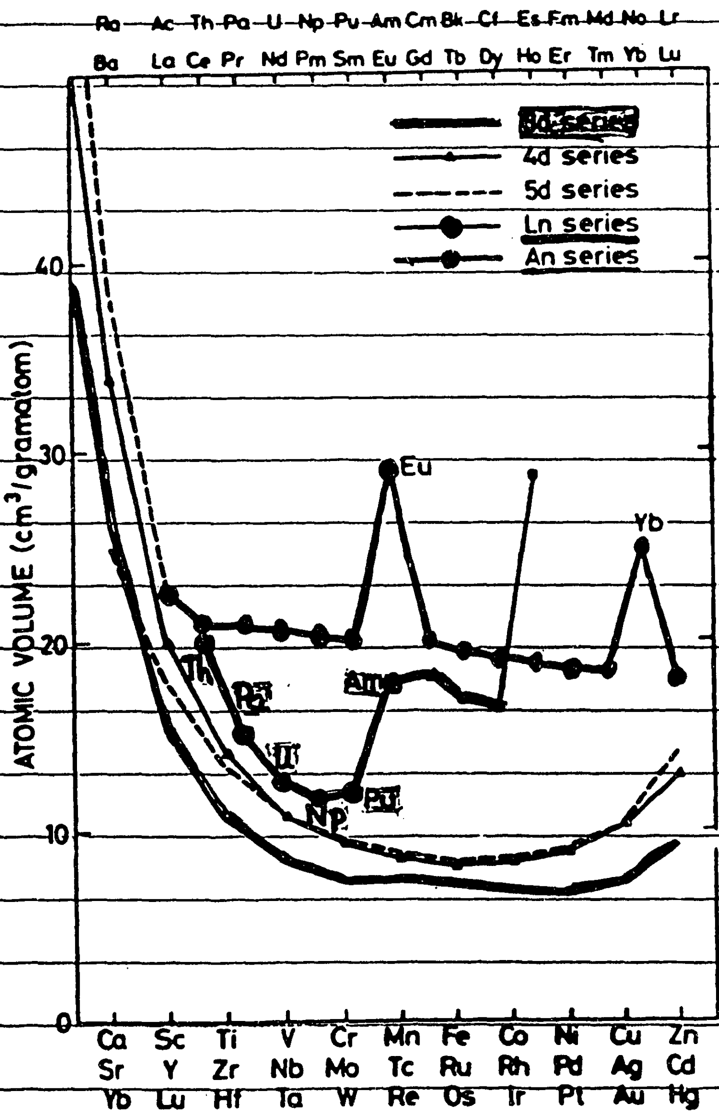

5f states localize between U and Am

What can XANES contribute to our understanding of 5f states in actinide compounds?

XANES : electronic structure information

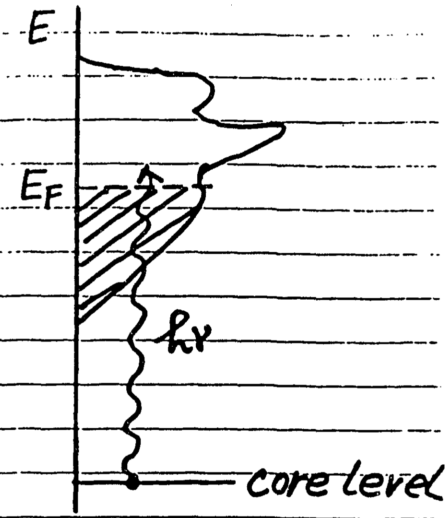

- XA process:

$$\mu \propto |\langle f|e \cdot \vec{r}|i\rangle|^2 \cdot \rho(E_F)$$

– monitors density of unoccupied final states at E_F with $\Delta l = \pm 1$

XA threshold	probes
K, L_I	p states
$L_{II,III}$, $M_{II,III}$	d states
$M_{IV,V}$, $N_{IV,V}$, $O_{IV,V}$	f states

- In case of bandlike, non-TM solids:

  – XANES reflects l-projected unoccupied partial density of states.

- In case of highly correlated, open-shell systems: 3d, 4f, 5f

  – XANES reflect Coulomb and/or exchange interactions between the open shells.

- XAS is high-energy spectroscopy

i.e. energy separation ΔE between different core-ionized final states is usually much larger than the mixing energy V of these states in the ground state:

$$\Delta E \gg V$$

example:

$EuCu_2Si_2$ homogeneously-mixed valent, $\bar{v} \simeq 2{,}5$

$a|4f^6\rangle + b|4f^7\rangle$; $V \simeq 10$ meV

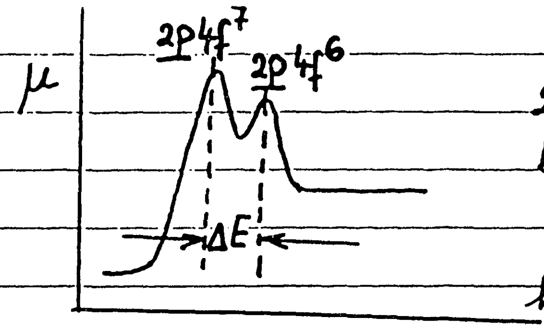

2 final states separated by $\Delta E \simeq 7$ eV.

↳ $\Delta E \gg V$

- Note:

Mössbauer spectroscopy is low-energy spectroscopy since only nucleus is excited, and difference in hyperfine interactions between different final states is $\ll V$.

e.g. isomer shift S between $Eu^{2+}(4f^7)$ and $Eu^{3+}(4f^6)$ differs only by

$$\Delta S \simeq 1 \times 10^{-6} \text{ eV}$$

$$\Delta S \ll V$$

↳ single Mössbauer line measures unperturbed ground state of $EuCu_2Si_2$.

● Example: L_{III}-XANES of Dy^{II}, Dy^{III}, and Dy^{IV} compounds

Dy: [Xe] $4f^{10}6s^2$ $\qquad 2p \xrightarrow{E1} 5d$

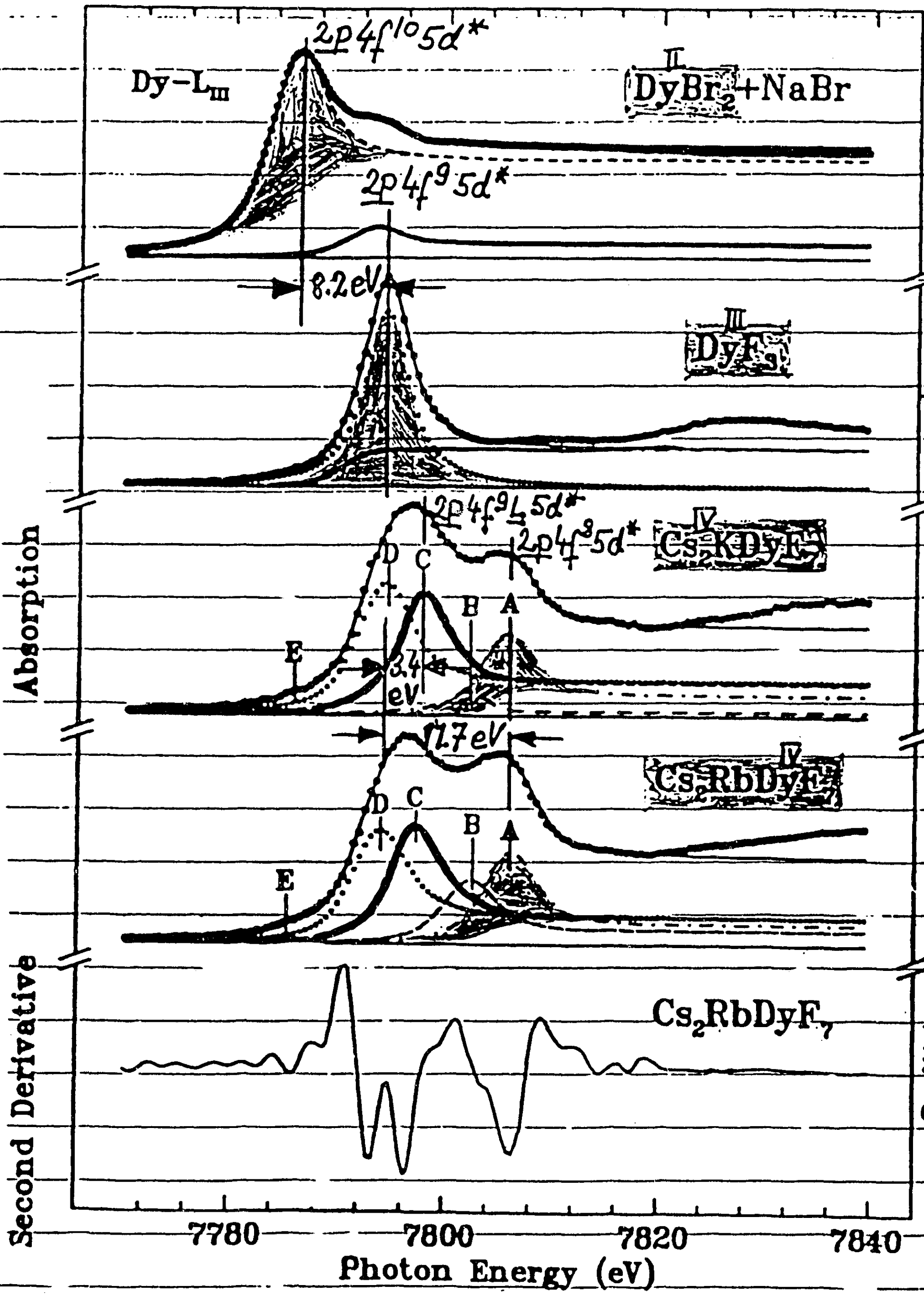

White line + absorption edge

Ref: Z. Hu, G. Kaindl et al., unpubl.

■ White line shift ΔE = 8.2 eV between Dy^{III} and Dy^{II}

= 11.7 eV — " — "Dy^{IV}" — " — Dy^{III}

■ Component $\underline{C}$ due to 4f covalency populated under the influence of the 2p core hole: $\underline{2p}4f^9\underline{L}5d^*$.

L_{III}-XANES

$$2p^6\,4f^n\,5d^m \xrightarrow{E1} 2p^5\,4f^n\,5d^{m+1}$$

- White line (WL) due to high density of states of unoccupied 5d states at E_F.

- WL shift ΔE

$$\Delta E = \Delta U_{cf} + \Delta U_{cd} - \Delta U_{fd}$$

– measures difference in Coulomb energies U between the two compounds or final states.

U_{cf} = core hole / 4f attraction

U_{cd} = core hole / 5d* –"–

U_{fd} = 4f / 5d* repulsion

– U_{cd} should not vary much chemically

↳ $\Delta E \cong \Delta U_{cf} - \Delta U_{fd}$

↑

main term

L_{III}-XANES spectra of various U compounds

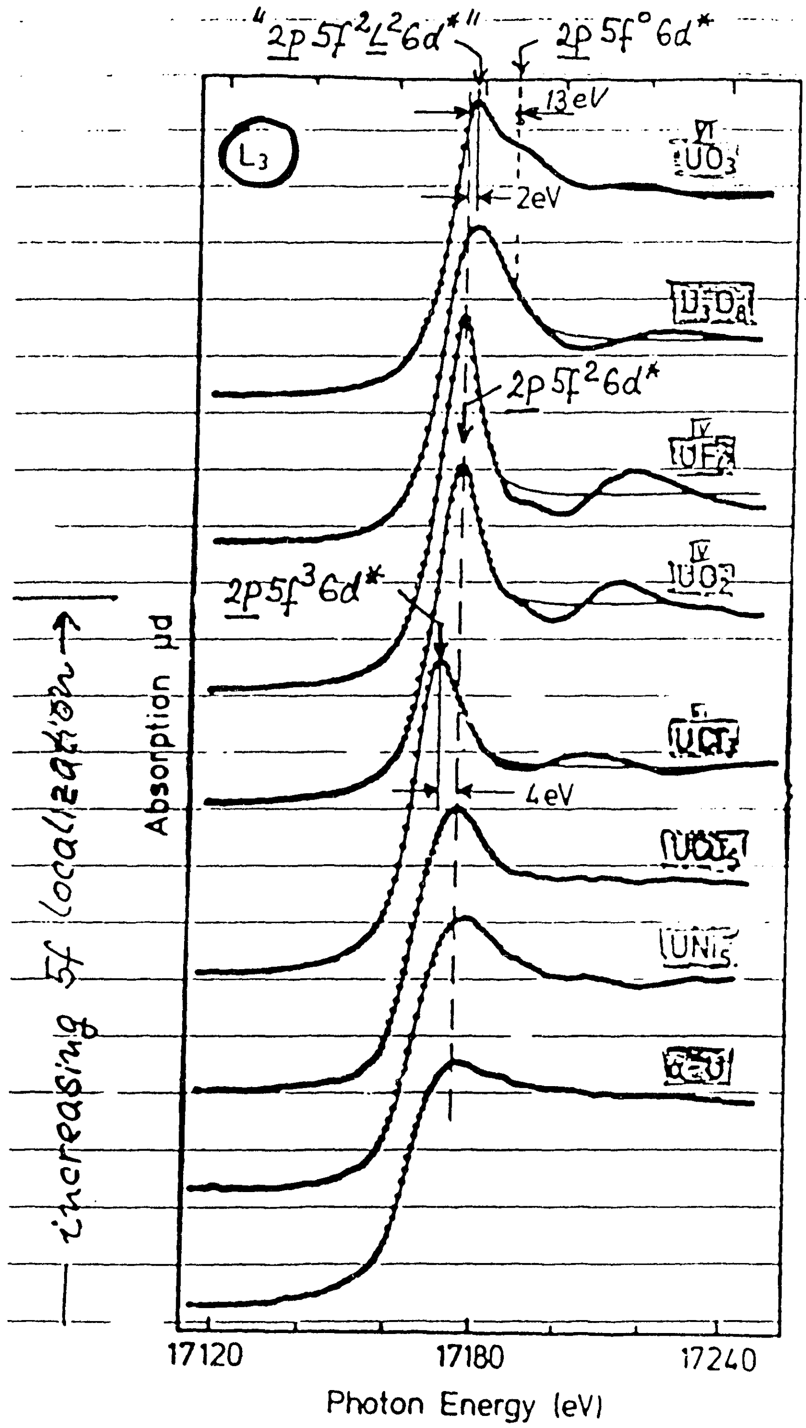

5f covalency

2 final states

$5f^2$ / $5f^3$ } 4eV shift between U^{III} and U^{IV}

localized / itinerant } 2 eV shift

← 5f band like

WL damped

- Width and relative weight of white line vary
  ↳ 6d density of states
- Position of W.L. changes by ≅ 17 eV
  ↳ 5f occupancy and localization

(B) Useful XA thresholds in Actinides

XANES spectra of UF_4 at various thresholds

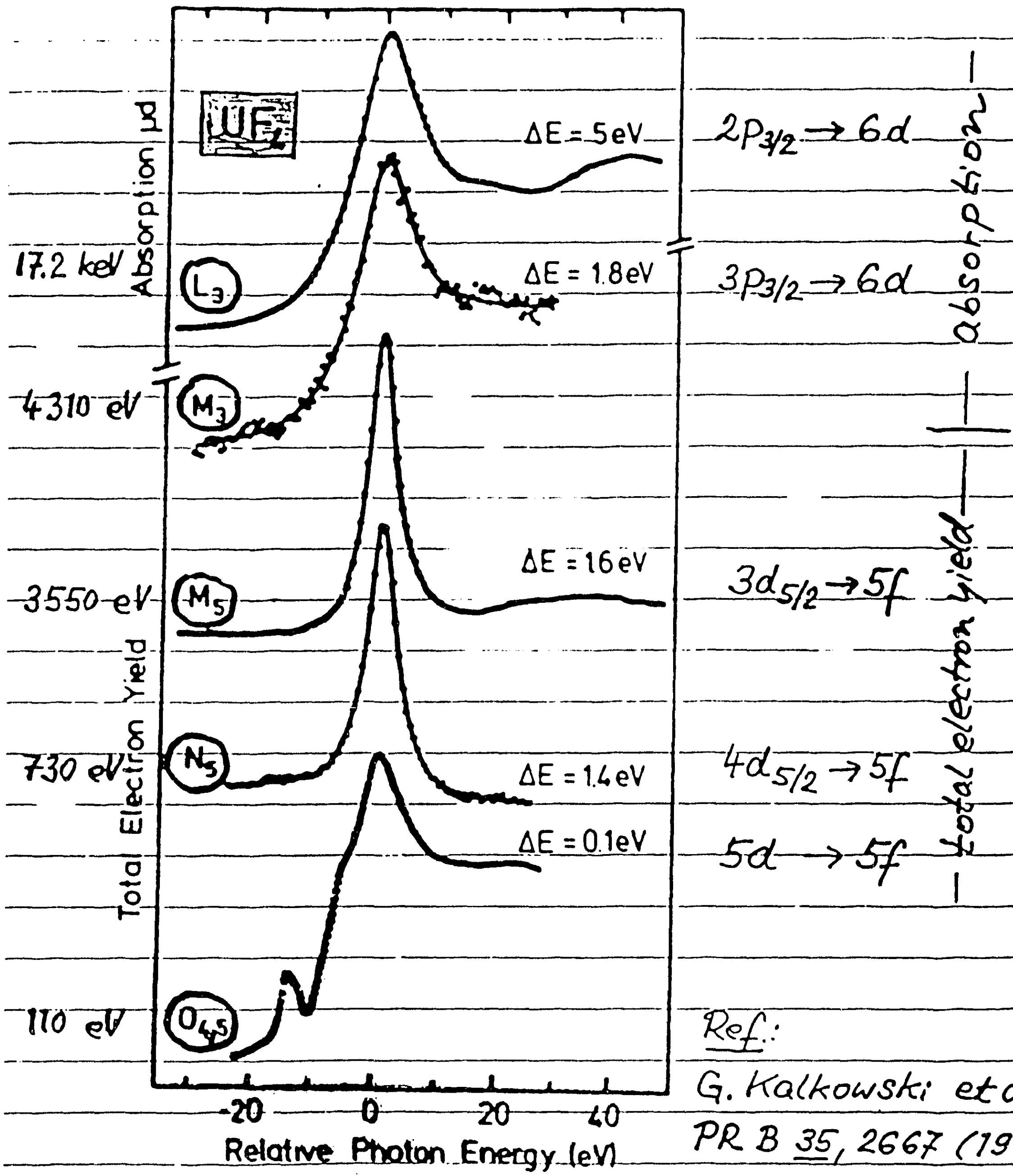

Ref.:
G. Kalkowski et al.
PR B 35, 2667 (1987)

- M_{III} provides very similar information as L_{III}.
- at $O_{4,5}$ multiplet splitting resolved
  $5d^9 5f^3$ final state

- Analogous results at M_{III} measured in absorption

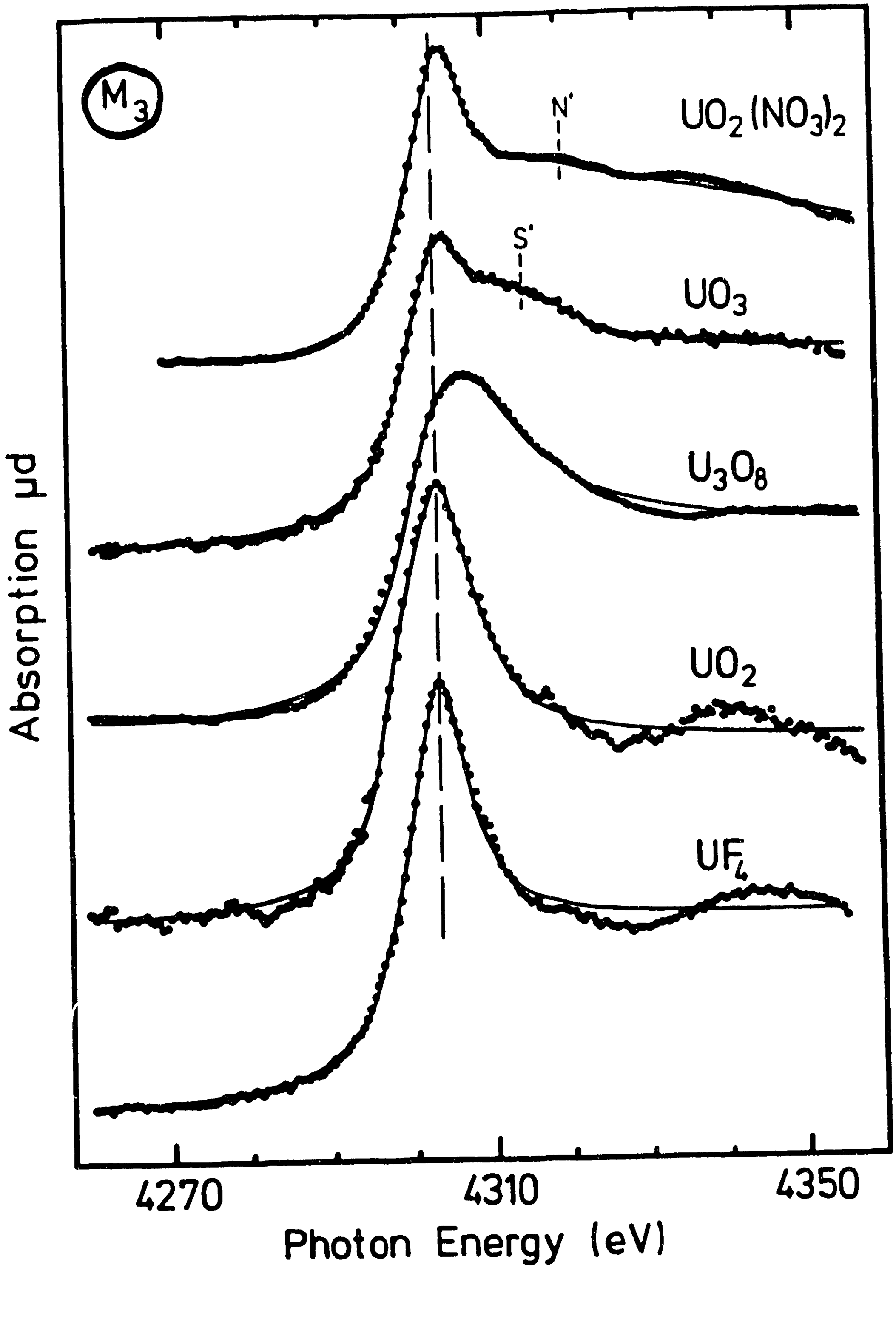

- Analogous results at M_{III} measured in total-electron yield

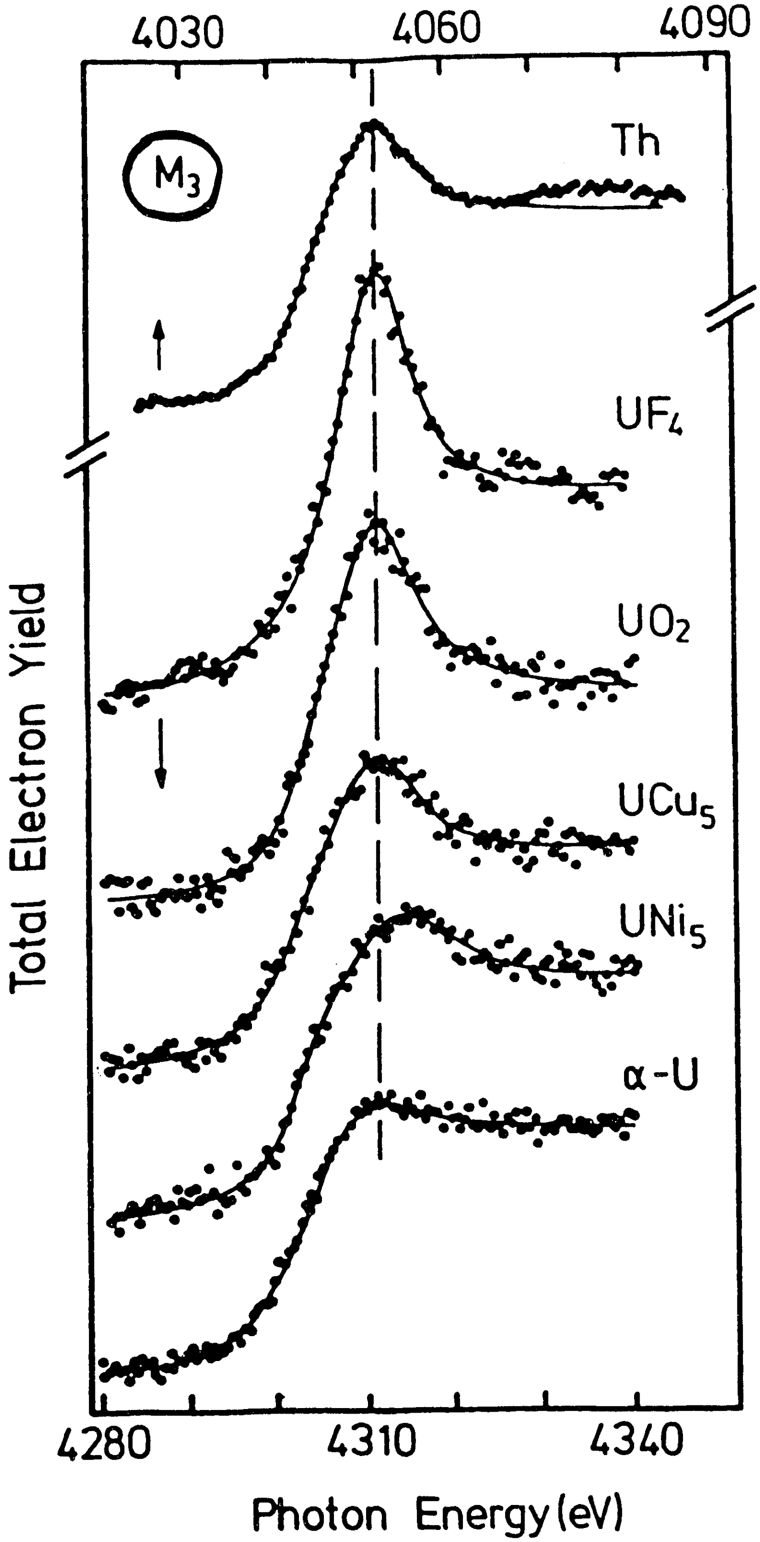

XANES spectra at the $M_{IV,V}$ thresholds

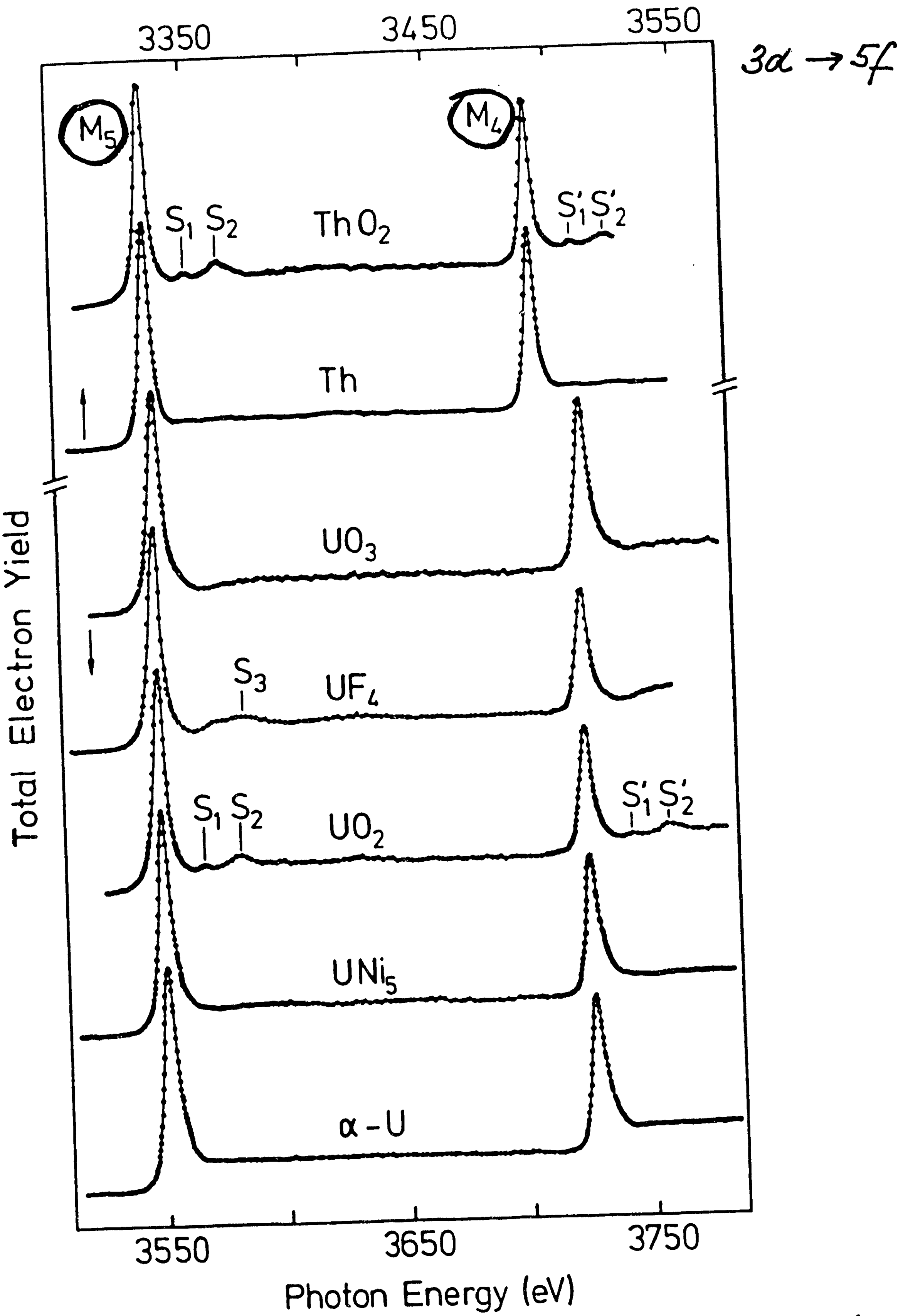

- *Multiplet splitting cannot be resolved*

XANES at the $N_{IV,V}$ thresholds

$4d^{10}5f^{n} \longrightarrow 4d^{9}5f^{n+1}$

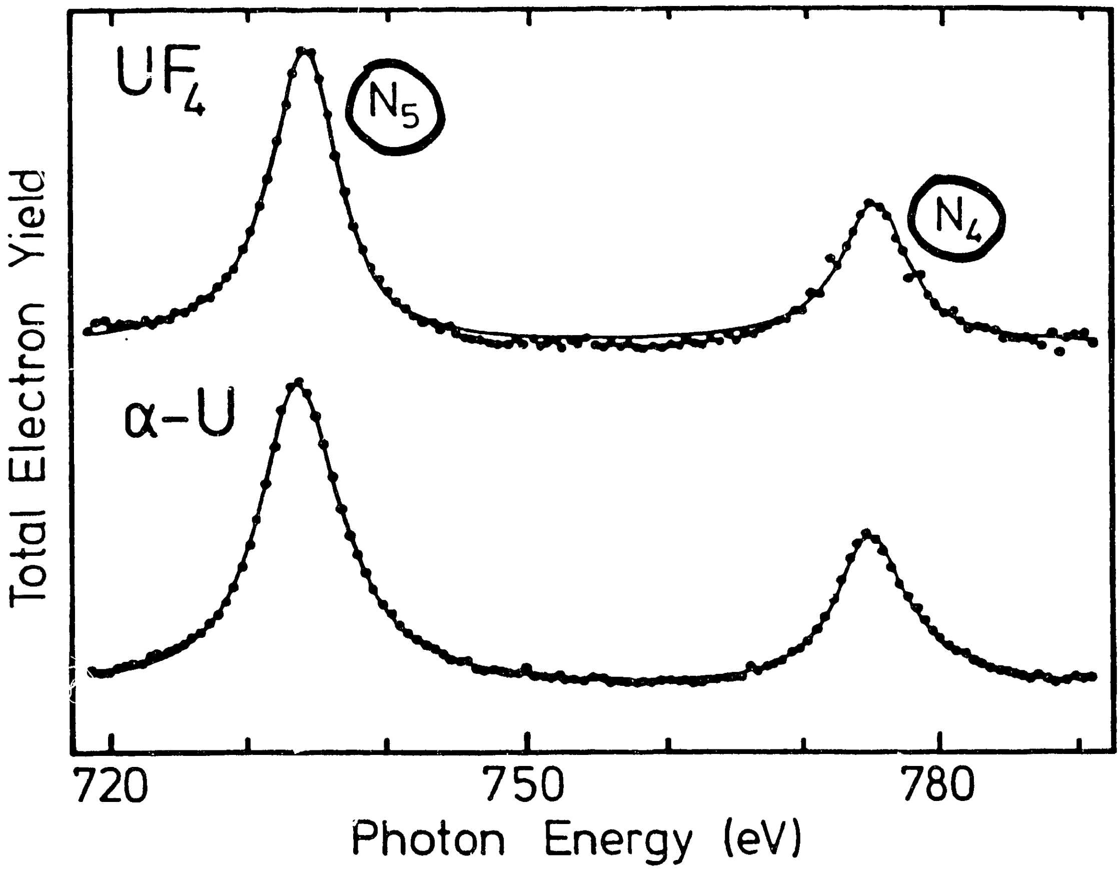

- No multiplet splitting resolvable
- No edge jumps
  WL dominate

XANES spectra at $U_{IV,V}$ thresholds

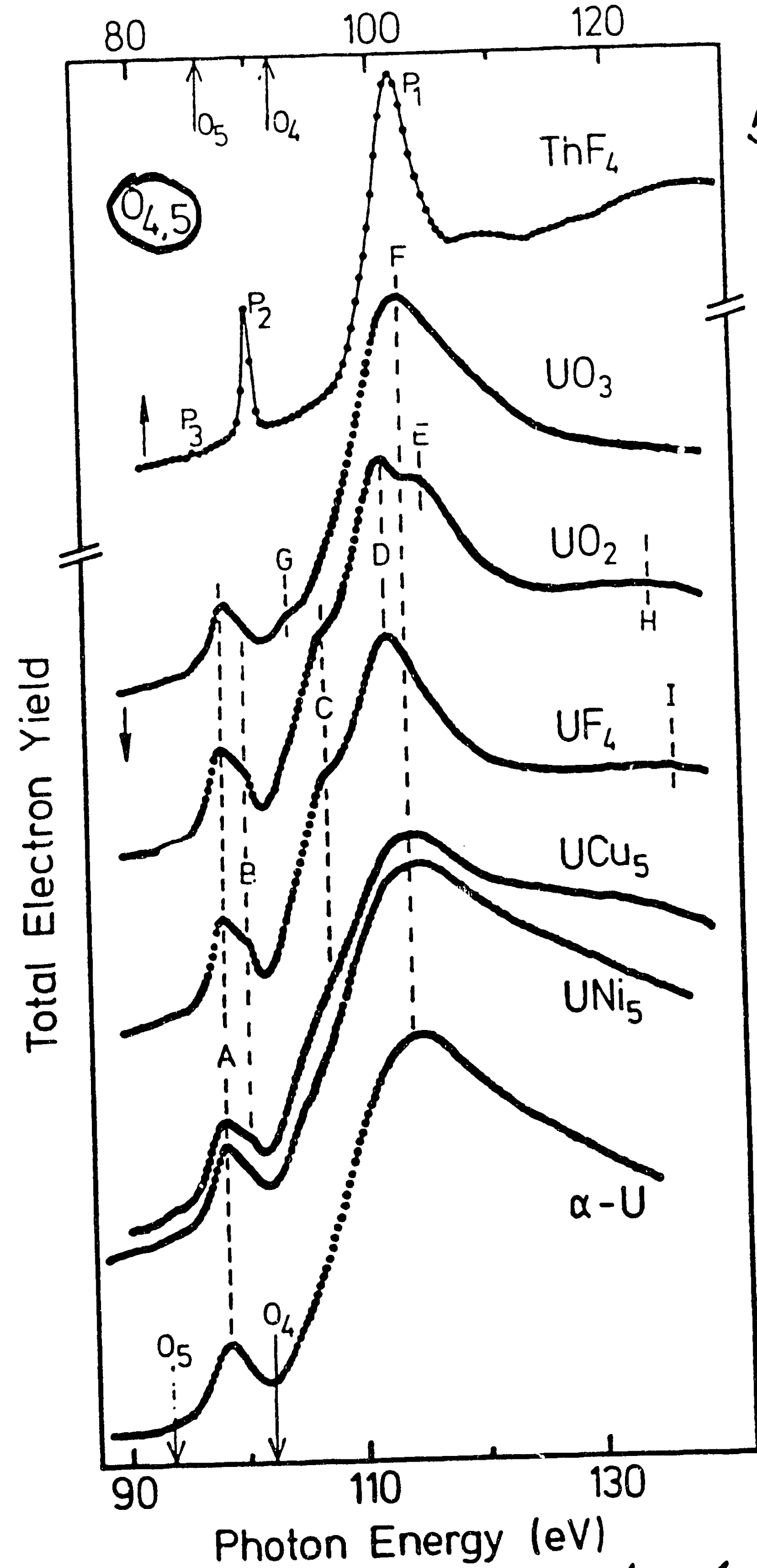

$5d^{10}5f^{n} \rightarrow 5d^{9}5f^{n+1}$

theory by A. Kotan et al. (1992).

Ref.: G. Kalkowski et al. PR B 35, 2667 (87)

- Multiplet splitting resolved washed out with increasing 5f delocalization

(C) L-edge XA in hot actinides: Np, Pu, Am,...

Experimental

- XANES studies at L-thresholds of Th, U, Np, Pu, Am
  $16.3\ keV \leq h\nu \leq 23.1\ keV$

absorption line with 3 ionization chambers:

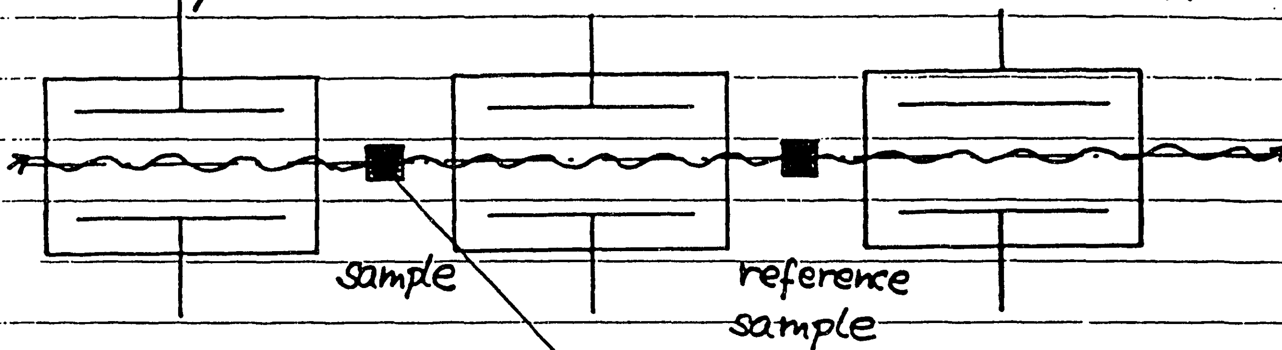

- 3-fold encapsulated absorbers

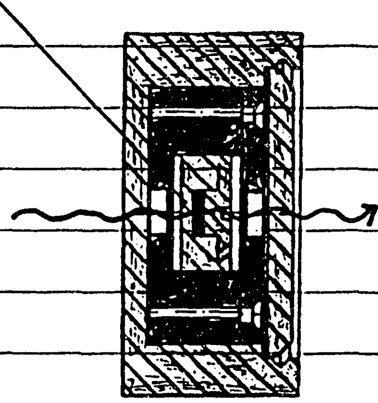

	max. sample mass (mg)	max. activity (μCi)
Np^{237}	5	3.1
Pu^{239}	5	304
Am^{241}	2	7.000

Diamond-anvil high-pressure setup for U-L_{III} XANES studies

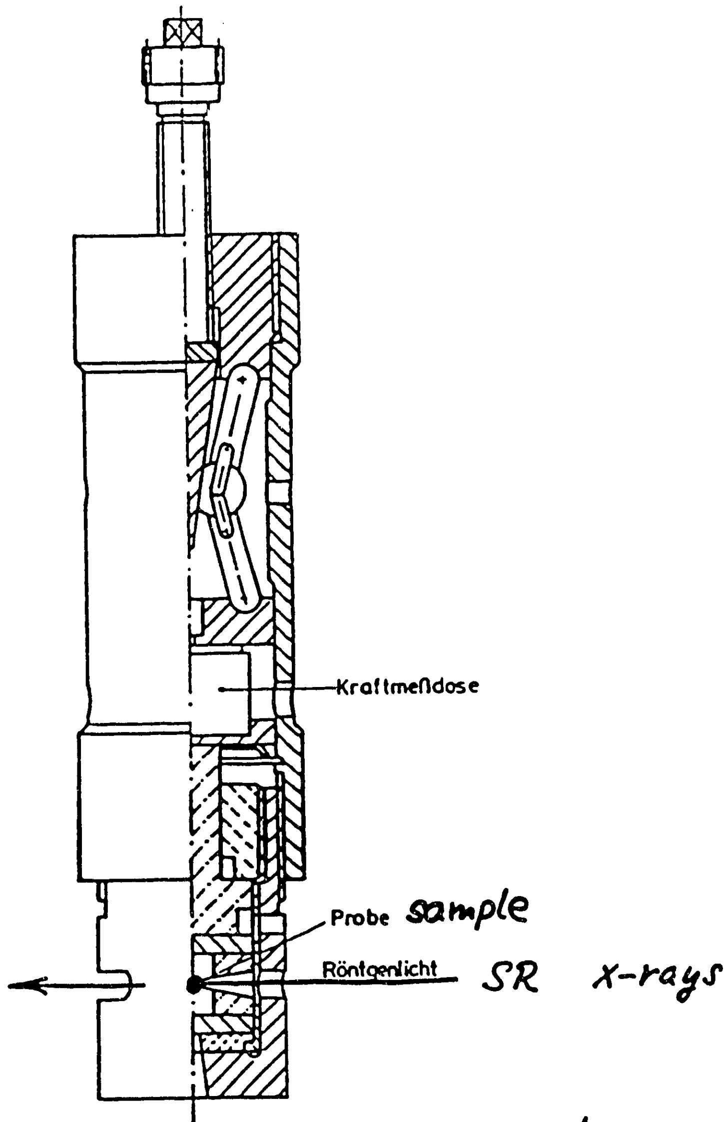

- external pressures up to $\simeq$ 500 kbar.

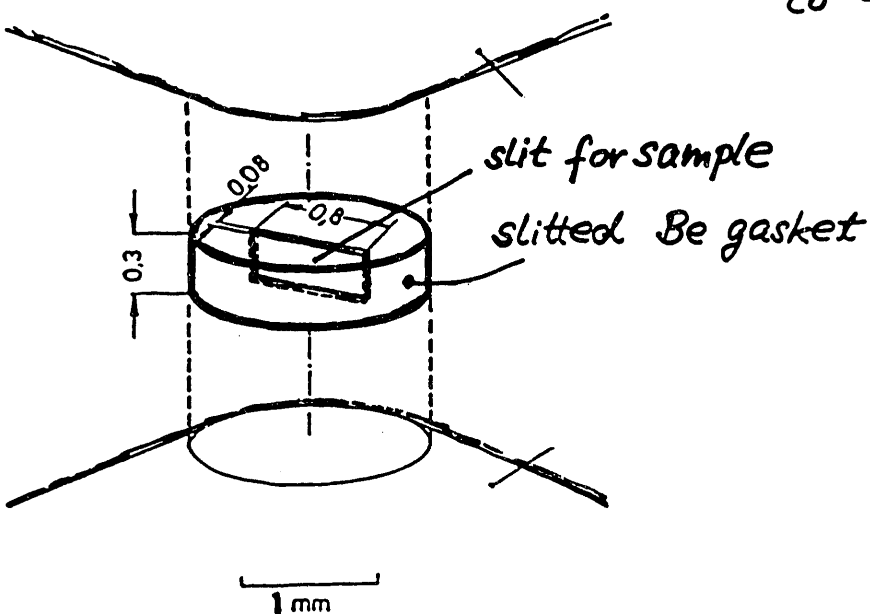

● Comparative L_{III}-XAS study of U, Np, Pu chalcogenides and pnictides

Ref.: G. Kalkowski et al., Solid State Comm. **64**, 793 (87).

U $\qquad\qquad$ Np^{237} $\qquad\qquad$ Pu^{239}

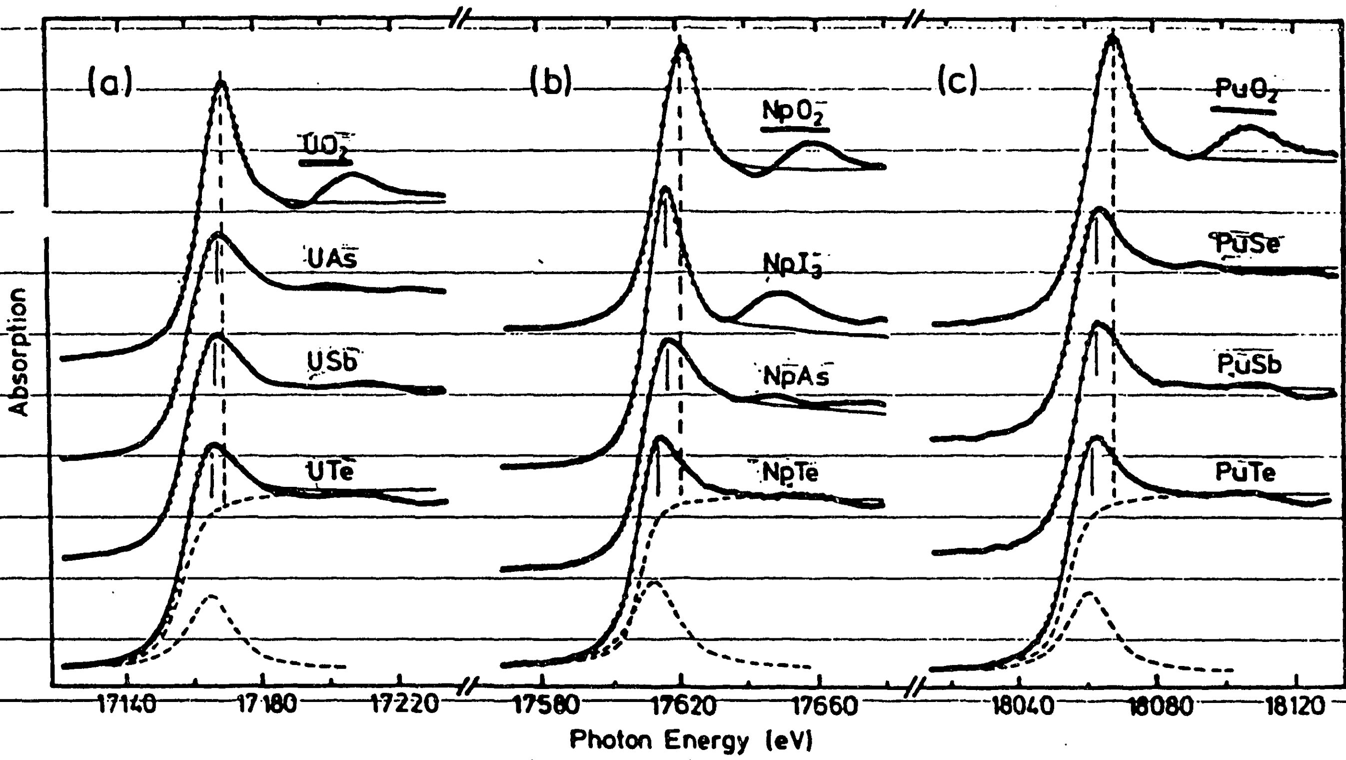

● UO_2, NpO_2, PuO_2 : tetravalent, localized 5f
$\quad 5f^2 \quad 5f^3 \quad 5f^4$ $\qquad$ serve as reference compounds

● W.L. of other compounds shift to lower energies relative to dioxides

e.g. $UO_2 - UAs$: $\Delta E = 3.5\ eV$

$NpO_2 - NpI_3$: $\Delta E = 3.9\ eV$

↳ higher 5f occupancy

Related L_3-XANES studies of ^{241}Am compounds

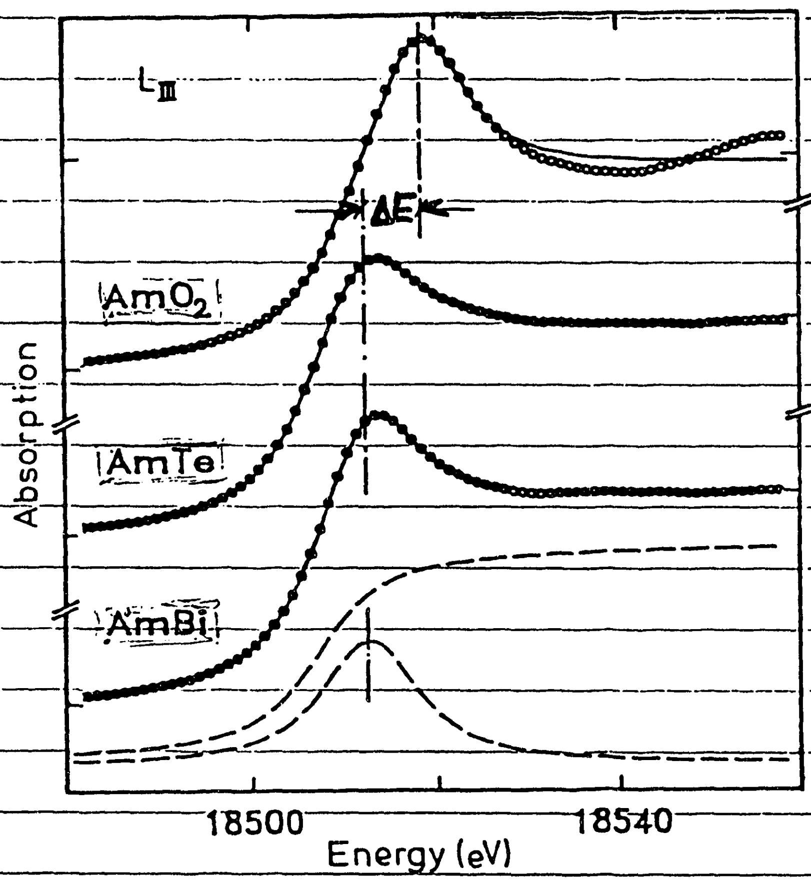

$\Delta E \cong -6\ eV$

Ref.: S. Bertram + et al., unpublished

L_3 shifts for U, Np, Pu, Am compounds relative to those of the respective dioxides

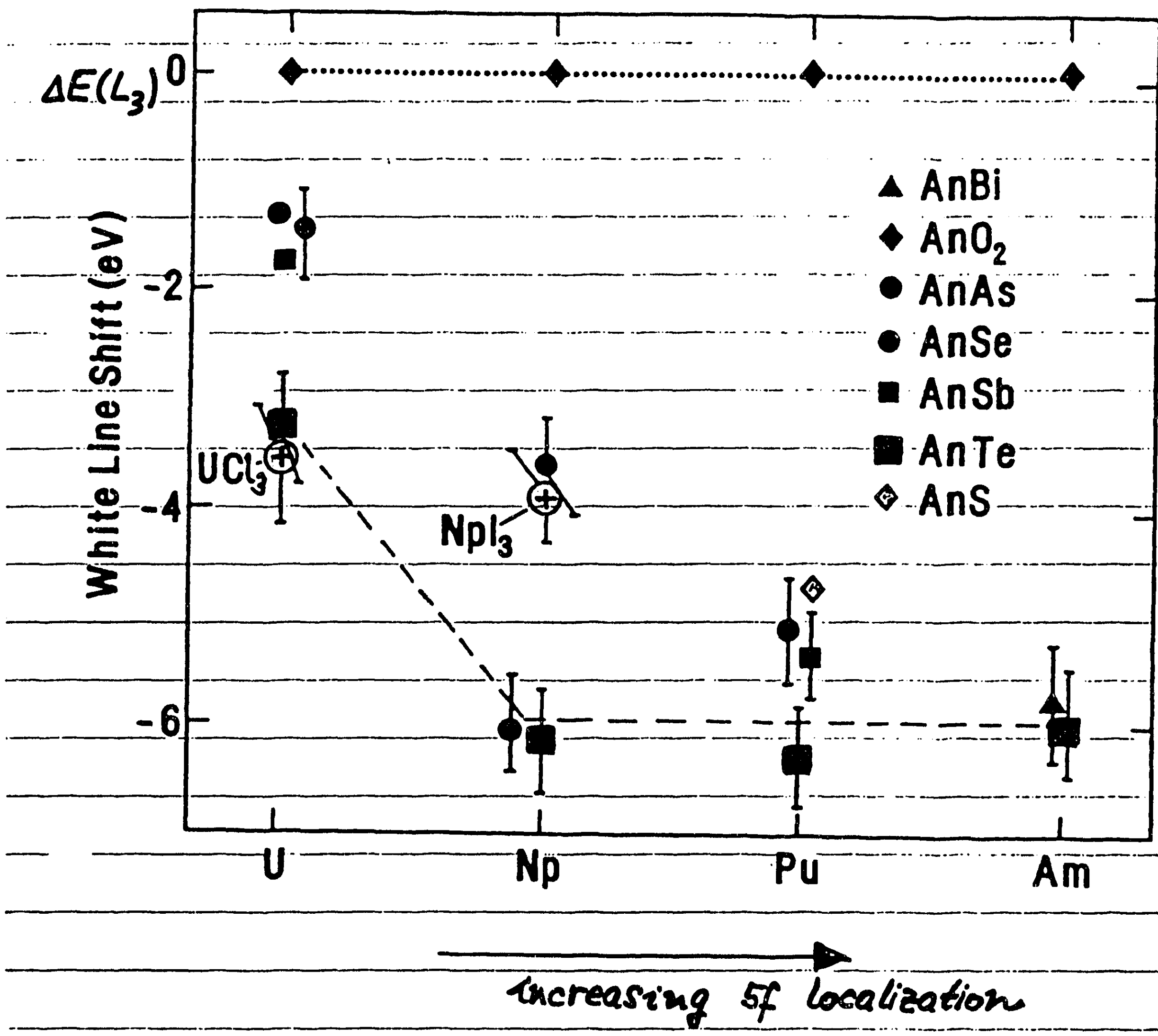

- ΔE between $U^{IV}O_2$ and $U^{III}Cl_3$ (3.5 eV) and $Np^{IV}O_2$ and $Np^{III}I_3$ (3.9 eV) agree well with theoretical predictions (Herbst & Wilkins, 1988).

Pu compounds

- PuSb n-form factor → rather localized $5f^5 (3^+)$
  agrees with L_3-shift $\Delta E(L_{III}) = -5.3$ eV

- PuTe 3+ with strong covalent mixing ?
  (temperature-independent χ +
  semiconductor-like resistivity)
  not supported by L_3-shift:
  $\Delta E(L_{III}) = -6.3$ eV
  ↳ favors a mixed-valent state for
  PuTe, with V between 2 and 3
  5f occupancy > 5

U compounds

comparison with

- PE results for USb, UTe < B. Reihl et al. (1981)
- Magneto-optical studies of US, USe, UTe < W. Reim et al. (1984)

↳ higher 5f localisation in UTe as compared to USb, US, and USe.

Agrees well with present L_3-shift results.

- USb: n-scattering shows large covalent mixing of 5f with Sb-p states < Lander et al. (1978), well reproduced by L_3-shifts.

- USb, UTe: Relativistic energy-band calculations <Brooks et al., 1986)

	n(fp)	n(f)
USb	0.53	2.42
UTe	0.27	2.57

n(fp) ↑ number of 5f electr. in band states; n(f) ↑ total f count

Compare very well with L_3-shift results.

(D) Detailed L_{III}-XANES study of Np compounds

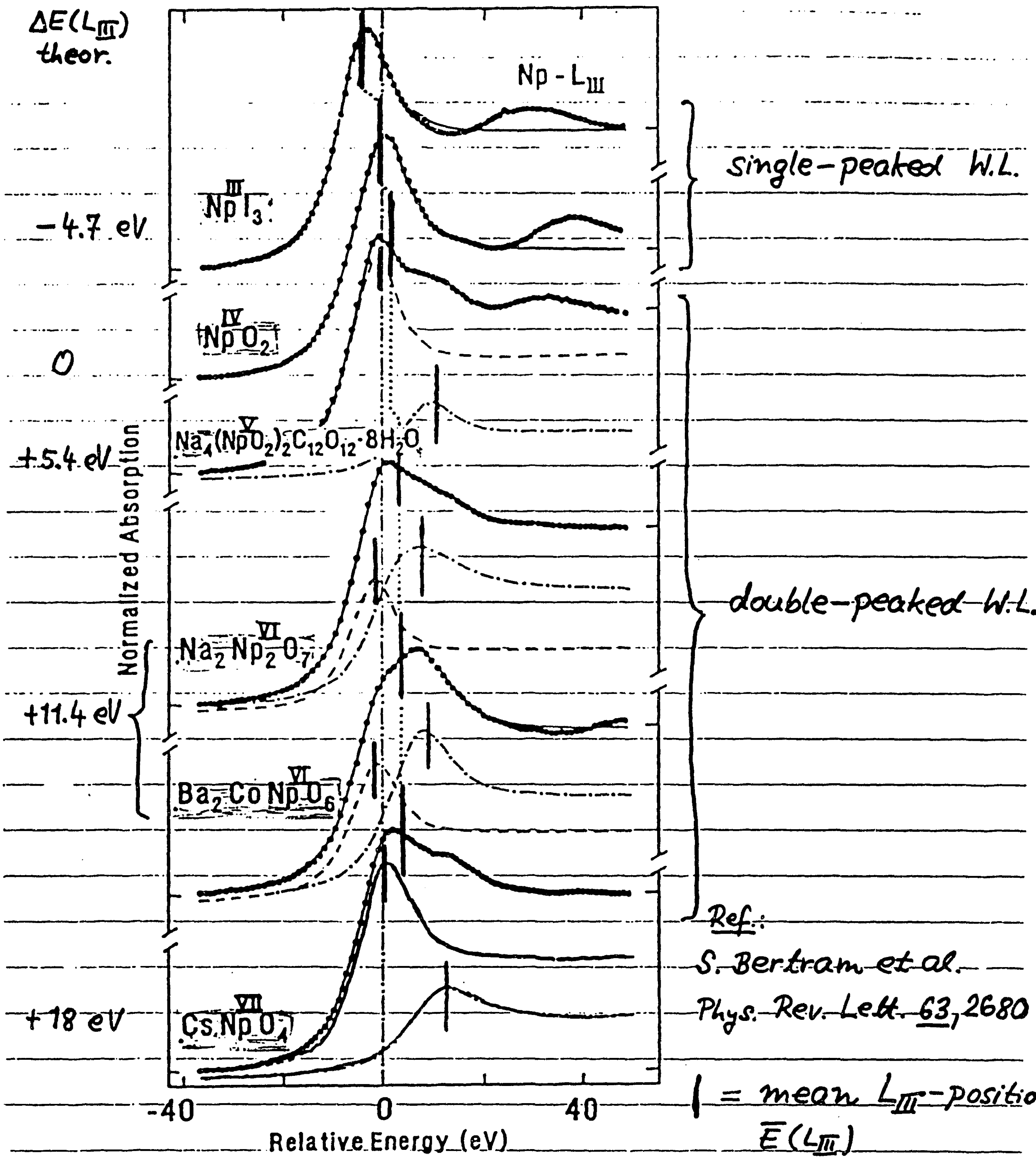

Ref.: S. Bertram et al. Phys. Rev. Lett. 63, 2680

| = mean L_{III}-position $\bar{E}(L_{III})$

↳ Interpretation due to final states with different 5f occupancies as a consequence of a strongly covalent 5f groundstate

Comparison with Ce^{IV}-compounds: CeF_4
CeO_2

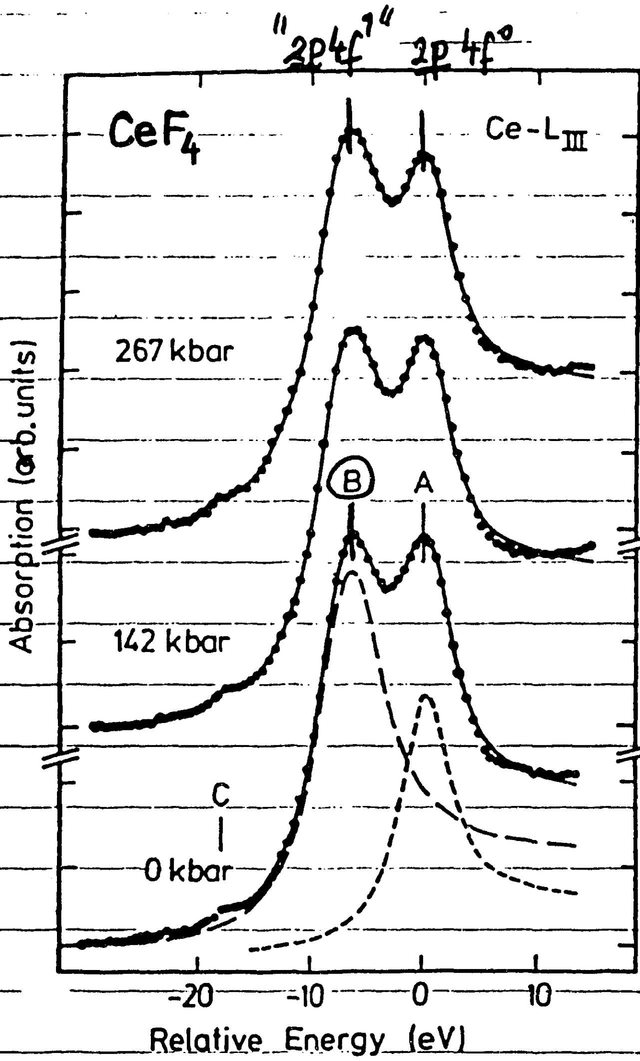

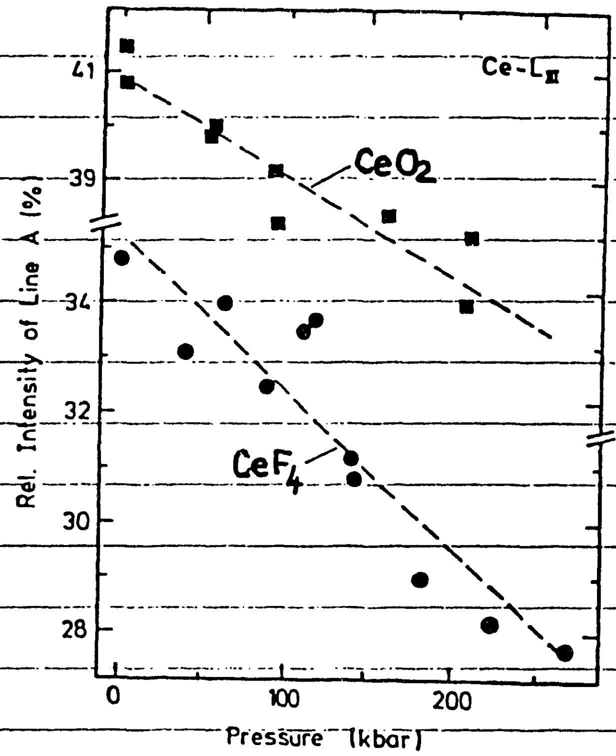

Ref.: G. Kaindl et al., Phys. Rev. B 38, 10174 (88)

- 4f covalency increases with pressure
  $\hookrightarrow$ relative intensity of component B increases ($\underline{2p}\ 4f^1$)

Analogous High-pressure Effects on
L_{III} - XANES Spectra of $U^{VI}O_3$

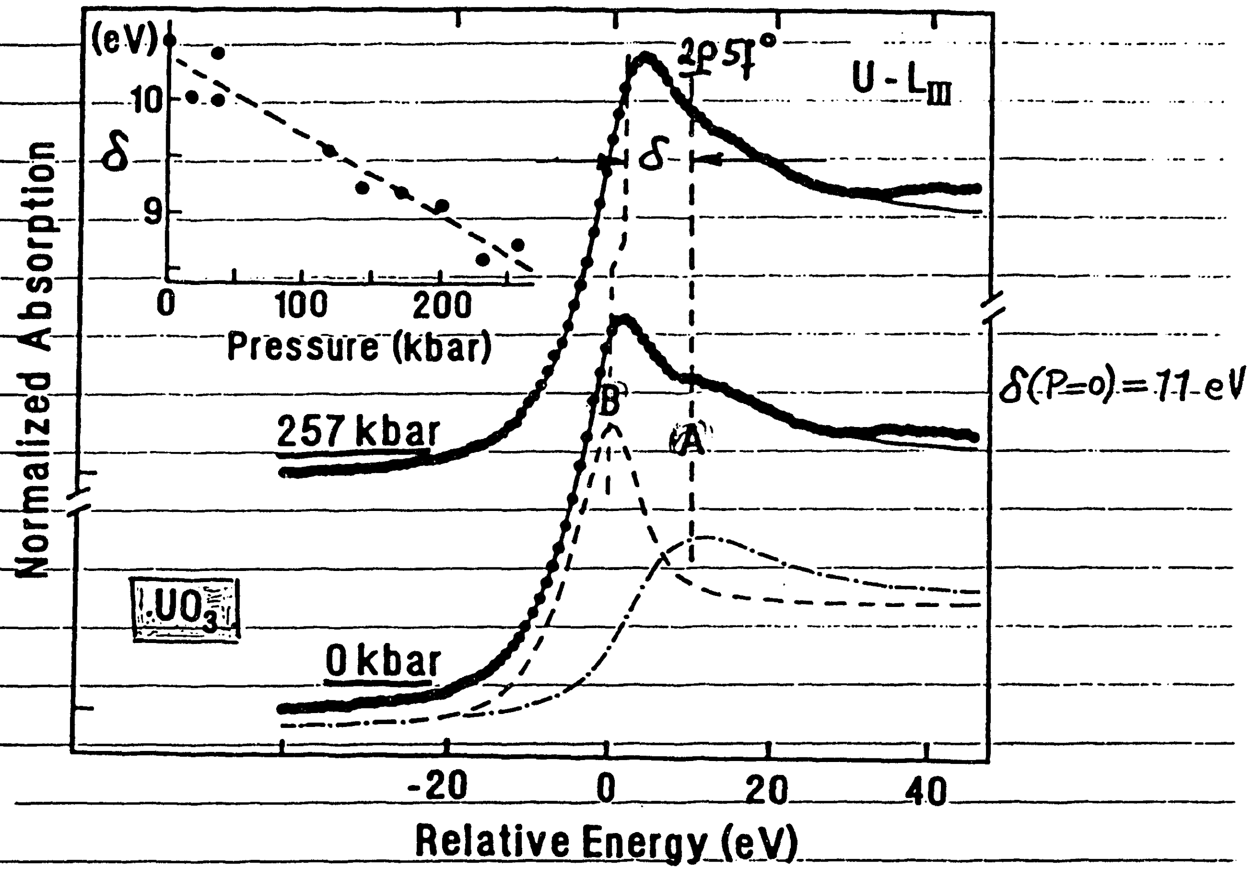

- Separation of peaks, δ, decreases with pressure
- Weight of peak B increases with pressure
  ↳ increase in covalency.
- → A and B due to different core-ionized final states with different 5f occupancies (5f° and "5f²").
- $\Delta E(L_{III})$: experimental : 11 eV (for P=0)
  theoretical : 11.1 eV

L_{III} XANES spectra of metallic Np compounds

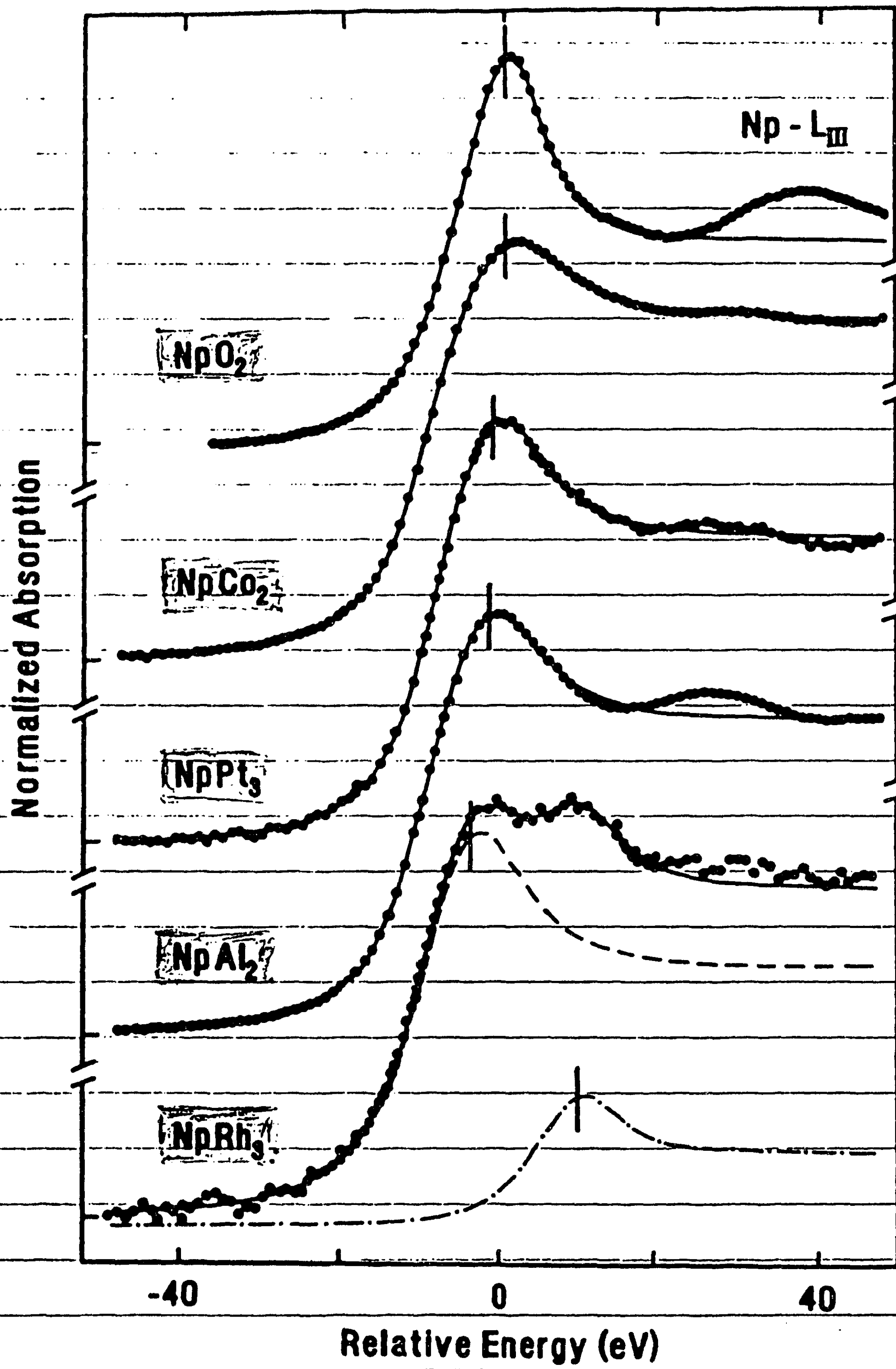

strongly localized

Ref.: S. Bertram + et al., unpublished

Correlation between $\overline{\Delta E}(L_{III})$ and Mössbauer isomer shift

— isomer shift $S \propto \Delta\langle r^2\rangle \ \Delta\rho(0)$

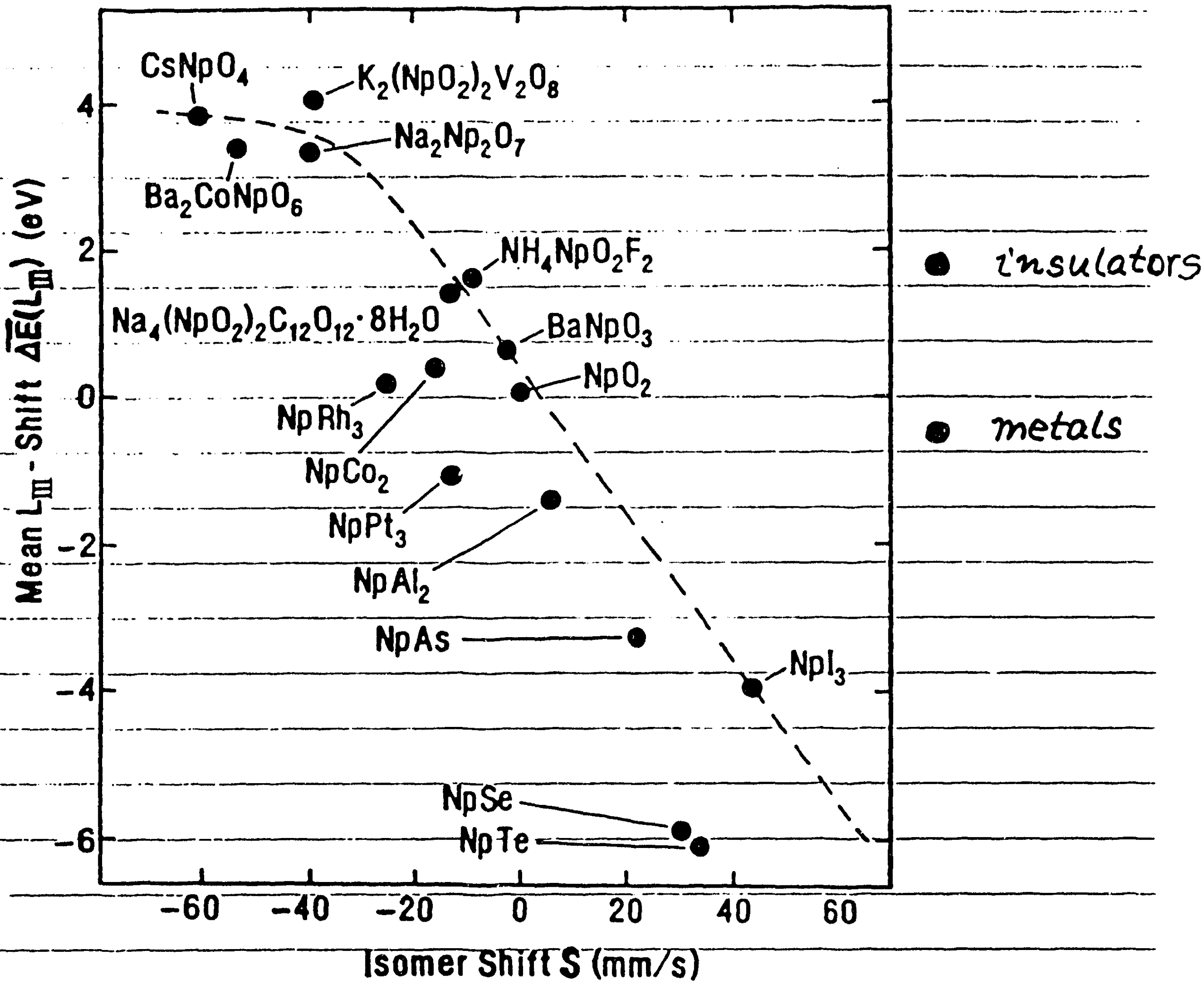

- Since $\Delta\langle r^2\rangle < 0$ for the 59-keV Mössbauer transition of Np^{237}, the systematic deviation of the metallic compounds is due to the contribution of the conduction electrons to the charge density at the nucleus.
- $\overline{\Delta E}(L_{III})$ monitors 5f-occupancy n_{5f} and 6d-occupancy n_{6d}, but is insensitive to conduction electron density (n_{7s}).

(E) High-Pressure L_{III}-XANES studies of U compounds

USb : semimetal < NaCl → CsCl crystallogr. phase transition at 8 GPa $\Delta V/V \simeq -8\%$

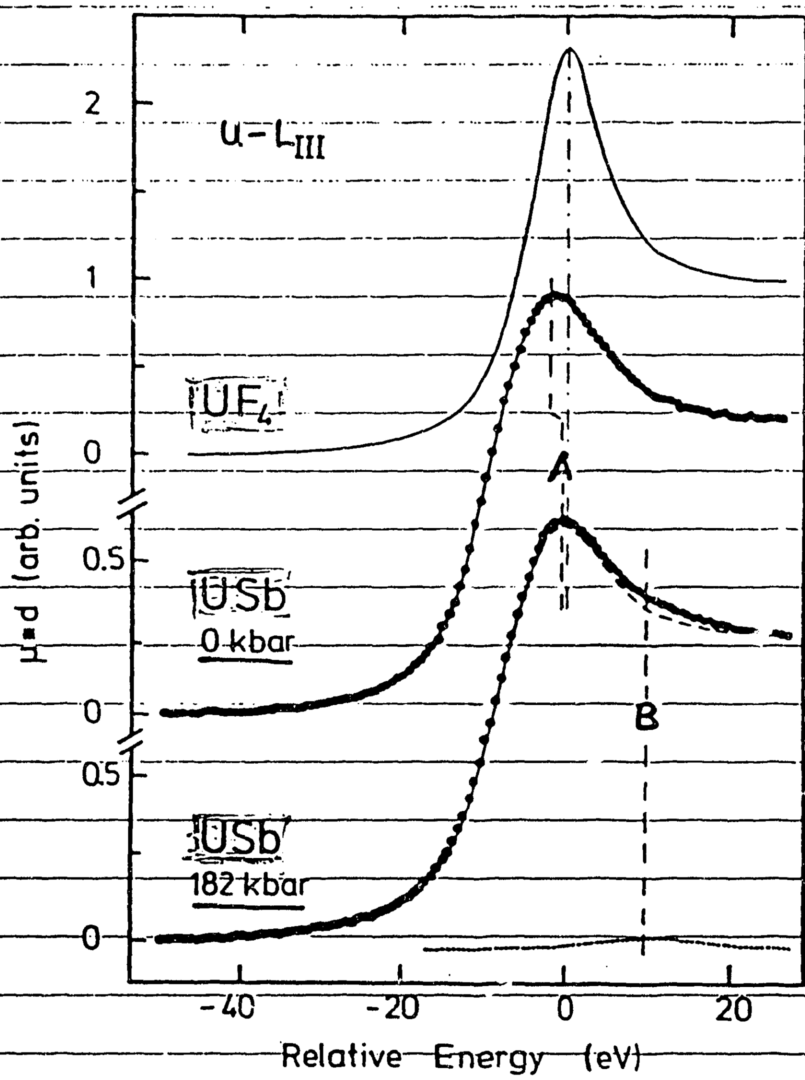

- White line A shifts to higher energy with pressure due to decrease in U_{fc}.
- Satellite B appears at higher pressures in the CsCl phase.

$\frac{dE}{dP} = 9\times10^{-2}$ eV/GPa ; $\frac{dE}{dP} = 6.3\times10^{-2}$ eV/GPa ;

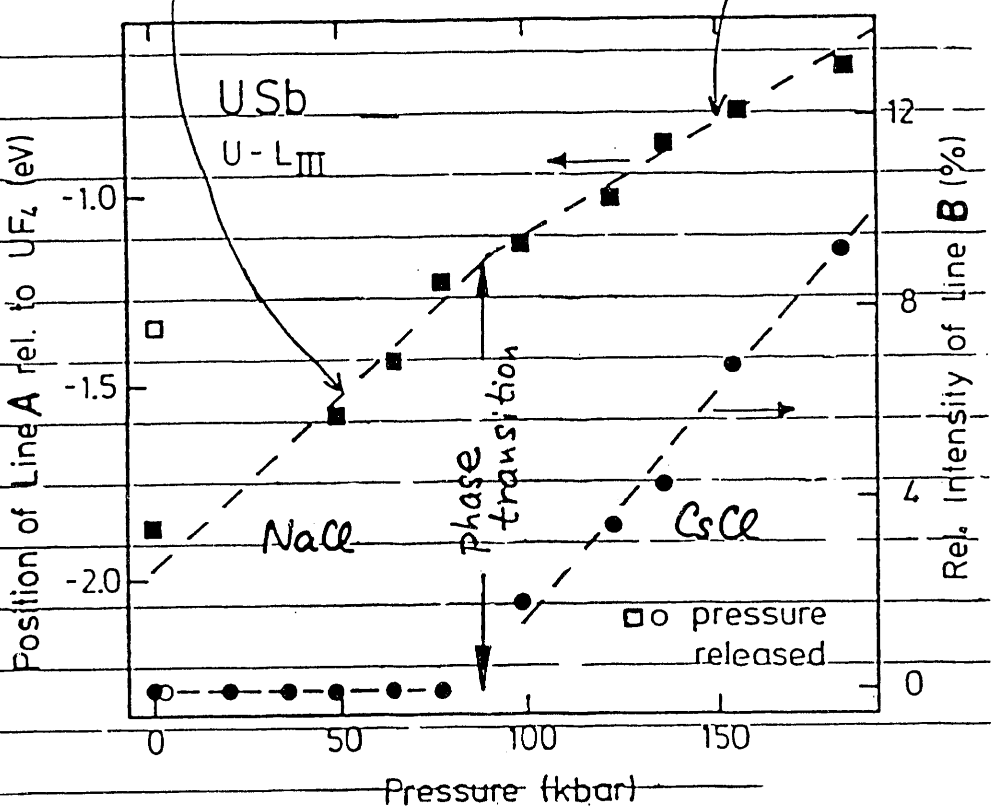

UTe metallic ; $c_{12} < 0$; Kondo effect

most localized U compound studied

shift by 2.8 eV between 0 and 18.8 GPa

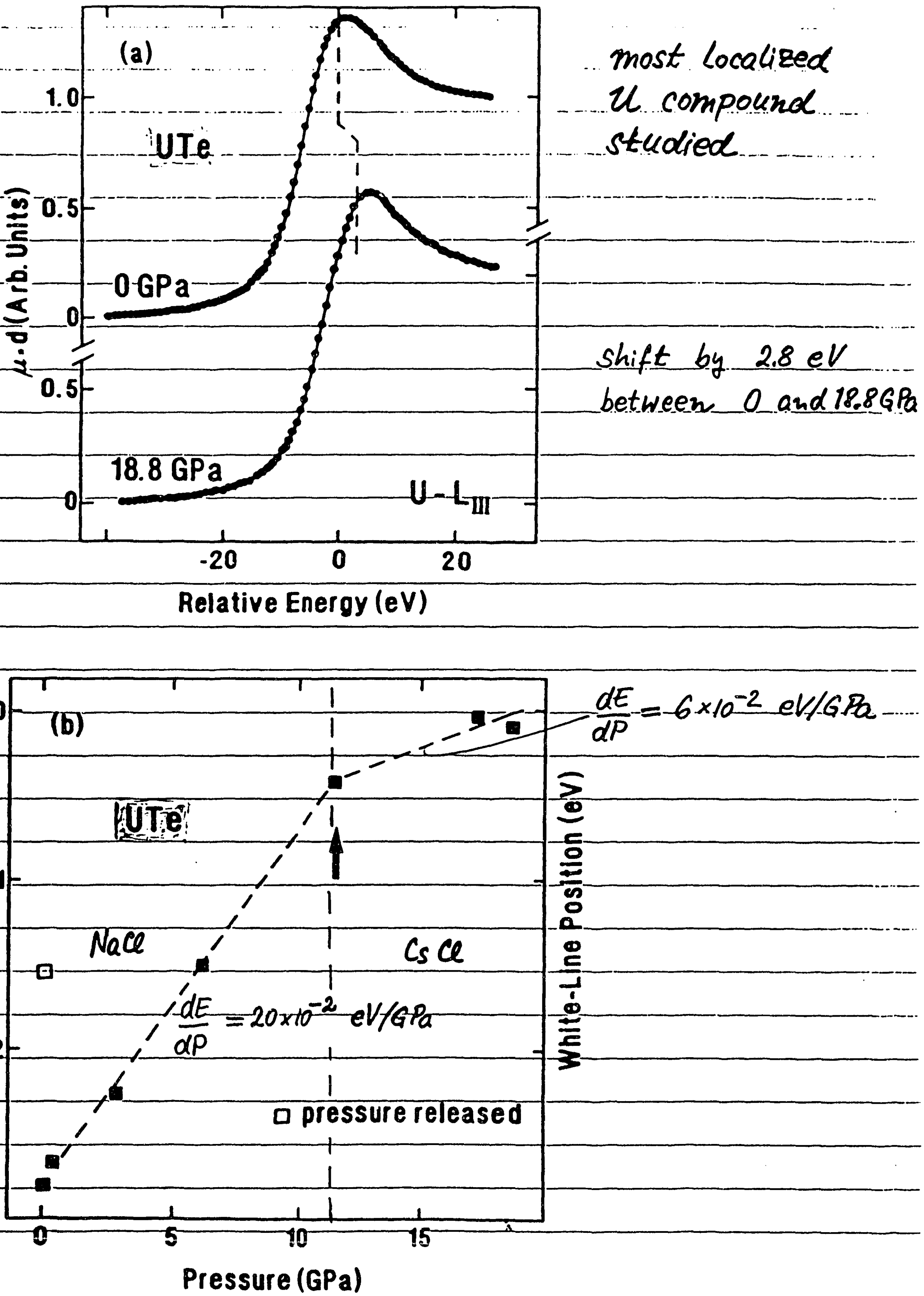

UC, UN delocalized 5f states

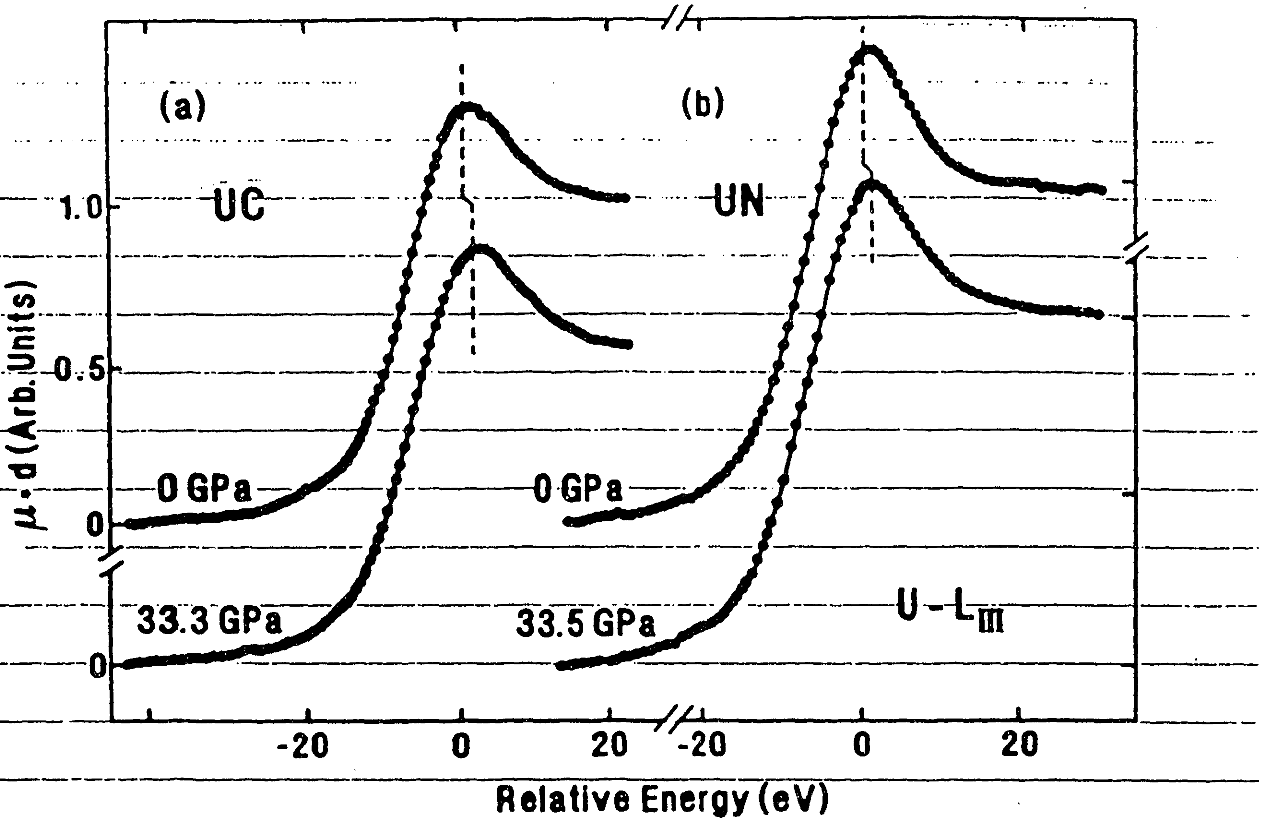

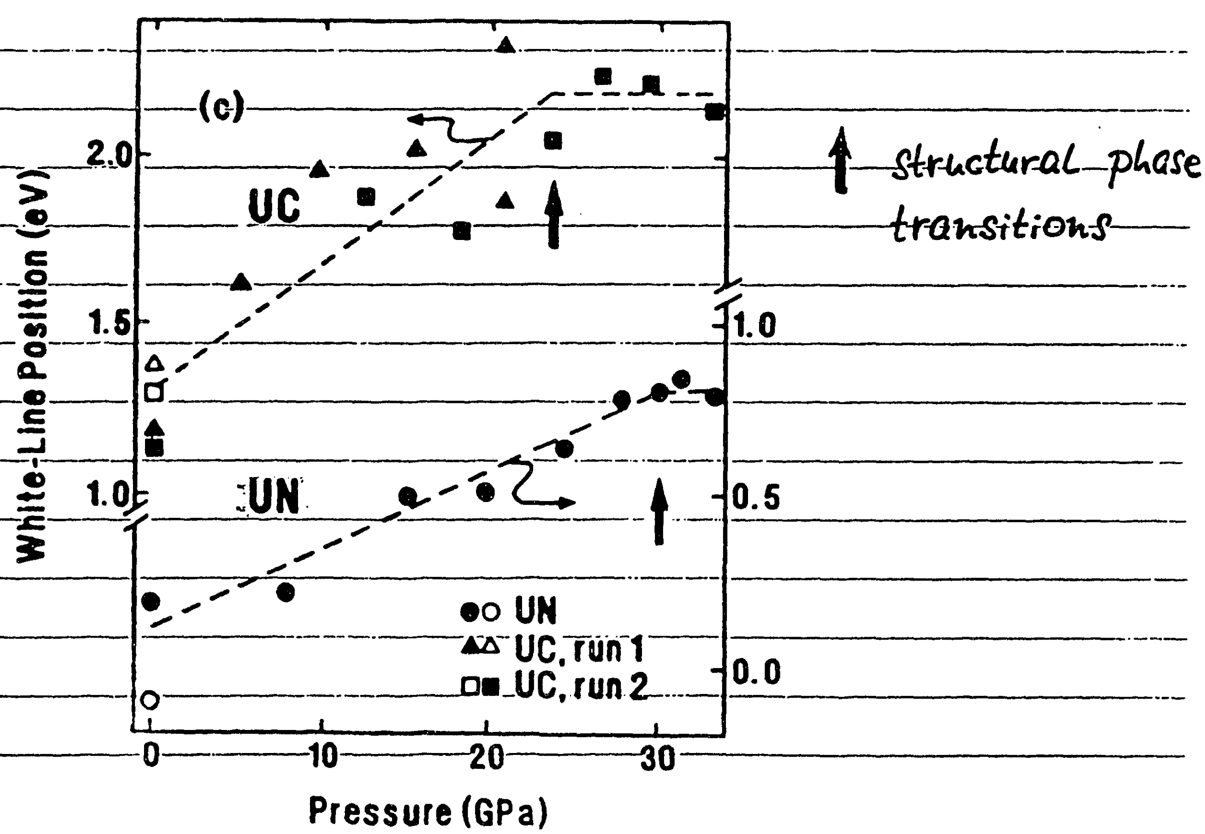

Summary and outlook

- XANES at various XA thresholds of An elements from XUV to hard x-ray region provides wealth of information on correlated 5f electronic structure.
- Without actinide beamline only L (and M)-edge studies feasible.
- L_{III}-XANES of light An compounds monitors 5f occupancy (valency) and 5f localization (covalency)
- L_{III}-XANES well suited for high-pressure studies
- Many-body theory needed for An-XANES results.
- Bright future with actinide beamline:
  - XANES studies at soft XA thresholds
  - Study of 5f magnetism by use of circular polarized light: magnetic circular dichroism.

Surface as a New Stage for Studying Actinides: Theoretical Study of the Surface Electronic Structure of Uranium

E. Tamura
Department of Chemistry and Material Science, L-268
Lawrence Livermore National Laboratory, P.O. Box 808
Livermore, CA 94550

Apart from traditional interests in surfaces—for example, studies of the physical properties of an interface between the vacuum and the bulk—the surface has been recognized as a new stage for constructing materials. They may be completely new materials or already known (but well controlled like defect-free single crystals). The advantage of this technique is that one can very easily control the lattice constants of crystals or even their structures by choosing suitable substrates for crystal growth. Although the crystals may grow only several layers, keeping the substrate lattice constant, they can normally be good representatives for studying the bulk properties of metals, and one can, of course, investigate a variety of interesting surface properties by varying the layer thickness.

As a prototype, we study theoretically the system in which U grows epitaxially on Pt(111) surfaces. Because relativistic effects play an important role in this system (generally for elements $Z > 50$), we first construct the fully relativistic, spin-polarized, surface Green function by the layer-KKR method. Once the Green function is obtained, one can essentially calculate any type of physical quantity: (spin-polarized) angle-resolved photoelectron current in UPS experiments, scattering intensities (also polarization) of electrons in LEED techniques, etc. Furthermore, the momentum-resolved, layer-projected density of states (DOS) can be easily calculated from the Green function itself, which is also helpful in analysis of experimental surface-spectroscopy data. Since our formalism is fairly general, we also discuss magnetically polarized systems and related surface-spectroscopy techniques.

Surface as a New Stage for Studying Actinides:
Theoretical Study on Surface Electronic Structure of Uranium

E. Tamura

*Department of Chemistry and Material Science, L-268,
Lawrence Livermore National Laboratory, P.O.Box 808,
Livermore CA 94550.*

Discussion

I) Surface Spectroscopies and Sample Preparation

II) Theories of Surface Spectroscopies

III) Theoretical Study on U/Pt(111)

I) Surface Spectroscopies and Sample Preparation

Surface Spectroscopies

1. Strongly Interacting Probe

Low energy electrons: LEED

Vacuum Ultraviolet: UPS

etc.

2. Weakly Interacting Probe

High energy electron: RHEED

X-ray: XPS and Related Techniques
(The excited electrons are low-energetic or
the signals are well-separated from the bulk signals.)

etc.

Sample Preparation

Choice of substrate plays an important role!

1. Lattice Constant

2. Reactivity

Celebrated Epitaxial Growth
(Layer-by-layer growth)

II) Theories of Surface Spectroscopies

The surface Green function plays a powerful role! $G(E, \underset{\sim}{k}^{\parallel})$

Layer KKR

0. Layer-projected Density of States
(Spectral Function of the quasiparticles)

$$N(E, \underset{\sim}{k}^{\parallel}) = -\frac{1}{\pi}\, \mathrm{Im}\, \mathrm{tr}\, G(\underset{\sim}{r}, \underset{\sim}{r}'; E, \underset{\sim}{k}^{\parallel})$$

1. LEED $\quad \underset{\sim}{k}^{\parallel}$

$$I(E, \underset{\sim}{k}^{\parallel}) = |G(\underset{\sim}{r}_D, \underset{\sim}{r}_S ; E, \underset{\sim}{k}^{\parallel})|^2$$

$$|\longrightarrow|^2$$

2. UPS $\quad \underset{\sim}{k}^{\parallel}$

$$I(E, \underset{\sim}{k}^{\parallel}) = -\frac{1}{\pi}\, \mathrm{Im} \langle \phi_{LEED} | \Delta G \Delta^{+} | \phi_{LEED} \rangle$$

$|\rightsquigarrow|^2 \qquad \Delta$: interaction $\underset{\sim}{\alpha} \cdot \underset{\sim}{A}(\underset{\sim}{r})$

3. XPS and Related Techniques

$$I(\omega) = \int dE\, d\underset{\sim}{k}^{\parallel}\, d\underset{\sim}{k}'^{\parallel}\, \mathrm{tr}\, G(E+\omega, \underset{\sim}{k}^{\parallel}) \Delta\, G(E, \underset{\sim}{k}^{\parallel}) \Delta^{+}.$$

4. .....and any

Write any graph.

III) Theoretical Study on U/Pt(111)

Pt Substrate

UPS $\vartheta_e = 0$ $\vartheta_{ph} = 0$ Circular. P.L

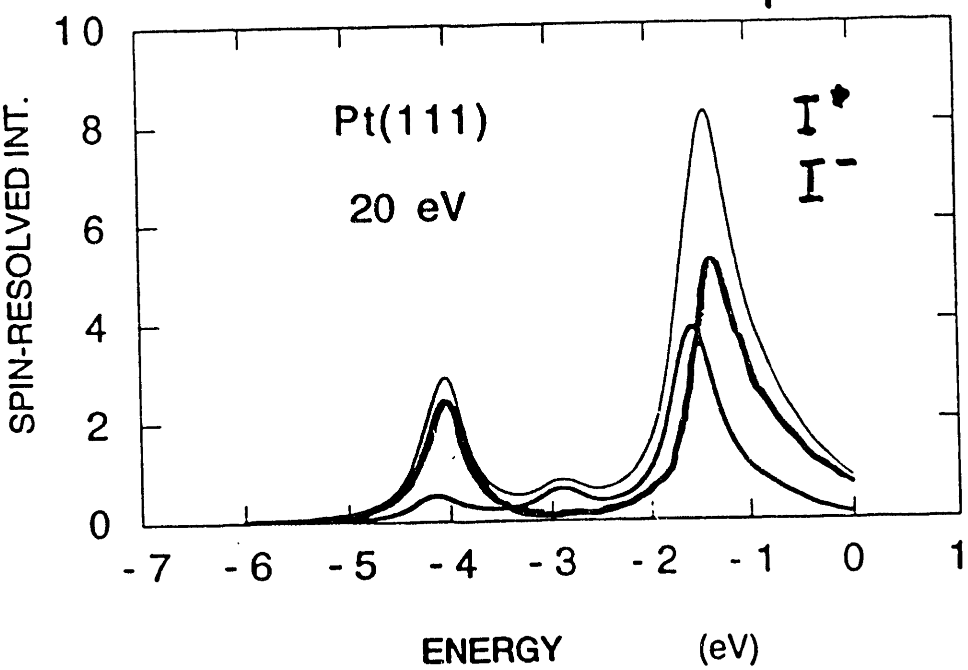

Pt (111) Layer DOS

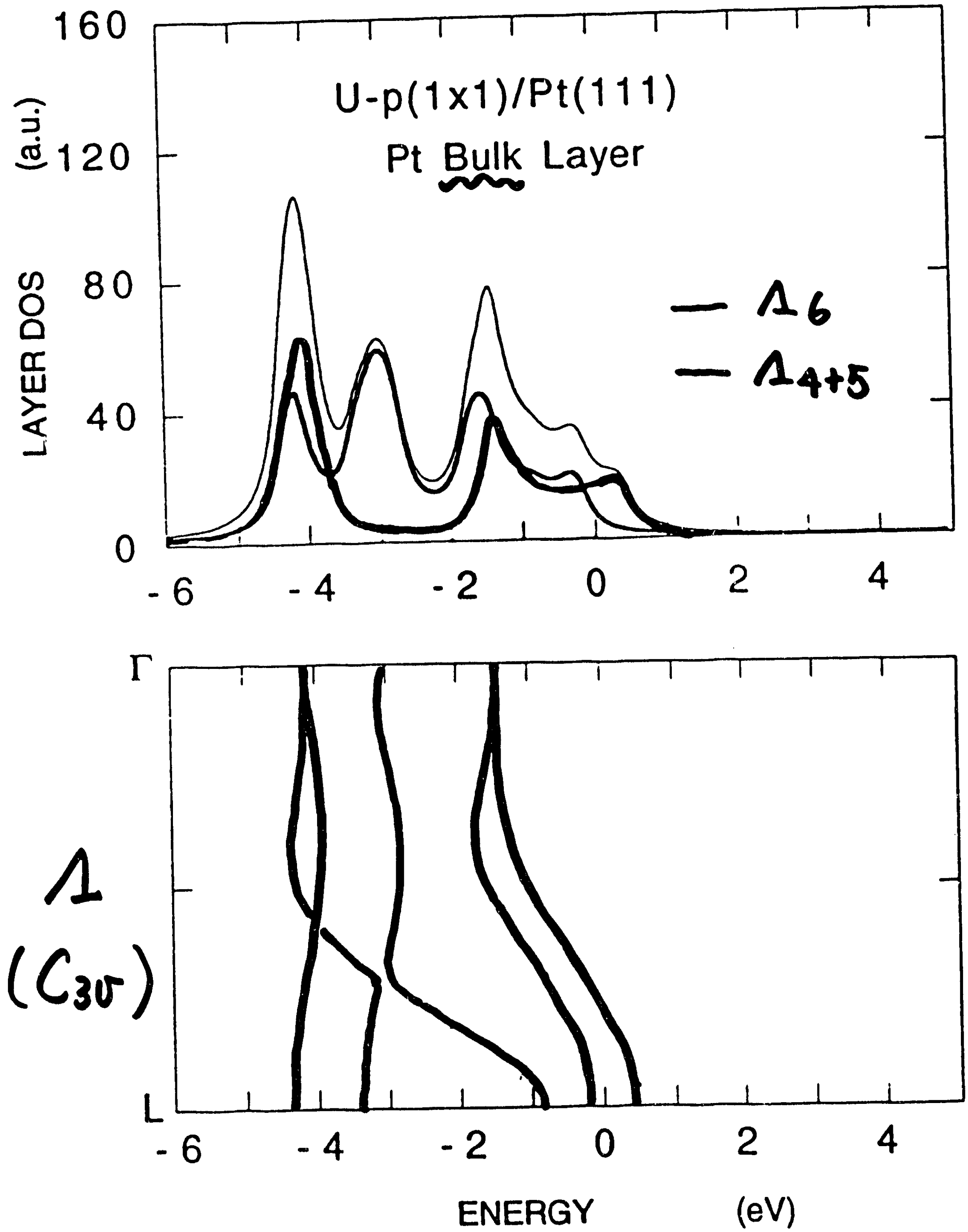

Group Theoretical Consideration

Dipole selection rule

$x+iy$

$\langle f \,|\, Y_1^1 \,|\, i \rangle$

Table C_{3v} -*symmetry*

Λ_6	$\Uparrow$ $\lvert\alpha\rangle$	$\Downarrow$ $\lvert\beta\rangle$	Λ_6
Λ_6^1	$Y_l^0\lvert\alpha\rangle$ $\frac{1}{\sqrt{2}}(Y_3^3 - Y_3^{-3})\lvert\alpha\rangle$	$Y_l^0\lvert\beta\rangle$ $\frac{1}{\sqrt{2}}(Y_3^3 - Y_3^{-3})\lvert\beta\rangle$	$0 \le l \le 3$
Λ_6^2	$\frac{-1}{\sqrt{2}}(Y_3^3 + Y_3^{-3})\lvert\alpha\rangle$	$\frac{1}{\sqrt{2}}(Y_3^3 + Y_3^{-3})\lvert\beta\rangle$	
Λ_6^3	$Y_l^1\lvert\beta\rangle$ $-Y_l^{-2}\lvert\beta\rangle$	$Y_l^{-1}\lvert\alpha\rangle$ $Y_l^2\lvert\alpha\rangle$	$1 \le l \le 3$ $2 \le l \le 3$
Λ_{4+5}	$e^{-i\phi}\lvert\alpha\rangle$	$e^{i\phi}\lvert\beta\rangle$	Λ_{4+5}
Λ_{4+5}^3	$Y_l^{-1}\lvert\beta\rangle$ $Y_l^2\lvert\beta\rangle$	$Y_l^1\lvert\alpha\rangle$ $-Y_l^{-2}\lvert\alpha\rangle$	$1 \le l \le 3$ $2 \le l \le 3$

Initial **Final** by ↻ light Y_1^1

Λ_6 — $\Uparrow$ +100% → Λ_6

Λ_{4+5} — $\Downarrow$ −100% ↗

1 MonoLayer U on Pt (111)

U - Layer DOS

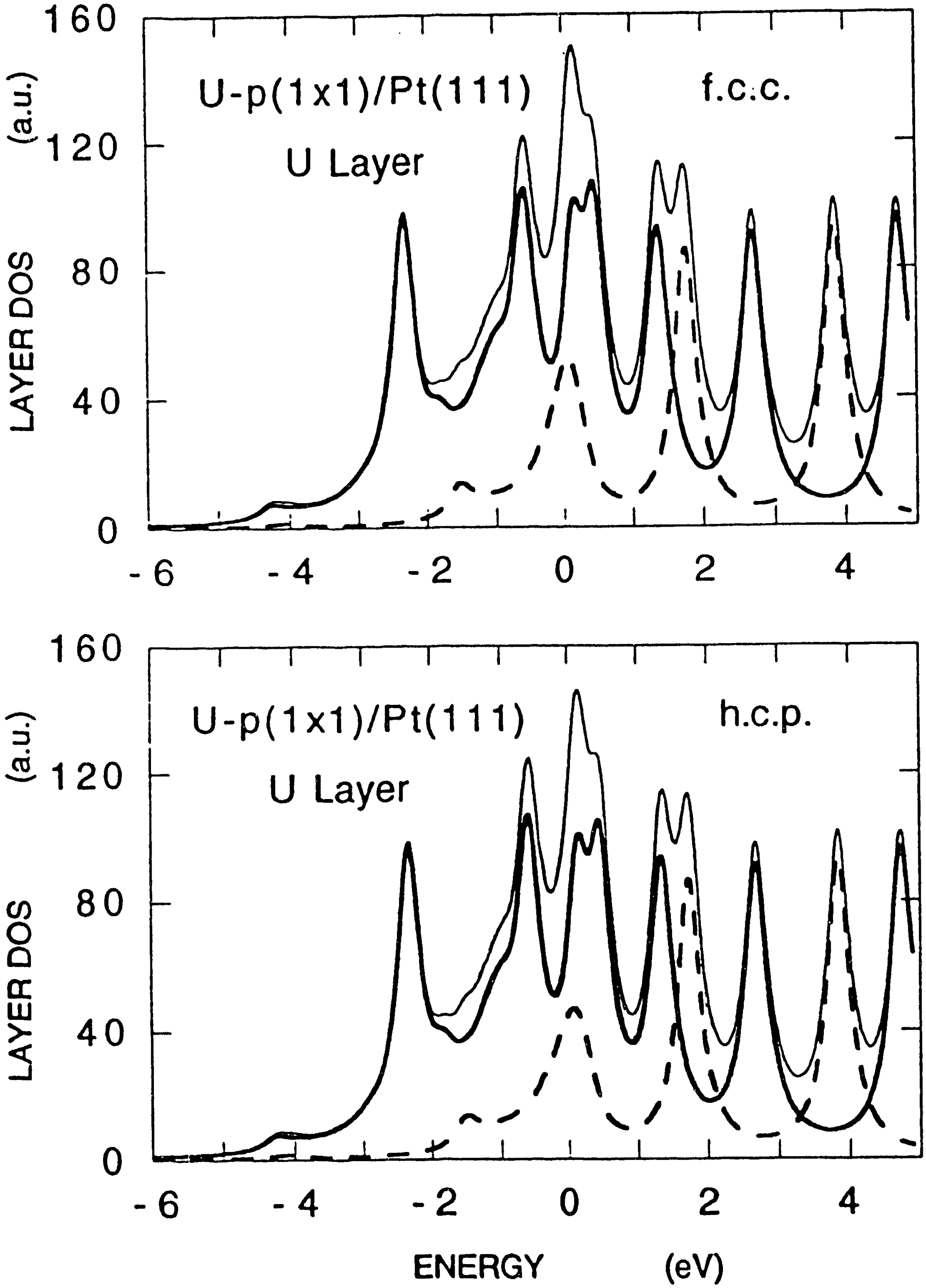

C A B C ...

B C ...

B A B C ...

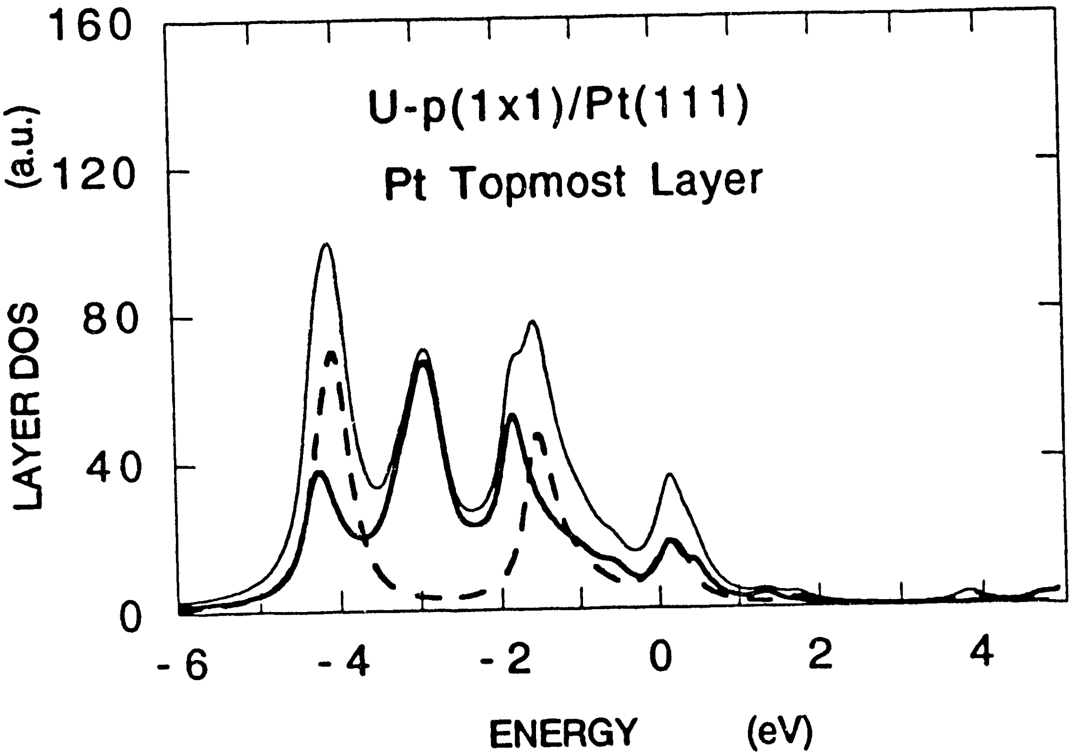
U-p(1x1)/Pt(111)
Pt Topmost Layer
160
120
80
40
0
LAYER DOS (a.u.)
- 6
- 4
- 2
0
2
4
ENERGY (eV)

Spin Polarized LEED

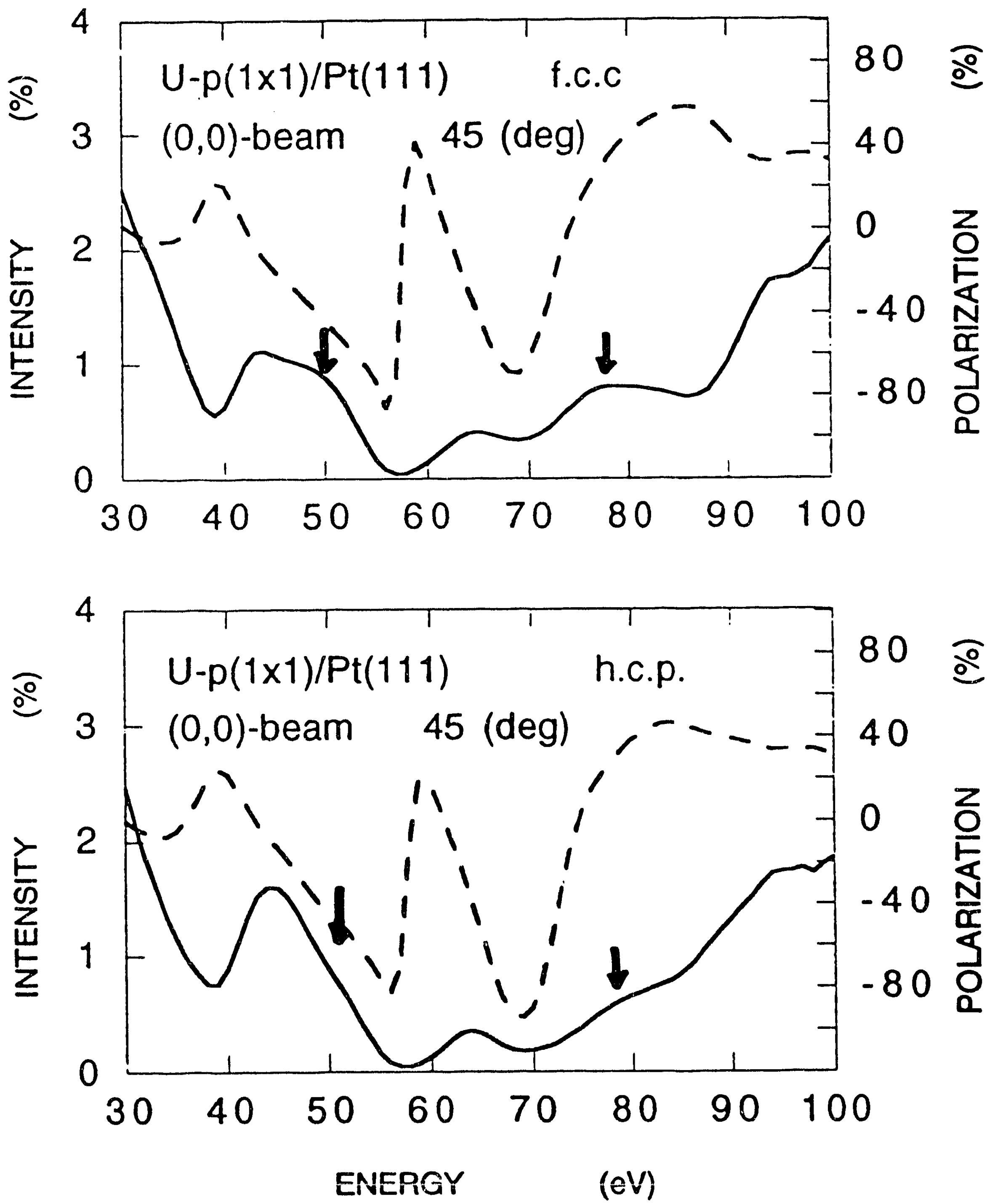

UPS $\vartheta_e = 0$ $\vartheta_{ph} = 0$ C.P.L.

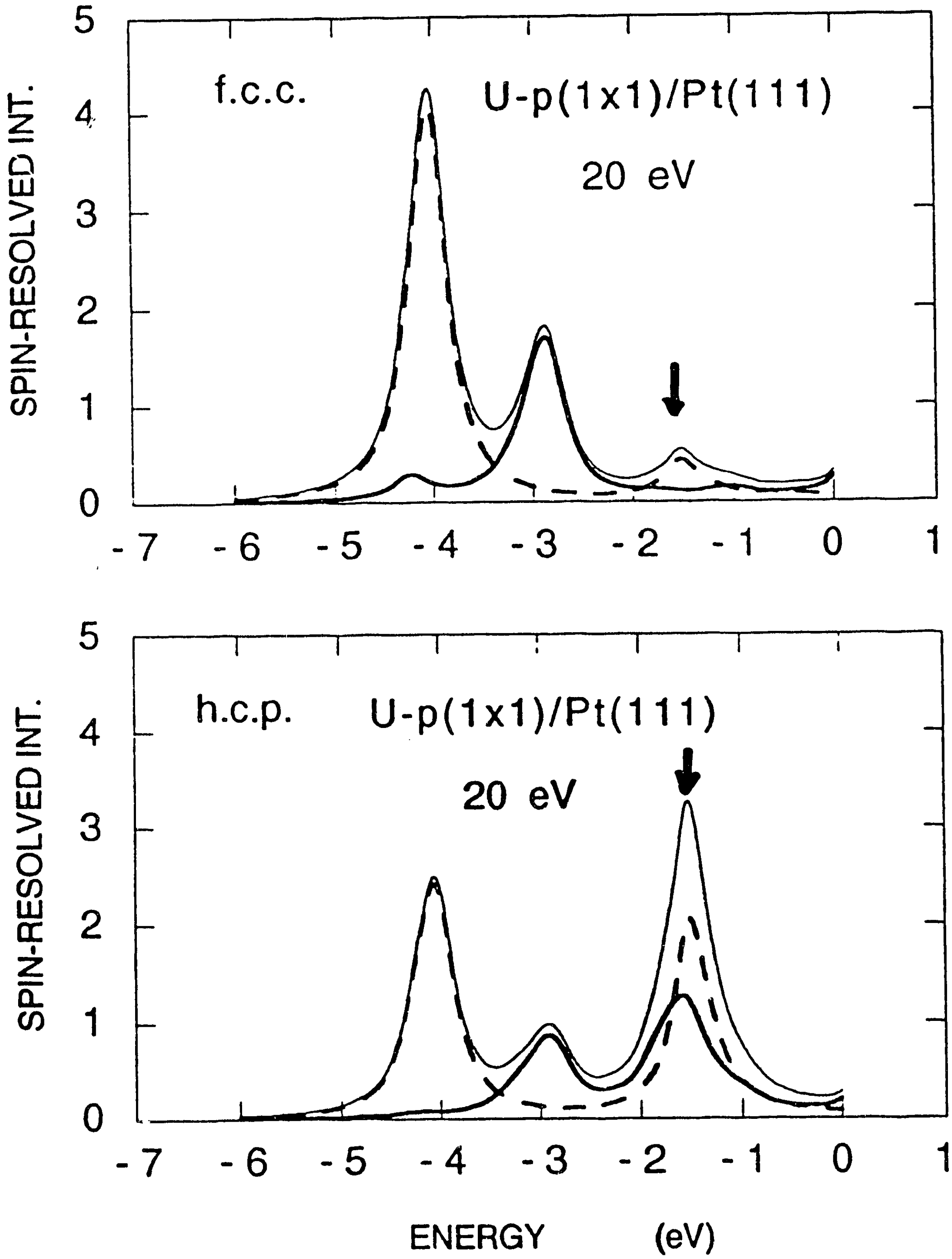

U(111) f.c.c. Bulk Layer DOS

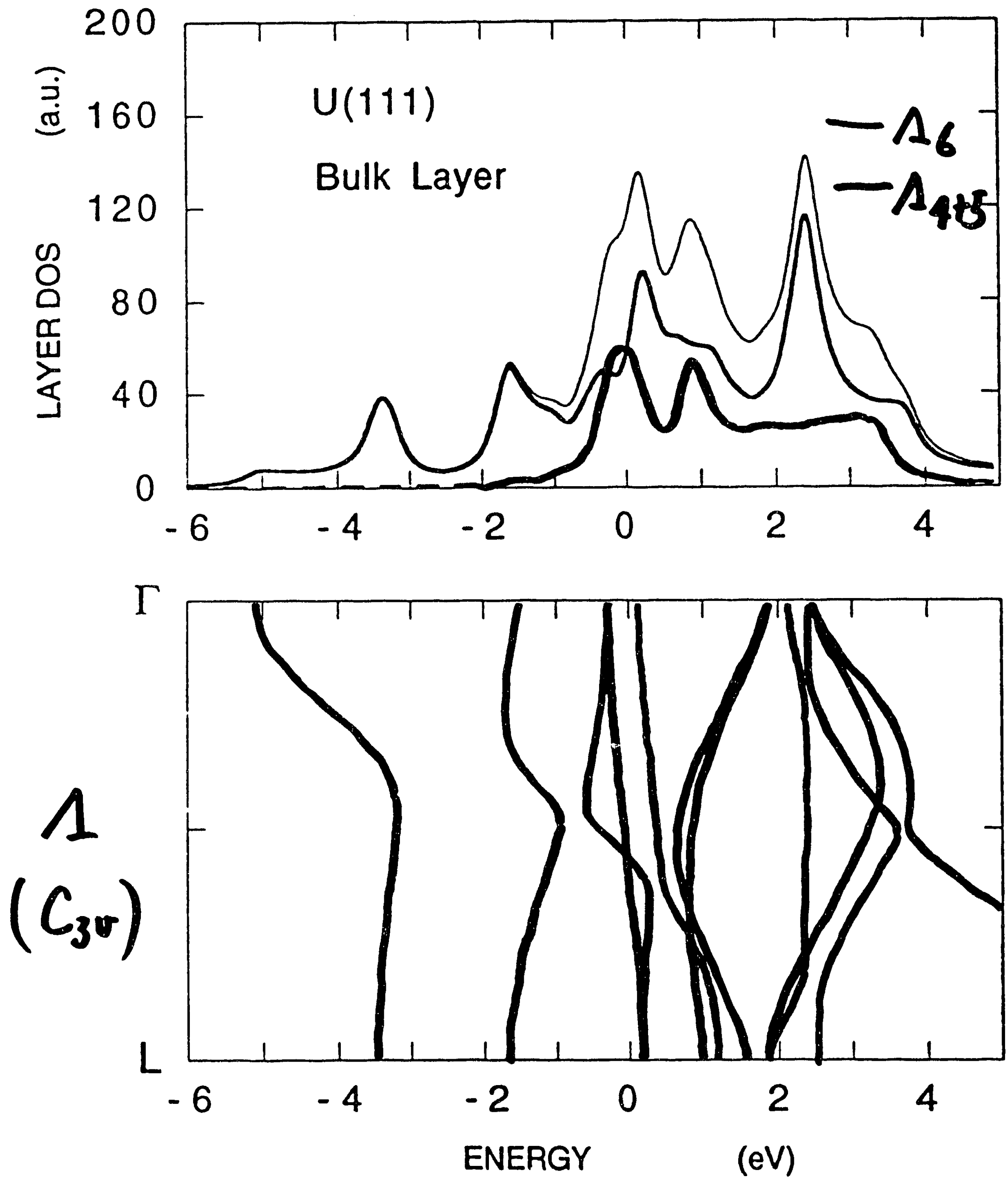

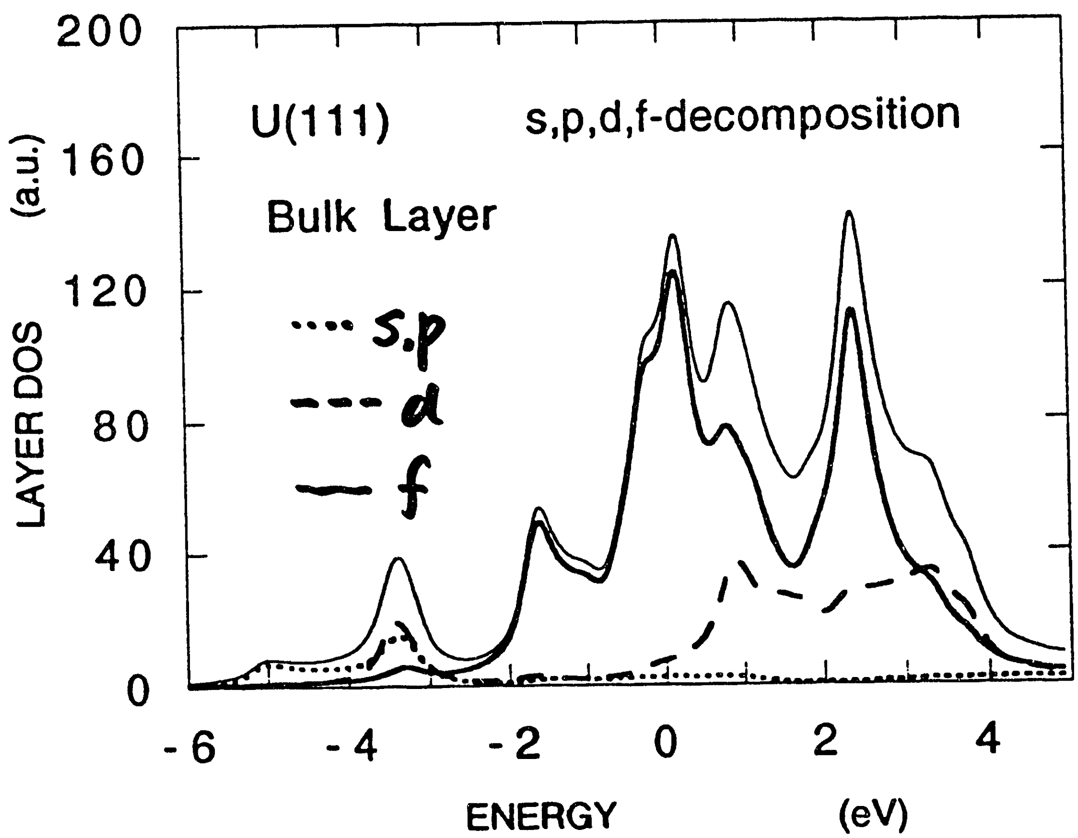

U(111)
s,p,d,f-decomposition
Bulk Layer
s.p
d
f
LAYER DOS (a.u.)
ENERGY (eV)
200
160
120
80
40
0
-6
-4
-2
0
2
4

U(111) f.c.c.

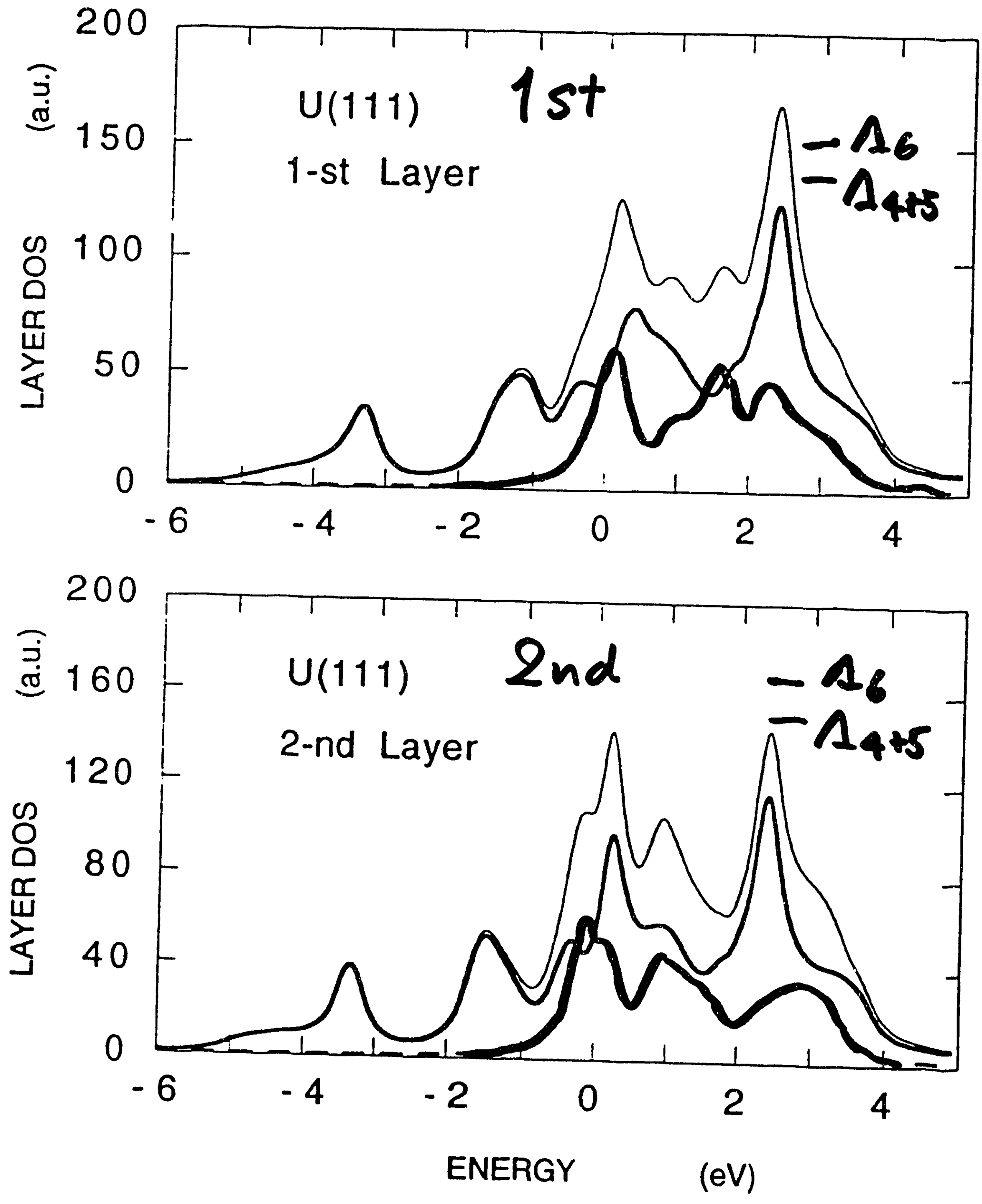

U(111)
1st
1-st Layer
— Δ_6
— Δ_{4+5}
LAYER DOS (a.u.)
0
50
100
150
200
-6
-4
-2
0
2
4
U(111)
2nd
2-nd Layer
— Δ_6
— Δ_{4+5}
LAYER DOS (a.u.)
0
40
80
120
160
200
-6
-4
-2
0
2
4
ENERGY (eV)

Ups $\vartheta_e = 0$ $\vartheta_{ph} = 0$ C.P.L.

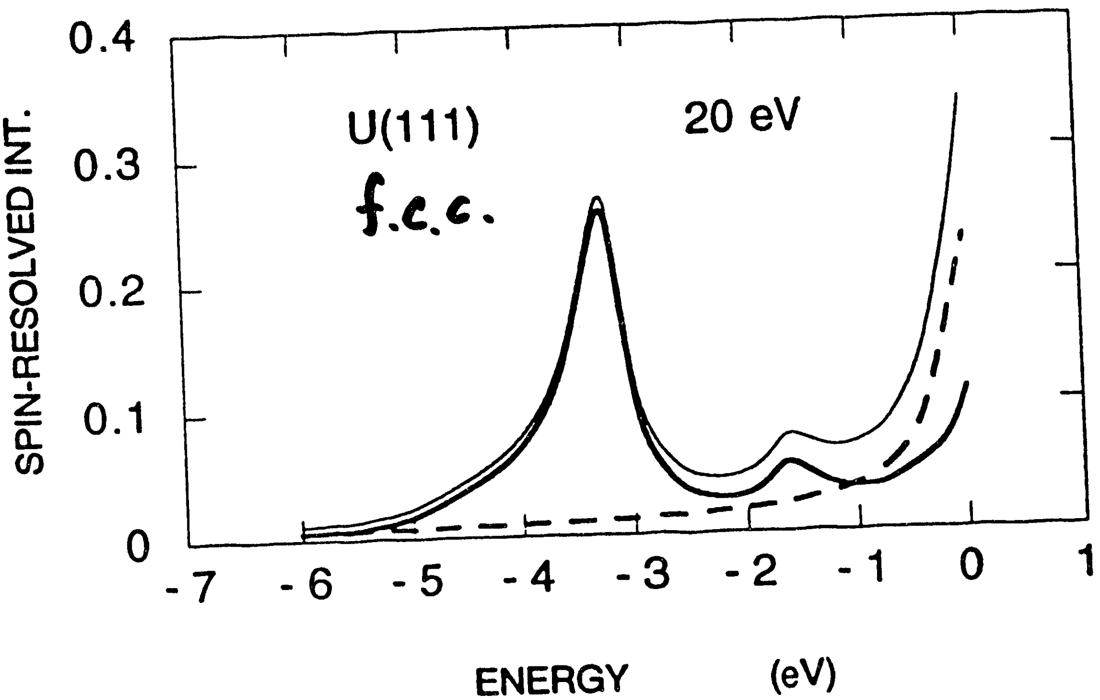

Conclusion

Do it on the SURFACE !!!!

Spin analysis is highly recommended!

Thanks to J. van Ek
who provided self-consistent uranium potentials for various lattice constants.

Magnetic X-ray scattering experiments at resonant energies

G.H. Lander

Commission of the European Communities, Joint Research Centre,
Institute for Transuranium Elements,
Postfach 23 40, D-7500 Karlsruhe, Fed. Republic of Germany

The cross sections for magnetic scattering of electromagnetic radiation were derived many years ago but are in general ~ 10^{-6} of the familiar cross sections for charge scattering. The brilliance of present and projected synchrotron sources now make this technique one of considerable promise.[1,2] The X-ray technique is complementary to the more usual technique of neutron scattering, and gives the possibility to separate spin and orbital moments, and to use the high instrinsic wavevector resolution to observe subtle effects in both the magnetic and crystal structures.[3]

An important discovery of resonant magnetic scattering was made by Gibbs et al.[4,5] in holmium. This occurs when the incident photon energy is tuned to certain absorption edges. A consequence is an enormous (> 10^5 in the case of actinides) enhancement[6] of the intensity, making the technique of particular importance in the study of f element magnetism. Resonance occurs when the an electron is excited into a shell in which there are already spin-polarized electrons. The relevant edges are shown in the Table.

We are examining the resonance itself to learn more about whether the predominant 'atomic' physics description[7] contains information on the condensed-matter properties of the material. In Fig. 1 we show the intensities of the magnetic reflections as a function of energy as the latter is varied through the M_V and M_{IV} absorption edges for the antiferromagnets USb and NpAs. The ratio of the intensities at the two edges can be calculated from first principles,[8] and has been shown to be a sensitive measure of the 5f-occupancy and degree of crystal-field mixing in the electronic ground-state wavefunctions.

Table I

Representative elements of the different possible magnetic series, together with the possible strong (E1) dipole transitions for resonant magnetic scattering, and the relevant X-ray energies and wavelengths ($E = 12.398/\lambda$).

		transition	edge	E (keV)	λ (Å)	edge	E (keV)	λ (Å)
3d	Fe	p-d	LII	0.72	17.22	LIII	0.707	17.54
4d	Rh	p-d	LII	3.146	3.94	LIII	3.004	4.13
5d	Pt	p-d	LII	13.27	0.93	LIII	11.56	1.07
4f	Gd	d-f	MIV	1.22	10.16	MV	1.19	10.42
5f	U	d-f	MIV	3.73	3.32	MV	3.55	3.49

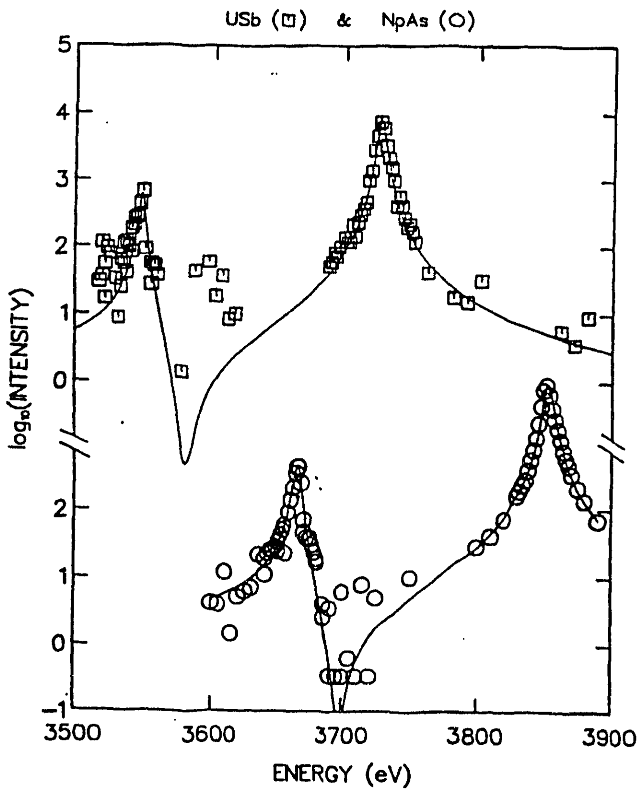

Integrated intensities as a function of energy for the antiferromagnetic reflections of USb (top curve) and NpAs (bottom curve)

The resonant scattering can be used also to examine the magnetic structures. Because the wavevector resolution of X-ray from the synchrotron is intrinsically so good, the technique is extremely powerful and has already given valuable information on the spatial correlations in systems such as the heavy fermion URu_2Si_2, in which the moments are $< 0.1\ \mu_B$ and the magnetism is not truly 'long range' in the same sense as the crystal structure.[9] A similar situation has been found by us in examining the complex magnetism in the solid solution

$U_{0.85}Th_{0.15}Sb$ with both neutrons and X-rays at resonant energies.[10] More recently we have been examining the correlations that develop *above* T_N in antiferromagnetic NpAs and find that they are different as viewed by X-rays and neutrons. This raises the question of the surface sensitivity of the X-ray technique (the neutrons are a bulk probe). There are already indications that the near-surface volume (the penetration depth here is 2000 - 3000 Å) behaves differently from the bulk,[11] and we anticipate more studies of this sort.

The prospects for resonant scattering are bright. By chance, the largest effects occur in the actinides, so that we should be expoiting them aggressively, particularly at the new 3rd generation sources. New areas one can envision are surface and multilayer magnetism, examination of transcurium samples at the microgram level, and inelastic magnetic scattering within the range of ~100 to 1000 meV.

Acknowledgements

I would like to acknowledge a close collaboration with the group of W.G. Stirling from the University of Keele and Doon Gibbs of Brookhaven National Laboratory. All our experiments have been done at beam-line X22C at the NSLS.

References:

1. M. Blume, J. Appl. Phys. 57, 3615-3618 (1985)
2. M. Blume and D. Gibbs, Phys. Rev. B 37, 1779 (1988); S.W. Lovesey, J. Phys. C: Solid State Phys. 20, 5625-5639 (1987)
3. J. Bohr et al, Physica B 159, 93-105 (1989)
4, D. Gibbs et al, Phys. Rev. Letters 61, 1241-1244 (1988)
5. D. Gibbs et al Phys. Rev. B 43, 5663-5681 (1991)
6. D.B. McWhan et al, Phys. Rev. B 42, 6007-6017 (1990)
7. J.P. Hannon et al, Phys. Rev. Letters 61, 1245-1248 (1988); erratum ibid 62, 2644 (1989)
8. C.C. Tang et al, Phys. Rev. B (Sept. 1, 1992)
9. E.D. Isaacs et al, Phys. Rev. Letters 65, 3185 (1990)
10. J.A. Paixão et al, Phys. Rev. B (in press)
11. J.P. Hill et al, Phys. Rev. Letters 66, 3281 (1991)

Magnetic Scattering of X-rays

The strongest interaction between photons and matter is through the charge (Thomson) term.

However the relativistic nature of electromagnetic radiation means that interactions between between space and spin wave functions cannot be distinguished - so that there is a term sensitive to the electron spin state.

This 'magnetic' interaction is weaker by the term

$\hbar\omega/mc^2 \sim 0.016$ for 8 keV photons.

This was recognised by Gell-Mann & Goldberger in 1954

First experiments by de Bergevin & Brunel (CNRS, Grenoble) in 1981 with standard x-ray tubes.

But - synchrotrons have ~ 8 orders of magnitude more intensity than sealed x-ray tubes.

(3) **Polarisation of the photons.**

Magnetic scattering results in σ to π rotation of the plane of polarisation. This means that it may be isolated by polarisation analysis.

Beams from a bending magnet line are highly linearly polarised (σ). The magnetic cross section contains terms that allow the separation of the spin **S** and orbital **L** components of the magnetisation. This separation can be done only in certain cases with neutrons, e.g. our own work on UFe_2

(4) **Tunability.**

We have a constant, or nearly so, flux of photons over a wide range of energies.

This allows us to bring the energy near an absorption edge and observe
RESONANT MAGNETIC SCATTERING.

We should emphasize that a complete theory for resonant scattering is not yet available.

There are **4 features** of synchrotron radiation that are of particular interest.

(1) **Intensity**

This may allow us to see magnetic scattering from samples that are of *nanogram* size.

It may also allow the observation of the arrangements of spins on the surface by using grazing incidence techniques.

(2) **Wavevector resolution**

This can be up to 10 times better than possible with neutrons (because of the naturally high collimation of the photon beams). This allows the study of phase transitions (e.g. Ho, Er etc) to be performed with high precision. Lattice effects can also be studied.

For both of these effects *good* crystals are needed !

URu_2Si_2 – E. Isaacs, B. Gaulin et al.

Magnetic scattering of photons

In the limit of high photon energy the cross section is:

$$\frac{d\sigma}{d\Omega} = \left(\frac{e^2}{mc^2}\right)^2 \operatorname{tr}\left(\left\langle M_c - \frac{i\hbar\omega}{mc^2} M_m \right\rangle P \left\langle M_c - \frac{i\hbar\omega}{mc^2} M_m \right\rangle^+\right)$$

where $\langle M_c \rangle = e(\vec{Q}) \cdot \vec{X}$ charge density

$$\langle M_m \rangle = \underbrace{\tfrac{1}{2} \vec{L}(\vec{Q})}_{\text{orbital contribution}} \cdot \vec{A} + \underbrace{\vec{S}(\vec{Q})}_{\text{spin contribution}} \cdot \vec{B}$$

$\vec{A}$ and $\vec{B}$ depend on geometry.

Note that magnetic part is weak.

Modified by $i \frac{\hbar\omega}{mc^2}$

i — out of phase by $\pi/2$

$\frac{\hbar\omega}{mc^2}$ ratio of incident photon energy to rest mass of electron

$mc^2 = 511$ keV

so with $\hbar\omega = 8$ keV

magnetic amplitude is down to $\sim 1\%$

P is density matrix for incident polarization.

AIIM

Association for Information and Image Management

1100 Wayne Avenue, Suite 1100
Silver Spring, Maryland 20910

301/587-8202

Centimeter

1 2 3 4 5 6 7 8 9 10 11 12 13 14 15 mm

1 2 3 4 5

Inches

1.0 1.1 1.25 1.4 1.6 1.8 2.0 2.2 2.5 2.8 3.2 3.6 4.0 4.5 5.0 5.6 6.3

MANUFACTURED TO AIIM STANDARDS

BY APPLIED IMAGE, INC.

3 of 5

The determination of **magnetic structures** appears possible, <u>but</u> the intensities are very small. These experiments are difficult.

Magnetic structures are much easier done with **neutrons**.

Neutrons can easily determine magnetic structures from powders, none yet with X-rays.

X-rays are and will be used to study in more detail systems already known, and special examples, e.g. surfaces and very small samples.

Antiferromagnets already examined:

MnF_2	Ho	UAs
(Cr)	Dy	UO_2
	Tm	USb
	Er	URu_2Si_2
	Sm	$U_{0.85}Th_{0.15}Sb$
	Gd - Y	NpAs
	Ho - Y	

Resonant Magnetic Scattering

We now come to the 'tunability' of a synchrotron source, i.e. the fact that photons of all wavelengths are emitted and not just a characteristic wavelength (e.g. Cu Kα at $\lambda = 1.5418$ Å)

X-ray resonances arise from electric multipole transitions between core levels and unoccupied electronic states near the Fermi edge.

Take L_{III} in Ho   8.07 keV, 1.54 Å

E1   dipole $2p_{3/2} \rightarrow 5d_{5/2}$

E2 quadrapole $2p_{3/2} \rightarrow 4f_{5/2}$

A strong enhancement of the scattering amplitude occurs so that

$$\langle M_m \rangle \Rightarrow \frac{\langle M_m \rangle}{\left(\frac{E_1 - E_2 - \hbar\omega}{\Gamma/2} - i \right)}$$

at resonance $\hbar\omega = E_1 - E_2$

Γ is width.

Resonant Scattering

The increase in the amplitude as a result of resonance will depend on:

(a) The lifetime effects

(b) The extent of overlap of the wavefunction of excited and existing unpaired electron states.

(c) The order of the multipole interaction.

e.g. Ho L_{III}	$2p_{3/2} \longrightarrow 5d_{5/2}$	small occupied DOS	E1 large matrix element
	$2p \longrightarrow 4f$	large DOS	E2 small matrix element

Gibbs et al PRL <u>61</u>, 1241 (1988)
see enhancement of ~ 50

Hannon et al. PRL <u>61</u>, 1245 (1988)
interpret data and emphasize that dipole (E1) + large DOS will give a big effect.

Resonance Exchange Scattering in UAs.

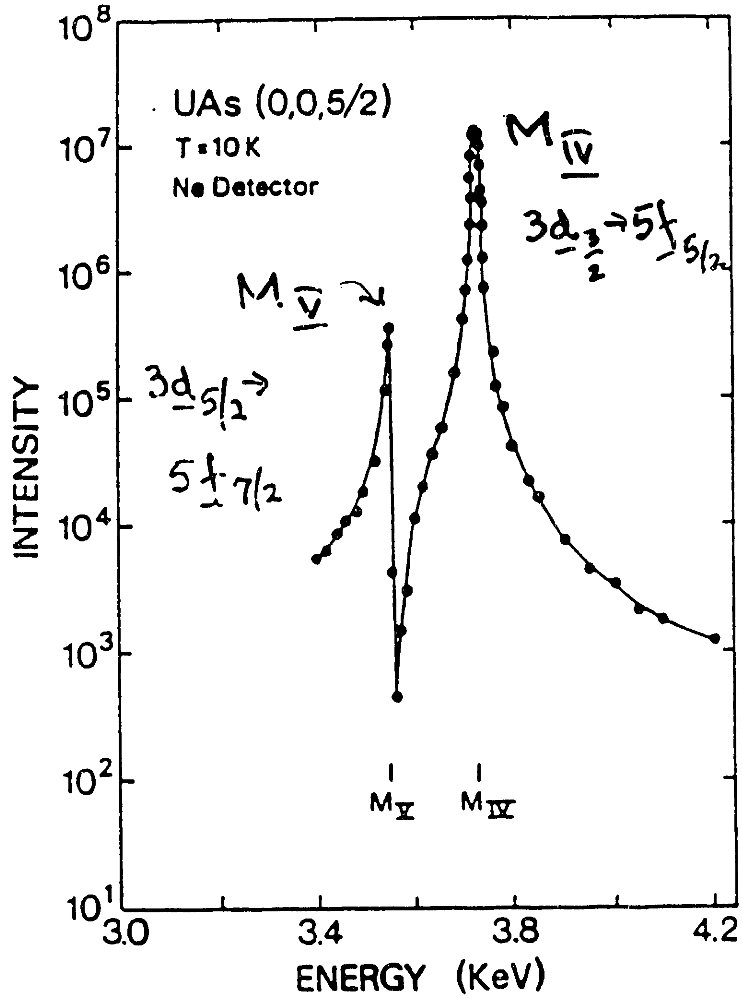

Notice the <u>enormous</u> increase in intensity at $M_{\underline{IV}}$.

Isaacs et al, Phys. Rev. Lett. <u>62</u>, 1671 (1989)
McWhan et al., Phys. Rev. B <u>42</u>, 6007 (1990)
Exp. at NSLS, Brookhaven Nat. Lab, USA.

Resonances — where will they be useful ?

$$\boxed{\underset{(keV)}{E} = \frac{12.4}{\lambda\ \text{Å}}}$$

		Edge	transition	E (keV)	λ (Å)
* 3d	Fe	L_{II}, L_{III}	2p → 3d	0.72	17.2
4d	Rh	$L_{II}, - L_{III}$	2p - 4d	3.15	3.94
5d	Pt	L_{II}, L_{III}	2p - 5d	13.27	0.93
* 4f	Ho	$M_{IV}\ M_{V}$	3d − 4f	1.35	9.2
* 5f	U	M_{IV}, M_{V}	3d − 5f	3.73	3.3

Clearly, actinides are the best

$\lambda = 3.3$ Å can get a few reflections
poor penetration
low incident intensity
& strongly absorbed by air

$$\left.\begin{array}{ll} M_{IV} & 3d_{3/2} \rightarrow 5f_{5/2} \\ M_{V} & 3d_{5/2} \rightarrow 5f_{7/2} \end{array}\right\}$$

Bragg's law $2d \sin\theta = \lambda$
for most materials $d_{max} \sim 4$ Å, $\lambda \lesssim 6$ Å

Analogue in absorption measurements is <u>circular dichroism</u>.

Here because it is a $q = 0$ measurement one must separate the normal and 'magnetic' contributions to the absorption

This is done by using circular polarisation (which has an imaginary component i) and reversing the applied field direction $\pm \vec{H}$ and measuring the <u>difference</u> in absorption.

G. Schütz et al. at Hamburg.
PRL <u>58</u>, 737 (1987)
PRL <u>62</u>, 2620 (1989)

Tang et al (1991) BD 4651 Phys. Rev. (1992)

UO_2

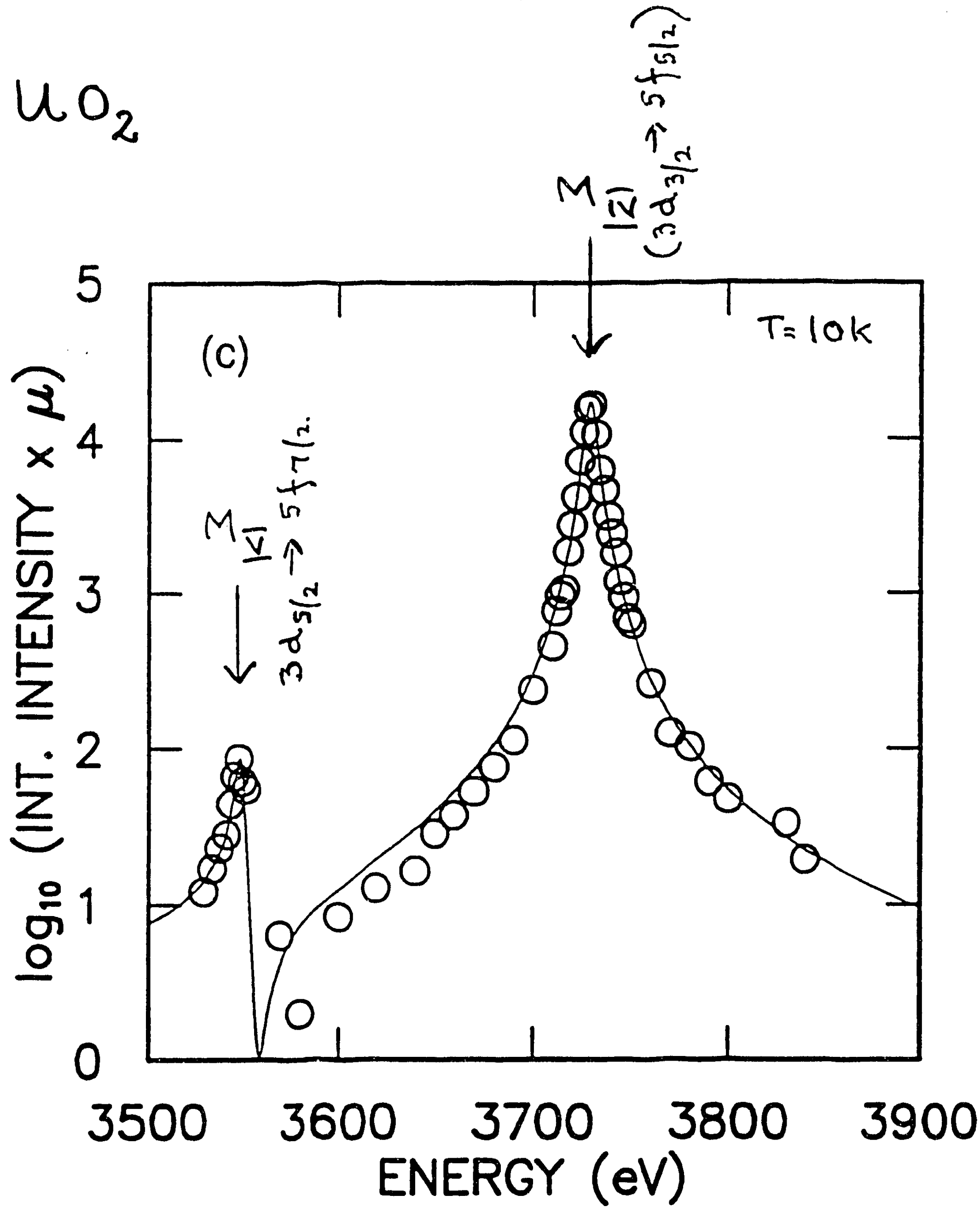

Solid line is fit with 2 resonances.

"Atomic physics" describes resonance behaviour.

widths close to resolution and expected core-hole lifetimes (~5 eV)

Ratios of heights give "Branching Ratios"

Tang et al (1991) BD4651

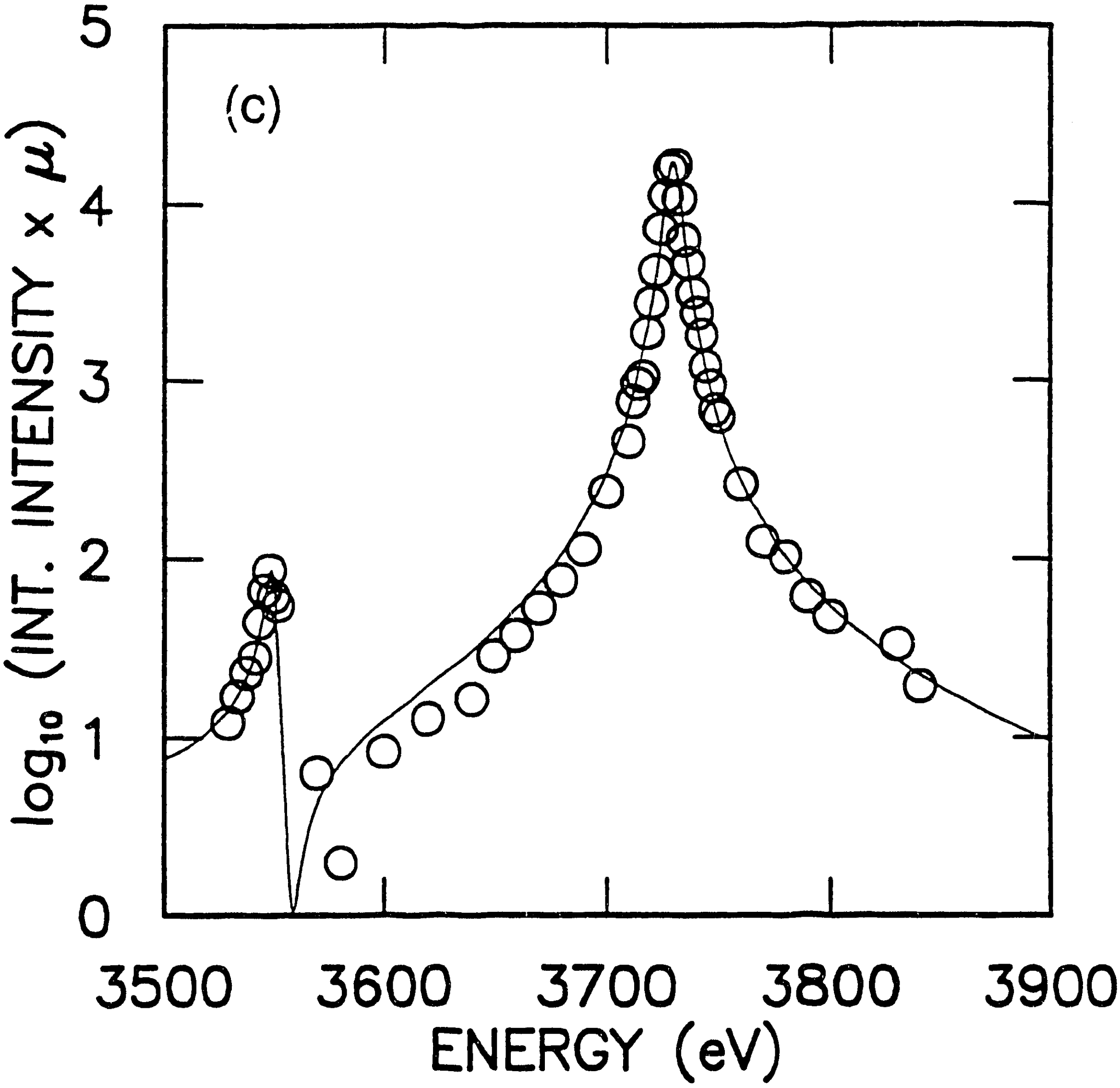

separation is binding energy

⇒ spin-orbit splitting of 5f shell.

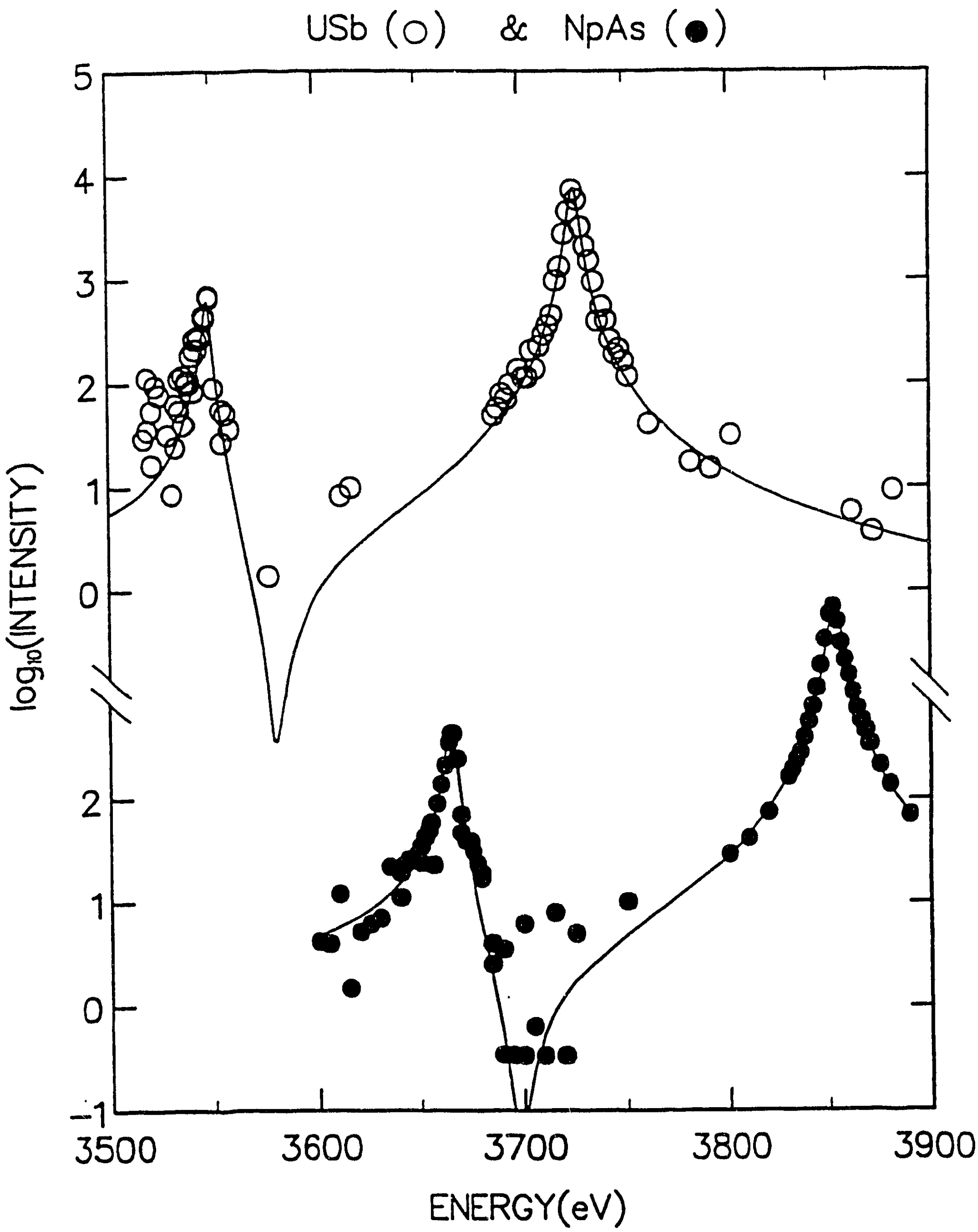
USb (○) & NpAs (●)
5
4
3
2
1
0
2
1
0
-1
log10(INTENSITY)
3500
3600
3700
3800
3900
ENERGY(eV)

Calculation of branching ratios

by Paolo Carra of the ESRF, Grenoble.

"ab initio" <u>atomic</u> calculations

all transitions possible for the transitions

$$5f^2\ ({}^3H_4) \longrightarrow 3\underline{d}^9\ 5f^3$$

and $$5f^3\ ({}^4I_{9/2}) \longrightarrow 3\underline{d}^9\ 5f^4$$

then, convoluted with Lorentzian shape

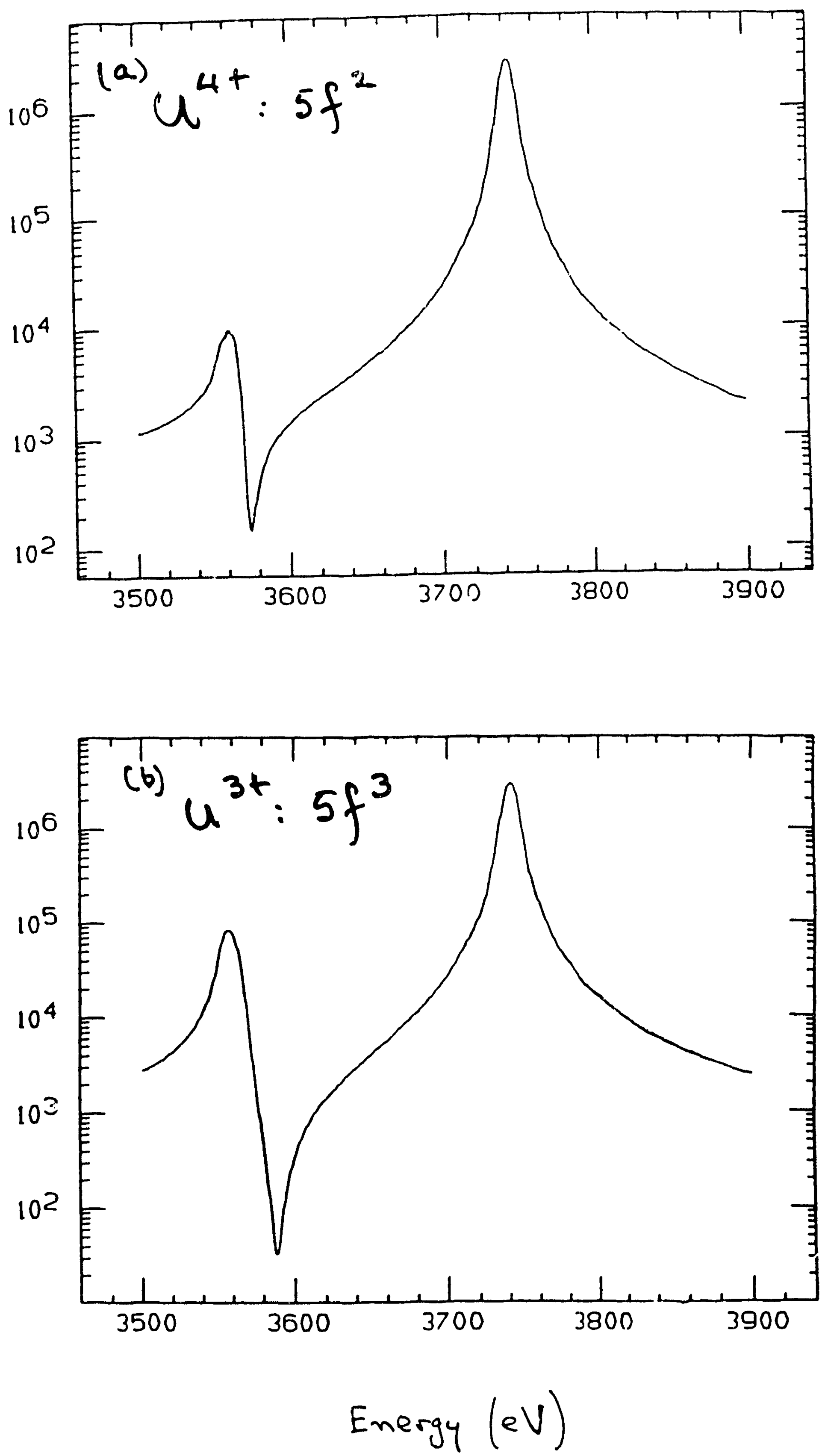
(a) U^{4+} : $5f^2$
10^6
10^5
10^4
10^3
10^2
3500
3600
3700
3800
3900
(b) U^{3+} : $5f^3$
10^6
10^5
10^4
10^3
10^2
3500
3600
3700
3800
3900
Energy (eV)

Variation (Branching ratio)^2
vs 5f electron occupation.

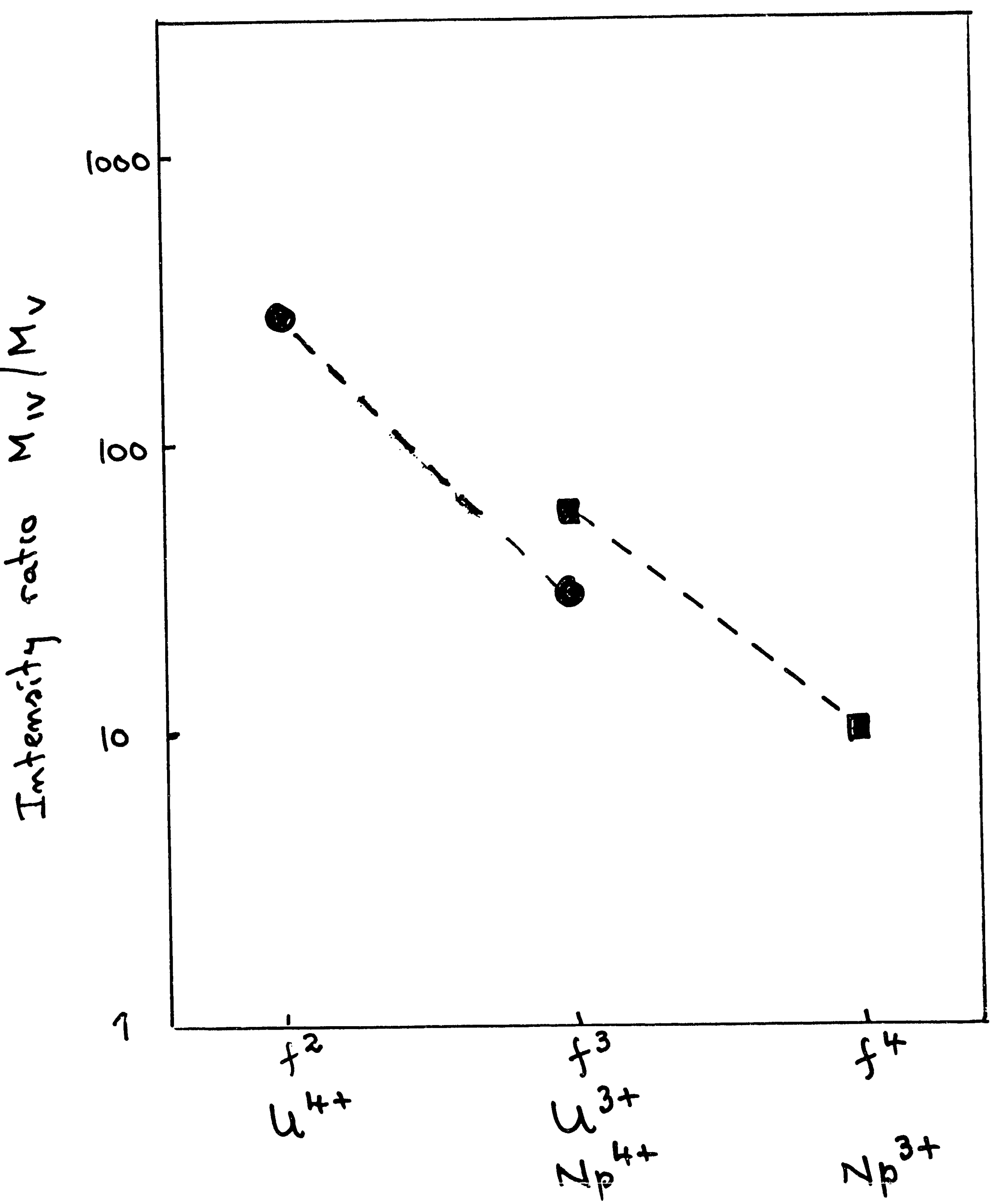

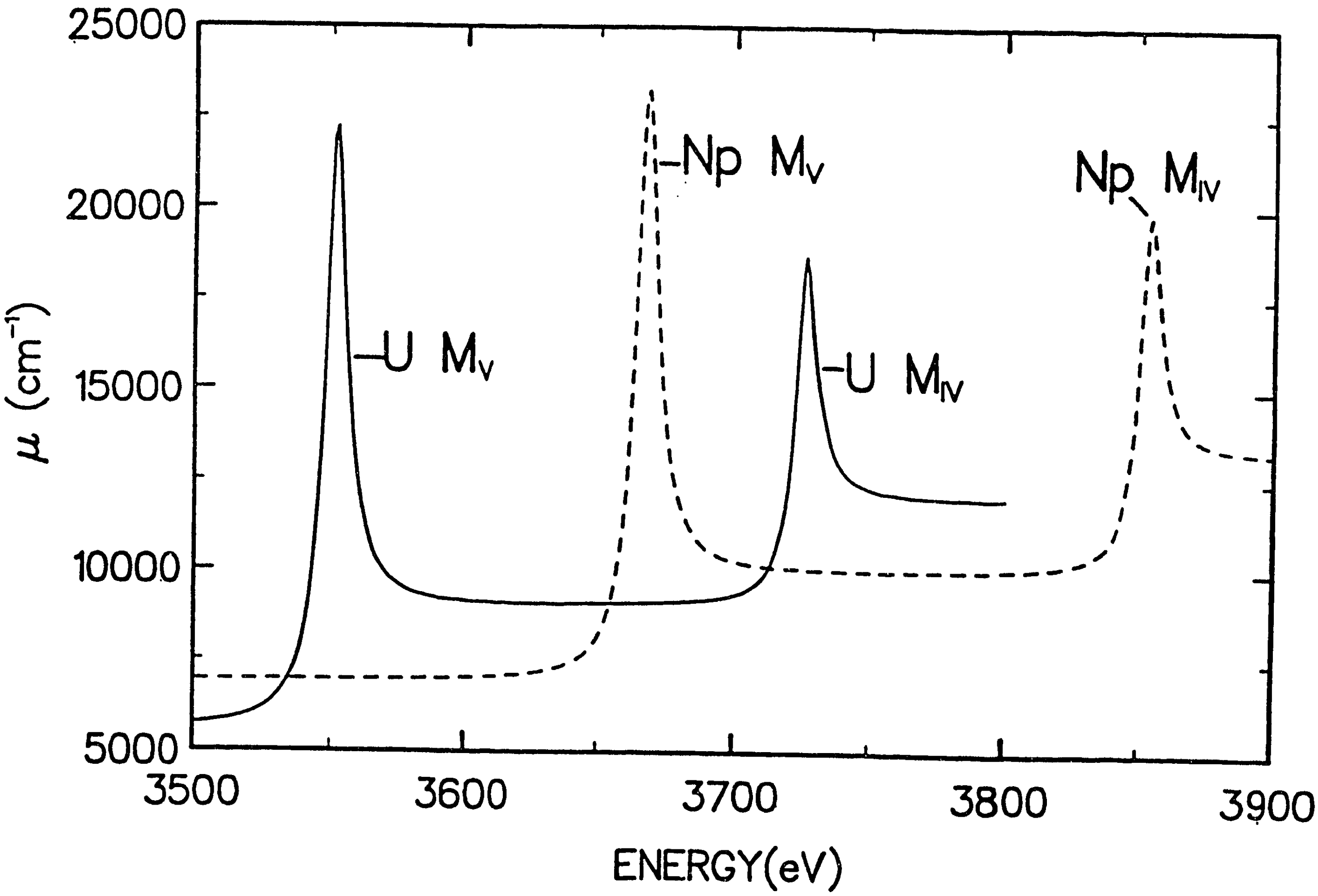

Absorption of $\mu = 2\times10^4$ cm^{-1}

means attenuation of beam $e^{-\mu t}$

$I/I_0 = 0.2 \quad t \approx 8000$ Å (0.8 μm)

Penetration (if $2\theta_B = 60°$) ~ 2000 Å

Near surface probe.

$U_{0.85}Th_{0.15}Sb.$

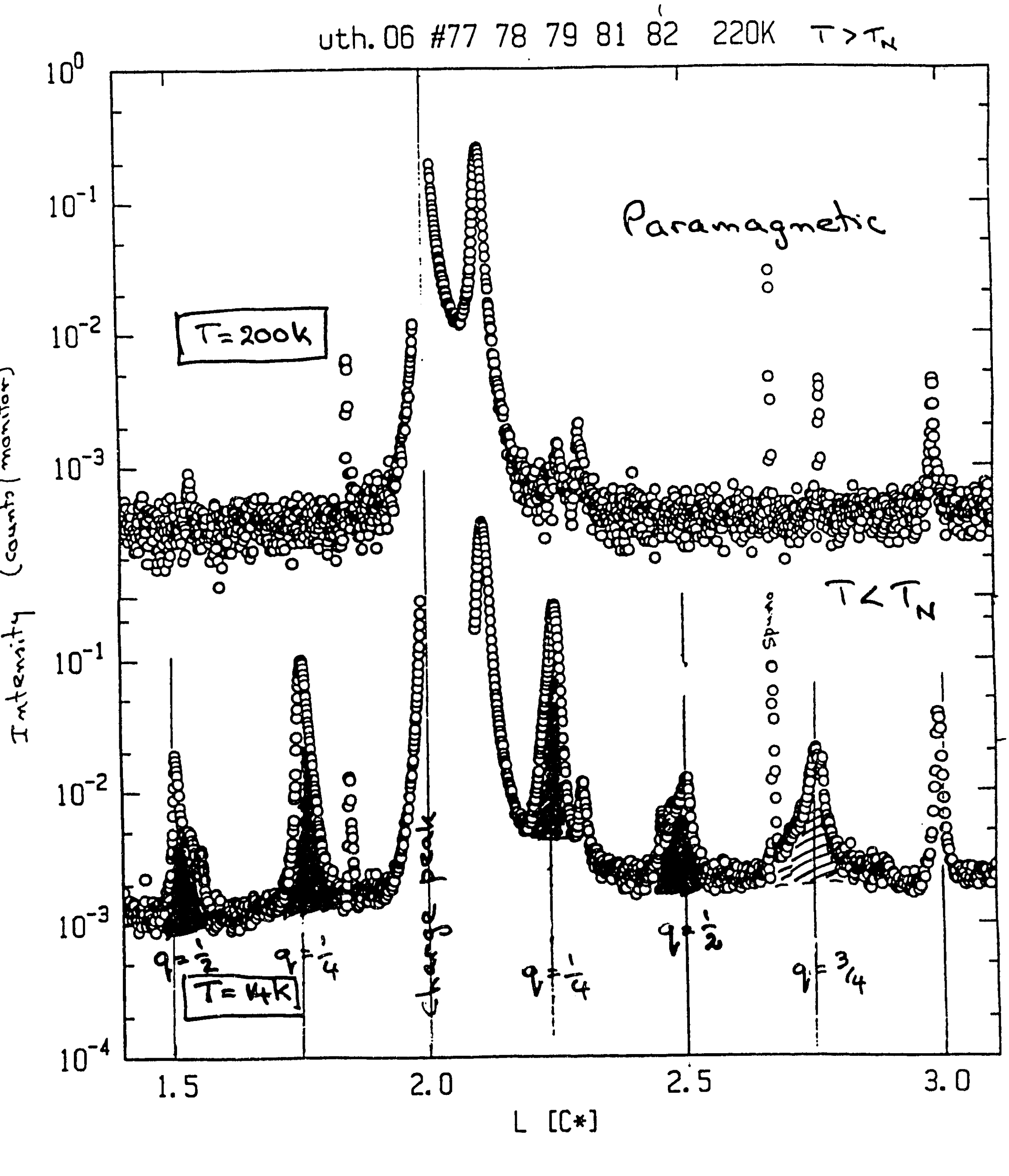

Future Prospects

Intensity

Surface magnetism

Critical scattering (helped also by resolution)

Nanogram quantities of actinides (using resonance)

Inelastic scattering ?

Resolution

New details of magnetic structures and coupling to the lattice. Correlation lengths.

Polarization

Separation of L and S

Tunability

We need a complete theory to be able to relate moments to the signal measured.

Branching ratio - new information on the electronic structure.

Orbital moment

Prospects

(1) Need 3.5 – 5 keV possibility of circular polarization

(2) Can use Be window at sample but want as little as possible in beam.

At BNL we lose a factor of 60 !

(3) Presently have a 'flake' of NpAs, 1.5 × 1.5 × 1 mm ~ 12 mg.

> 20,000 cts/sec in mag. peak.

we can estimate that exp. can be done on nanogram samples

The magnetism of higher actinides is unknown

⟹ gives us information on electronic structure.

BEAMLINE INSTRUMENTS FOR RADIOACTIVE MATERIALS

Hideo OHNO, Hiroyuki KONISHI, Katsumi KOBAYASHI*
and
Shigemi SASAKI

Office of Synchrotron Radiation Facility Project
Japan Atomic Energy Research Institute (JAERI)
Tokai-mura, Naka-gun, Ibaraki 319-11, Japan

*Photon Factory (PF)
National Laboratory for High Energy Physics (KEK)
Oho 1-1, Tsukuba, Ibaraki 305, Japan

Objective

Physics and chemistry of actinides are increasing their interest. Many successful experiments have been performed on the so-called "heavy fermion", or narrow band system particularly on uranium by using synchrotron radiation. It would be of great interest to extend photoemission studies beyond uranium and to study localization of the 5f electrons quantitatively with a certain experimental method to separate the spin and orbital components.

Recently, we constructed a new beamline at the Photon Factory, KEK. The aim of construction is to study unsealed radioactive materials, to obtain the know-how on design and installation of a beamline and to investigate necessary optics and instrumental specifications of the SPring-8 beamline for radioactive material research.

Outlines

The beamline is designed to accept radiations emitted from a bending magnet. Outline of the beamline is schematically shown in Figs. 1 and 2. The basic design of the front end is similar to those of the conventional type in the KEK-PF. The beamline is divided into two branch beamlines by means of a fixed mask. One is a soft x-ray [1.6-6 keV] beamline, BL-27A, which adopts a focusing optical system with a bent-cylindrical CVD-SiC mirror and an InSb (111) flat double-crystal monochromator. All the optical components are installed in ultra-high vacuum. The first crystal of the monochromator is cooled using a heat pipe. The BL-27A has two tandem experimental stations. The upstream station is located at halfway to the focusing point in order to get a large beam size (>20 mm x 5 mm) for the irradiation of biological samples. The downstream station is located at the focus point to be used for photoelectron spectroscopy. The estimated photon flux is $5x10^{10}$cps for 3 keV x-rays with a energy resolution of $4x10^{-4}$ for 200 mA beam current. The other is an x-ray [4-17 keV] beamline, BL-27B. The BL-27B is designed for XAFS and XRD. Horizontal focusing is achieved by a Si(111) sagittally focusing double-crystal monochromator and vertical focusing is achieved by a downstream bent mirror. The flux of 10 keV x-rays is estimated to be $1x10^{11}$cps with a energy resolution of $2x10^{-4}$ for 200 mA beam current.

There are some new design concepts for this beamline different from those of the conventional beamlines. Firstly, two monitor chambers (RI ports) for an eventual radioactive contamination are installed. The radioactivity of those monitors will be checked at regular intervals. Secondly, two additional fast closing valves and a buffer chamber are installed as shown in Fig.2 in the soft x-ray beamline. These are against an eventual accident of scattering of the radioactive samples as well as an event of the vacuum failure. Thirdly, a capton foil mounted on SUS wires of 200 meshes is inserted in front of the experimental area of the soft x-ray beamline. Although the radiations of the VUV region of the energy less than 300 eV are cut by the foil, more than 80% transparency is guaranteed for soft x-rays of the energy above 1 keV.

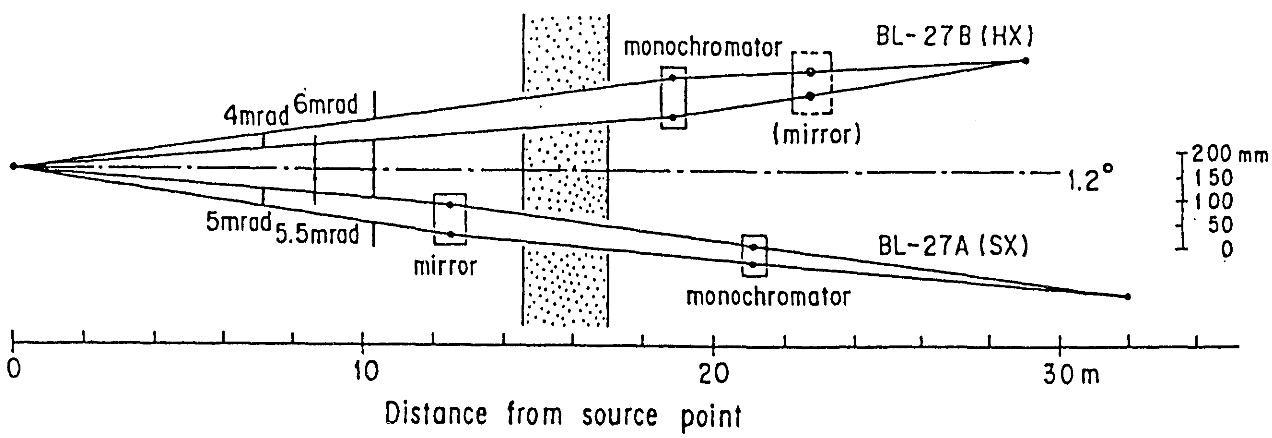

Figure 1. Layout of optical components for BL-27A&B.

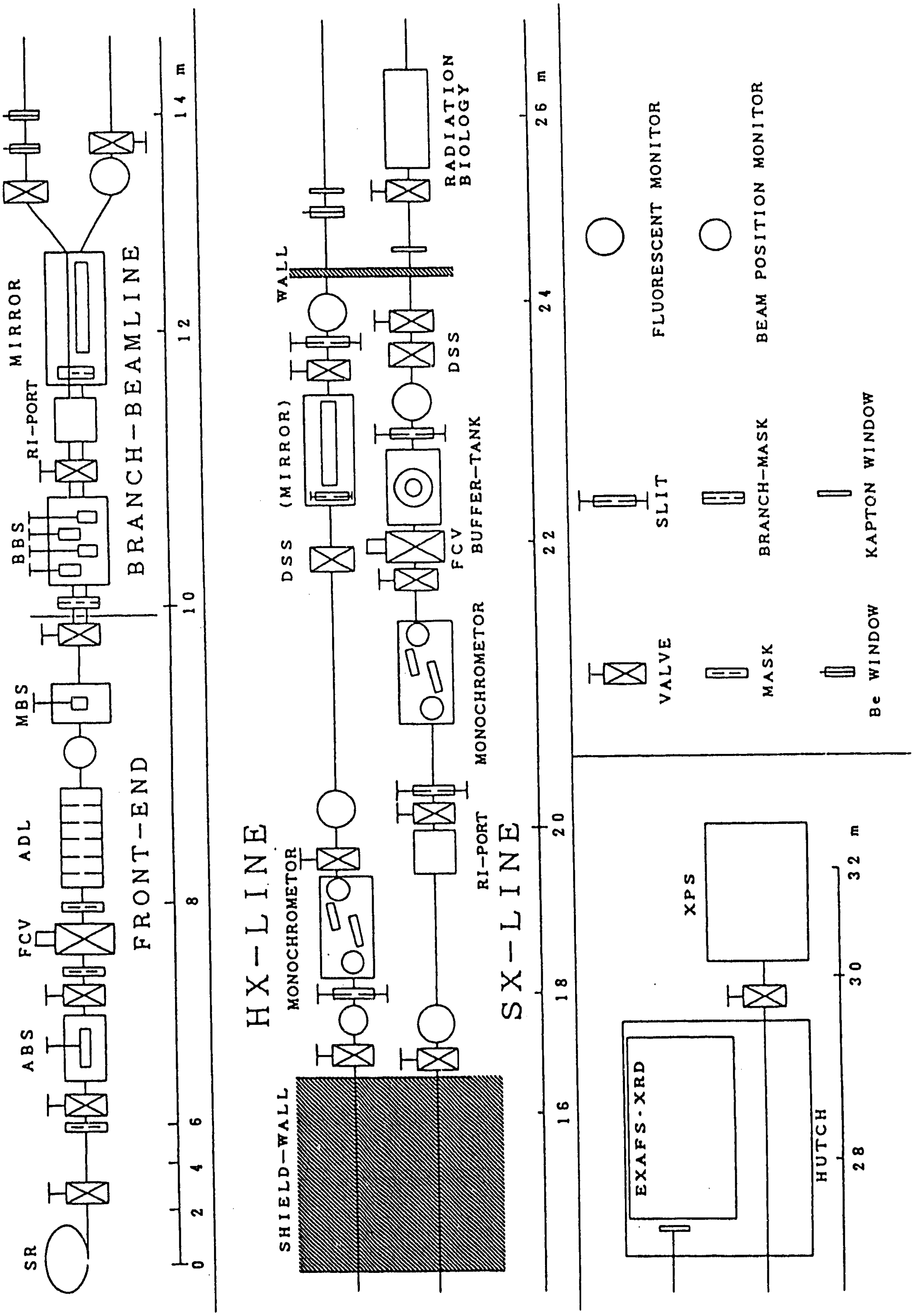

Figure 2. Schematic view of BL-27 showing the layout of beamline components.

BEAMLINE INSTRUMENTS FOR RADIOACTIVE MATERIALS

Hideo OHNO, Hiroyuki KONISHI, Katsumi KOBAYASHI*
and
<u>Shigemi SASAKI</u>

Office of Synchrotron Radiation Facility Project
Japan Atomic Energy Research Institute (JAERI)
Tokai-mura, Naka-gun, Ibaraki 319-11, Japan

*Photon Factory (PF)
National Laboratory for High Energy Physics (KEK)
Oho 1-1, Tsukuba, Ibaraki 305, Japan

Objectivis

1. **To sudy radioactive materials irradiated with high energy particle beams**
2. **To study actinoid compounds**
3. **To study bio-specimens includes radioisotopes as tracers**

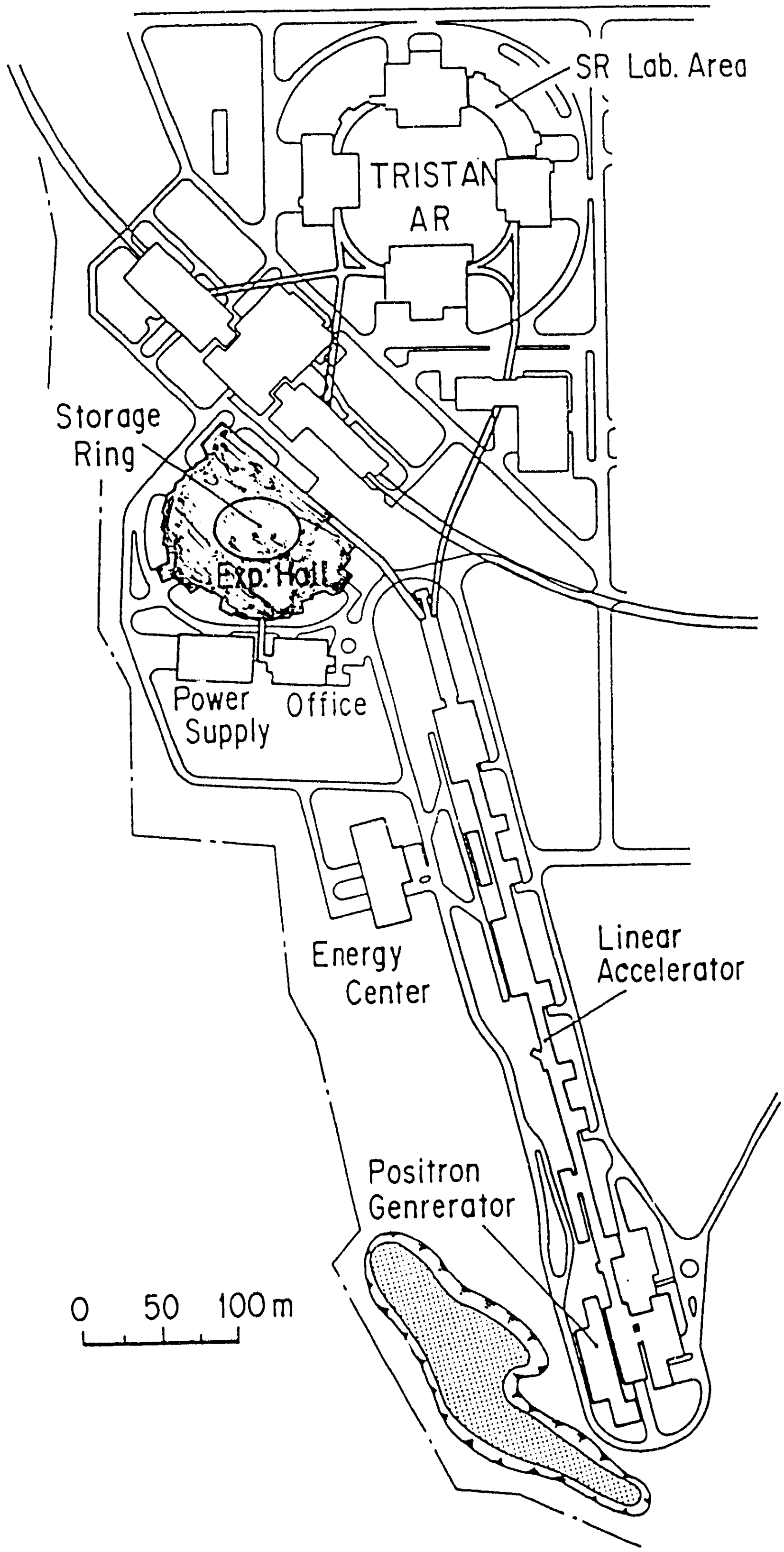

Plan View of the Photon Factory

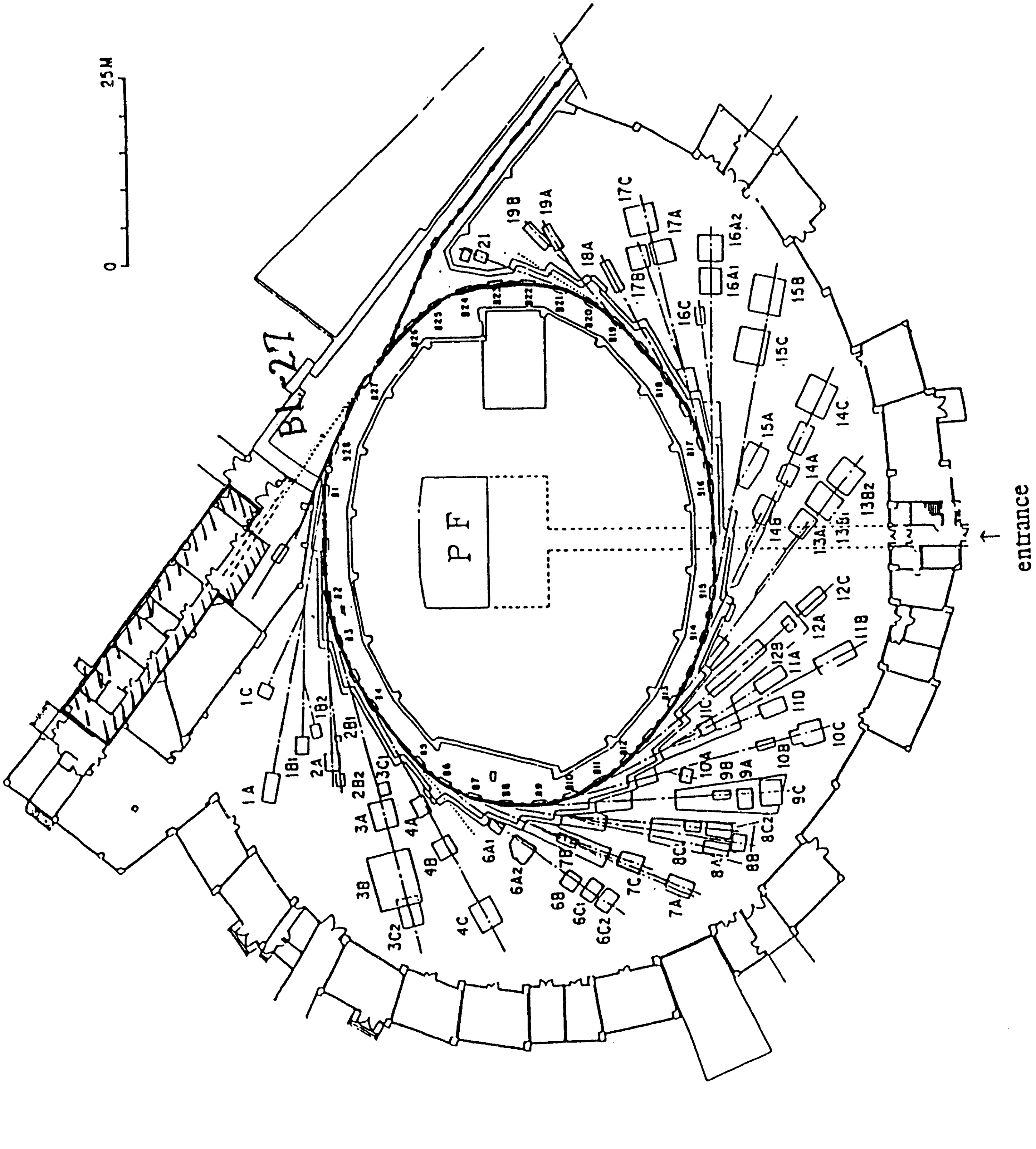

0
25M
BL-27
PF
entrance
1A
1B1
1B2
1C
2A
2B1
2B2
3A
3B
3C1
3C2
4A
4B
4C
6A1
6A2
6B
6C1
6C2
7A
7B
7C
8A
8B
8C1
8C2
9A
9B
9C
10A
10B
10C
11A
11B
11C
11D
12A
12B
12C
13A
13B1
13B2
14A
14B
14C
15A
15B
15C
16A1
16A2
16C
17A
17B
17C
18A
19A
19B
21

The BL-27 consists of two branch beamlines, BL-27A and BL-27B.

BL-27A (Soft X-ray Line)

Energy region :	1.8 - 6 keV
Acceptance angle :	5 mrad
Optical devices :	douple crystal monochromator InSb(111)
	SiC bent cylindrical mirror
Stations :	Radiation Biology Studies
	X-ray Photoelectron Spectroscopy (XPS)

BL-27B (Hard X-ray Line)

Energy region :	4 - 20 keV
Acceptance angle :	4 mrad
Optical devices :	double crystal monochromator Si(111)
	with sagittal focusing mechanism
Station :	XAFS
	X-ray Diffraction

Characteristics of BL-27

1. **Kapton Film Window (7.9 μm thick)**

2. **Two Fast Closing Valves**

3. **RI Ports : Special components for quick survey of the radioactive contamination in the beamline**

4. **Specially Designed Masks**

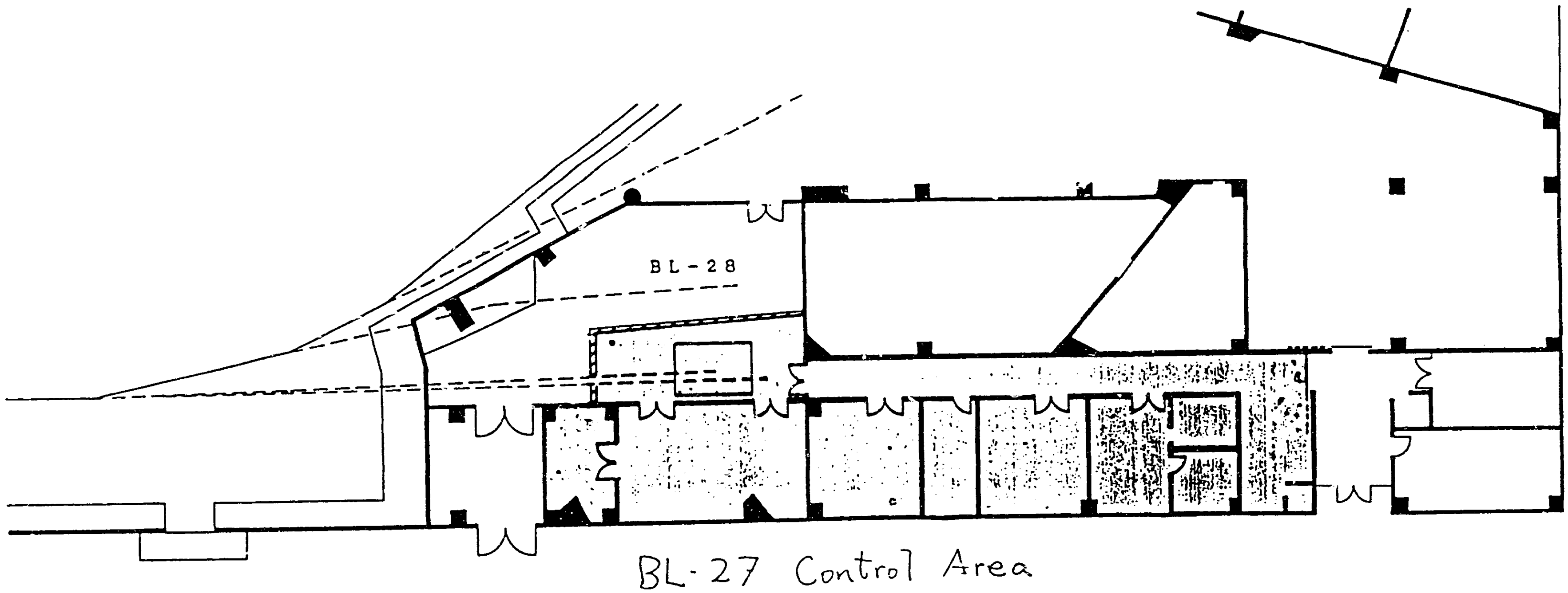

ＢＬ－２７汚染管理区域想定図

ＢＬ－２７で使用する核燃料物質及びＲＩの種類、形状、量について
(Elements & Compounds which can be used at BL-27)

１、アクチノイド系物質

元素　Ｕ、Ｔｈ

主な化学形態

酸化物　ＵＯ２ＣＯ３、ＵＯ２Ｃ２Ｏ４、ＵＯ２ＳＯ４、ＣｕＵ３Ｏ、ＣｕＣＯ４
ＣｕＵ３Ｏ10、ＵｘＯｙ
Ｔｈ（ＣＯ３）２、Ｔｈ（ＳＯ４）２、Ｔｈ（Ｃ２Ｏ４）２、ＴｈｘＯｙ等

炭化物　ＵｘＣｙ、ＴｈｘＣｙ

窒化物　ＵｘＮｙ、ＴｈｘＮｙ

その他の金属間化合物 (Metallic compounds)

２，ＲＩ含有物質 (Matters including following radio-isotope)

主な核種

２群　Ｎａ－22、Ｓｉ－32、Ｃａ－45、Ｔｉ－44、Ｖ－49，Ｍｎ－54，
Ｃｏ－56，Ｃｏ－57，Ｃｏ－58，Ｃｏ－60　Ｎｉ－63，Ｚｎ－65，
Ｇｅ－68、Ａｓ－73、Ｓｒ－85，Ｓｒ－89，Ｙ－88，Ｙ－91，Ｚｒ－88，
Ｚｒ－95，Ｎｂ－93，Ｎｂ－95、Ｔｃ－95、Ｔｃ－97，Ａｇ－105，
Ａｇ－110，Ｓｎ－113，Ｓｎ－119、Ｓｂ－123，Ｓｂ－124，Ｃｓ－134，
Ｃｓ－137，Ｂａ－133、Ｃｅ－139、Ｃｅ－141，Ｃｅ－144，Ｈｆ－172，
Ｈｆ－175，Ｈｆ－181，Ｔａ－179、Ｔａ－182，Ｗ－181，Ｗ－185，
Ｗ－188、Ｐｔ－193，Ａｕ－195　、Ｔｌ－204，

３群　Ｐ－32，Ｐ－33，Ｓ－35，Ｖ－48，Ｃｒ－48，Ｍｎ－52，Ｃａ－47，
Ｆｅ－52，Ｆｅ－55，Ｆｅ－59，Ｎｉ－57，Ｎｉ－66，Ｃｕ－64，
Ｃｕ－－67，Ｚｎ－62，Ｚｎ－69m，Ｚｎ－72，Ｇｅ－69，Ｇｅ－77，
Ａｓ－71，Ａｓ－72，Ａｓ－74，Ａｓ－76，Ａｓ－77，Ｓｒ－82，
Ｓｒ－91，Ｙ－87，Ｙ－90，Ｙ－93，Ｚｒ－89，Ｚｒ－97，Ｎｂ－90，
Ｍｏ－99、Ｔｃ－95，Ｔｃ－96，Ｔｃ－99m，Ｐｄ－100，Ｐｄ－103，
Ｐｄ－109、Ａｇ－111、Ｓｎ－121，Ｓｎ－125，Ｓｂ－119，Ｓｂ－120，
Ｓｂ－122，Ｓｂ－126，Ｓｂ－127，Ｓｂ－128，Ｃｓ－129，Ｃｓ－131，
Ｃｓ－132，Ｃｓ－136，Ｎｄ－147，Ｔａ－183、Ｗ－－178，Ｗ－187，
Ｐｔ－188，Ｐｔ－191，Ｐｔ193m，Ｐｔ－195m，Ｐｔ－197，
Ａｕ－196，Ａｕ－198，Ａｕ－199

４群　Ｈ－3，Ｃ－14

３、形状、取扱い量

別紙

Schematic Layout of Beam Line for RI and Actinoid experiments (BL-27)

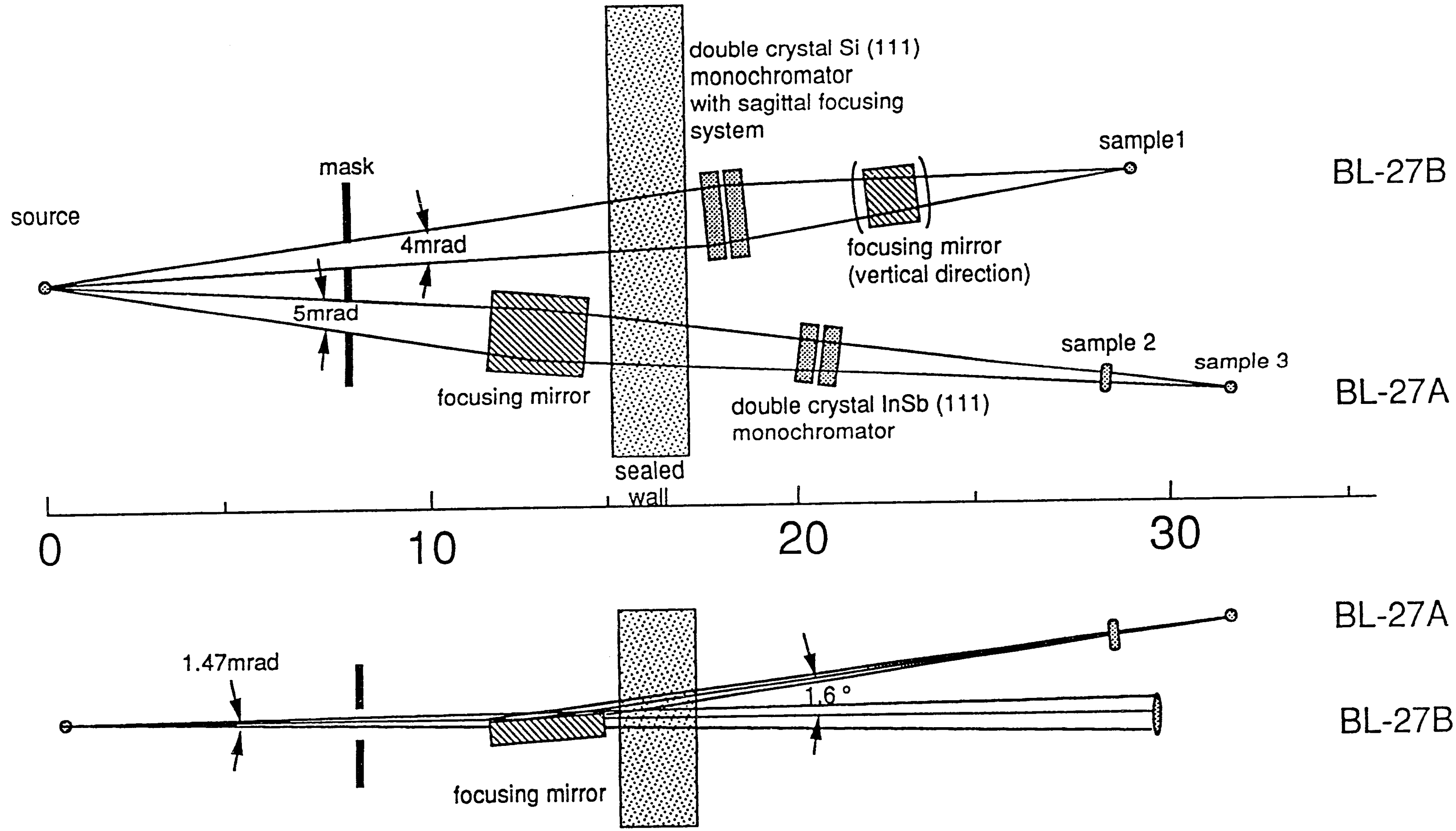

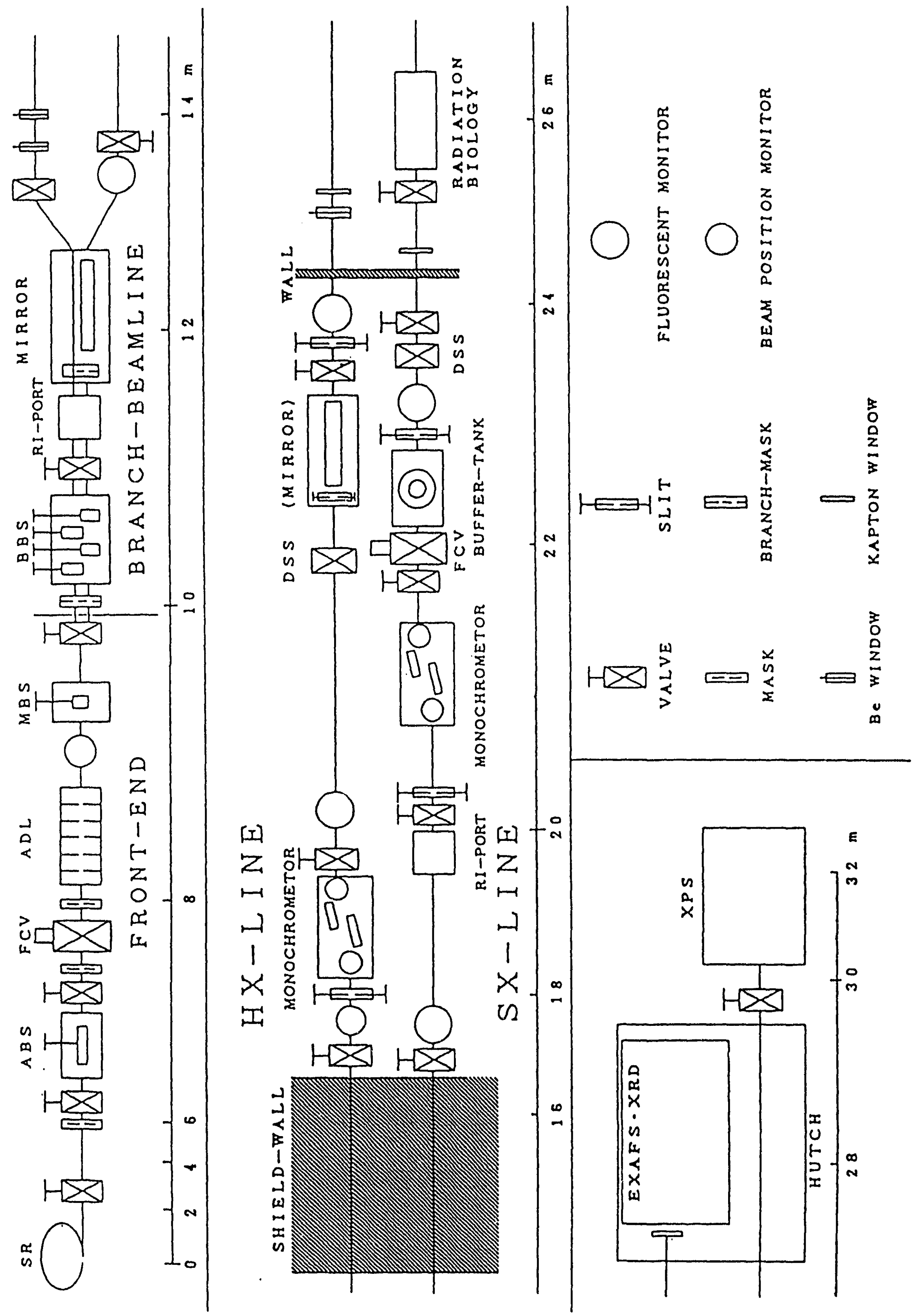
SR
ABS
FCV
ADL
MBS
BBS
RI-PORT
MIRROR
FRONT-END
BRANCH-BEAMLINE
0
2
4
6
8
10
12
14 m
SHIELD-WALL
HX-LINE
MONOCHROMETOR
DSS
(MIRROR)
WALL
SX-LINE
RI-PORT
MONOCHROMETOR
FCV
BUFFER-TANK
DSS
RADIATION
BIOLOGY
16
18
20
22
24
26 m
EXAFS·XRD
HUTCH
XPS
28
30
32 m
VALVE
SLIT
FLUORESCENT MONITOR
MASK
BRANCH-MASK
BEAM POSITION MONITOR
Be WINDOW
KAPTON WINDOW

カプトン窓概観図
(Kupton Window for Soft X-ray Beamline)

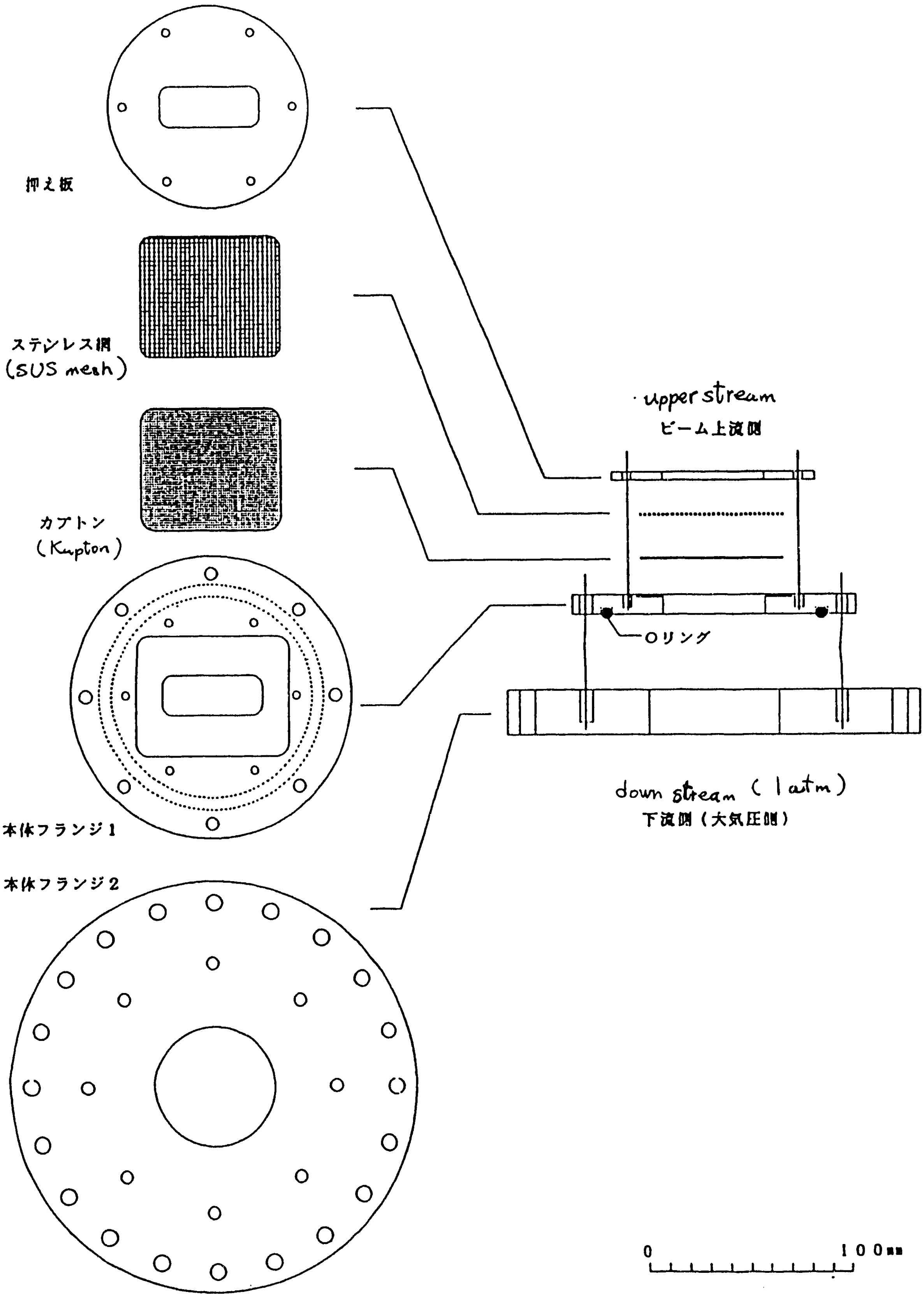

Kapton Window

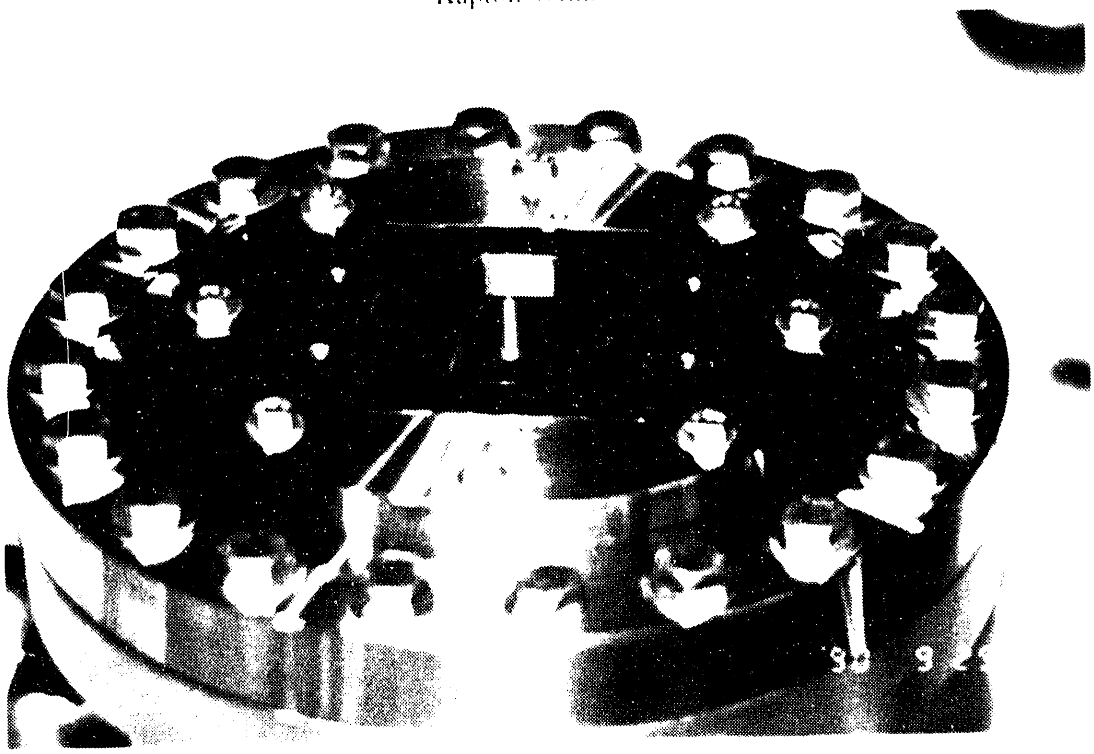

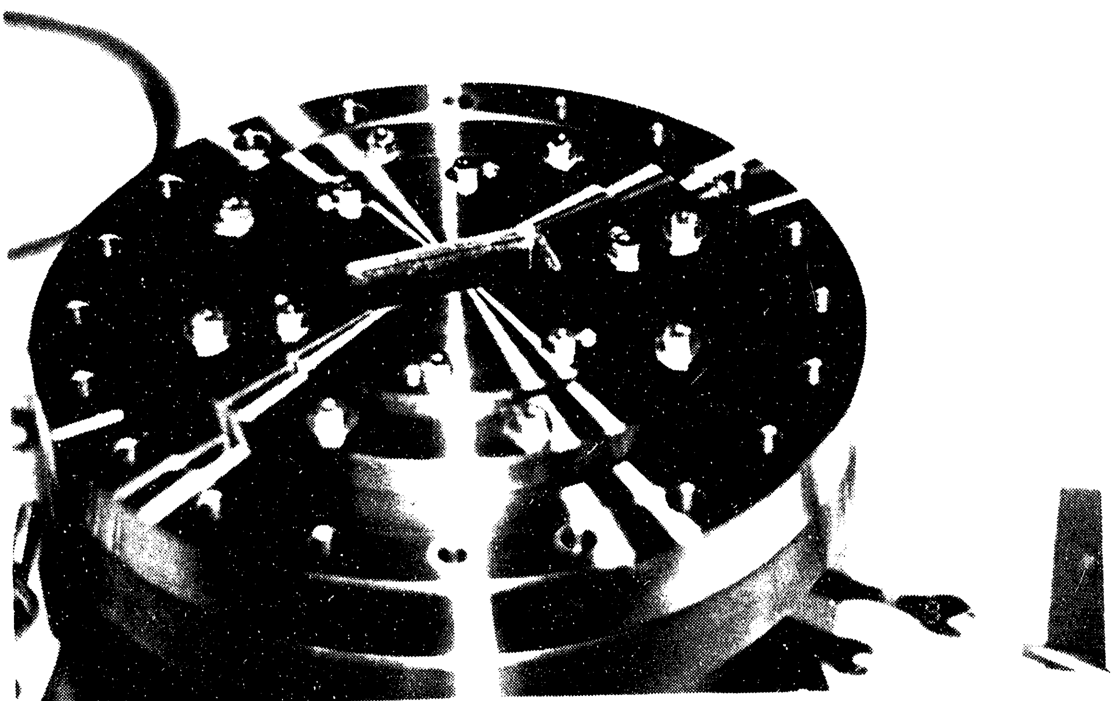

CBB 9210-8166

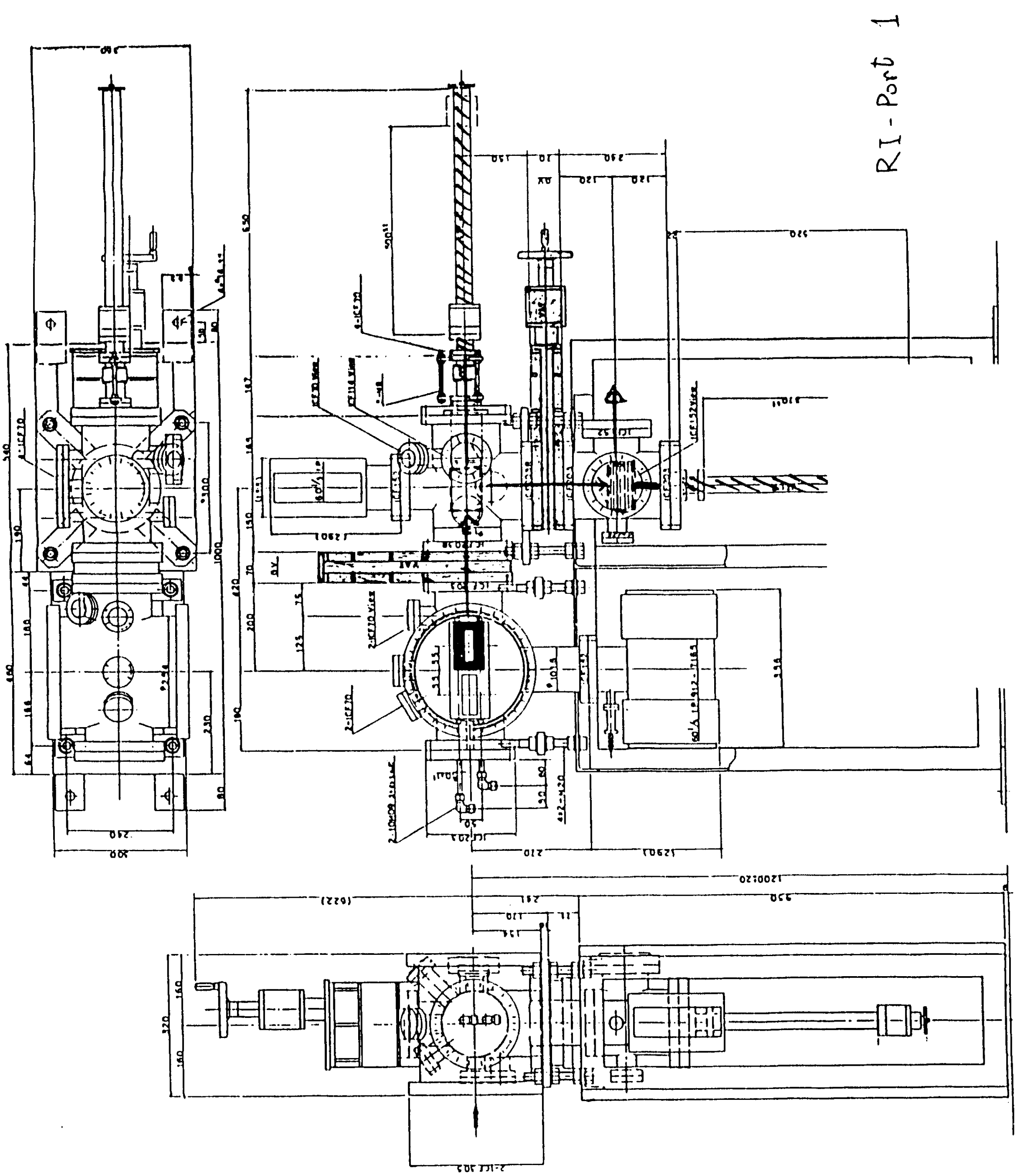
RI-Port 1

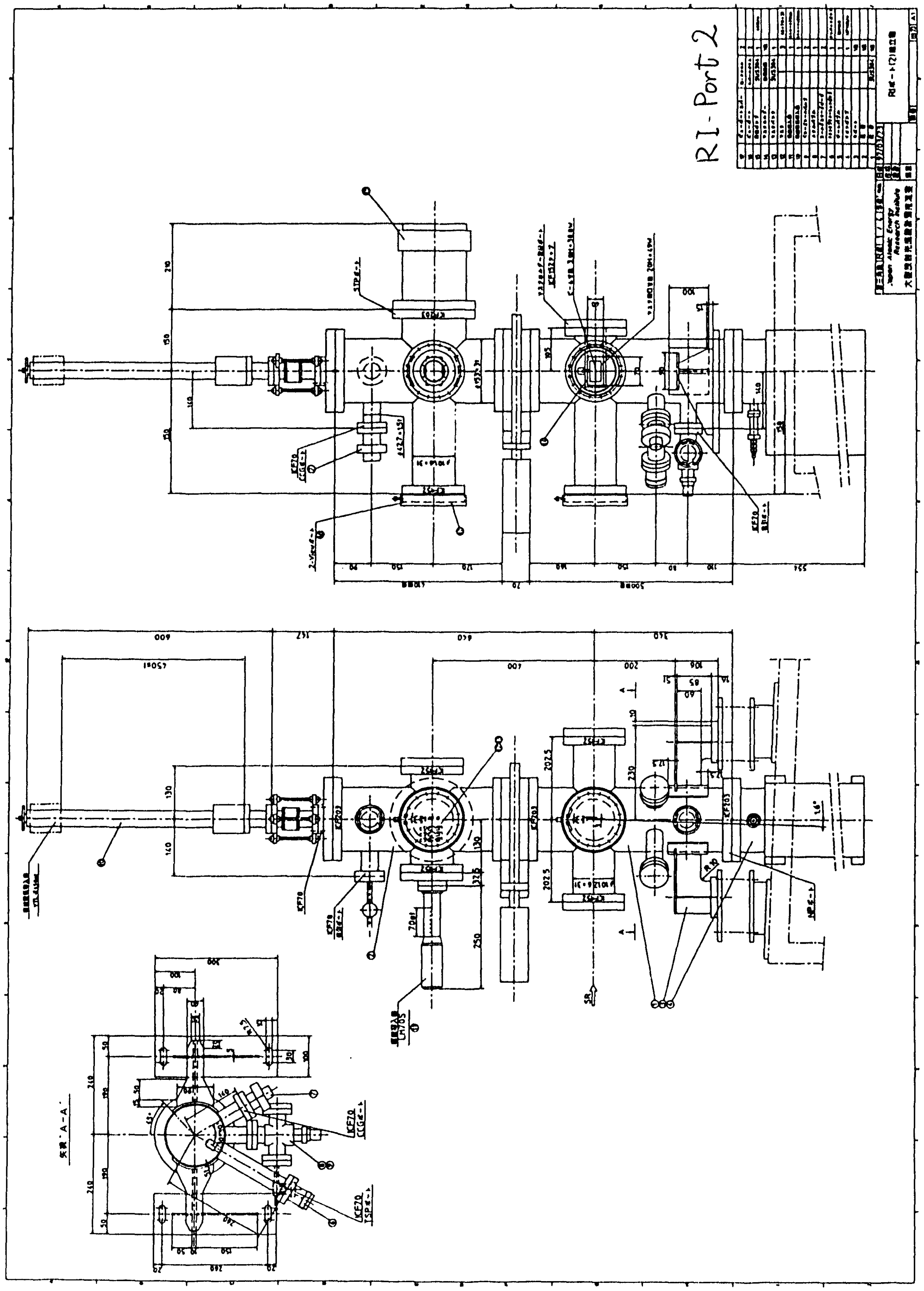
RI-Port 2

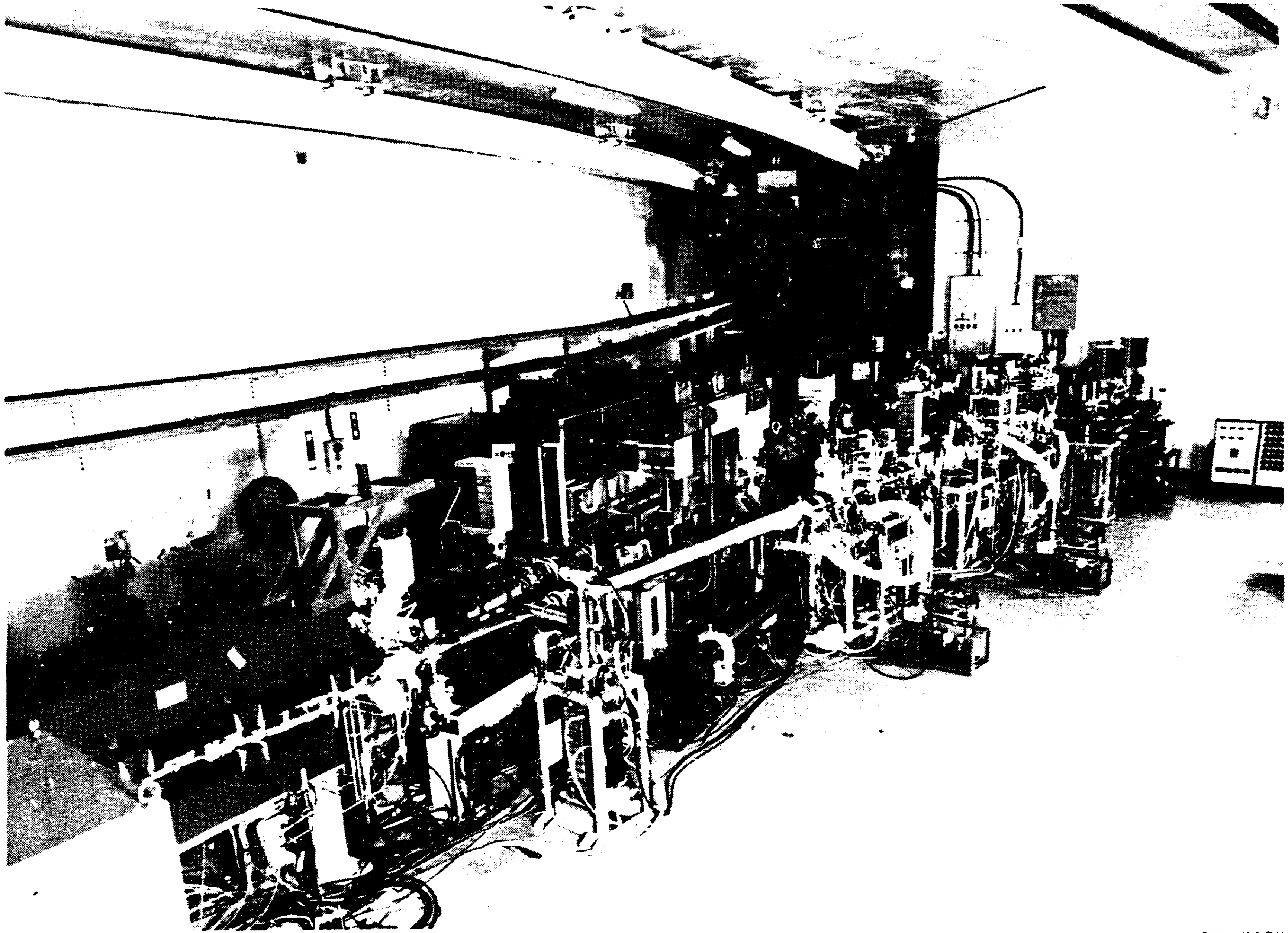

CBB 9210-8128

Front End of BL-27

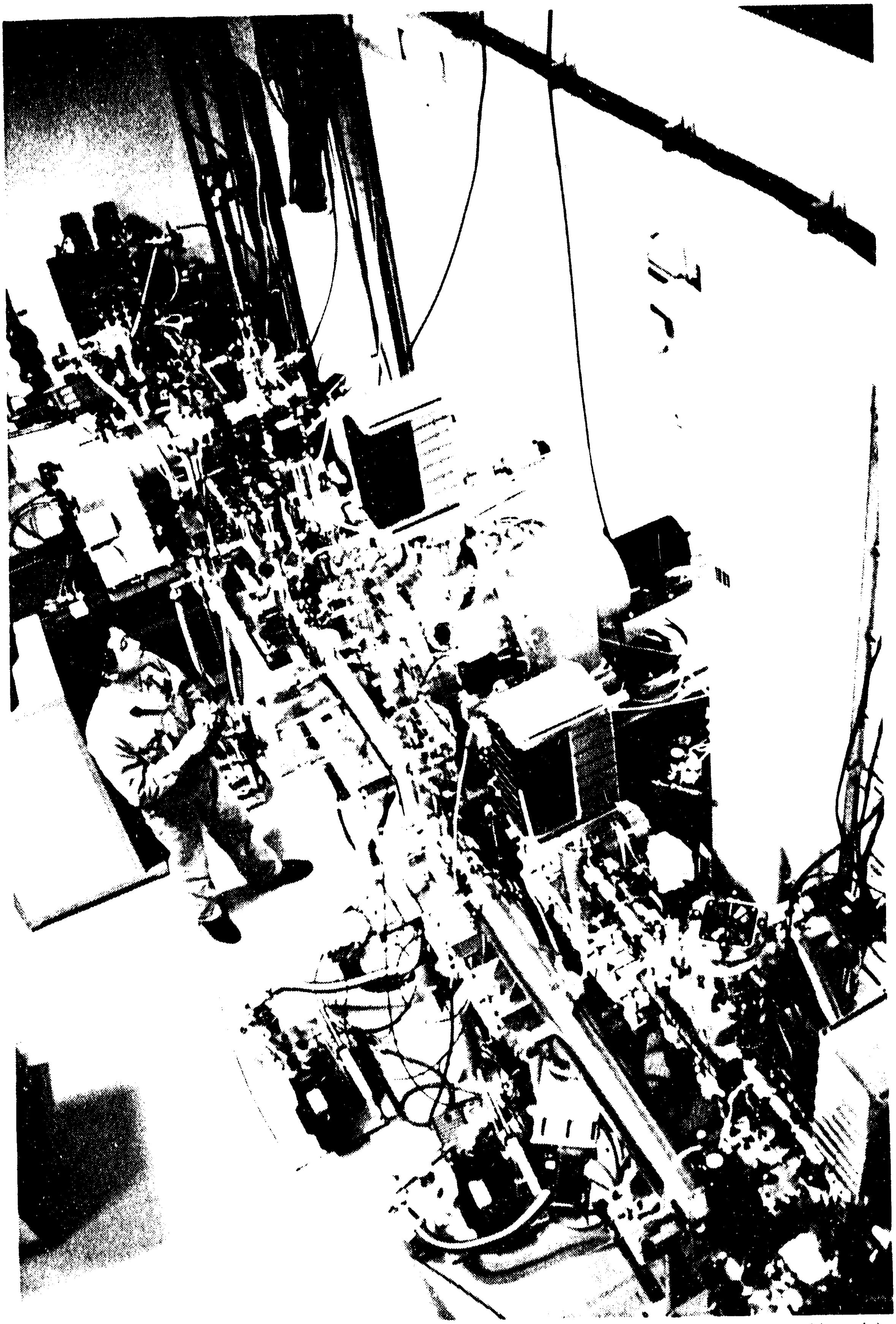

CBB 9210-8136

Downstream Parts of BL [illegible]

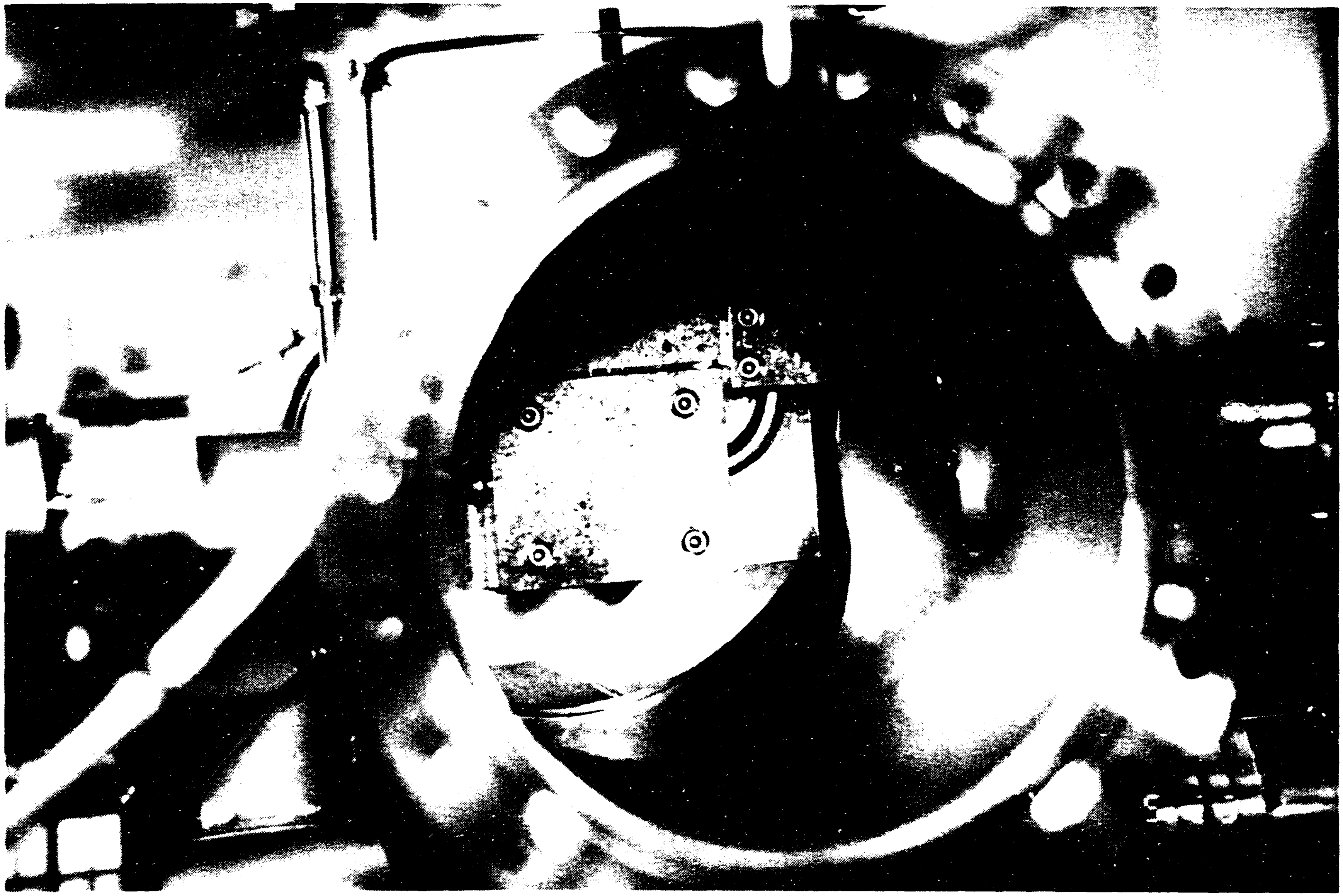

CBB 9210-8132

Backside view of ABS

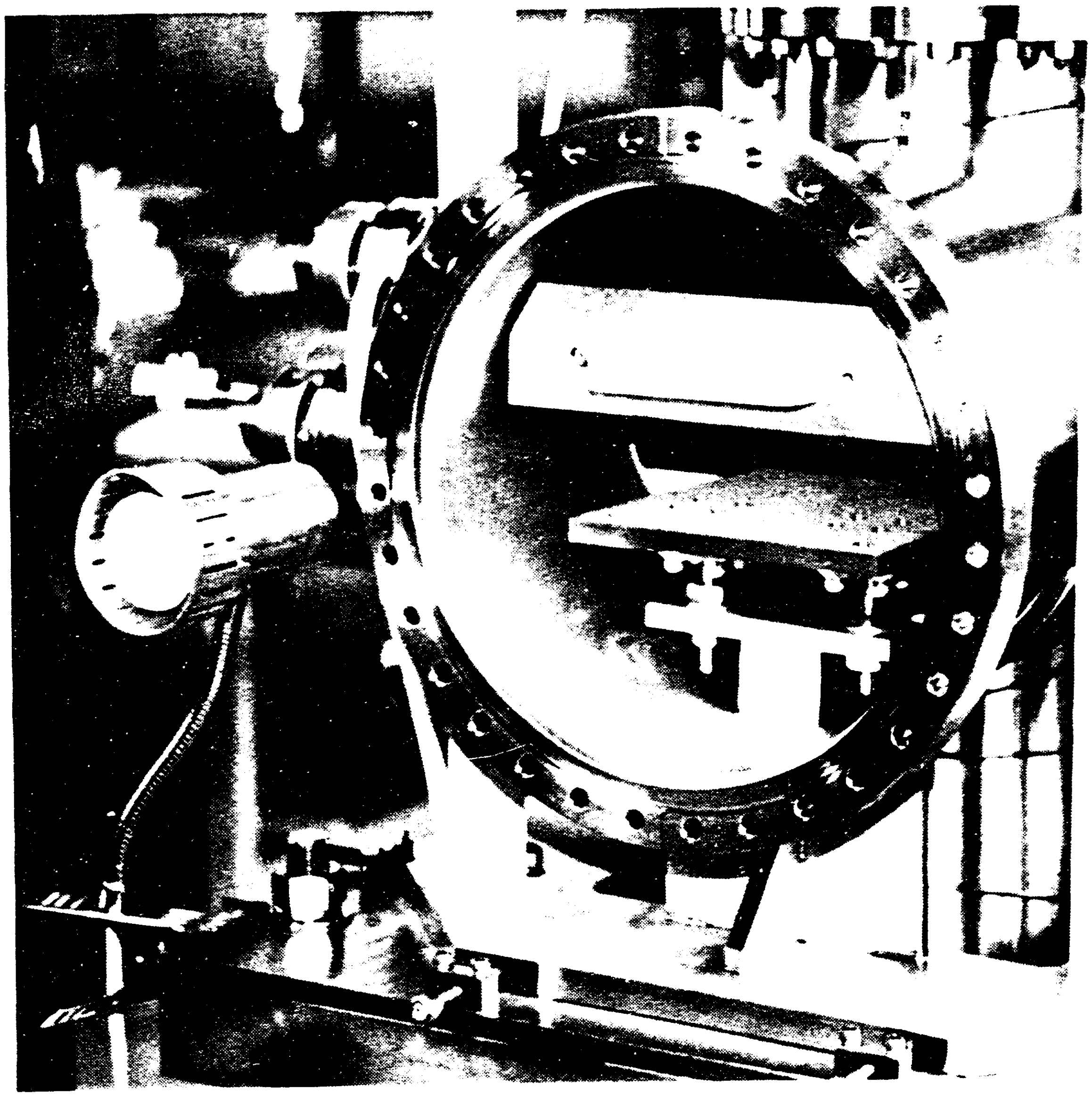

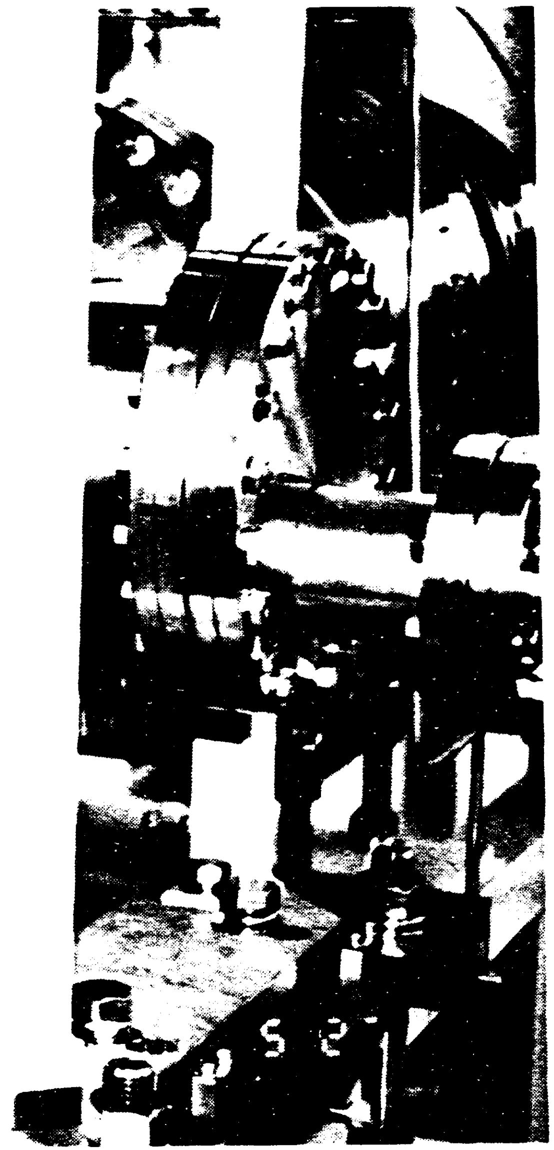

CBB 9210-8134

Main Beam Shutter MBS

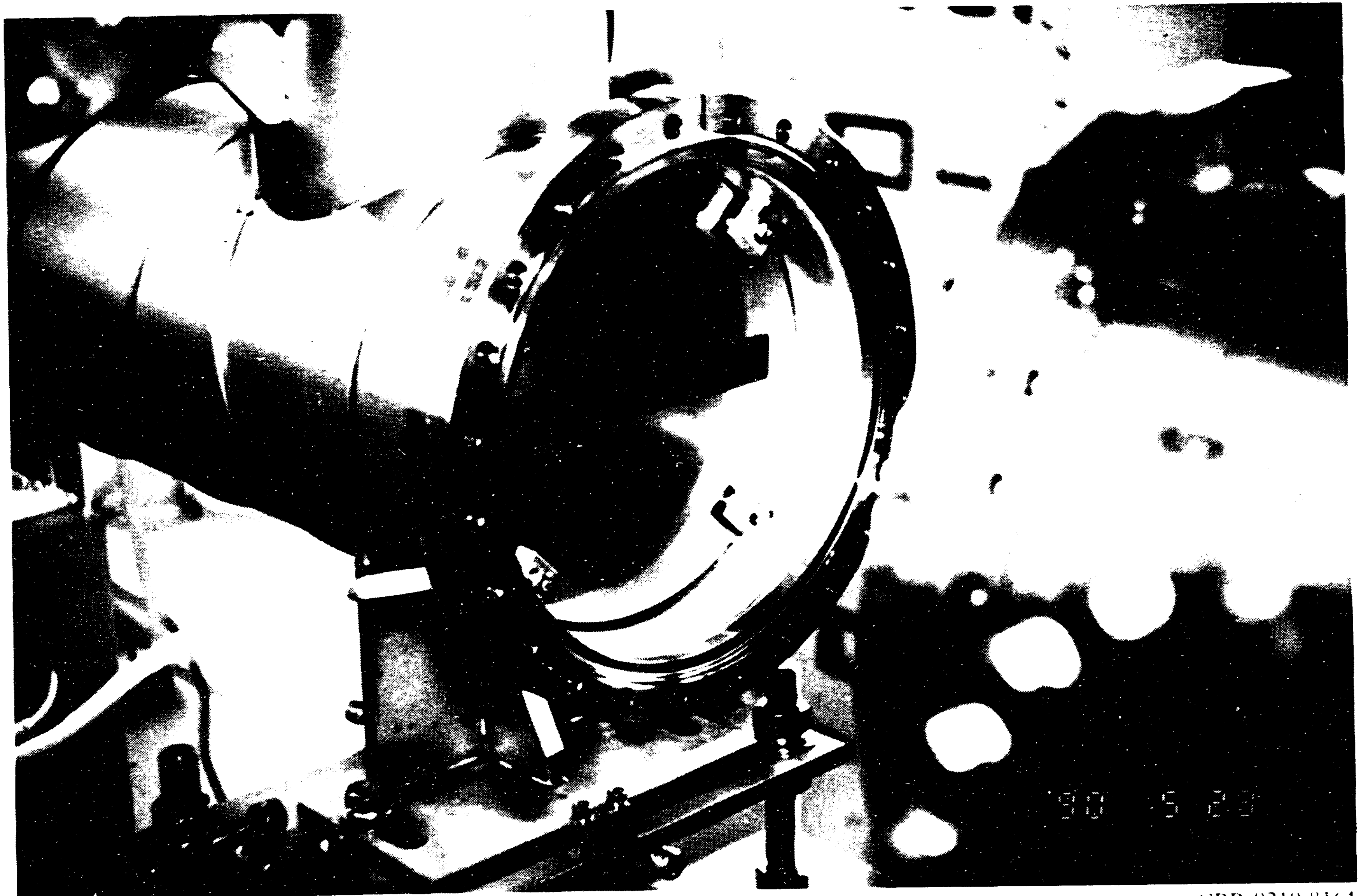

CBB 9210-8164

ADI

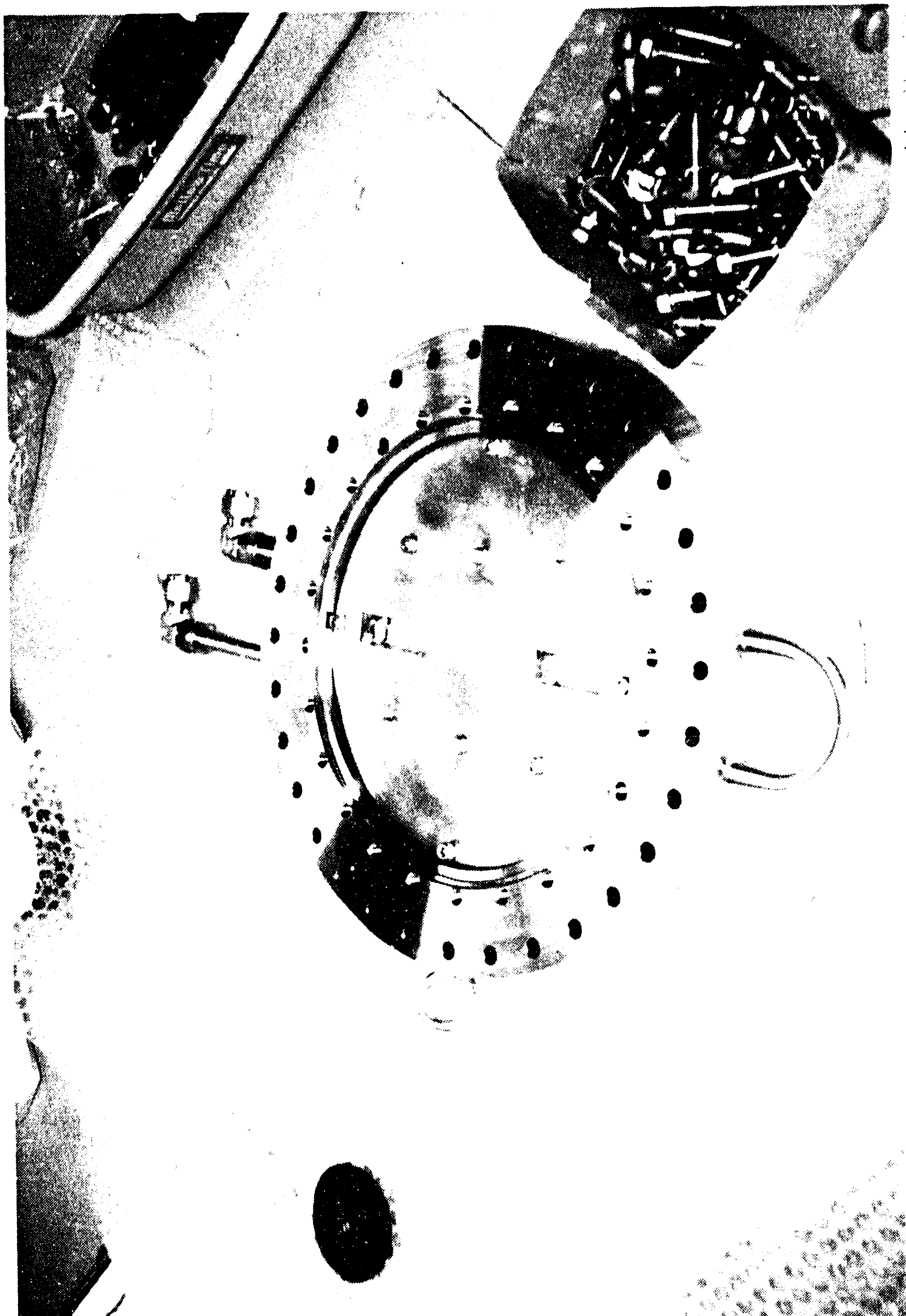

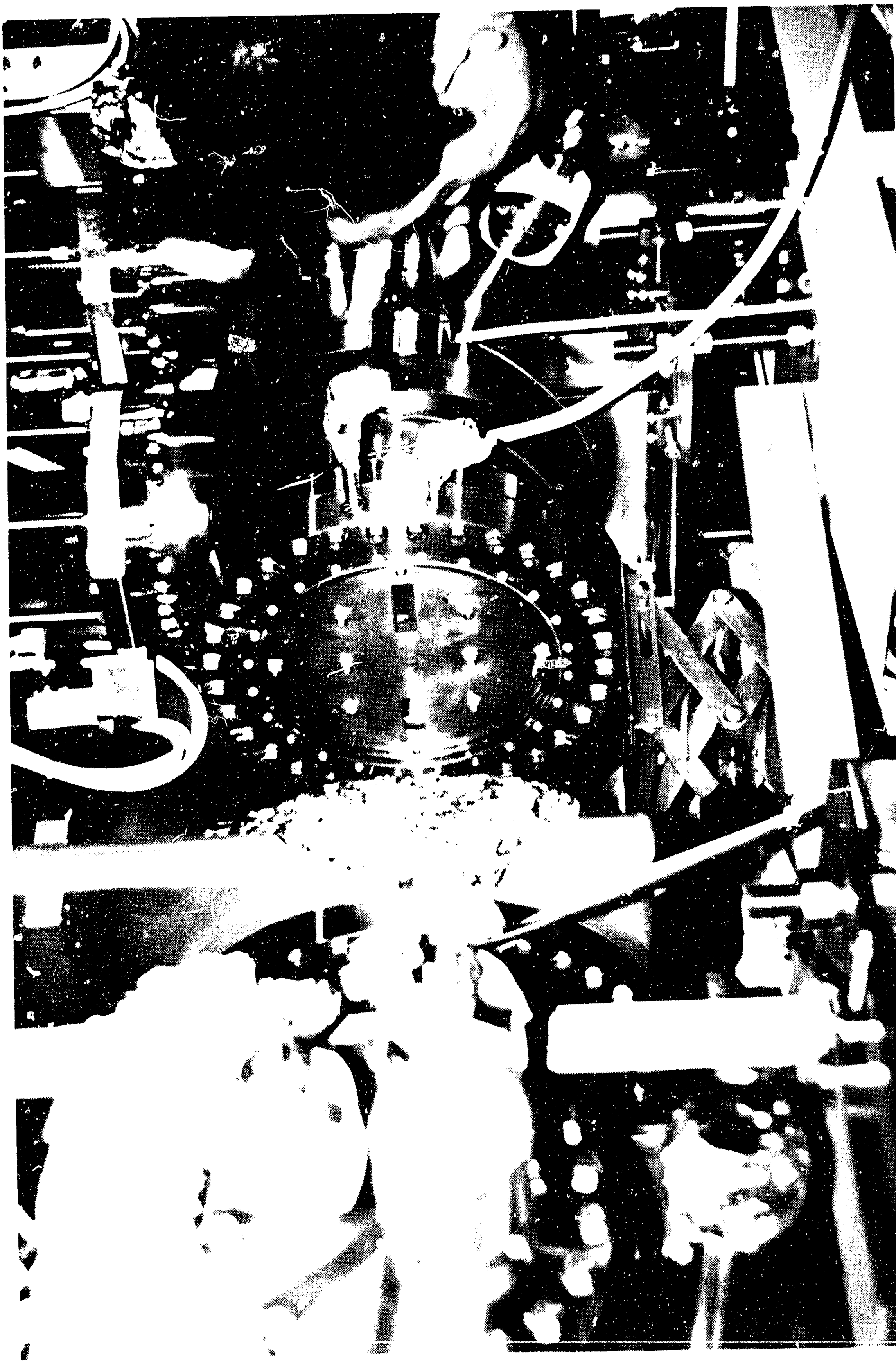

CBB 9210-8138

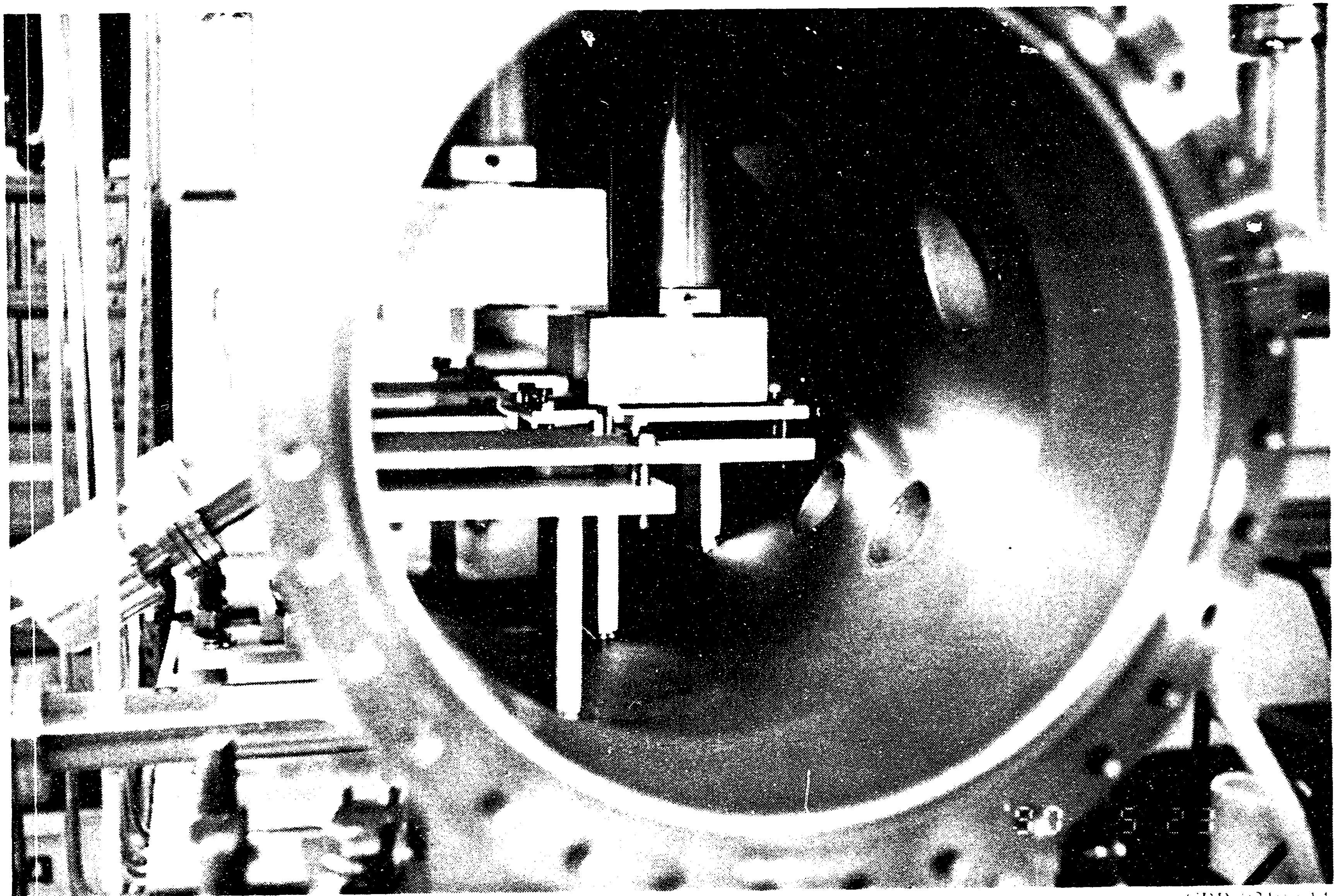

CBB 9210-8140

Frontside View of BBS (Branch Beam Shutter)

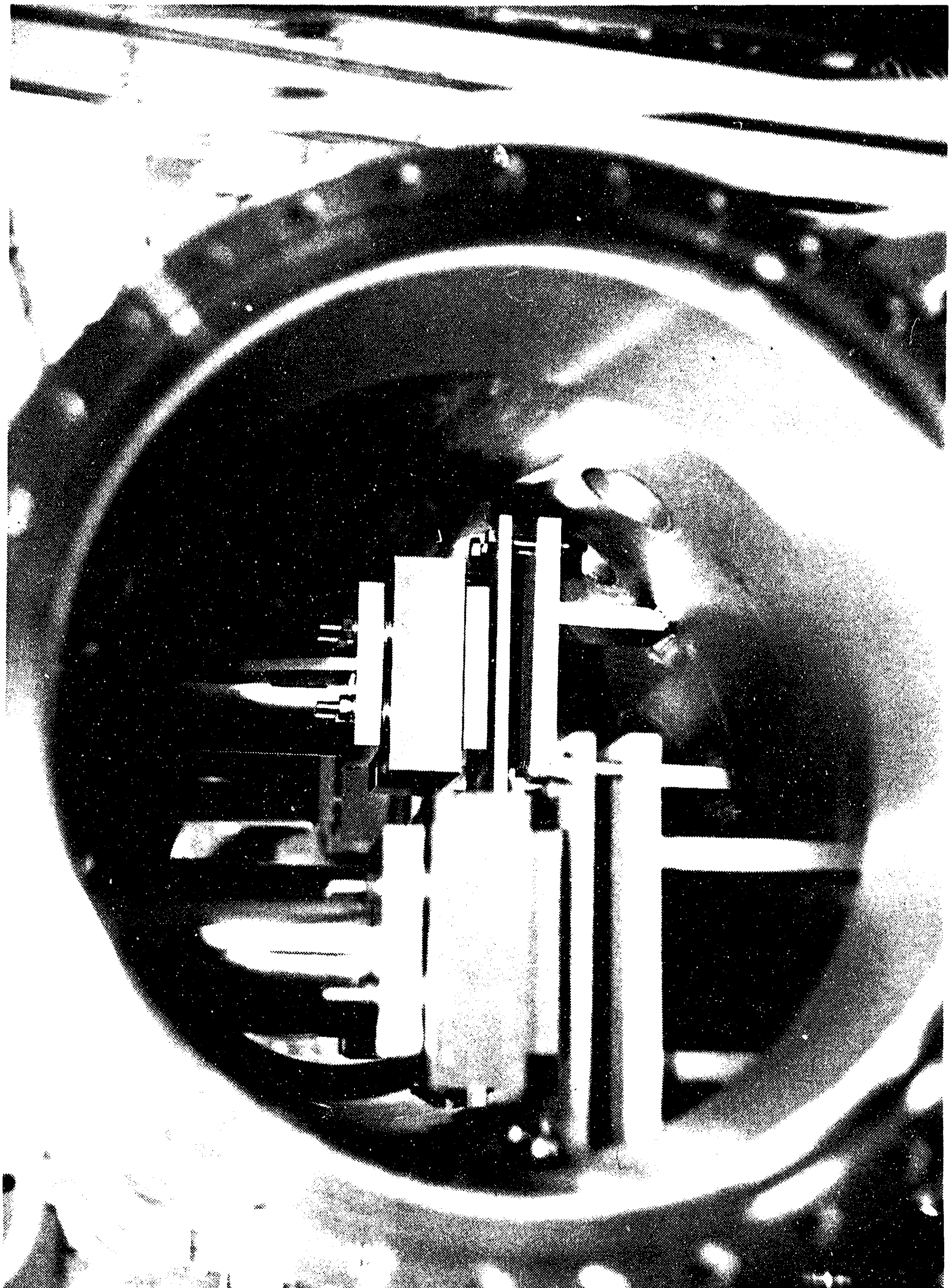

CBB 9210-8142

Backside view of BBS

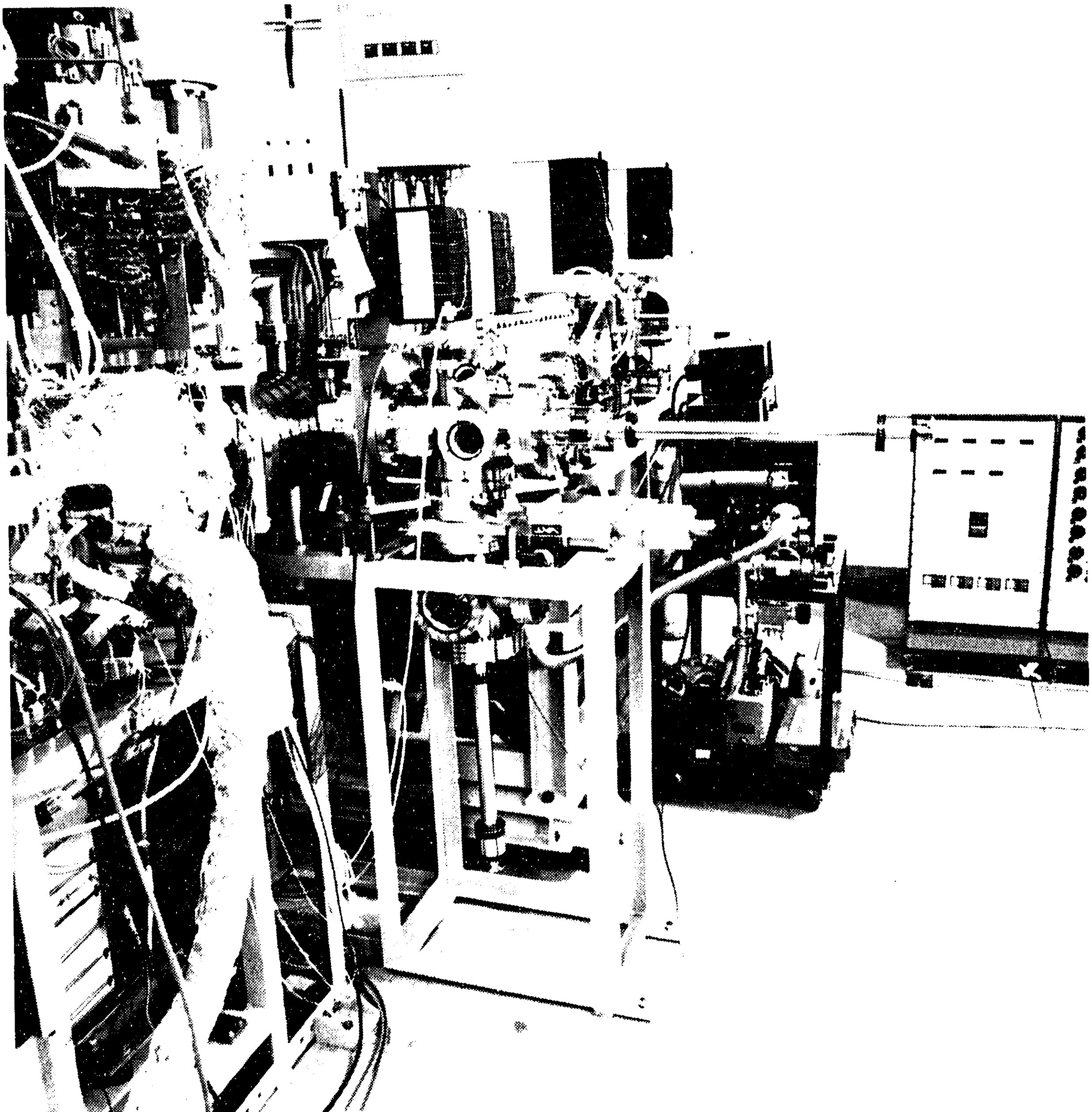

CBB 9210-8144

RI-Port 1

CBB 9210-8146

Inside of RI-Port

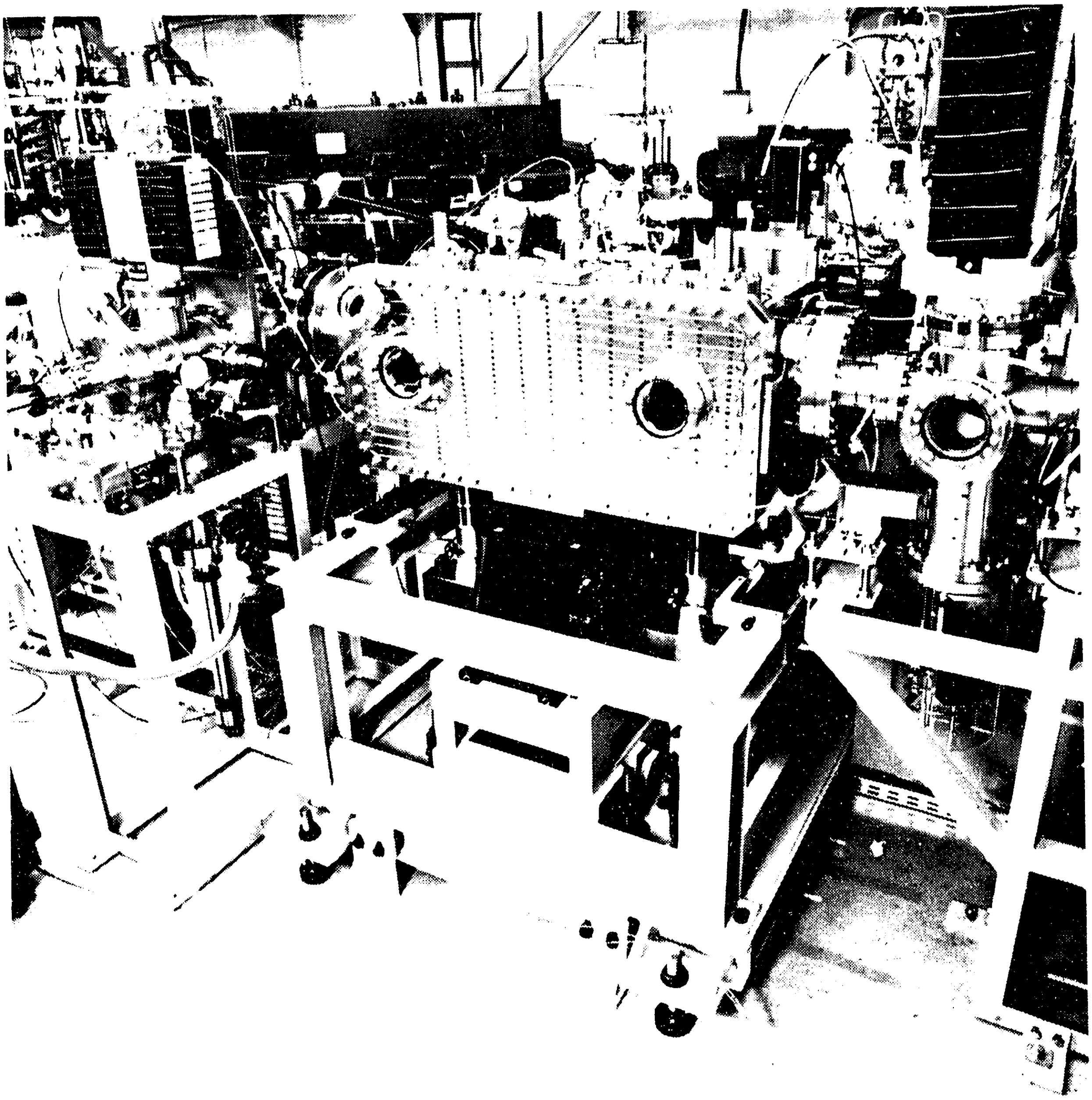

CBB 9210-8148

Mirror Chamber

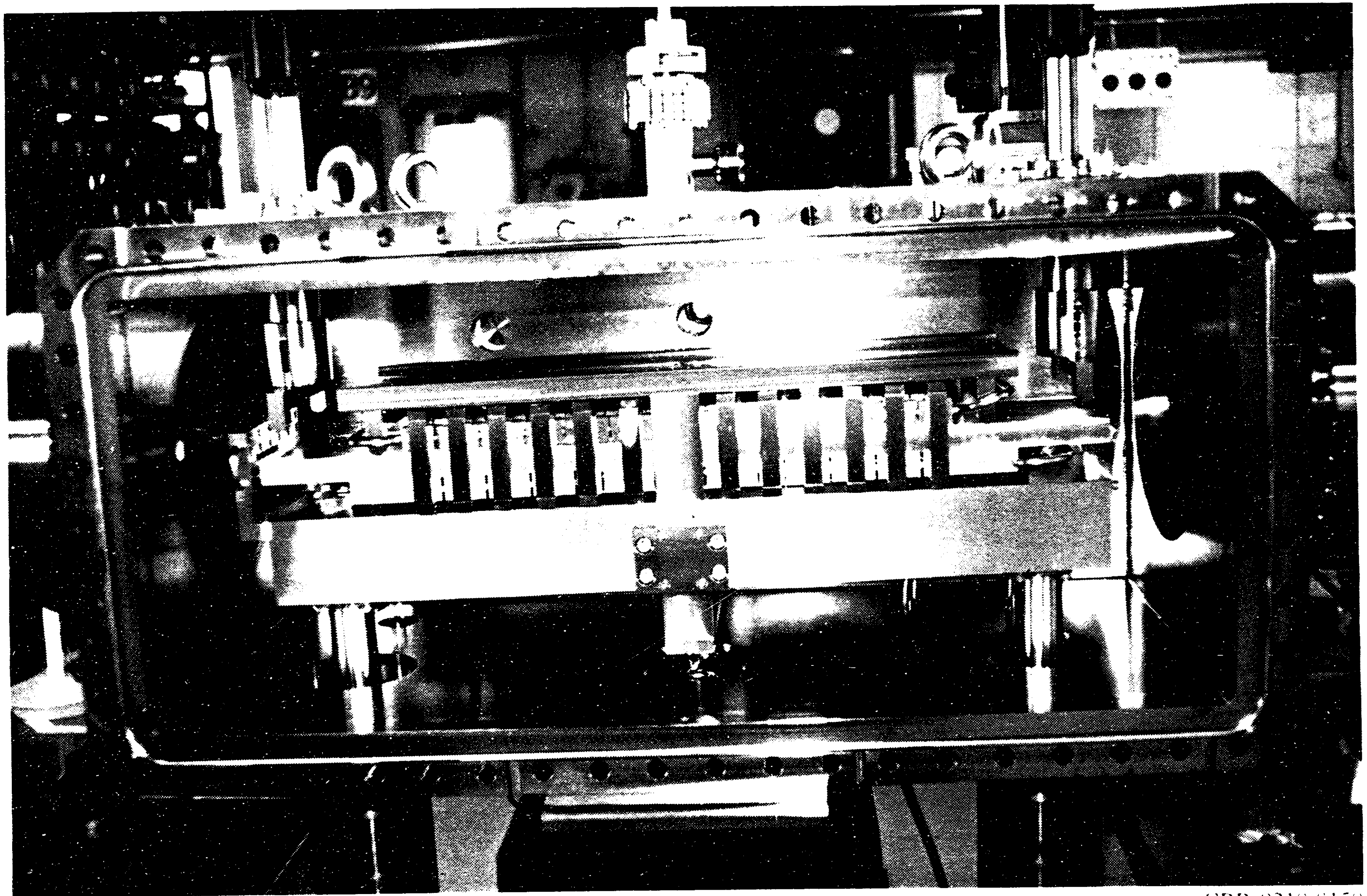

CBB 9210-8150

Inside of Mirror Chamber

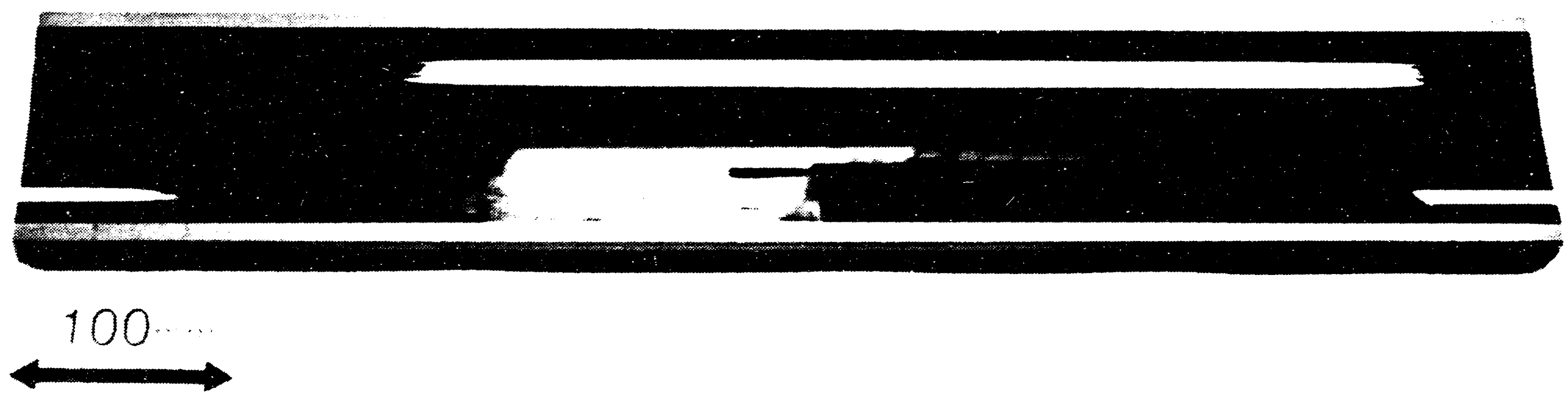

SiC Mirror

CBB 9210-8152

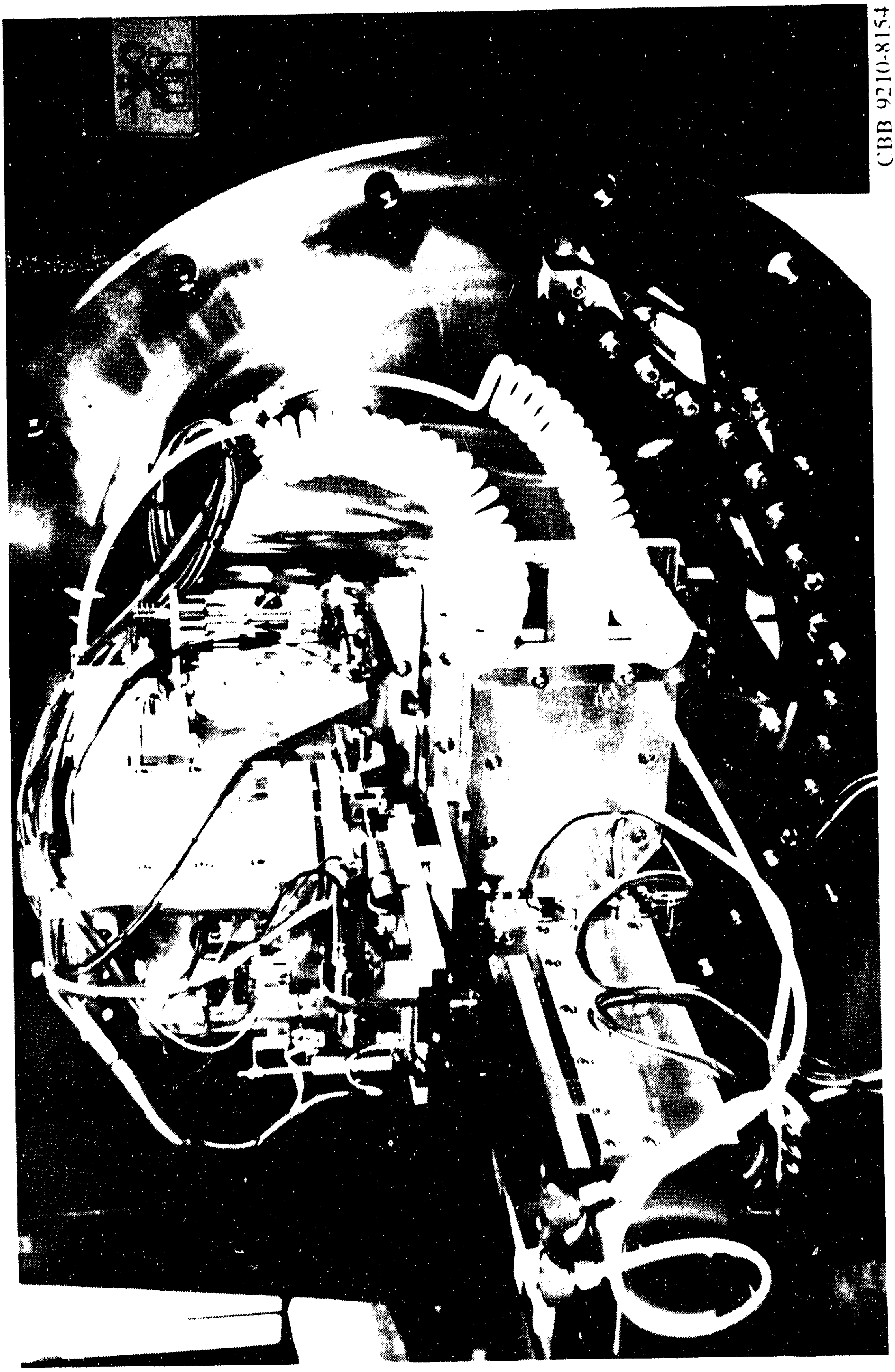

CBB 9210-8154

Hard X-Ray Monochromator

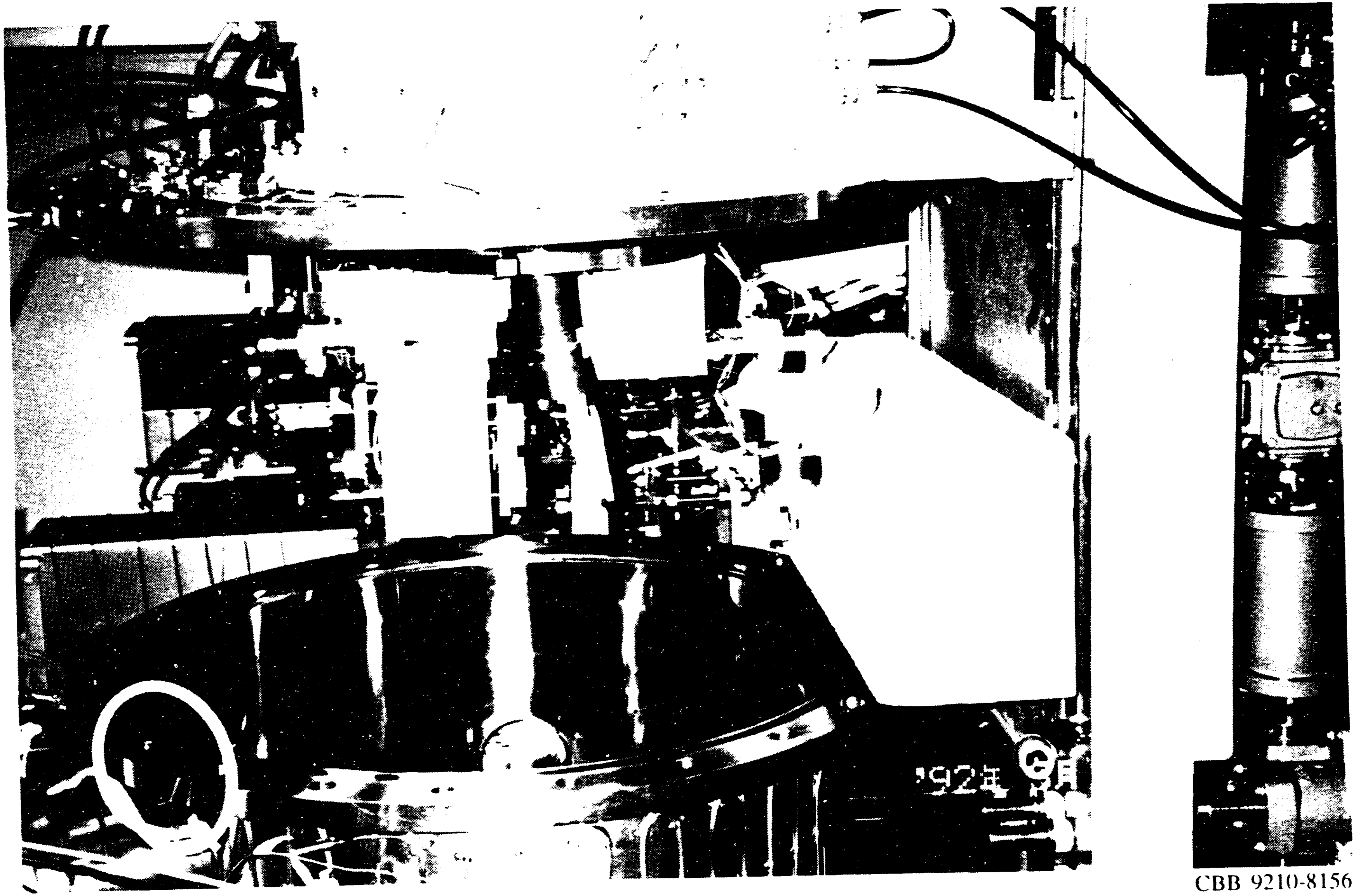

CBB 9210-8156

Soft X-Ray Monochromator

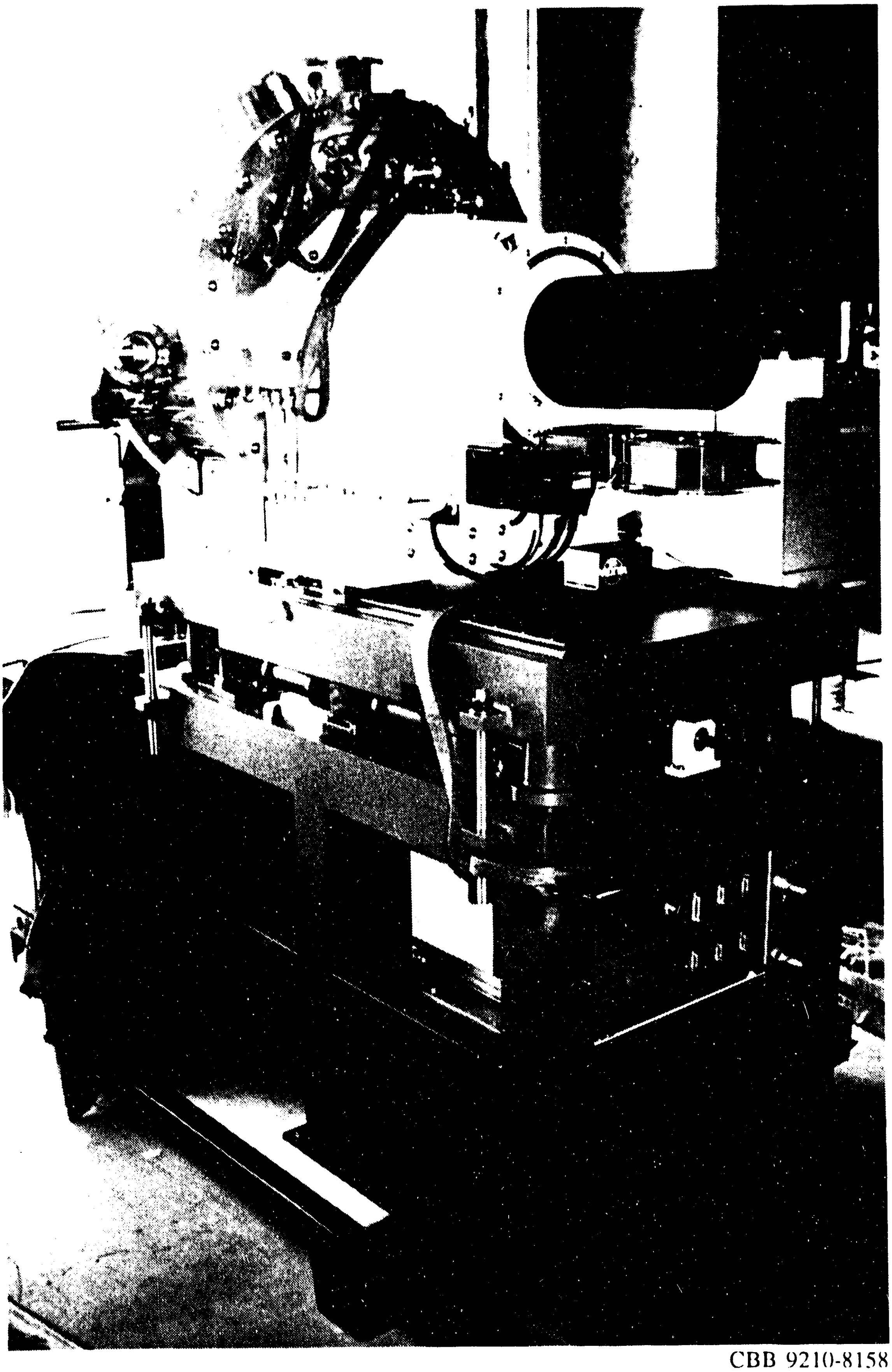

CBB 9210-8158

Soft X-Ray Monochromator with Heat Pipe

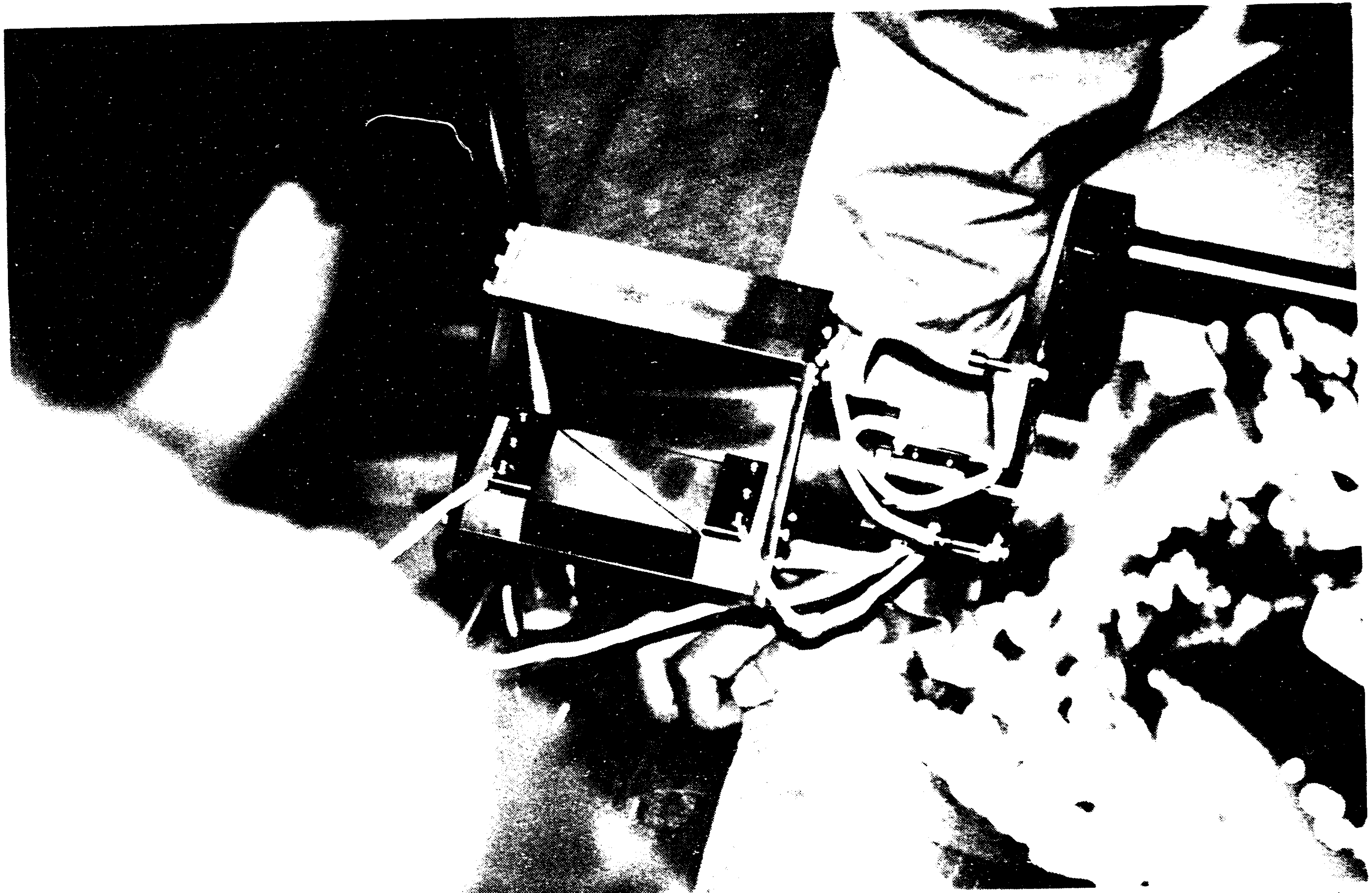

CBB [illegible]

Beam Position Monitor

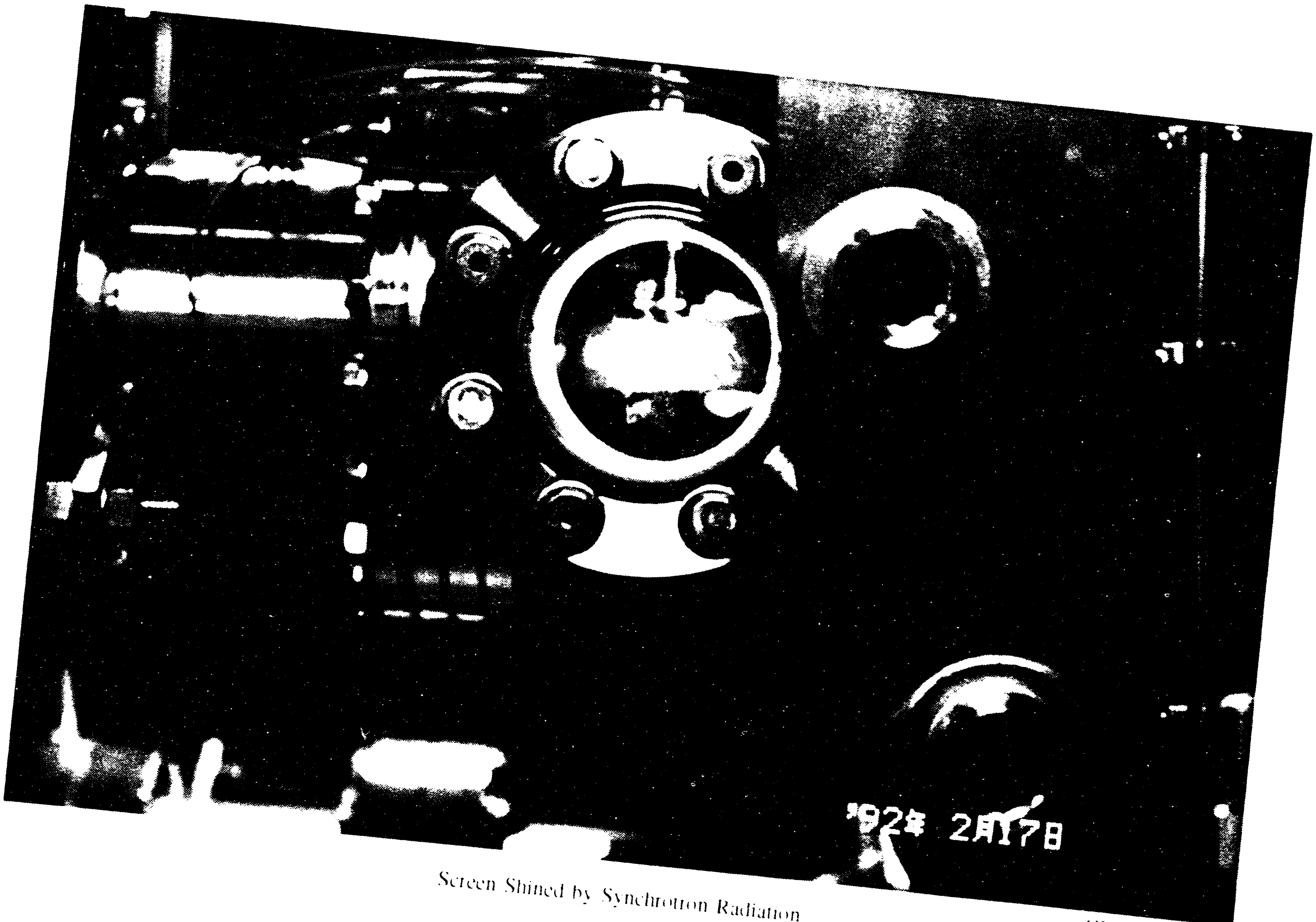

Screen Shined by Synchrotron Radiation

CBB 9210-8162

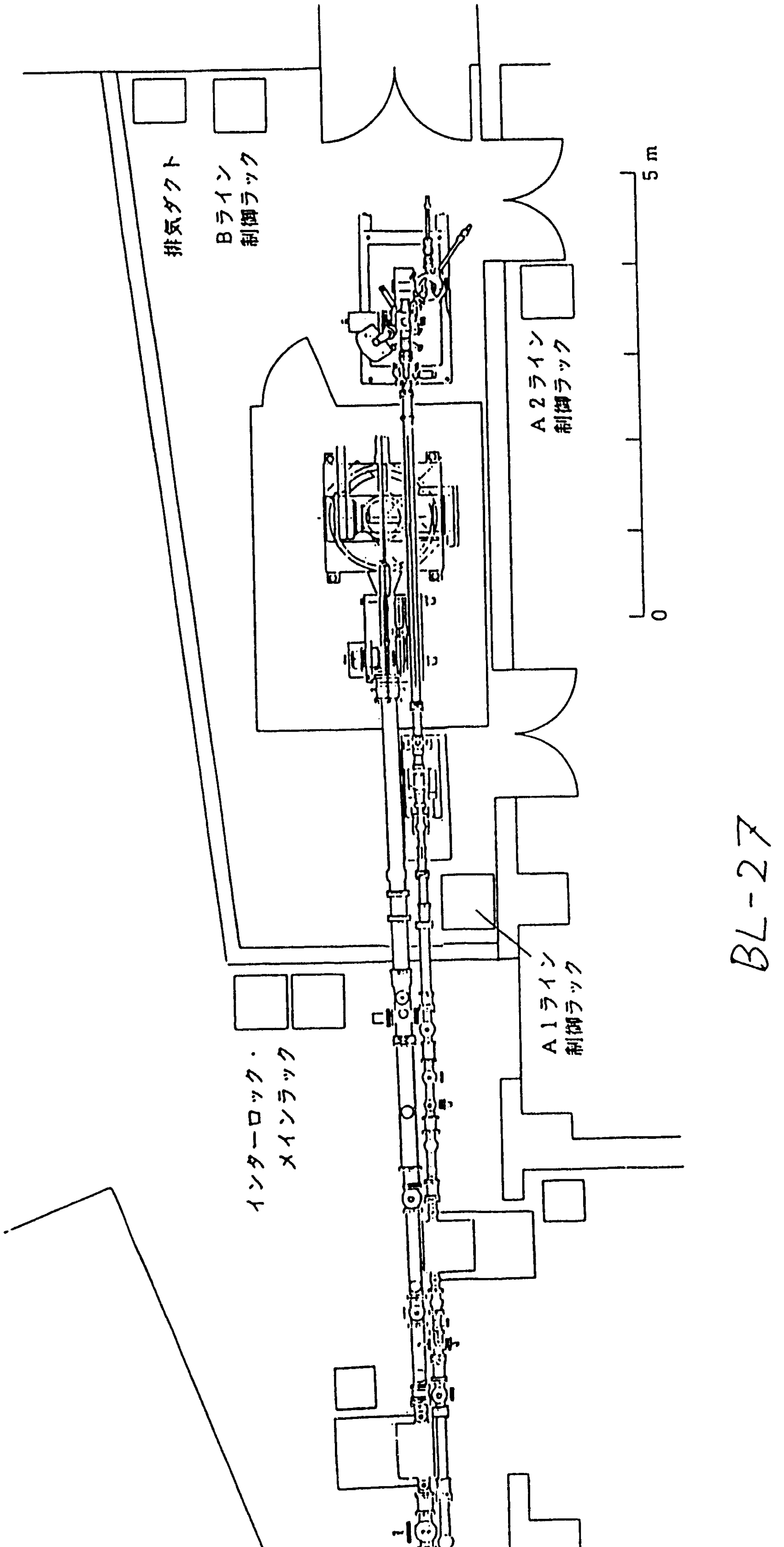
排気ダクト
Bライン
制御ラック
A２ライン
制御ラック
A１ライン
制御ラック
インターロック・
メインラック
5 m
0
BL-27

Abstract for the ALS Workshop on "*Synchrotron Radiation in Transactinium Research*," October 1–2, 1992, Berkeley, California

"The Search for X-Ray Absorption Magnetic Circular Dichroism in Actinide Materials: Preliminary Experiments using UFe_2 and U–S"

J.G. Tobin, G.D. Waddill, T. Gouder, and C. Colmenares, Department of Chemistry and Materials Science, Lawrence Livermore National Laboratory, Livermore, California

Recently we began a series of experiments using near-edge-x-ray-absorption-fine structure (NEXAFS) looking for magnetic-circular-dichroism (MCD) in the magnetic actinide materials UFe_2 and U–S. These experiments were performed at SSRL using the University of California/National Laboratories PRT Beamline 8–2[1,2]. This SGM beamline permits us to access the 2p → 3d transition of Fe (B^F = 707, 720 eV) and the 4d → 5f transition of U (B^F = 736, 778 eV). Absorption experiments with circularly-polarized x-rays[2] should allow direct, elementally-specific interrogation of the magnetic and related electronic structure of these materials, in analogy with the results from magnetic x-ray scattering[3]. Our initial experiments utilized NEXAFS[4], but in the future they will also be expanded to include core-level photoemission[5] as well. The preliminary results for these systems will be presented, as well as a simplified, single-electron theoretical framework for approximate spin analysis of NEXAFS-MCD[4,6,7]. The limitations of this approach will be discussed in light of results from many-body calculations[8].

Finally, we will describe how the orders-of-magnitude improvement in brightness at the ALS, plus the establishment of a dedicated transactinium facility will open the door for an unprecedented opportunity for both basic science using 5f elements, as well as improving the overall understanding of the physical and chemical properties of actinide materials.

References

1. K.G. Tirsell and V.P. Karpenko, Nucl. Instrum. Meth., A291, 511 (1990).
2. L.J. Terminello, G.D. Waddill, and J.G. Tobin, Nucl. Instrum. Meth. (1992).
3. D.B. McWhan, C. Vettier, E.D. Isaacs, G.E. Ice, D.P. Siddons, J.B. Hastings, C. Peters, and D. Vogt, Phys. Rev. B 42, 6007 (1990).
4. J.G. Tobin, G.D. Waddill, and D.P. Pappas, Phys. Rev. Lett., 68, 3642 (1992).
5. G.D. Waddill, J.G. Tobin, and D.P. Pappas, Phy. Rev. B–Rapid Comm., 46, 552 (1992).
6. J.G. Tobin, G.D. Waddill, P.A. Sterne, and D.P. Pappas, In preparation.
7. J.G. Tobin and G.D. Waddill, submitted to Phys. Rev. B–Rapid Comm., 1992.
8. H. Ogasawara, A. Kotani, and B.T. Thole, Phys. Rev. B 44, 2169 (1991).

Acknowledgements

This work was performed under the auspices of the U.S. Department of Energy by Lawrence Livermore National Laboratory under contract number W-7405-ENG-48. This work was supported by Karen Clark.

The Search for X-Ray Absorption Magnetic Circular Dichroism in Actinide Materials: Preliminary Experiments using UFe_2 and S/U

James G. Tobin
Chemistry and Materials Science Department
Lawrence Livermore National Laboratory

Collaborators
G.D. Waddill, LLNL
T. Gouder, LLNL
C.A. Colmenares, LLNL
A.Chaiken, LLNL
A. Jankowski, LLNL

ALS Workshop on "Synchrotron Radiation in Transactinium Research"
October 1–2, 1992, Berkeley, CA

X-ray absorption magnetic circular dichroism in actinide materials

- Preliminary study
  - Polycrystalline UFe_2 and sulphur on polycrystalline U at SSRL

- Magnetic uranium compounds
- Beamline 8–2 at SSRL (moving to ALS)
- MCD effects in x-ray absorption and photoemission
  - Experiments with 3d materials
  - Projections for 5f systems
- Photoemission of S/U and UFe_2
- Near-edge x-ray absorption of S/U and UFe_2

Ferromagnetic uranium compounds

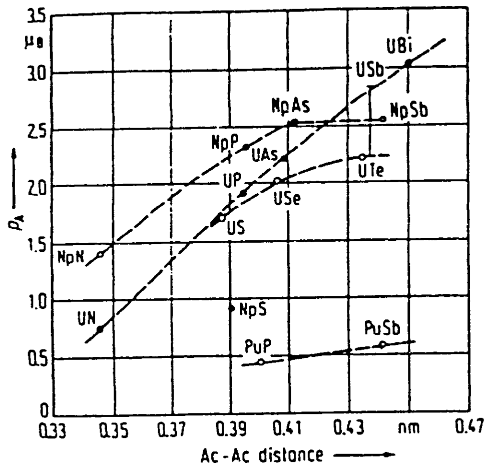

Ordered magnetic moments of actinide monopnictides and monochalcogenides. Open circles – ferromagnetic; closed circles – antiferromagnetic. From Landolt Bornstein III/12c

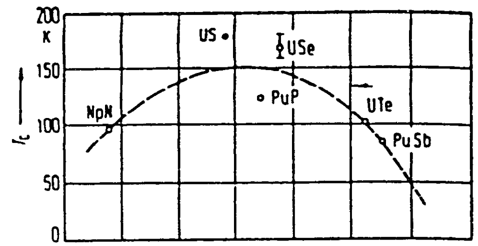

Magnetic transition temperatures of actinide monopnictides and -chalcogenides.

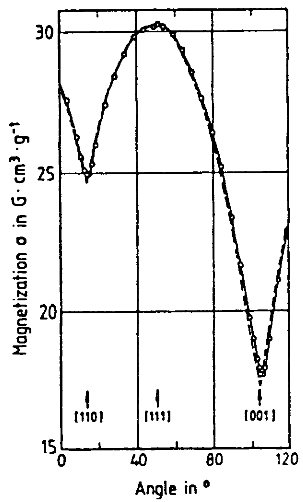

Magnetization of a uranium monosulfide crystal (specimen C1) as a function of relative angle in the (1$\bar{1}$ 0) plane at 75K. Gmelin Handbook in Inorganic Chemistry, 8th Ed.

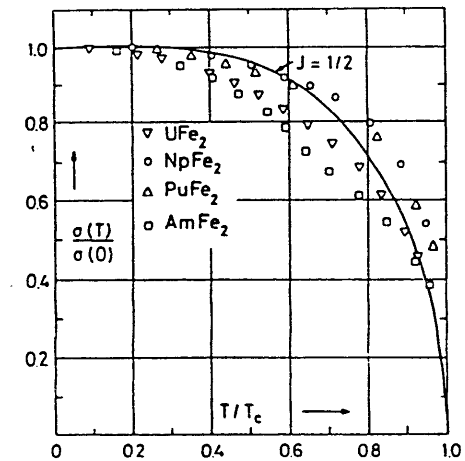

Reduced magnetization $\sigma(T)/\sigma(0)$ *vs.* reduced temperature T/T_C for four ferromagnetic AFe_2-type intermetallic compounds. "The Physics of Actinide Materials," P. Ersos and J.A. Robinson. For UFe_2; T_C = 172K

Spherical Grating Monochromator Beamline (8-2) at SSRL

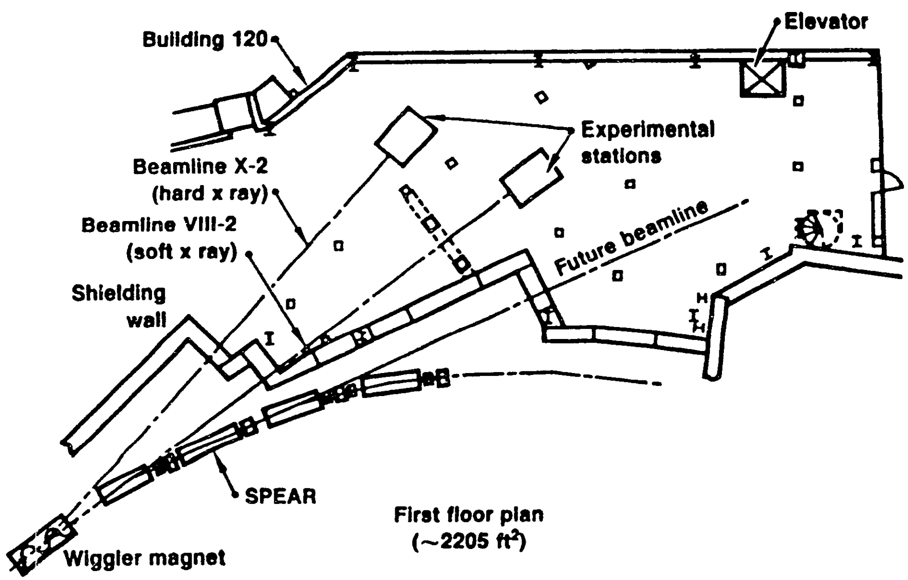

First floor plan
(~2205 ft²)

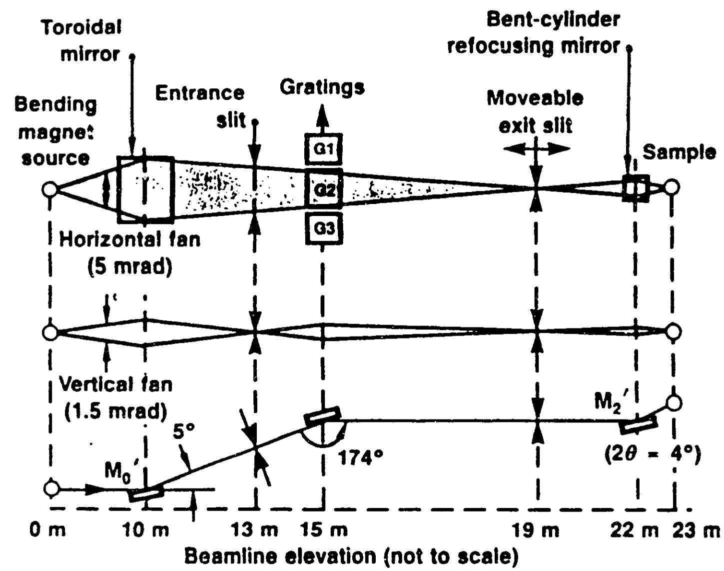

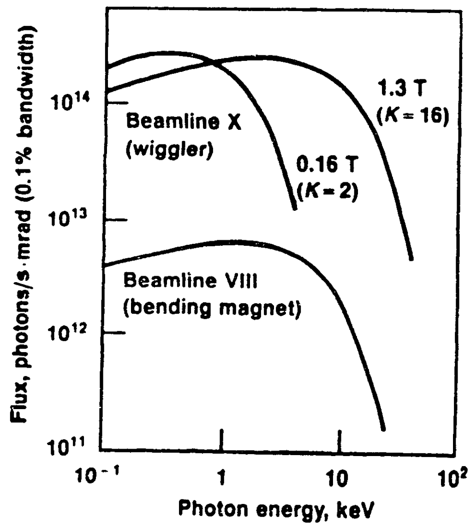

Outputs of the Beamline VIII bending magnet and Beamline X wiggler for SPEAR operating at 3 GeV and 100 mA. Changing the wiggler magnetic field (measured in teslas) changes the deflection parameter K and the output spectra.

Three Beamlines

X-2 Wiggler

VIII-1 Torroidal Grating Mono

VIII-2 Spherical Grating Mono

Nanoscale magnetics: Beamline 8–2

High resolution x-ray absorption by gases

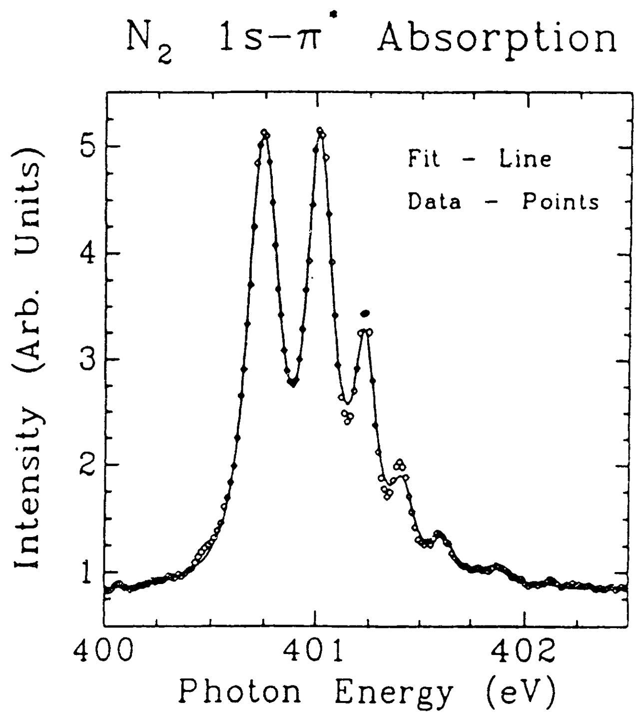

Terminello, Waddill, and Tobin

Helicity selection and detection

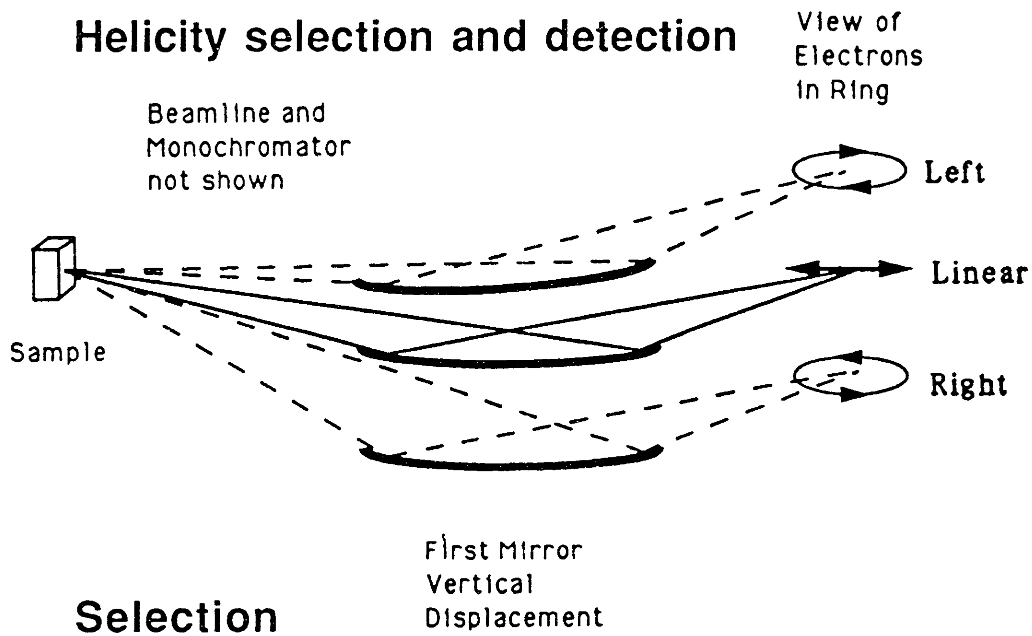

Selection

— Originally moved first mirror

— Now move selection aperture

Detection

— CoPd multilayers in Io section

In collaboration with Jo Stöhr et al., of IBM-Almaden Research and M. Rowen of SSRL

Transmission multilayer structures produce useful phase retardation in the $h\nu \approx 50 - 300$ eV range.

Kortright, *et al.*, Appl. Phys. Lett., 60, 2963 (1992)

Kortright and Underwood, NIM, A291, 272 (1990)

transmitted field amplitude ratio $t_s/t_p = |t_s/t_p| e^{-i\Delta}$

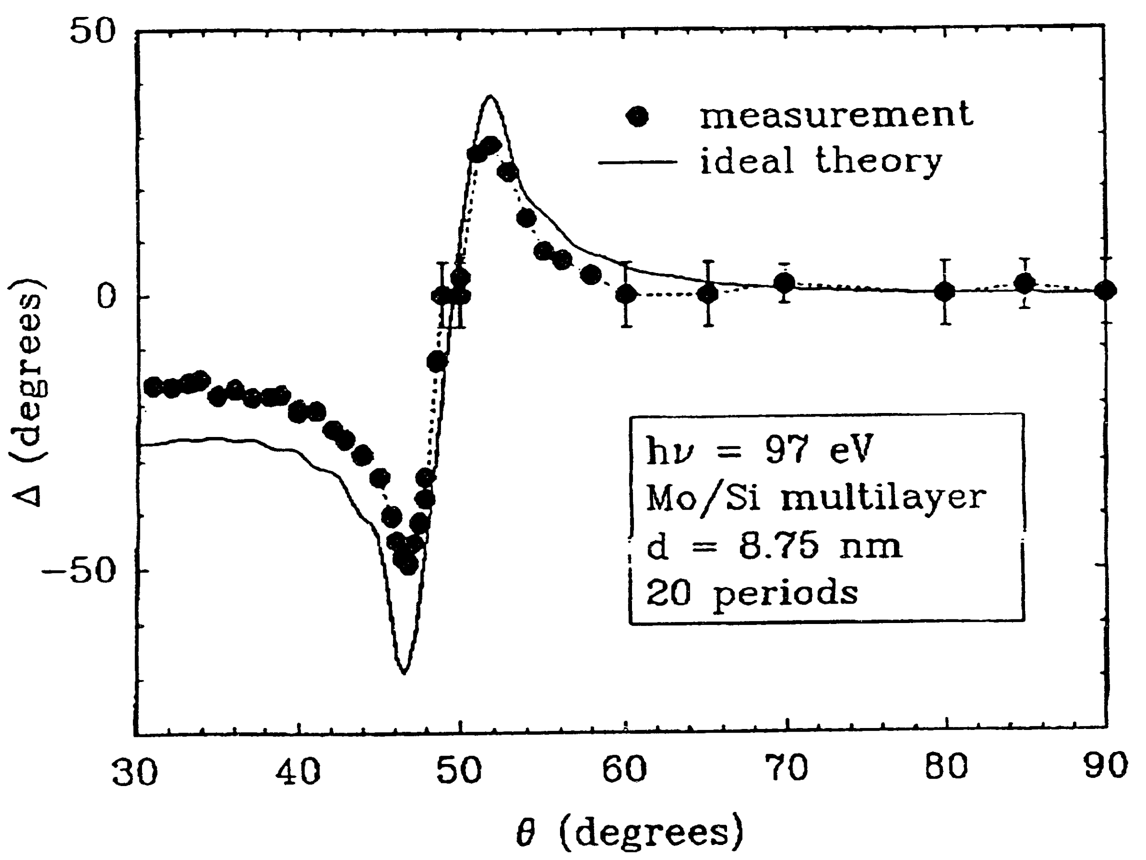

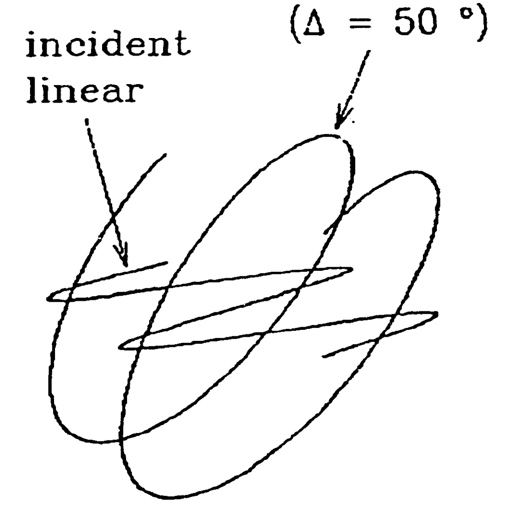

transmitted intensity ≈ 20%

Nanoscale magnetics – Vector alignment

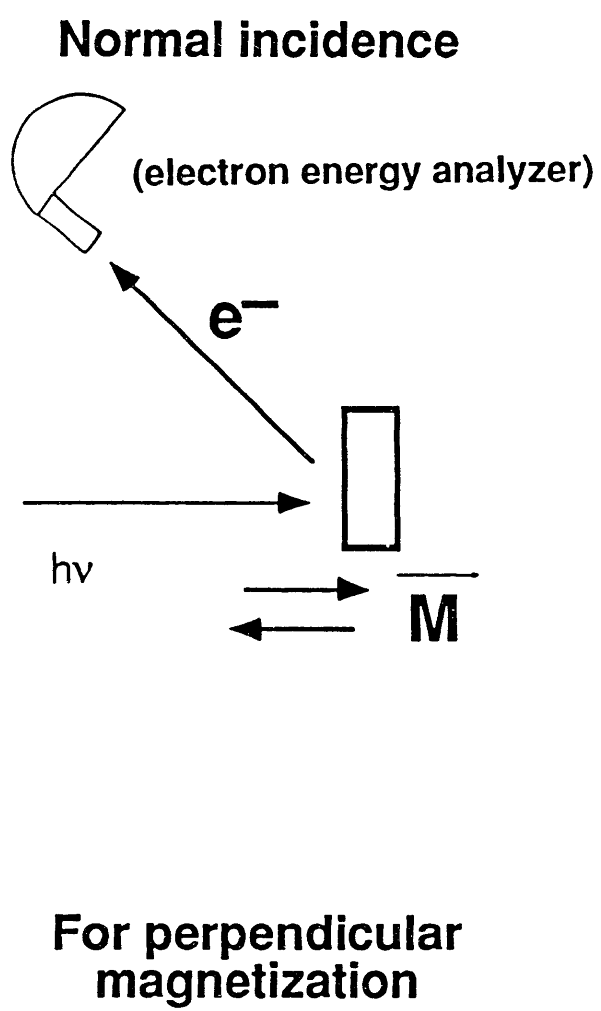

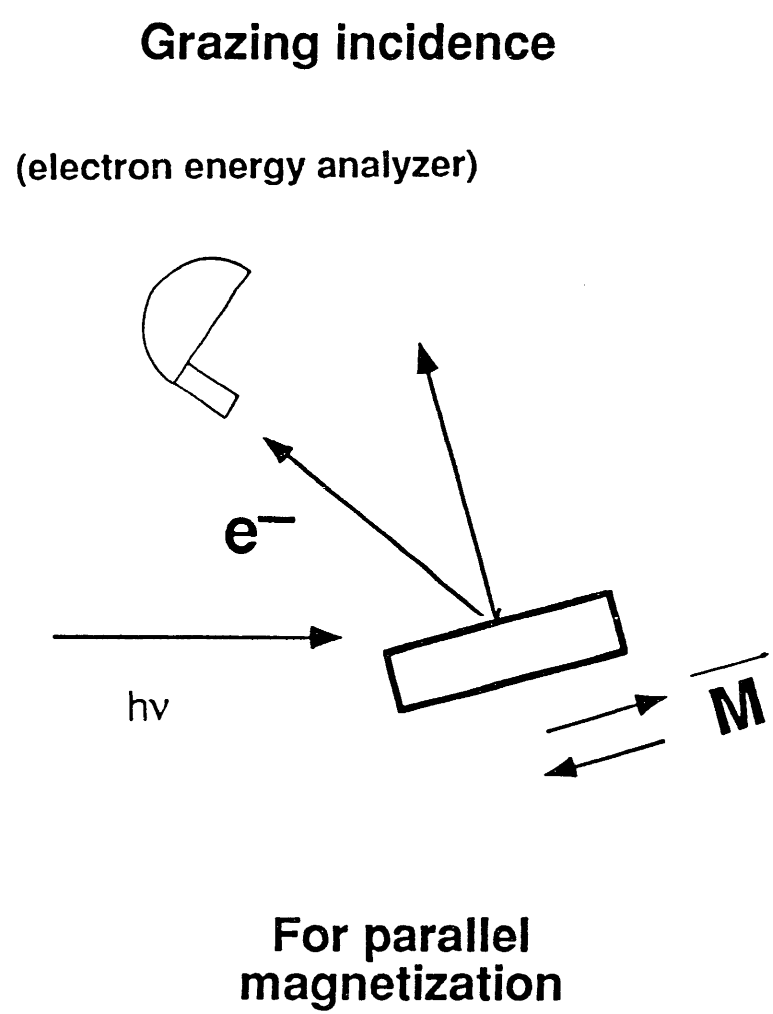

Nanoscale magnetics – Photoemission

Photoemission

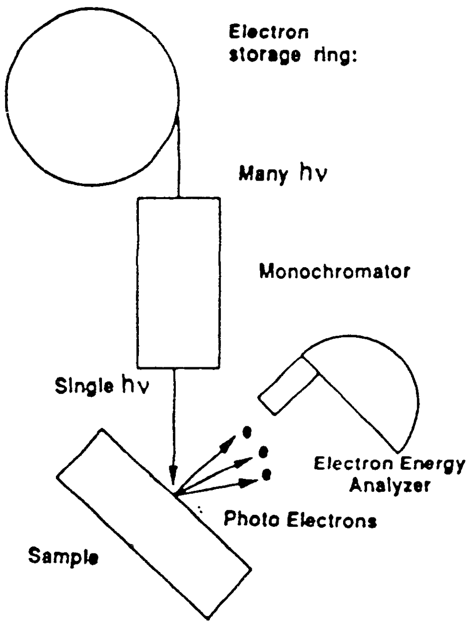

1. Fix photon energy
2. Choose helicity – above, in, or below plane or ring
3. "Align" magnetization and helicity vectors
4. Vary kinetic energy of accepted electrons

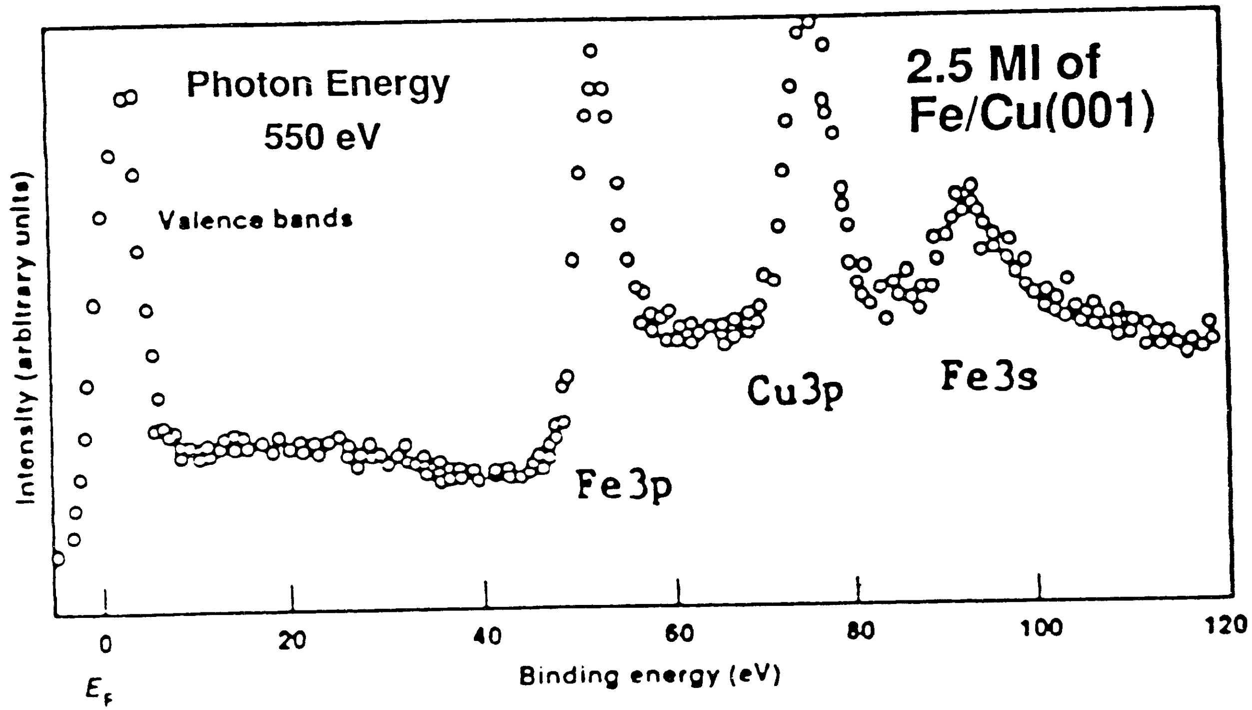

Nanoscale magnetics – Absorption of x-rays

Electron emission

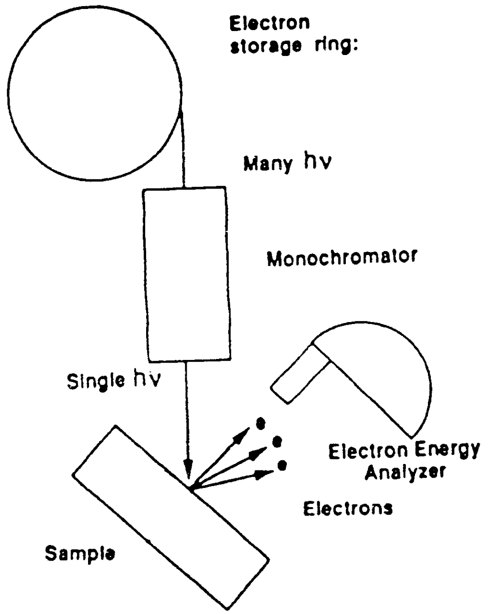

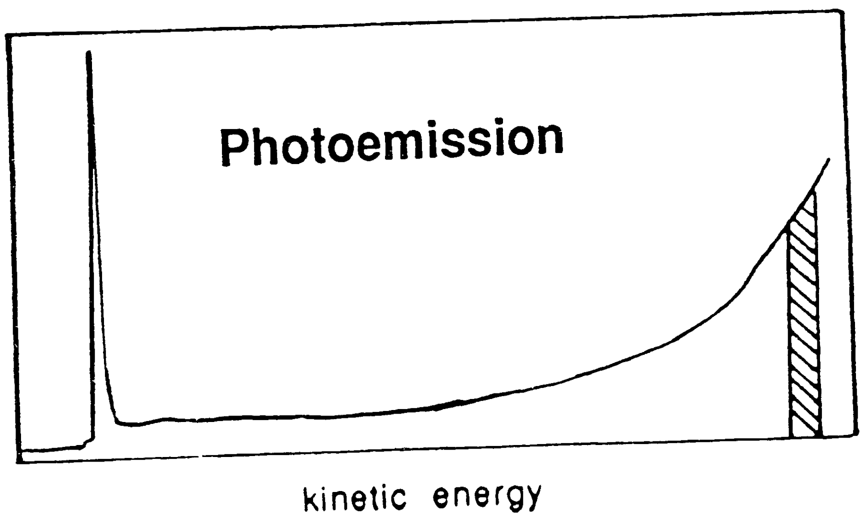

1. Choose low Ke window
2. Choose helicity: above, in, or below plane or ring
3. "Align" magnetization and helicity vectors
4. Scan photon energy (LV)

Absorption spectrum

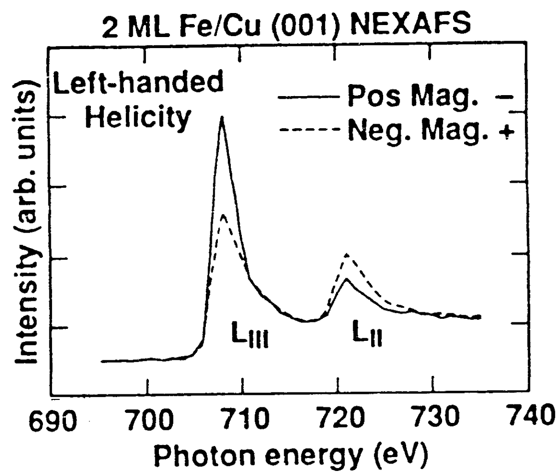

X-Ray Magnetic Circular Dichroism - Near Edge X-Ray Absorption Fine Structure

Electric dipole selection rules

right circular pol : $\Delta m_l = +l, \Delta m_j = +l, \Delta m_s = 0$

left circular pol: $\Delta m_l = -l, \Delta m_j = -l, \Delta m_s = 0$

Fe 2p → 3d

$$BR = \frac{I(2p^{3/2})}{I(2p^{3/2}) + I(2p^{1/2})}$$

P	M	PvsM	BR_{exp}	BR'_{exp}
L	O	+	0.64	0.58
L	I	–	0.83	0.75
R	I	+	0.65	0.59
R	O	–	0.83	0.75
LIN			0.74	0.67

Experiment
→ giant effect

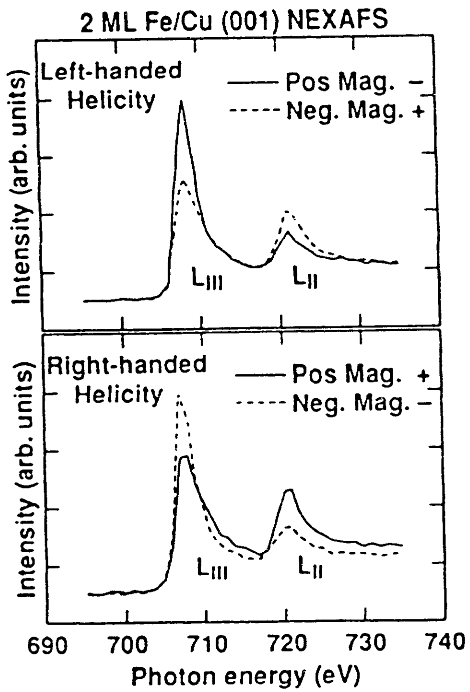

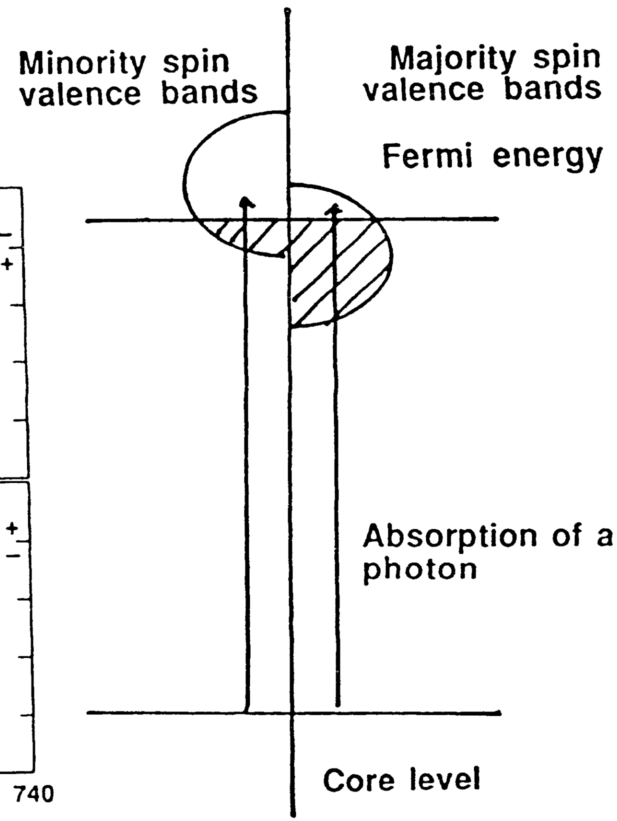

Tobin, Waddill, and Pappas, Phys. Rev. Lett. 68, 3642 (1992)

NEXAFS MCD–simplified, approximate analysis

$$BR_{TH} = \frac{3+2(1-\alpha)\beta+2(1-\beta)\alpha}{6}$$

$$MM = 2(10-n)\left[\frac{3BR'-2}{2\beta-1}\right] = 2(10-n)\left[\frac{3BR'-2}{P}\right]$$

BR	=	Branching ratio
α	=	Spin-down polarization
β	=	Right circular polarization
MM	=	Magnetic moment
P	=	$2\beta - 1$, circular polarization
BR'	=	Normalized branching ratio
n	=	Configuration # (n = 6 for Fe)

Assumptions include:
- Single electron picture
- Nonstatistical effects can be "normalized out" in BR
- Only $p \rightarrow d$ transition, electric dipole
- No coupling of majority and minority density of states
- Dominant octahedral crystal field splitting (or isotropic potential)
- Complete orbital quenching
- $g = 2$

BR'	Parallel	Antiparallel
EXP	0.595	0.75
THEORY*	0.60	0.73

* 2μB/Fe atom, 90% circular polarization

Nanoscale magnetics: NEXAFS MCD

Temperature studies:
Loss of remanent magnetization

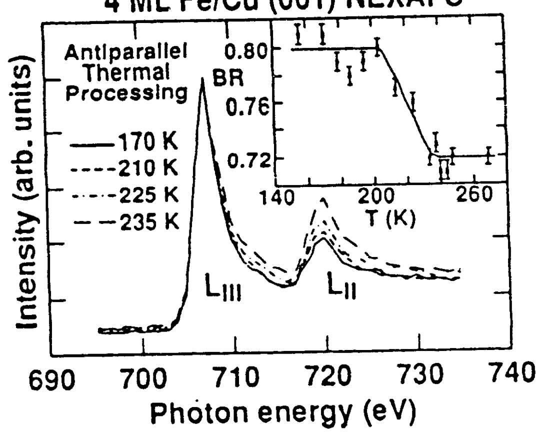

4 ml Fe/Cu(001)
Negative magnetization, negative helicity

Nanoscale magnetics: Core level photoemission → exchange splitting

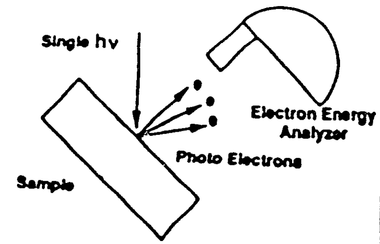

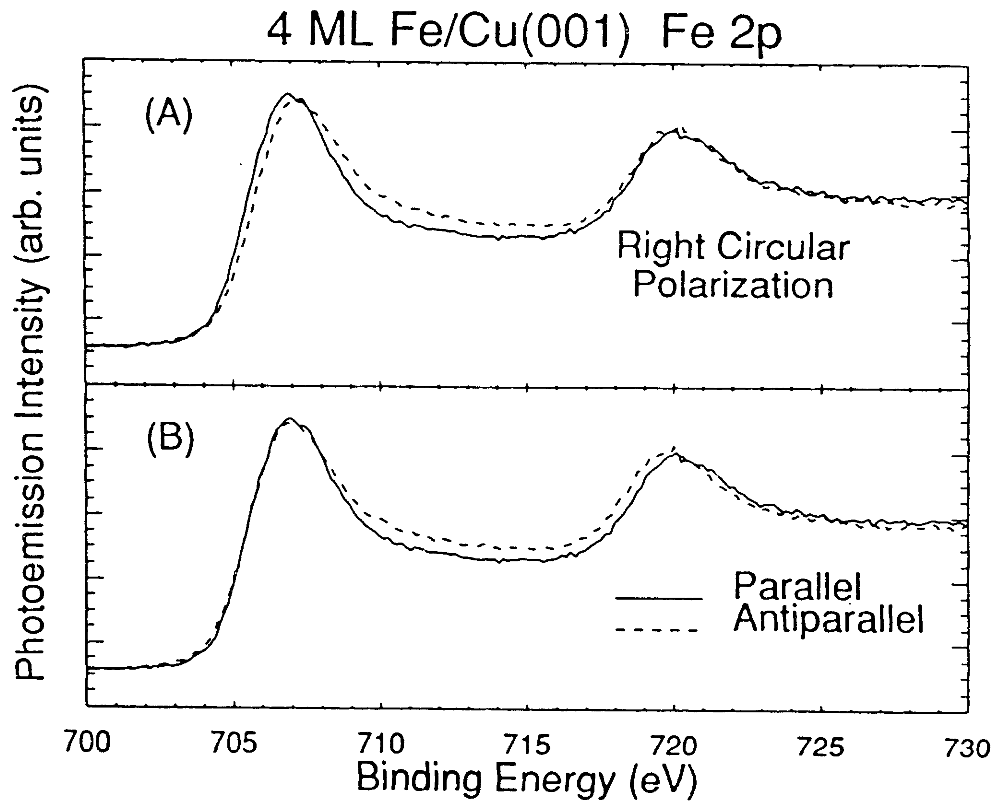

X-Ray Magnetic Circular Dichroism: Core Level Photoemission

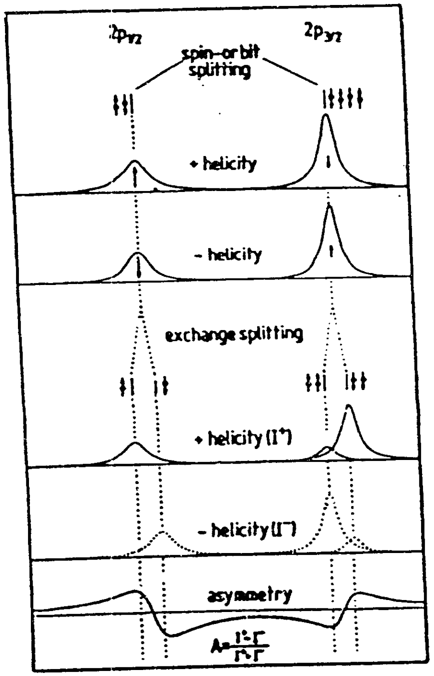

Spin orbit and exchange splitting

Baumgarten et al., PRL, 65, 492 (1990)
Bulk Fe PES

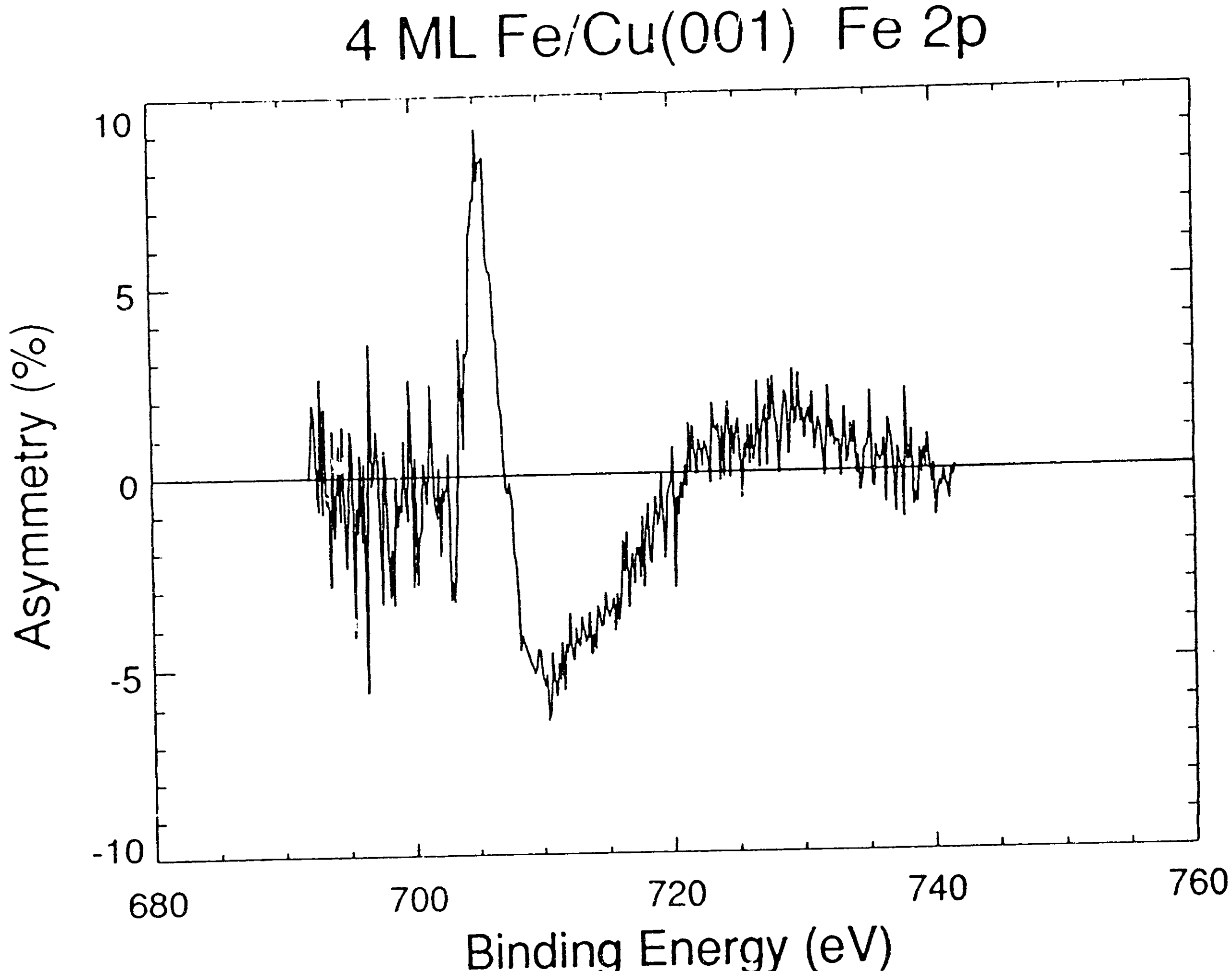

Asymmetry of the photoemission intensity observed for parallel (I_P) and antiparallel (I_A) orientation of photon spin and sample magnetization, $A = (I_P - I_A)/(I_P + I_A)$.

X-Ray Magnetic Circular Dichroism: Core Level Photoemission

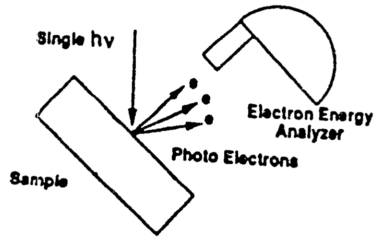

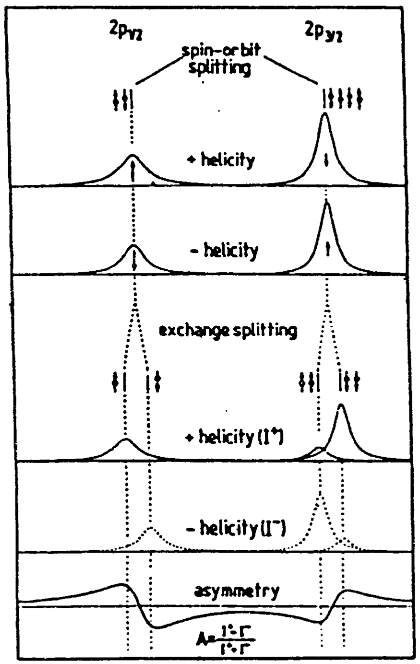

From Baumgarten, et al., PRL 65, 492 (1990) [Bulk Fe Pes]

2 ML Fe/Cu(001)

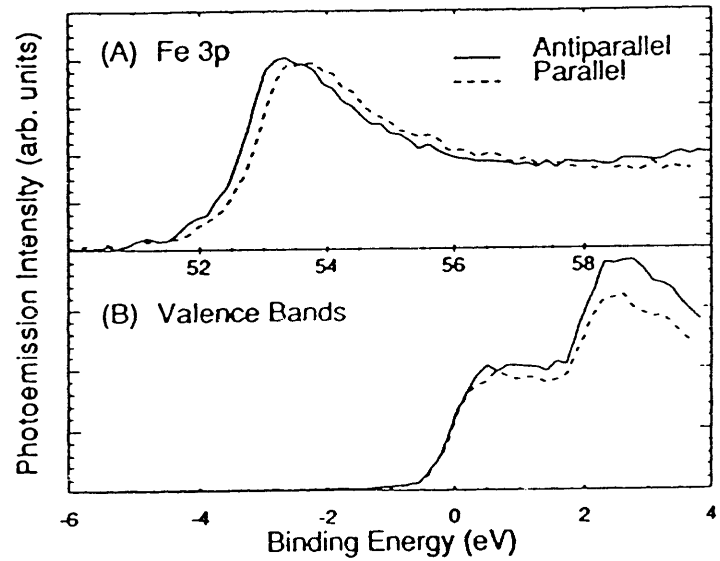

New data:
Preliminary analysis

2 ML Fe/Cu(001) Fe 3p

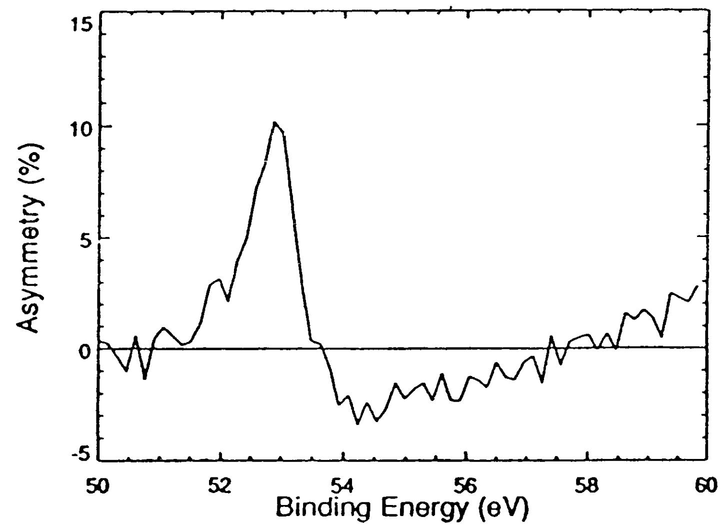

Spin-Dependent
Core Level Photoemission

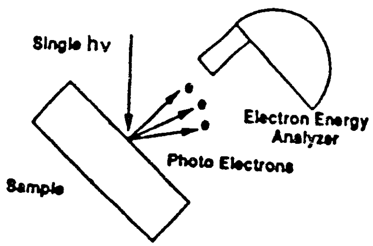

Fe

3d ↑↓ ↑ ↑ ↑ ↑

4s ↑↓

3p ↑↓ ↑↓ ↑↓

3s ↑↓

Spin Alignment

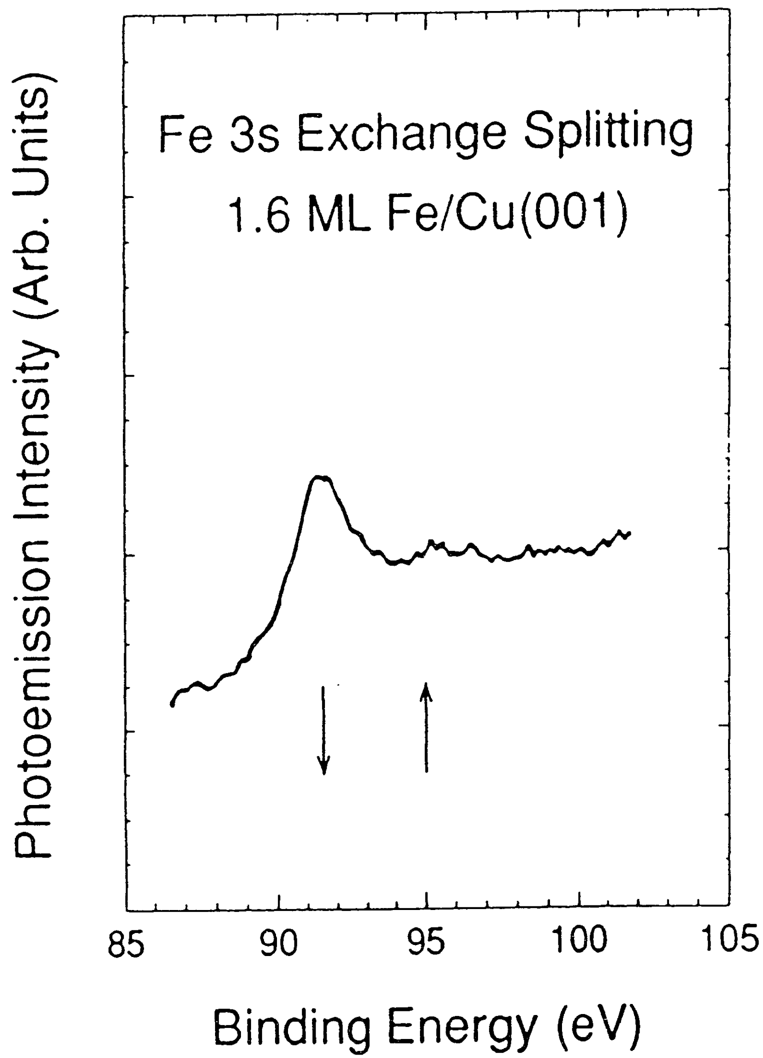

Angle-resolved photoemission spectra with hν = 190 eV of the Fe 3s exchange splitting for 1.6 ML Fe/Cu(001). The splitting is ~3.8 eV.

MCD–NEXAFS and photoemission of Fe/Cu(001)

- Giant effect in NEXAFS MCD
- Simplified approximate analysis: $BR_{TH} = \dfrac{3 + 2(1-\alpha)\beta + 2(1-\beta)\alpha}{6}$
- Perpendicular moment at low coverage–NEXAFS
- Parallel moment at high-coverage–NEXAFS
- Core-level photoemission $\rightarrow$ exchange splitting
  — Ultrathin film value < bulk Fe

X-ray absorption MCD in actinides: Projections

Calculations

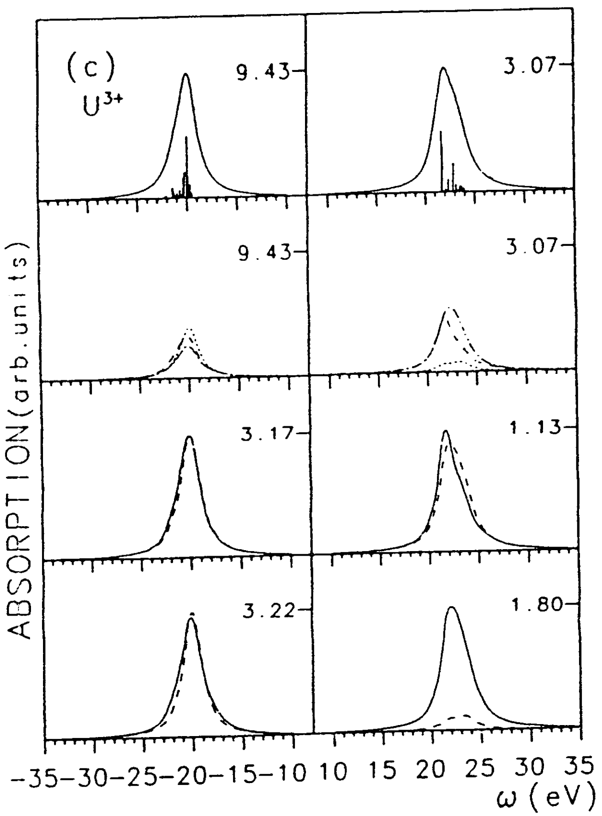

Fig. 1. The top panels: calculated 4d → 5f x-ray absorption spectra. The right sides correspond to 4d3/2 components and the left sides to 4d5/2. The second panels: the same curves, on the same scale, for each ΔJ final state. The third panels: MXD spectra for linearly polarized light. The bottom panel: MXD spectra for circularly polarized light at T = 0 K, RCP (solid curves) and LCP (dashed curves). From Ogasawara, Kotani and Thole, Phys. Rev. B., 44, 2169 (1991).

Simple one-electron picture
d → f transitions

$BR_{TH} = {}^2/_5[1 + (1 - \alpha)\,\beta + (1 - \beta)\,\alpha]$

α = % down spin polarization; $0 \leq \alpha \leq 1$
β = % right spin polarization; $0 \leq \beta \leq 1$

Only appropriate for systems without spin-orbit splitting
(e.g., L = 0 $Gd^{+3}(4f^7)$ and
L = 0 $Am^{+2}(5f^7)$, $Cm^{+3}(5f^7)$)

Resonant photoemission at SSRL

S/Poly-U

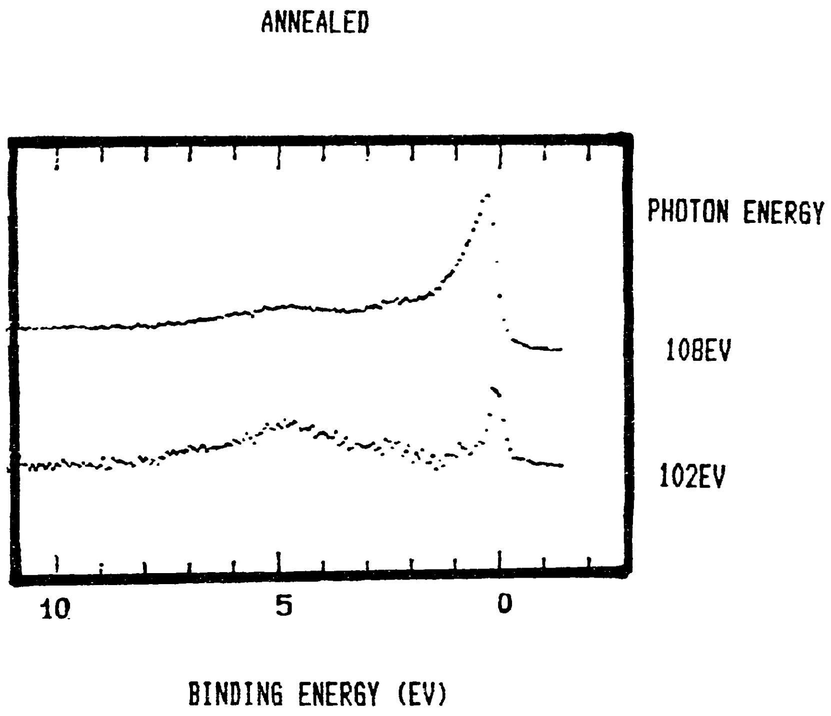

Polycrystalline UFe_2

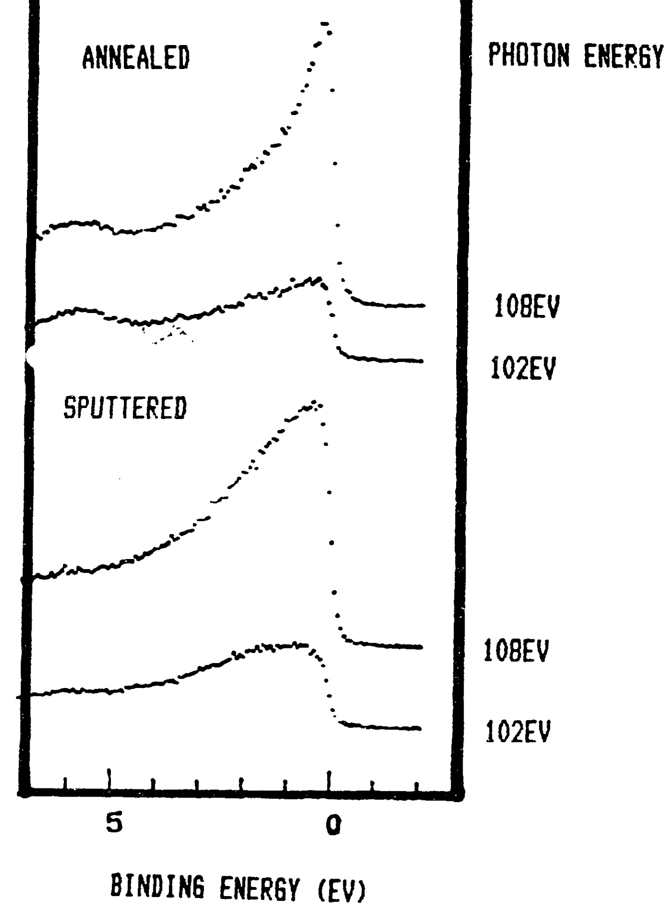

Actinides — Proposed MCD studies

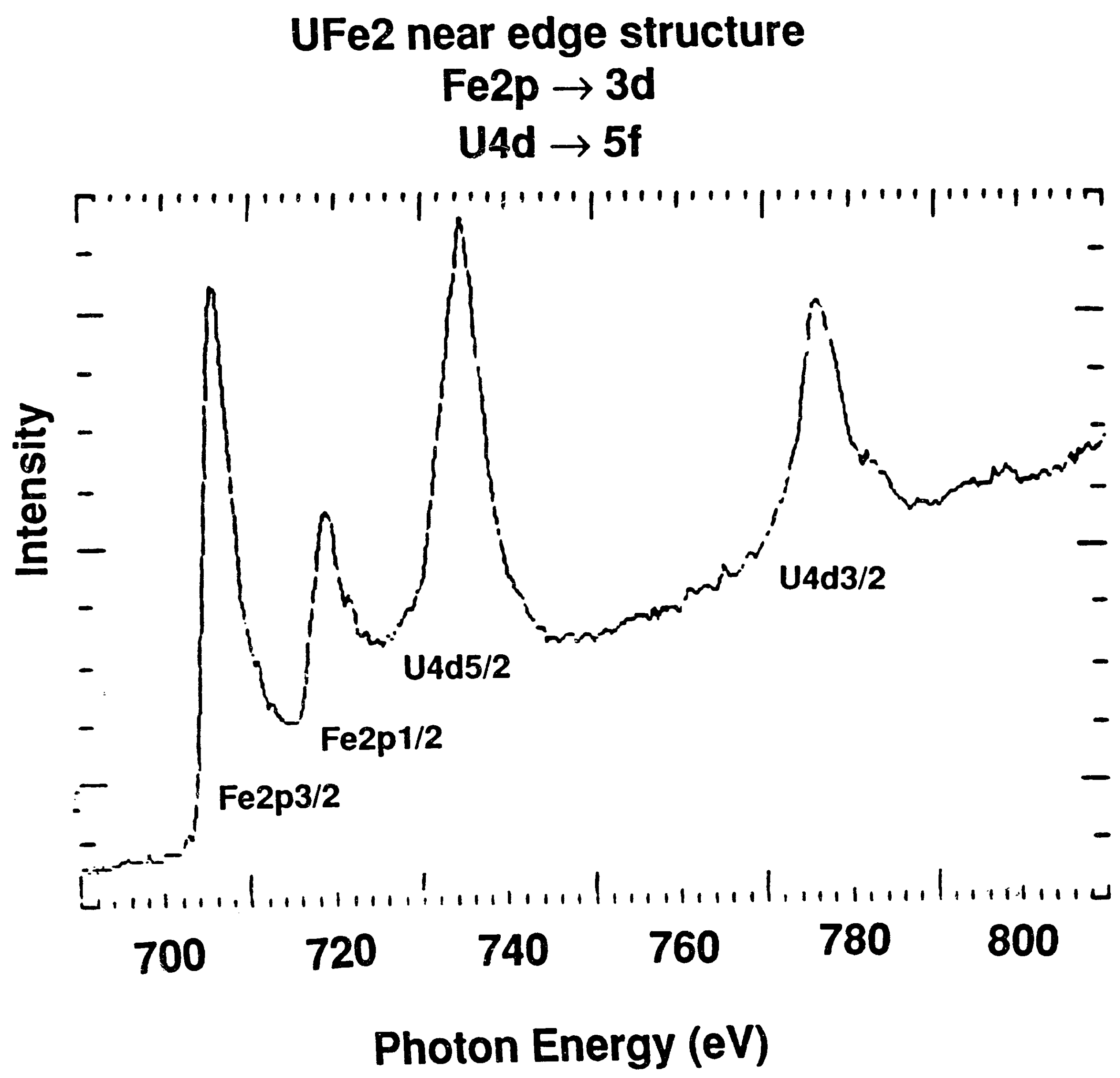

Tobin, Waddill, Gouder, and Colmenares

Probing for MCD in S/Poly-U

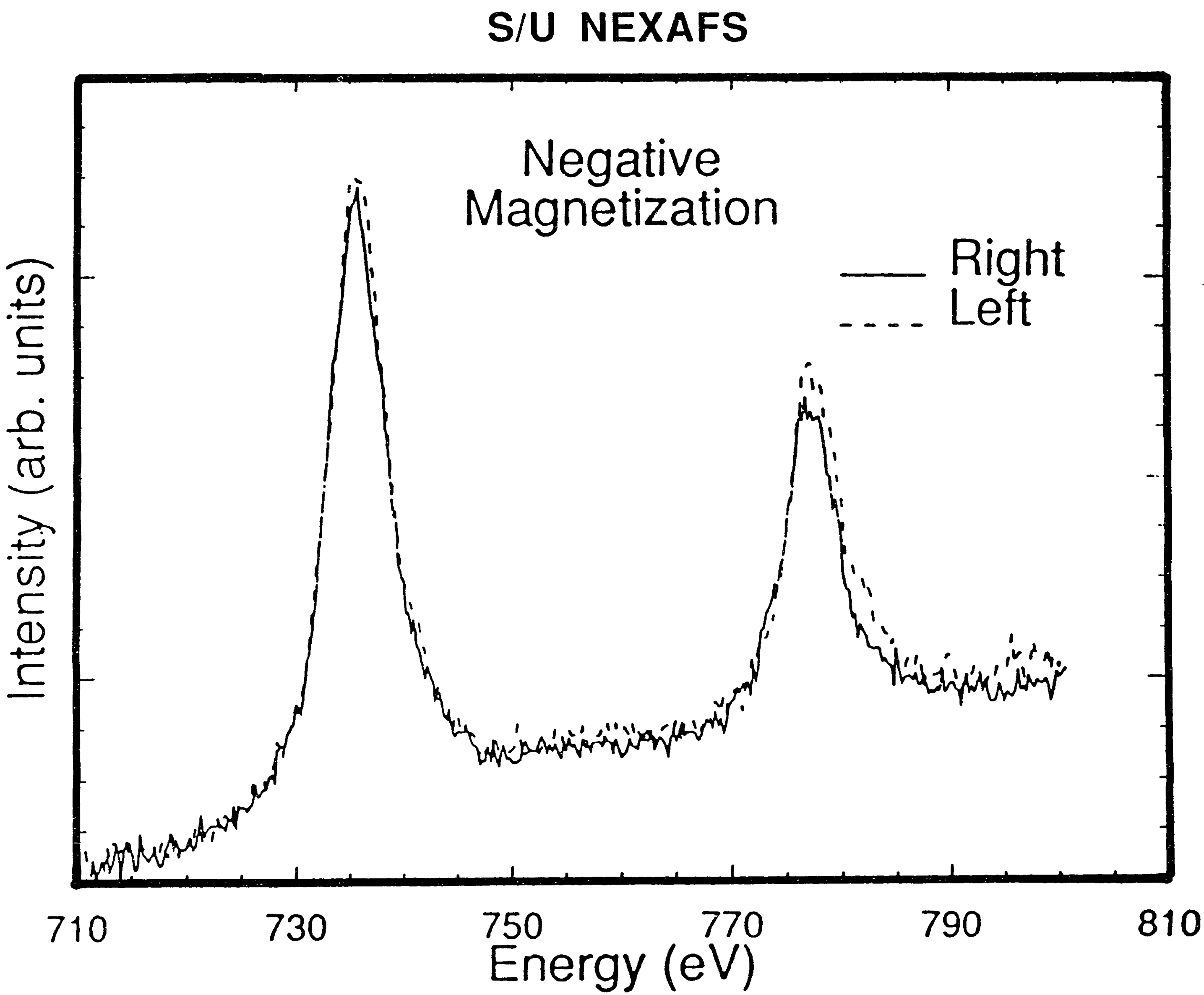

MCD in uranium compounds – prospects

- Elemental specificity: Useful for complex systems
- 100x brightness improvement in move to ALS
- Multilayers: Chaiken and Jankowski (in development...)
- Microscopic samples with ALS spectromicroscopy facility?
- X-ray absorption and photoemission with uranium
  - $4d \rightarrow 5f$ B^F = 778, 736 eV
  - $5d \rightarrow 5f$ B^F = 103, 94 eV
- Actinide facility: Expand beyond U^{238}
  - Chalcogenides and pnictides of actinide elements often exhibit strong magnetic effects. MCD measurements will provide stringent benchmarks for modeling of such systems and MCD may provide additional analytical capabilities for monitoring corrosion.

The Laser Plasma Laboratory Light Source: A Source of Preliminary Transuranic Data

A.J. Arko, J.J. Joyce and R.J. Bartlett

Los Alamos National Laboratory, Los Alamos, NM 87545

The 5f electron series of elements is unique in the periodic table with its richness of narrow band phenomena. Electron spectroscopy, particularly photoemission using tunable light, offers the best means of exploring the electronic structure of the 5f's. While it has indeed been employed extensively in the study of uranium and its compounds, it is the elements beyond uranium which seem to offer the best potential for understanding the localization-delocalization mechanism. However, the inherent dangers of working with highly radioactive materials at a soft X-ray synchrotron source (sample encapsulation is not possible in the soft X-ray regime) have prevented, at least up to now, the utilization of this technique for transuranics. X-Ray Photoemission Spectroscopy in the laboratory has proven to be a valuable resource, but it cannot address many of the unique properties of the 5f's which can only be probed with tunable light. In particular, it is resonant photoemission which is the most powerful tool for separating the orbital character of of the photoelectron features.

The proposed transuranic beamline will solve most of the above problems provided that the performance in the 80 eV to 200 eV range, the region of the 5f resonances, is adequate, and provided that sufficient beam time is available for users. To a large extent, however, many of the measurements can be accomplished on a rather inexpensive poor man's light source, sometimes called the laser plasma light source. The integrated output intensity of this source is related to the power of the laser light impinging on the target, combined with the collection solid angle of the first mirror. With the right set of parameters it can equal the intensity of a bending magnet beamline over a limited range of photon energies. Thus, much of the work can be done in one's own laboratory without the need to transport radioactive samples in an era when the public is overly sensitized to the dangers of radioactivity. Only crucial experiments can be reserved for the undulator beamline which is likely to be over-subscribed in any case.

A schematic diagram of the Laser plasma source is given below (see Fig. 1). A high

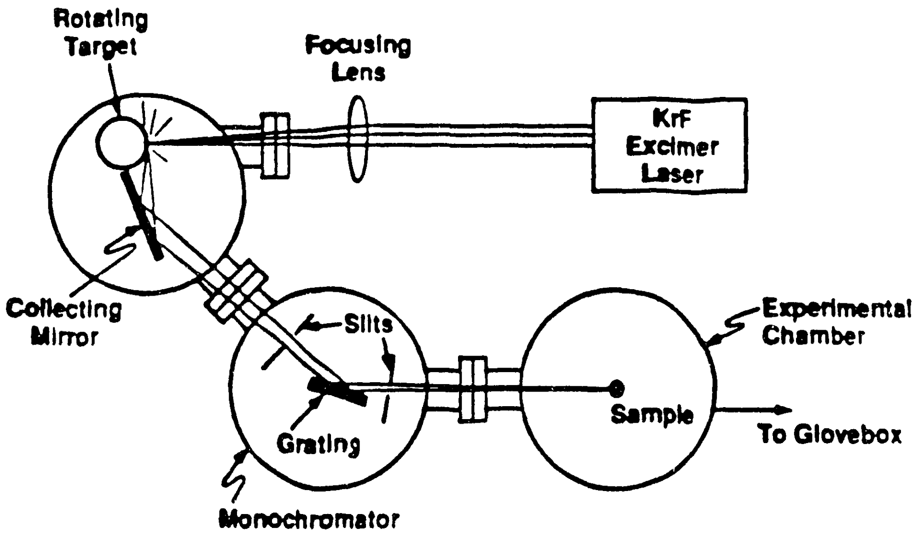

Fig. 1 Schematic of the Laser Plasma Light Source.

inten[illegible] [illegible]imer laser light (700 mJ/pulse, 30 nsec/pulse, 200 Hz) is focused on to a metal target to [illegible] high temperature plasma in a ≈100 micron area of the target. Some metals such as gold will re-radiate a continuum of light, essentially black body radiation, which can be collected and focused on a monochromator, and subsequently focused on a sample for purposes of photoelectron spectroscopy. Because the entire light source, together with the monochromator and the spectrometer, must fit within the confines of one's laboratory, one cannot have the luxury of high-resolution monochromators such as a TGM. Instead, a compact variable-grooved grating monochromator from Hettrick Scientific, with a resolving power of about 500, and an energy range from ≈30 to ≈200 eV, with fixed entrance and exit slits, will be employed. Thus it should be possible to obtain about 200 meV resolution in the region of the 5f resonances. This is still only about a factor of 2 worse than some of the best resolutions presently reported in this energy range at this time. The data collection system will consist of multi-channel charge integration rather than pulse counting, since the individual electrons will be too closely bunched during a single pulse to separate them out.

In order to enable us to work with highly radioactive transuranic materials in our laboratory it will still be necessary to develop a glove-box and sample transfer system whereby a specimen surface can be prepared in a "hot" sample preparation chamber (see Fig. 2). After the surface is prepared, the sample can then be transferred into the spectrometer chamber via a series of right angle transfers thereby avoiding direct line of sight from the specimen chamber, and further insuring that only the small sample holder, rather than the entire transfer arm, is the only contamination introduced into the spectrometer chamber. In this way we feel that contamination can be kept to a minimum. Once the sample is in the chamber and cooled to some low temperature, subsequent cleaning can be effected with a light laser pulse on the sample.

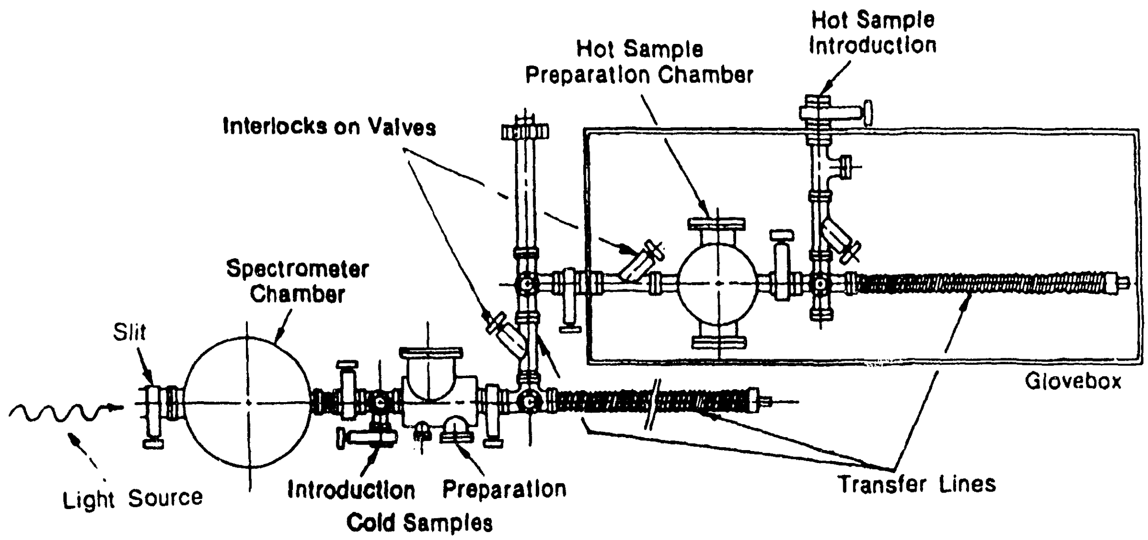

Fig. 2 Schematic diagram of transuranic spectrometer and glove box system, showing the series of right angle transfers to avoid line of sight into the spectrometer.

A potentially useful side benefit of the laser source is the prospect of doing pump-and-probe experiments with two lasers to study empty states at high resolution. Because of the high photon intensity per pulse (≈10^8 photons) at the sample, combined with the slow rep rate, one can actually do better in the way of usable photon flux than is possible at bending magnet sources by at least 3 orders of magnitude, primarily because one is only able to use ≈10^3 bunches at best at a synchrotron.

* Work supported by the U.S. Department of Energy

The Laser Plasma Light Source: A Source of Preliminary Data for the Transuranics

A.J. Arko and J.J. Joyce
+ R.J Bartlett

Work Supported by the U.S. Department of Energy

Need For Tunable Light

* **Resonance -- Separate out f-component**
* **Cross-section variation (Cooper Minima)**
* **Angle-Resolved Studies**
* **Surface vs Bulk Studies**
* **CFS and CIS Spectra**
* **Pump and Probe**

Why the Need for the LPLS?

* **Primary reason is safety!**

  a) Highly radioactive samples
  b) Cannot use windows in the XUV range
  c) Real risk of contaminating an expensive ring
  d) Many suffer in case of contamination

* **LPLS is very inexpensive**

* **Only a few individuals involved**

* **No need to transport samples**

* **Security at LANL already in place**

* **Long term Storage of Samples**

Undulator will in any case be over-subscribed

In no way can this source replace the undulator if the safety considerations are resolved!

* **Intensity 1 to 2 orders of magnitude down**

* **No polarization**

* **Cannot reach ultra-high resolution**

But it does have a favorable time structure for time resolved studies!

Schematic Diagram of Laser System

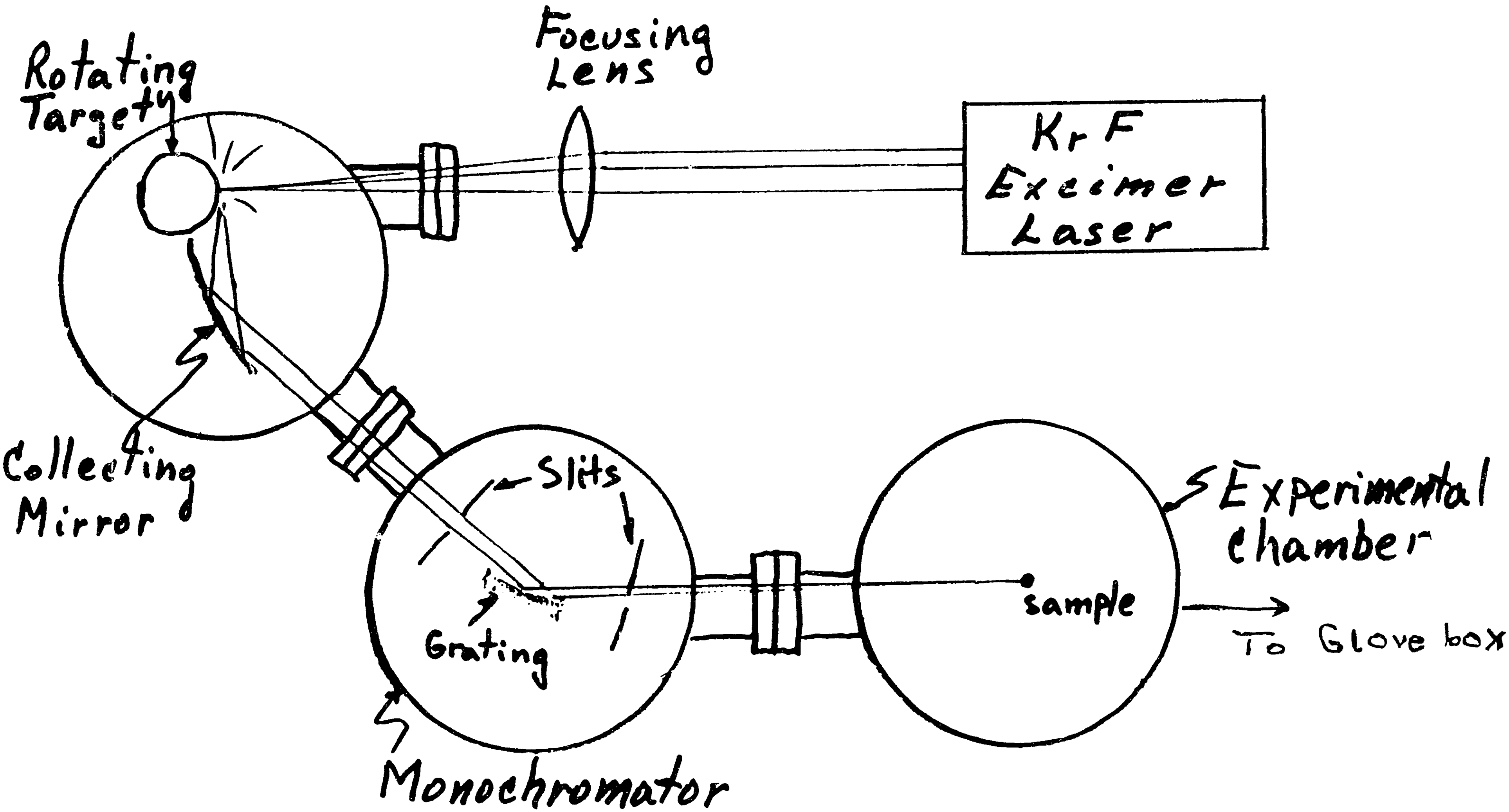

Specifications

I. The Laser (Lambda Physik)

Type	KrF
Power per pulse...........................	620 mJ
Pulse duration.............................	30 Nsec
Rep Rate....................................	200 Hz
Focused spot size........................	30 microns

II. The Target (Acton Research)

Rotating Metal Drum	gold, samarium, yterbium, Al
Spot temp.	≈ 180,000 K
Pulses per drum	≈ 60,000,000
Useful measuring time	≈ 80 hrs

III. The Monochromator (Hettrick Scientific)

Type	Grazing incidence, Non-Rowland
Grating......................................	Spherical, Variable Groove Density
Angle of Incidence........................	4°
Resolving Power...........................	500 - 1000
Energy Range..............................	30 - 200 eV
Peak Energy................................	100 eV
Peak Intensity..............................	1011 Photons/sec

IV. The Analyzer (VSW Angle Resolved)

50 mm Radius
Multichannel detection
Charge Integration

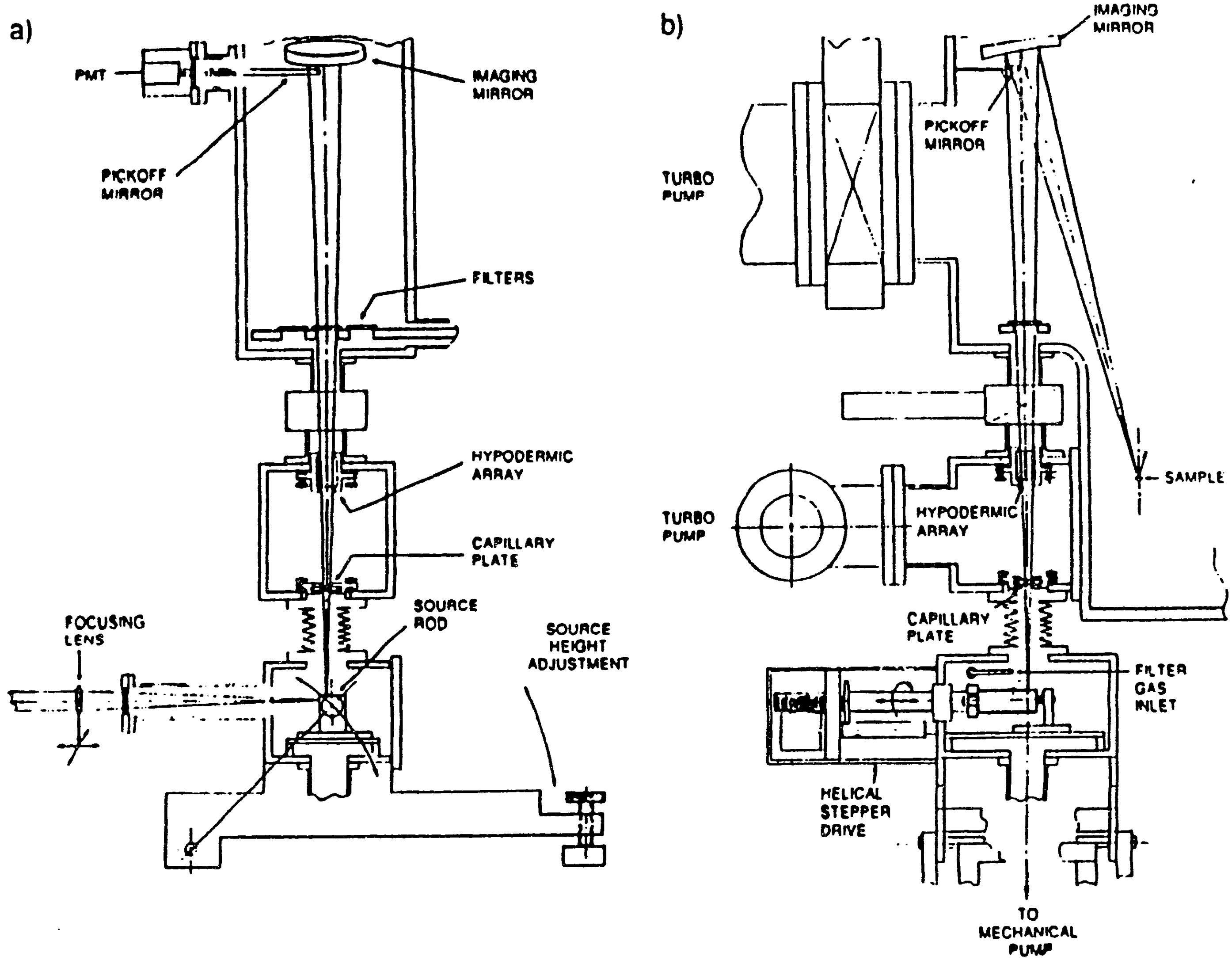

Schematic representation of the Laser Plasma Light Source, (a) side view, (b) front view.

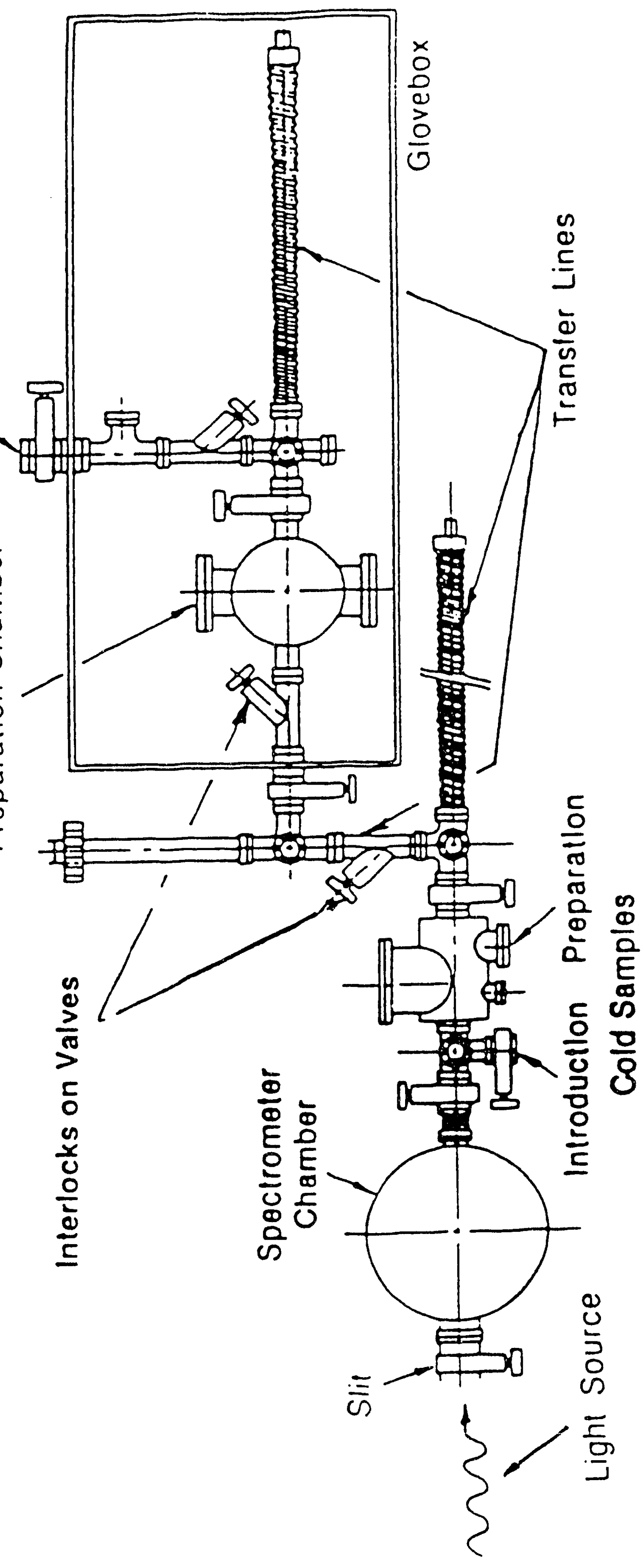
Glovebox
Transfer Lines
Hot Sample
Introduction
Hot Sample
Preparation Chamber
Interlocks on Valves
Spectrometer
Chamber
Introduction
Preparation
Cold Samples
Slit
Light Source

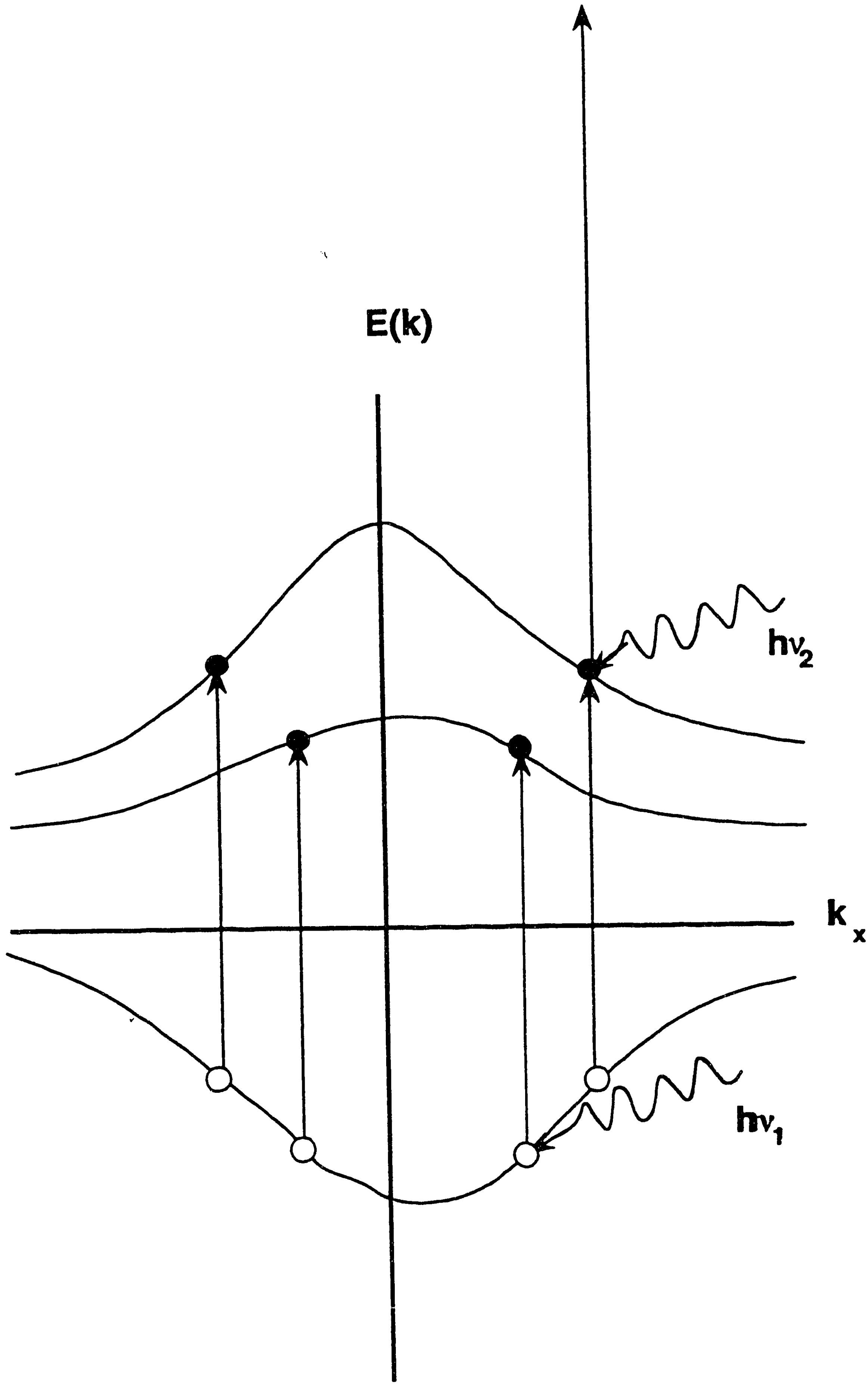
E(k)
hν2
kx
hν1

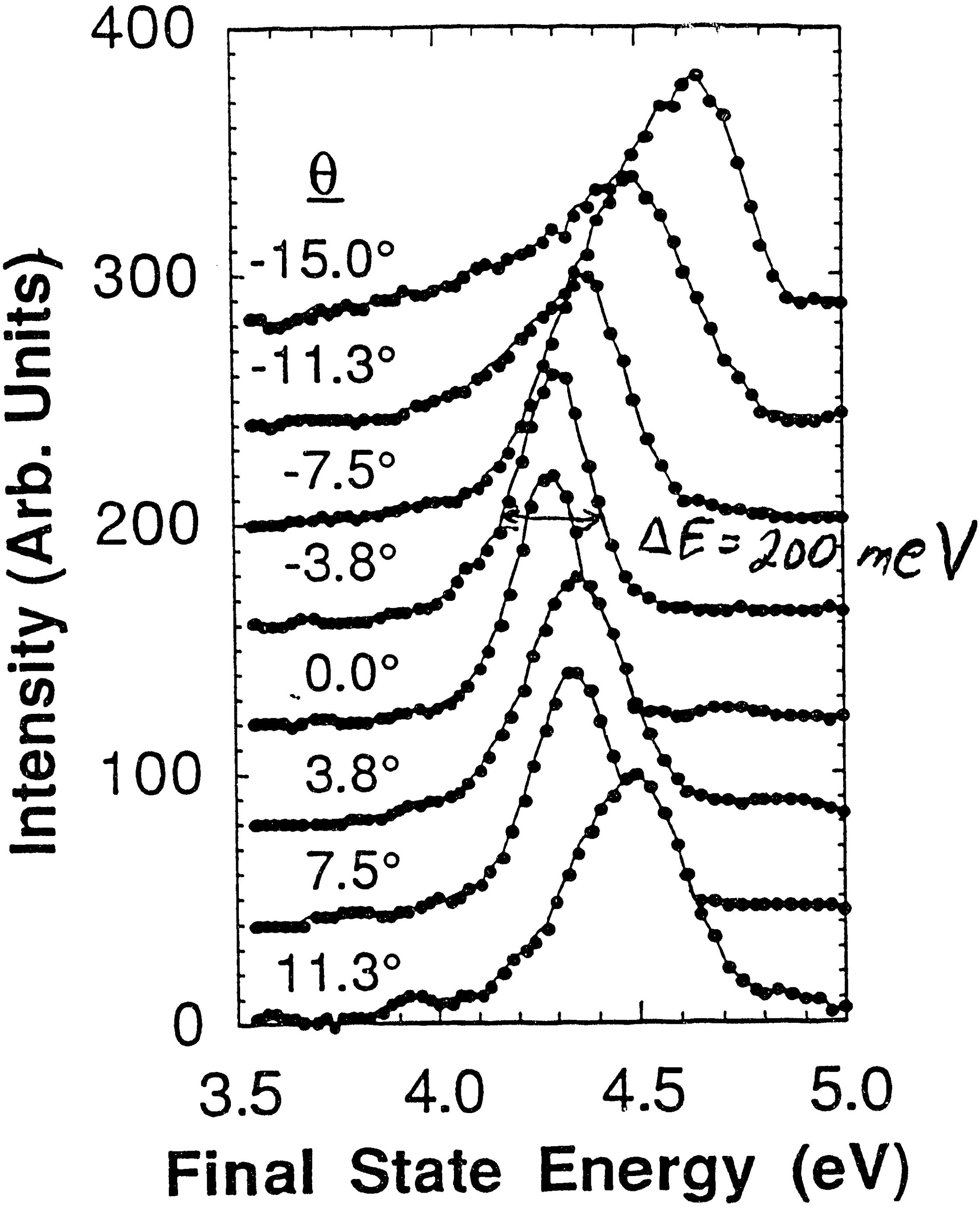

Intensity (Arb. Units)
Final State Energy (eV)
θ
-15.0°
-11.3°
-7.5°
-3.8°
0.0°
3.8°
7.5°
11.3°
ΔE = 200 meV
0
100
200
300
400
3.5
4.0
4.5
5.0

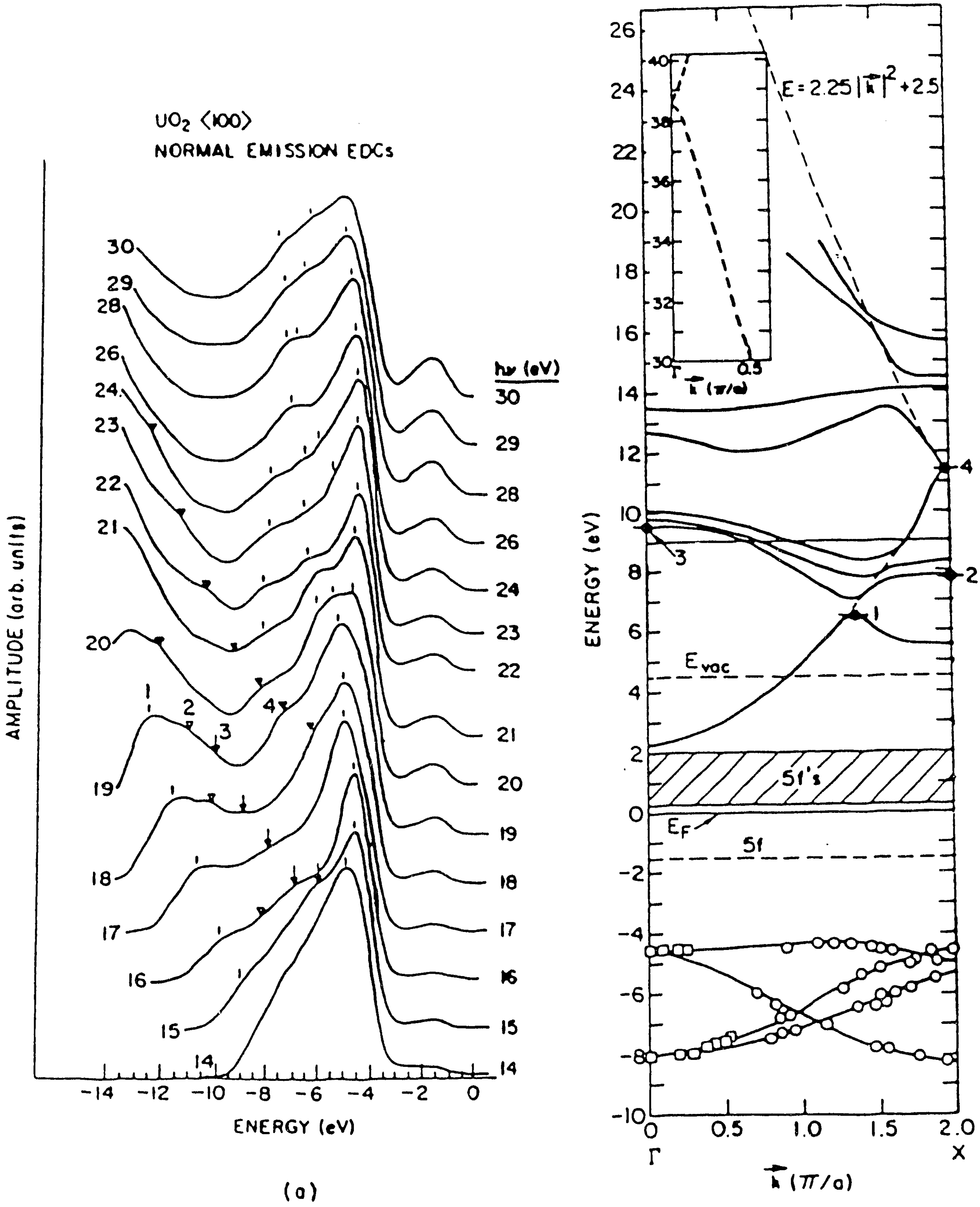

UO2 ⟨100⟩
NORMAL EMISSION EDCs
AMPLITUDE (arb. units)
ENERGY (eV)
hν (eV)
5f's
E_vac
E_F
5f
ENERGY (eV)
E=2.25|k|²+2.5
k (π/a)
Γ
X

(a)

(b)

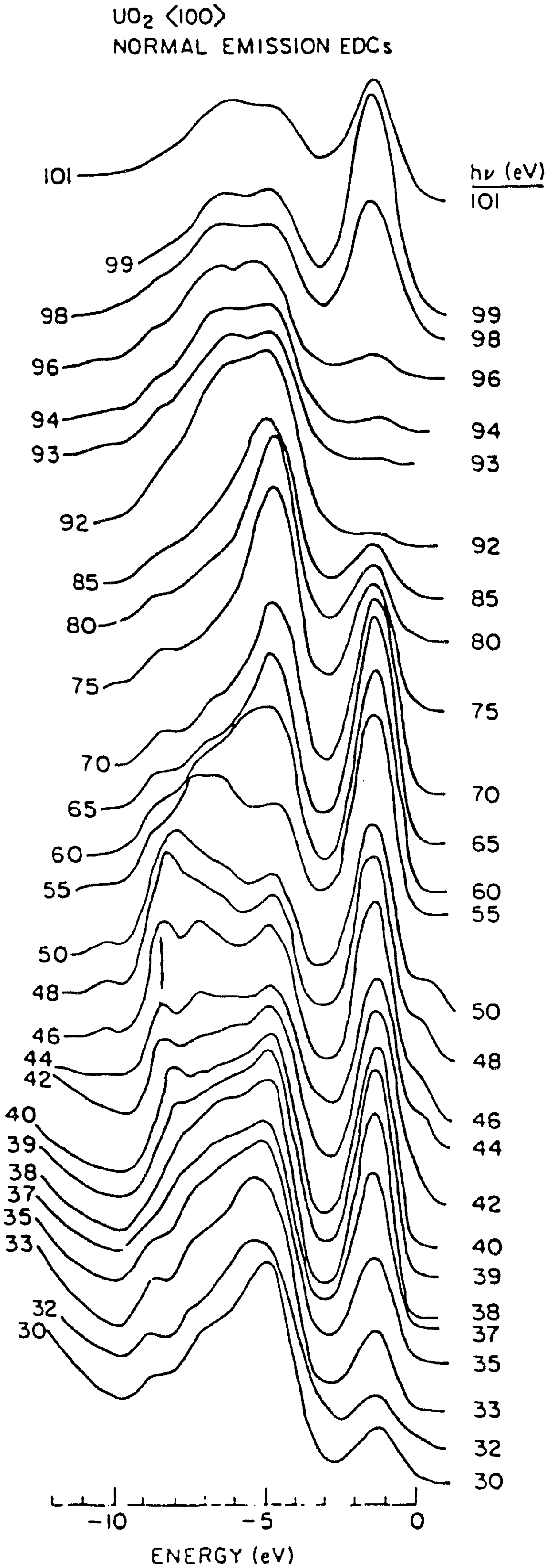

UO_2 ⟨100⟩
NORMAL EMISSION EDCs
hν (eV)
101
99
98
96
94
93
92
85
80
75
70
65
60
55
50
48
46
44
42
40
39
38
37
35
33
32
30
−10
−5
0
ENERGY (eV)

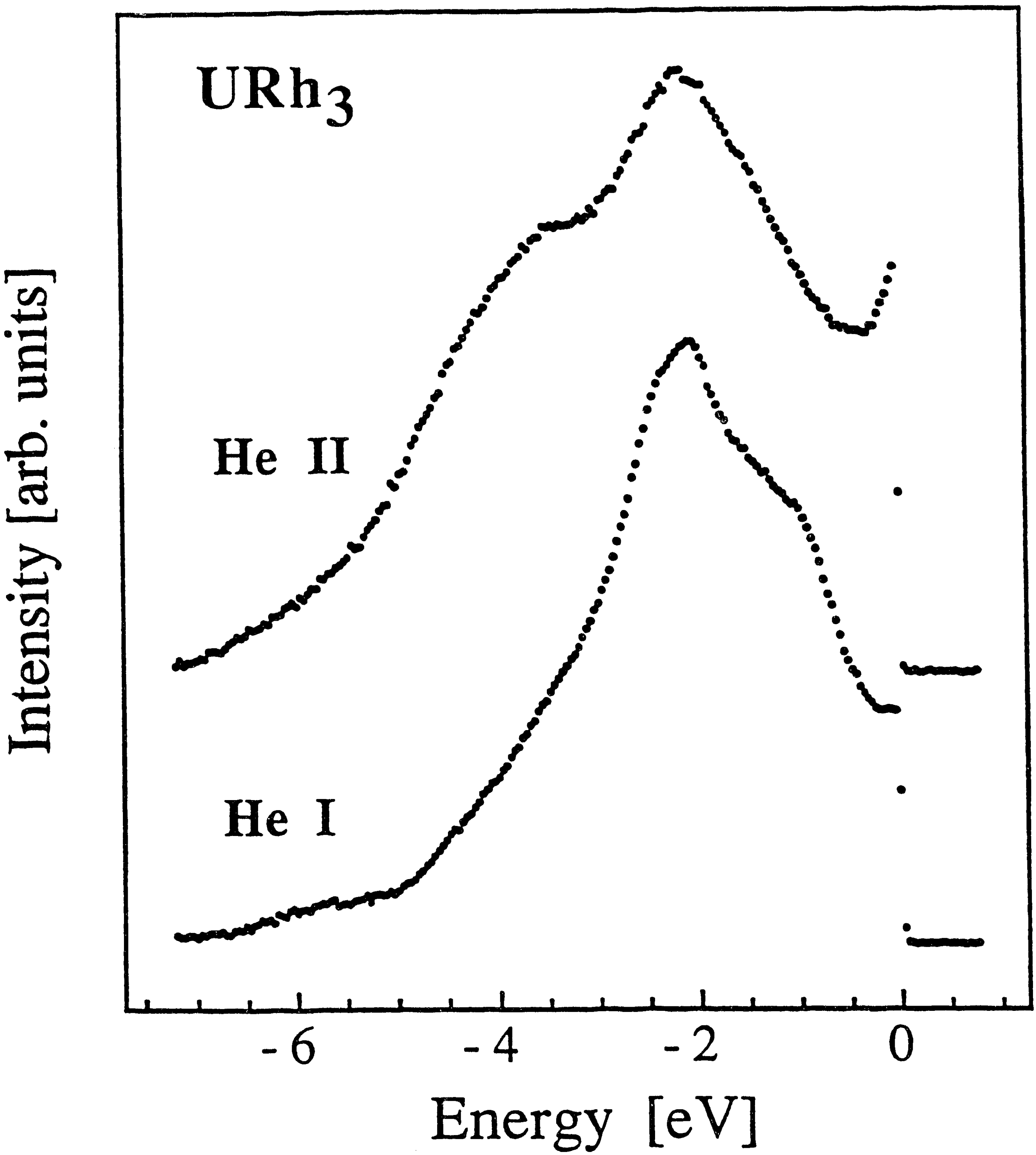

URh3
He II
He I
Intensity [arb. units]
-6
-4
-2
0
Energy [eV]

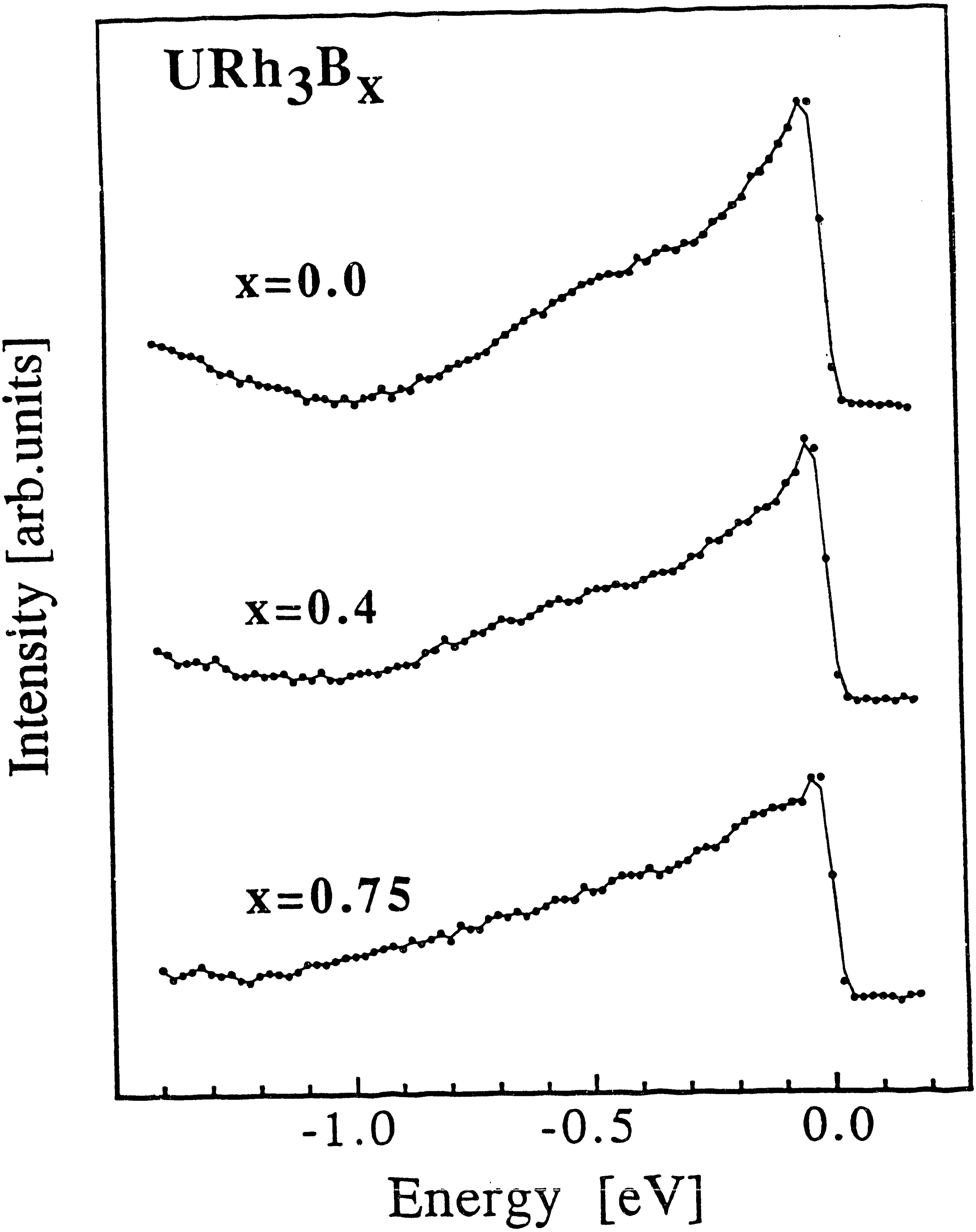

URh3Bx
x=0.0
x=0.4
x=0.75
Intensity [arb.units]
-1.0
-0.5
0.0
Energy [eV]

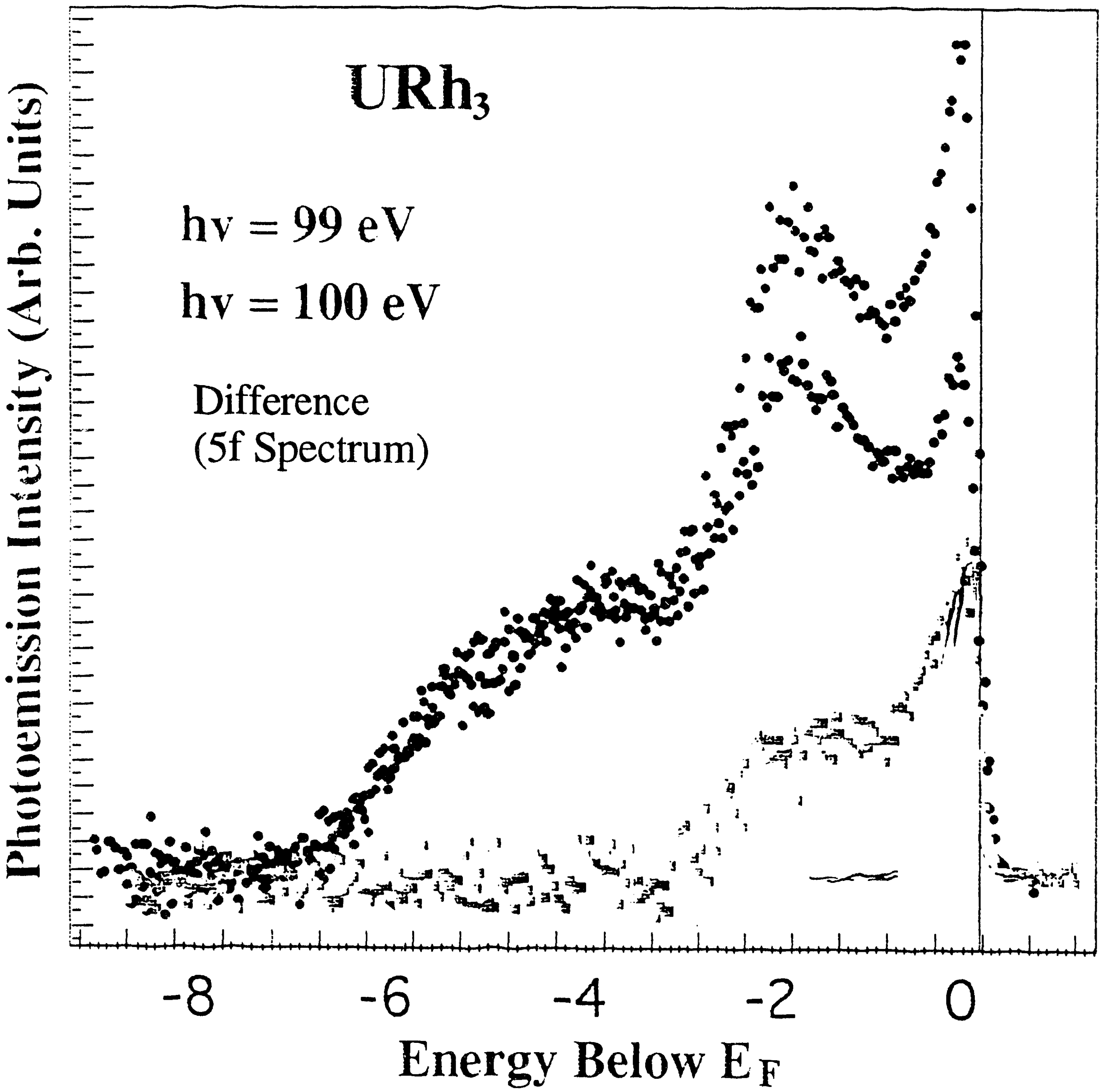
URh$_3$
hv = 99 eV
hv = 100 eV
Difference
(5f Spectrum)
Photoemission Intensity (Arb. Units)
-8
-6
-4
-2
0
Energy Below E$_F$

Cross Sections in UBe_{13}

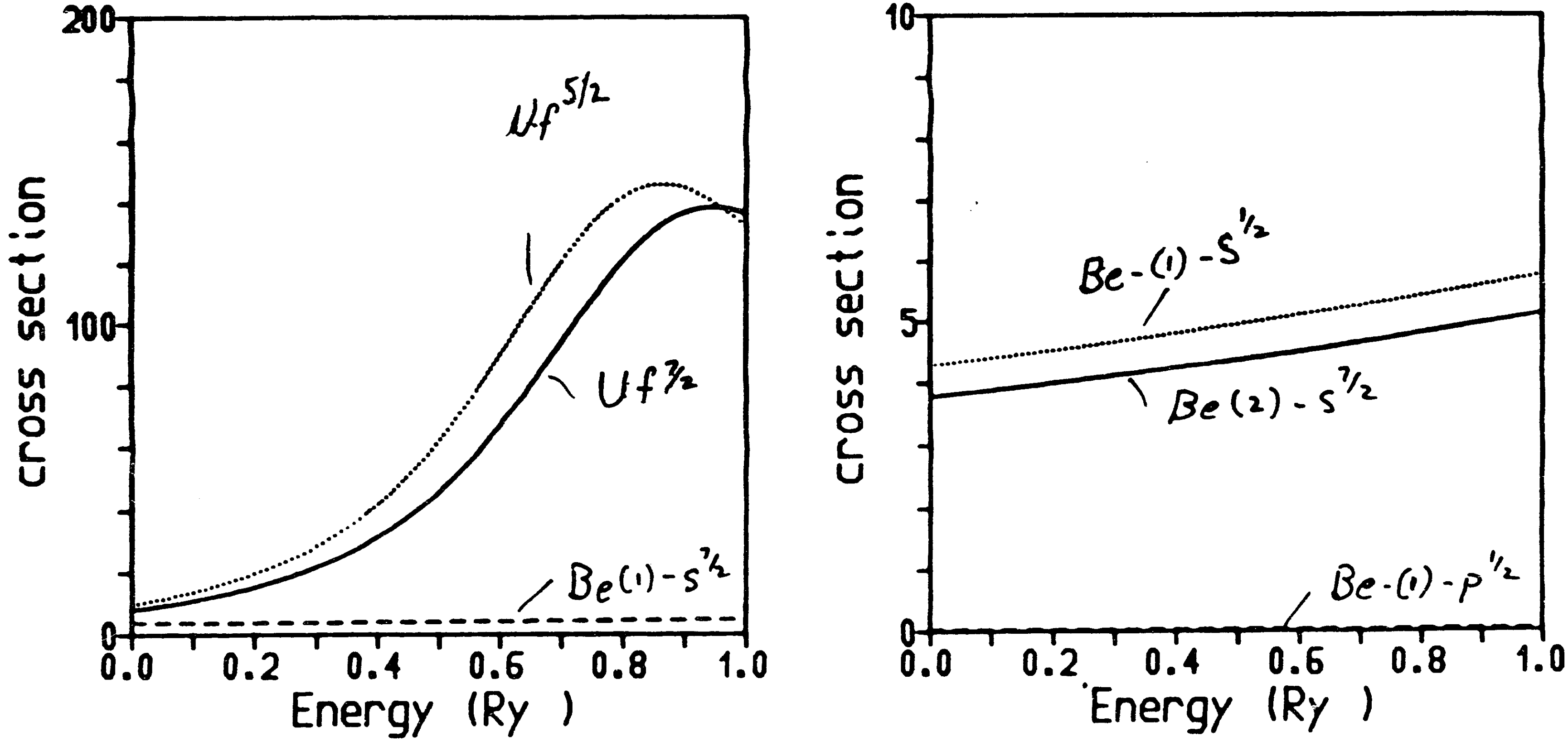

Boring, Weinberger, Albers, Schadler

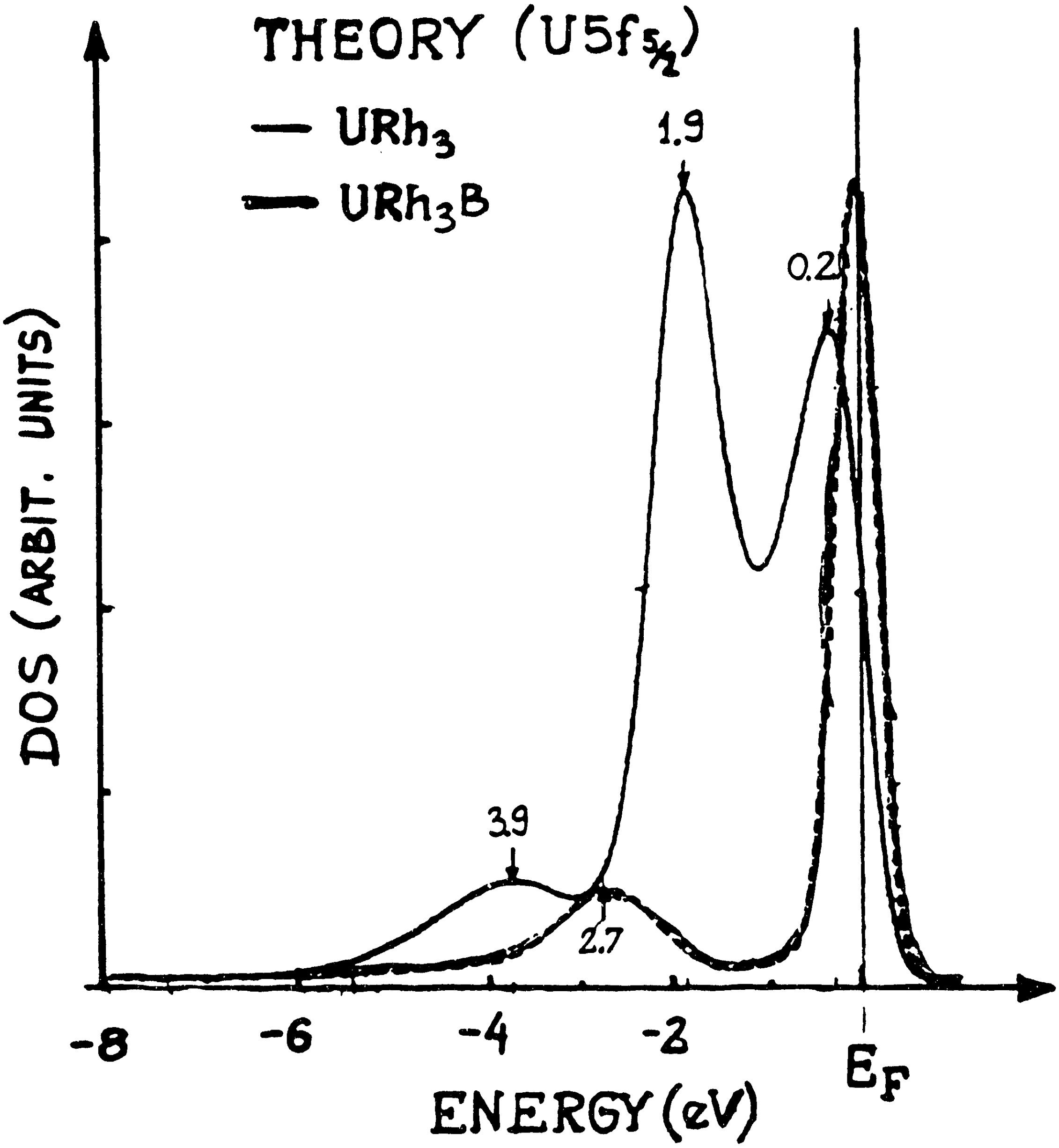

THEORY (U5f5/2)
URh3
URh3B
1.9
0.2
3.9
2.7
DOS (ARBIT. UNITS)
-8
-6
-4
-2
EF
ENERGY (eV)

D. D. Koelling

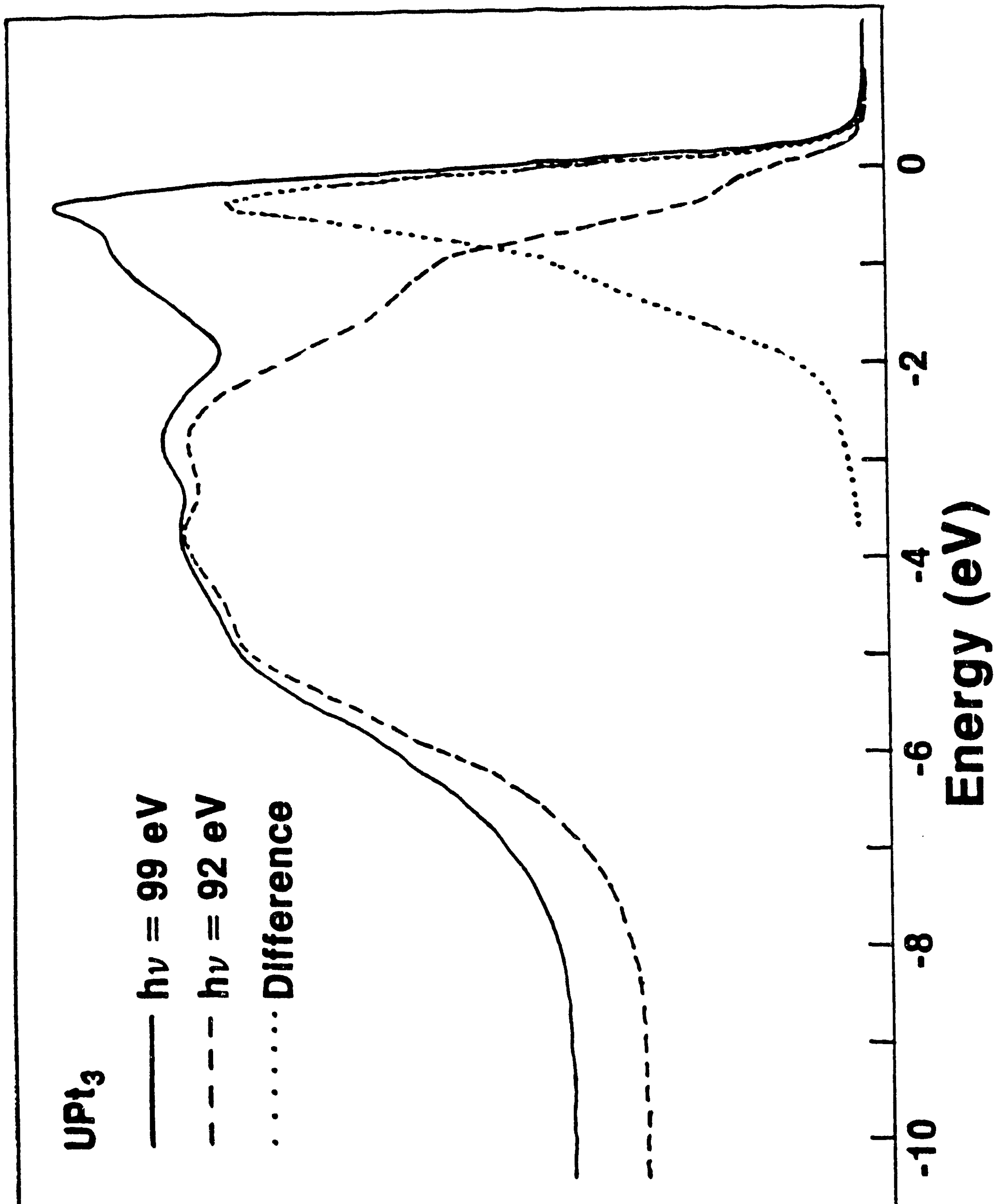
UPt3
hν = 99 eV
hν = 92 eV
Difference
-10
-8
-6
-4
-2
0
Energy (eV)
Amplitude (Arbitrary Units)

AIIM

Association for Information and Image Management

1100 Wayne Avenue, Suite 1100
Silver Spring, Maryland 20910
301/587-8202

Centimeter

Inches

MANUFACTURED TO AIIM STANDARDS
BY APPLIED IMAGE, INC.

4 of 5

Data from "upt3.5f 108"

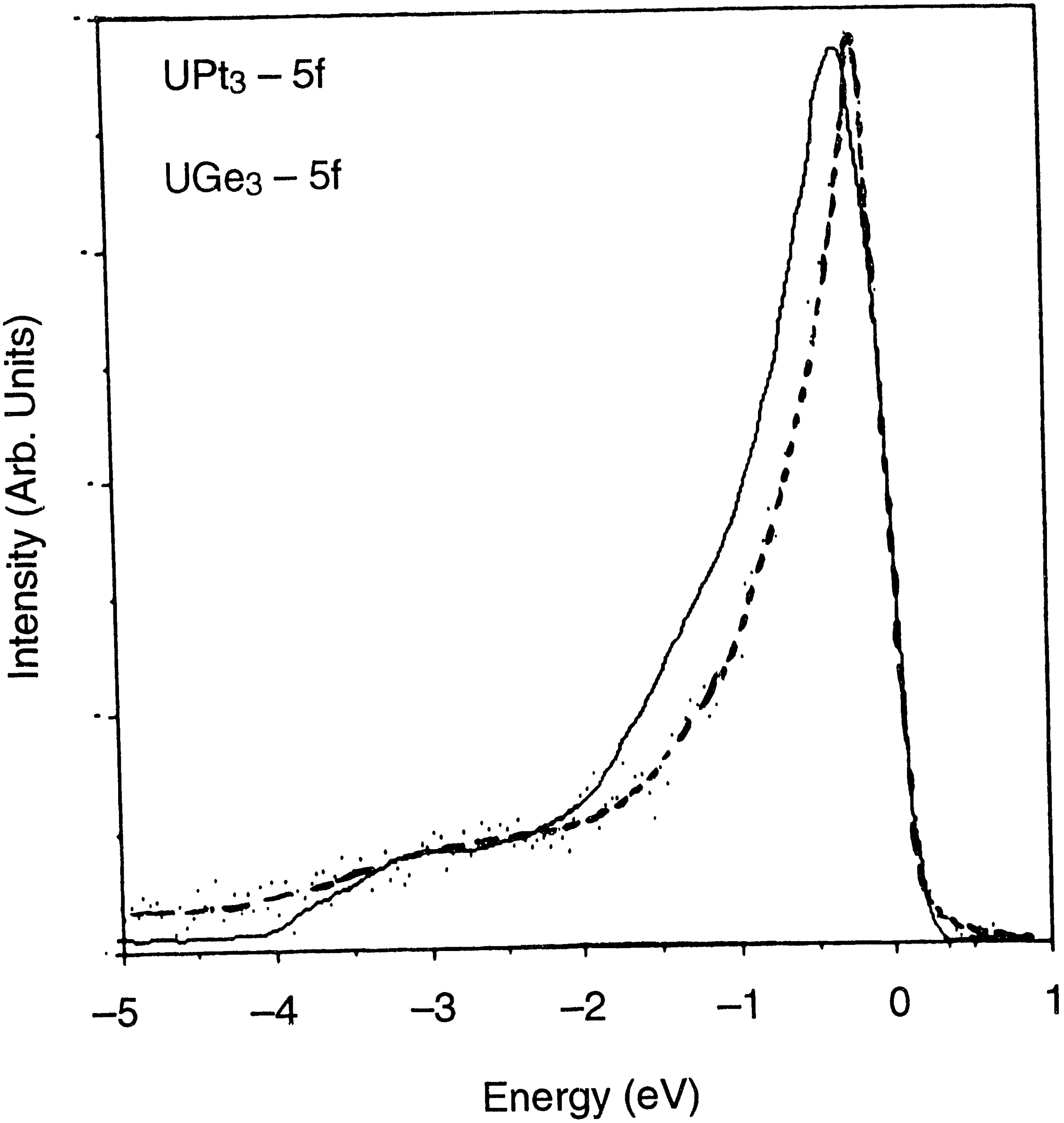

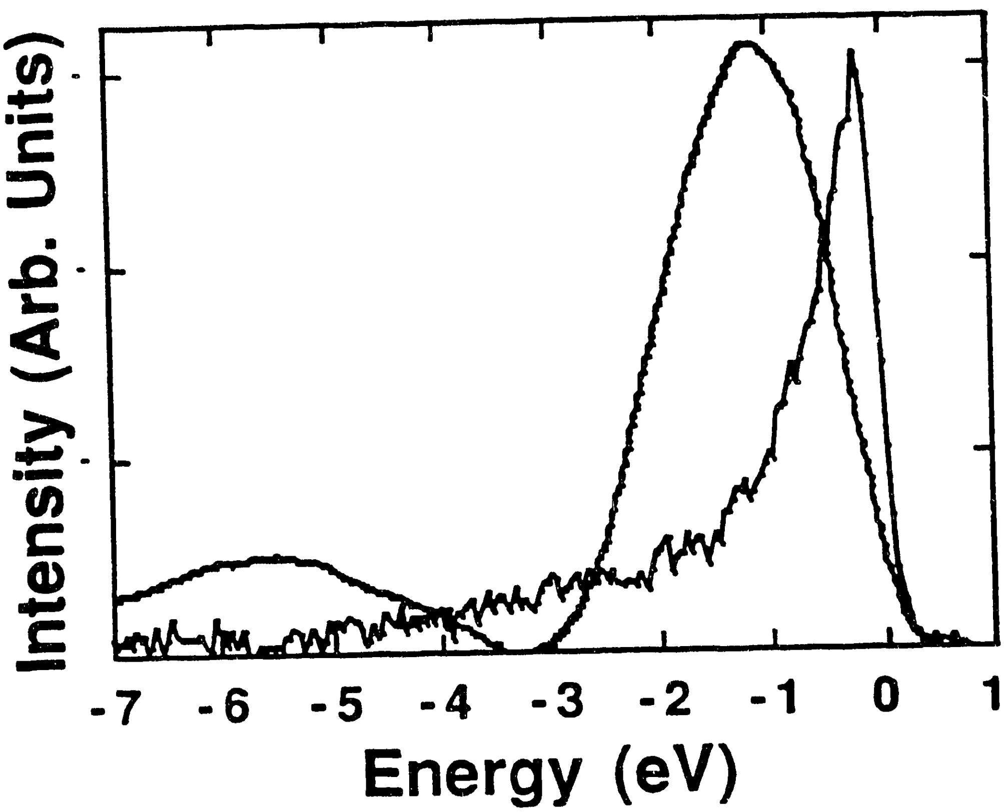
Intensity (Arb. Units)
-7 -6 -5 -4 -3 -2 -1 0 1
Energy (eV)

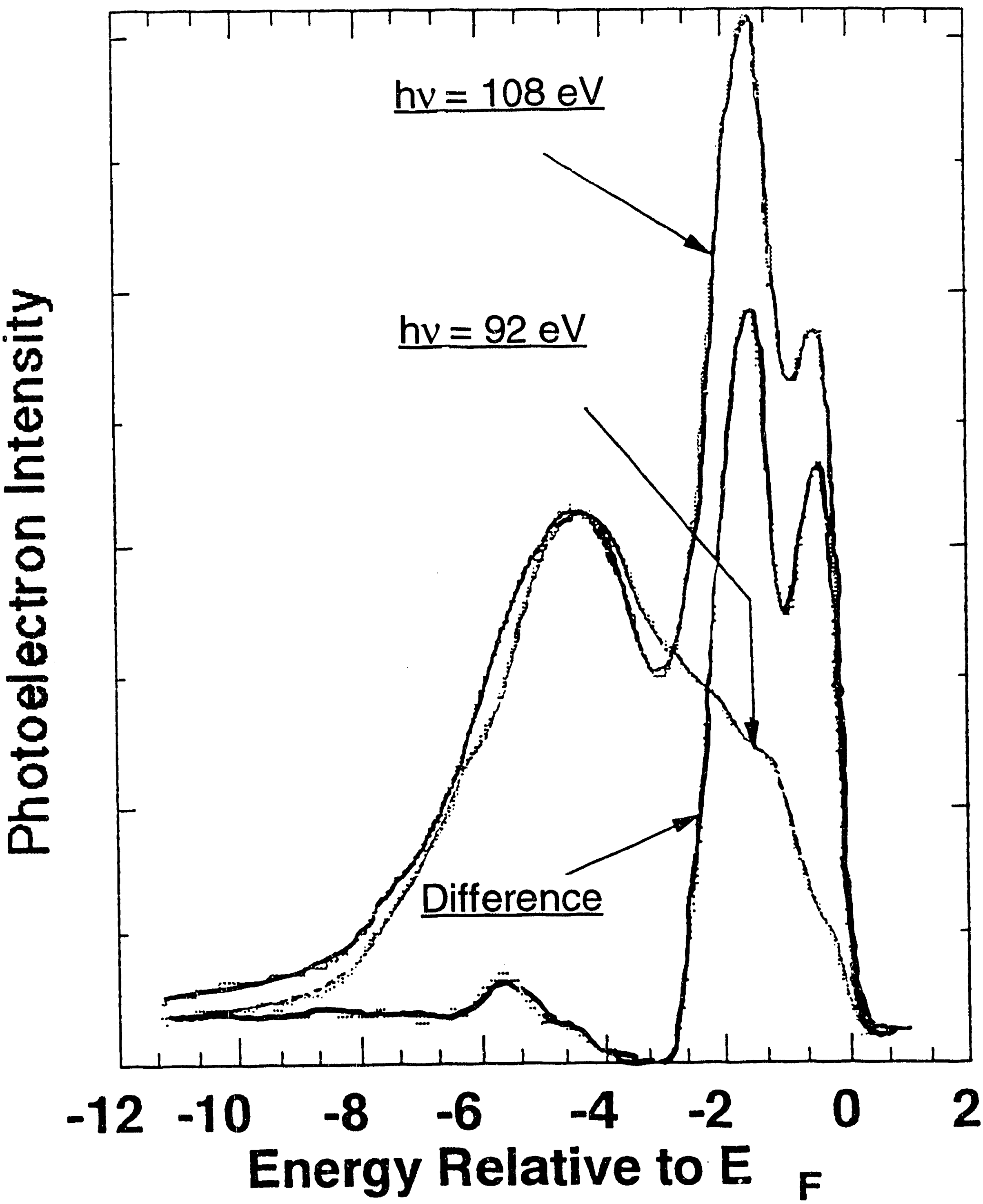
hν = 108 eV
hν = 92 eV
Difference
Photoelectron Intensity
-12
-10
-8
-6
-4
-2
0
2
Energy Relative to E_F

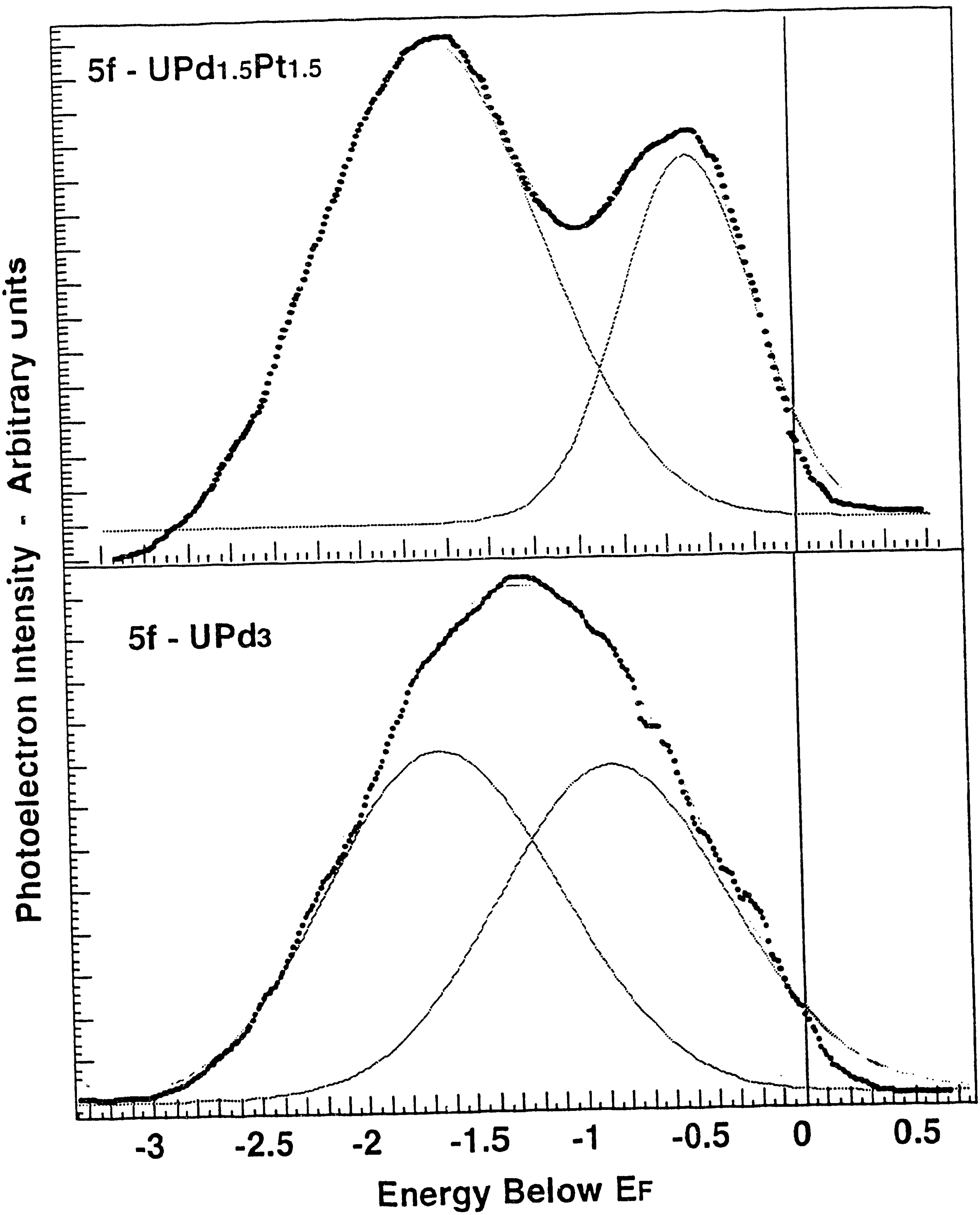

5f - UPd1.5Pt1.5
5f - UPd3
Photoelectron Intensity - Arbitrary units
-3
-2.5
-2
-1.5
-1
-0.5
0
0.5
Energy Below EF

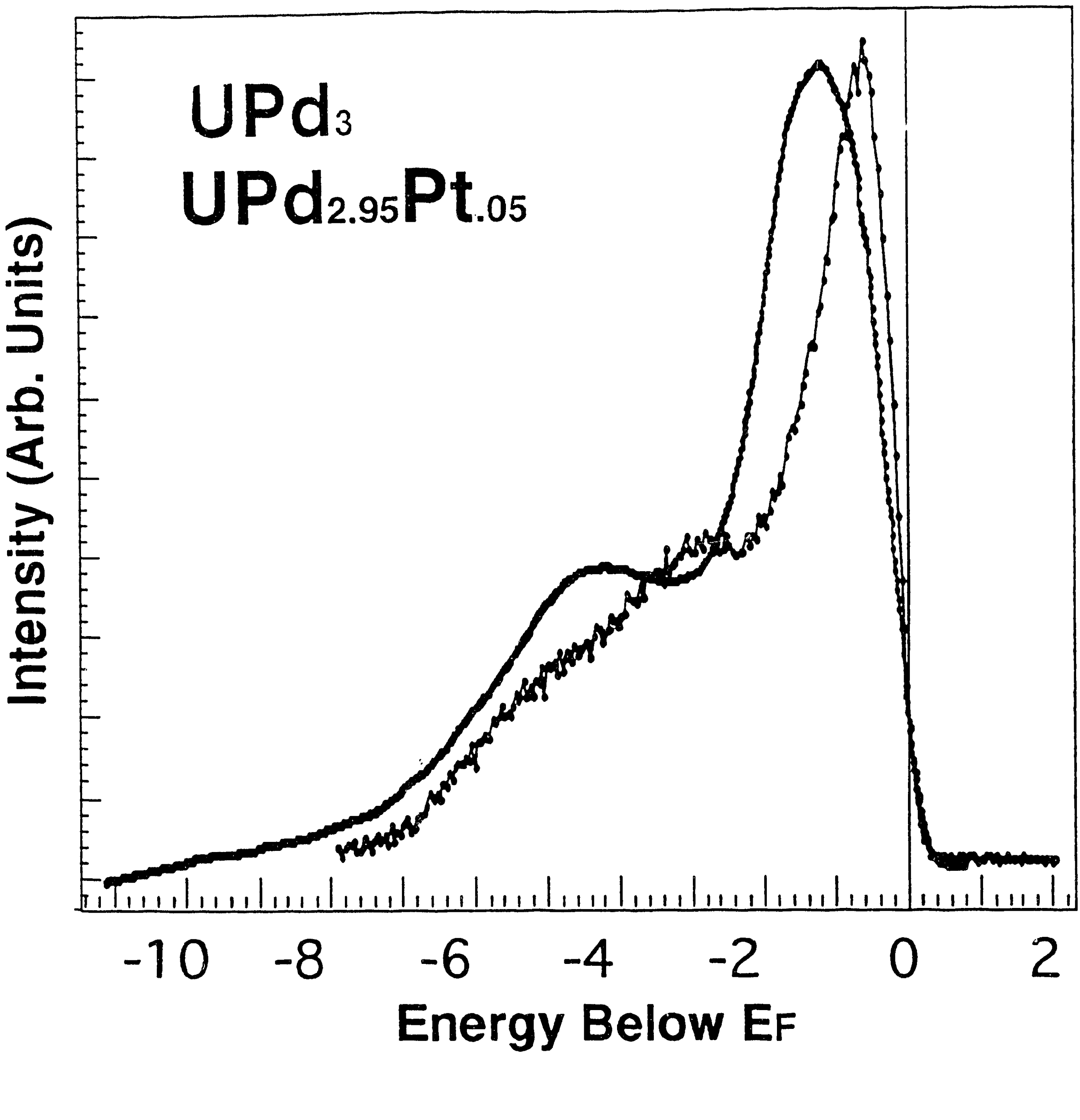

UPd3
UPd2.95Pt.05
Intensity (Arb. Units)
-10
-8
-6
-4
-2
0
2
Energy Below EF

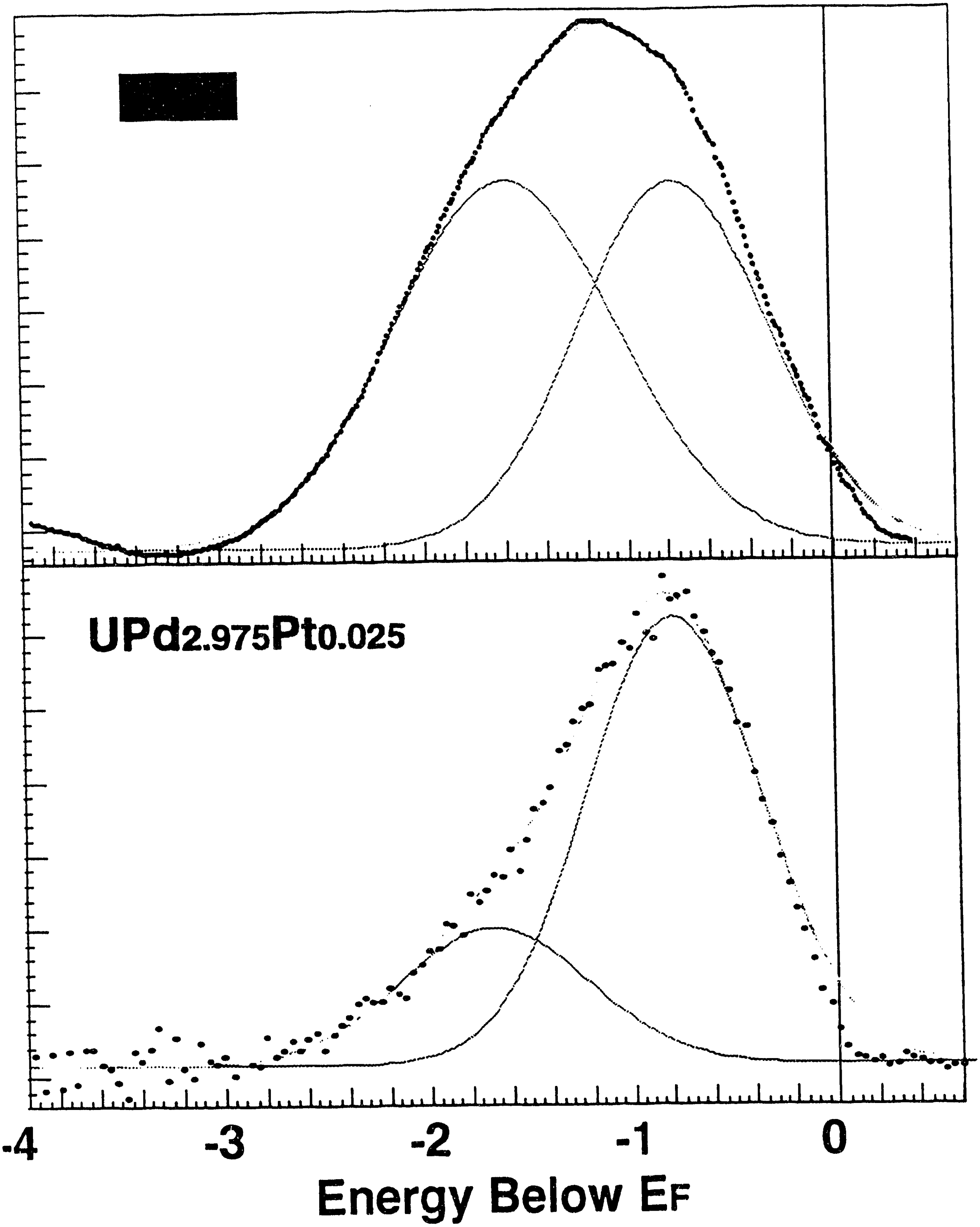
[redacted]
UPd2.975Pt0.025
-4
-3
-2
-1
0
Energy Below EF

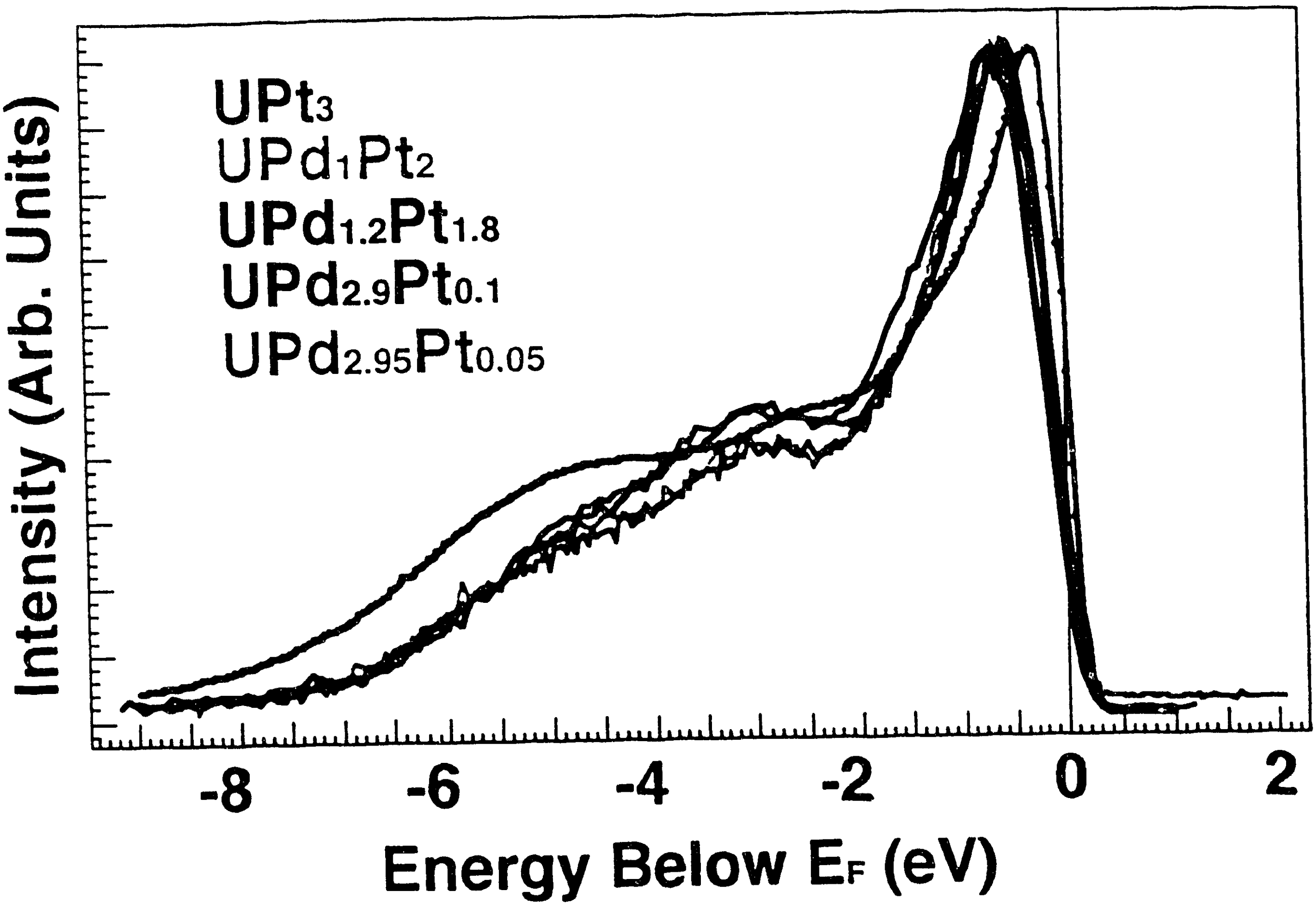

UPt3
UPd1Pt2
UPd1.2Pt1.8
UPd2.9Pt0.1
UPd2.95Pt0.05
Intensity (Arb. Units)
-8
-6
-4
-2
0
2
Energy Below EF (eV)

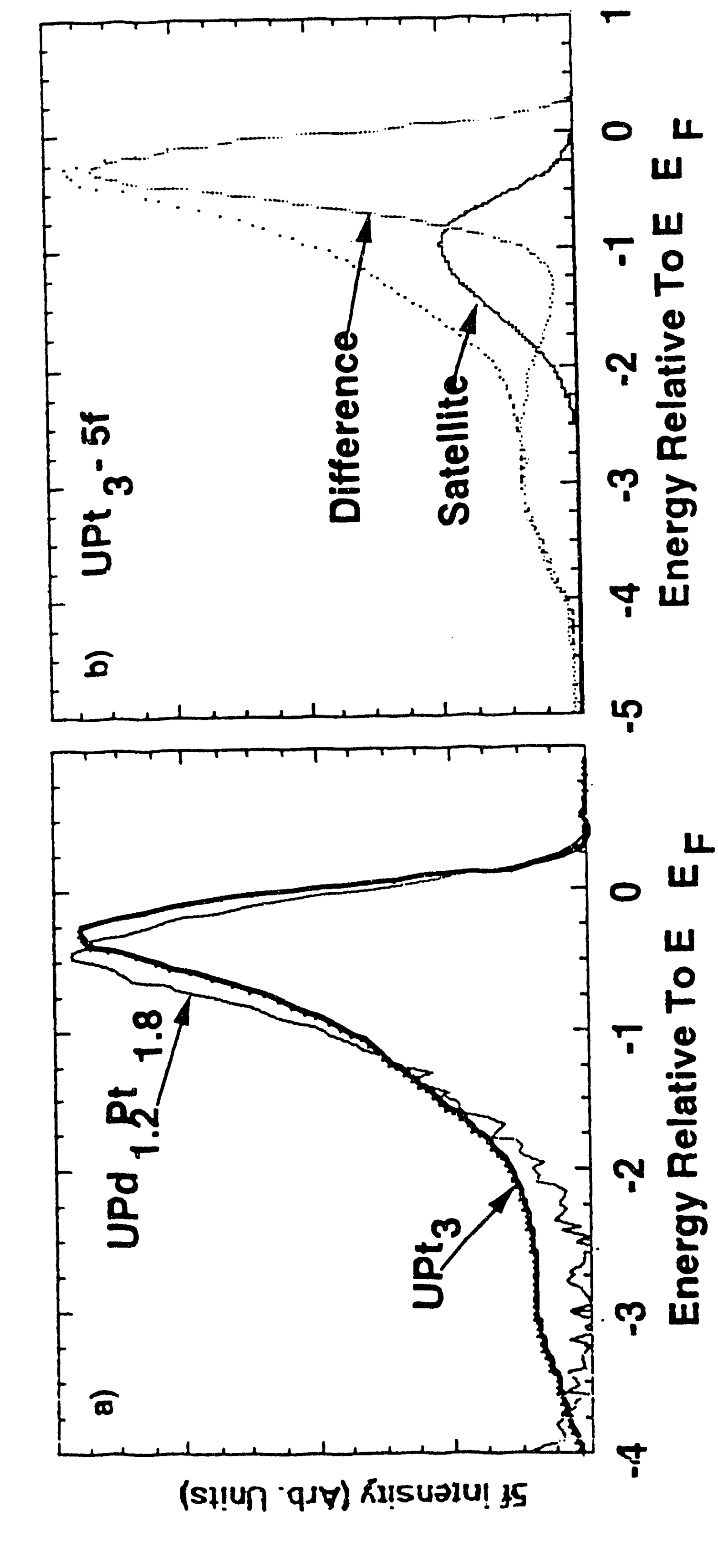
a)
UPd$_{1.2}$Pt$_{1.8}$
UPt$_3$
Energy Relative To E$_F$
5f intensity (Arb. Units)
b)
UPt$_3$ - 5f
Difference
Satellite
Energy Relative To E$_F$
-4
-3
-2
-1
0
-5
1

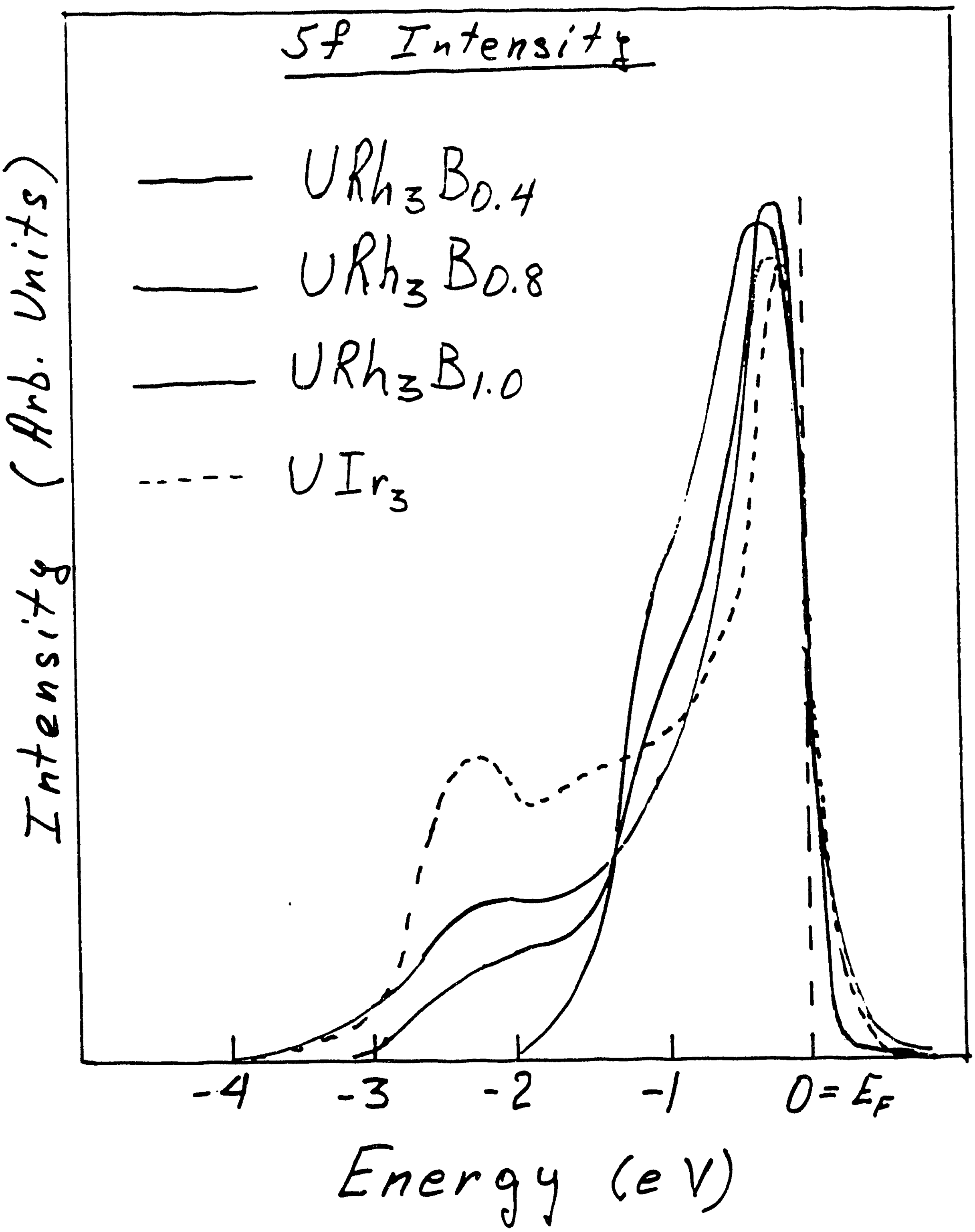

5f Intensity
URh3B0.4
URh3B0.8
URh3B1.0
UIr3
Intensity (Arb. Units)
-4
-3
-2
-1
0 = EF
Energy (eV)

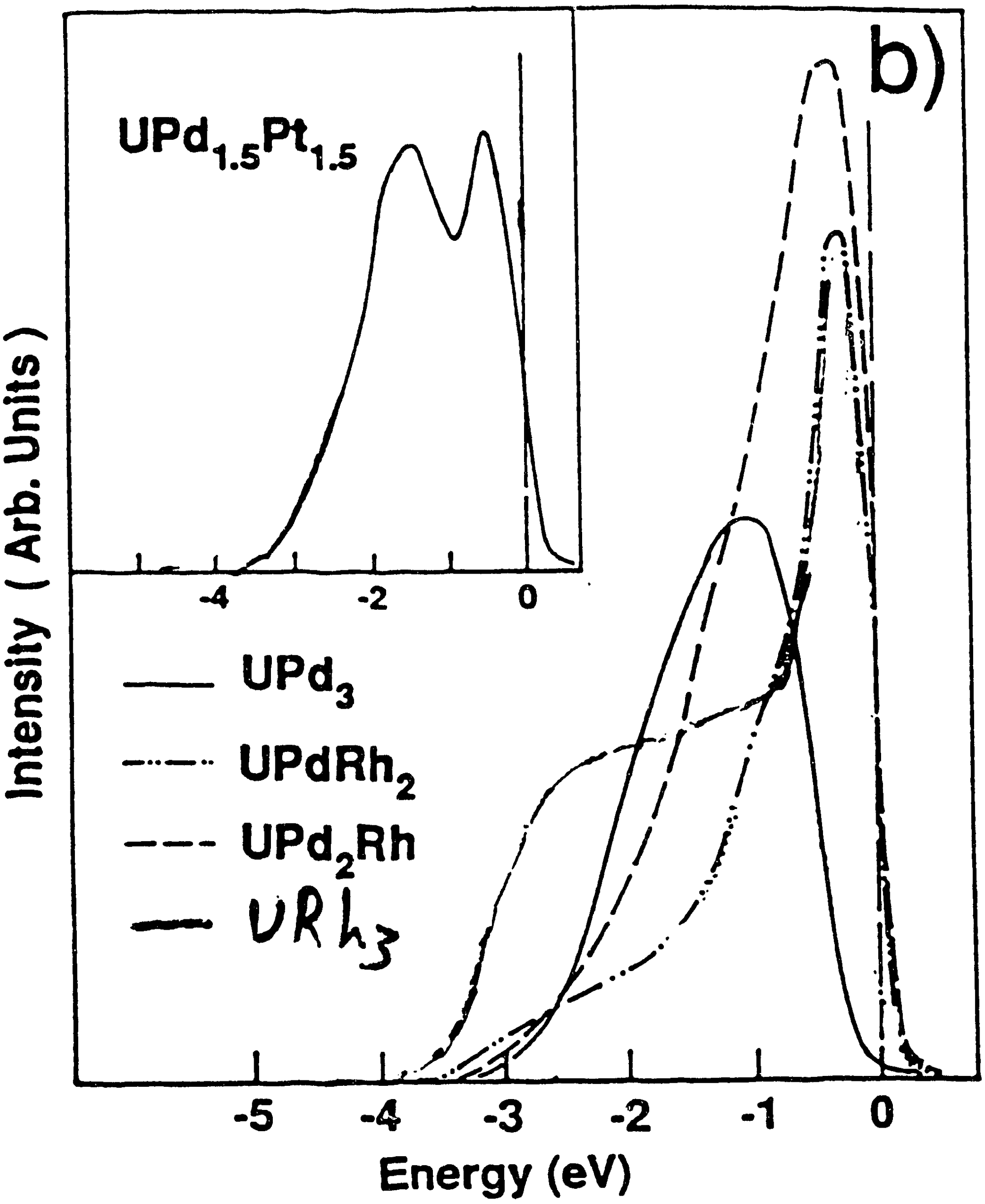

b)
UPd$_{1.5}$Pt$_{1.5}$
-4
-2
0
UPd$_3$
UPdRh$_2$
UPd$_2$Rh
URh$_3$
Intensity (Arb. Units)
-5
-4
-3
-2
-1
0
Energy (eV)

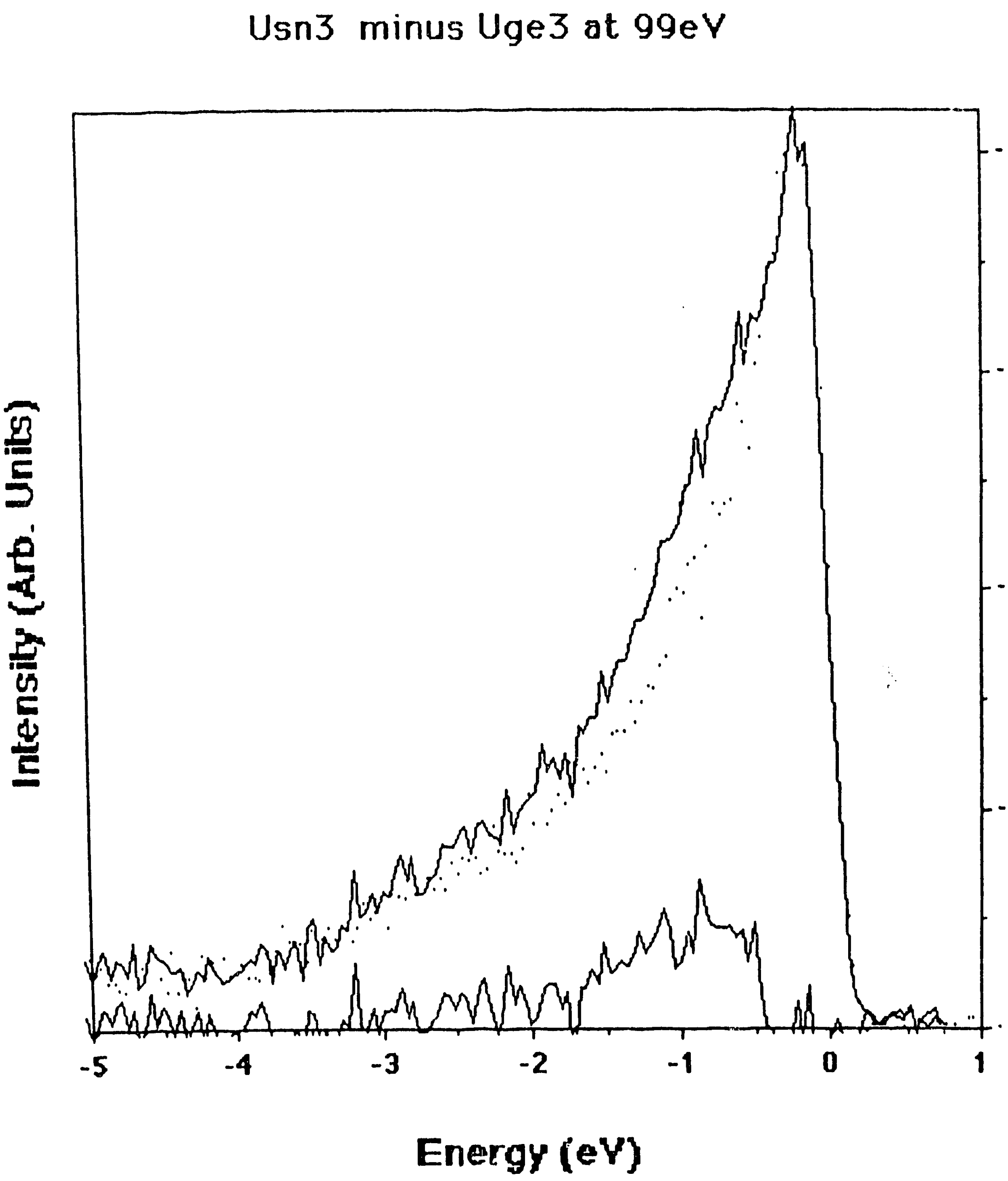

Usn3 minus Uge3 at 99eV
Intensity (Arb. Units)
-5
-4
-3
-2
-1
0
1
Energy (eV)

Res-Anti.CeSb.DIFF1
hv=120 - hv=113 normalized to 'd' feature at -2 eV

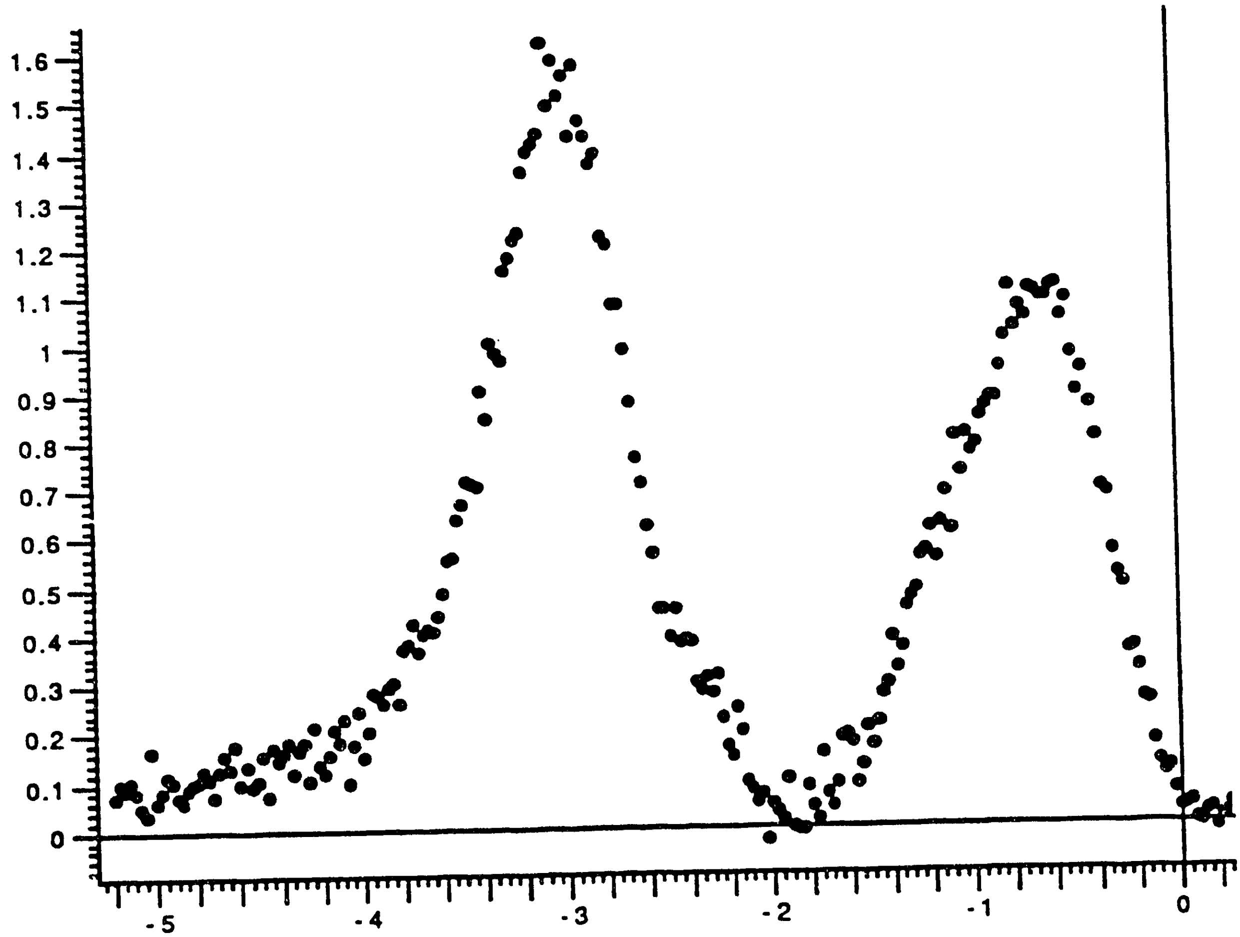

CeSb T ~ LN_2

Inten + Ke adj. for d Feature @ -2eV to line-up: Res → hν=120eV
Anti Res → hν=113eV

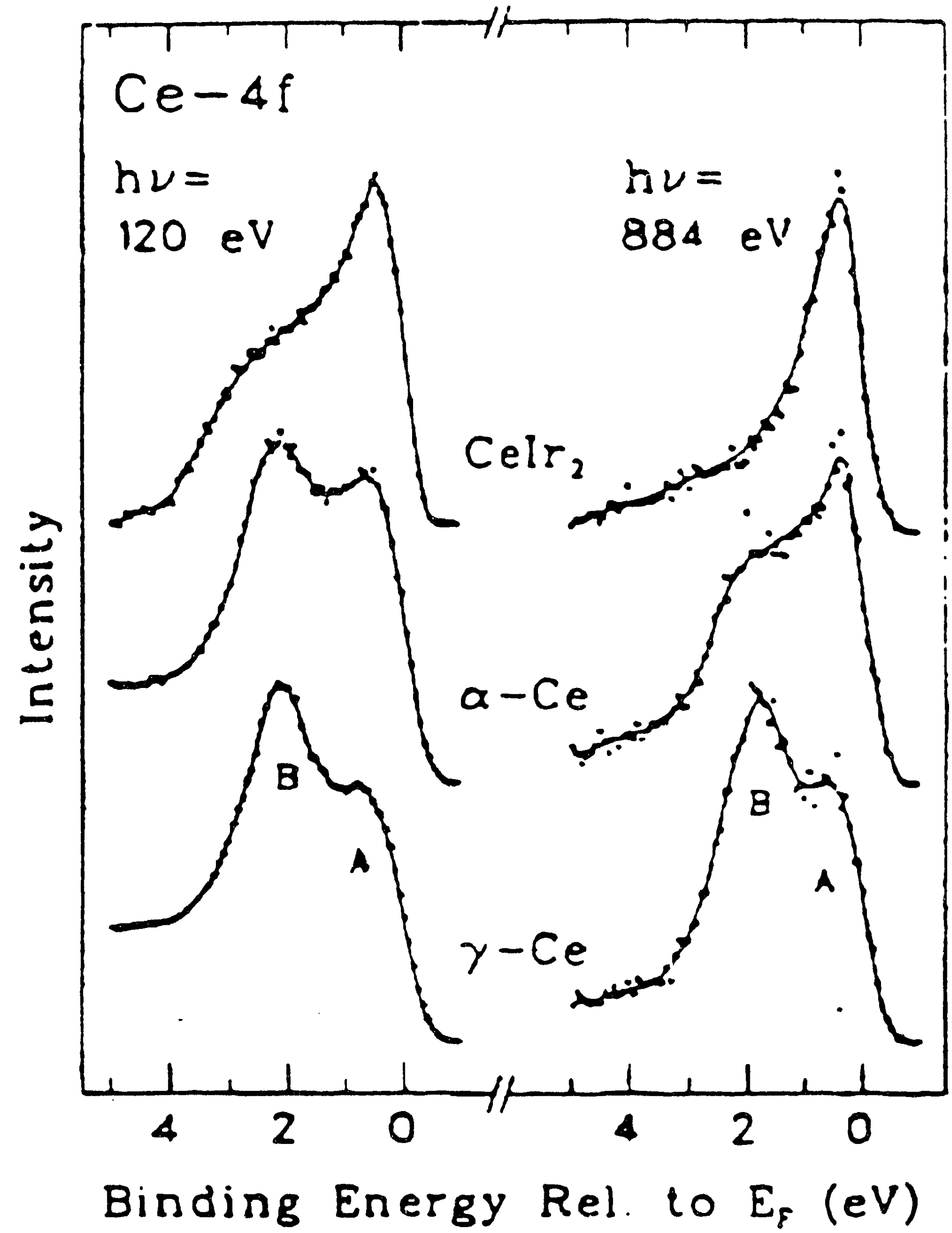

Resonant Ce 4f PE spectra of γ-Ce metal, α-Ce metal, and $CeIr_2$, taken at the Ce 4d (left panel) and Ce 3d (right panel) thresholds, with 700 meV spectral solution in both cases. The solid lines through the data points serve as a guide to the eyes.

ResAntiRes.CeSb.Diff

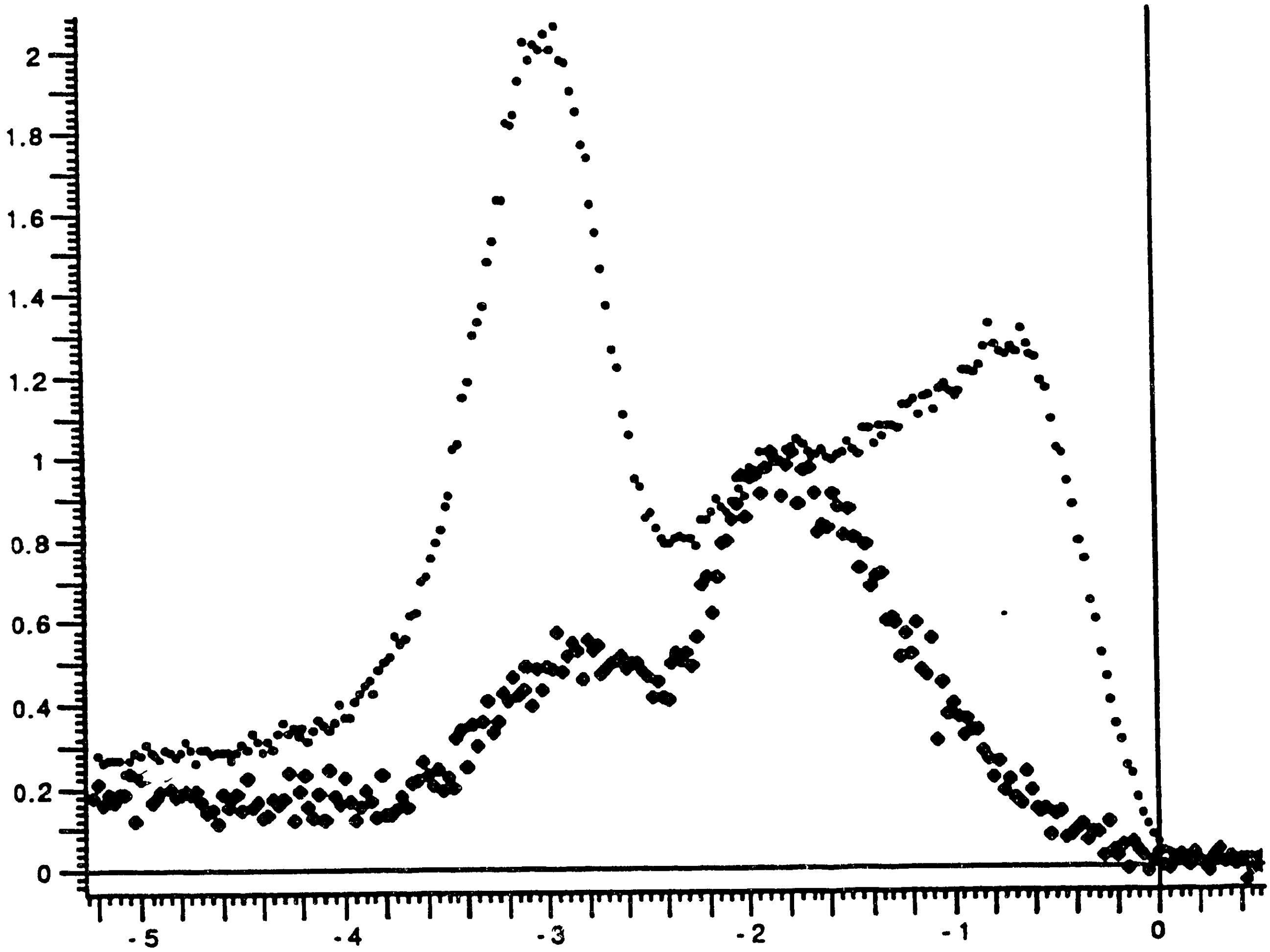

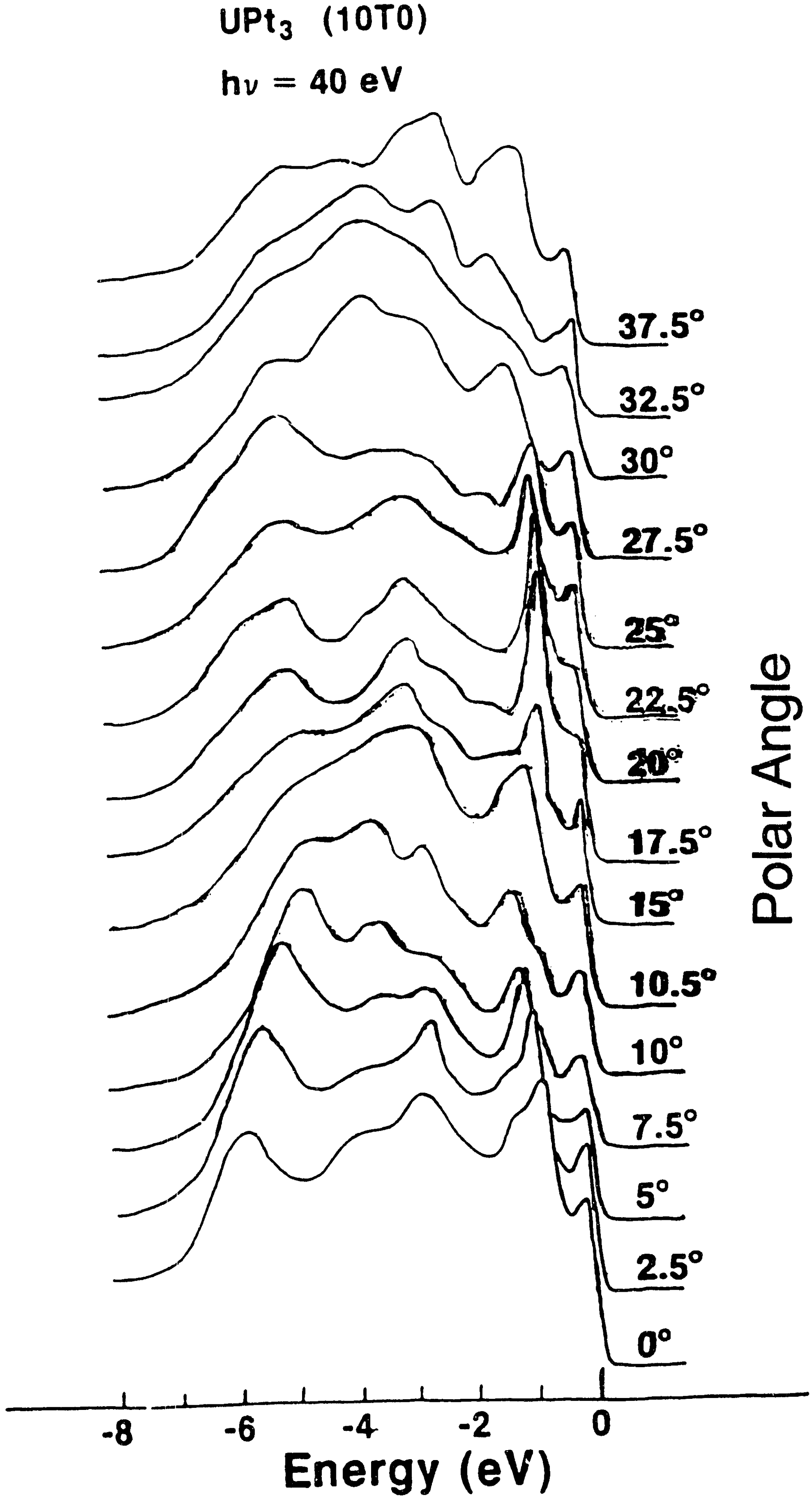
UPt$_3$ (10T0)
hν = 40 eV
37.5°
32.5°
30°
27.5°
25°
22.5°
20°
17.5°
15°
10.5°
10°
7.5°
5°
2.5°
0°
Polar Angle
-8
-6
-4
-2
0
Energy (eV)

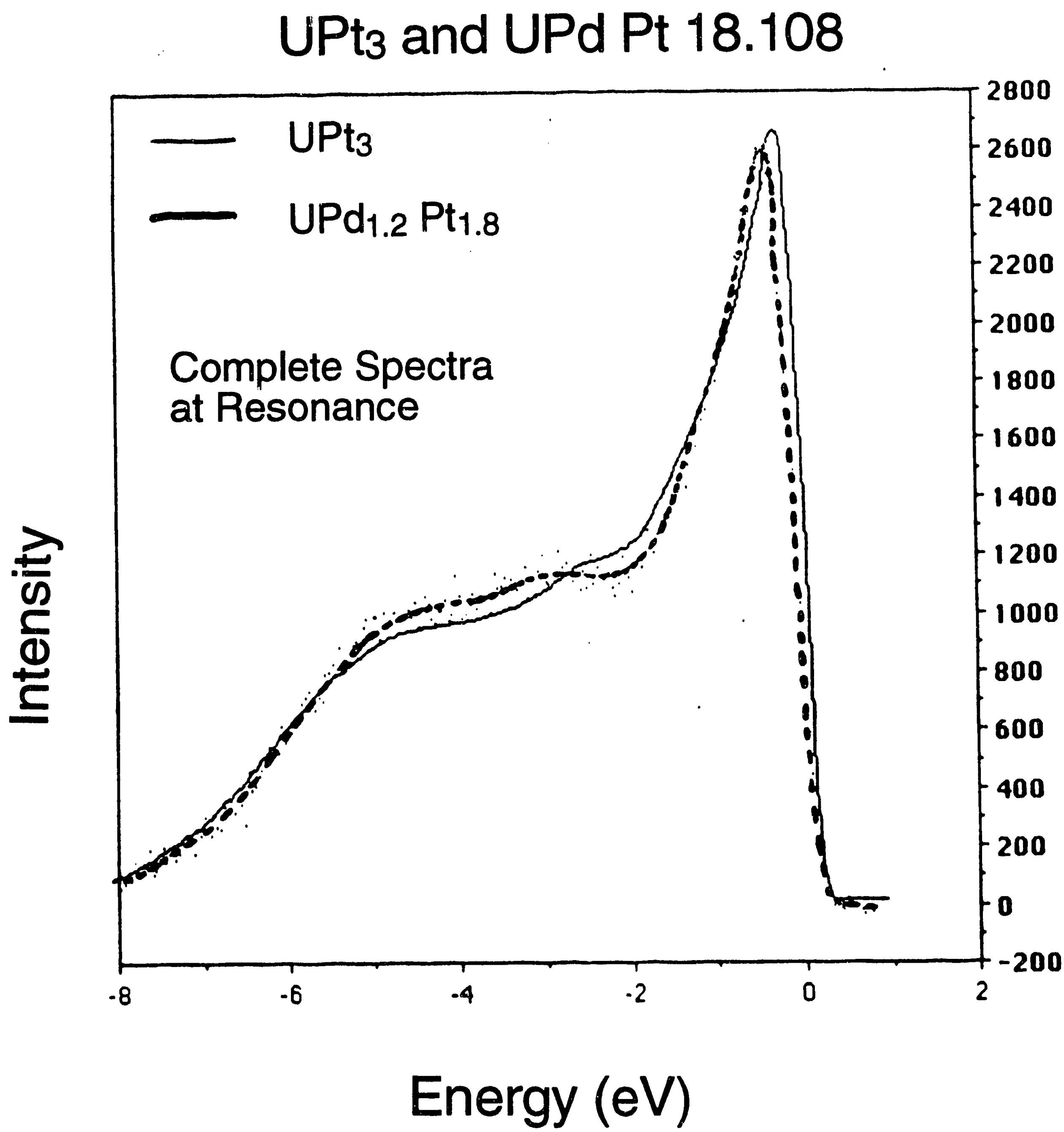
UPt3 and UPd Pt 18.108
UPt3
UPd1.2 Pt1.8
Complete Spectra
at Resonance
Intensity
2800
2600
2400
2200
2000
1800
1600
1400
1200
1000
800
600
400
200
0
-200
-8
-6
-4
-2
0
2
Energy (eV)

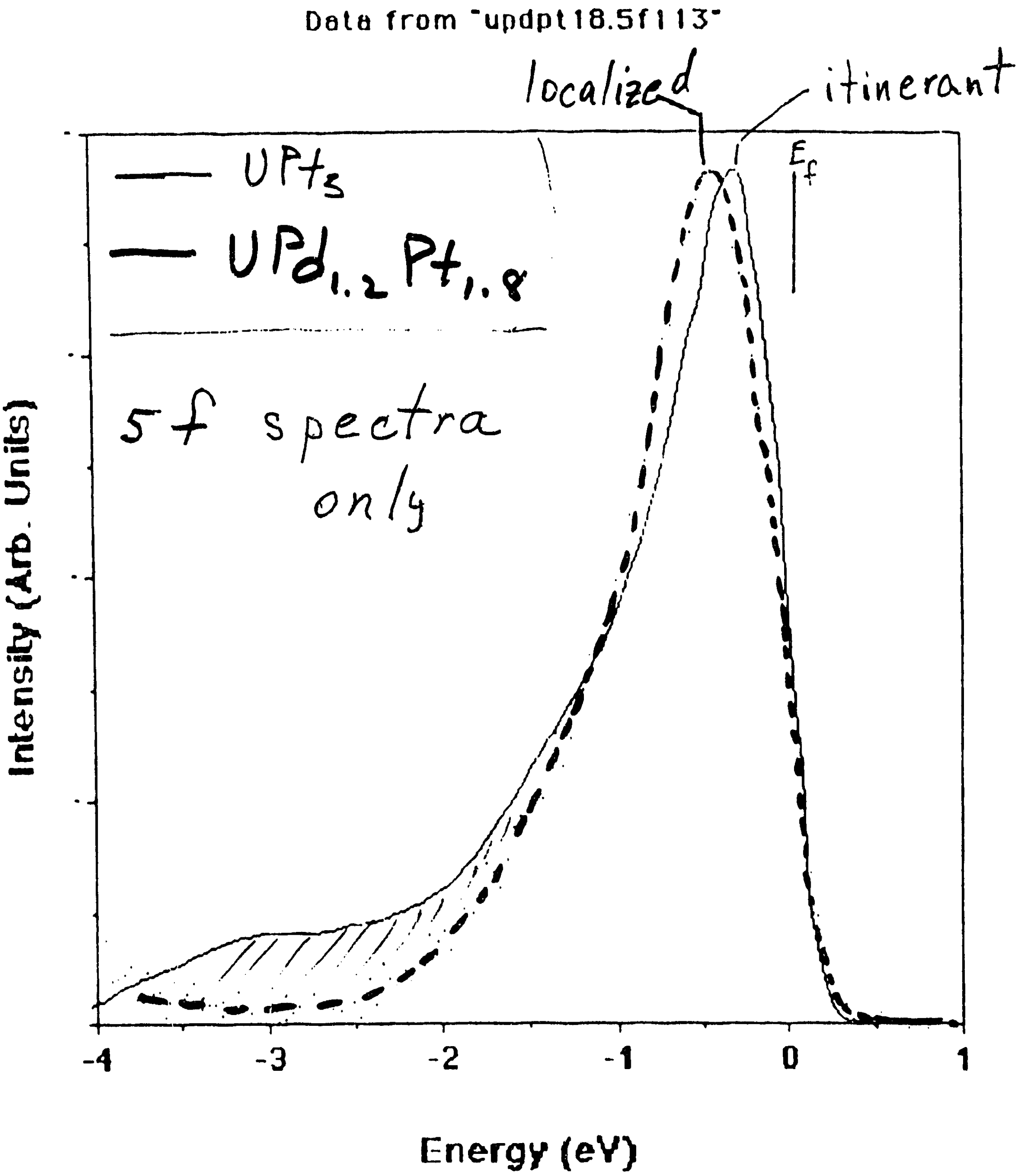
Data from "updpt18.5f113"
localized
itinerant
UPt3
UPd1.2Pt1.8
5f spectra only
Ef
Intensity (Arb. Units)
-4
-3
-2
-1
0
1
Energy (eV)

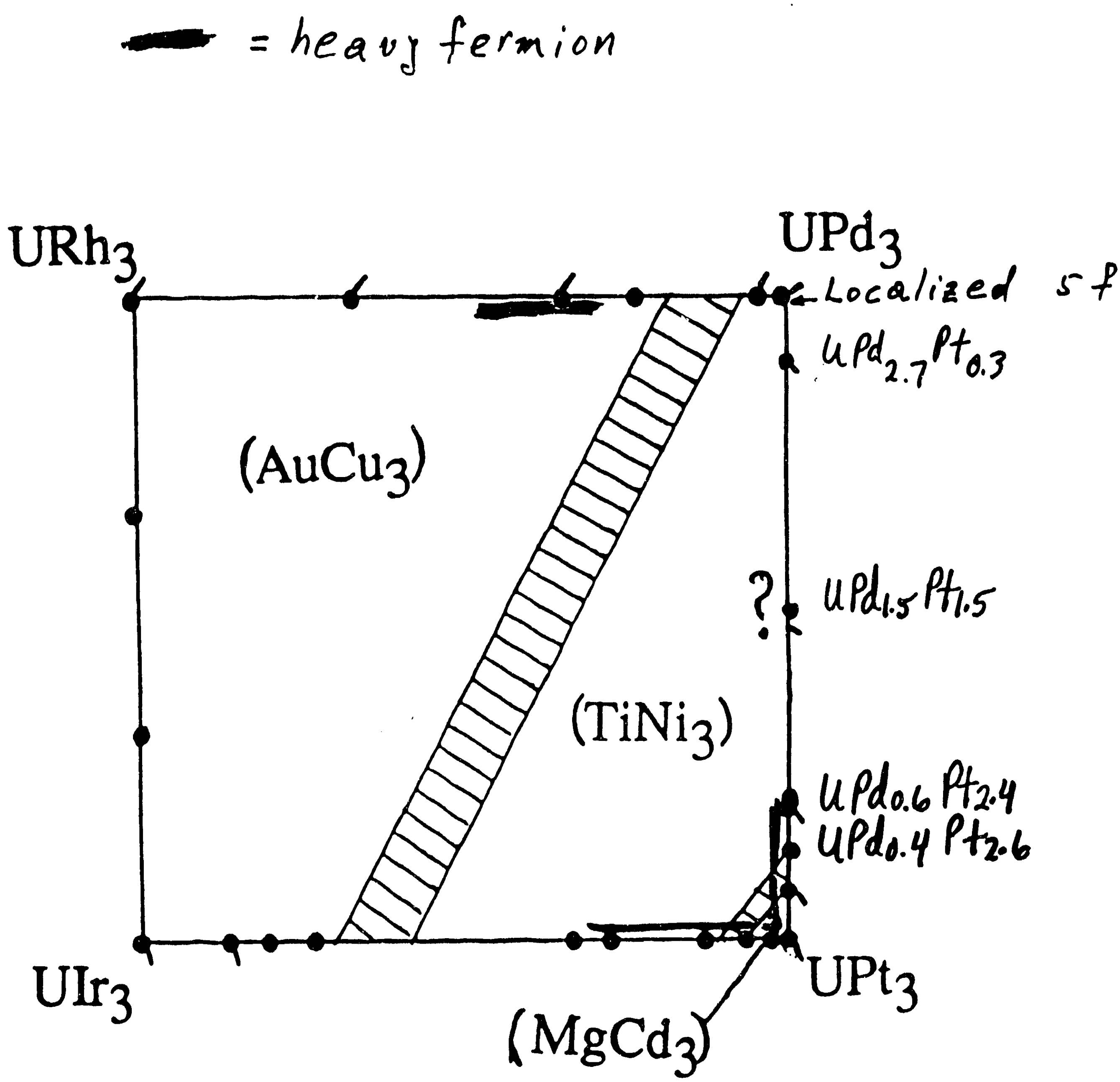
= heavy fermion
URh3
UPd3
Localized 5f
UPd2.7Pt0.3
(AuCu3)
?
UPd1.5Pt1.5
(TiNi3)
UPd0.6Pt2.4
UPd0.4Pt2.6
UIr3
UPt3
(MgCd3)

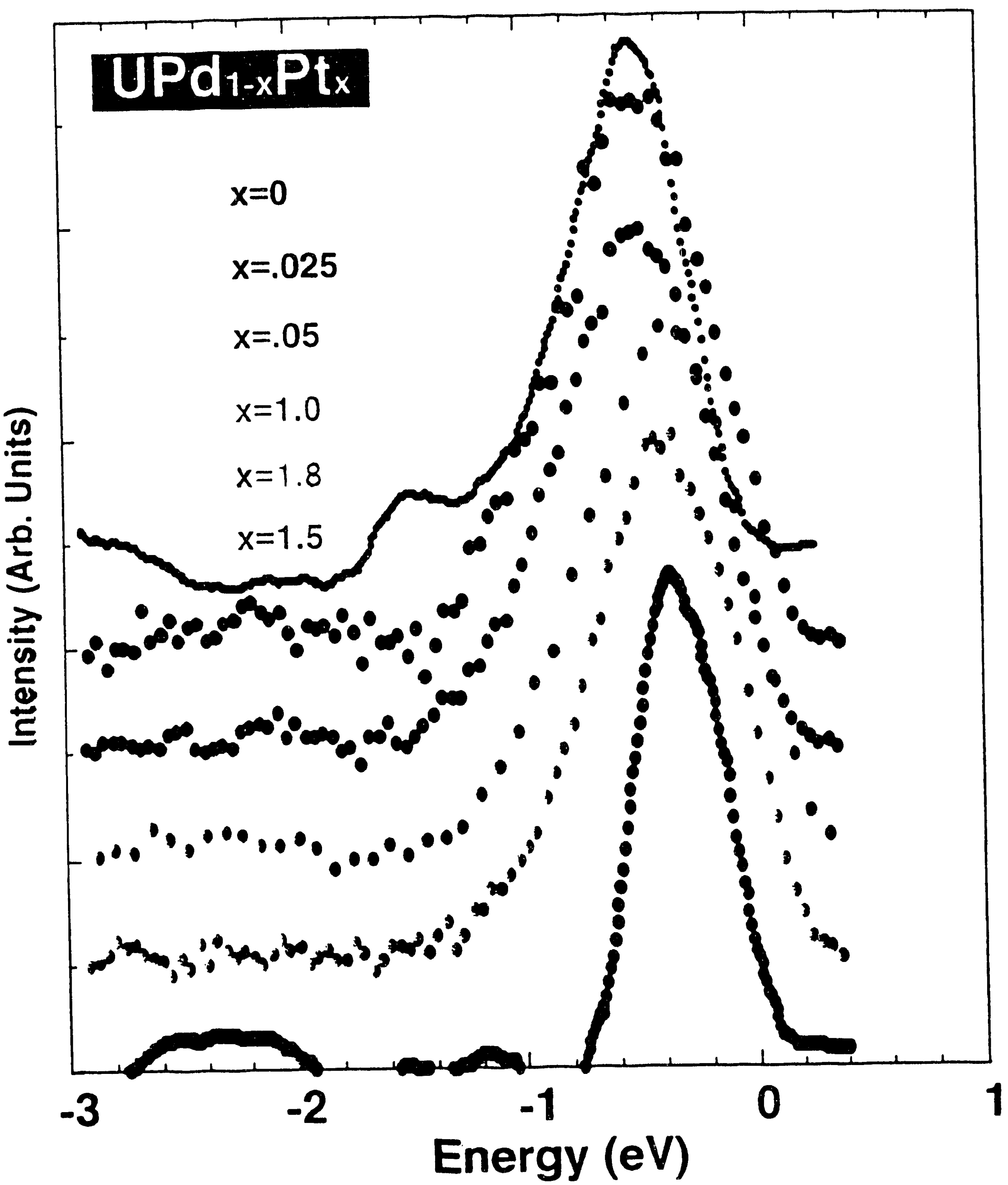
UPd1-xPtx
x=0
x=.025
x=.05
x=1.0
x=1.8
x=1.5
Intensity (Arb. Units)
-3
-2
-1
0
1
Energy (eV)

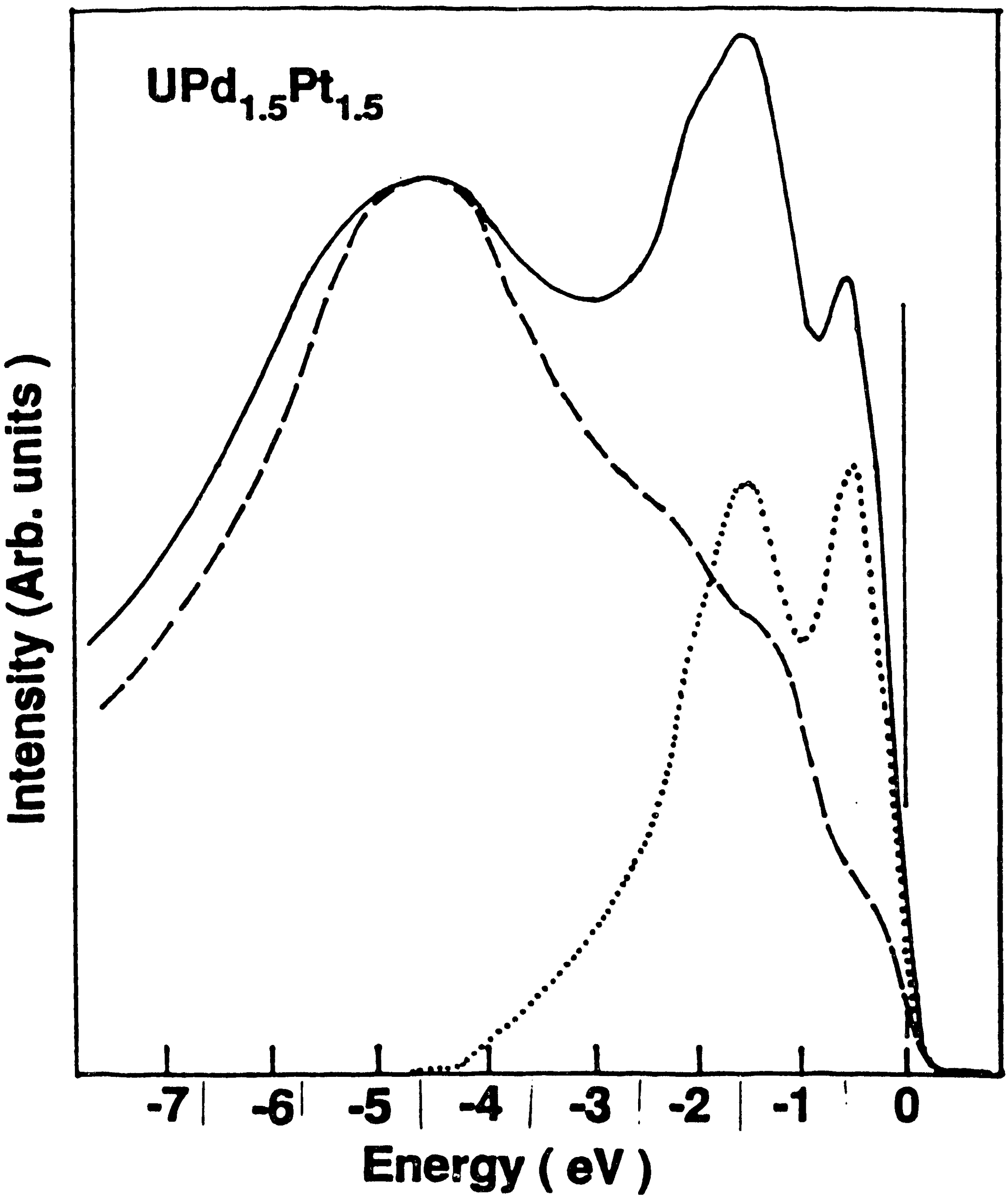

UPd$_{1.5}$Pt$_{1.5}$
Intensity (Arb. units)
-7
-6
-5
-4
-3
-2
-1
0
Energy (eV)

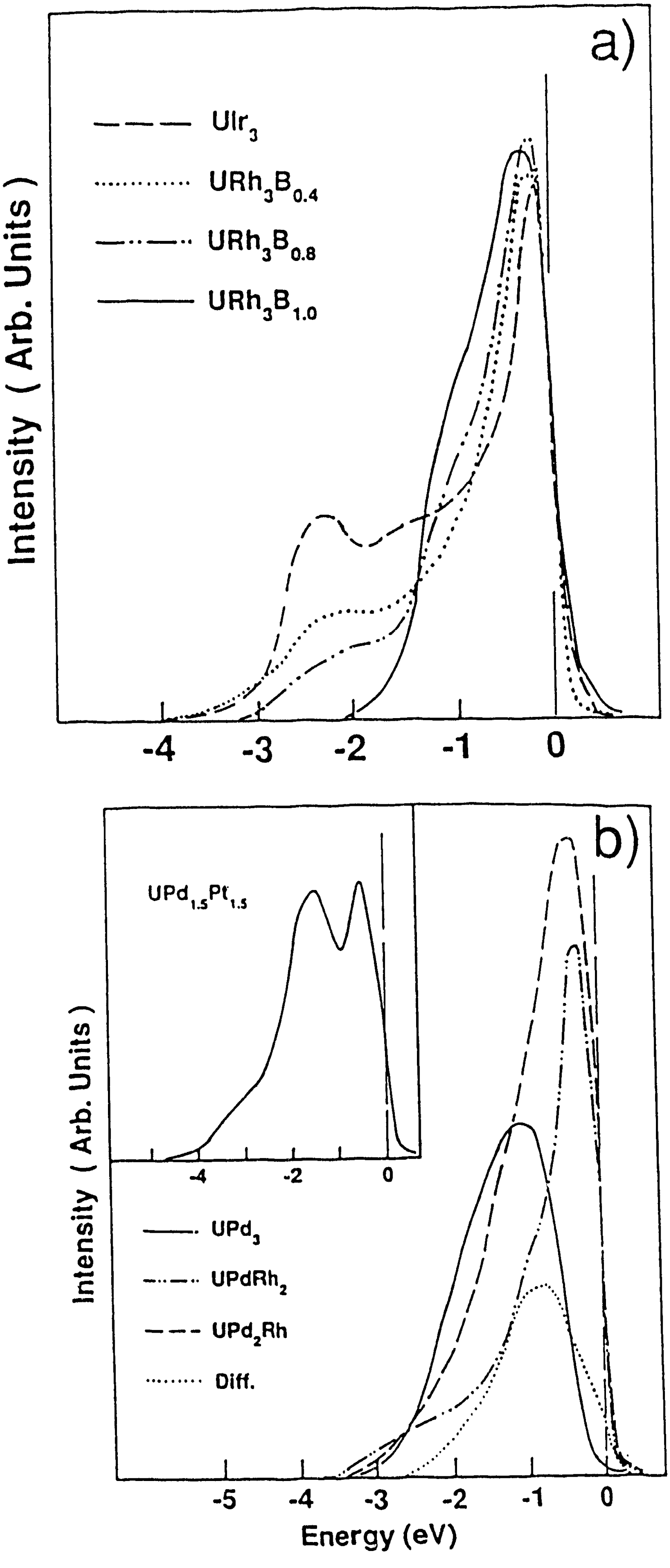
a)
UIr3
URh3B0.4
URh3B0.8
URh3B1.0
Intensity (Arb. Units)
-4
-3
-2
-1
0
b)
UPd1.5Pt1.5
-4
-2
0
UPd3
UPdRh2
UPd2Rh
Diff.
Intensity (Arb. Units)
-5
-4
-3
-2
-1
0
Energy (eV)

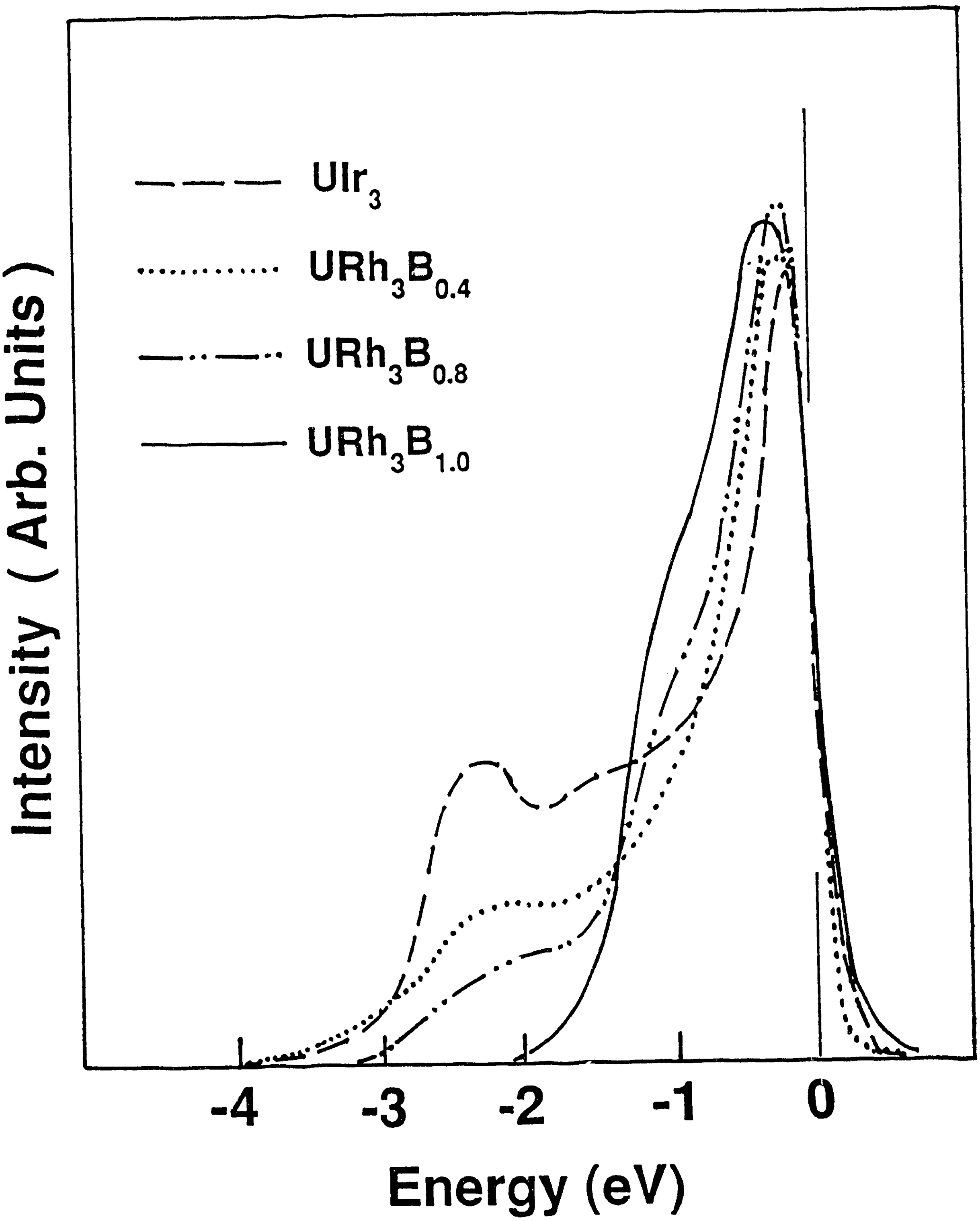

UIr3
URh3B0.4
URh3B0.8
URh3B1.0
Intensity (Arb. Units)
-4
-3
-2
-1
0
Energy (eV)

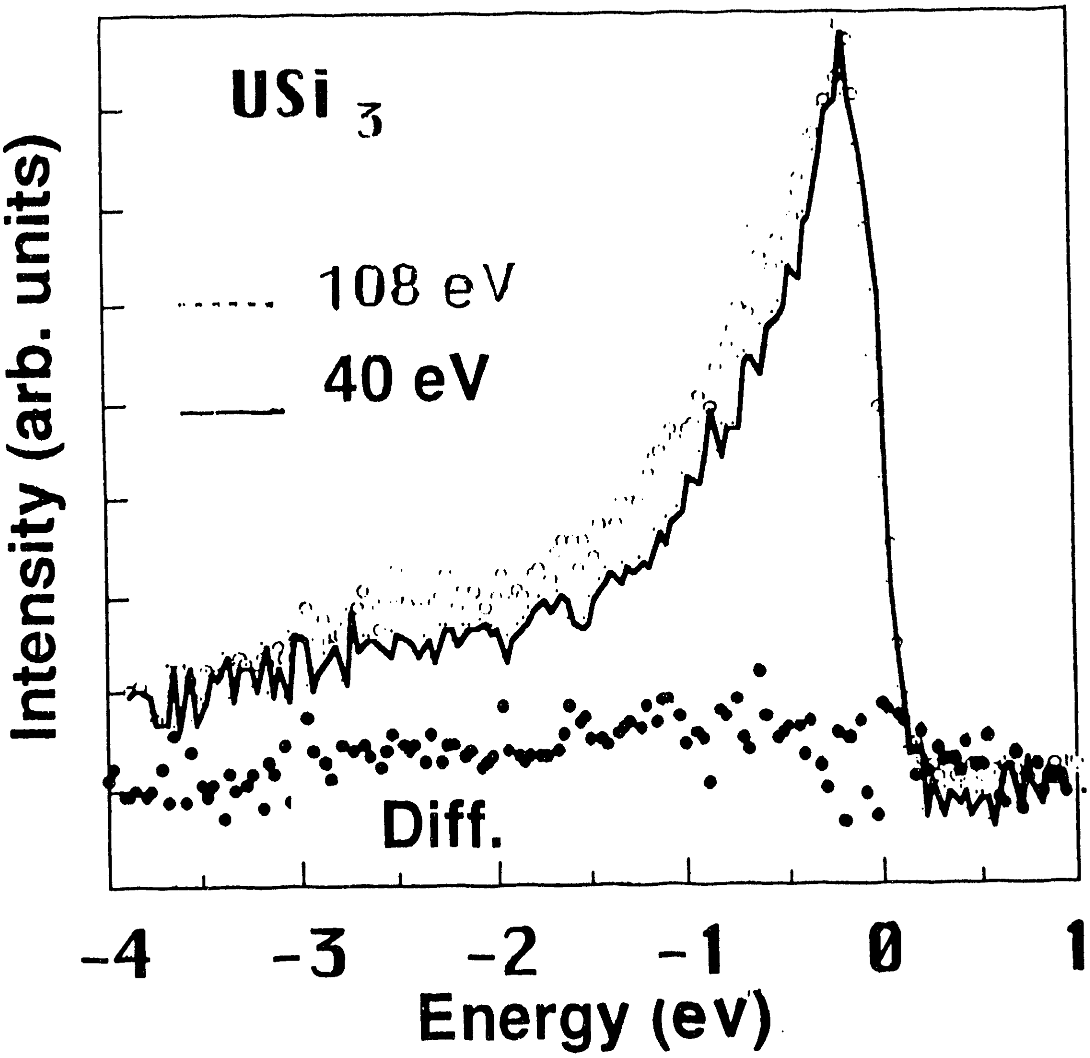
USi 3
108 eV
40 eV
Diff.
Intensity (arb. units)
-4
-3
-2
-1
0
1
Energy (eV)

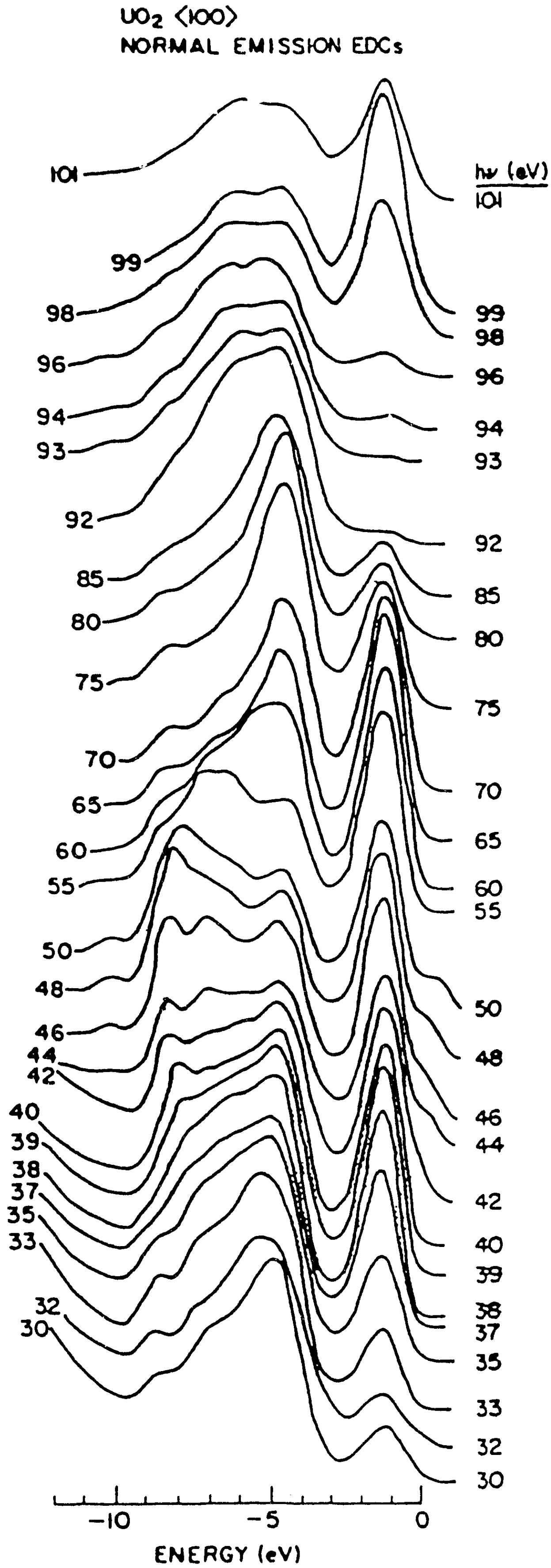

UO2 ⟨100⟩
NORMAL EMISSION EDCs
hν (eV)
101
99
98
96
94
93
92
85
80
75
70
65
60
55
50
48
46
44
42
40
39
38
37
35
33
32
30
−10
−5
0
ENERGY (eV)

ELECTRON SPECTROSCOPY OF HEAVY FERMION ACTINIDE MATERIALS *

J.W. Allen

Randall Laboratory, University of Michigan, Ann Arbor, MI 48109–1120

The actinides belong to the general category of materials often called by the term "narrow band," by which it is meant that correlations induced by Coulomb interactions play an important role in determining their properties. The 5f electrons of the actinides are generally regarded as being more localized than the transition metal 3d electrons, but less localized than the rare earth 4f electrons. Given that the band model seems to be a good starting point for describing the 3d electrons of the elemental transition metals, but that the atomic model seems to be the proper starting point for describing the 4f electrons of the rare earth elements, it is perhaps not surprising that the full range of bandlike to atomic behavior seems to be found in actinide elements and compounds. For the elements, the usual understanding is that, as one progresses to the right across the actinide row, the transition from bandlike to atomic occurs between Pu and Am. As with the transition metals, atomic behavior can be induced by making compounds. For example, an atomic model is a better starting point than band theory for describing the 3d and 5f electrons of NiO and UO_2, respectively.

Heavy fermion behavior is a narrow band property, found in both rare earth and actinide materials, and perhaps even transition metal materials, which highlights the tension between the band and atomic viewpoints especially well. The defining characteristic is that the T-linear specific heat coefficient γ, which is proportional to the density of states at the Fermi energy for an electron gas is found to be 50 to 1000 times larger than for a free electron gas. Phenomenologically, the large γ suggests a very small bandwidth. Band calculations for such materials do find reduced bandwidths but the predicted γ-values are still 20 to 50 times less than the measured values. A quite different approach which has met with great success for rare earth materials models the 4f electrons as strongly correlated atomic states, hybridized with bandlike conduction band states. This approach leads to the Kondo picture in which the rare earth magnetic moment is quenched by formation of a many-body singlet ground state, but where spin fluctuations occur on the scale of the Kondo temperature T_K. The evolution of the spin entropy over the energy and temperature range T_K gives a T-linear specific heat contribution with coefficient $\gamma \sim 1/T_K$. In this picture, heavy Fermion behavior is naturally explained by very small T_K values associated with the quenching of atomic magnetic moments. However, the story comes full circle again with the realization that low temperature electrical properties display the translational symmetry of the lattice, and that f-electron Fermi surfaces in fair to excellent agreement with predictions of band theory have been found for some heavy fermion materials.

Spectroscopic studies of Kondo behavior have centered on Ce and Yb materials. The signature of Kondo behavior in the single-particle f spectrum, measured by photoemission spectroscopy (PES) and inverse photoemission spectroscopy (IPES), is the appearance of a peak near the Fermi energy E_F called the Kondo resonance. In Ce, for example, the resonance lies between a $4f^1 \rightarrow 4f^0$ atomic ionization peak below E_F in the PES spectrum and a $4f^1 \rightarrow 4f^2$ atomic affinity peak above E_F in the IPES spectrum. The separation of the affinity and ionization peaks signals the atomic Coulomb repulsion U. The spectral weight of the Kondo resonance increases with T_K and for materials with a small number of f-electrons like Ce (or U), most of the weight lies in the IPES spectrum. Such a three peaked structure is observed in Ce compounds and has been interpreted from the view of the impurity Anderson model within its Kondo regime[1]. The Hamiltonian parameters found from fitting the 4f spectra, and also the 3d core level spectra of Ce and Yb materials, lead to T_K values of the right order of magnitude for small T_K materials, and in good agreement with experiment for moderate to large T_K materials. No other picture at present offers such a unifed view of spectroscopic and low temperature properties.

A confusing complication, however, is that the PES spectra of small T_K materials display much more spectral weight near E_F than expected for the small-T_K resonance. In fact, the model predicts spectral weight near E_F due to other mechanisms[1] than the resonance itself, but there is currently controversy[2] as to whether these mechanisms do indeed explain spectra taken with ever-better resolution[3]. There is also controversy[2] as to whether the temperature dependence[3] of the resonance is or is not consistent with theory for Ce and Yb materials.

For actinides, due to the difficulty of obtaining and handling highly radioactive samples, heavy fermion research, and most electron spectroscopy, centers on uranium and its compounds. In general, the 5f spectra of heavy-fermion uranium materials do not resemble those of rare earth materials. There is a very large amount of spectral weight around E_F with a rather bandlike appearance, and there are not well separated ionization and affinity peaks. The only evidence[4] of the importance of the Coulomb interaction U is that the widths of both the PES and IPES 5f spectra exceed that predicted in band calculations, and the primary evidence[4] for the applicability of the impurity Anderson approach has been that dilution of uranium by a non-5f element like Y causes no change in the 5f PES spectrum measured at modest resolution.

Recently an exception[5,6,7] has been found in the system $Y_{1-x}U_xPd_3$. UPd_3 is not a heavy-fermion material but it is the only uranium intermetallic with a 5f spectrum which suggets an Anderson model. The 5f spectrum has a gap around E_F with peaks below and above E_F which are interpreted, respectively, as a $5f^2 \rightarrow 5f^1$ ionization peak and a $5f^2 \rightarrow 5f^3$ affinity peak. In the alloy system it is found that E_F shifts toward the ionization peak asa x is decreased. This phenomenon is called "Fermi level tuning" and occurs[5] because Y^{3+} replaces U^{4+}, the ionization state correpsonding to $5f^2$. For $x < 0.3$ the transport properties[6] develop characteristic Kondo behavior, with T_K increasing as x decreases. This is qualitatively consistent with the Anderson impurity model, which predicts that T_K increases as the 5f ionization energy relative to E_F decreases. For the same range of decreasing x, the 5f IPES spectrum displays a growth of weight near E_F which produces an un-gapped spectrum much like that of concentrated heavy-Fermion materials, and which has been interpreted as the Kondo resonance[7]. As with small T_K Ce systems, there is extra weight near E_F which must be rationalized by various additional mechanisms in the model. Another exciting finding[6] is that the transport properties display unusual features consistent with non-Fermi liquid behavior arising from the quadrupolar Kondo effect. Thus this alloy system both provides the first example of a uranium system for which the Anderson/Kondo scenario works even qualitatively, and joins the high temperature superconducting cuprates as a possible example of non-Fermi liquid behavior.

Spectroscopy using synchrotron radiation has been essential in all the work described above, and will continue to be a driving experimental force. Resonant photoemission[8], which utilizes a 5f PES cross-section enhancement occuring when the photon energy is tuned through an absorption threshold, provides the means for extracting the 5f PES spectrum in systems with strong competing emission from other elements or in systems where the 5f element is very dilute. Related absorption edge and core level studies also provide useful information about the 5f electronic states. With the advent of insertion device beamlines and matching monochromators, these studies can be carried out with increasingly better resolution, and also at higher energy absorption edges, where the resonance contrast can be higher, or where the higher kinetic energy of the outgoing electrons permits less surface sensitive spectra to be taken. Angle-resolved photoemission spectroscopy (ARPES) has had less impact in studies of heavy-Fermion materials because the low energy scale associated with the large γ–values has required resolutions not normally achievable. Also, in the higher photon energy range where resonant photoemission is usually performed, adequate k-resolution requires angle resolution better than that allowed by present signal to noise ratios. This situation too will be improved by the intensity and resolution of the new generation of beamlines and monochromators, and angle-resolved resonant photoemission spectroscopy studies should become feasible. For both heavy-Fermion and non-Fermi liquid behavior it will be very important to study the details of ARPES lineshapes very near E_F. Finally, none of these powerful techniques have been applied to actinides other than Th or U. A great advance in understanding actinide electronic structure generally can be anticipated if such studies can be made on the entire actinide sequence.

Much energy has been wasted in debate as to whether the atomic or the band approach is the better choice. It is obvious that the experimental properties display features of both approaches and that what is required is a unified explanation. One anticipates, for example, that the Kondo resonance of the impurity model should have additional spectral structure associated with dispersing excitations that make up a renormalized band structure which defines the Fermi surface[9]. To test such ideas will require ultra high resolution angle resolved photoemission studies of states very near E_F, as may be possible with future synchrotron-based spectroscopy.

* This work is supported by the U.S. National Science Foundation Low Temperature Physics Program under Grant No. DMR-91–08015, and by the U.S. Dept. of Energy under Contract No. DE-FG02–90ER45416.

1. J.W. Allen, S.-J. Oh, O. Gunnarsson, K. Schönhammer, M.B. Maple, M.S Torikachvili and I. Lindau, Adv. in Phys. **35**, 275 (1986).
2. J. J. Joyce, A.J. Arko, J. Lawrence, P.C. Canfield, Z. Fisk, R.J. Bartlett and J.D. Thompson, Phys. Rev. Letters **68**, 236 (1992).
3. F. Patthey, J.-M. Imer, W.-D. Schneider, J.H. Beck and Y. Baer, Phys. Rev. B **42**, 8864 (1990).
4. J.W. Allen, S.-J. Oh, L.E. Cox, W.P. Ellis, M.S. Wire, Z. Fisk, J.L. Smith, B.B. Pate, I. Lindau and A.J. Arko, Phys. Rev. Lett. **54**, 2365 (1985); J.-S. Kang, J.W. Allen, M.B Maple, M.S. Torikachvili, B.B. Pate, W.P. Ellis and I. Lindau, Phys. Rev. Lett. **59**, 493 (1987).
5. J.-S. Kang, J. W. Allen, M.B. Maple, M.S. Torikachvili, W.P. Ellis, B.B. Pate, Z.-X. Shen, J.J. Yeh and I Lindau, Phys. Rev. B **39**, 13529 (1989).
6. C.L. Seaman, M.B. Maple, B.W. Lee, S. Ghamaty, M.S. Torikachvili, J.-S. Kang, L.-Z. Liu, J.W. Allen and D.L. Cox, Phys. Rev. Lett. **67**, 2882 (1991).
7. L.-Z. Liu, J.W. Allen, C.L. Seaman, M.B. Maple, Y. Dalichaouch, J.S. Kang,-M.S. Torikachvili and M.A. Lopez de la Torre, Phys. Rev. Lett. **68**, 1034 (1992).
8. J.W. Allen in *Synchrotron Radiation Research: Advances in Surface and Interface Science*, edited by Robert Z. Bachrach, Vol 1: Techniques (Plenum Press, New York, 1992), p. 253.
9. G. Zwicknagl, J. Magn. Magn. Mat. **76&77**, 16 (1988).

"Heavy Fermion"

from large specific heat γ

Recall for free Fermions

$$C_{el} = \frac{\partial}{\partial T}\int \varepsilon f^0(\varepsilon) N(\varepsilon)\, d\varepsilon$$

$$\cong \underbrace{\left[\frac{\pi^2}{3}k_B^2 N(\varepsilon_F)\right]}_{\gamma} T + \cdots$$

Simple picture [we know it's too simple]

$$\delta \bar{E} \sim \left[k_B T N(\varepsilon_F)\right] \times k_B$$

$$C \sim \underbrace{\left[2k_B^2 N(\varepsilon_F)\right]}_{\sim\gamma} T$$

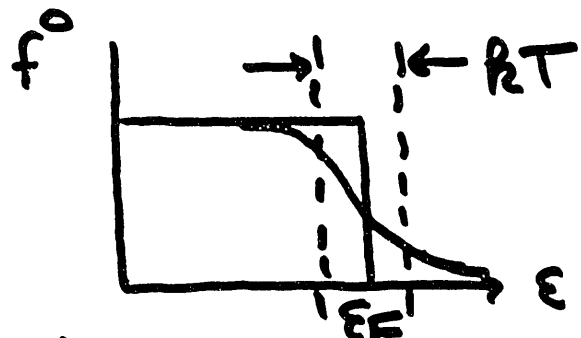

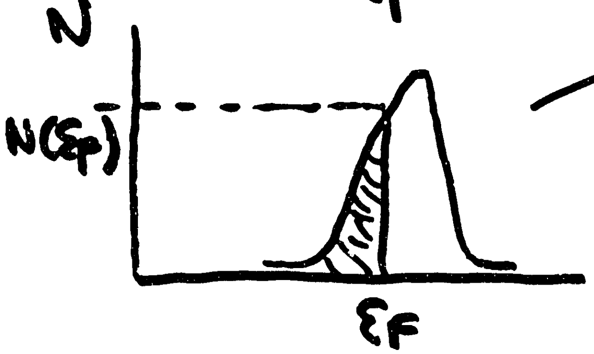

- Big γ, big $N(\varepsilon_F)$
  big mass
  narrow bands
- $\gamma \sim$ low en.
  Fermi excitation

$N(E_F) \sim m$

typically 0.5 to 5 mJ/mole K^2

"Heavy-Fermion" Materials

- large specific heat γ

  $C_{el} \cong \gamma T + \dots$

  $\gamma \sim$ mass for free Fermions

- some superconductors

  speculation of unusual pairing

d (Å)	Material	$\gamma\left(\frac{mJ}{mole\,K^2}\right)$	$T_{s.c.}$
4.43	$CeAl_3$	1620	......
5.13	UBe_{13}	1100	.85
4.1	$CeCu_2Si_2$	1000	.6
4.1	UPt_3	450	.5

↳ large metal-metal spacing

$\Rightarrow$ Anderson (impurity) model

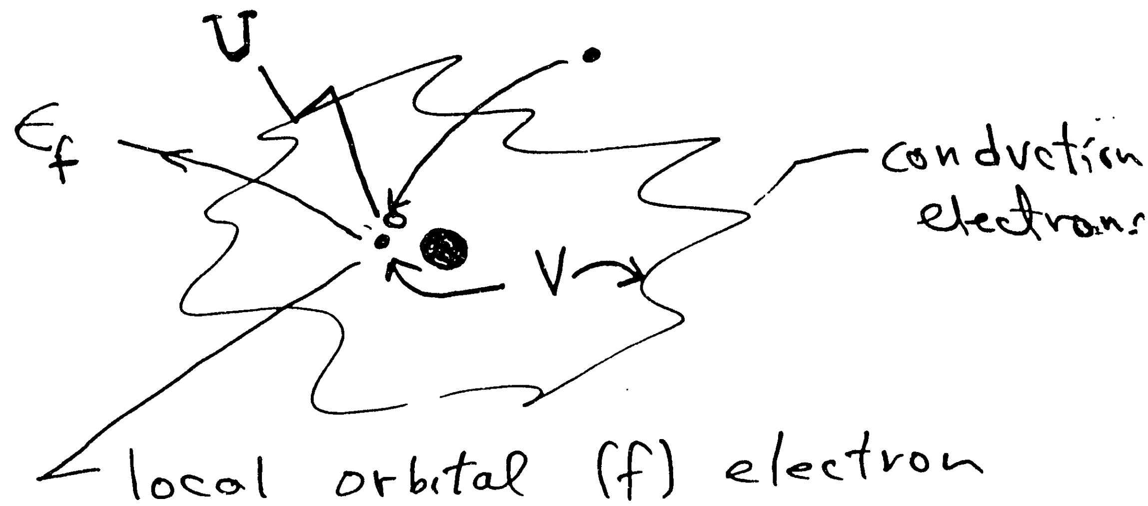

1-channel Kondo

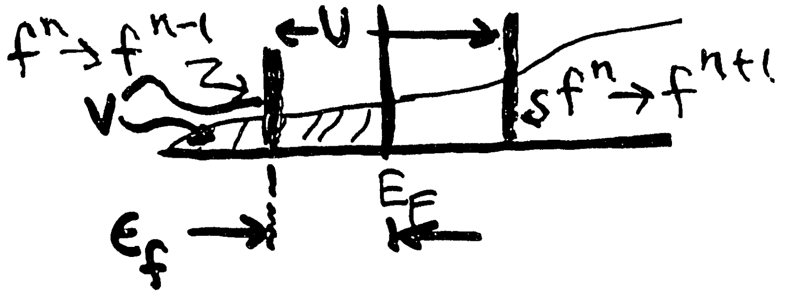

Anderson impurity model - f-electron ion in metal

FOR LOW ENERGIES $\longrightarrow \mathcal{H} = -2J\, \underset{\sim}{S}_I \cdot \sum_{\underset{\sim}{k}} \underset{\sim}{\sigma}_k$

f^n local moment

conduction electron spins

$$\boxed{J = \rho \frac{V^2}{\epsilon_f}}$$

GROUND STATE SINGLET

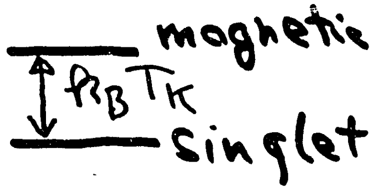

LOCAL MOMENT SCREENED DYNAMICALLY

"KONDO CLOUD" of conduction electrons

$\to kT_K \sim D \exp\left(-\frac{1}{J}\right)$

FOR $T < T_K \simeq T_F^*$ - LOCAL FERMI LIQUID

renormalized conduction electrons

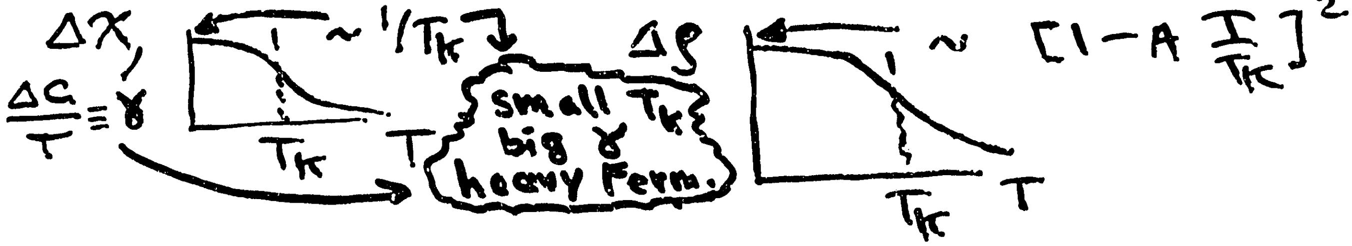

RARE EARTH PARADIGM

4f SPECTRUM & KONDO RESONANCE (Suhl / Abrikosov)
(1st rigorous derivation Gunnarsson / Schönhammer 1983

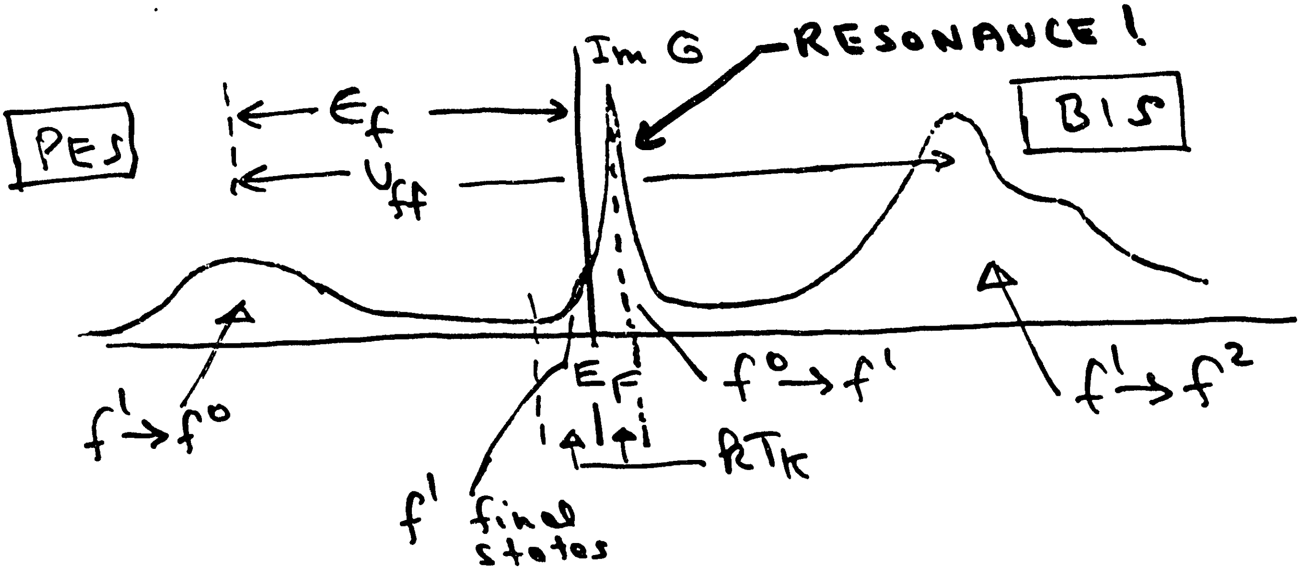

- RESONANCE WEIGHT $\sim (1-n_f)\, n_f$ PES
  $\sim (1-n_f)\, N_f$ BIS
  small for small T_K
  large for large T_K $\sim n_f \left[\frac{kT_K}{\rho V^2}\right]$ PES

- RESONANCE SHOWS OTHER ENERGY SCALES
  Δ_{LS} and Δ_{CEF} for $4f^1$
  fine structure - gives extra weight

- ALSO EXTRA WEIGHT $f^2 \to f^1$ from f^2 in ground state - important for small T_K materials

- SHOULD ALSO SHOW LATTICE EFFECTS (dispersion) as fine structure - but not observed yet. [But extra width]

$\boxed{\text{THE FIRST ORDER CASE}}$ (early 80's)

(Allen, Fuggle, Gunnarsson / Schönhammer, Maple)

- UNIFIED DESCRIPTION OF HIGH ENERGY SPECTRAL WEIGHTS AND THERMODYNAMICS

  4f Photoemission

  4f Inverse photoemission (BIS)

  3d XPS

  3d XAS

  $\chi(0)$, γ

- SEMIQUANTITATIVE DESCRIPTION OF CERIUM α-γ PHASE TRANS

  KONDO VOLUME COLLAPSE
  (Allen – Martin)

  (relevance to Plutonium ?)

Adv. in Phys. 35, 275 (1986)

Theory — Gunnarsson Schönhammer

GOOD SPECTRA FITS AND $\chi(0) \sim 1/T_K$ ALSO.

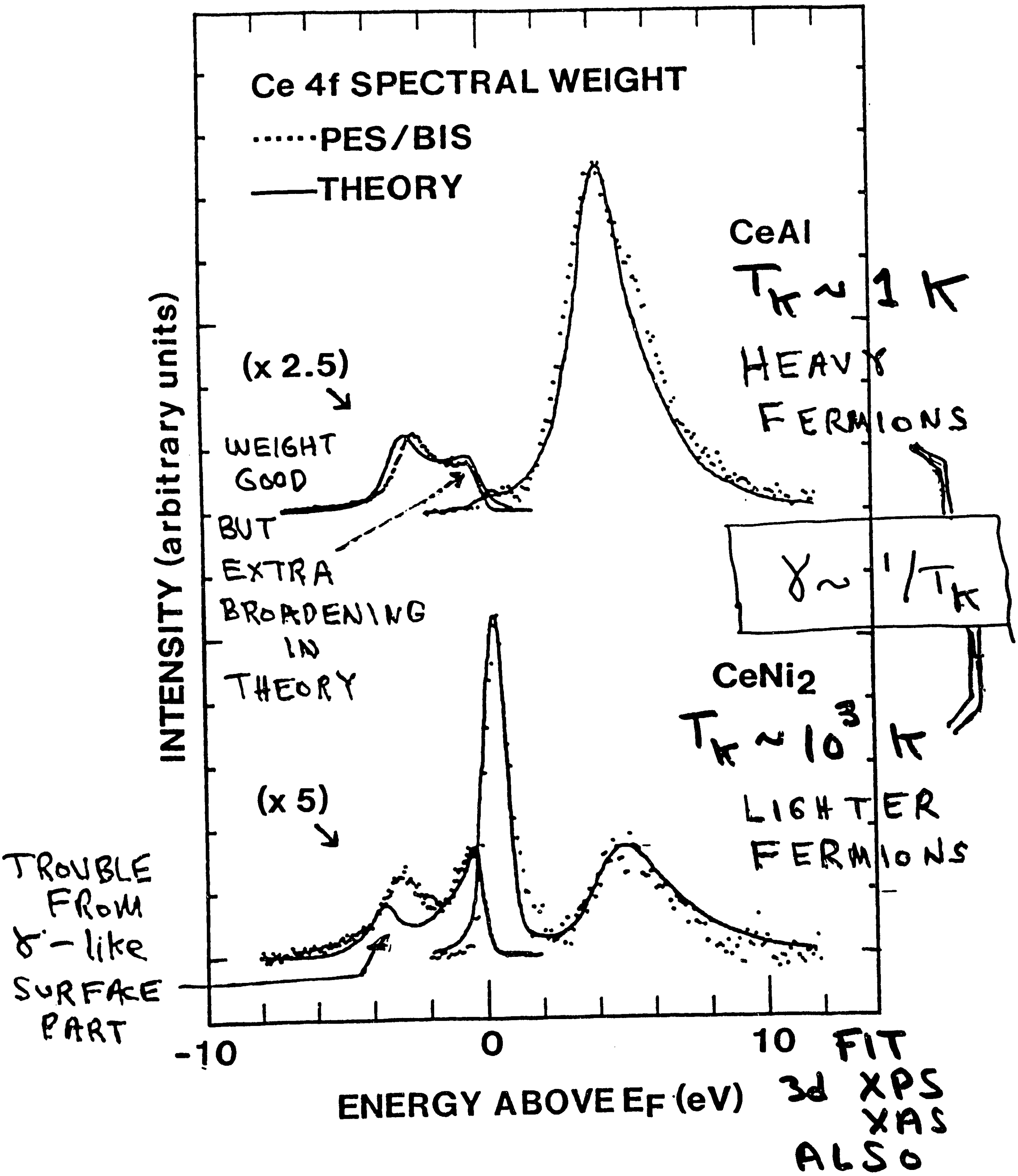

Analysis with Gunnarsson / Schönhammer
Adv. in Physik

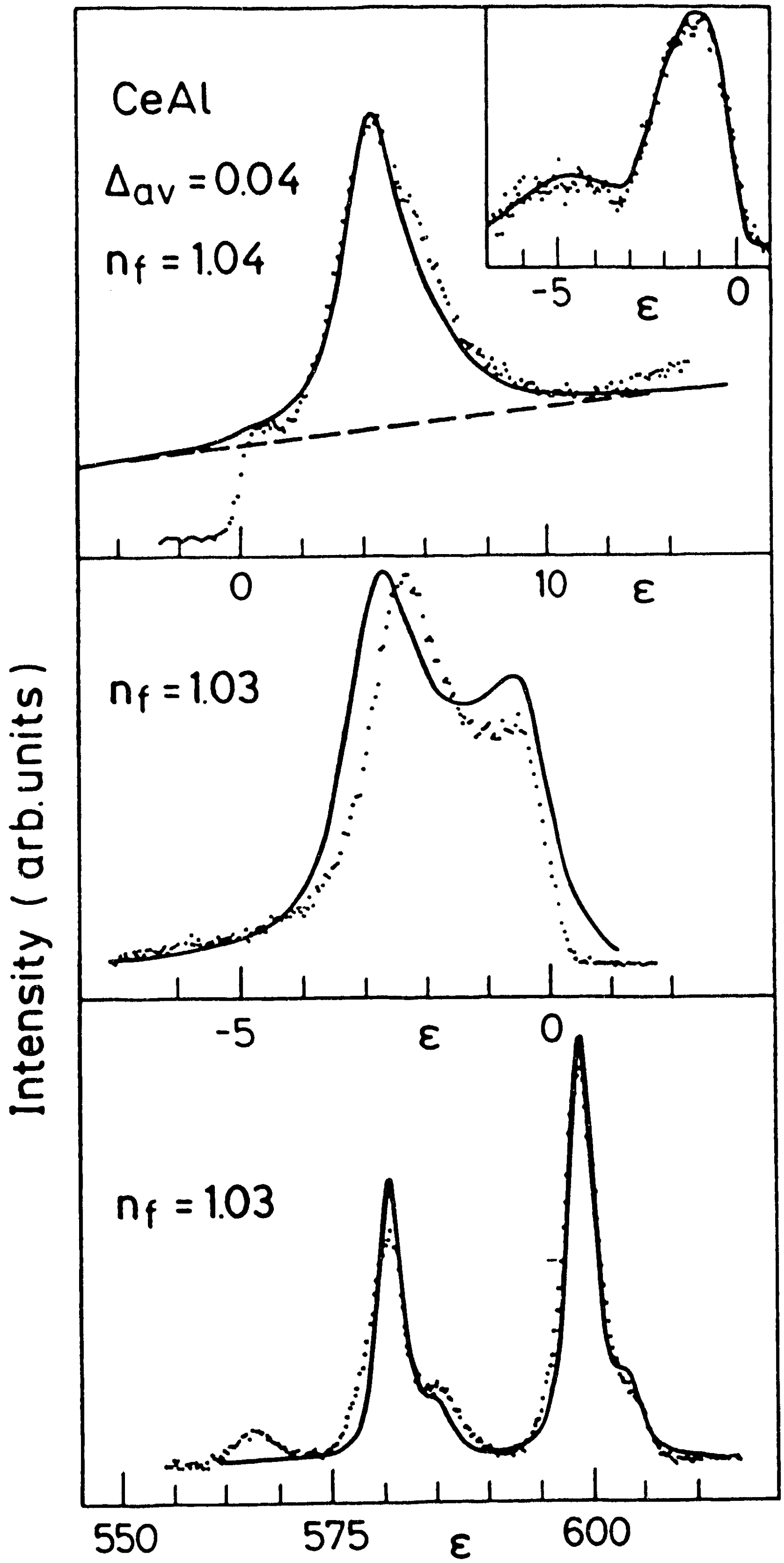

CeAl
γ-like
$T_K \lesssim 1\,K$

WEIGHT NEAR E_F TOO LARGE FOR KONDO RESONANCE

BUT FIT EASILY ANYWAY!

FIT PES, BIS AND Ce 3d XPS CORE LEVELS
NEED ALL THREE TO GET HAMILTONIAN PARAMETERS;

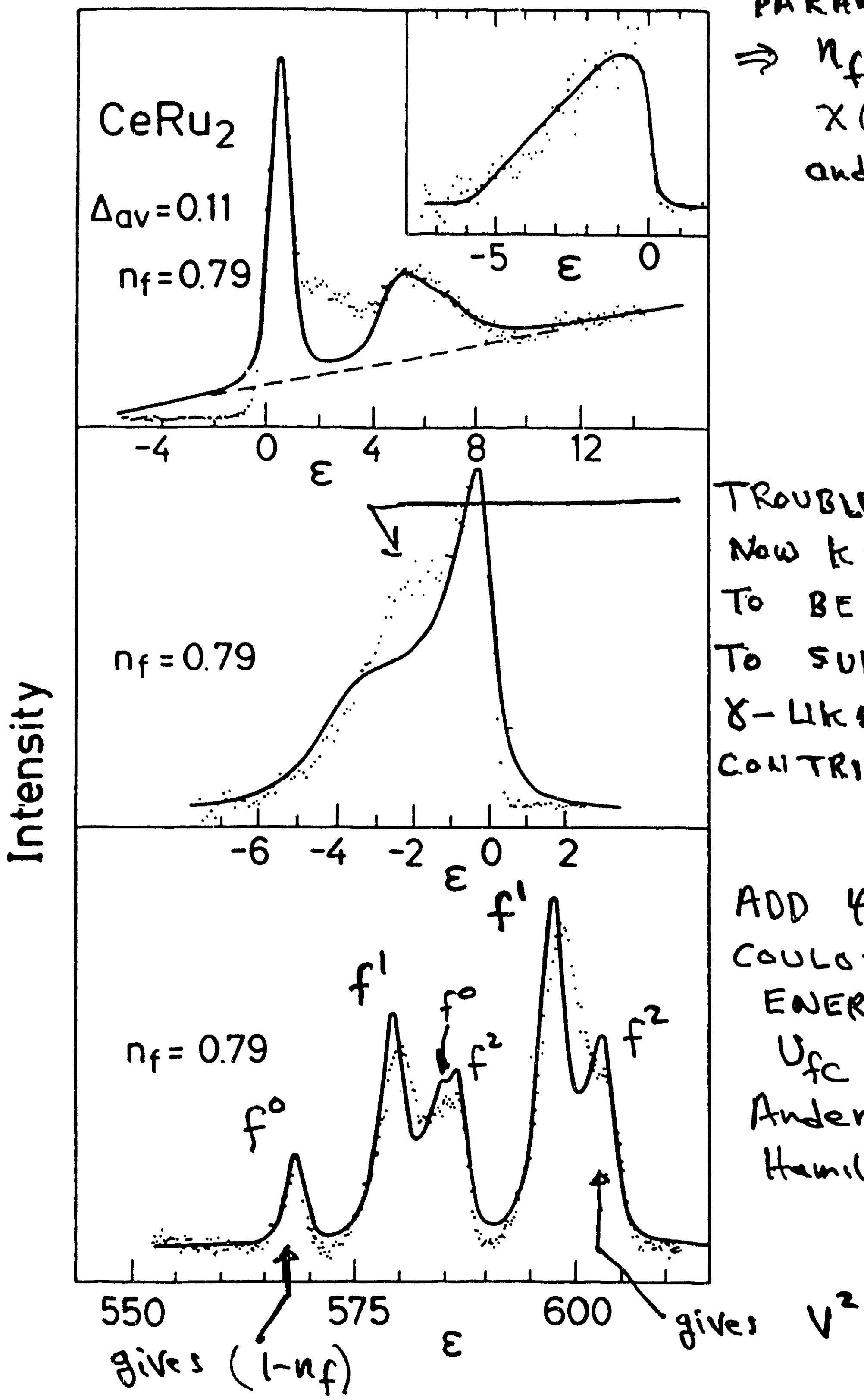

$\Rightarrow n_f$, $\chi(0)$, and T_K

TROUBLE HERE NOW KNOWN TO BE DUE TO SURFACE γ-LIKE CONTRIBUTION

ADD 4f–CORE COULOMB ENERGY U_{fc} to Anderson Hamiltonian

CALCULATE PHASE BOUNDARY

SCALE SPECTROSC. Δ's by 1.12 TO MATCH χ(u) EXACTLY. AFTER THAT— NO ADJUSTMENTS

P-V isotherms

& equal area construction.

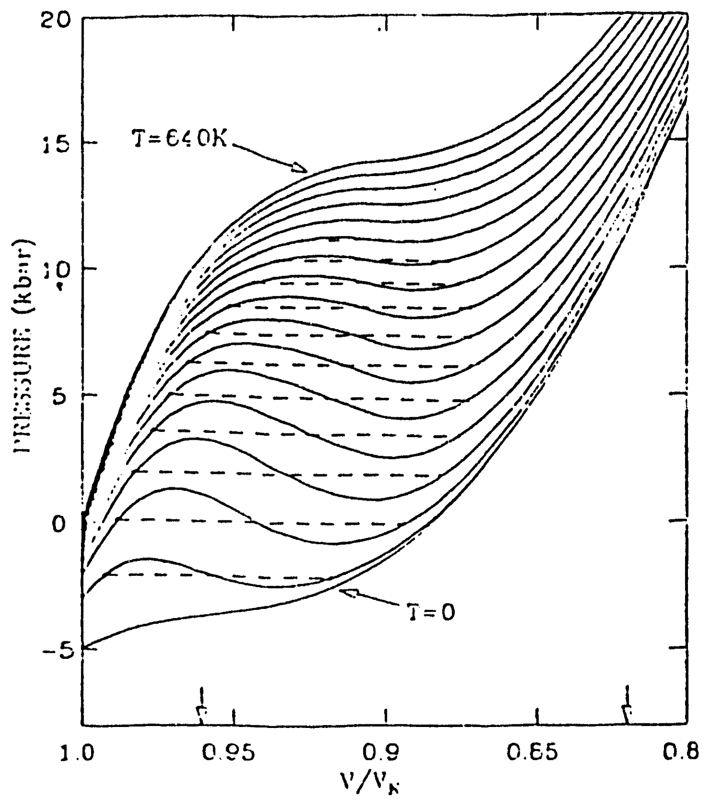

Ce KONDO VOLUME COLLAPSE CALCULATED FROM SPECTROSCOPY

(Liu/Allen Phys. Rev. 1992)

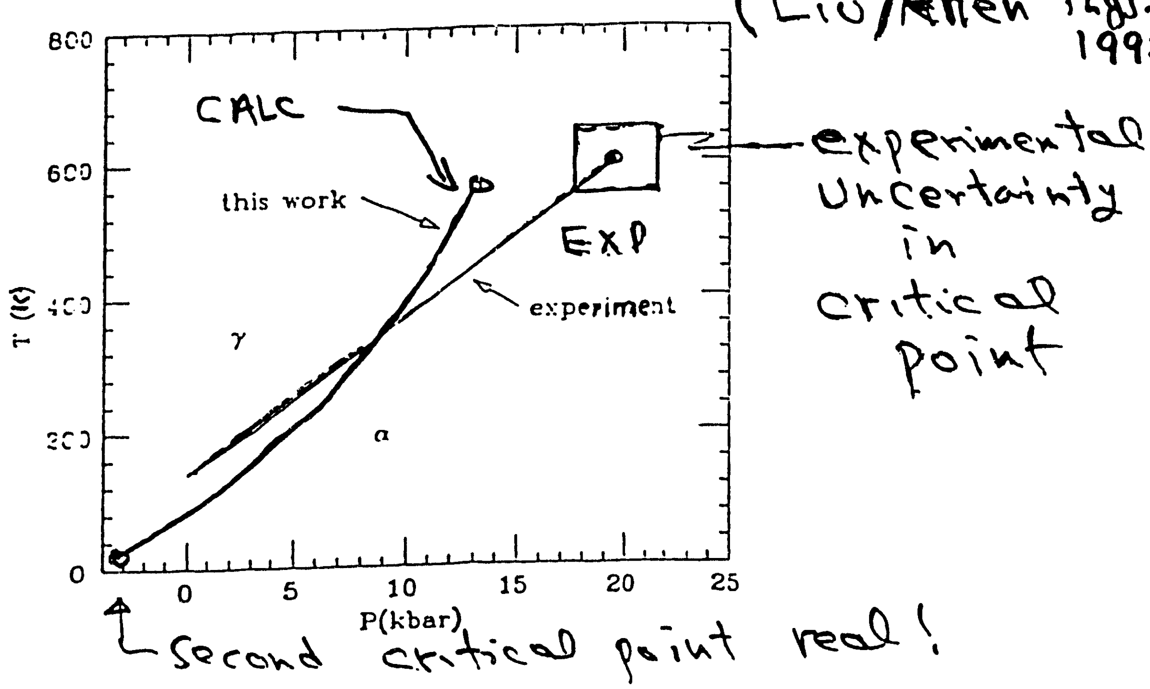

MORE DETAILED STUDIES

- HIGH RESOLUTION PHOTOEMISSION
- T-DEPENDENT PHOTOEMISSION & BIS
- SURFACE SHIFTS OF PARAMETER VALUES
  → surface valence changes

OUTCOME ?

- CONFIRM
- REFINE
- DESTROY

NEW FOCUS

Yb the one-hole analog of Ce $4f^1$

- main Kondo resonance in photoemission – high res possible & large T-dependence predicted

→ Photoemission – synchrotrons – will be important for heavy actinides

Quasi particle bands for $CeCu_2Si_2$

(d'Ambrumenil + Fulde 1985)

(Zwicknagl 1988)

- very near E_F
- Σ constructed from single-site Anderson ℓ (Kondo) scattering phase shifts — modify LDA

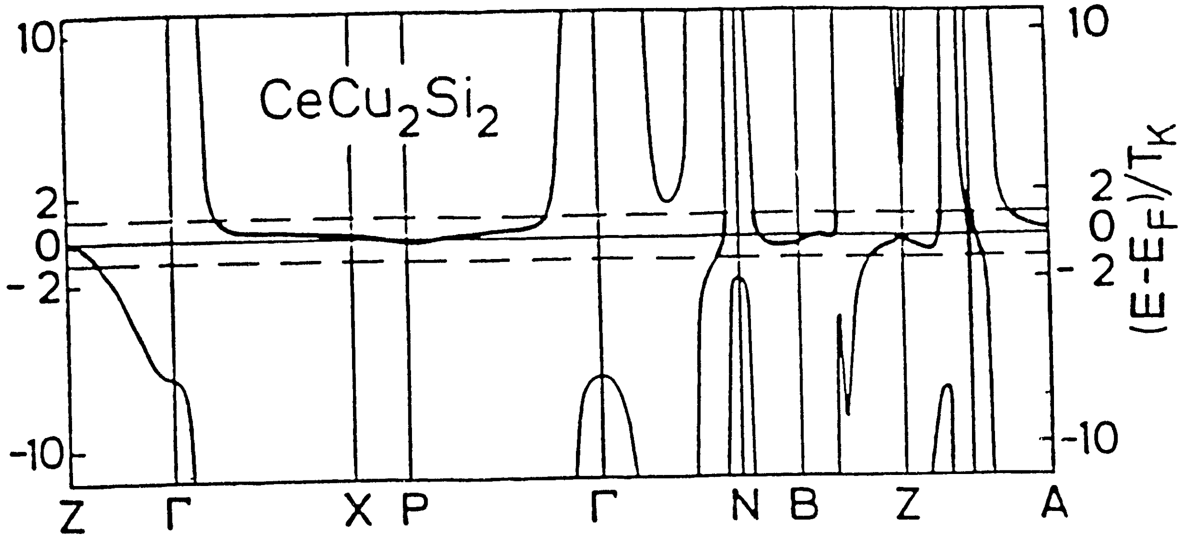

Note: energy scale is

$\frac{E - E_F}{T_K}$ & $T_K \sim 1$ meV

IN PRINCIPLE

RESONANCE HAS "BAND STRUCTURE"

NOT OBSERVED YET BY PES / BIS

WHERE IS THE "U" in Uranium ?

CeAl
small T_K
"heavy" Fermions

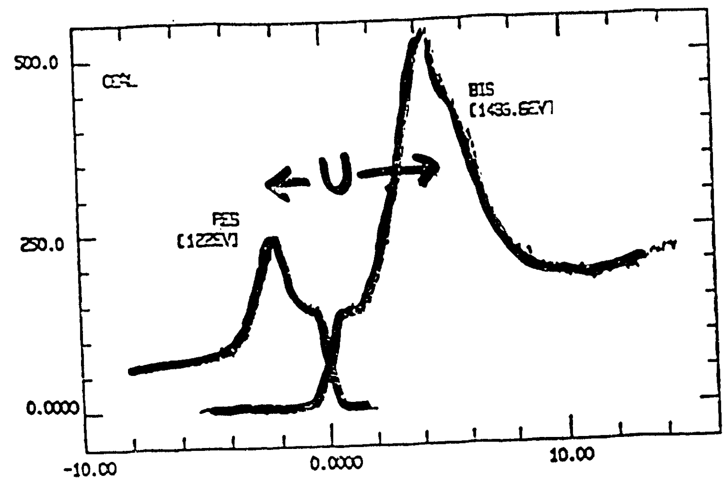

Heavy Fermion
UBe_{13}
(Weillard et al
1984)

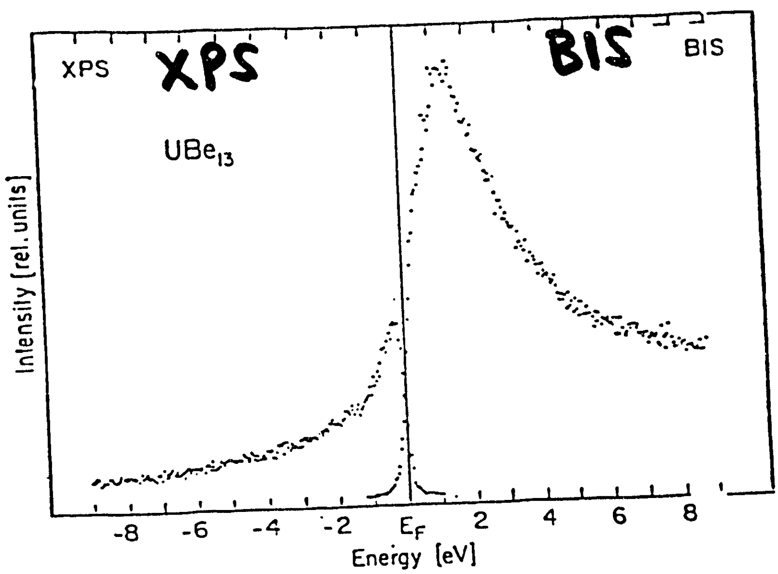

$CeRu_2$
big T_K
"light Fermions"

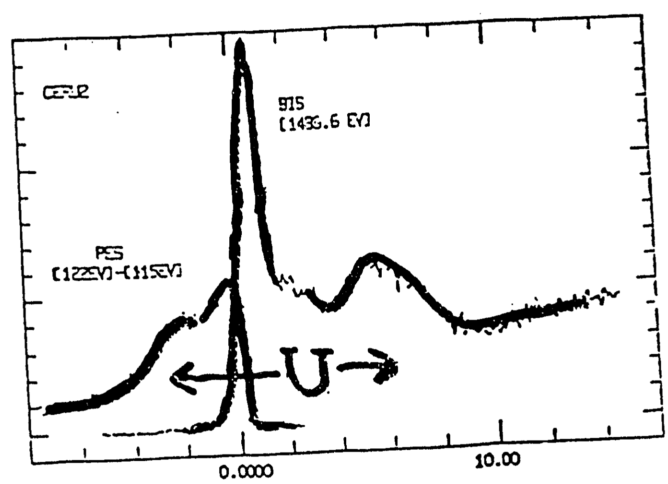

HEAVY FERMION U - MATERIALS

(1) BOTH LDA and SPECTRUM HAVE TOO MUCH 5f WEIGHT AROUND E_F TO EASILY UNDERSTAND LARGE γ.

(2) BUT SPECTRUM MUCH BROADER THAN LDA BOTH ABOVE AND BELOW E_F.

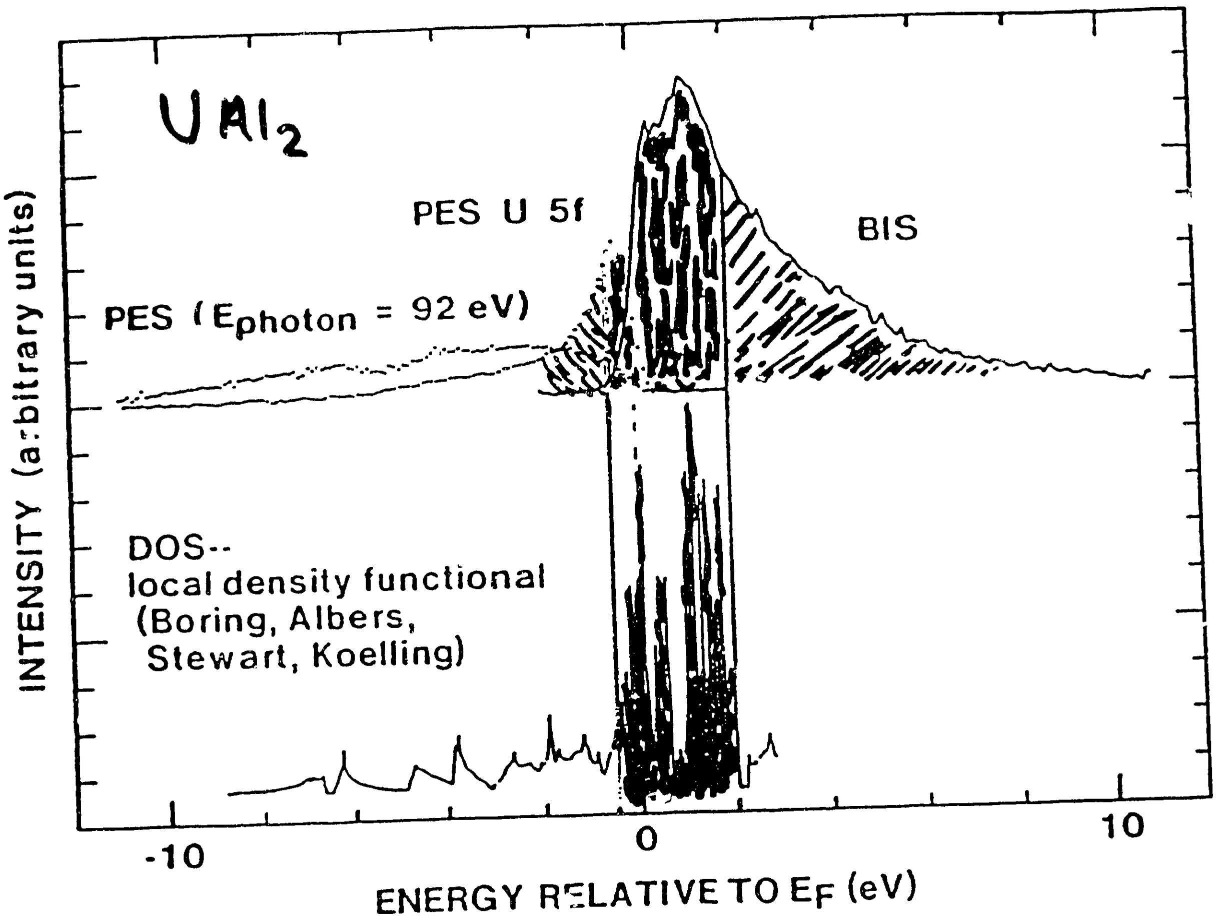

(2) IS ONLY EVIDENCE of U_{ff} !!

Uranium seems different from Ce, spectroscopically

ALLEN et al. PRL '85

Heavy Fermion $Y_{1-x}U_xAl_2$

5f SPECTRUM INDEPENDENT OF X

Impurity Anderson ok for starting point

Kong et al. PRL '87

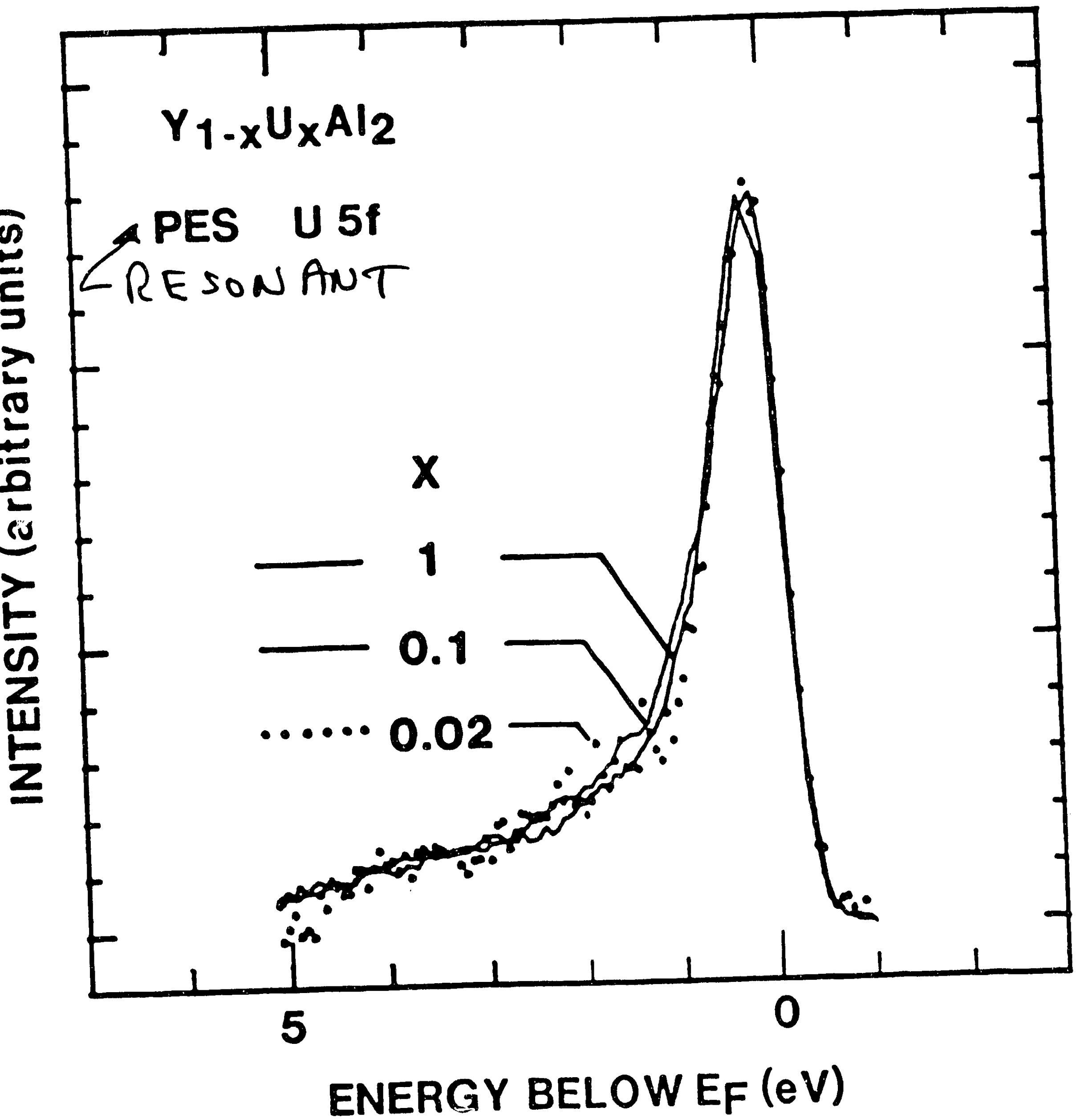

$\boxed{Y_{1-x} U_x Pd_3}$

LOW T_c (actually no T_c)

$\boxed{\text{HIGH EXCITEMENT!!}}$

TWO "FIRSTS":

- NON-FERMI LIQUID KONDO
  $x < 0.3$

- SPECTROSCOPY / TRANSPORT qualitatively correlated with impurity Anderson model

PEOPLE

UNIV. of MICHIGAN
L. Z. Liu
J.-S. Kang
R.O. Anderson

OHIO STATE UNIV.
D.L. COX

SAN DIEGO STATE UNIV.
M.S. Torikachvili

U. CAL. SAN DIEGO
C.L. Seaman
M.B. Maple
Y. Dalichaouch
M.A. Lopez dela Torre
B.W. Lee
S. Ghamaty

UPd$_3$ – REFERENCE COMPOUND

Baer et al.
SS Com. 36, 387
(1980)

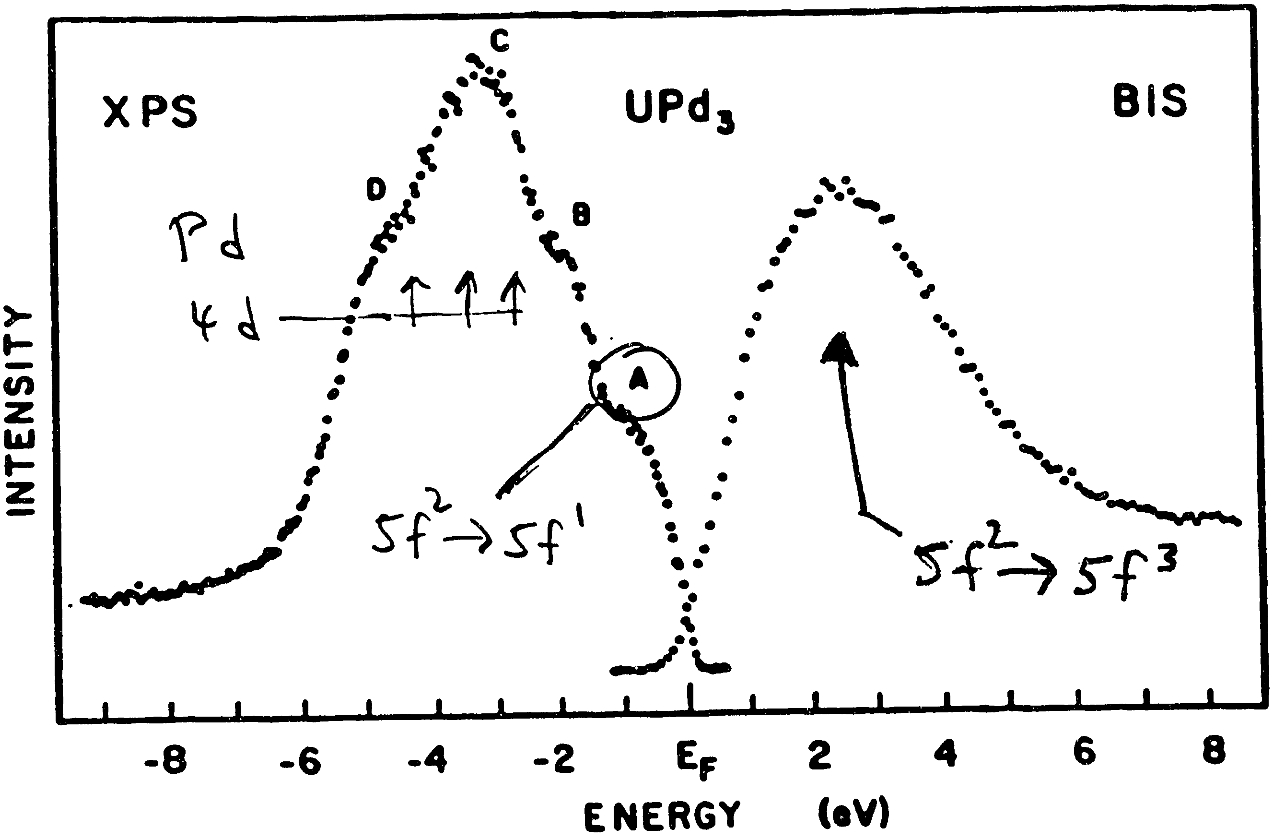

THE ARCHTYPE "LOCALISED 5f" SYSTEM $\Updownarrow$ U^{4+}

- f^2 Δ_{CFS} neutron scat.
- ≈ 0 5f weight at E_F
  $\Rightarrow$ correlation gap U
- other evidence

$Y_{1-x}U_xPd_3$

(J.-S. KANG thesis)

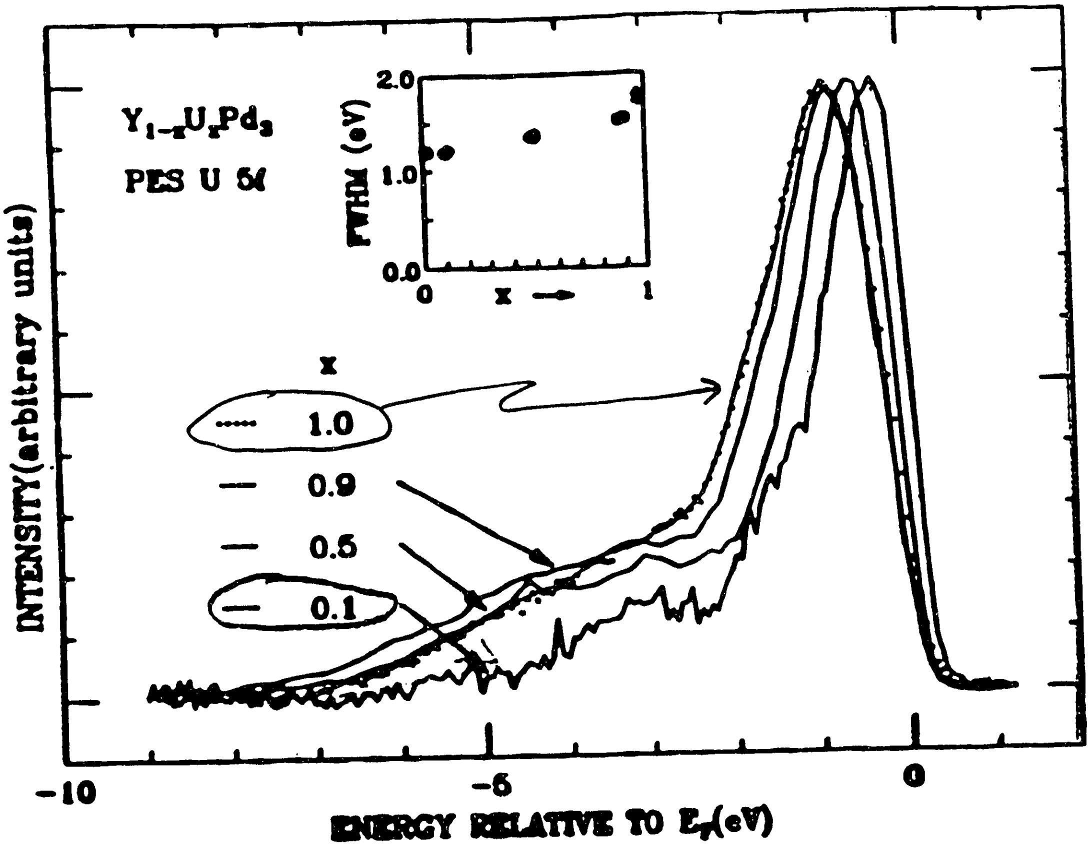

<u>UNEXPECTED ACTION!!</u>

- 5f peak narrows & shifts to E_F..
- Change <u>not</u> especially correlated with crystal structure transition

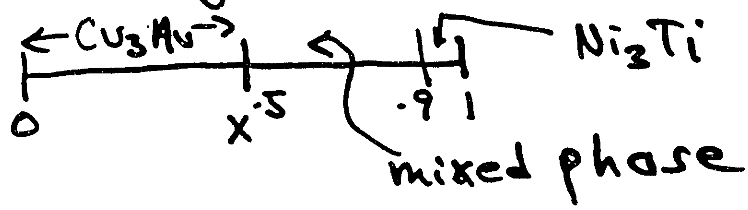

"Fermi-level Tuning"

Kang et al PRB $\underline{39}$, 13529 (1989)

Idea: Y^{3+} replaces U^{4+}

in $Y_{1-x} U_x Pd_3$

as x changes $1 \rightarrow 0$

Cond. elec./cell decreases by 1

E_F decreases by $\cong \dfrac{\sim 1 \text{ elec/cell}}{\sim 1 / \text{eV cell}} \cong 1 \text{ eV}$

band theory YPd_3 $D(\varepsilon)$ near E_F

HOPE! A paradigm impurity system for spectroscopy & transport

So

test picture spectroscopically

U-M — L.Z. Liu

do transport (UCSD) – C. Seaman

$$T_K \sim E_F \exp\left(\frac{-\epsilon_f}{\rho N_f V^2}\right)$$

$\Rightarrow T_K$ increases as X decreases (ϵ_f decreases)

2-CHANNEL KONDO (quadrupolar Kondo) D. COX idea

EXAMPLE: U^{++} $5f^2$ Γ_3 doublet of $J=4$ (cubic)

$$\xrightarrow{\text{hybridization}} |\underline{k}\,;\Gamma_7\,5f^1\rangle$$

- non-Kramers doublet; no magnetic dipole electric quadrupole
- group theory $\rightarrow$ each channel of quadrupole couples to 2 channels of Γ_8 conduction band quartet

$$\longrightarrow H = -2J\,\underset{\sim}{S}_I \cdot \sum_{\underset{\sim}{k}} [\underset{\sim}{\sigma}_{k1} + \underset{\sim}{\sigma}_{k2}]$$

pseudo spins

O never can get singlet — so never get Fermi liquid!

O FIND LOCAL NON-FERMI LIQUID

$$\frac{\Delta C}{T} \sim -\ln \alpha T \qquad \frac{\rho(T)}{\rho(0)} \simeq 1 - A\sqrt{T}$$

$$\Delta S(0) = \frac{R}{2}\ln 2$$

NON F.L. SURVIVES IN LATTICE ? NOT KNOWN

UCSD PHASE DIAGRAM FROM TRANSPORT

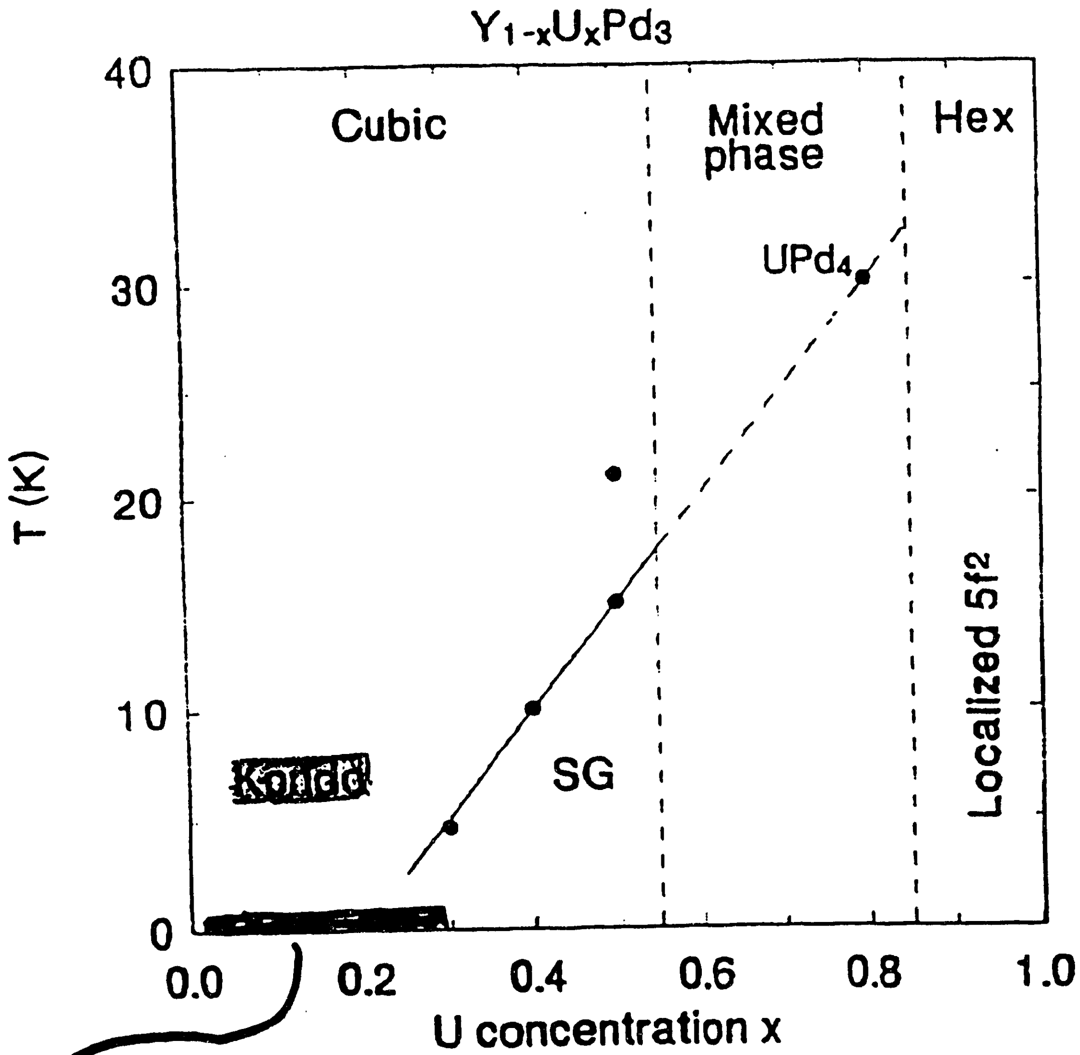

- EXCITING RESULTS FOR $X < 0.3$
- NON-FERMI LIQUID KONDO IN TRANSPORT PROPERTIES
- KONDO RESONANCE in BIS spectrum

RESISTIVITY

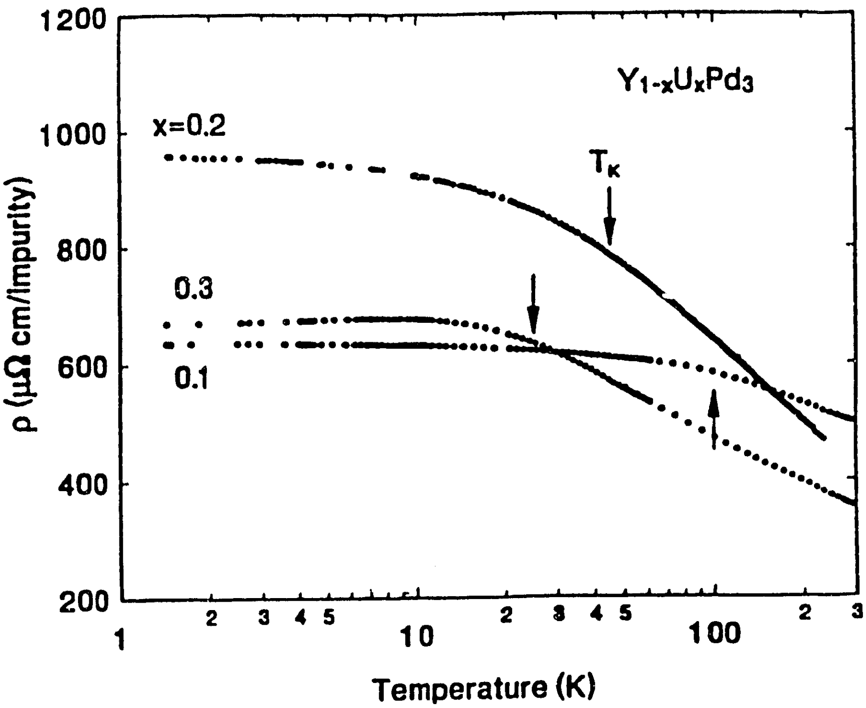

Log T behavior shows Kondo effect

T_K increases as x decreases

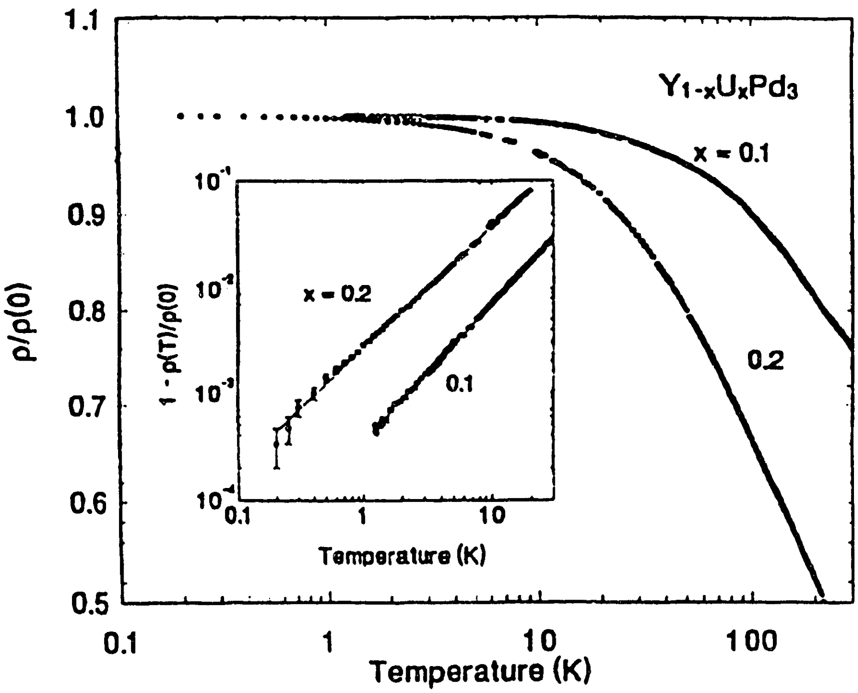

Low T linear behavior for $x \leq 0.2$

Non-fermi liquid

(but not $\sqrt{T}$)

$Y_{1-x} U_x Pd_3$ Results

COMPLEX PHASE DIAGRAM (Seamon ?
UCSD

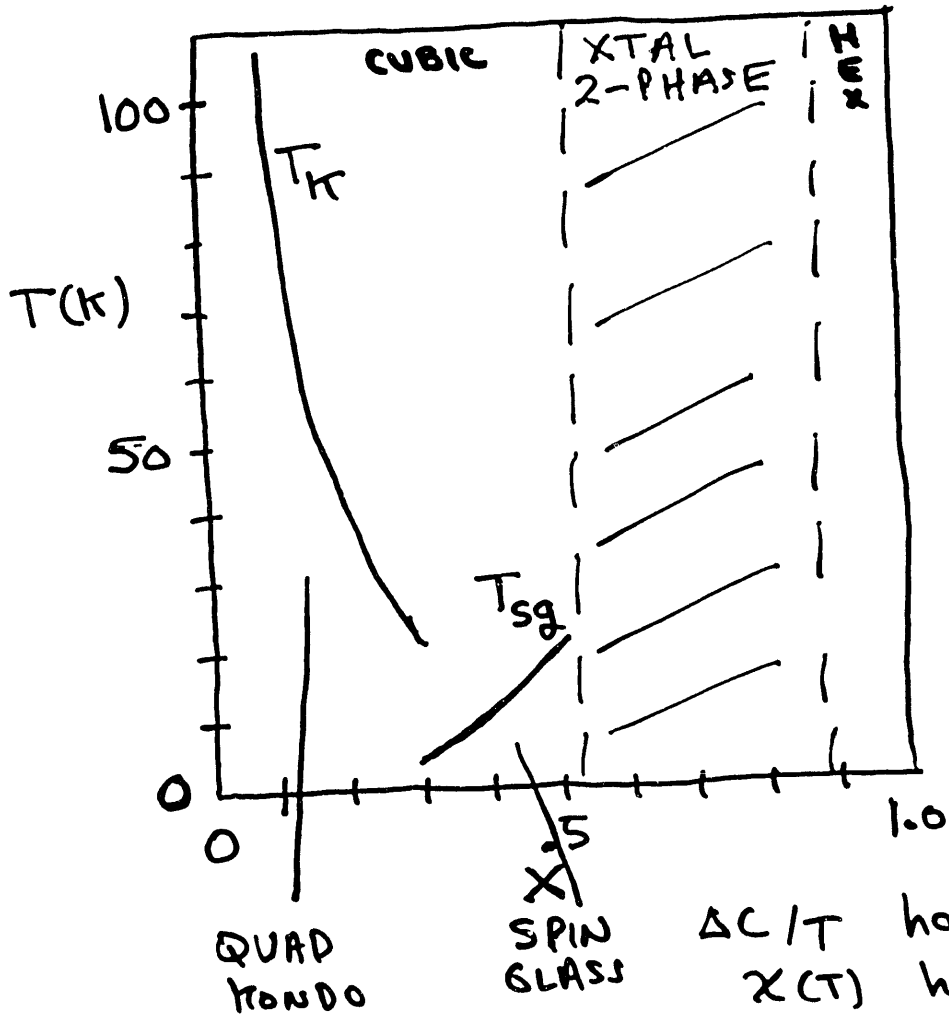

PRL
published
1991

$\Delta C/T$ has max
$\chi(T)$ hysteretic

FOR X < 0.3

(QUADRUPOLAR) KONDO GROUND STATE

(QUADRUPOLAR) KONDO RESONANCE

CORE LEVEL XPS

$Y^{3+}_{1-x} U^{4+}_x Pd_3$

Qualitatively ok

Shifts for Pd, Y same direction

≈ same magn.

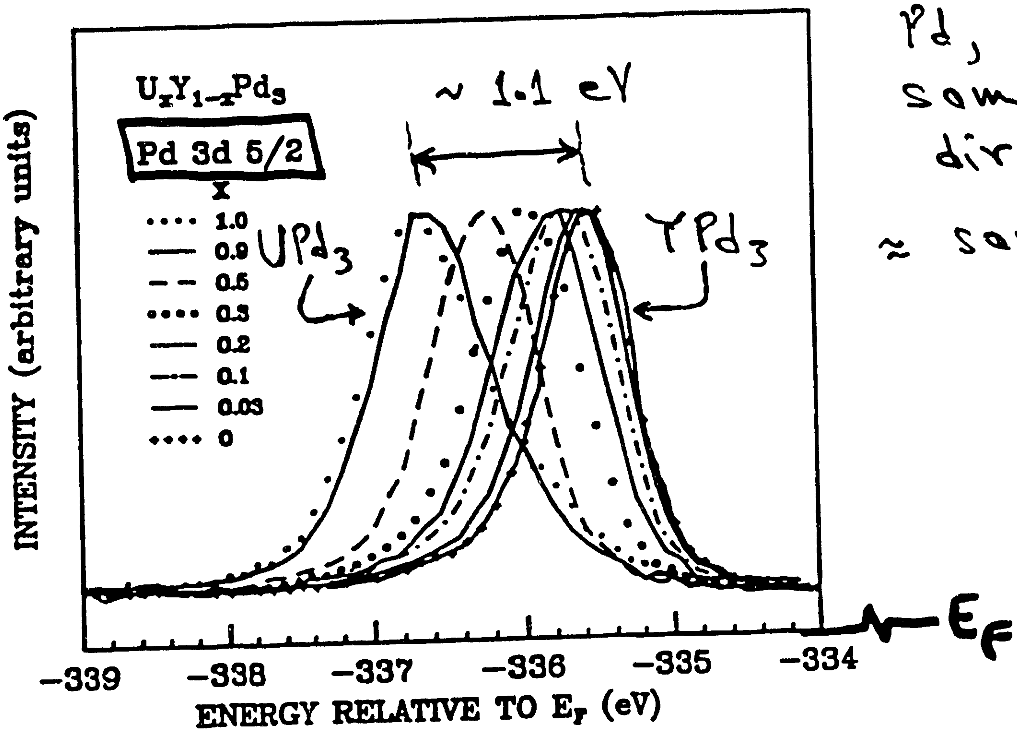

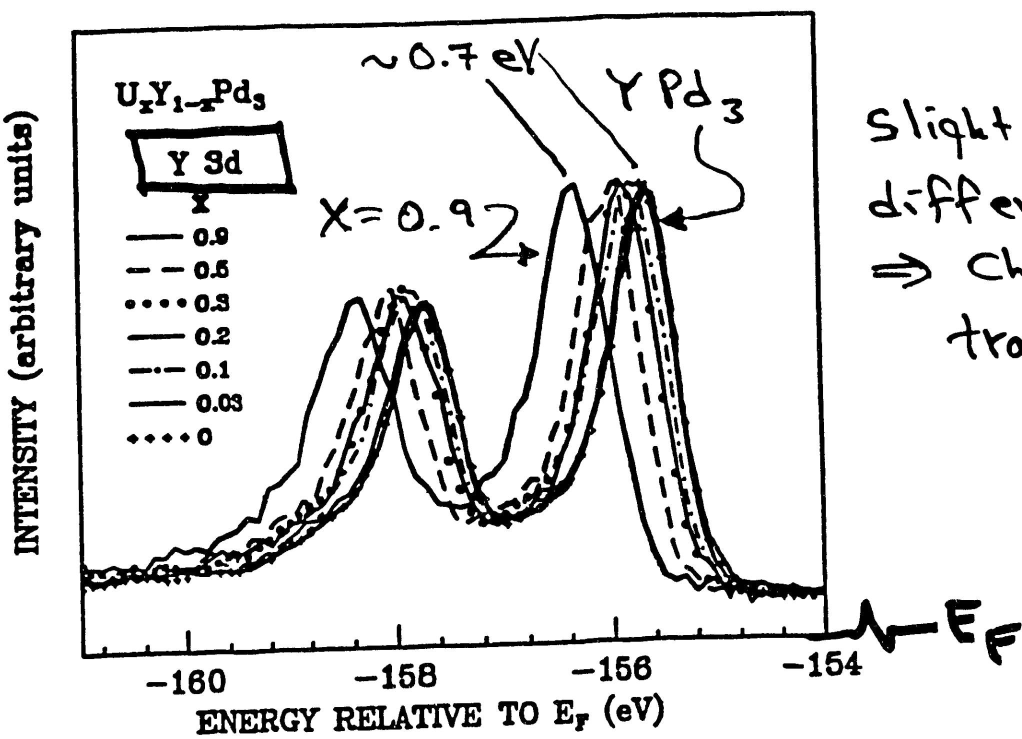

Slight magn. difference ⇒ Charge transfer

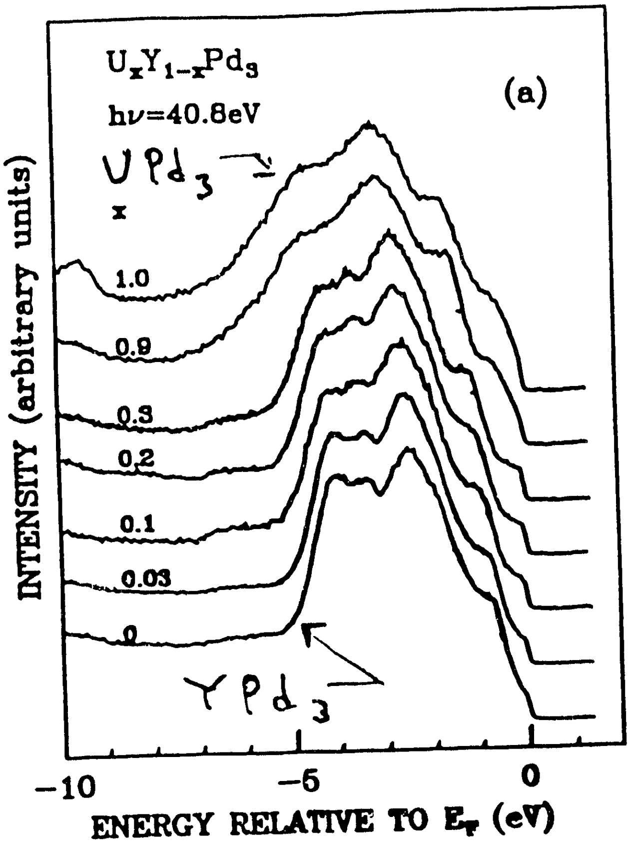

VALENCE BAND

PES $h\nu = 40.8$ eV

RES ~ 100 meV

5f cross-section small

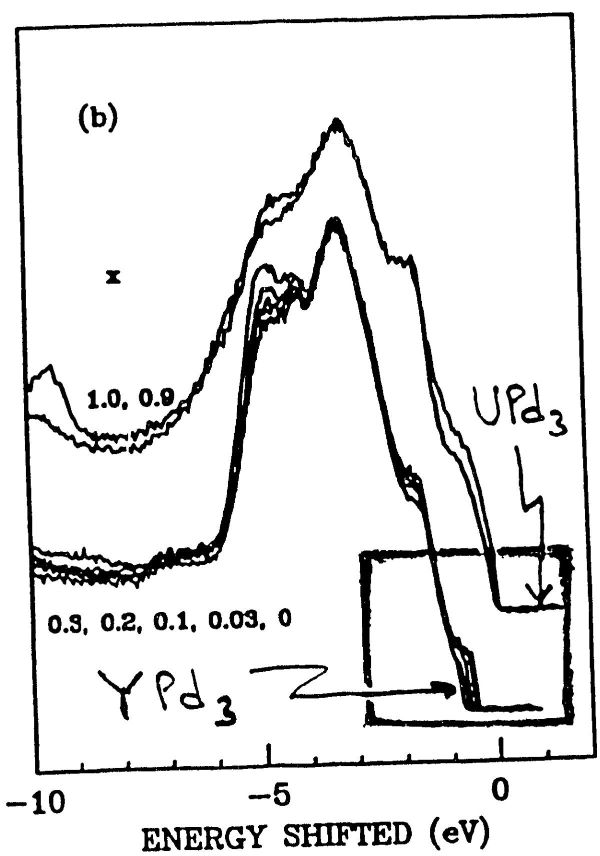

ALIGN VALENCE BAND FEATURES

See E_F shift as x changes $1 \rightarrow 0$

$\Delta E_F \cong 0.8$ eV

BIS data - 8 samples

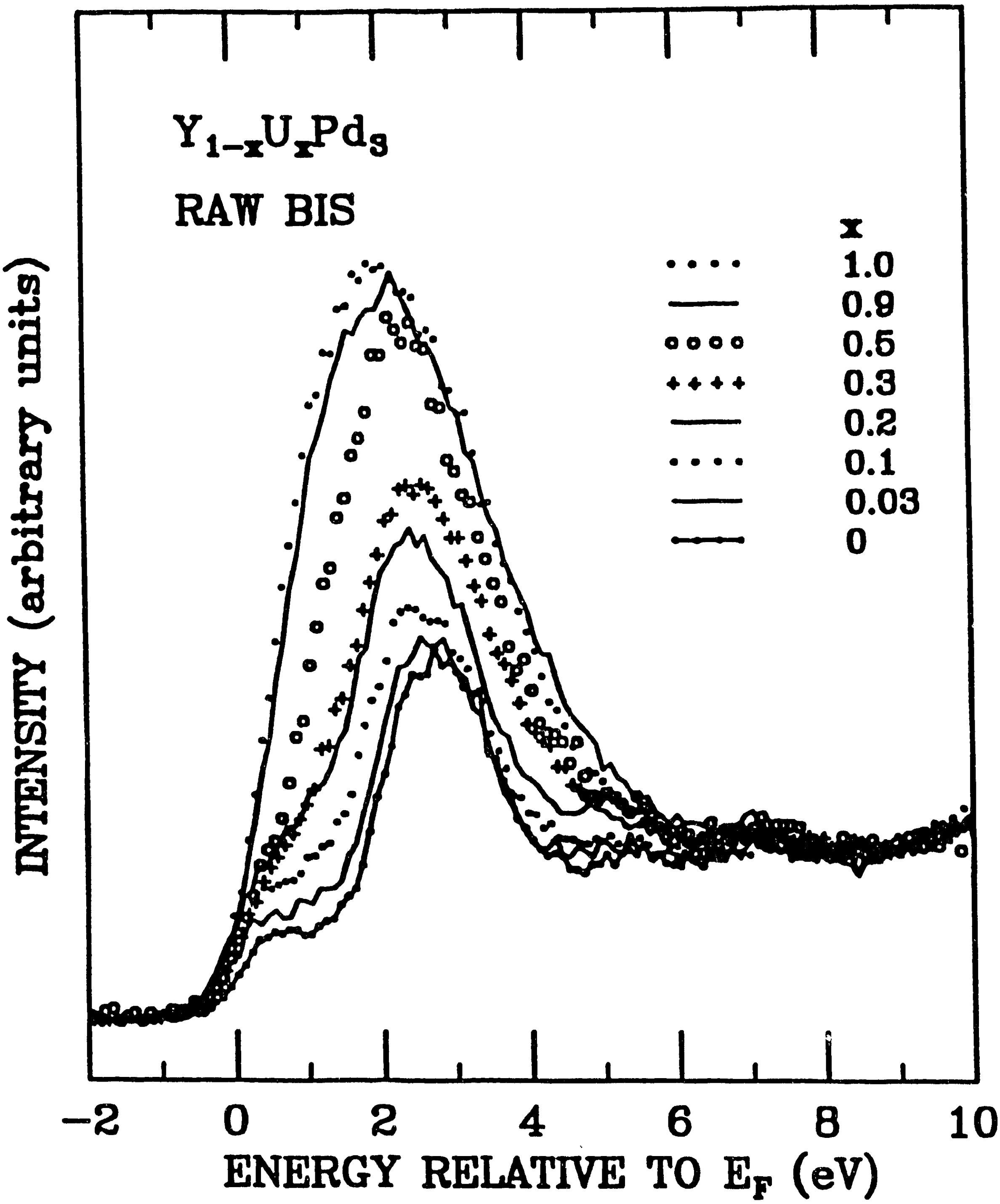

BIS / PES

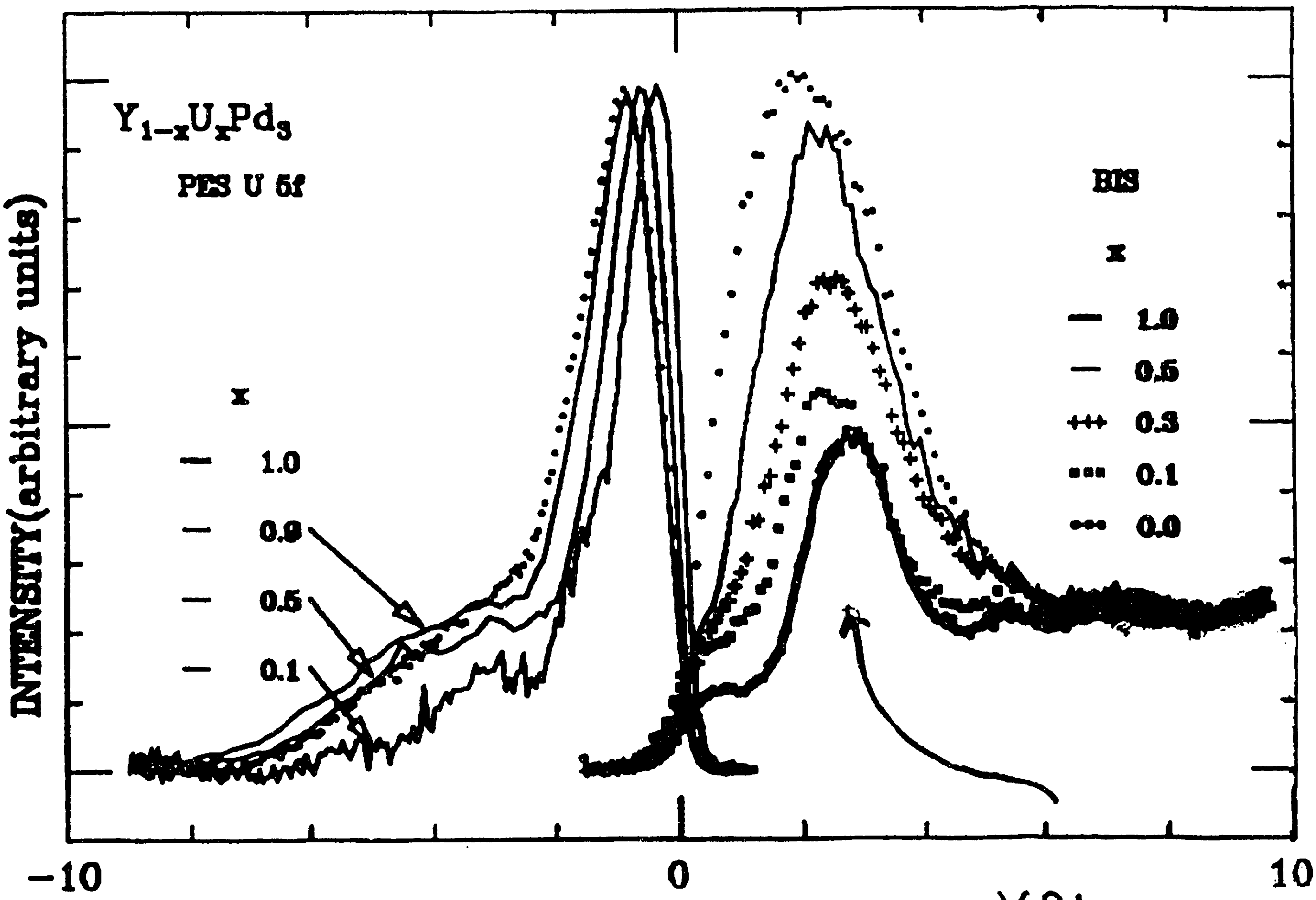

XPd_3
Xd — Pd 4
antibonding
peak

LDA for YPd_3
(König 1983)

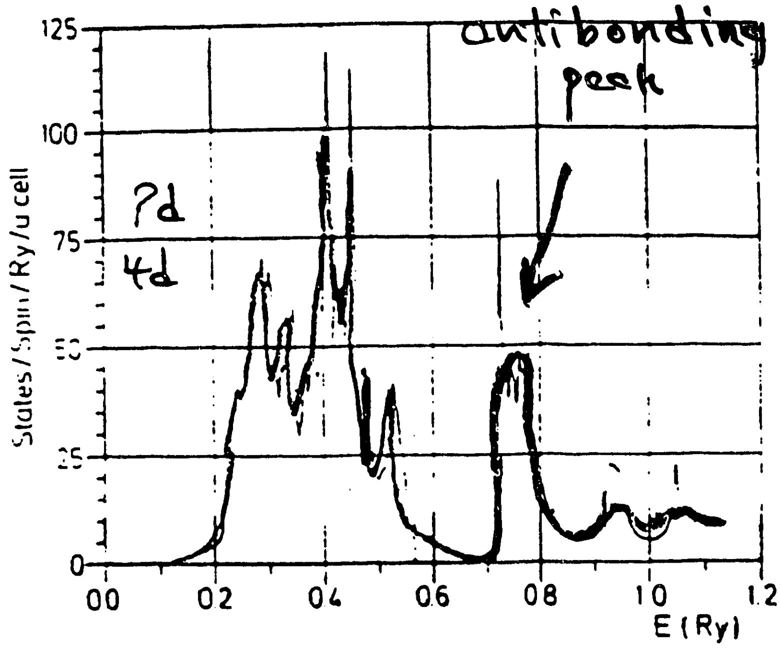

EXTRACTED 5f BIS

- Assume Y U isoelectronic
- shift X = 0 curve by E_F shift in valence band PES
- subtract from X ≠ 0 curves

NOTE – doesn't affect result near E_F

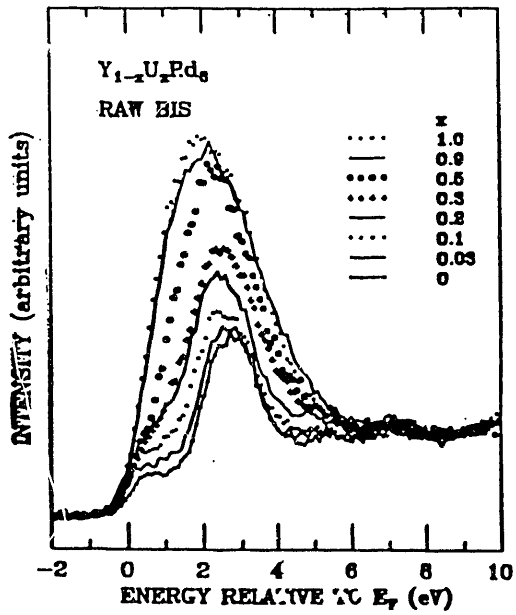

CENTROID SHIFTS AWAY FROM EF

For X ≤ 0.3
ρ(T) shows Kondo with T_K increasing
we observe growth of E_F weight!
Interpret as Kondo resonance!

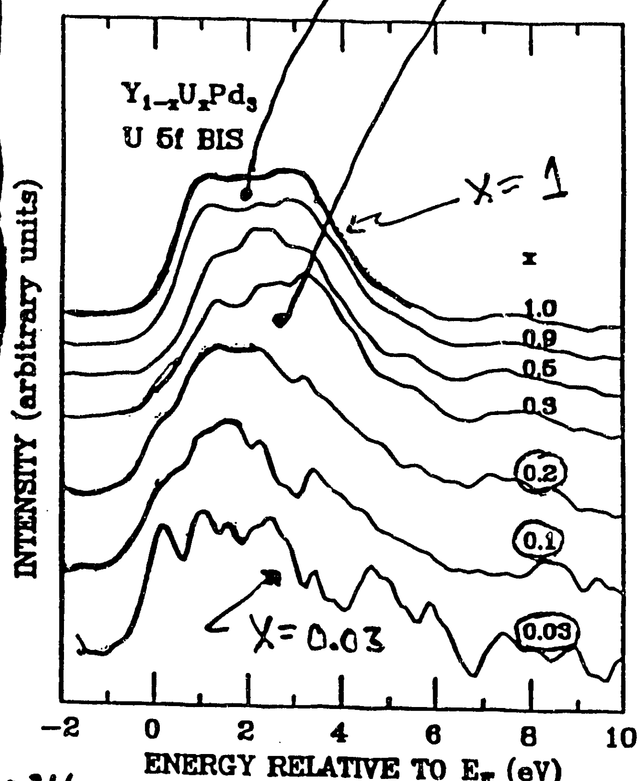

Liu et al

published – PRL 68, 1034 (1992)

DETAIL PES / BIS near E_F

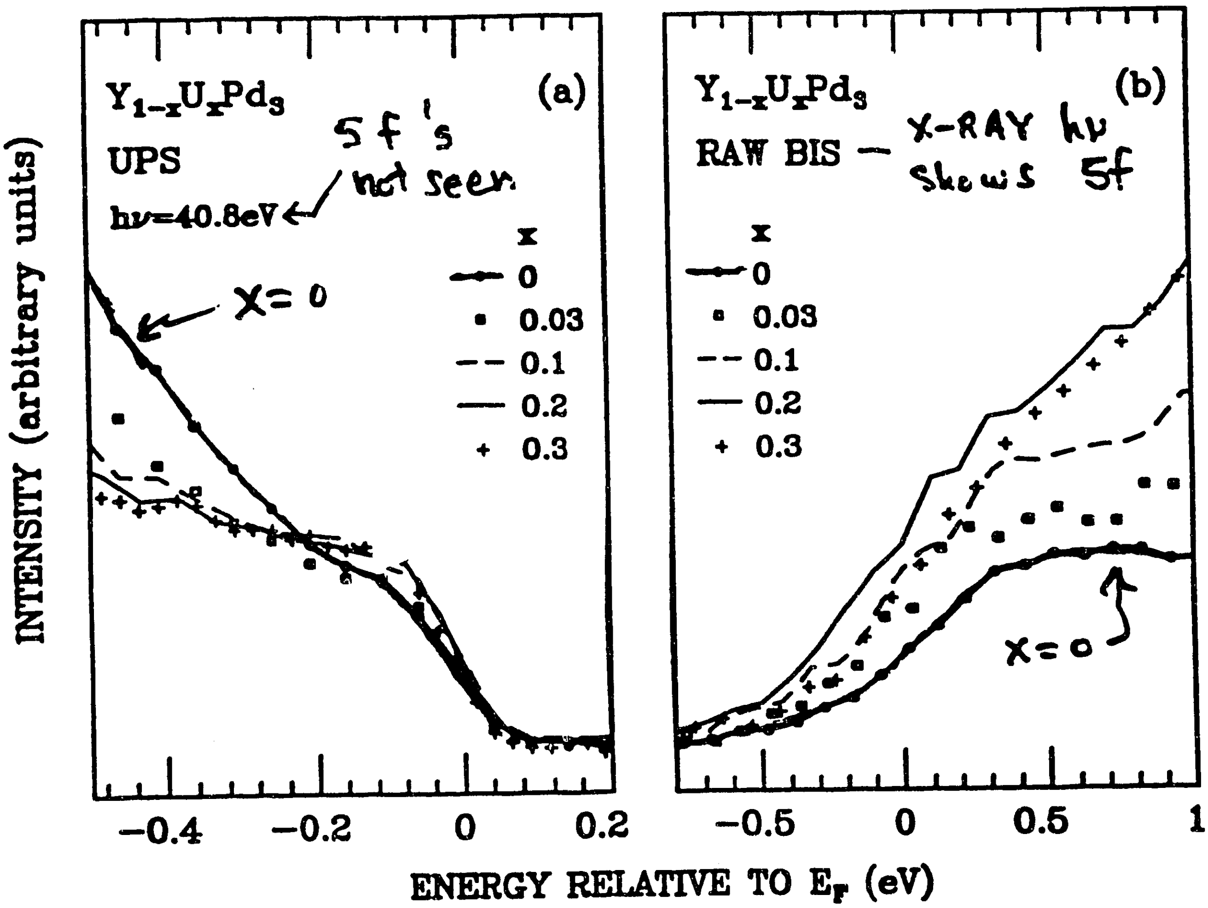

- $E_F \longrightarrow$ as x increases
- DOS rather flat & constant with x
- BIS increases then decreases as x increases

GROWTH OF E_F weight gives gapless spectrum in diluted material like heavy Fermion UPt_3 as U is diluted

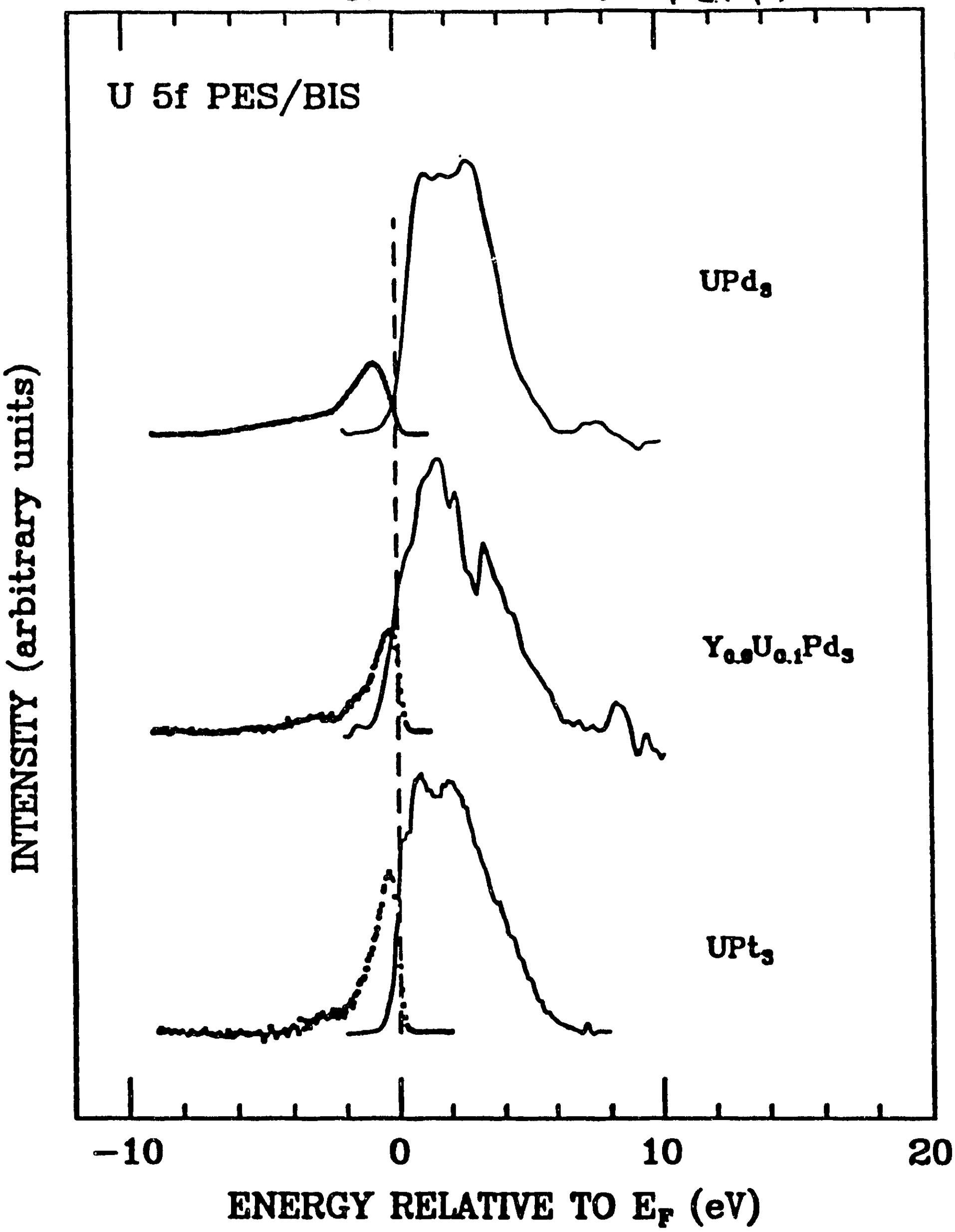

⟹ SUPPORT FOR KONDO RESONANCE / ANDERSON model PICTURE of ALL Heavy Fermion Uranium materials

(Allen et al PRL '85)

DIFFERENCES FROM Ce

① $U_{eff} \sim 2$ eV [~ 6 eV for Ce]

Correlation Gap much smaller
($f^3 \to f^2$ important)

② • Ce^{3+} $4f^1$ largest splitting is
$\Delta_{SPIN\ ORBIT} \sim 0.25$ eV
⇒ SIMPLE RESONANCE SIDEBANDS

• But $U^{4+}(5f^2)$ or $U^{3+}(5f^3)$ has many multiplets, ~ 1–2 eV range
⇒ SPREAD OUT SIDEBAND STRUCTURE
& MUCH MORE WEIGHT FOR SAME T_K – FILLS IN GAP, GIVES BANDLIKE LOOK

③ Hybridization $\langle 5f^n | \mathcal{H} | 5f^{n-1}; \underset{\sim}{k} \rangle$ greatly reduced by overlap factors [Hirst, Cox] even tho $\langle f | H | \underset{\sim}{k} \rangle$ larger than for Ce.

Allows small T_K and big m^*.

$Th^{4+}_{1-x} U^{4+}_x Pd_3$

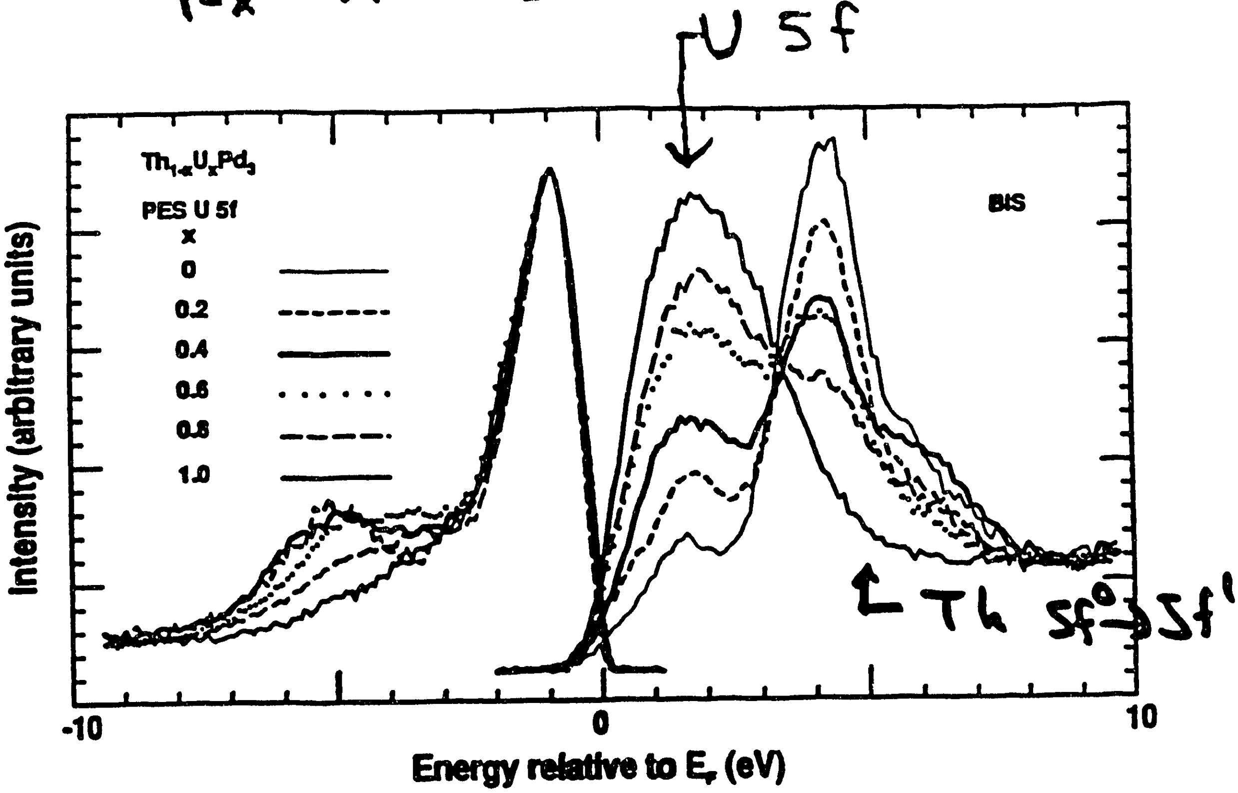

U and Th same valence

$\Rightarrow$ NO E_F SHIFT

Pd core levels — no shift in $Th_{1-x}U_xPd_3$

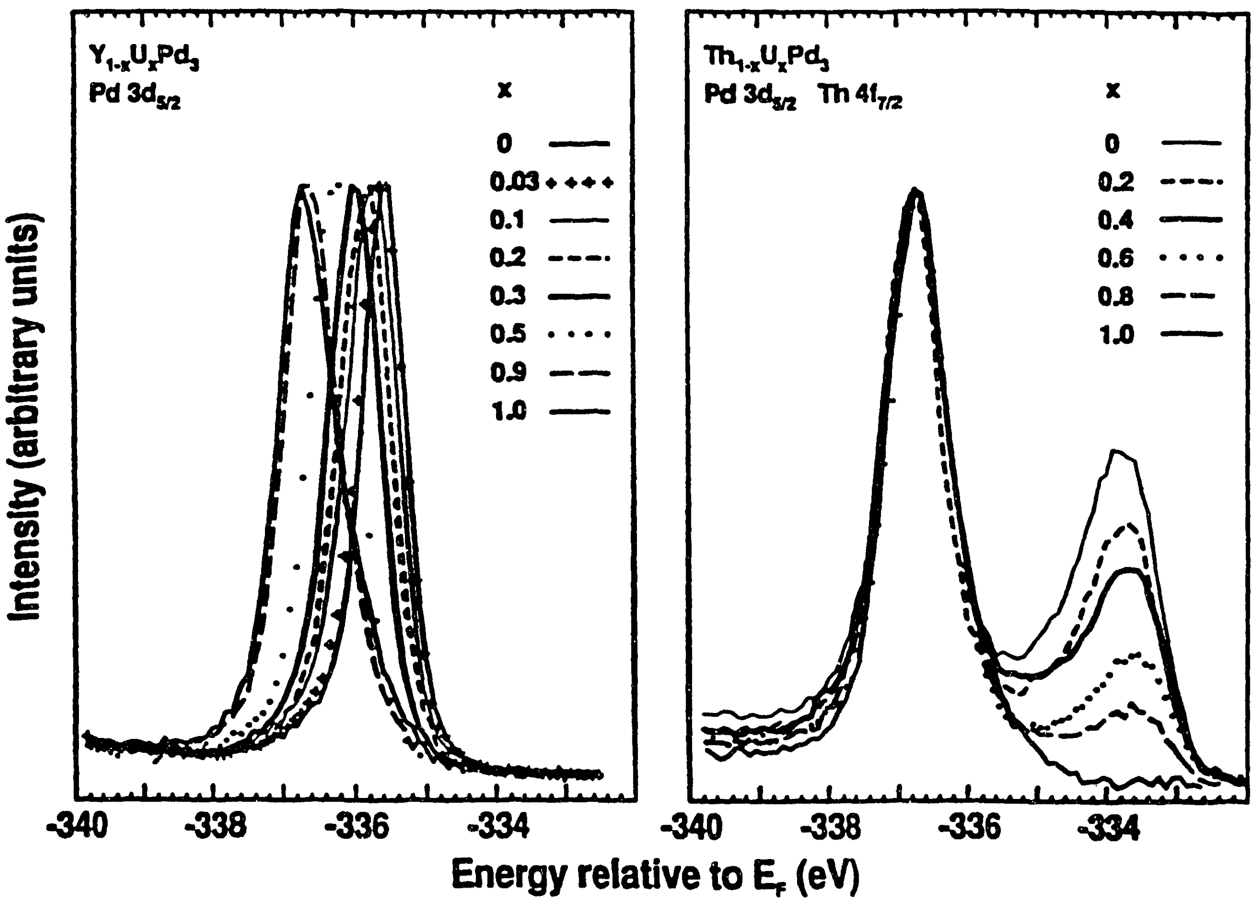

Fermi Level Tuning
DOMINATES inter-site interactions

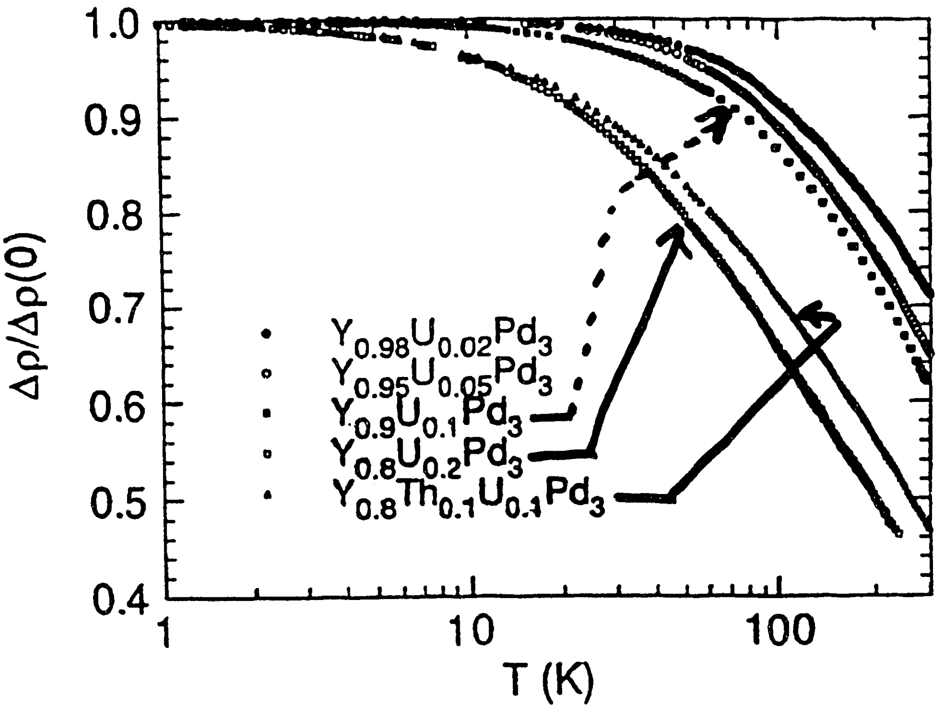

decrease U 0.2 to 0.1
but preserve total 4+ with Th
$\Rightarrow E_F$ not shifted
observe $T_K \cong$ same !
and much different from
$Y^{3+}_{0.9}U^{4+}_{0.1}Pd_3$ where E_F shifts

OVERVIEW

Strongly interacting fermion systems :
typically MULTIPLE ENERGY SCALES
appear in $G(\omega)$

Aim : trace

hi energy scales (tends to be charge) ⟶ emergent low energy scales (tends to be spin)

Interacting ground state properties

ACTIVITY

RARE EARTHS

Details of impurity Anderson model
surface shifts (Kaindl)
LDA $V(\epsilon)$ for fitting data
Lattice effects "on hold"

} Ce $\alpha-\gamma$ trans. — KONDO VOLUME COLLAPSE

ACTINIDES

? ? ? ~~?~~ ~~?~~ ~~?~~

compare spectra to LDA
dilution studies
looking for paradigm — FOUND! $Y_{1-x}U_xPd_3$

T-metal oxides

Mott-Hub. insulators
impurity Anderson ⟶ lattice effects ?
HTSC metals — normal state issues
MI transition

Study of Thin Layers of Actinides. Present Status and Future Use of Synchrotron Radiation*

T. H. Gouder and C. A. Colmenares
University of California
Lawrence Livermore National Laboratory
Livermore, California 94550

The study of actinide thin layers is a very important but yet unexplored field in the surface science of these materials. The low coordination environment of the surface should produce band narrowing[1,2] and this could ultimately result in the localization of the 5f-electrons, even for the light actinides. The wide surface concentration range which can be covered by thin layer deposition allows chemical and physical properties to be determined as a function of surface composition. The interaction of a dilute U surface phase with gas molecules is an important subject in the field of catalysis, where actinide surface atoms could act as promoters and local reaction centers.[3] From a more applied view point, thin layers offer the opportunity to study non-buried interfaces between actinides and the substrate material, thus allowing surface science to investigate the behavior of actinide-containment material interfaces under corroding conditions: interduffusion, oxidation and phase separation can particularly be addressed by this technique.[4]

We will present an XPS/UPS study of the U deposition on Pt. We will discuss the mode of growth of the surface phase, surface compound formation and bulk diffusion of the surface actinide atoms. U immediately reacts with the Pt substrate to form a surface alloy and this is shown by the narrowing of the Pt5d lines (Figure. 1), which is attributed to the dilution of Pt atoms in a U matrix.

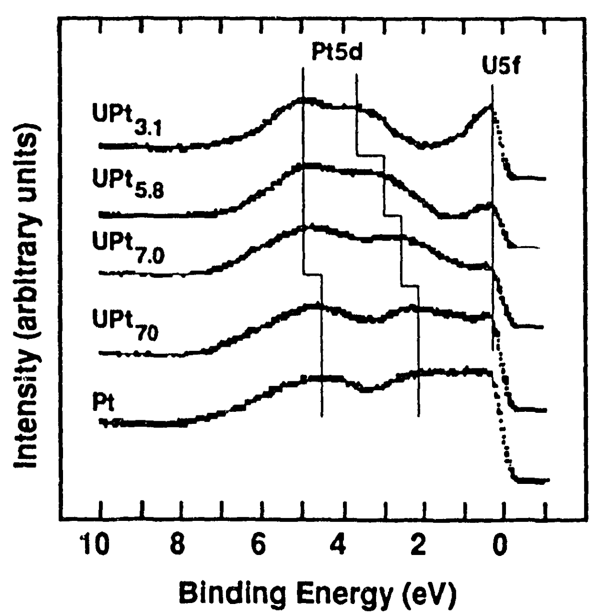

Fig. 1. HeII spectra resulting from the deposition of uranium onto a platinum surface at room temperature.

For the more concentrated U phase the U5f electrons are delocalized, as shown by the 5f emission at E_F. It is not possible to investigate a very dilute U system by conventional laboratory spectroscopy because of the strong Pt signal, thus it is necessary to resort to synchrotron radiation studies. In addition, we will address the interaction of the surface alloy with the gas phase, in particular the decomposition of the surface alloy in the presence of O_2. We will discuss the use of thin layers of U on an inert support (graphite) to study the U surface reaction with O_2 and CO, at high gas dosages, without a bulk to act as a sink for O and C. In particular we will present a study of the conversion of UO_2 into the U oxycarbide, which is a solid solution of UO and UC (Figure 2).

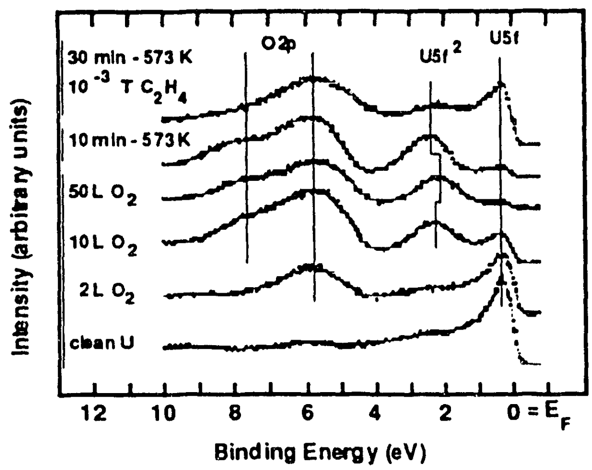

Fig. 2. HeII spectra of the formation of UO_2 followed by its conversion to oxycarbide by exposure to C_2H_4 at 573K.

These results may be of importance for the use of U in catalytic applications. Finally we will discuss the use of synchrotron radiation in the study of diluted actinide systems and thin layers.

1. K. P. Kämper, W. Schmitt, G. Güntherodt and H. Kuhlenbeck, Phys. Rev. B **38** (1988), 9451.

2. J. E. Inglesfield, Rep. Prog. Phys. **45** (1982), 223.

3. R. A. van Santen, *"Theoretical Heterogeneous Catalysis,"* World Scientific (1991), Singapore, New Jersey, London, Hong Kong.

4. T. Gouder, C. A. Colmenares, *"Thin Layers of Uranium on Polycrystalline Platinum and Their Interaction of O_2,"* submitted for publication to Surface Science.

*This work was performed under the auspices of the U.S. Department of Energy by Lawrence Livermore National Laboratory under contract No. W-7405-Eng-48.

Thin Layers of Actinides

Chemical Reactivity and Electronic Structure

Outline

1. Introduction

   - Research Interests
   - Choice of Substrates
   - Sample Preparation

2. Status Quo / Outlook

   XPS/AES/UPS - Synchrotron

   - Electronic Structure   U - Pd / U-Pt
   - Chemical Reactivity
     - U - Pt: O_2 , CO
     - U - Pd: O_2

3. Conclusion

Uranium Thin Layers: Research areas

Chemical Reactivity

Electronic Structure

* System

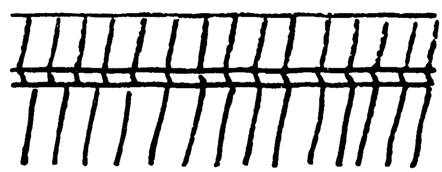

An

Interface

Substrate

* Subjects

- Diffusion
- Dissolution

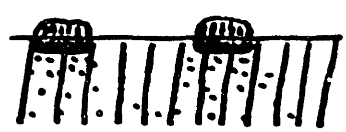

Containment
Nuclear
Materials

- Interface
  Decomposition

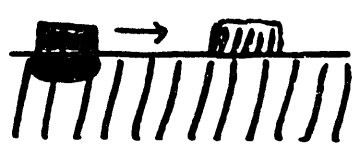

Corrosion

- Surface properties
  - * 5f - localization
  - * Local Reaction Centers (Catalysis)

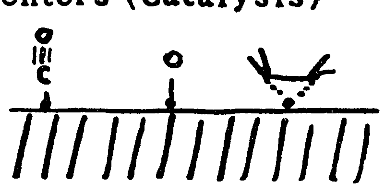

Strategy

Clean Systems

Characterization

Electronic Structure : 5f localization

Surface Reactions

Gas Adsorptions

Chemical Applications

5f Localization in Chemical Systems

* Dilution (Alloys): | increase mean An-An distance
  | avoid hybridization: [UPt_3]

* Partial Oxidation: $Z_{eff} \uparrow$ UO_2,

* Decrease Dimensionality:

  * Surface

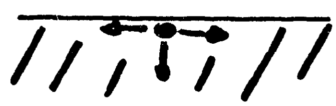

  * Thin Layer

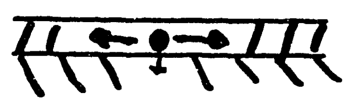

High interaction - low interaction

  * Cluster

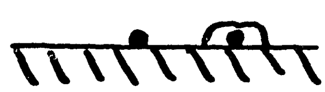

Solid → Atomic like

Electronic Structure - 5f Localization

5f - Levels in Pure Elements (Metals)

Th	Pa	U	Np	Pu	Am	Cm

Delocalization — Localization

5f - Levels in Chemical Systems

* 5f - 5f overlapping -> An-An distance
  -> An-An coordination

* 5f - ligand hybridization

Surface Reactivity

- Subject

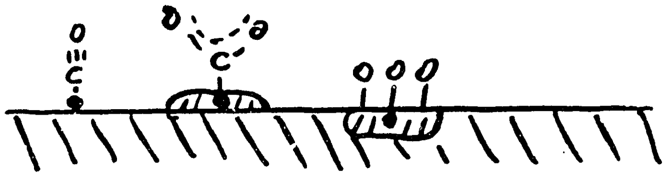

* An - Adsorbate Bonding

6d7s - 5f

- Reactivity of An Systems (-> Catalysis - Corrosion)

* Concentrated Bulk An

- 6d7s electrons -> early TM : strong bonding
- 5f electrons -> late TM : weak bonding

$\Longrightarrow$ catalysis

* Diluted Bulk An

- for [U] ↗ reactivity ↘ UNi_x <-> CO
- surface segregation

* Diluted Surface An

- low reactivity molecular chemisorption
- stable surface phase

Choice of Substrate

* Interaction Substrate - U (-> 5f localization)

- Strength

Low Medium Strong

- Type U 6d / U5f hybridization
  - localized system
    -> Pd
  - heavy fermion systems ?
    -> Pt

* Chemical Reactivity

group VIII metals : Ni, Pd, Pt

group 1b : Cu

* Containment Materials - Passivation

Ti, Mo, Binary Systems

Cluster Deposition

* Sputter Deposition

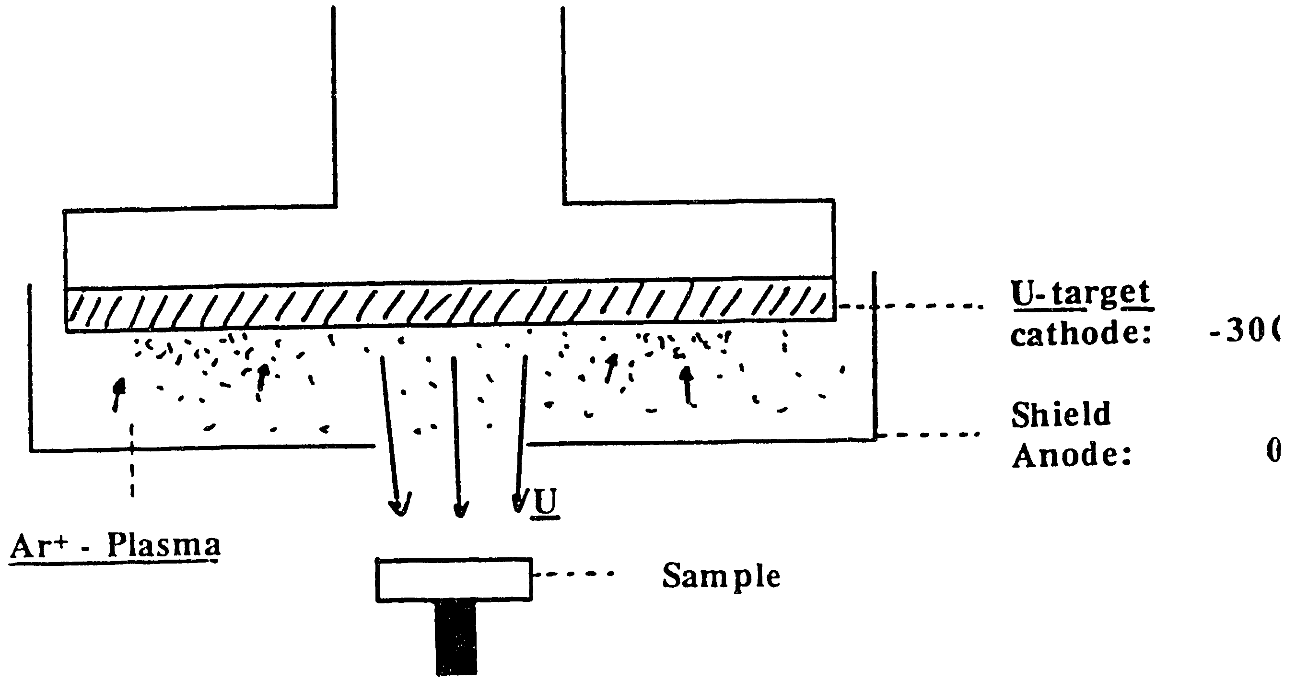

Source: | Target Current: 5 mA
Ar-Pressure: 5 10^{-3} Torr
Impur. Pressure: < 10^{-9} Torr

Particles: | Atoms / Ions
Clusters

U deposition on Pd at RT - AES study

* U Overlayer: 30 sec - 10 mA U: 5 A

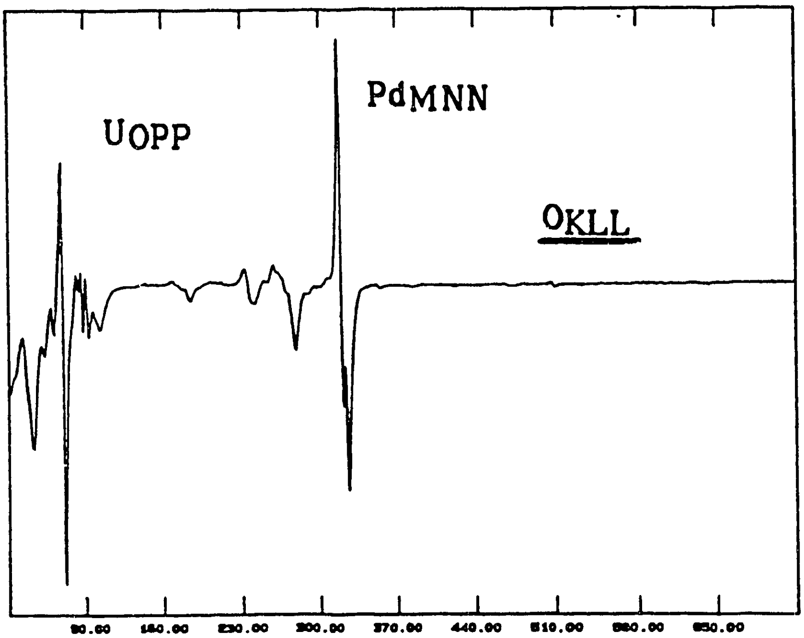

* UO_2 Overlayer: 10 L O_2

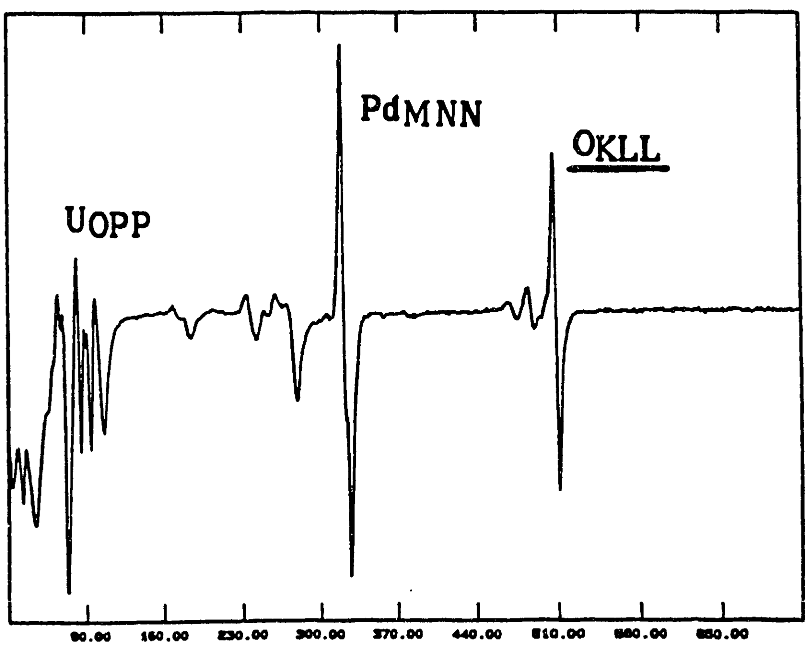

Electronic Structure of U-surface phase

- Experiment

* U-Pd	AES:	Deposition/Annealing
	XPS/UPS:	e^- - Structure
* U-Pt	UPS	

- Summary/Future work

  * Synchrotron

U - Pd system : Surface Reconstruction

- AES - Study of U-Pd Annealing

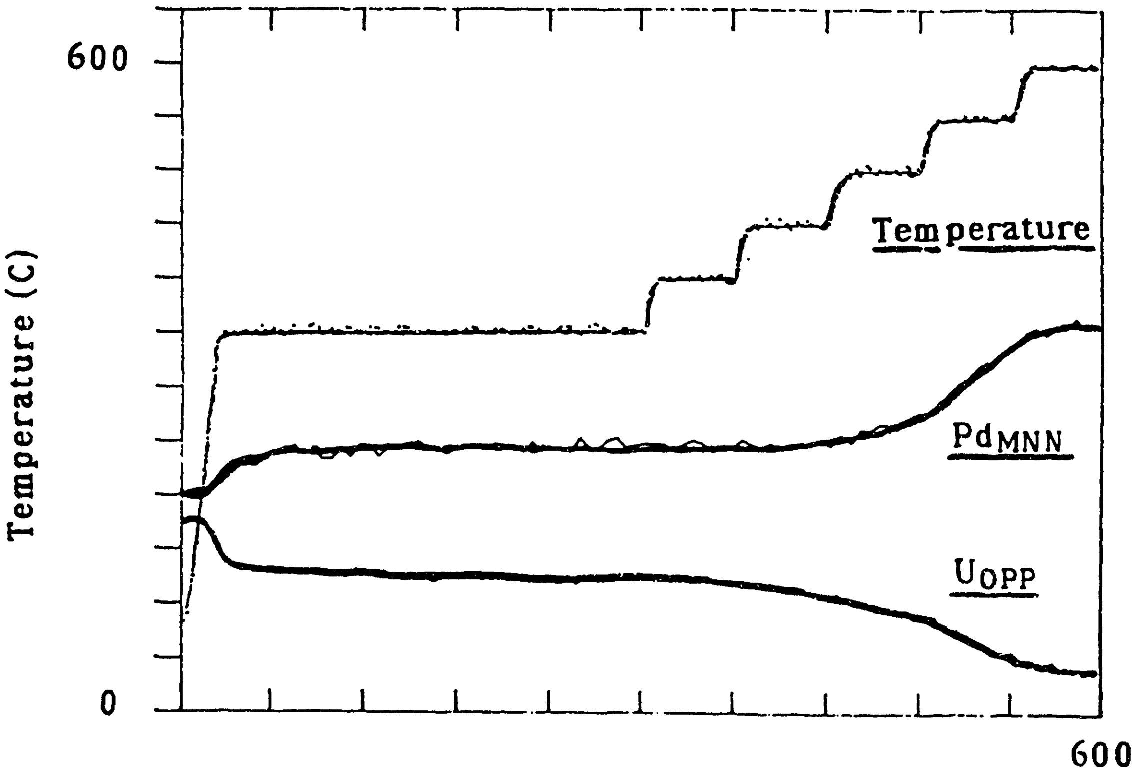

(U deposition at RT)

* low temperature diffusion

  - I_U ↘ 75%

  - step height ↗ with U coverage

    → U surface diffusion
    → Formation of surface compound

* high temperature diffusion

  - I_U ↘ 0 %

    → U bulk diffusion

U - Pd: Annealing

U4f

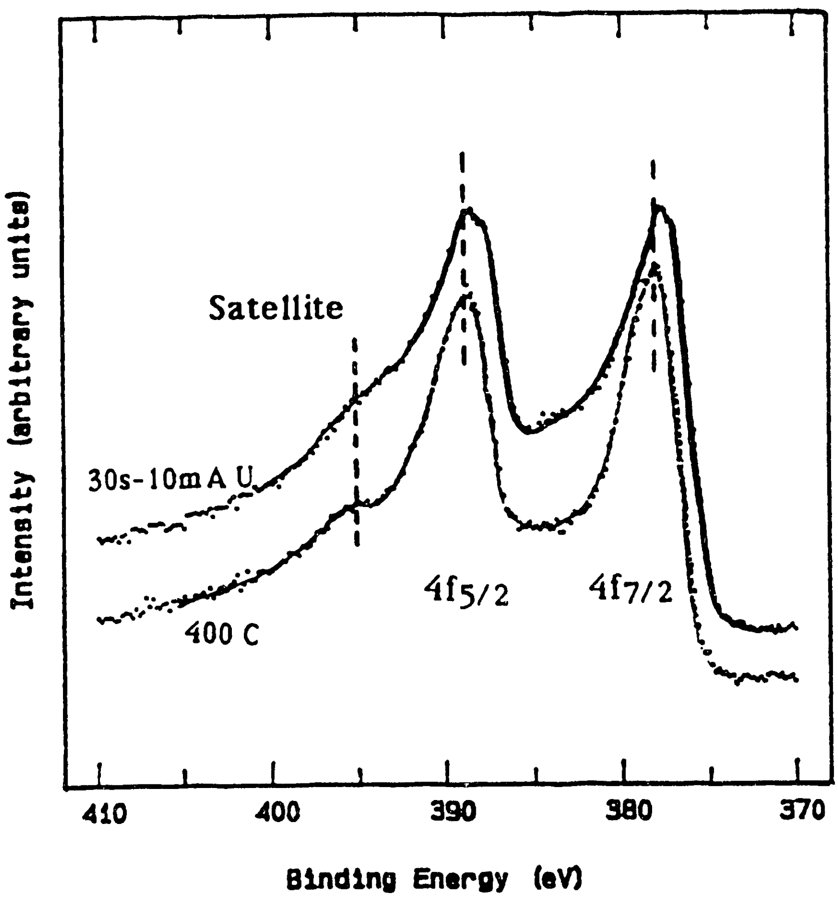

* RT deposition

- Asymmetrical shape → DOS at E_F
- Broad peak → inequivalent U atoms
- 6 eV satellite → 5f localization

* Annealing 200 C, 400 C

- Asymmetry
- Sharper peaks → 5f localization
- 6 eV satellite

U - Pd: Annealing

Pd3d

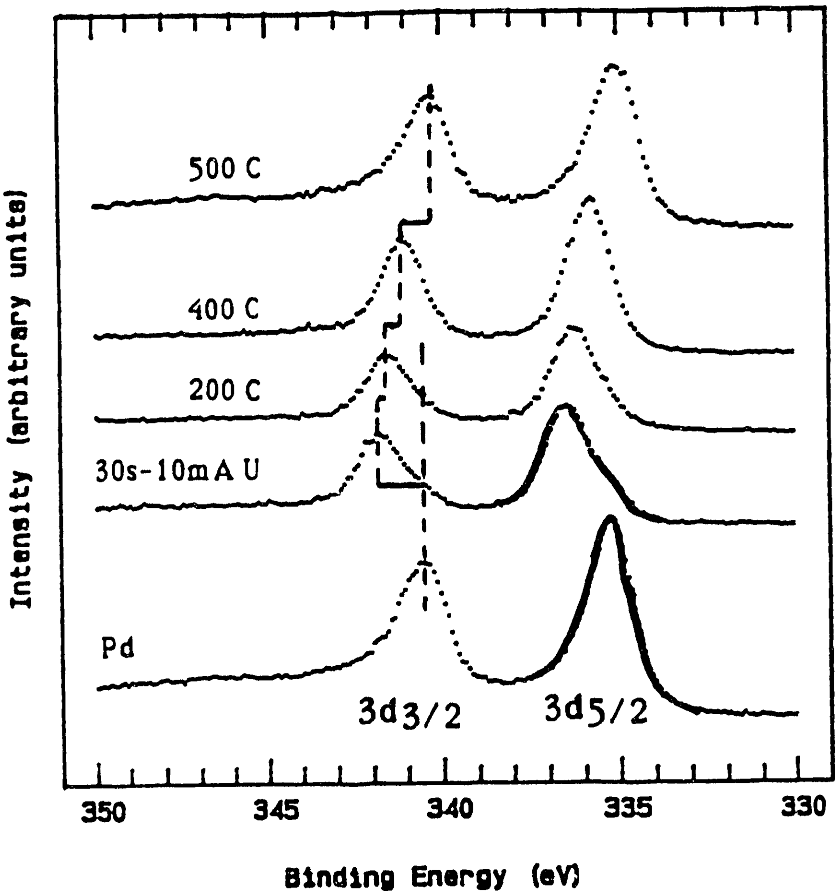

* RT deposition
  - High BE shift (85%) --> U-Pd surface layer
  - Non shifted (15%) --> Pd-bulk
  - Asymmetry --> Pd4d DOS at E_F

* Annealing 200 C, 400 C
  - BE decreases --> U diffusion
  - Pd_{met} peak disappears

→ Continuous shift <-> Dilution <-> Variable stoichiometry

U - Pd: Increasing [U]

Pd3d - high resolution

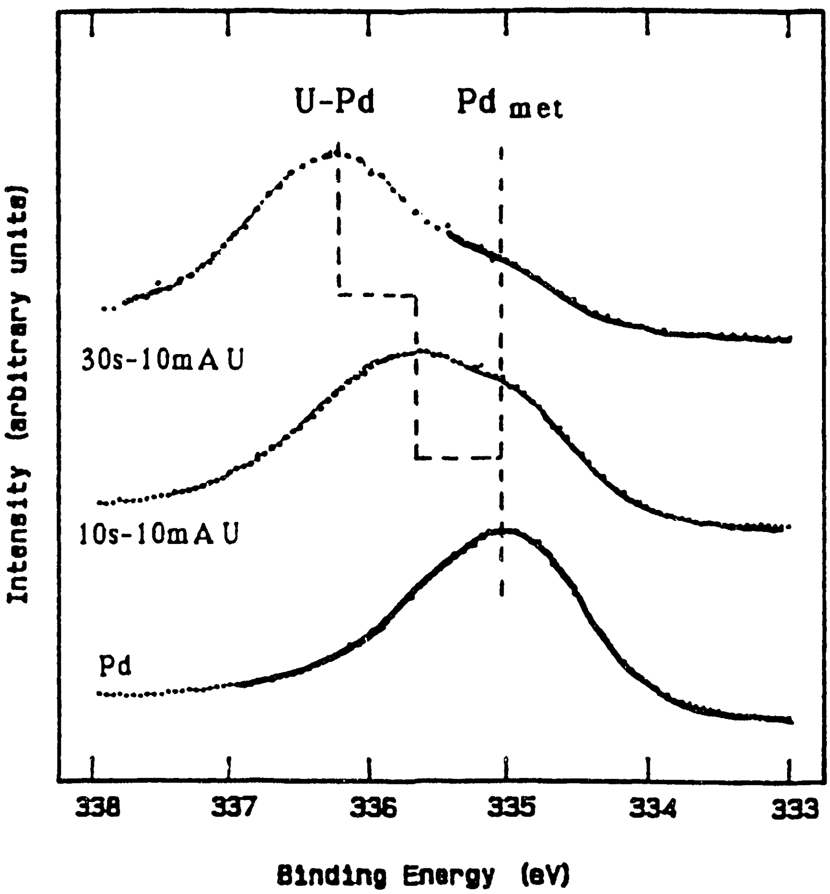

* for [U]

- Binding Energy $\quad$ Pd3d $_{U-Pd}$
- Intensity $\quad$ Pd3d $_{Pd\ metal}$

U - Pd: Annealing

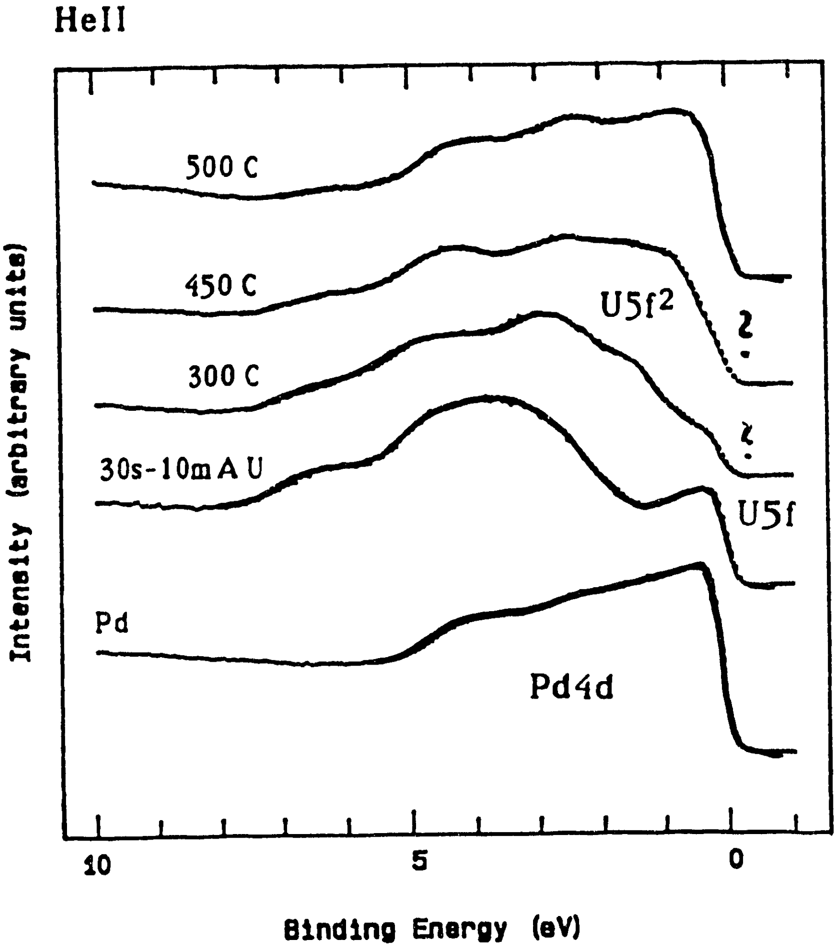

* <u>RT deposition</u>
  - I_{EF} <--> U5f → U5f delocalized
  - BE (Pd4d) → U-Pd bonding
  - Pd4d narrows → Pd dilution (?)

* <u>Annealing 200 C, 400 C</u>
  - I_{EF} ↘ → U5f localization
  - U5f² at 1.4 eV → UPd_3
  - Pd4d broadens → U dilution

U - Pt: Increasing Temperature

HeII

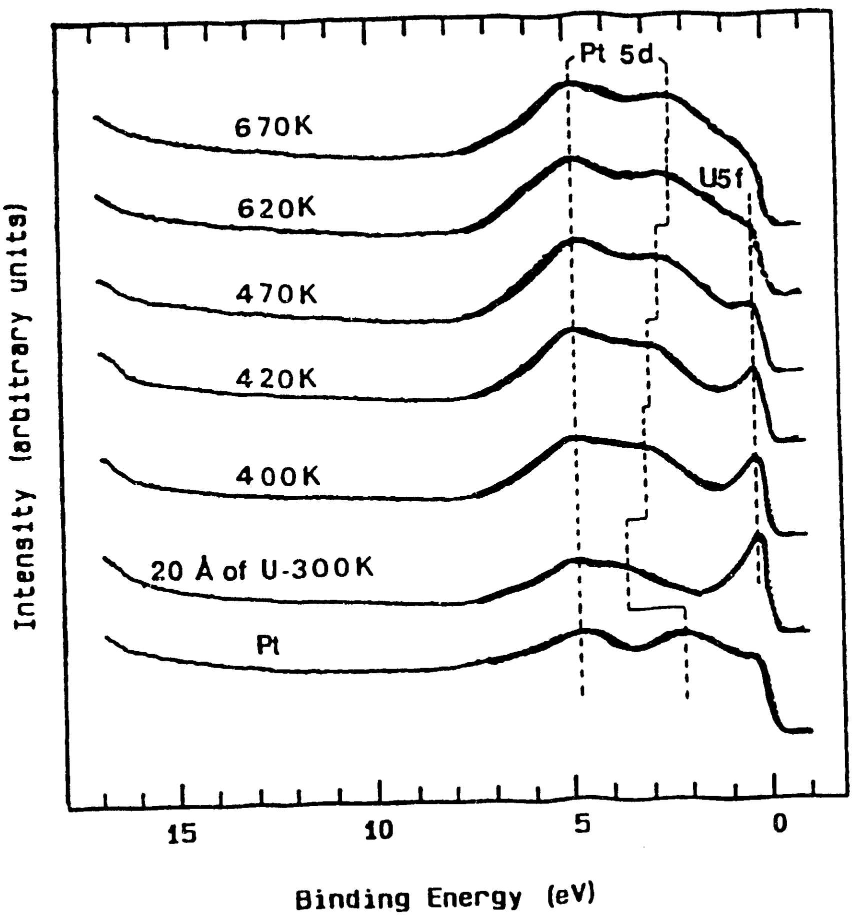

* With T ↗ : I_{EF} ↘

  - [U] ↘

  ⟹ U - Pt reaction

  ⟹ High Interaction System

* BE (Pt5d) ↘ : pure Pt

  ⟹ U responsible for high BE

Electronic Structure: Summary

* Status Quo

  - High Purity surface phase
  - Surface U: 5f delocalized <---> high [U]
  - Bulk diffusion <---> continuous stoichiometry

* Future Work

  - Systems
    - Low [U]
    - s.c. Studies: well defined surfaces
    - Heavier Actinides (Np, Pu): approach localization threshold

  - Synchrotron Studies
    - Low [U] /high TM d-signal <-> Resonant PE
    - High Energy Resolution <-> High Photon Current
    - Band Mapping
    - Depth Resolution - XPS: vary hn

Surface-Gas Interaction

- Experiment

    * U-Pt / O_2, CO Interaction
    * U-Pd / UO_2 Dissolution

- Summary/Future work

    * Synchrotron

CO on U - Pt at RT

HeII

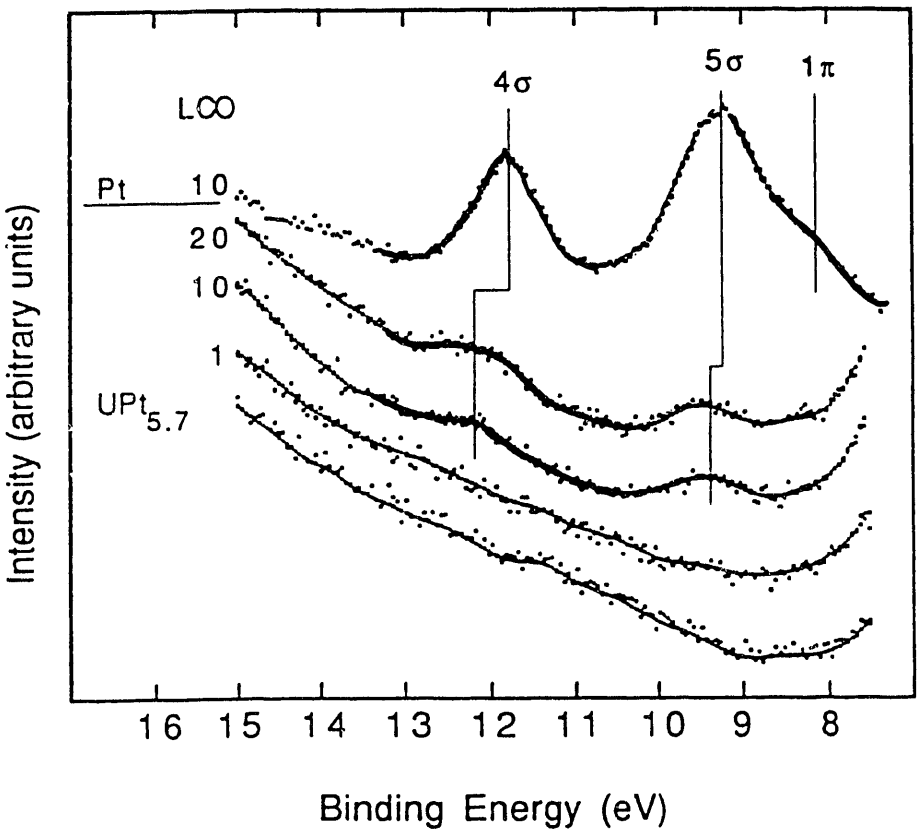

* O2p: dissociative adsorption
* CO 4σ,1π: molecular chemisorption

$\Delta 4\sigma - 1\pi \uparrow$: changed e- structure of CO

→ Modification of Pt by U

O2 on U - Pt

HeII

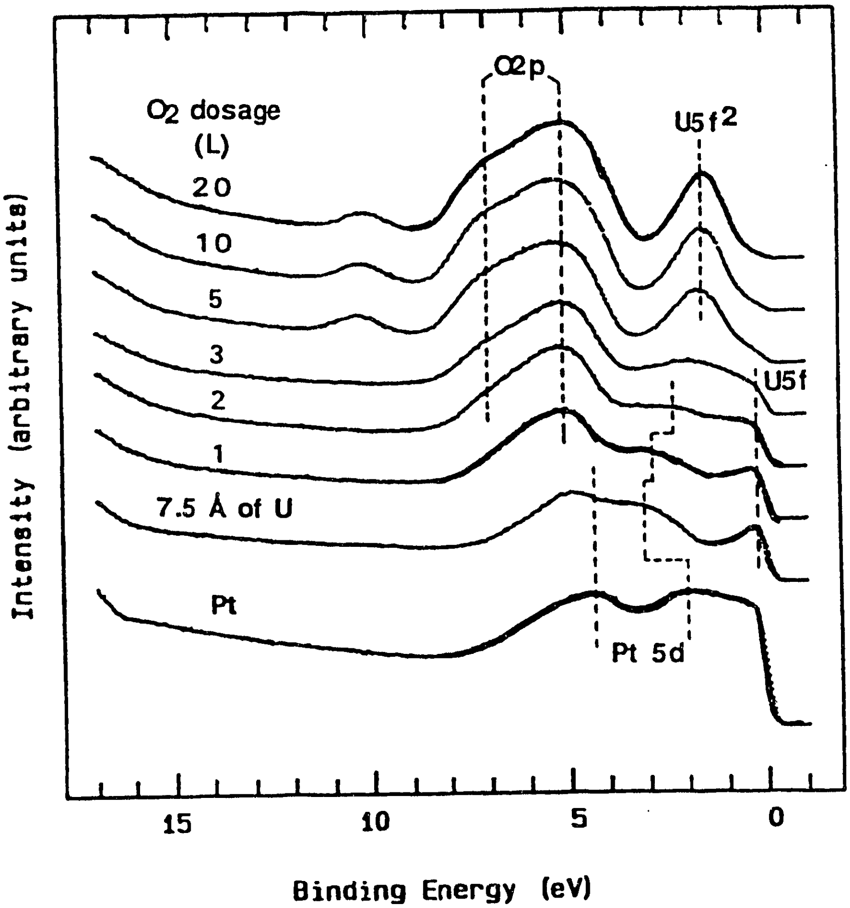

* O2p↑: oxide formation UO_2 ; UO_{2+x}

* I_{EF} ↘ | U oxidized
no Pt5d

* Pt5d | I ↘
BE ↘

oxidation: total attenuation of Pt signals

Pd - UO_2: Annealing

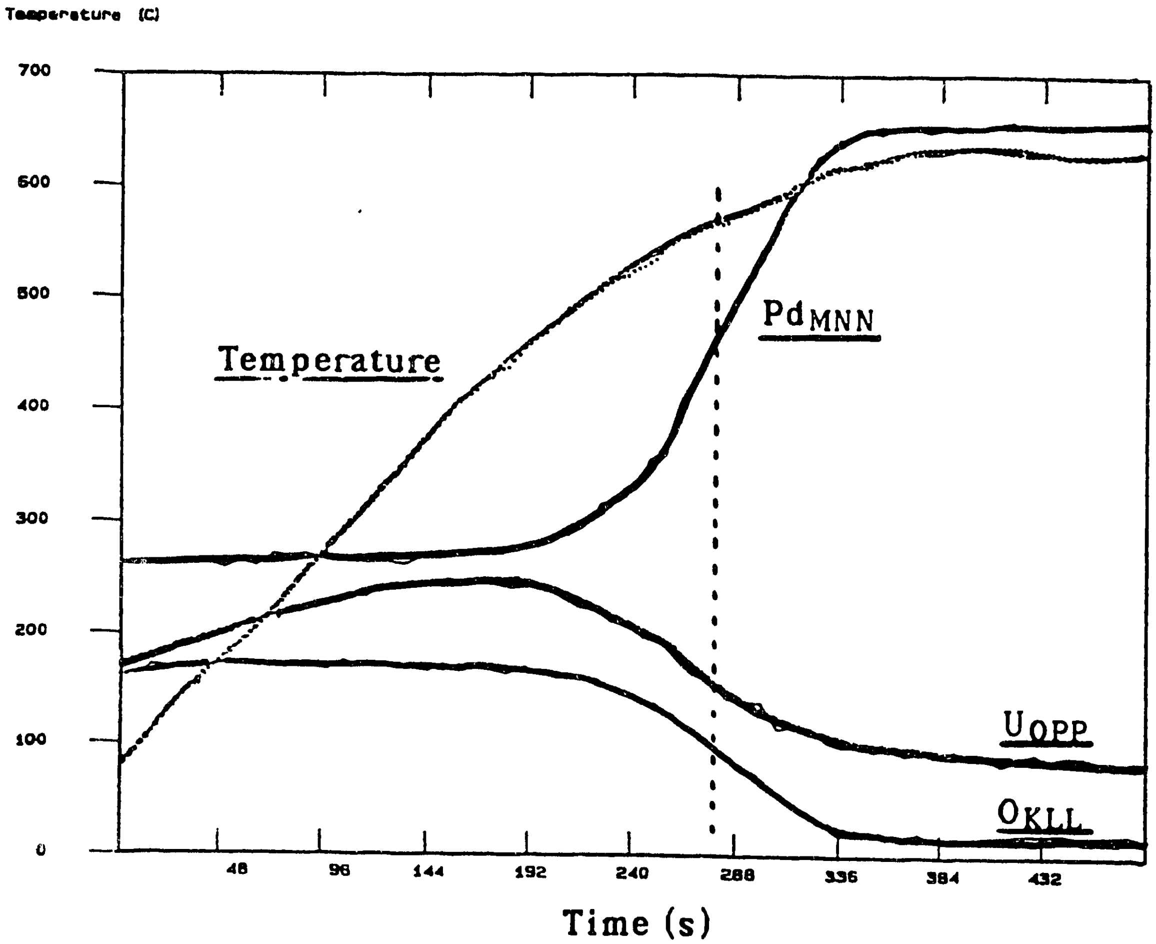

* at 550 C: Dissolution of UO_2

$$Pd + UO_2 \rightarrow Pd - U - O$$

$$\rightarrow Pd - U , O$$

➜ ΔH_f Pd - U formation : driving force ?

Surface-Gas Interaction/Summary

* Status Quo

- U-Pt: Molecular adsorption at RT -> Reactivity
- U-Pt / O_2: U surface segregation
- U-Pd : UO_2 dissolution

* Future Work

- <u>Systems</u>
  - Low [U]
  - Heavier Actinides (Np, Pu)
  - H_2O, CO_2, ... Corrosion

- <u>Synchrotron Studies</u>
  - Low [U] /high TM d-signal <-> Resonant PE
    evolution of 5f ↗ gas adsorption (CO, CO_2)
  - Depth Resolution - XPS: vary hν

Conclusion

Chemical Reactivity - Electronic Structure

Identify Role of 5f Electrons in Chemical Bonds

- well characterized systems/experiments
- highly diluted An system
- study of heavier actinides <-> realistic An systems

Actinide Beamline

HIGH RESOLUTION ELECTRON SPECTROSCOPY OF HIGHLY RADIOACTIVE ACTINIDES: CONSEQUENCES FOR A FUTURE TRANSURANIUM BEAMLINE

J.R. Naegele

Commission of the European Communities, Joint Research Centre
Institute for Transuranium Elements, Postfach 2340
D-7500 Karlsruhe, Germany

The intermediate position of the 5f actinide series between the 4f and 3d series is well established as e.g. nicely exhibited in a so-called "Nearly Periodic Table of Transition Elements [1]. The transition from delocalized to localized behaviour of the electrons in the unsaturated shell occurs at the beginning and end of the 4f and 3d series, respectively, whereas for the actinides that transition is observed in the middle of the series around Pu and Am[2]. This uniqueness of the actinides is strikingly demonstrated by their electronic properties resulting in a very rich complexity of physical properties[3]; Heavy Fermion behaviour is mentioned in particular. Thus the actinides offer an ideal opportunity to study the gradual change in localization of 5f electrons, i.e. correlation effects.

Photoemission spectroscopy using ultraviolet (UPS) and X-ray light (XPS) either from conventional laboratory light or synchrotron sources is well accepted to determine in a quite straightforward way the electronic structure of solids. Because of the unique electronic structure of the actinides with particular emphasis on the influence of the 5f electrons and of the great importance of actinides with respect to nuclear safety, an electron spectrometer for XPS, AES, EELS and particular high resolution UPS on highly radioactive materials has been built up at the Institute for Transuranium Elements. A commercial Leybold-Heraeus LHS-10 spectrometer has been modified to meet safety and vacuum requirements under glove box conditions[4,5]. The spectrometer is divided into three parts: preparation chamber (1), analysis chamber (2) and pumping section (3).

(1) A new preparation chamber was designed for pressures better than 10^{-8} Pa and mounted into a closed glove box. An integrated baking system is shielded by water cooling to allow for baking to 200 C in the closed glove box. All necessary "in-situ" sample surface preparation, like sputtering or scraping, is performed solely in the preparation chamber. Thus most of the radioactive waste is kept back in the preparation chamber.

(2) A new μ-metal analysis chamber together with the excitation sources (X ray and UV rare gas discharge sources) and the hemispherical electron energy analyzer are mounted into a generally open glove box frame.

(3) The UHV-pumping systems are also mounted into an open glove box system underneath the analysis and preparation chamber compartments. The roughing pumps are placed outside of the glove box system; the vacuum lines are fed through absolute filters into the glove box system to keep back potential radioactive contaminants.

The activity level in the analysis chamber was kept for about two years below the critical value beyond which one can no longer open the analysis side without closing the glove box. Afterwards the analysis glove box had to be closed in case of repair. For this purpose a repair glove box system has been installed. Recently, after extensive measurements on a very brittle PuSe single crystal, the contamination level was so seriously enhanced that the noise counting rate induced by radioactivity within the energy analyzer reached 1500 c/sec which prevented any further successful measurements. In a time consuming procedure, the energy analyser was successfully cleaned up in the repair glove box and transferred back to the analysis chamber.

Based on the experience collected now for more than 10 years at the Institute for Transuranium Elements the following statements concerning a future synchrotron beam line for transuranium elements can be made:

- A contamination of the storage ring can under all circumstances be completely excluded by e.g. using fast closing valves in connection with a "delay-line" as described in a feasibility study[6,7].
- The photoemission experiment should not be dependent in particular on laboratory infrastructure, i.e. atmosphere, water and gas supply, radiation monitors, decontamination means etc.. A possible solution would be to introduce the experiment into a small test chamber including an entrance lock[7].
- Facilities for handling and storage of radioactive samples and contaminated spectrometer parts, as well as for repair purposes ("repair box"), are desirable [7].
- The radioactivity level within the analysis chamber must be kept for an extended time (>5y) as low as possible because of risk of storage ring contamination in case of unexpected accidents and low background count rate. This can be achieved by placing a special transfer chamber between the analysis and preparation chamber as proposed in a feasibility study[7].
- The analyzer system should have an entrance lens system to minimize the background count rate originating from the radioactivity of the sample itself.
- The highly focussed photon-beam of the storage ring will permit the use of very small samples (diameter< 1mm) and thus cause much less radioactive waste produced by cleaning processes in the preparation chamber.

The performance of the spectrometer at the Transuranium Institute is described. Particular emphasis is given to high resolution UPS: at T = 80 K, a pass energy of 2 eV, the Fermi edge of gold showed a width of 45 meV at a maximum counting rate of 1.4 10^4 c/s. Recently, the spectrometer has been modified to cool the sample with liquid He. The spectrometer resolution has been measured by UPS on Ar gas showing a width of about 20 meV for the Ar 3p lines. It is pointed out that the high resolution in combination with high counting rates is essential for the very highly reactive actinide materials because of the fast oxidation of the surface due to the segregation of bulk oxygen impurities to the surface. High intensity synchrotron light from the ALS will provide a resolution of 10 meV or even better provided the sample can be cooled to liquid He temperatures. It is shown that this is important for measurements on Heavy Fermion materials.

UPS/XPS valence band and XPS core level spectra are presented for the following materials[4,5,8-10]: UO_2, PuO_2, Pu_2O_3, Am_2O_3, Th, U, Np, α-Pu, δ-Pu, Am, Pu_xAm_{1-x}, PuSe, UNi_2 and UMn_2.

All actinide oxides have localized 5f electrons and should therefore display $5f^{n-1}$ final state multiplets[11]. The oxygen 2p and the 5f emissions are clearly identified by their excitation probabilities[12] varying specifically with the photon excitation energy. Surprisingly no 5f multiplets but just a single actinide 5f peak are observed. Using the calculated multiplet intensities[11], it is shown that phonon broadening of about 1 eV prevents completely the resolution of the multiplet components and explains the characteristic variation of the 5f emission intensity along the series.

Phonon broadening is certainly of minor importance for metallic actinide systems, in contrast to highly ionic semiconducting actinide compounds like the oxides. Thus for metals, much sharper structures are observed, in particular close to the Fermi level. Whereas all elemental actinide metals[4,5,8-10] from U to α-Pu show similar valence band and 4f core level spectra due to itinerant 5f states pinned at the Fermi level, Am is the first metal in the actinide series showing a withdrawl of the 5f states from the Fermi level, i.e. a 5f final state triplet due to localization of the 5f electrons[9]. The 5f multiplets are resolved because neither phonon nor the life-time broadening conceil their structures because of the low 5f density of states at the Fermi level. Discrepancies between the experimentally observed 5f multiplet components and calculated intensities are discussed.

Of particular interest are those cases for which the 5f electrons are intermediate between delocalization and localization. With respect to this, examples of δ-Pu, Am_xPu_{1-x} and PuSe will be presented and discussed in detail even if the final description of the 5f electrons is not yet well established. The 4f core level and valence band spectra show similar 5f derived features for the three compounds:

- The 4f core levels exhibit, in addition to the metallic α-Pu 4f lines, a satellite at roughly 4 eV higher binding energy (the intensity of which is obliviously dependent on the degree of the 5f localization that is relatively small in δ-Pu, increasing in Am_xPu_{1-x} with x and more pronounced in PuSe).
- Three sharp structures appear in the vicinity of the Fermi level at 0.9 and 0.6 eV binding energy and directly at the Fermi level; the width of these structures is of order of 100 to 150 meV. In δ-Pu, the narrowing of the 5f state compared with α-Pu is quite clearly observed; a similar effect is observed in Am_xPu_{1-x}. In PuSe, an additional broad 5f derived structure is observed at 2 eV binding energy.

In PuSe, unusually strong temperature variations are observed for the 4f core levels as well as for the triplet structure in the vicinity of the Fermi level that cannot be explained by the common Fermi edge broadening.

A final consistent explanation is hard to give on the basis of conventional photoelectron spectroscopy using classical synchrotron radiation and laboratory UV-sources. But it is shown how the availability of the ALS will definitely improve the situation in actinide reasearch. That is further proved by the example of synchrotron[13] and conventional[5] photoemission experiments on UMn_2.

Finally, because of the importance of the actinides for the nuclear industry and related safety aspects, recent gas adsorption studies on Pu[14] and photoelectron studies on $(U/Pu)O_2$ fuel pellets and their dissolution residues[4] are reported. In this respect the availability of the ALS will open new possibilities for analytical investigations.

1. J. L.Smith and E.A.Kmetko, J.Less-Common Metals, **90**, 83 (1983).
2. H.L.Skriver, O.K.Andersen and B.Johansson, Phys.Rev. Lett. **41** 42 (1978).
3. Handbook on the " *Physics and Chemistry of Actinides*" edited by A.J.Freeman and G.H.Lander, Vol. 1 and 2 (North-Holland, Amsterdam, 1984 and 1985)
4. J.R.Naegele, J.Phys. (Paris) **45**, C2-841 (1984).
5. J.R.Naegele, J.Nucl.Mat. **166**, 59 (1989).
6. A.Savoia,P.Perfetti and J.R.Naegele, Proc. Int.Workshop on "*Perspectives on the Use of Synchroton Radiation in Transuranium Research*", Karlsruhe 1985, edited by G.Kaindl and C.Laubschat (Freie Universität Berlin, 1985), p.40.
7. A. Savoia and P.Perfetti, Feasibility Study "*Energy and Angle Dependent Photoemission Spectroscopy on Highly Radioactive Actinide Solids Using Synchrotron Radiation*", Research Contract No. CR/01/83 of the Commission of the EC,1986.
8. J.R.Naegele, J.Ghijsen and L.Manes, in "*Actinides-Chemistry and Physical Properties*", in: " Structure and Bonding", edited by L.Manes, Vo. 59/60 (Springer, Berlin,1985) p.197.
9. J.R.Naegele, L.Manes, J.C.Spirlet and W.Müller, Phys.Rev. Lett. **52**,1834 (1984).
10. J.R.Naegele,L.E.Cox and J.W.Ward, Inorg.Chim.Acta **139**,327(1987)
11. F.Gerken and J.Schmidt-May, J.Phys.F **13**, 1571 (1983).
12. J.J. Yeh and I.Lindau, Atomic Data and Nuclear Data Tables **32**, 1 (1985).
13. J.R.Naegele, J.Ghijsen, R.L.Johnson and V.Sechovsky, Phys.Scripta **35**, 877 (1987).
14. T.Almeida, L.E.Cox, J.W. Ward and J.R.Naegele, submitted to Surf. Sci..

Electron spectrometer (UPS/XPS/AES) for highly radioactive materials

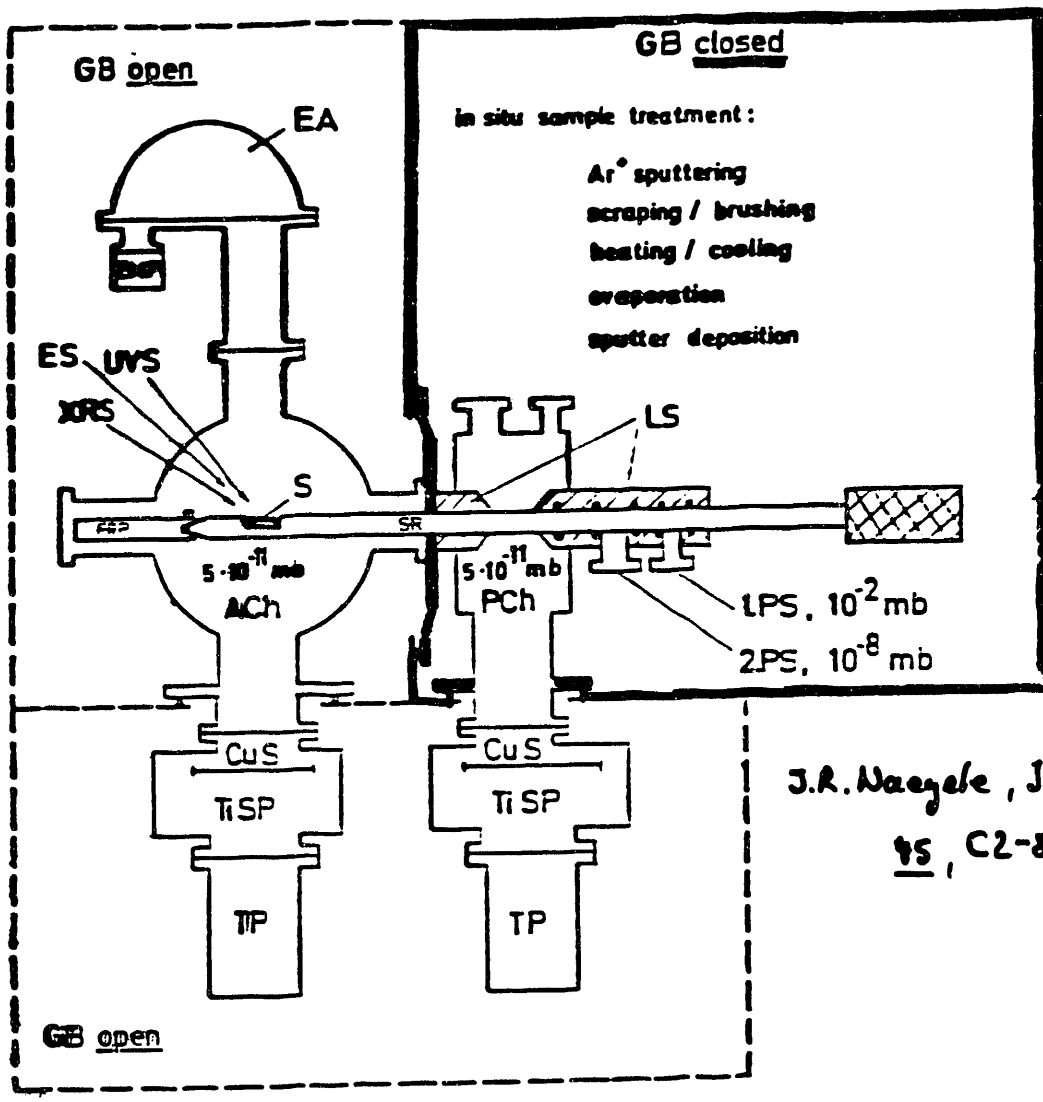

J.R. Naegele, J.d. Physique 45, C2-841 (1984)

ACh analysing chamber
CuS copper shield
EA electron energy analyser
EMP electron muliplier
FRP final rod piece
GB glove box
LS lock system, differentially pumped
PCh preparation chamber
S sample
Sr sample rod
TiSP titanium sublimation pump
TP turbopump
UVS UV source (rare gas discharge source)
XRS X-ray source (Mg or Al anode)
ES electron source
1.PS 1. differential pumping stage
2.PS 2. differential pumping stage

Photon energy dependent valence band spectra of UO_2 demonstrating cross sections

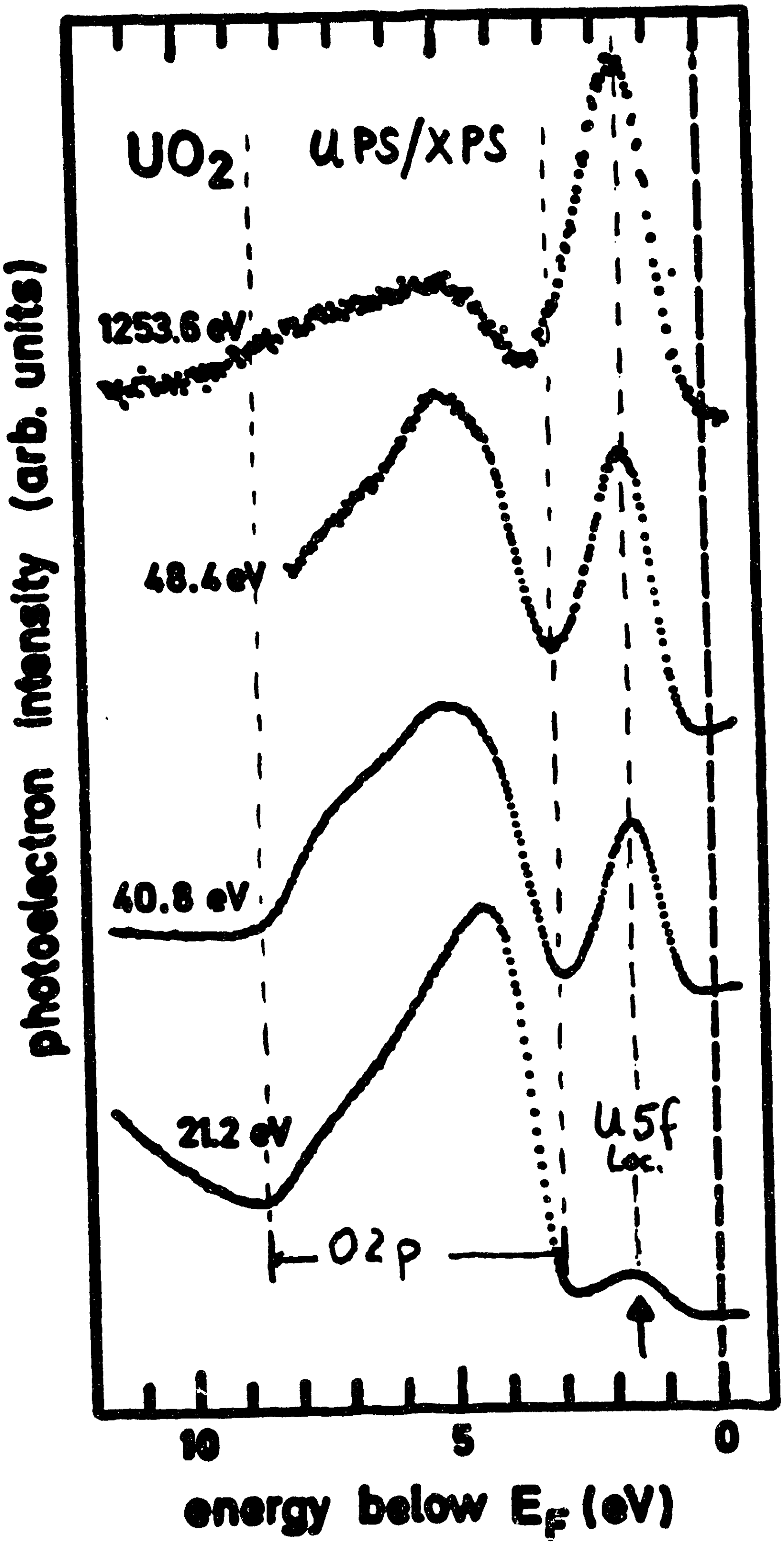

UPS a: 21.2 eV

b: 40.8 eV

c: 48.4 eV

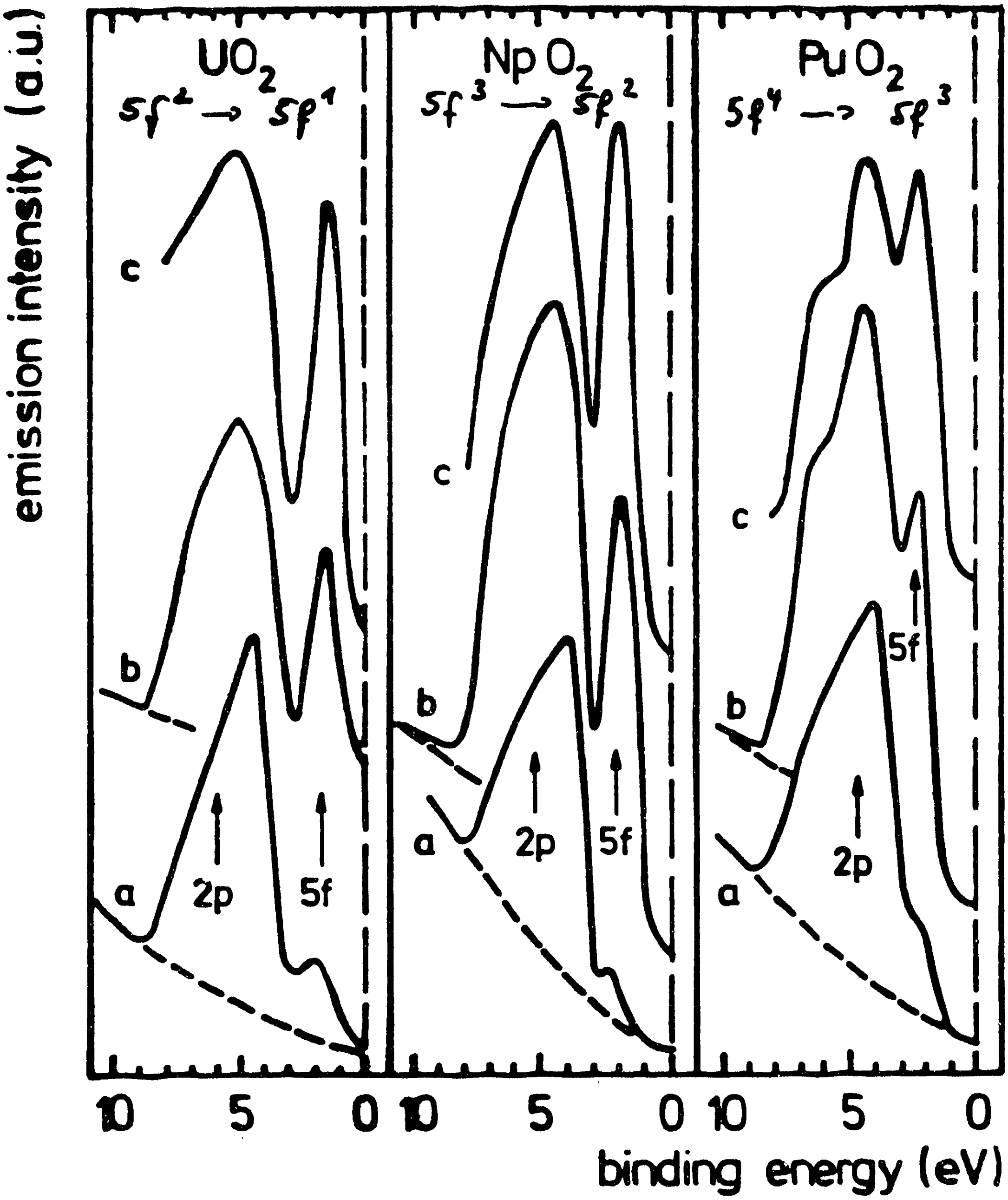

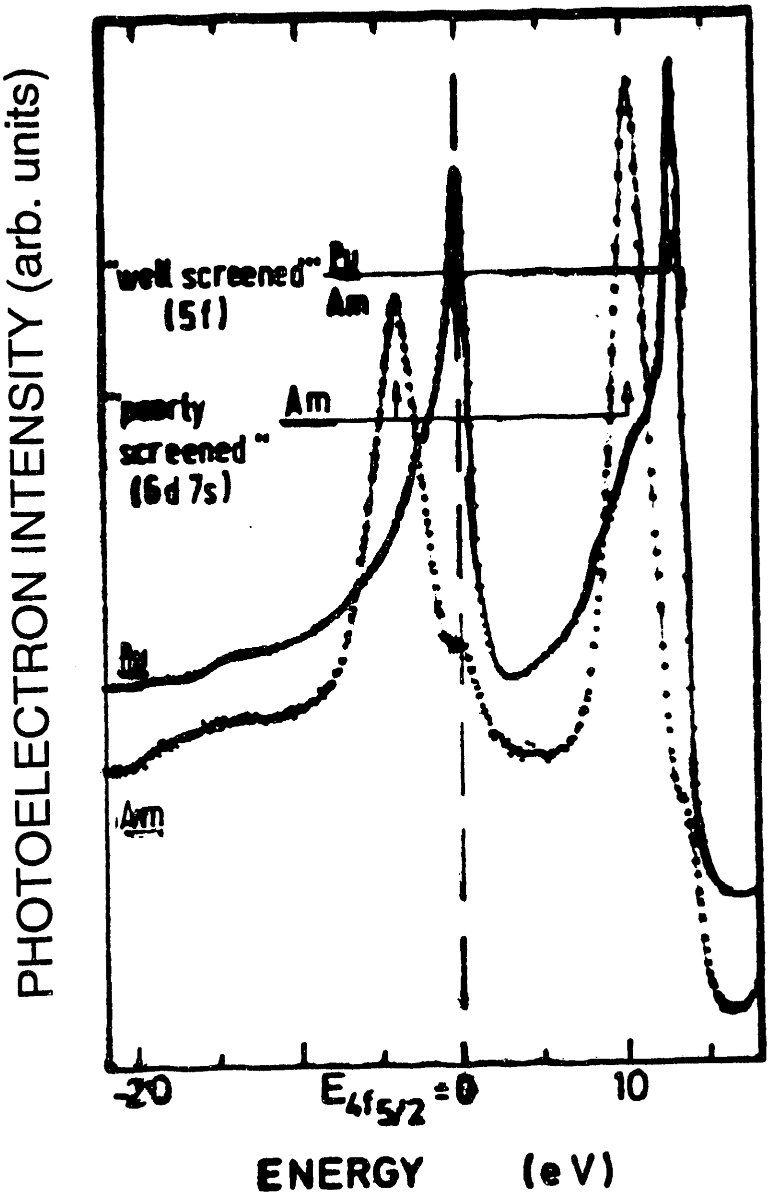

XPS 4*f*-core-level spectra of Am and Pu metal.

PHOTOELECTRON SPECTRA OF THE CONDUCTION BAND OF ACTINIDE METALS

hν = 40.8 eV (UPS)

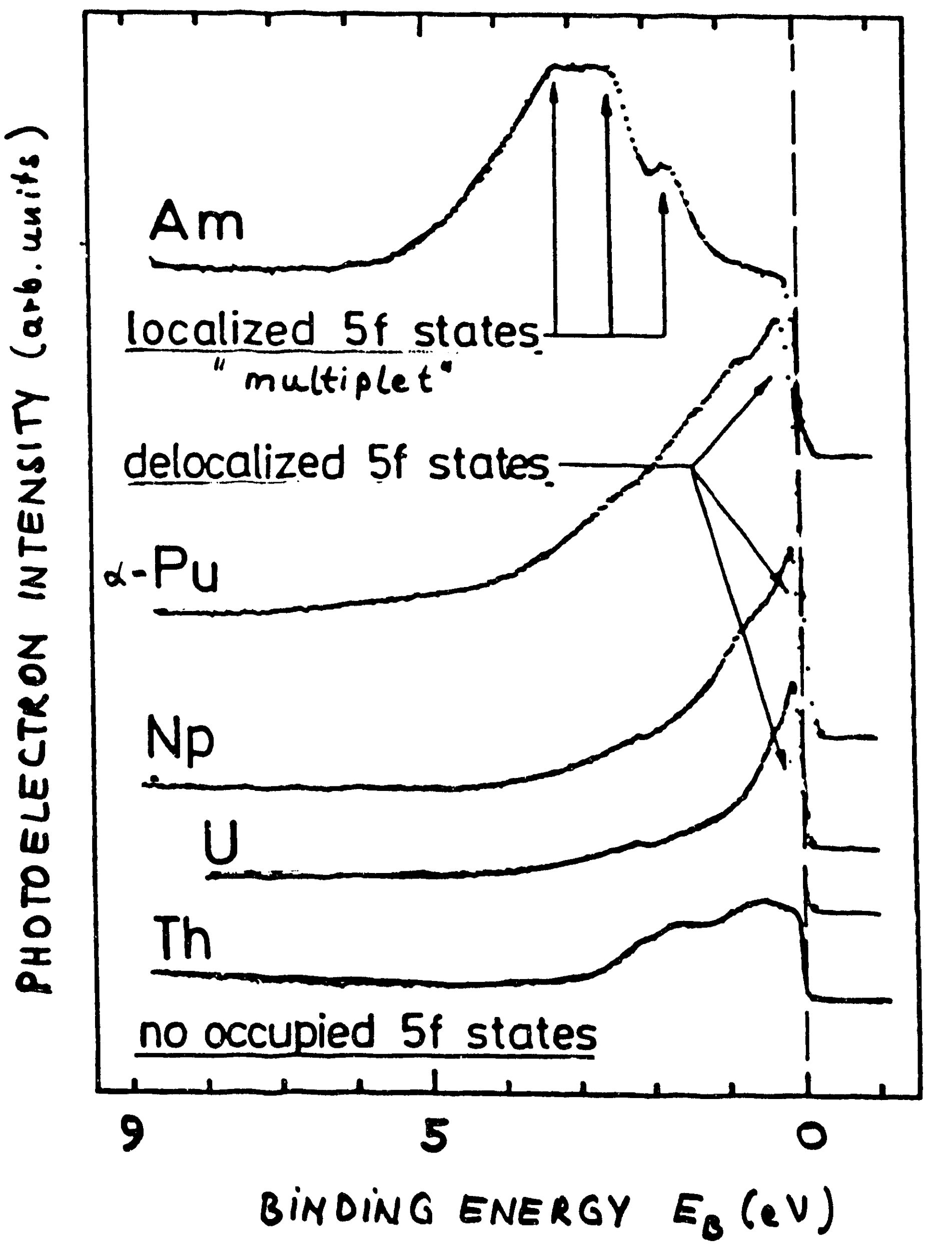

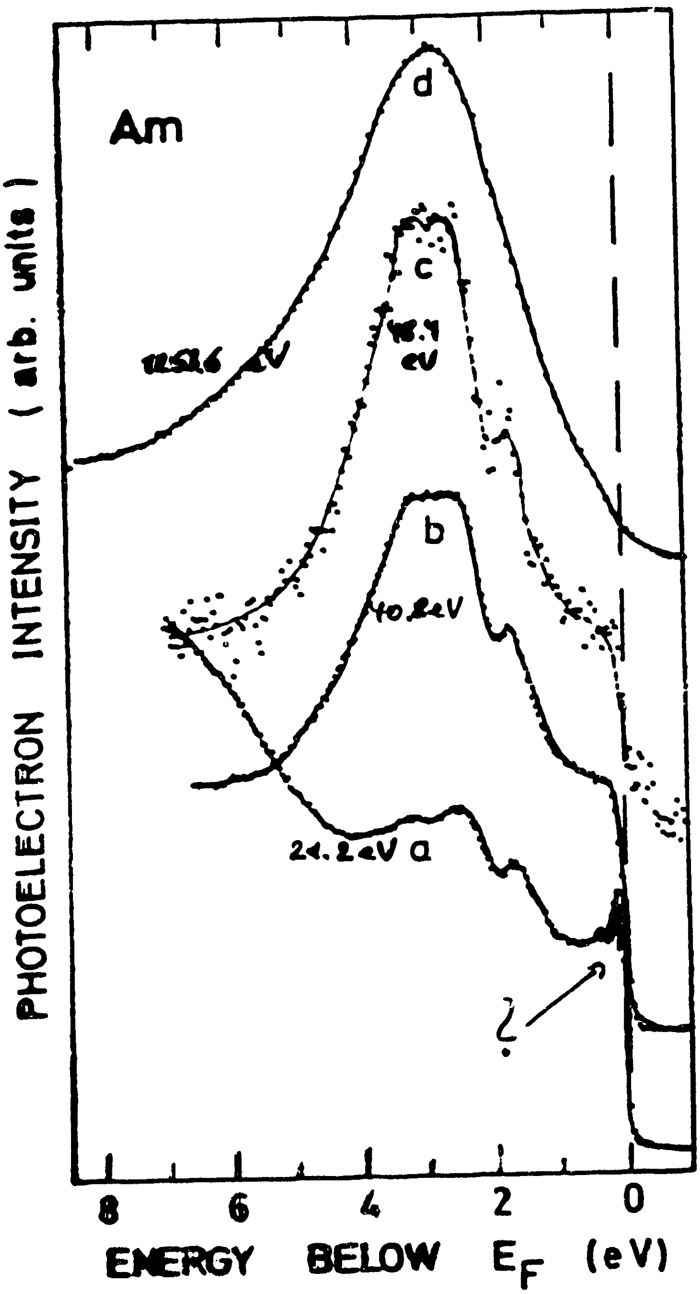

a: 21.2 eV

b: 40.8 eV

c: 48.4 eV

d: 1253.6 eV

AIIM

Association for Information and Image Management
1100 Wayne Avenue, Suite 1100
Silver Spring, Maryland 20910
301/587-8202

Centimeter

1 2 3 4 5 6 7 8 9 10 11 12 13 14 15 mm

1 2 3 4 5

Inches

1.0 1.1 1.25 1.4 1.6 1.8 2.0 2.2 2.5 2.8 3.2 3.6 4.0 4.5 5.0

PHOTOELECTRON SPECTRA OF THE CONDUCTION BAND OF UMn_2

$h\nu$: variable 16.7 - 48.4 eV (UPS)

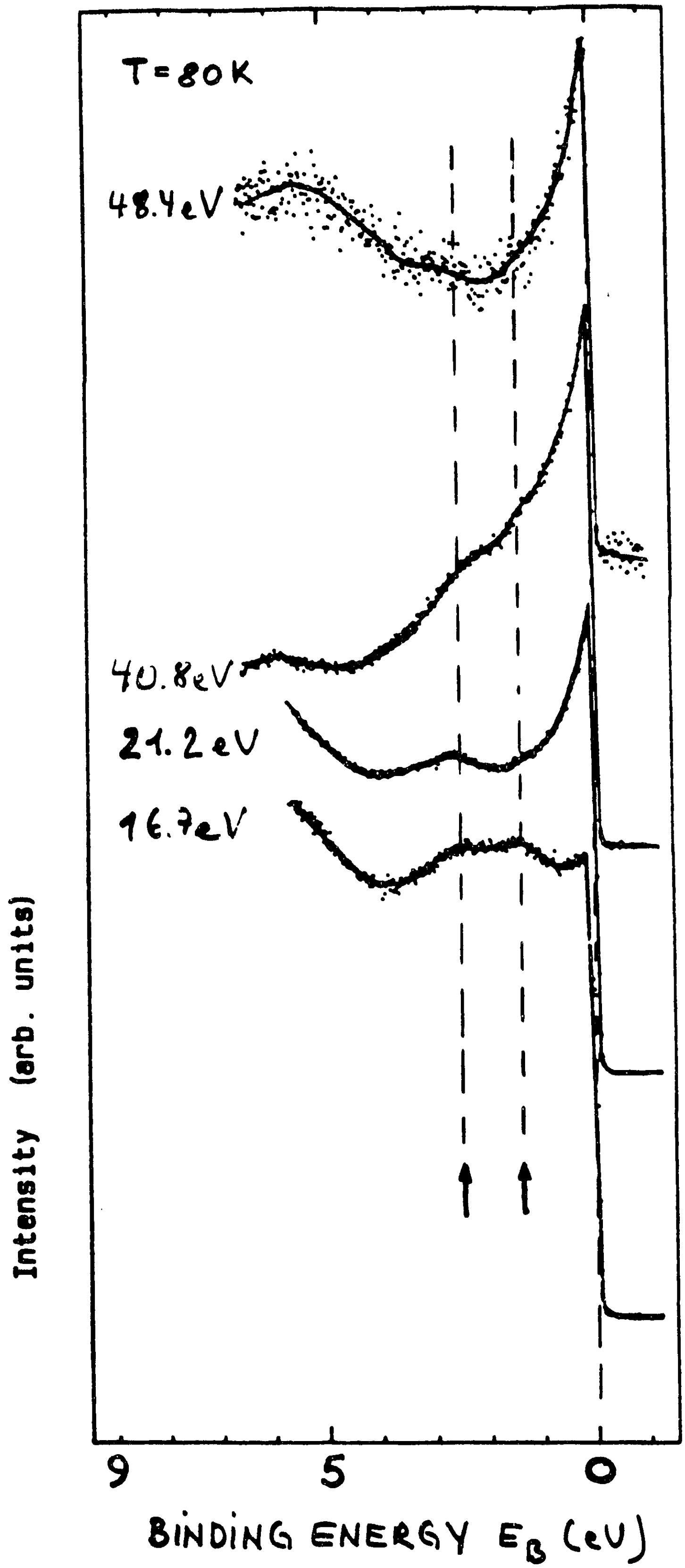

XPS 4f core level spectra
(U/Pu) O_2

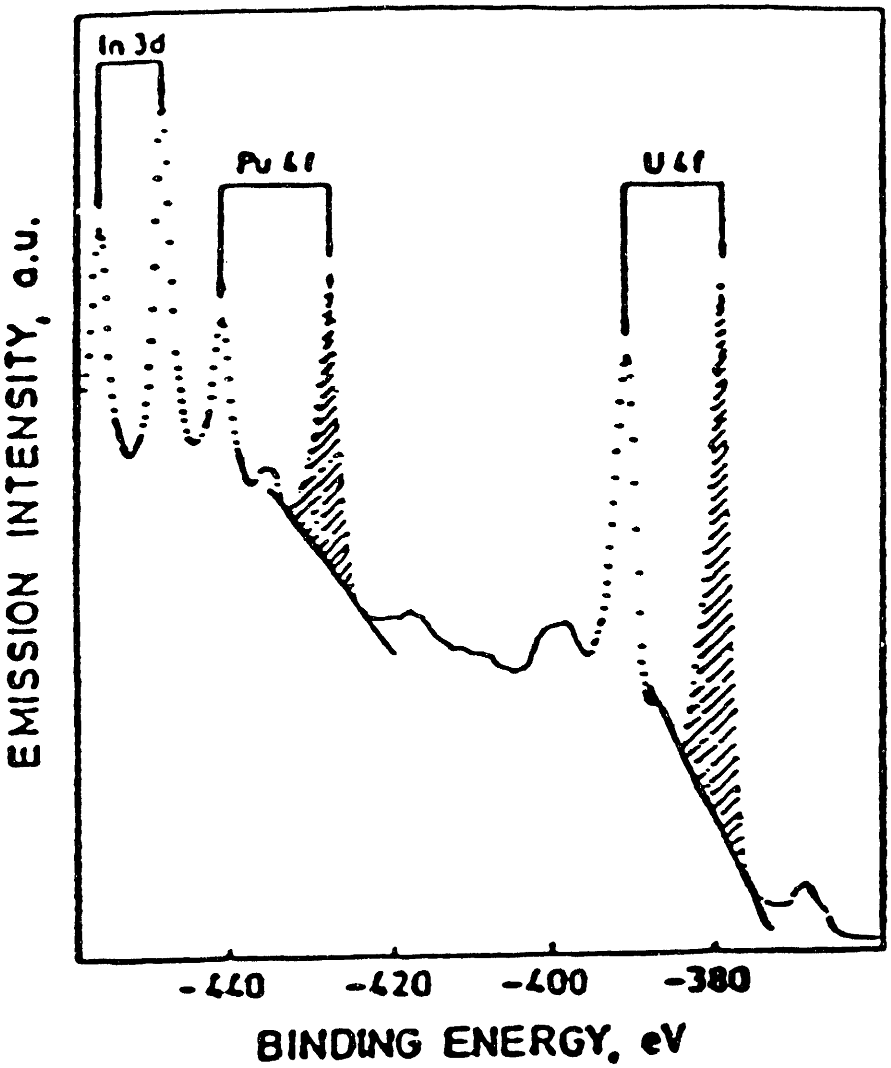

The spectra for the dissolution residues (in HNO_3) of $(U/Pu)O_2$ are displayed here. They show a ~ 10% enhanced Pu surface concentration compared with virgine $(U/Pu)O_2$.

PHOTOELECTRON SPECTRA OF THE Np 4f CORE LEVELS FORMATION OF SURFACE Np_2O_3 OXIDE ON Np METAL

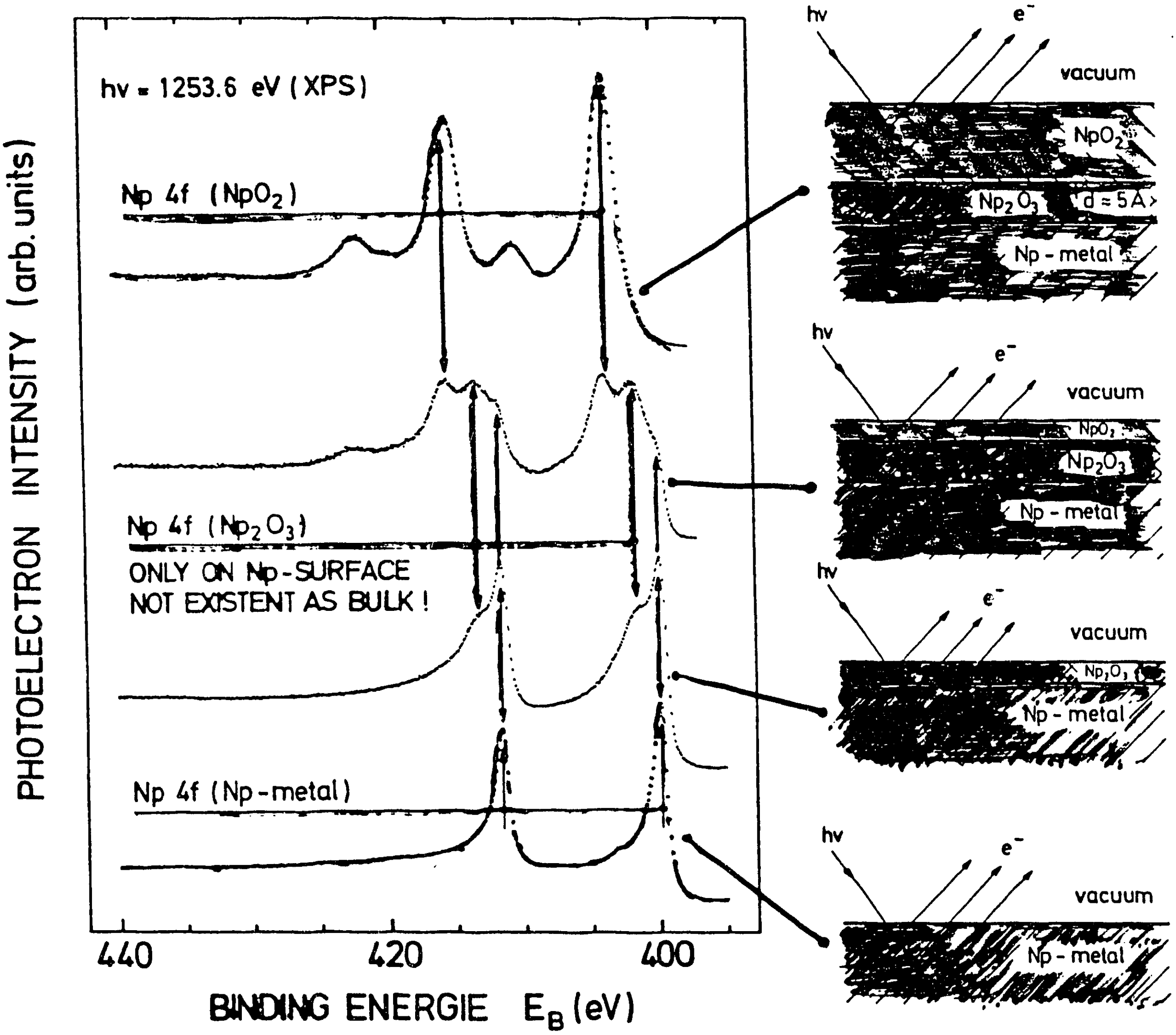

Np_2O_3 NOT EXISTENT AS BULK PHASE !

O_2 adsorption on Pu metal

UPS (HeII: 40.8eV) valence band spectra

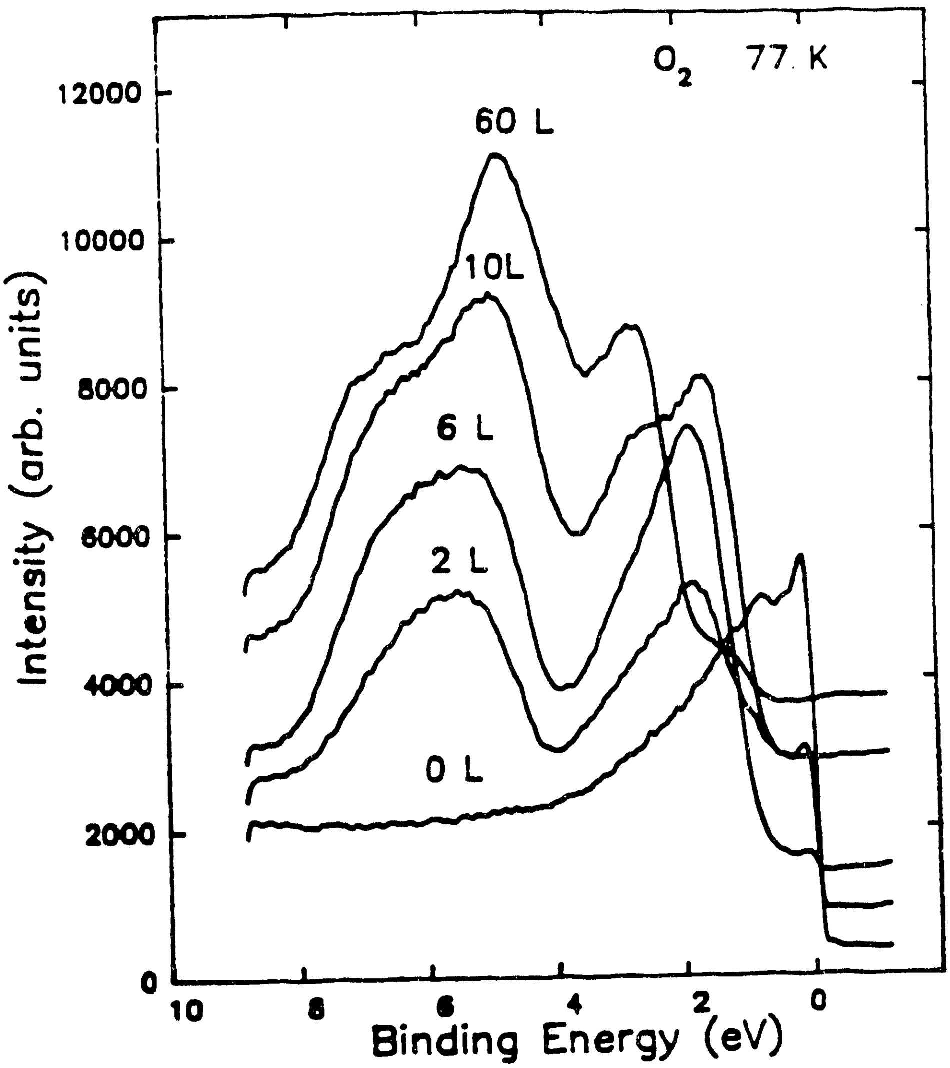

Conduction Band Spectra of PuSe
scraped surface d: XPS $\Delta E = 1.1$ eV
UPS $\Delta E = 45$ meV

a (16.8 eV)
b (21.2 eV)
c (40.8 eV)

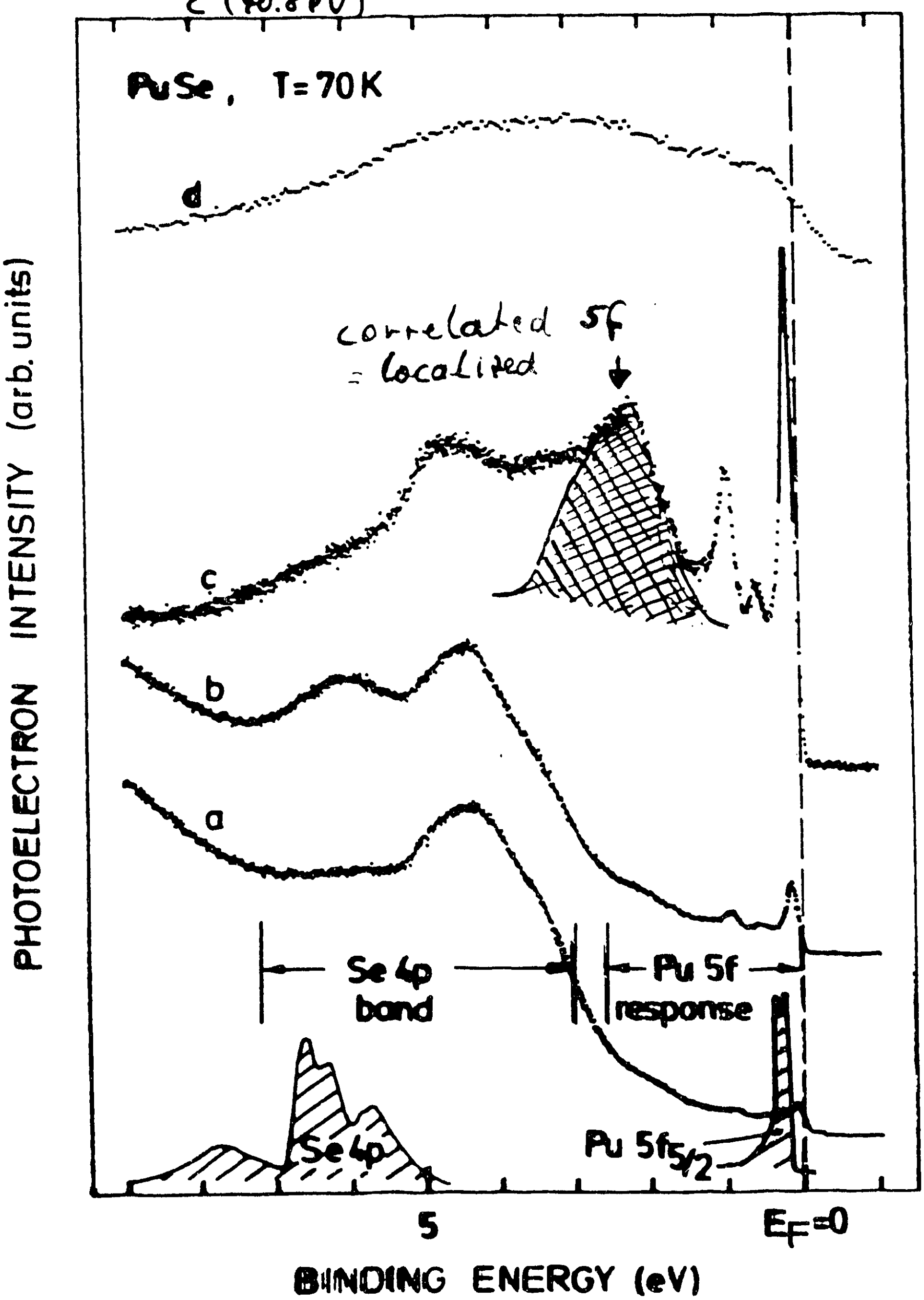

J.R. Naegele, F. Schiavo, J.-C. Spirlet
Institute for Transuranium Elements,

to be published

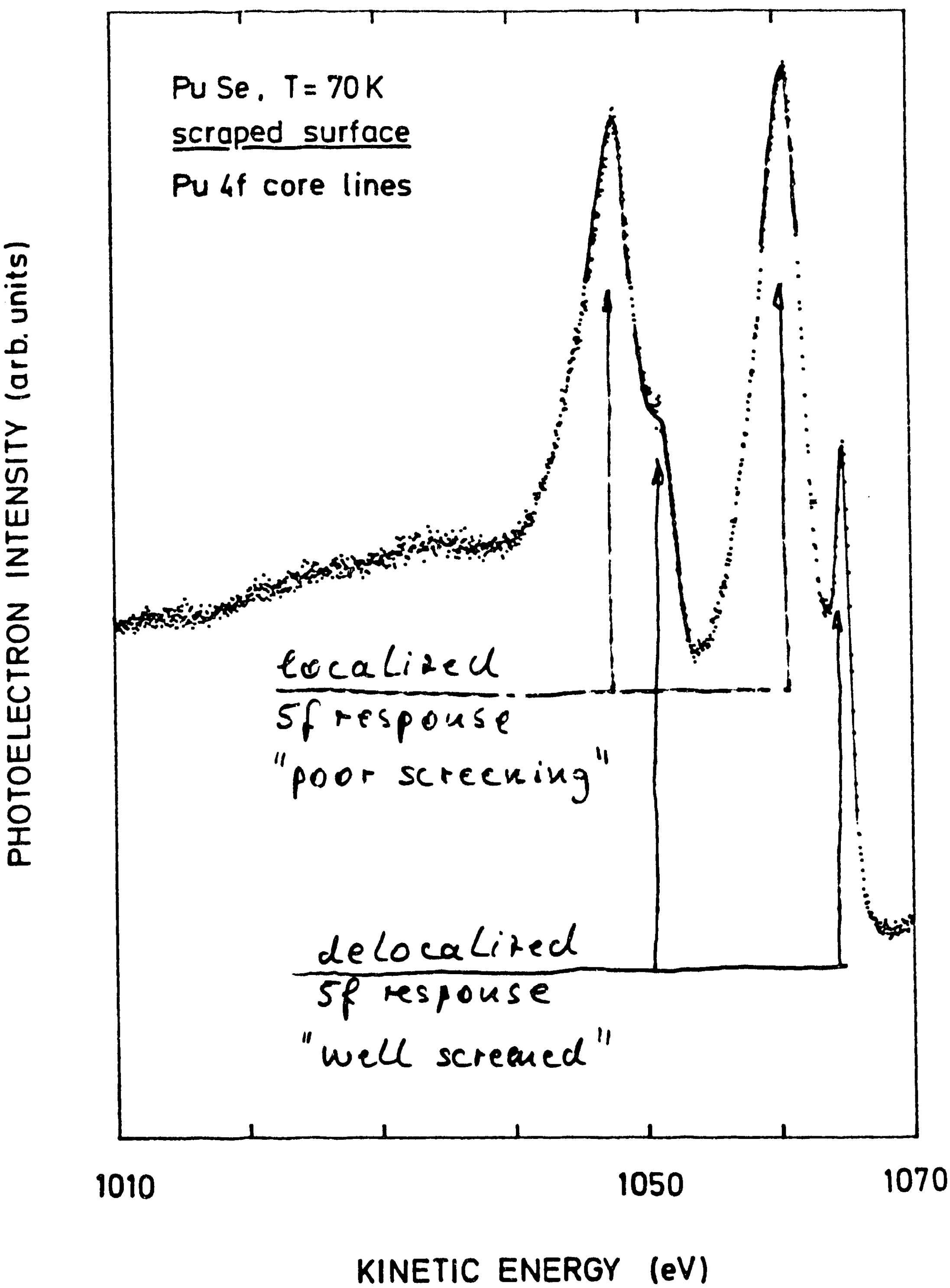

J.R. Naegele, F. Schiavo, J.-C. Spirlet
Institute for Transuranium Elements
to be published

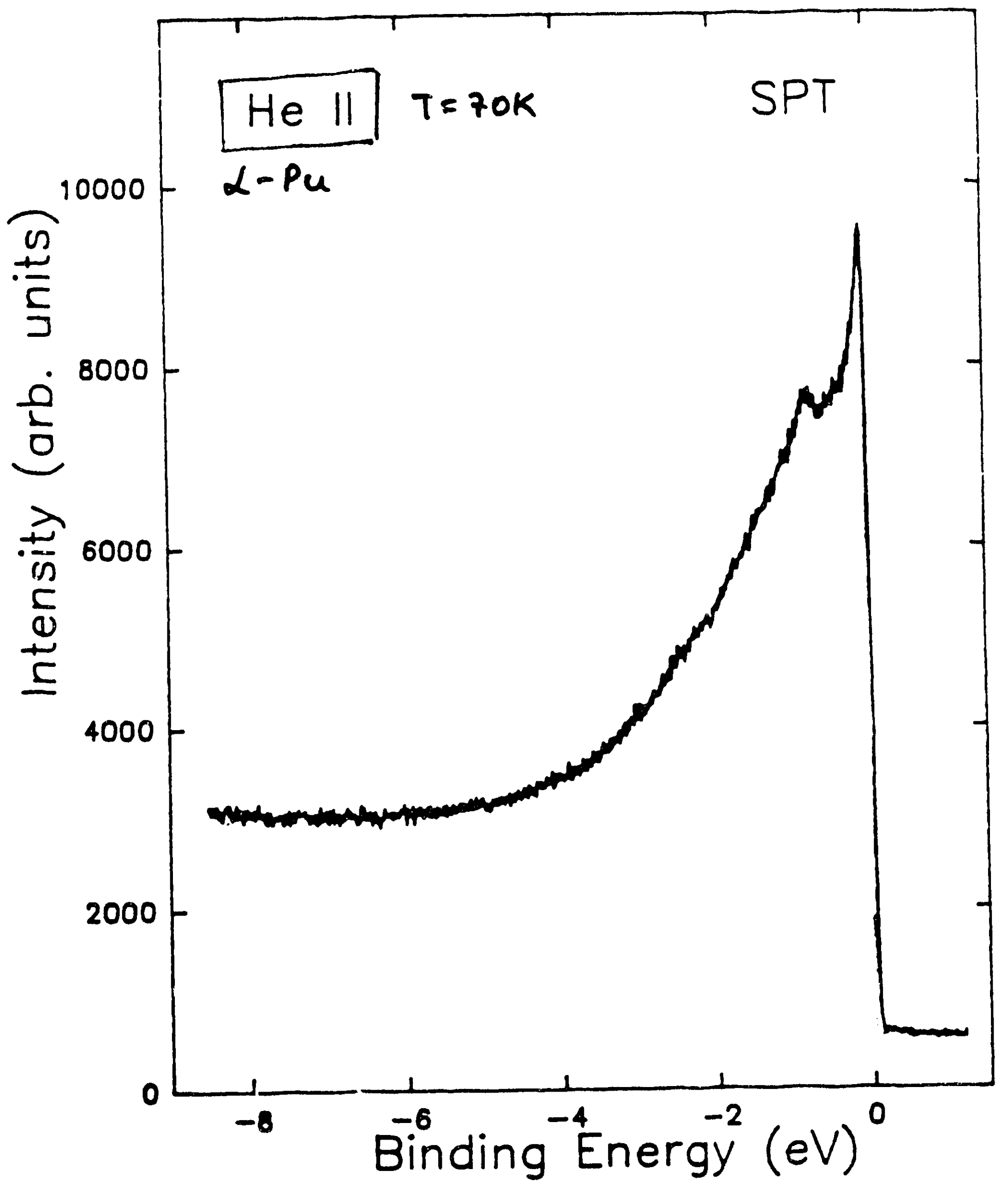
He II
T=70K
SPT
α-Pu
Intensity (arb. units)
10000
8000
6000
4000
2000
0
-8
-6
-4
-2
0
Binding Energy (eV)

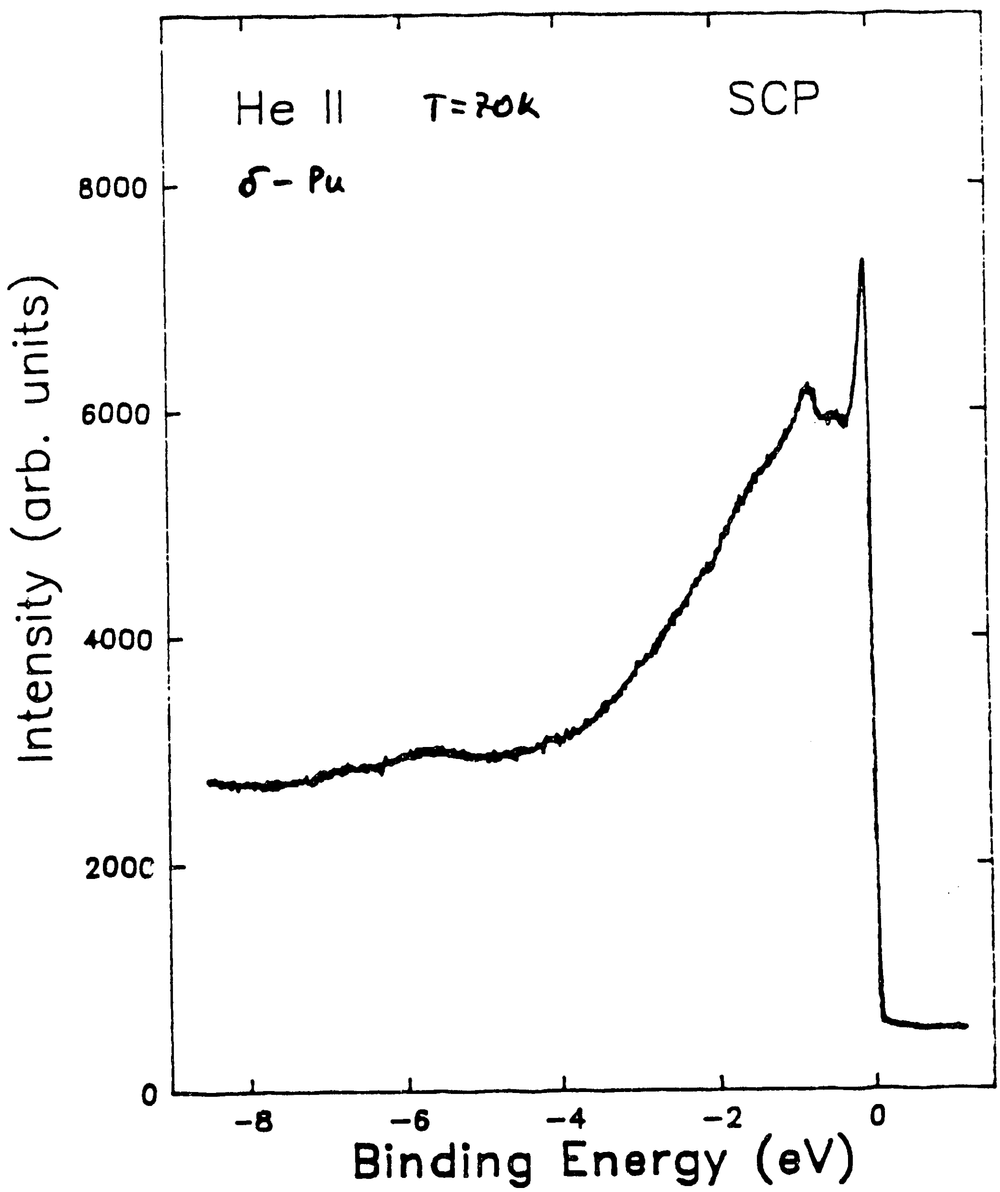
He II
T=70K
SCP
δ - Pu
Intensity (arb. units)
8000
6000
4000
2000
0
-8
-6
-4
-2
0
Binding Energy (eV)

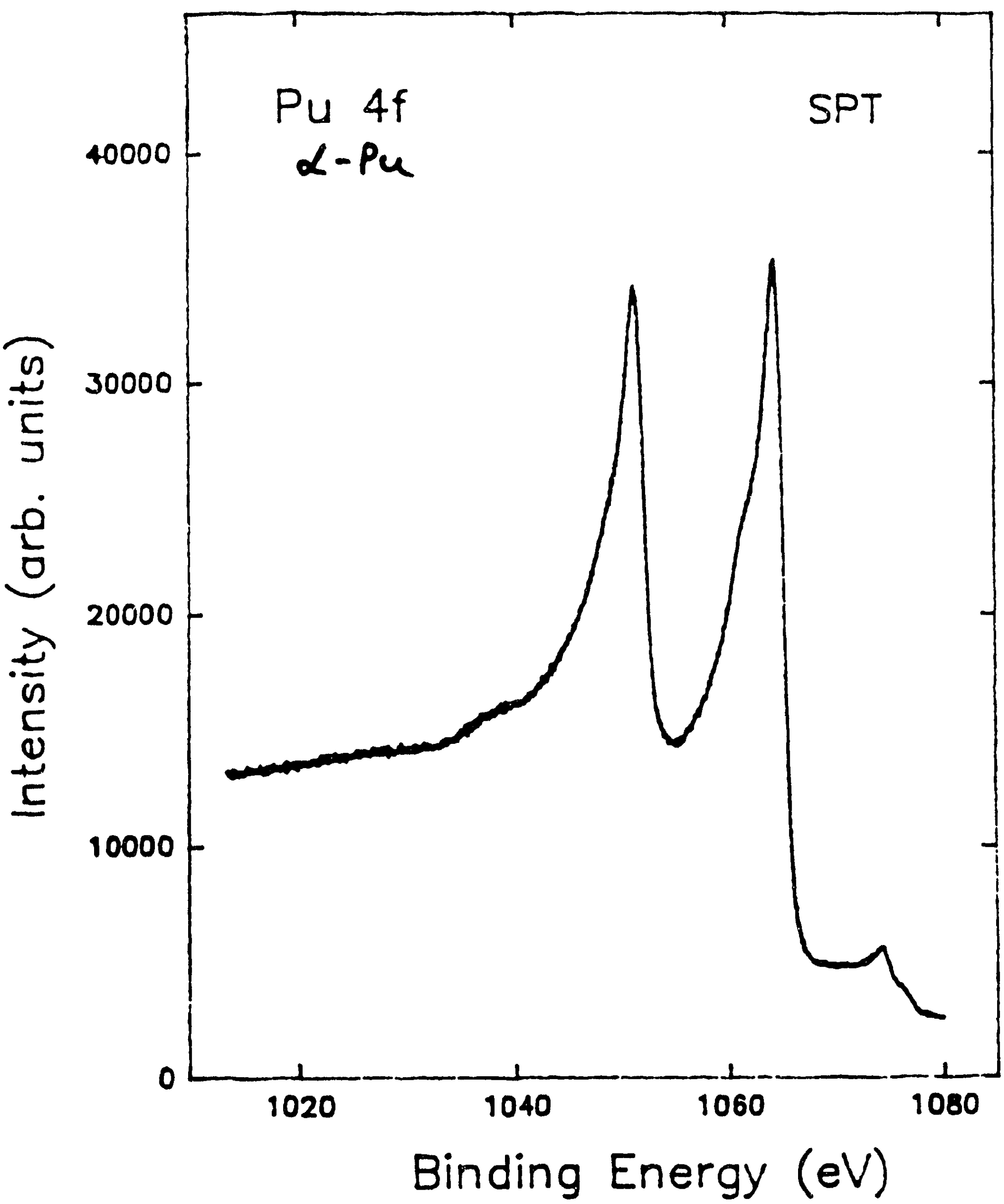
Pu 4f
α-Pu
SPT
40000
30000
20000
10000
0
Intensity (arb. units)
1020
1040
1060
1080
Binding Energy (eV)

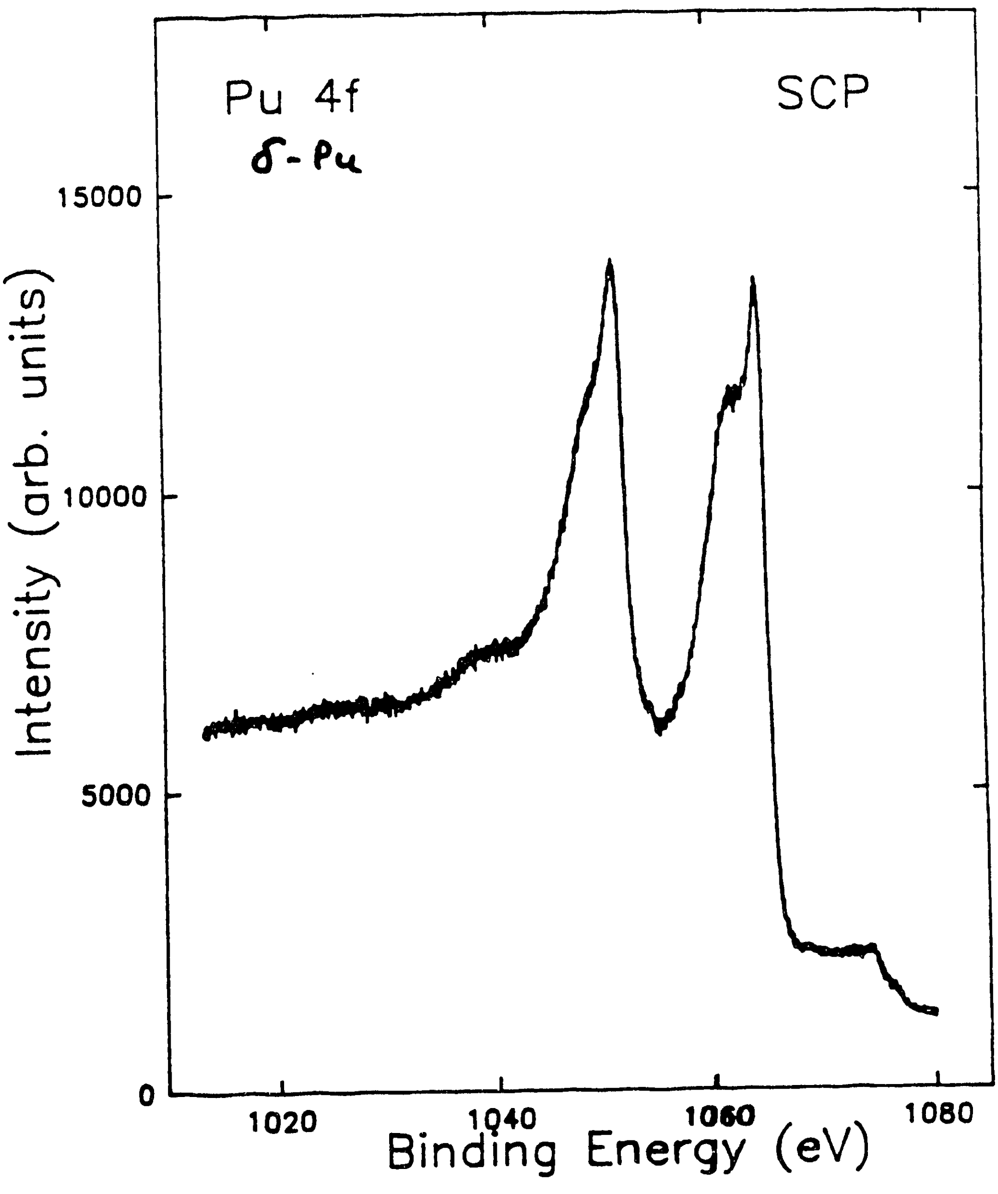

Pu 4f
δ-Pu
SCP
15000
10000
5000
0
Intensity (arb. units)
1020
1040
1060
1080
Binding Energy (eV)

$Am_{1-x} Pu_x$

XPS (Al K_α : 1486.6 eV) An 4f levels

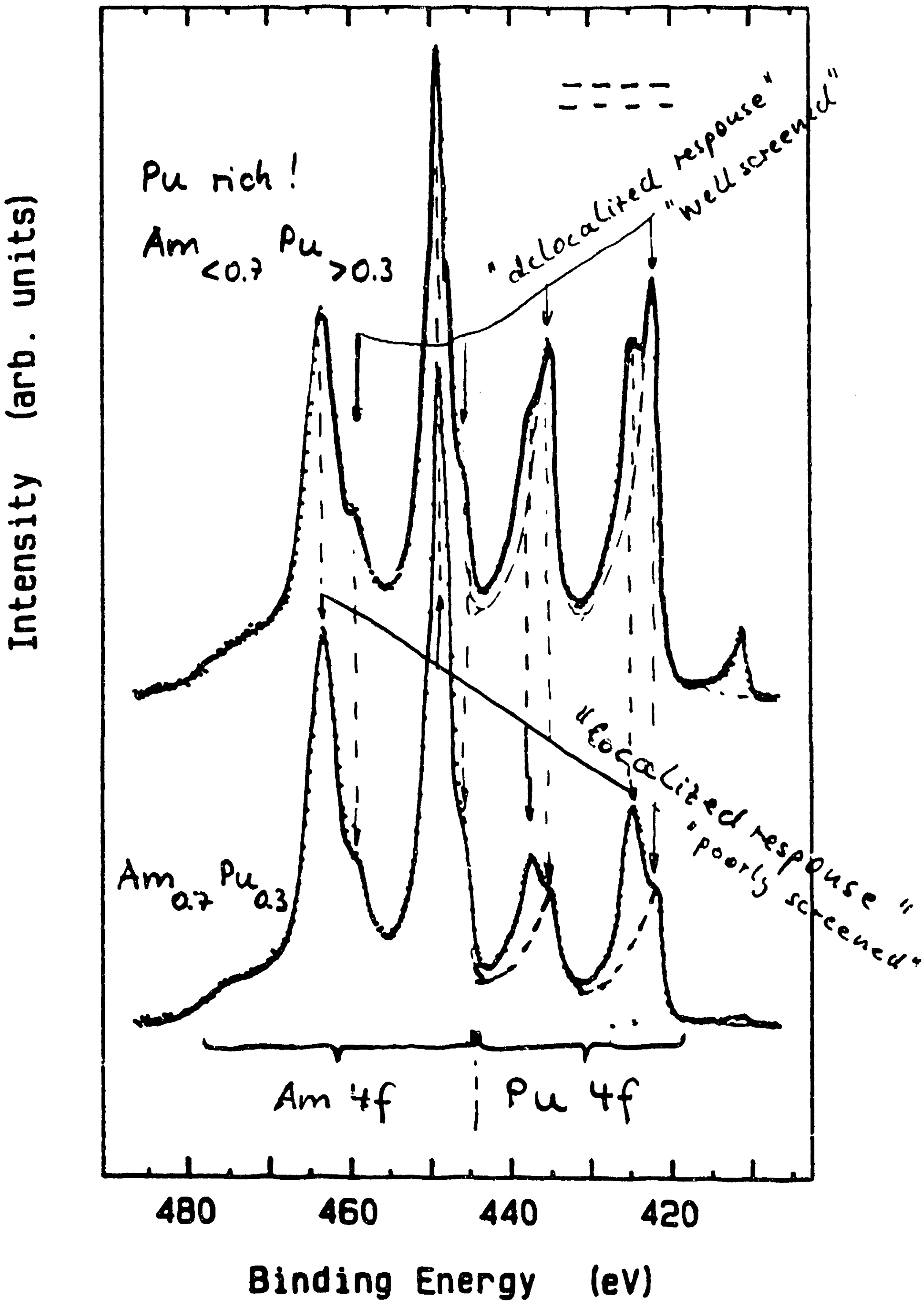

Electronic Structure and Correlated-Electron Theory for Actinide Materials

Bernard R. Cooper
Department of Physics
West Virginia University

The central feature of the electronic and related solid-state behavior for actinide materials is the f-electron localization that occurs as the f transition shell is filled. From the point of view of theory this translates into the development of correlation (fluctuation) effects in the electronic behavior that cannot be captured by the time-averaged potentials used in band theory. We have treated several aspects of this question in recent years and will discuss two of these: (1) the relevance of surface electronic structure behavior as a probe of the development of correlation effects as the f electrons begin to have some localized character, (2) the effects of band-f hybridization and coulumb exchange in transferring f spectral density into (or out of) the band sea thereby causing moment washout and driving the approach to the heavy fermion state. Both these effects can be probed experimentally by photoemission.

ELECTRONIC STRUCTURE AND CORRELATED-ELECTRON THEORY FOR ACTINIDE MATERIALS

Bernard R. Cooper
Department of Physics, West Virginia University

The central feature of the electronic and related solid-state behavior for actinide materials is the *f*-electron localization that occurs as the *f* transition shell is filled. This translates into the development of correlation (interconfigurational fluctuation) effects in the electronic behavior that cannot be captured by the time-averaged potentials used in band theory. We have treated several aspects of this question in recent years and will discuss two of these.

(1) The relevance of surface electronic structure behavior as a probe of the development of correlation effects as the *f* electrons begin to have some localized character.

(2) The effects of band-*f* hybridization and coulomb exchange in transferring *f* spectral density into (or out of) the band sea thereby causing moment washout and driving the approach to the heavy fermion state.

Both these effects can be probed experimentally, and I will discuss the ongoing relationship between theory and experiment in these developing areas of research.

As increase atomic number, Coulomb correlation energy (effects on energy of instantaneous rather than time-averaged motion of electrons) becomes large relative to the f-electron bandwidth, and the itinerant (band) description is no longer valid for the f electrons.

As the atomic number increases, the added $5f$ electrons are not able to screen completely the increased nuclear charge, and therefore the occupation number of the $5f$ level increases more rapidly than the increase in atomic number, i.e., nonlinear effect → threshold for localization.

Instead the localized description of the ionic $5f$ electrons (i.e., large spin-orbit and Hund's rule coupling of L, S (maximized) and J (minimized) [really intermediate coupling closer to L-S than to j-j] interacting with their environment through the crystalline electric field and the exchange interactions via the conduction electrons) becomes more appropriate. The increased importance of correlation effects favors magnetic ordering as opposed to solid-state bonding.

J. L. Smith & Z. Fisk, 1982

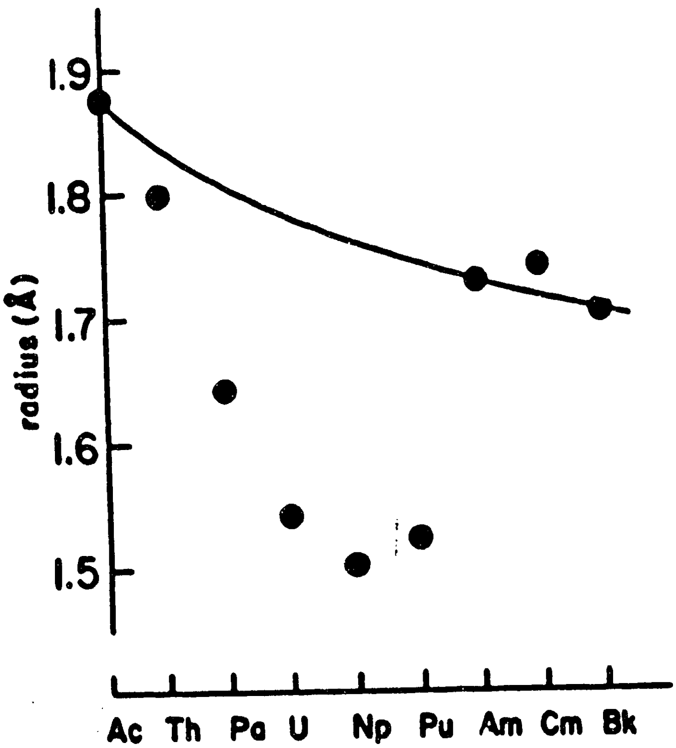

The known radii of the atomic volumes of the actinide atoms for the room-temperature phases of the pure metals. The line shows the assumed actinide contraction (similar to the lanthanides) based upon the radii of Ac, Am, Cm, and Bk. It is the tri-valent sign that would occur without f-electron bonding. Curium above the line is the same as for gadolinium in the lanthanides, where the tri-valent line is well defined.

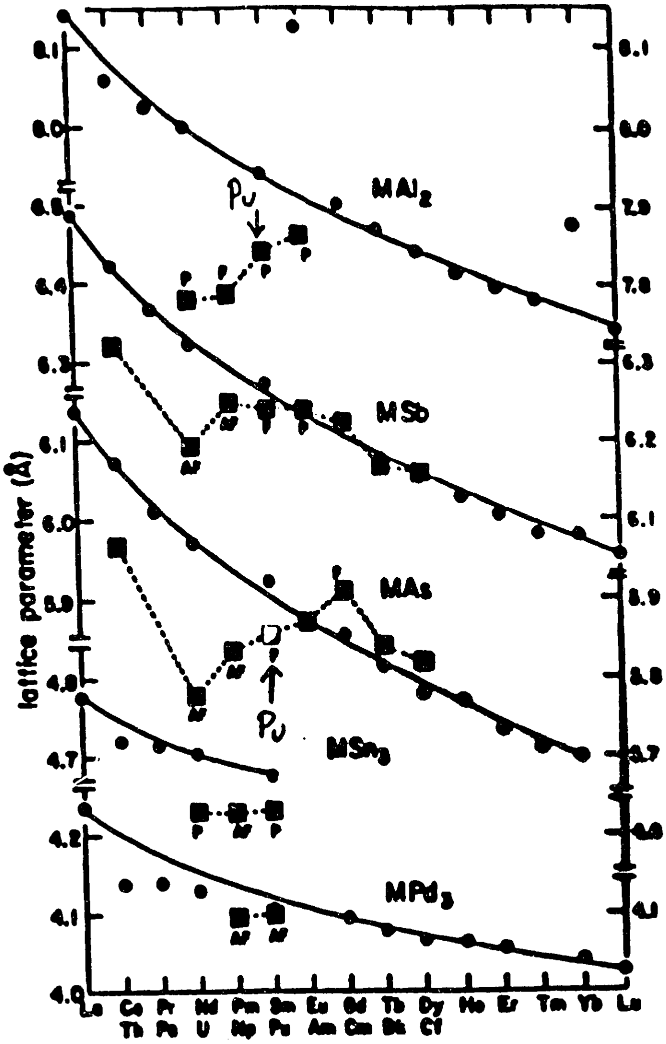

The lattice parameters for five families of lanthanide (circles) and actinide (squares) compounds. As in the pure elements, the presence of the f-band causes a size depression below the smooth line connecting the lanthanide compounds, which is the same line (unlike the pure elements) as for the actinide compounds. Magnetic behavior is indicated by P-paramagnetic, AF-antiferromagnetic, and F-ferromagnetic.

Will discuss two regimes of behavior as go from fully itinerant toward somewhat localized f-electron behavior.

(1) Light actinide elements (uranium, neptunium, plutonium, americium)---increased localization on going from bulk to surface behavior for *f*-electrons → beginnings of importance of correlation effects, possible increased importance of polarization effects (possible magnetic ordering coordinated with surface reconstruction) compared to bonding effects.

(2) Development of significant correlation effects as *f*-electrons localize further and hybridization of *f*-electrons with non-*f* band electrons becomes dominant effect on *f* state broadening as compared to direct *f*-*f* overlap---approach to the heavy fermion state, associated magnetic effects, importance of orbital aspects of coulomb exchange between *f* electrons and band electrons on top of hybridization.

CHANGE IN f-ELECTRON BEHAVIOR OF LIGHT ACTINIDES BETWEEN BULK AND SURFACE

Theoretical electronic (band) structure results (O.Eriksson, Y.G. Hao, B.R. Cooper) on changes in surface relative to bulk for Pu compared to U.

plus

L. Cox experimental results on α-Pu photoemission difference between 85° (almost normal) and 15° to surface (Mg Kα x-rays, 1253.6 eV).

Raise interesting questions:
(1) of possible structure and magnetic ordering changes at surface compared to bulk for Pu,
(2) of surface for U behaving in more Pu-like way than bulk of Pu, i.e. possibly having complicated reconstructions,
(3) of how the "conflict" between greater density/band broadening for increased cohesion (bonding) versus less density/band narrowing (localization, minimizing adverse effects of occupation of antibonding states and increasing gains of polarization/magnetic ordering energy) develops as $5f$ occupation increases---does surface of uranium contract relative to bulk to increase bonding while that of plutonium expands to accommodate occupation of antibonding states, but decrease anti-bonding effects by developing magnetic ordering??

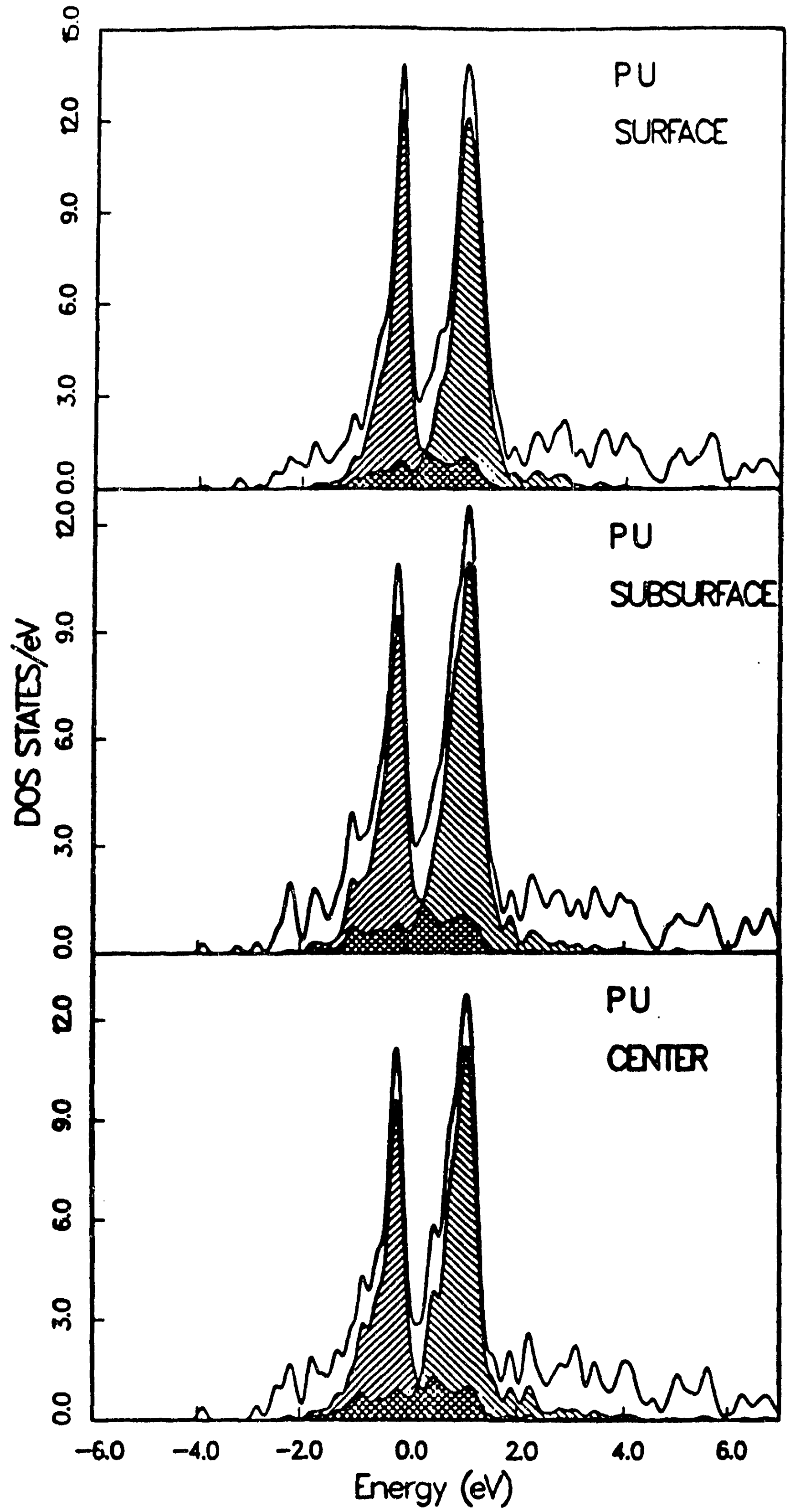
PU
SURFACE
PU
SUBSURFACE
PU
CENTER
DOS STATES/eV
Energy (eV)
0.0
3.0
6.0
9.0
12.0
15.0
-6.0
-4.0
-2.0
0.0
2.0
4.0
6.0

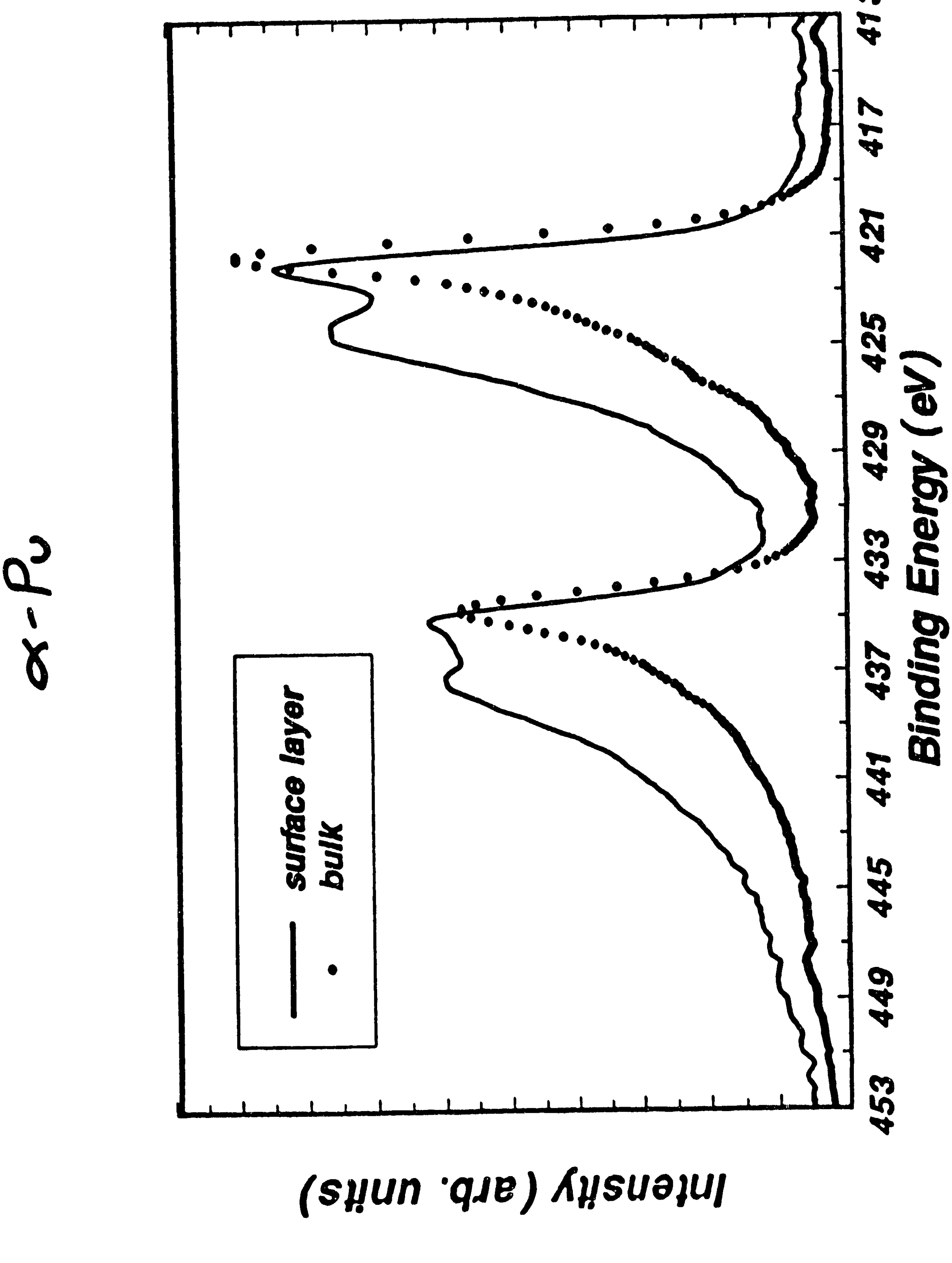
α-Pu
surface layer
bulk
453
449
445
441
437
433
429
425
421
417
413
Binding Energy (eV)
Intensity (arb. units)

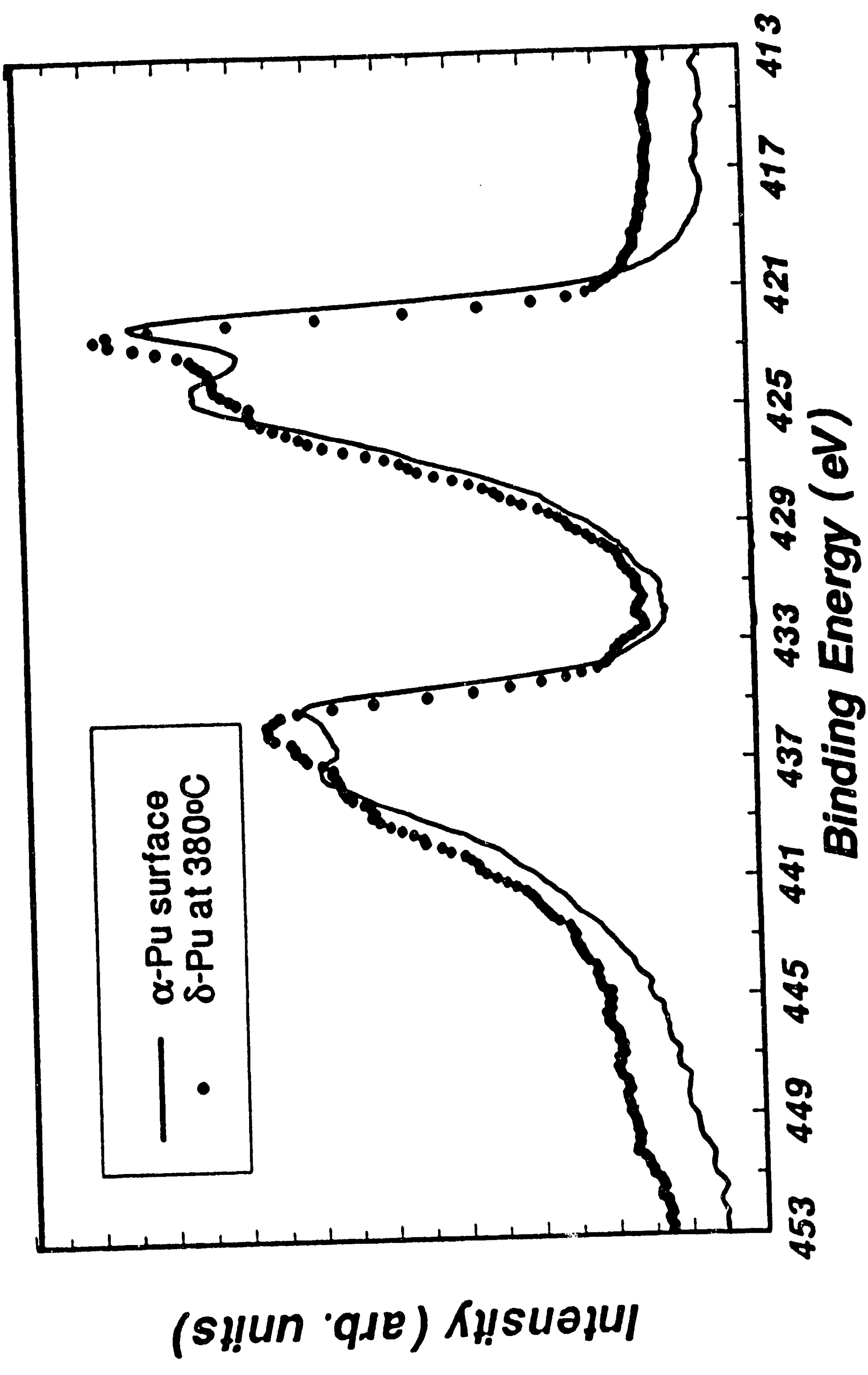
α-Pu surface
δ-Pu at 380oC
Binding Energy (eV)
Intensity (arb. units)
453
449
445
441
437
433
429
425
421
417
413

Table 1

Theoretical lattice constants of the Pu monolayer, and bulk Pu* (a.u.).

	paramagnetic	spin polarized	spin and orbital polarized
bulk (fcc)	7.60	-	-
monolayer (square)	7.93 (4.3% expansion over bulk)	8.10	8.13 (7.0% expansion)

* For the experimental α density the lattice constant of fcc Pu is ~ 8.1 a.u. and for the δ density it is ~ 8.8 a.u.

Table 3

Magnetic moments (μ_B) $m(\ell)$, $\ell = s, p, d$, and f, from spin polarized scalar-relativistic Pu at two densities, a=8.1 and a=7.6. S denotes the surface-layer, S-1 the subsurface-layer and C the center- (bulk) layer.

a=8.1 (experimental α density)

	m(s)	m(p)	m(d)	m(f)
C	0.011	-0.006	0.186	4.434
S-1	-0.023	0.002	-0.228	-4.529
S	0.022	0.001	0.244	4.921

a=7.6

	m(s)	m(p)	m(d)	m(f)
C	0.004	-0.010	0.174	3.539
S-1	-0.013	0.001	-0.185	-3.646
S	0.020	0.001	0.225	4.357

slab is not thick enough. Bulk moment should be zero.

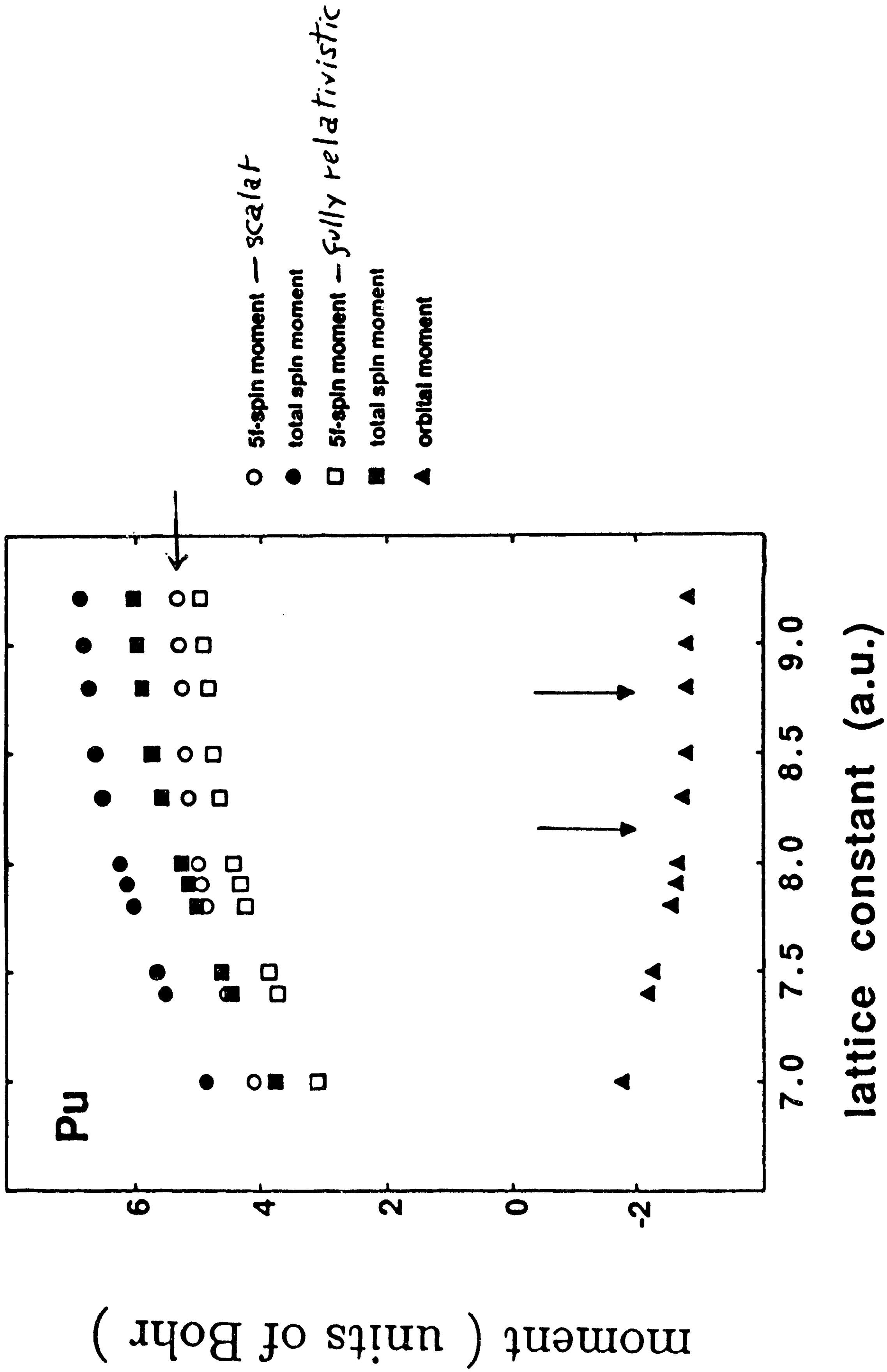

Pu
5f-spin moment — scalar
total spin moment
5f-spin moment — fully relativistic
total spin moment
orbital moment
lattice constant (a.u.)
moment (units of Bohr)
7.0
7.5
8.0
8.5
9.0
6
4
2
0
-2

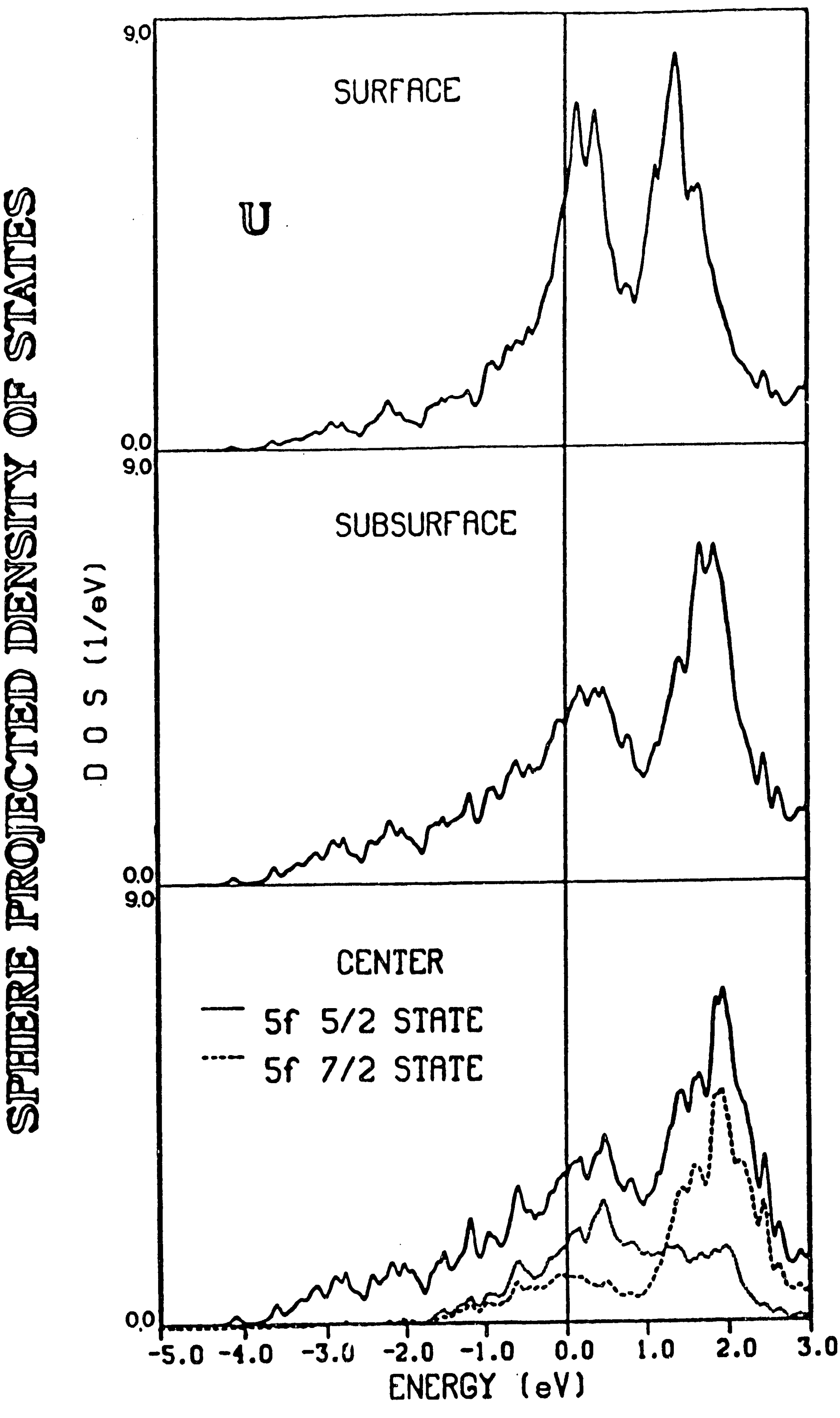

SPHERE PROJECTED DENSITY OF STATES
D O S (1/eV)
U
SURFACE
SUBSURFACE
CENTER
5f 5/2 STATE
5f 7/2 STATE
9.0
0.0
9.0
0.0
9.0
0.0
-5.0
-4.0
-3.0
-2.0
-1.0
0.0
1.0
2.0
3.0
ENERGY (eV)

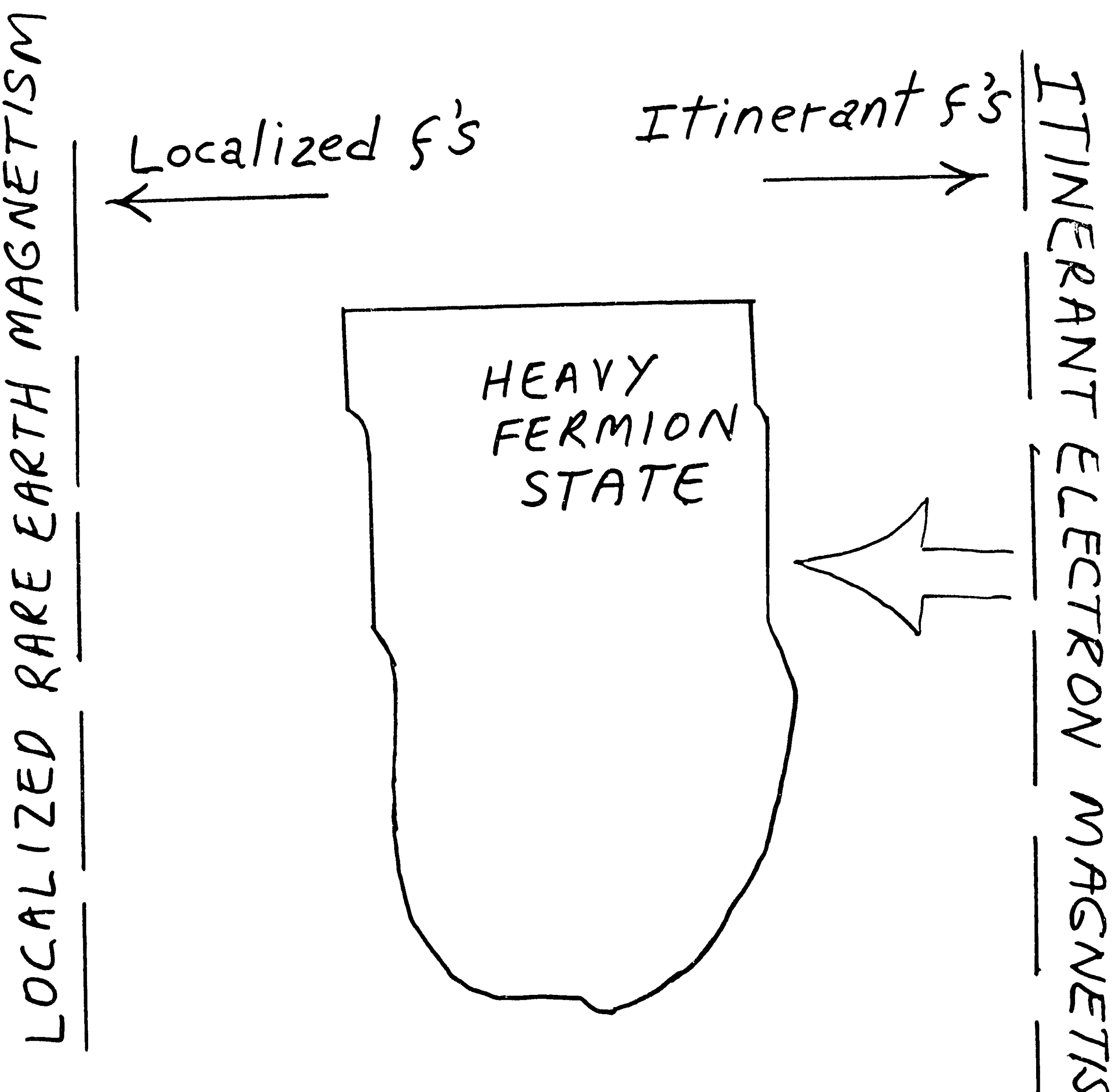

LOCALIZED RARE EARTH MAGNETISM
Localized f's
Itinerant f's
ITINERANT ELECTRON MAGNETISM
HEAVY FERMION STATE

Heavy Fermion Antiferromagnets

(1) Reduced Néel Temperature
(2) Reduced Ordered Moment
(3) Sensitivity of T_N to Chemical Composition

We have developed theory and ab initio computational technique allowing us to use the prediction of reduced ordered moment (and reduced T_N) behavior as a diagnostic tool defining the approach to (or departure from) the correlated- electron heavy-fermion state with changing chemical environment in an isostructural series of compounds.

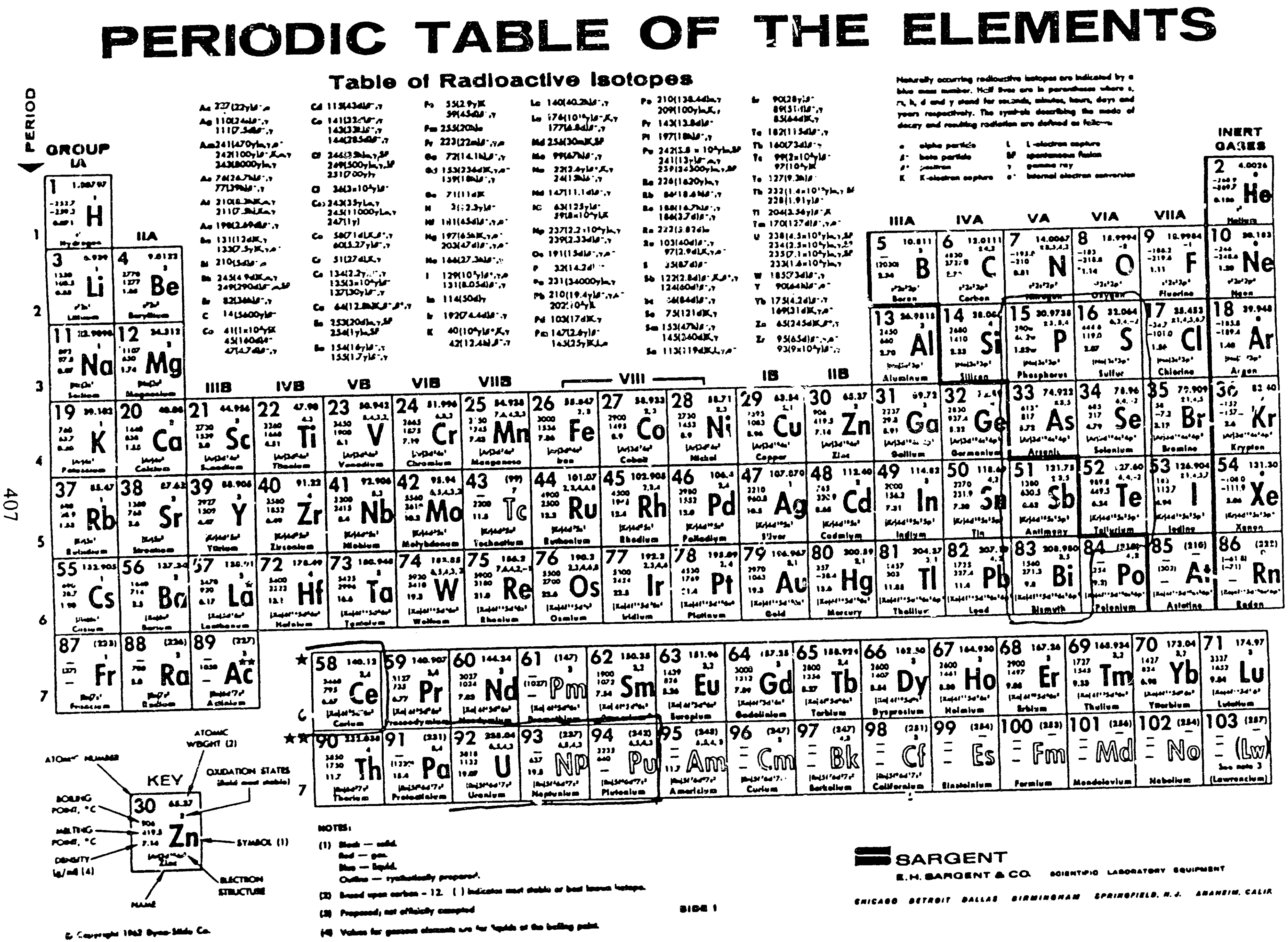
PERIODIC TABLE OF THE ELEMENTS
Table of Radioactive Isotopes
GROUP IA
IIA
IIIB IVB VB VIB VIIB VIII IB IIB
IIIA IVA VA VIA VIIA
INERT GASES
PERIOD
1 H Hydrogen
2 He Helium
3 Li Lithium
4 Be Beryllium
5 B Boron
6 C Carbon
7 N Nitrogen
8 O Oxygen
9 F Fluorine
10 Ne Neon
11 Na Sodium
12 Mg Magnesium
13 Al Aluminum
14 Si Silicon
15 P Phosphorus
16 S Sulfur
17 Cl Chlorine
18 Ar Argon
19 K Potassium
20 Ca Calcium
21 Sc Scandium
22 Ti Titanium
23 V Vanadium
24 Cr Chromium
25 Mn Manganese
26 Fe Iron
27 Co Cobalt
28 Ni Nickel
29 Cu Copper
30 Zn Zinc
31 Ga Gallium
32 Ge Germanium
33 As Arsenic
34 Se Selenium
35 Br Bromine
36 Kr Krypton
37 Rb Rubidium
38 Sr Strontium
39 Y Yttrium
40 Zr Zirconium
41 Nb Niobium
42 Mo Molybdenum
43 Tc Technetium
44 Ru Ruthenium
45 Rh Rhodium
46 Pd Palladium
47 Ag Silver
48 Cd Cadmium
49 In Indium
50 Sn Tin
51 Sb Antimony
52 Te Tellurium
53 I Iodine
54 Xe Xenon
55 Cs Cesium
56 Ba Barium
57 La Lanthanum
72 Hf Hafnium
73 Ta Tantalum
74 W Wolfram
75 Re Rhenium
76 Os Osmium
77 Ir Iridium
78 Pt Platinum
79 Au Gold
80 Hg Mercury
81 Tl Thallium
82 Pb Lead
83 Bi Bismuth
84 Po Polonium
85 At Astatine
86 Rn Radon
87 Fr Francium
88 Ra Radium
89 Ac Actinium
58 Ce Cerium
59 Pr Praseodymium
60 Nd Neodymium
61 Pm Promethium
62 Sm Samarium
63 Eu Europium
64 Gd Gadolinium
65 Tb Terbium
66 Dy Dysprosium
67 Ho Holmium
68 Er Erbium
69 Tm Thulium
70 Yb Ytterbium
71 Lu Lutetium
90 Th Thorium
91 Pa Protactinium
92 U Uranium
93 Np Neptunium
94 Pu Plutonium
95 Am Americium
96 Cm Curium
97 Bk Berkelium
98 Cf Californium
99 Es Einsteinium
100 Fm Fermium
101 Md Mendelevium
102 No Nobelium
103 (Lw) (Lawrencium)
KEY
ATOMIC NUMBER
ATOMIC WEIGHT (2)
OXIDATION STATES (Bold most stable)
BOILING POINT, °C
MELTING POINT, °C
DENSITY (g/ml) (4)
SYMBOL (1)
ELECTRON STRUCTURE
NAME
NOTES:
(1) Black — solid. Red — gas. Blue — liquid. Outline — synthetically prepared.
(2) Based upon carbon - 12. ( ) indicates most stable or best known isotope.
(3) Proposed; not officially accepted
(4) Values for gaseous elements are for liquids at the boiling point.
SIDE 1
SARGENT
E. H. SARGENT & CO. SCIENTIFIC LABORATORY EQUIPMENT
CHICAGO DETROIT DALLAS BIRMINGHAM SPRINGFIELD, N. J. ANAHEIM, CALIF.
© Copyright 1962 Dyna-Slide Co.

Going from uranium to cerium to heavy rare earth, the peak positions of the f-wave functions decrease while the peak values of the f-wave functions increase. This indicates that the f states are becoming more and more localized

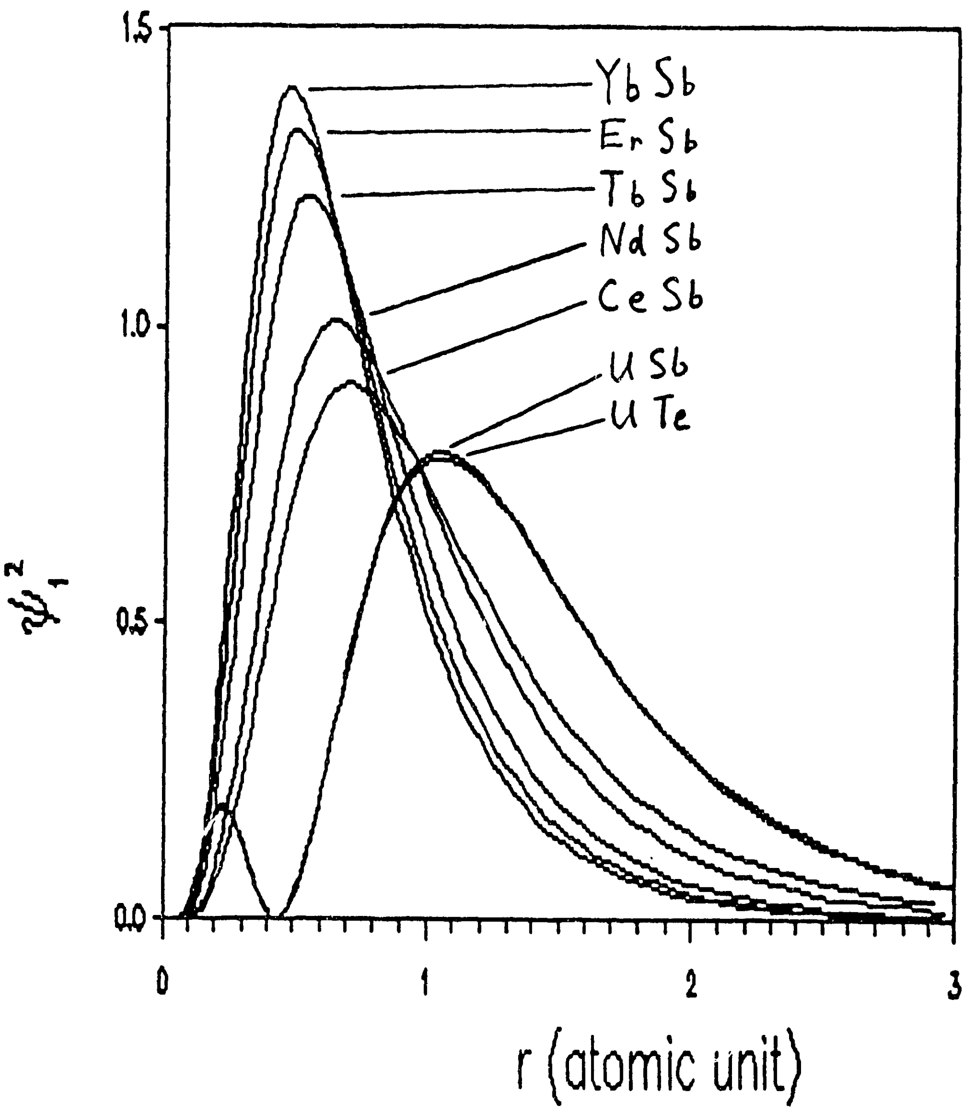

Reason for f states being more delocalized in uranium than in rare earths: the existence of the 4f shell in uranium pushes its 5f states outward, since ϕ_{5f} and ϕ_{4f} must be orthogonalized.(Having the same angular part Y_{3m}, their radius parts must be orthogonalized.)

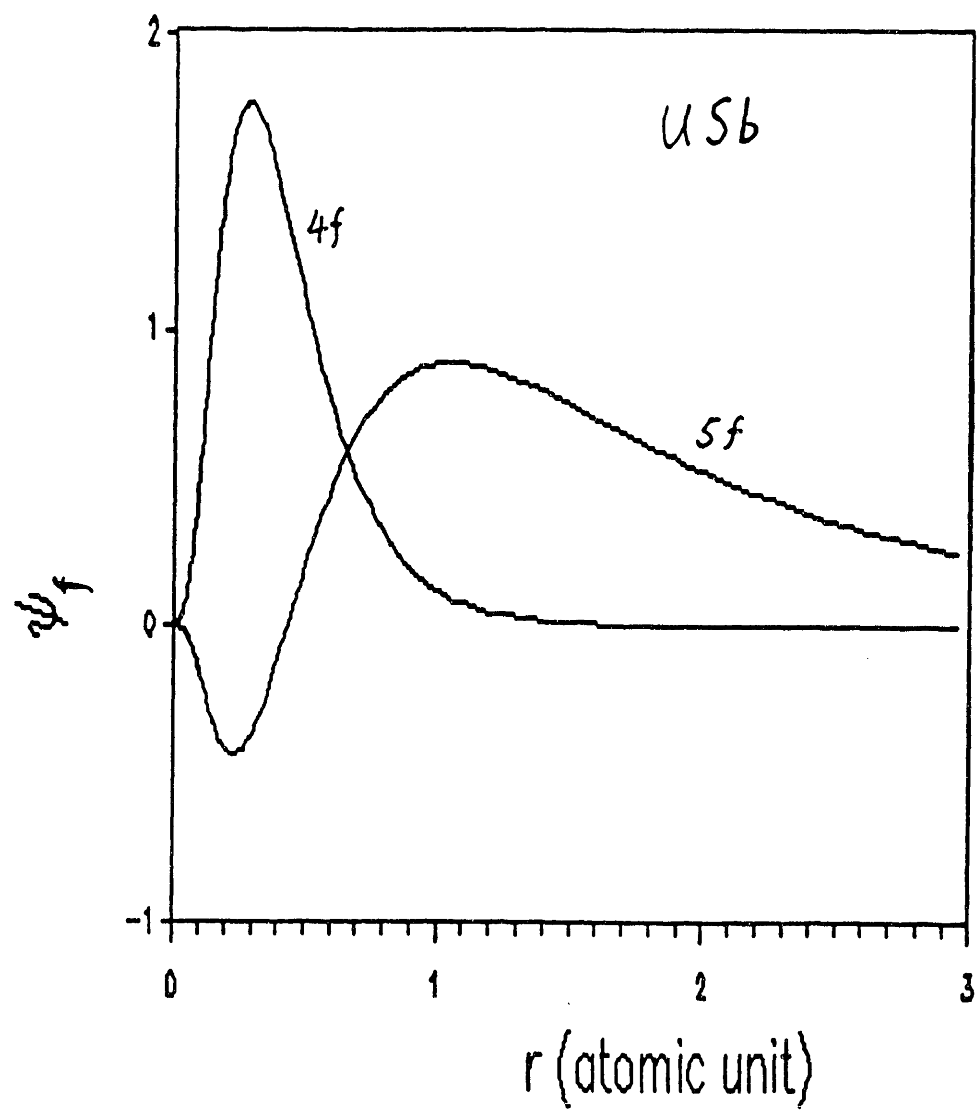

Starting from the true Hamiltonian:

$$H = \sum_i \nabla_i^2 + V_0(r_i) + \frac{1}{2}\sum_{i\neq j}\frac{1}{r_{ij}}$$

$V_0(r_i)$: potential from nuclei and core electrons

$1/r_{ij}$: Coulomb interaction involving all valence and f- electrons

Second quantization + Hartree-fock approximation

$$\downarrow$$

$$\begin{aligned}
H &= H_0 + H_1 \\
H_0 &= \sum_k \epsilon_k b_k^+ b_k + \sum_{Rm} \epsilon_m c_m^+(R) c_m(R) + \frac{U}{2}\sum_{\substack{R \\ m\neq m'}} n_m(R) n_{m'}(R) \\
H_1 &= \sum_{kmR} [V_{km} e^{-i\mathbf{k}\cdot\mathbf{R}} b_k^+ c_m(R) + \ h.c.] \ + \\
&\quad \sum_{kk'}\sum_{nn',R} J_{nn'}(\mathbf{k},\mathbf{k}') e^{-i(\mathbf{k}-\mathbf{k}')\cdot\mathbf{R}} b_k^+ c_n^+(R) b_{k'} c_{n'}(R)
\end{aligned}$$

V_{km}: band-f hybridization

$J_{nn'}(\mathbf{k},\mathbf{k}')$: band-$f$ exchange

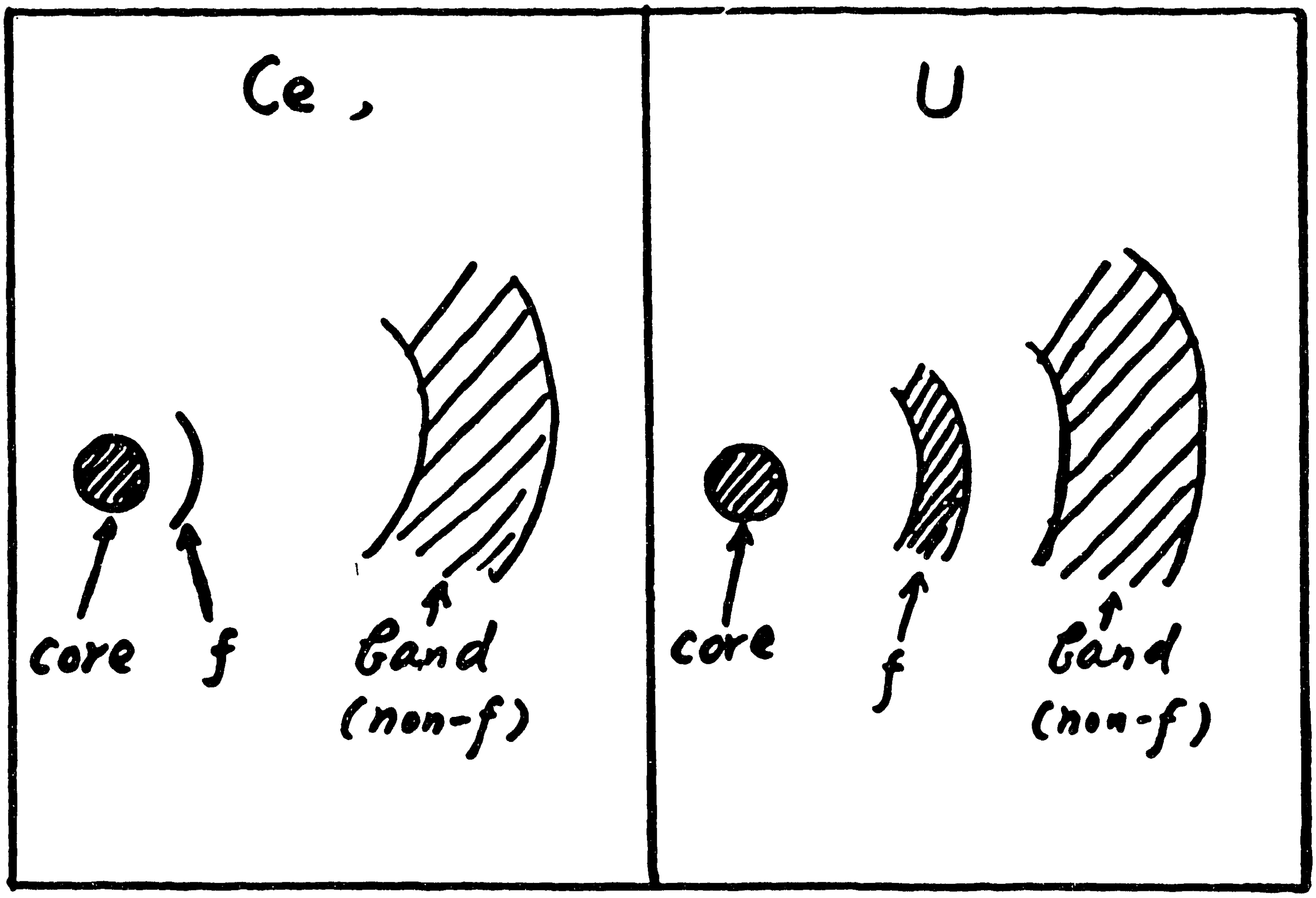
Ce ,
core
f
band
(non-f)
U
core
f
band
(non-f)

- In our present treatment, hybridization(mixing of f-electrons with non-f band electrons) is treated differently for cerium and neodymium(slightly delocalized f-electrons) than for uranium(more delocalized f-electrons). Hybridization is negligible for heavy rare earths.
- Coulomb exchange is treated in the same way for the rare earths and uranium.
- The two-ion "exchange" and the magnetic ordering are treated the same way for rare earths and uranium — behavior is projected onto a "site-centered" ionic basis, and thereby effects of hybridization giving interconfigurational fluctuations(correlations, not time averaged) are included.
- For cerium and uranium materials we have also done calculations using spin and orbitally polarized band theory (only effects of hybridization giving correlation included are time averaged – LDA).

TECHNIQUE FOR RARE EARTHS

(1) Evaluate the hybridization from the starting point that the f-states are viewed as resonance states confined to the core.

(a) Perform a warped linear-muffin-tin-orbital (LMTO) band structure calculation. The f states are treated as local states in such calculation.

(b) Extract a characteristic quantity, the resonance width, from the band structure calculation. Use this quantity to calculate the hybridization V_k between f-states and non-f band states.

$$\text{resonance width } \frac{\Gamma}{2} = \frac{|\psi_f(s)|^2}{|\kappa h_3(\kappa s)|^2}$$

$$\text{hybridization potential } \nu(\kappa) = -[\frac{\Gamma}{2\kappa\Omega}]^{1/2}$$

$$\text{hybridization } V_{km} = \nu(\kappa)(\Omega)^{1/2}[T_m(k)]^*$$

where ψ_f is the f-state wave function, h_3 the Hankel function, s the muffin-tin sphere radius, κ^2 the fermi energy, Ω the unit cell volume, and $T_m(k)$ is related to KKR structure function.

(2) Calculate the exchange interaction between the f-states and non-f band states. The LMTO scheme expands a large number of band wave functions in terms of a limited number of muffin-tin orbitals. Therefore $J_{nn'}(\mathbf{k}, \mathbf{k}')$ can be expanded in terms of the B tensor given below which is also limited in the number of its elements:

$$J_{nn'}(\mathbf{k}, \mathbf{k}') = \sum_{tt'=1,2} \sum_{\substack{lms \\ l'm's'}} X^{t*}_{lms}(\mathbf{k}) \, B_{n\ \ n'}^{lmst\ l'm's't'} \, X^{t'}_{l'm's'}(\mathbf{k}')$$

$$X^1_{lms}(\mathbf{k}) = a^k_{lms}$$
$$X^2_{lms}(\mathbf{k}) = \sum_{l'm's'} a^k_{l'm's'} S^k_{l'm's'\ lms}$$

$$B_{n\ \ n'}^{lmst\ l'm's't'} = \langle \chi^{t*}_{lms}(r_1) \psi^*_n(r_2) \mid \frac{1}{r_{12}} \mid \psi_n(r_1) \chi^{t'}_{l'm's'}(r_2) \rangle$$

where a^k_{lms} and $S^k_{l'm's'\ lms}$ are the band eigenvectors and KKR structure functions. The tensor $B_{n\ \ n'}^{lmst\ l'm's't'}$ is the integral between the f-wave function $\psi_n(r)$ and various muffin-tin orbitals $\chi^t_{lms}(r)$, where k, l, m, s stand for momentum, angular momentum, magnetic quantum number and spin respectively, and t is the type of muffin-tin orbital.

HYBRIDIZATION TECHNIQUE FOR URANIUM

Evaluate the hybridization from the starting point that the f-states are viewed as bands.

Start with the Bloch sum of the f-states:

$$\psi_{mk}(r) = \frac{1}{N^{1/2}} \sum_{R} exp(ik \cdot R)\psi_m(r - R)$$

The Hamiltonian matrix is constructed from $\psi_{mk}(r)$ and the Bloch sum of non-f states $\phi_{nk}(r)$:

$$H = \begin{pmatrix} H_f & V \\ V^* & H_c \end{pmatrix}$$

where

$$(H_f)_{mm'} = <\psi_{mk}(r) \mid H \mid \psi_{m'k}(r)>$$

$$(H_c)_{nn'} = <\phi_{nk}(r) \mid H \mid \phi_{n'k}(r)>$$

$$(V)_{mn} = <\psi_{mk}(r) \mid H \mid \phi_{nk}(r)>$$

The non-f part of the Hamiltonian H_c is singled out and diagonalized to give the nonhybridized non-f band states $\Phi_k^n(r)$,

$$\Phi_k^n(r) = \sum_{n'} \alpha_{nn'}^k \phi_{n'k}(r)$$

where $\alpha_{nn'}^k$ is the eigenvector and n the band index. The hybridization matrix elements are obtained by projecting V_{mn} onto $\Phi_k(r)$:

$$V_{km}^n = <\psi_{mk}(r) \mid H \mid \Phi_k^n(r)> = \sum_{n'} \alpha_{nn'}^k V_{mn'}$$

EXPRESSION FOR TWO-ION INTERACTION:

$$H(1,2) = -\sum_{n_1 n_1'} \sum_{n_2 n_2'} E_{n_1\ n_1'}^{n_2\ n_2'}(\mathbf{R_2} - \mathbf{R_1}) \times c_{n_2}^{+}(2) c_{n_2'}(2) c_{n_1}^{+}(1) c_{n_1'}(1)$$

$E_{n_1\ n_1'}^{n_2\ n_2'}$ is calculated using perturbation method:

$$E_{n_1\ n_1'}^{n_2\ n_2'}(\mathbf{R_2} - \mathbf{R_1}) =$$

$$\sum_{2nd\ order}^{4th\ order} \langle 0 \mid H_1 \frac{1}{E_0 - H_0} H_1 \frac{1}{E_0 - H_0} H_1 \cdots\ H_1 \mid 0 \rangle$$

where $\mid 0\rangle$ and E_0 are the ground state and its energy. For the ground state, all the ions are in the f^1 configuration and the band electrons form a closed Fermi sea. For the intermediate states, the ions can either be in f^1, f^2 or f^0 configuration. We have to take into account all the possible virtual excitation processes which exchange electrons(holes) between the two ions.

There are three types of processes:

Exchange-Induced (RKKY): J 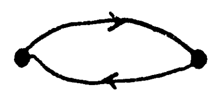 J

Hybridization-Induced: V^2 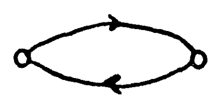 V^2

Cross Effect: V^2 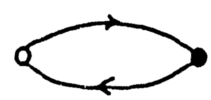 J

"Charge leakage" of f states in rare earths versus uranium:

YbSb	0.18%	
ErSb	0.25%	
TbSb	0.21%	localized
NdSb	0.60%	↓
CeSb	1.6 %	weakly delocalized
USb	4.0 %	↓
UTe	3.1 %	begin to show itinerancy

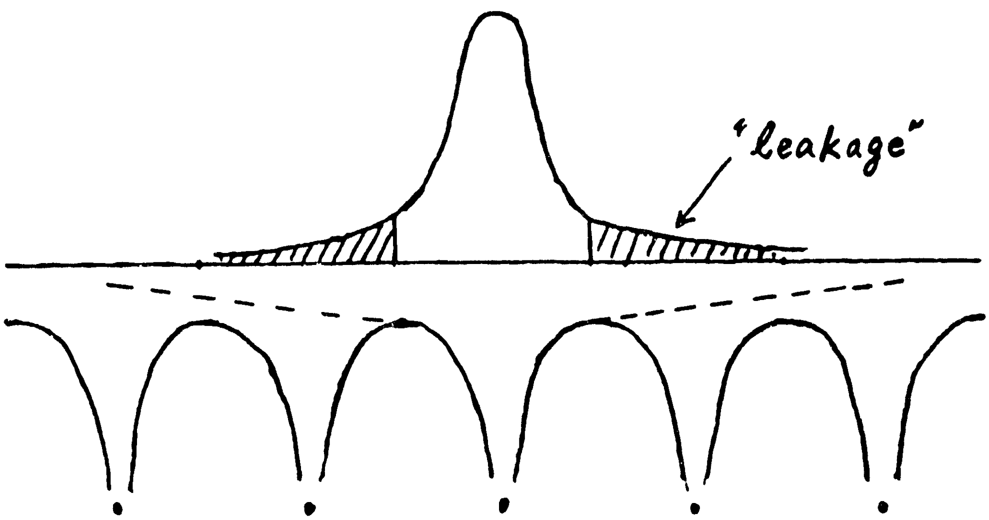

Influence: self banding of the f states in rare earths negligible; self banding of the f states in uranium substantial.

Essentially, we have learned how to exhibit magnetic ordering properties in the correlated-electron state by projecting onto a site-centered basis (free-ion states). This takes the form of having a complicated looking, highly anisotropic two-ion interaction with consequent observable properties. Note that the only correlation effects included are on-site (interconfigurational) correlations.

Since uranium f-electrons are substantially more delocalized than cerium f-electrons, we have developed a scheme for uranium that goes back and forth between a band and a site-centered picture for the f- electrons. The site-centered basis is not as adequate for capturing magnetic ordering effects in uranium systems as it is for cerium systems (i.e. there is a need for a "richer" basis, presumably containing band states).

For monopnictides and monochalcogenides, of NaCl-structure: For Cerium, coulomb exchange > hybridization (not a general rule); for uranium, hybridization > exchange.

Hybridization drives the system toward the heavy fermion state by merging the f-spectral density into the d-p band spectral density in the presence of interconfigurational correlation effects.

↓

Moment Washout

Coulomb exchange counteracts this moment reduction by acting through the orbital part of the RKKY interaction (brought about by the strong spin-orbital coupling).

HEART OF THE PHYSICS

The correlations we include are on-site correlations (U, configuration fluctuations). As the f-spectral density is pulled off-site by hybridization, U becomes ineffective; and ordered moment is lost because the cooperative hybridization (or really the cooperative hybridization/orbital exchange) giving ordered moment becomes ineffective the more the f-spectral weight is pulled off-site by hybridization (the larger the fraction of time off-site as reflected in broadening).

Hybridization $\rightarrow$ merges f-spectral density into d-p band spectral density

$$\downarrow$$

heavy fermion state

weak hybridization (e.g. CeSb) — f-moment "left behind" on-site very slightly diminished – primary effect is highly anisotropic magnetic ordering via dense f/d-p plasma – orbitally-coupled magnetism.

strong hybridization (e.g. CeTe, PuTe) — washes away on-site f-spectral density to be polarized – ordered moment drastically reduced and then destroyed – moment washout.

Band-f coulomb exchange acts to restore moment via orbitally corrected RKKY.
(Thus, our calculations for CeTe would predict an ordered low-temperature moment of a few hundredths of a Bohr magneton with hybridization only, but this increases to a few tenths of a Bohr magneton in close agreement with experiment when coulomb exchange is included.)

	US	USb	UTe	CeTe	CeBi	CeSb	NdSb	ErSb
T_N(K) (hybridization)		240	220	0.2	2.6	3.4	0.6	0
T_N(K) (exchange)		~20	~20	3.0	38	35	6.0	1.3
m (u_B)(low T moment)		3.3	3.3	0.35	2.1	2.1	3.3	8.9
T_N(K) (experiment)	178	213	104	2.2	26	18	16	3.6
m (u_B) (experiment)	1.55	2.85	2.25	0.3	2.1	2.1	3.0	7.0
m (u_B) (band theory)	1.52		1.65	0.96				

- The strong hybridization in itinerant uranium systems is responsible for the high ordering temperature.
- Polarized band theory is good for US, but UTe is too itinerant for site centered theory and not itinerant enough for band theory.
- The site centered treatment of magnetic ordering for uranium systems overestimates the way in which increased hybridization increases interionic coupling, and therefore this treatment overestimates the ordering temperature.
- In polarized band theory, the increase of hybridization causes band broadening, and this gives too low an ordered moment for UTe.
- Much weaker hybridization in rare earths than in uranium.
- Correlated electron theory works excellently for CeTe. Band theory fails because it neglects interconfigurational fluctuations.(correlations)
- Decreasing exchange going from light to heavy rare earths; hybridization is negligible for heavy rare earths.

Depression of superconductivity with Pr content in $Pr_x Y_{1-x} Ba_2 Cu_3 O_7$

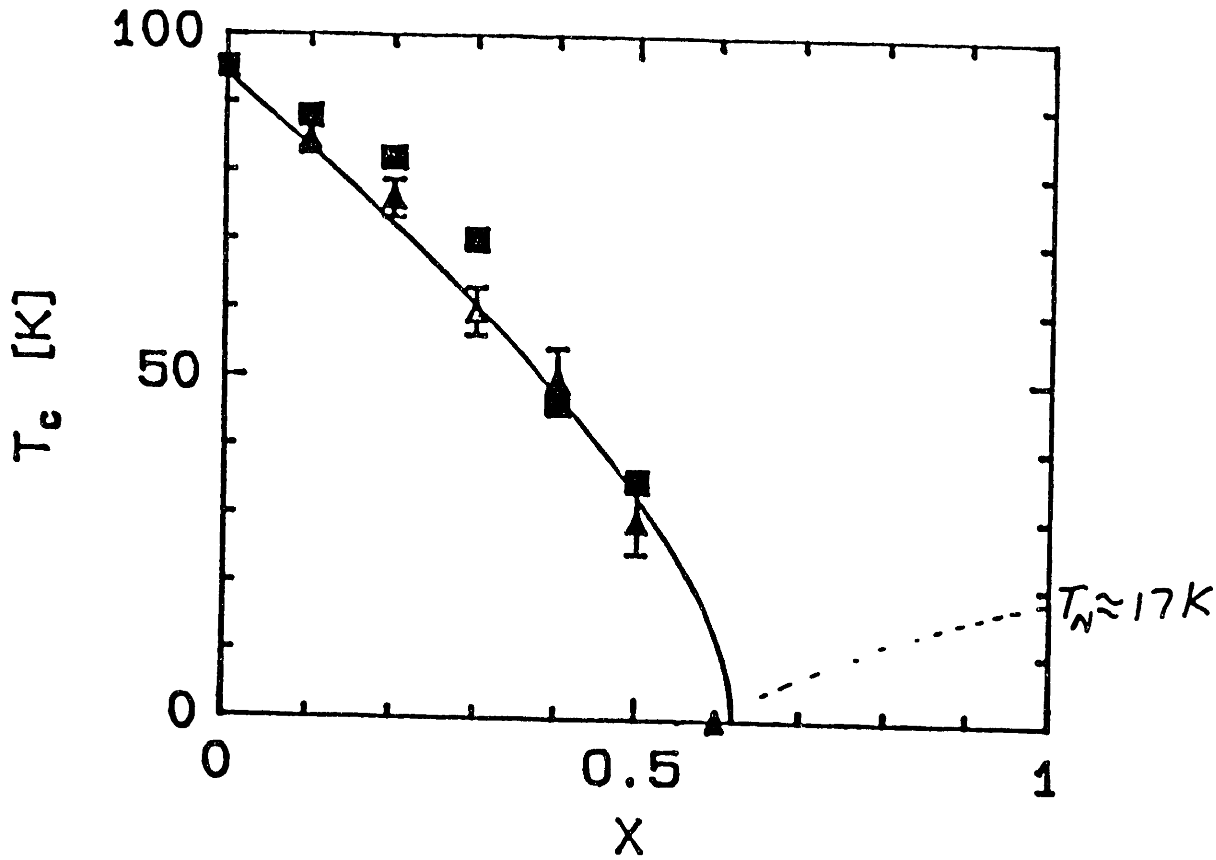

Jee et al (Temple U.), 1988

$C_m \sim Pr \quad T_N = 22K$

L. Soderholm

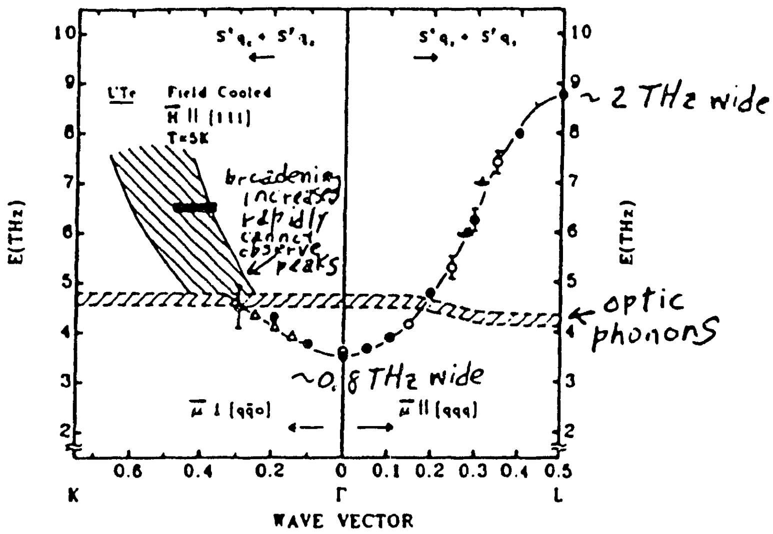

Dispersion curve for UTe along the q_l (parallel to the moment) and q_x (perpendicular to the moment) directions at 5 K. The narrow hatched line shows the optic-phonon frequency. The different symbols correspond to different spectrometer conditions. The wide hatched area on the left-hand side corresponds to the region where we are unable to assign specific peak positions.

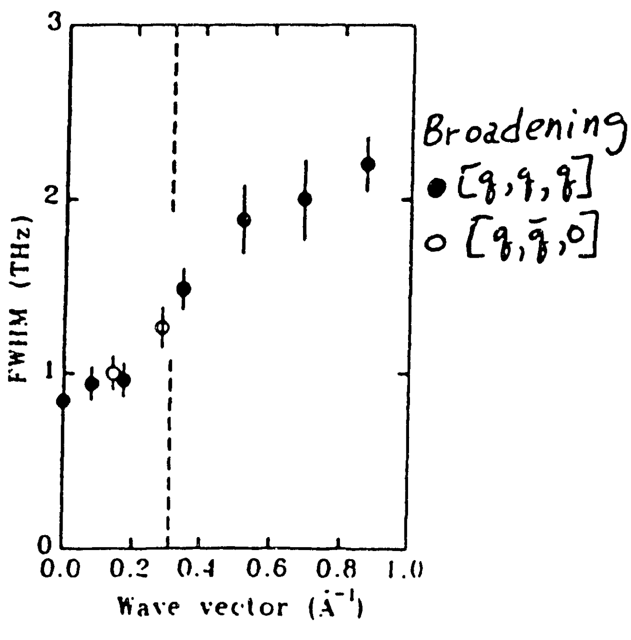

FWHM of Lorentzian damping function at 5 K for excitation peaks as a function of q in Å^{-1}. Solid points correspond to q_l, open points to q_x. The dashed vertical line indicates the wave vector at which the magnetic and optic-phonon excitation intersect.

We extended our previous theory for the magnetic behavior of hybridizing partially-delocalized f-electron systems to include hybridization-induced relaxation effects in the magnetic response. Each partially delocalized f-electron ion is coupled by hybridization to the band sea; and this both leads to a hybridization-mediated anisotropic two-ion interaction giving magnetic ordering and also gives a damping mechanism, via the coupling to the band sea, for the excitations of the magnetically ordered lattice. This coupling also provides a strong renormalization of the magnetic excitation energies obtained for the ionic lattice coupled by the two-ion interaction. To treat these effects on the magnetic response we have developed a formalism for calculating the dynamic susceptibility based on the projection-operator method developed by Mori and others.

We solve the problem by three steps :

(1) Two-ion coupling → mean-field level structure.

Solve the eigenvalue problem with H_0 in the mean-field theory to obtain a 10-energy-level structure (dispersionless).

(2) Two-ion coupling → RPA excitation dispersion.

perfectly sharp excitations

Solve the eqations of motion for $H_0-(H_0)_{MF}$ to get the dispersion of magnetic excitations in the Random Phase Approximation (RPA).

(3) **Hybridization relaxation to band bath → strong renormalization of excitation energies.**

Using the memory function method of Mori et al. to calculate the magnetic damping caused by H' (hybridization coupling of each uranium to band bath).

$$\mathcal{H}_0 = \sum_{k,M} \epsilon_k n_{k,M} + \sum_{M} \mathcal{E}_M n_M + \frac{U}{2} \sum_{M,M'} n_M n_{M'} + W\left[x \frac{(O_4^0 + 5O_4^4)}{60} + (1-|x|) \frac{O_6^0 - 21O_6^4}{2520}\right] - \sum_{j} E_{ij} \sum_{MM'} \sum_{NN'} J_{MM'}^{NN'} L_{MM'}^{(i)} L_{NN'}^{(j)},$$

Hybridization (ab initio)

$$\mathcal{H}' = -\mathcal{J} \sum_{k,k'} \sum_{M,M'} c_{k'M'}^{\dagger} c_{kM} c_M^{\dagger} c_{M'},$$

Hybridization double counted - affects dispersion.

Input: $T_C = 104$ K, ordered moment $2.6\mu_B$, ab initio $\mathcal{J}N(\epsilon_F) = -0.09$ (1990) (1991) ~ -0.2

UTe

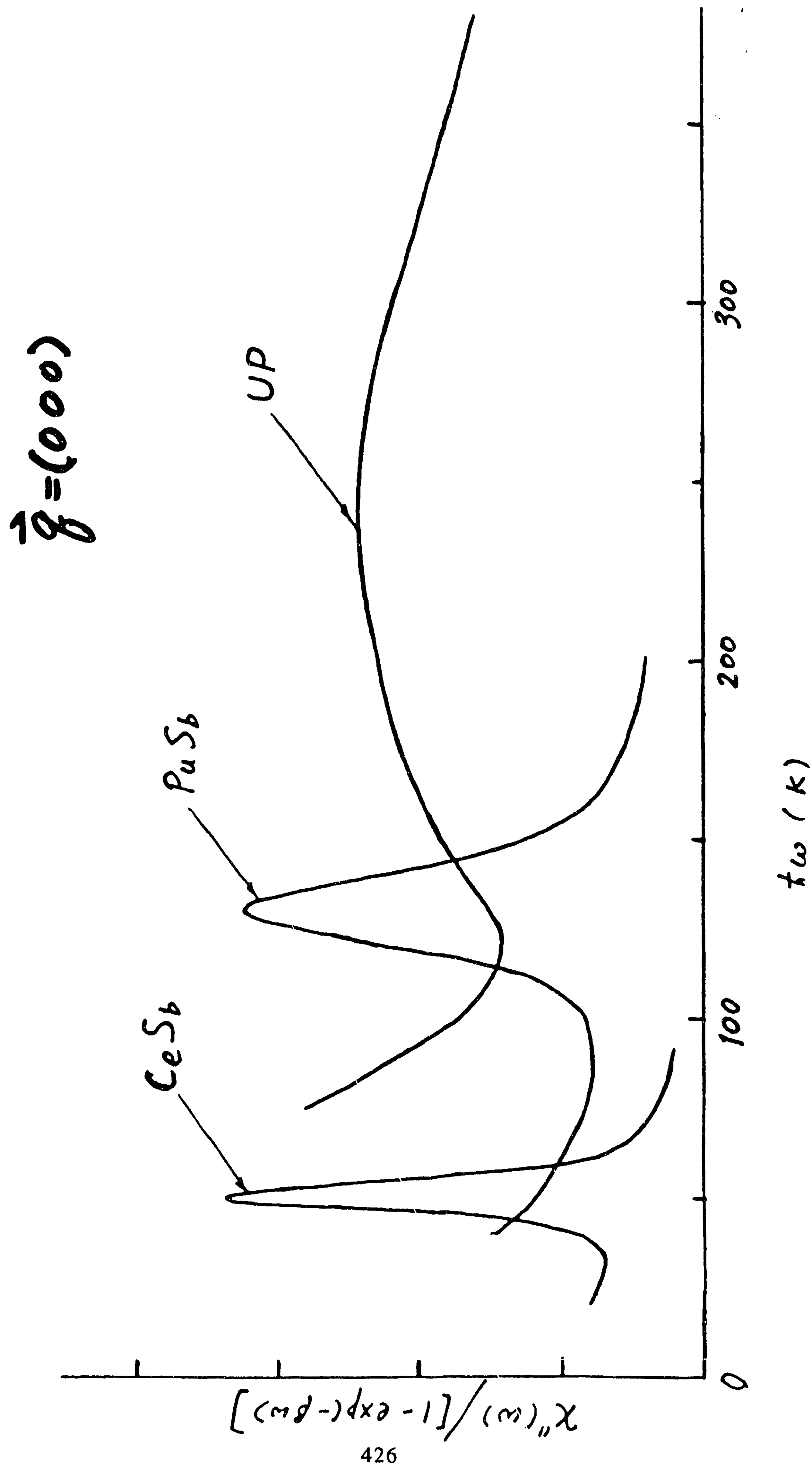

$\vec{q} = (000)$
UP
PuSb
CeSb
$\hbar\omega$ (K)
0
100
200
300
$\chi''(\omega)/[1 - \exp(-\beta\omega)]$

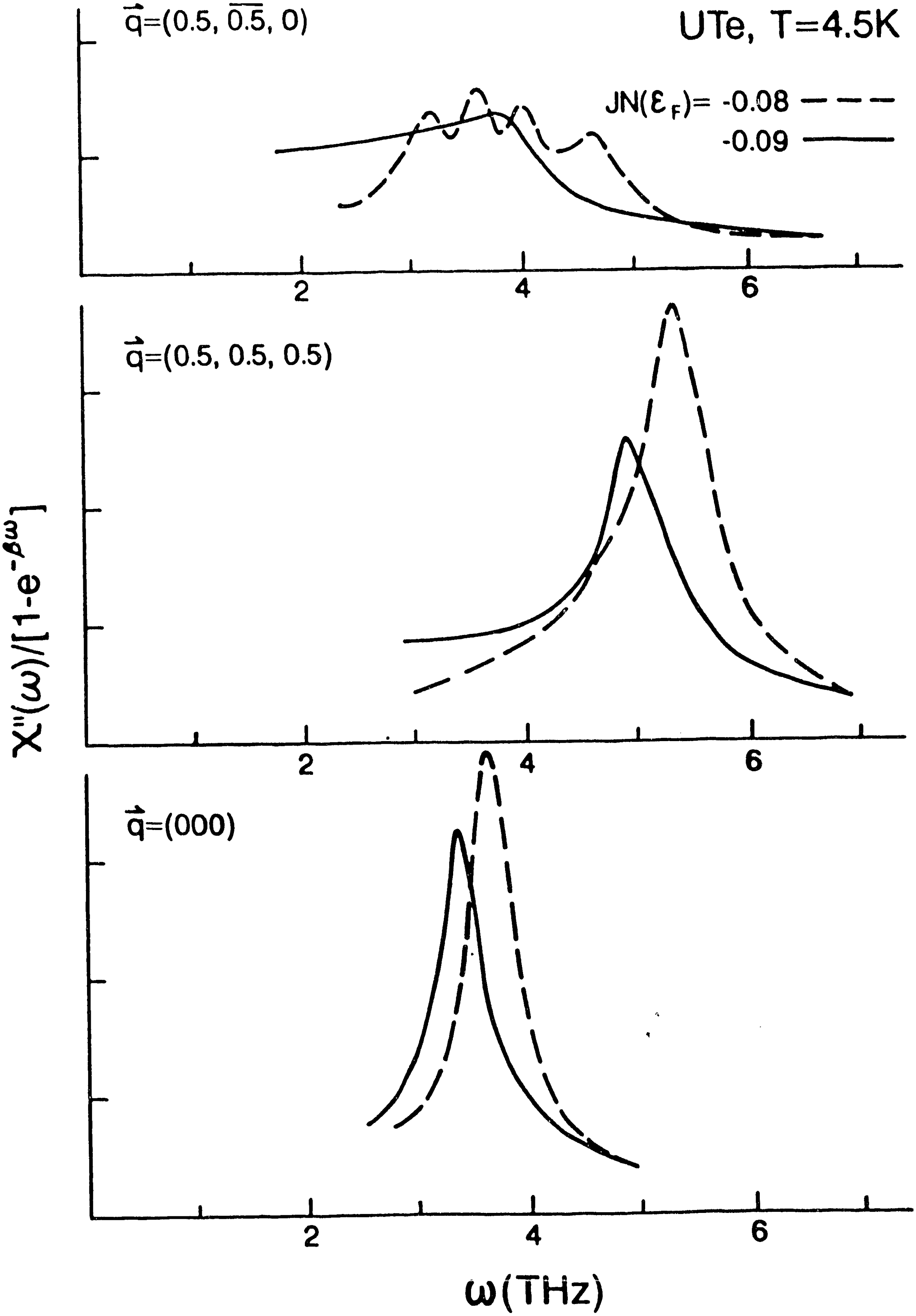

$\vec{q}$=(0.5, $\overline{0.5}$, 0)
UTe, T=4.5K
JN(ε$_F$)= -0.08
-0.09
$\vec{q}$=(0.5, 0.5, 0.5)
$\vec{q}$=(000)
X''(ω)/[1-e$^{-\beta\omega}$]
2
4
6
ω(THz)

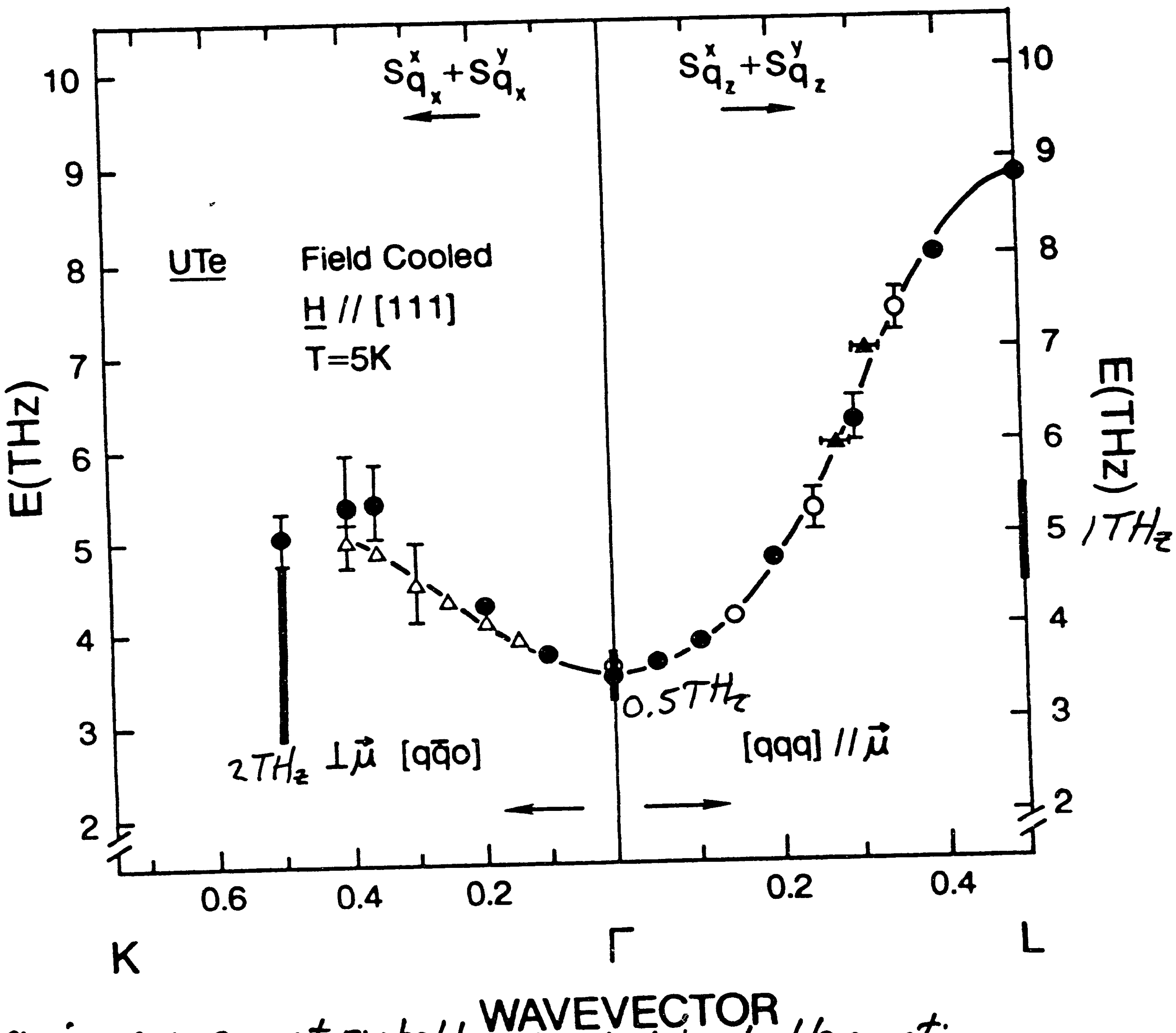

— dispersion agreement probably affected by double counting of hybridization

— broadening would roughly double with present $J N(\varepsilon_F)$.

Giant magneto-optic Kerr rotations occur in a number of cerium and uranium chalcogenides and pnictides (ETH experiments). Some of these materials (e.g. CeTe, UTe) show distinct evidence of correlated-electron behavior including incipient heavy fermion behavior. This leads us to ask two questions. What is the origin of the giant magneto-optic effects? What relationship, if any, exists between the giant magneto-optic behavior and the approach to the correlated-electron, heavy fermion state? We have found quantitative answers to these questions through comparison of absolute ab initio spin-and-orbitally polarized full-potential LMTO LDA calculations of the optical conductivity tensor in comparison with experiment. The giant magneto-optic behavior originates in the coupling of light to the large partially itinerant orbital polarization present in these materials. The approach to the heavy fermion state is characterized by a washout (broadening away) of what band theory would predict to be strong structure in the magneto-optic dispersion; and magneto-optic behavior appears to be a very sensitive probe of the approach to the heavy fermion state, presumably reflecting very sensitively the broadening that characterizes this approach.

- Conventional one-electron band theory is inadequate for an understanding of the giant magneto-optic behavior.
- To see if one-electron (band) theory is adequate, extend band theory to include explicit orbital polarization (Hund's second rule ala Brooks).

- With explicit orbital polarization, does band theory theory correctly give the experimental static magnetic moment (magnetization measurement/neutron diffraction) and dynamic magnetic moment (magneto-optic experiment)? See 28. Yes for US. No for UTe, CeTe

- Results for US, UTe and CeTe. incipient heavy fermion

more correlated

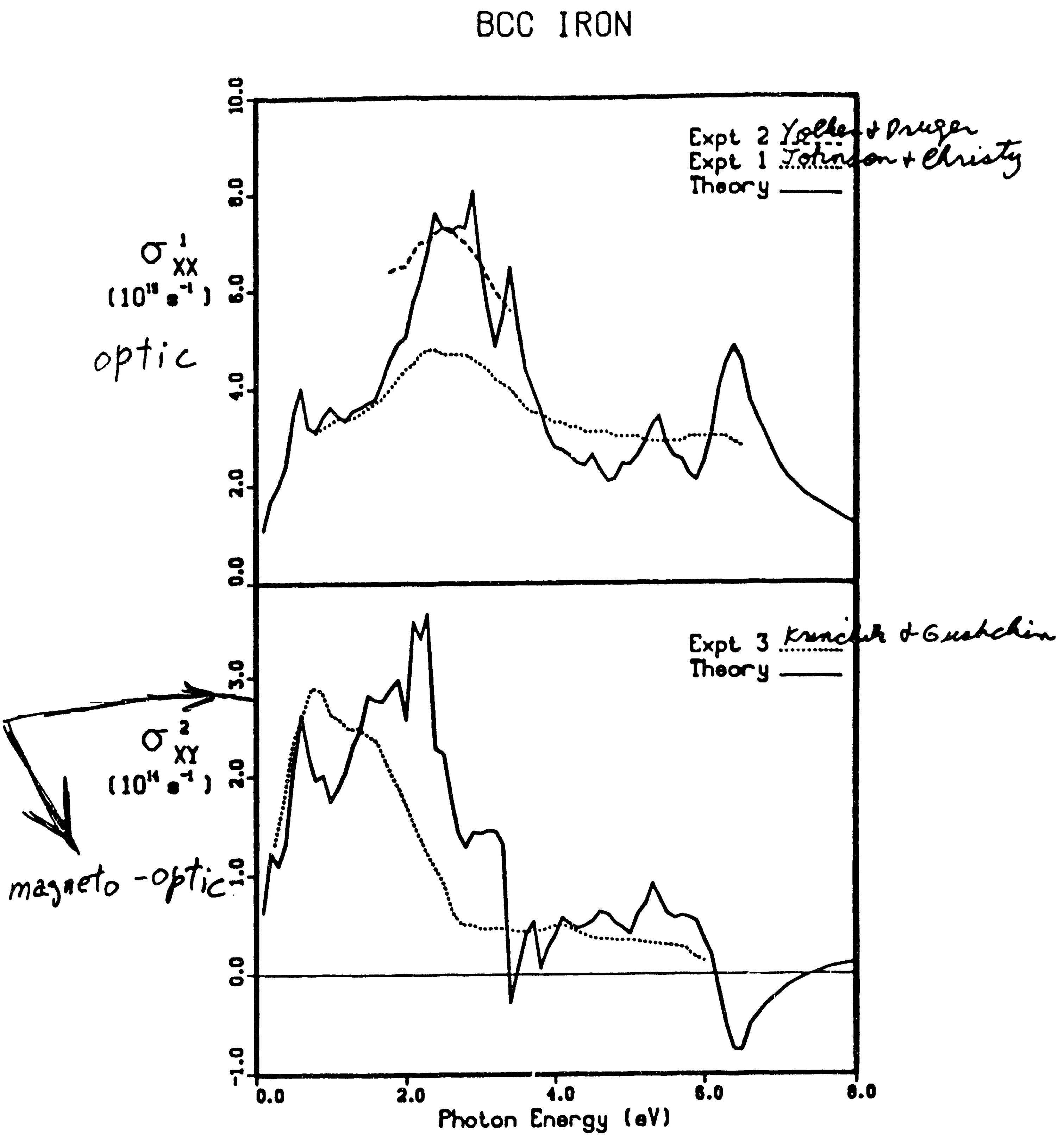

Band Theory works for iron - a good itinerant electron ferromagnet

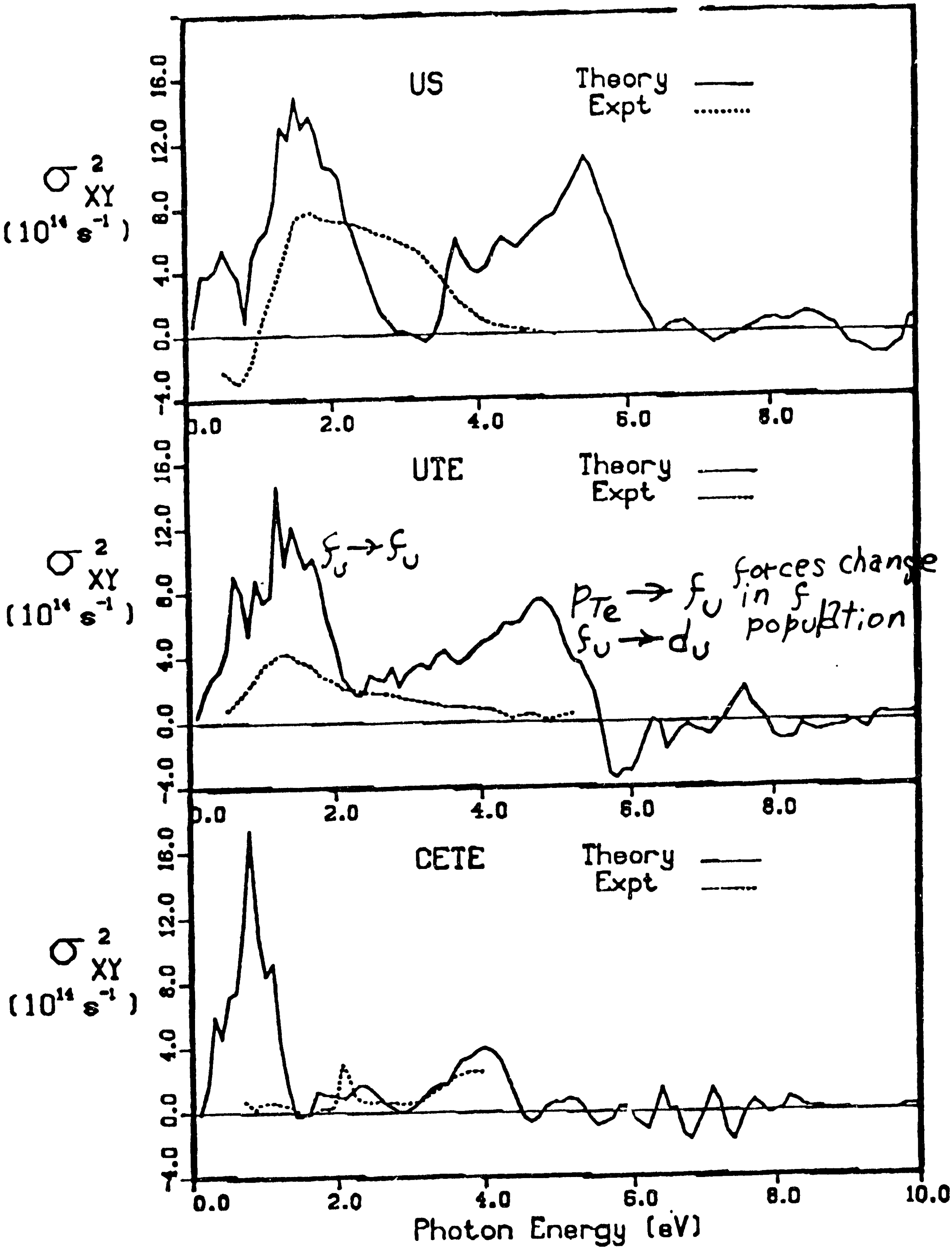
US
Theory
Expt
UTE
Theory
Expt
$f_U \rightarrow f_U$
$p_{Te} \rightarrow f_U$
$f_U \rightarrow d_U$
forces change in f population
CETE
Theory
Expt
σ^2_{XY} (10^{14} s^{-1})
Photon Energy (eV)

Summary of Key Results

- For static moment, band (i.e. one-electron) Theory is inadequate for understanding the diminished ordered moment associated with the approach to the highly-correlated electron state as in CeTe (an incipient heavy fermion - Ott and Hulliger) even when explicit orbital polarization is included.

$$\mathrm{US} \rightarrow \mathrm{UTe} \rightarrow \mathrm{CeTe}$$

- The Magneto-optic behavior is a more sensitive measure of the diminished ordered moment associated with strong correlation effects presumably because it provides a dynamic measure of the moment.

FCC CETE

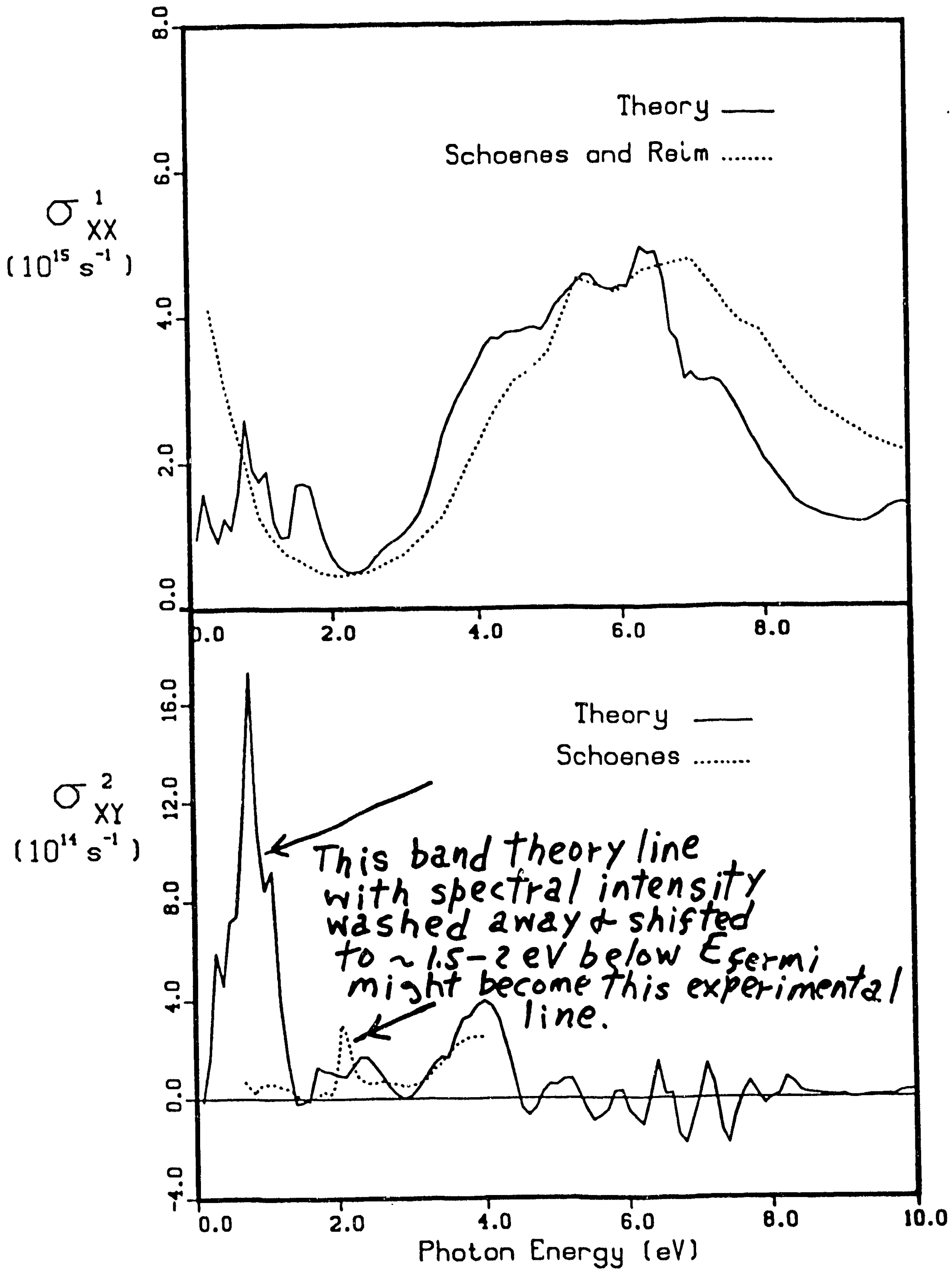

Raises questions to be explored in photoemission. Can extend Mori theory to magneto-optics and photoemission.

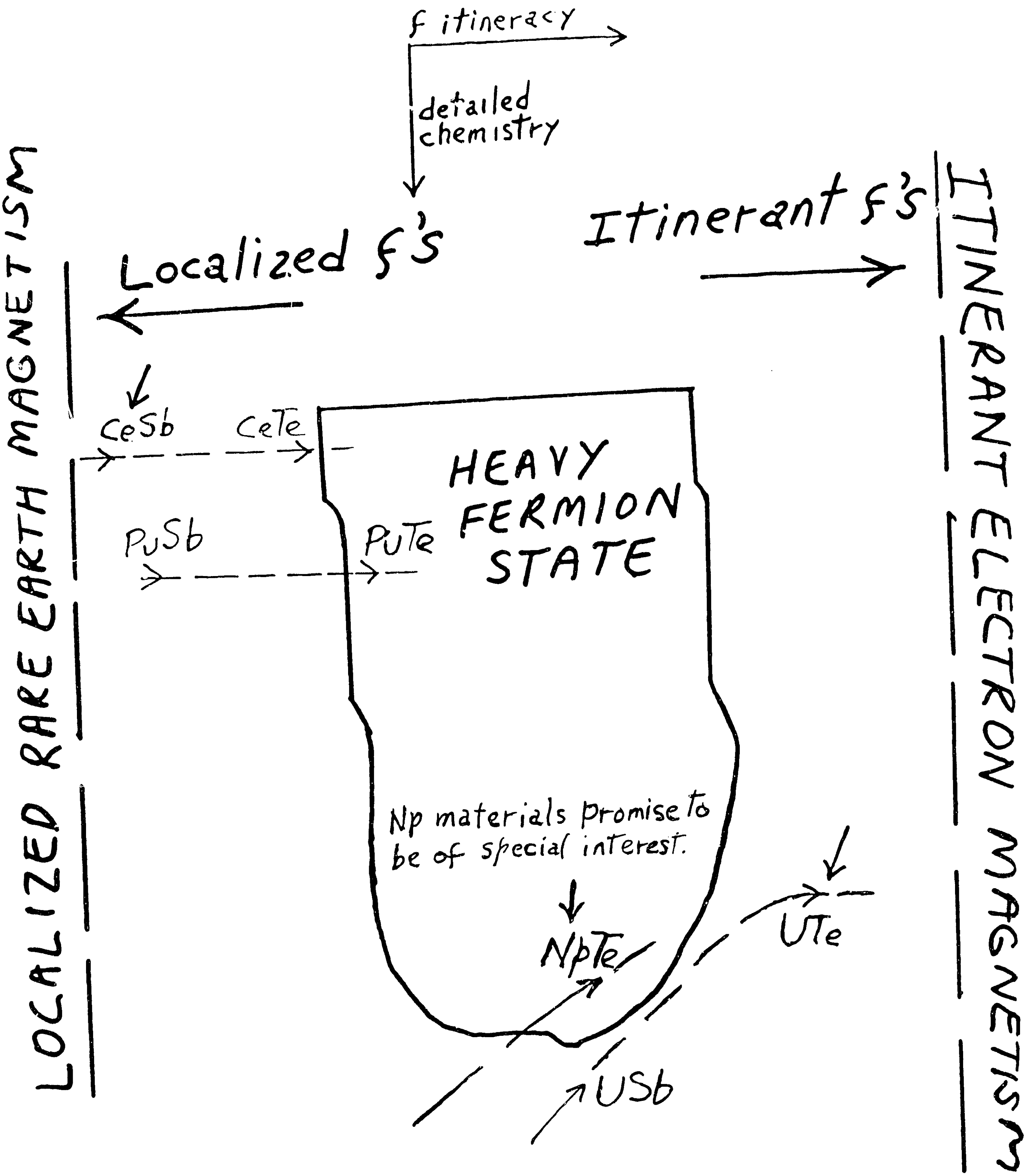

f itineracy
detailed chemistry
Localized f's
Itinerant f's
LOCALIZED RARE EARTH MAGNETISM
ITINERANT ELECTRON MAGNETISM
CeSb
CeTe
PuSb
PuTe
HEAVY FERMION STATE
Np materials promise to be of special interest.
NpTe
UTe
USb

HEAVY FERMION AND KONDO PHENOMENA IN ACTINIDE MATERIALS

M. Brian Maple

Department of Physics and Institute for Pure and Applied Physical Sciences
University of California, San Diego
La Jolla, CA 92093

Heavy fermion and Kondo phenomena in metals containing transition metal, rare earth, and actinide ions with partially-filled 3d, 4f, and 5f electron shells can be traced to the hybridization of the localized 3d, 4f, and 5f states and the conduction electron states. Since the spatial extent of the 5f wave functions is intermediate between that of the 4f and 3d wave functions, the strength of the hybridization for systems containing actinide ions is intermediate between that of systems containing rare eath and transition metal ions. In this intermediate regime, a rich variety of heavy fermion and Kondo phenomena in actinide systems are found, some of which are briefly summarized below.

Heavy Fermion Compounds

Heavy fermion compounds are formed from 4f- and 5f-elements (such as Ce, U, and Yb) which have an unstable f-configuration [1,2]. The "heavy fermion" state, characterized by an enormous electronic specific heat coefficient γ, develops below a characteristic "coherence temperature." While the high temperature behavior may be reasonably well accounted for in terms of an array of independent paramagnetic Kondo "impurity ions," the low temperature coherent Fermi liquid regime is not well understood. It is unstable against the formation of superconducting and low moment (~0.01 μ_B) antiferromagnetic states, which coexist on a microscopic scale in compounds such as UPt_3 [3-5] and URu_2Si_2 [6-8]. The superconducting state is particularly interesting. The power-law temperature dependences of thermodynamic and transport properties below T_c in heavy fermion superconductors indicate the existence of an anisotropic energy gap similar to that of superfluid ^3He. Additional evidence for a nonscalar ($l \neq 0$) order parameter is the observation of two or more distinct superconducting states in UPt_3 [3-5], $U_{1-x}Th_xBe_{13}$ [9,10], and, possibly, URu_2Si_2 [11], the origin of which may be due to the coupling of antiferromagnetic and multicomponent superconducting order parameters. However, it has not yet been definitively demonstrated that the multiple superconducting transitions in all of these materials are intrinsic features of unconventional superconductivity or associated with two different metallurgical phases. Antiferromagnetic fluctuations have also been proposed as the mechanism leading to Cooper pair formation in heavy fermion superconductors and have been shown to impede s-wave pairing. The magnetic and superconducting properties of heavy fermion compounds are also extraordinarily sensitive to chemical impurities and frequently yield striking results such as the non-monotonic decrease of T_c in $U_{1-x}Th_xBe_{13}$ [9,10], the transition from small to localized moment antiferromagnetic ordering in $U_{1-x}Th_xPt_3$ [12], the transition from SDW to local moment antiferromagnetic ordering in $URu_{2-x}Rh_xSi_2$ [13] and to ferromagnetic ordering in $URu_{2-x}Re_xSi_2$ [14].

Hybridization Gap Semiconductors

Another striking and related phenomenon observed in these unstable f-electron materials is the formation of an insulating ground state with a small energy gap of the order of several meV which is apparently associated with hybridization between localized f and conduction electron states (hence the terminology "hybridization gap semiconductor") or Kondo interactions (hence the name "Kondo insulator"). Materials which exhibit this behavior include, for example, SmB_6 [15], SmS [16], $CeFe_4P_{12}$ [17], UFe_4P_{12} [18], $Ce_3Bi_4Pt_3$ [19], and $U_3Sb_4Pt_3$ [20,21]. Apparently, the physics of such systems can be described by a lattice Hamiltonian consisting of a single half-filled conduction band which is crossed by an occupied magnetic level.

Multichannel Kondo Effect

While the exotic superconductivity of the heavy fermion materials has attracted the most attention, it is clear that no fundamental understanding can be achieved without a microscopic theory of the normal state properties. Recent experiments [22,23] on the $Y_{1-x}U_xPd_3$ system have led to important and exciting results that provide compelling evidence for a two-channel quadrupolar Kondo effect [24] with concomitant non Fermi liquid behavior. There may be a relation between the breakdown of Fermi liquid theory in $Y_{1-x}U_xPd_3$ and that which is believed to occur in the high T_c oxide superconductors. This work is important from several viewpoints. First, this is a new aspect of the Kondo problem and it enhances our fundamental understanding of magnetic moments in metals. Secondly, the behavior of the electrons cannot be described using Fermi liquid phenomenology which has traditionally been very successful in characterizing normal state properties of even highly correlated electronic materials. Finally, these results could have consequences for the concentrated heavy fermion systems which exhibit such anomalous behavior, and perhaps other highly correlated electronic systems. For the $Y_{1-x}U_xPd_3$ system at low temperatures $T << T_K$, where T_K is the Kondo temperature, the electrical resistivity varies nearly linearly with T, $\rho(T)/\rho(0) \approx 1 - T/(aT_K)$, and the electronic specific heat diverges logarithmically, $\Delta C/T \approx -(1/T_K)\ln T$ with a finite residual T = 0 entropy $S(0) \approx (R/2)\ln 2$. Electronic specific heat $\Delta C/T$ vs lnT data for $Y_{1-x}U_xPd_3$ samples with x = 0.1 and 0.2 are shown in Fig. 1.

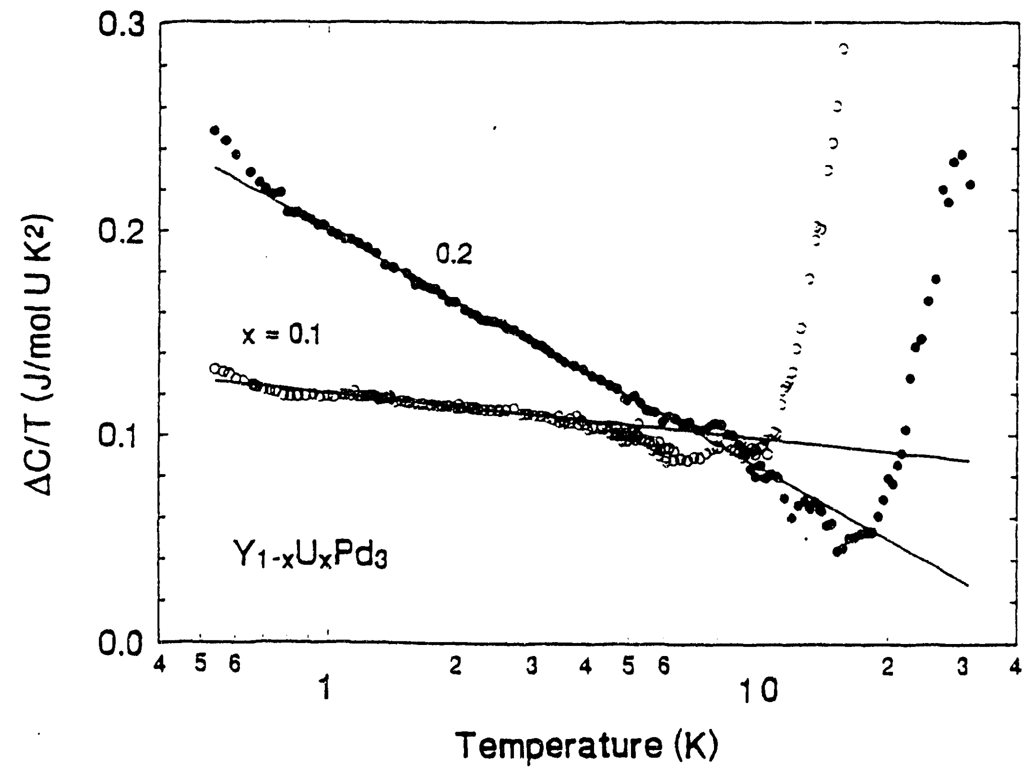

Figure 1. Electronic specific heat $\Delta C/T$ vs lnT data for $Y_{1-x}U_xPd_3$ samples with x = 0.1 and 0.2. The solid lines corespond to fits with T_K = 220 K and 42 K for x = 0.1 and 0.2, respectively [10].

*This work was supported by the U.S. Department of Energy under Grant No. DE-FG03-86ER45230 and National Science Foundation under Grant No. DMR 91-07698.

1. Z. Fisk, D. W. Hess, C. J. Pethick, D. Pines, J. L. Smith, J. D. Thompson, and J. O. Willis, *Science* **239**, 33 (1988).
2. Z. Fisk and M. B. Maple, *J. Alloys and Compounds* **183**, 303 (1992).
3. R. A. Fisher, S. Kim, B. F. Woodfield, N. E. Phillips, L. Taillefer, K. Hasselbach, J. Flouquet, A. L. Giorgi, and J. L. Smith, *Phys. Rev. Lett.* **62**, 1411 (1989).
4. K. Hasselbach, L. Taillefer, and J. Flouquet, *Phys. Rev. Lett.* **63**, 93 (1989).
5. R. N. Kleiman, P. L. Gammel, E. Bucher, and D. J. Bishop, *Phys. Rev. Lett.* **62**, 328 (1989).
6. T. T. M. Palstra, A. A. Menovsky, J. van den Berg, A. J. Dirkmaat, P. H. Kes, G. J. Nieuwenhuys, and J. A. Mydosh, *Phys. Rev. Lett.* **55**, 2727 (1985).
7. M. B. Maple, J. W. Chen, Y. Dalichaouch, T. Kohara, C. Rossel, M. S. Torikachvili, M. W. McElfresh, and J. D. Thompson, *Phys. Rev. Lett.* **56**, 185 (1986).
8. W. Schlabitz, J. Baumann, B. Pollit, U. Rauchschwalbe, H. M. Mayer, U. Ahlheim, and C. Bredl, Z. *Phys. B* **62**, 171 (1986).
9. H. R. Ott, H. Rudigier, Z. Fisk, and J. L. Smith, *Phys. Rev. B* **31**, 1651 (1985).
10. S. E. Lambert, Y. Dalichaouch, M. B. Maple, J. L. Smith, and Z. Fisk, *Phys. Rev. Lett.* **57**, 1619 (1986).
11. M. B. Maple, Y. Dalichaouch, B. W. Lee, C. L. Seaman, P. K. Tsai, P. E. Armstrong, Z. Fisk, C. Rossel, and M. Torikachvili, *Physica B* **171**, 219 (1991).
12. A. P. Rameriz, B. Batlogg, E. Bucher, and A. S. Cooper, *Phys. Rev. Lett.* **57**, 1072 (1986).
13. H. Amitsuka, T. Sakakibara, and Y. Miyako, J. Mag. Mag. Mat. **90 & 91**, 517 (1990).
14. Y. Dalichaouch, M. B. Maple, J. W. Chen, T. Kohara, C. Rossel, M. S. Torkachvili, and A. L. Giorgi, *Phys. Rev. B* **41**, 1829 (1990).
15. J. W. Allen, R. M. Martin, B. Batlogg, and P. Wachter, *J. Appl. Phys.* **49**, 2078 (1978).
16. A. Jayaraman, P. Dernier, and L. D. Longinotti, *Phys. Rev. B* **11**, 2783 (1975).
17. M. S. Torikachvili, M. B. Maple, and G. P. Meisner, in H. Eckern, ed., *Proc. LT-17*, North-Holland, Amsterdam, 857 (1984).
18. G. P. Meisner, M. S. Torikachvili, K. N. Yang, M. B. Maple, and R. P. Guertin, *J. Appl. Phys.* **57**, 3073 (1985).
19. M. F. Hundley, P. C. Canfield, J. D. Thompson, Z. Fisk, and J. M. Lawrence, *Phys. Rev. B* **42**, 6842 (1990).
20. T. Takabatake, S. Miyata, H. Fujii, Y. Aoki, T. Suzuki, T. Fujita, J. Sakurai, and T. Hiraoka, *J. Phys. Soc. Japan* **59**, 4412 (1990).
21. P. C. Canfield, A. Lacerda, J. D. Thompson, G. Sparn, W. P. Beyermann, M. F. Hundley, and Z. Fisk, *J. Alloys and Compounds* **181,** 77 (1992).
22. C. L. Seaman, M. B. Maple, B. W. Lee, S. Ghamaty, M. S. Torikachvili, J.-S. Kang, L. Z. Liu, J. W. Allen, and D. L. Cox, *Phys. Rev. Lett.* **67**, 2882 (1991).
23. C. L. Seaman, M. B. Maple, B. W. Lee, S. Ghamaty, M. S. Torikachvili, J.-S. Kang, L. Z. Liu, J. W. Allen, and D. L. Cox, *J. Alloys and Compounds* **181**, 327 (1992).
24. D. L. Cox, *Phys. Rev. Lett.* **59**, 1240 (1987).

HEAVY FERMION AND KONDO PHENOMENA IN ACTINIDE MATERIALS

M. Brian Maple
University of California, San Diego

- Materials containing lanthanide, actinide, and transition metal ions with partially-filled 4f, 5f, and 3d electron shells
  $\Rightarrow$ correlated electron phenomena
- Dilute or concentrated
- Disordered or ordered (sublattice)
- Hybridization between localized 4f, 5f, and 3d states and conduction electron states
- Radial extent of 5f wavefunctions (~0.7 Å) intermediate between that of 4f and 3d wavefunctions (~0.4 Å,~0.9 Å)
  $\Rightarrow$ Hybridization of actinide ions intermediate between that of rare earth and transition metal ions
- Delicate balance between localized and itinerant character for actinide ions leads to rich variety of heavy fermion and Kondo phenomena

Three examples

- Heavy fermion superconductivity and magnetism
- Hybridization gap semiconductors (Kondo insulators)
- Multichannel Kondo effect (non-Fermi liquid)

Multichannel Kondo effect (non-Fermi liquid)

Nozieres and Blandin, '80

- Metallic matrix containing paramagnetic impurity ions

  m-channel Kondo effect

  m channels of conduction electrons interact via spin dependent exchange interaction with paramagnetic impurity ions
  $\Rightarrow$ overscreening of paramagnetic impurity spin for $T \ll T_K$
  $\Rightarrow$ local non-Fermi liquid

  Relevant to high T_c superconductivity in oxides
  Normal state properties (e.g., linear $\rho(T)$ curve)
  $\Rightarrow$ marginal or non-Fermi liquid behavior

- Two channel quadrupolar Kondo effect — *Cox, '87*

  Quadrupolar Kondo effect — electric analogue of magnetic Kondo effect

  System — $Y_{1-x}U_xPd_3$

Experimental evidence for two-channel quadrupolar Kondo effect in $Y_{1-x}U_xPd_3$

Coworkers:

U. California, San Diego	C. L. Seaman B. W. Lee S. Ghamaty
San Diego State U.	M. S. Torikachvili
U. Michigan	J. W. Allen L.-Z. Liu J.-S. Kang
Ohio State U.	D. L. Cox
Oak Ridge National Laboratory	H. A. Mook

UPd$_3$ Only actinide intermetallic compound consistent with localized 5f electrons (low T)

U^{4+} $5f^2$ ($^3H_4$) $^{2S+1}L_J$

INS: CEF levels (Shamir et al.,'78)

(Nonmagnetic ground state)

Small $\gamma \approx 5$ mJ/mol K^2 (Andres et al.,'78)

PES/BIS: Gap in 5f spectral weight about E_F

Low $N(E_F)$ (Baer et al.,'80)

(Reihl et al.,'88)

(Arko et al.,'88)

YPd$_3$ Small $\gamma \approx 3.5$ mJ/mol K^2 (Besnus et al.,'83)

$N(E_F) \approx 1$ state/eV cell (Koenig et al.,'83)

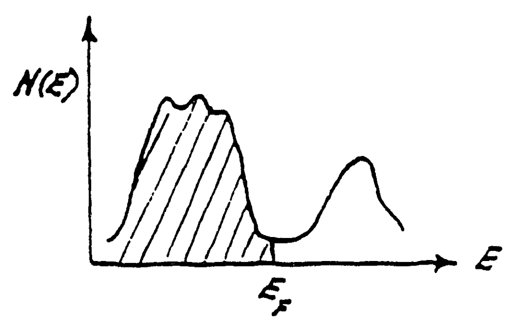

Y$_{1-x}$U$_x$Pd$_3$ PES (Kang et al.,'89)

Increase in $|E_{5f} - E_F|$ with x (~1 eV as $x = 0 \rightarrow 1$)

Interpretation: Fermi-level tuning

Substitution of $\underline{U^{4+}}$ for $\underline{Y^{3+}}$ $\Rightarrow$ increase in n

$\Rightarrow$ increase in E_F

Expectation: Moderate 5f-conduction electron hybridization (V_{kf})

$\Rightarrow$ Kondo effect

$$\mathcal{H}_{ex} = -2\mathcal{J}\mathbf{S}\cdot\mathbf{s}(0) \quad \textit{with } \mathcal{J}<0$$

$$\mathcal{J} \sim \frac{-\langle V_{kf}^2 \rangle}{|E_{5f} - E_F|}$$ should decrease in magnitude with x

$\Rightarrow T_K \sim T_F \exp[-1/N(E_F)|\mathcal{J}|)]$ should decrease with x

Motivated measurements of $\rho(T)$, $C(T)$, $\chi(T)$, $R(H)$ on polycrystalline $Y_{1-x}U_xPd_3$

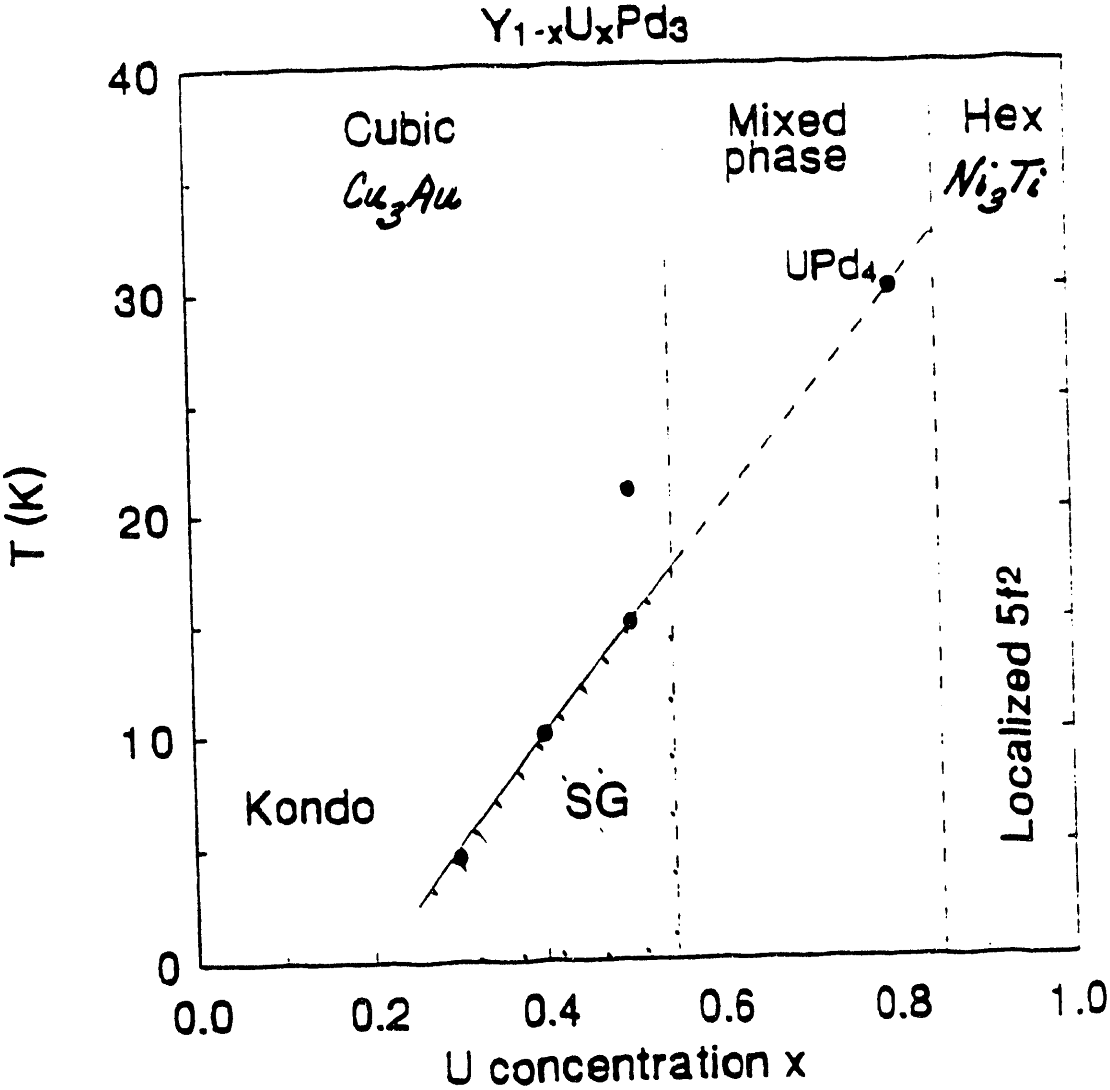

Structural change: Electronically driven

Kondo behavior ($x \leq 0.2$)

- T_K decreases with x (consistent with FLT and U^{4+})
- Unconventional low-T behavior (non-Fermi liquid)
- Comparison to m-channel Kondo model yields remarkable
  agreement with m = 2, S = 1/2 case
- Quadrupolar Kondo effect: Microscopic mechanism

Kondo Effect

$$\mathcal{H}_{ex} = -2\mathcal{J}\mathbf{S}\cdot\mathbf{s}(0); \qquad \mathcal{J} < 0 \qquad \text{(AFM)}$$

Moderate hybridization — **S** well defined (long-lived)
Single ion effect

$$T_K \sim T_F \exp\left[-1/N(E_F)|\mathcal{J}|\right]$$

T-dependent Kondo resonance

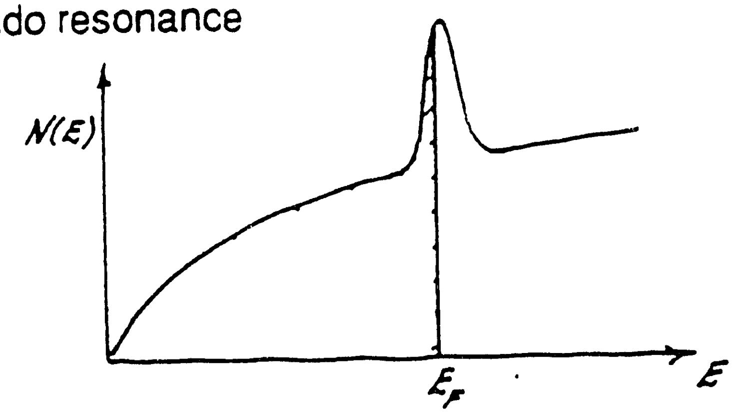

$T >> T_K$: Local moment — $\chi(T) \sim C/(T - \Theta_{CW})$; $|\Theta_{CW}| \sim 3 - 4\, T_K$

$$\rho(T) \sim -\ln T$$

$T << T_K$: Highly correlated many-body singlet ground state
Local Fermi liquid

$$\chi(T),\ C(T)/T \to \text{const} \propto N(E_F) \sim 1/T_K$$

$$S(0) \to 0$$

$\rho(T) \to \rho_0[1 - (T/T_0)^2]$ e.g., $Th_{1-x}U_x$ $T_K \gtrsim 100K$
Maple et al., '70

Two-Channel Kondo Effect (Nozieres & Blandin,'80)

$$\mathcal{H}_{ex} = -2\mathcal{J}\,\mathbf{S}.[\sigma_1 + \sigma_2]$$

$T << T_K$: Overscreening $\Rightarrow$ Critical state behavior
Local non-Fermi liquid

$\chi(T)$, $C(T)/T \rightarrow -(1/T_K)\ln T$

$\rho(T) \rightarrow \rho_0[1-(T/T_0)^n]$, $n = 1/2$

$S(0) = (R/2)\ln(2)$ — Tsvelik,'85
Sacramento & Schlottmann,'89
Affleck & Ludwig,'91

Quadrupolar Kondo Effect (Cox,'87)

S: Impurity pseudospin 1/2 (quadrupole moment)
σ_1, σ_2: time-reversed ($\uparrow,\downarrow$) channels which screen **S**

$$\left.\begin{array}{ll} \Gamma_1 \text{ —} & 5f^1, J=\frac{5}{2}, \Gamma_7 \\ \Gamma_4 \equiv & 5f^2, J=4, \Gamma_3 \\ \Gamma_5 \equiv & \end{array}\right\}$$ *mix via conduction* $j=\frac{5}{2}, \Gamma_8$ *partial waves*

Γ_3 — non-Kramer's, non-magnetic doublet

U^{4+} (Pr^{3+}) $^3H_4$ groundstate multiplet

$\chi \rightarrow \chi_{quadrupolar}$
$\chi_{magnetic} = \chi_{vV} \sim 1 - T^{1/2}$ (Cox, '91)

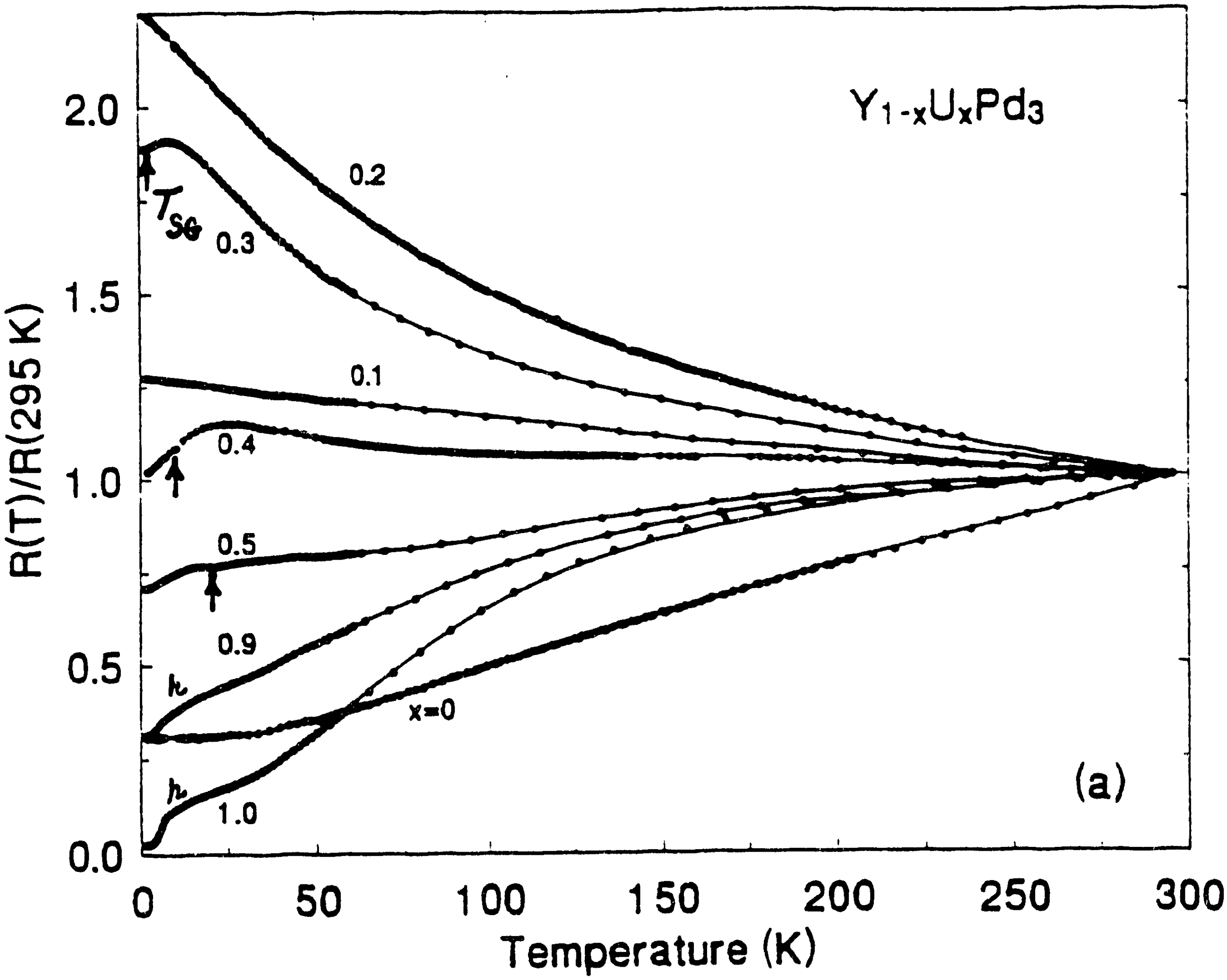
Y1-xUxPd3
R(T)/R(295 K)
Temperature (K)
0.2
0.3
0.1
0.4
0.5
0.9
x=0
1.0
T_{SG}
(a)
0.0
0.5
1.0
1.5
2.0
0
50
100
150
200
250
300

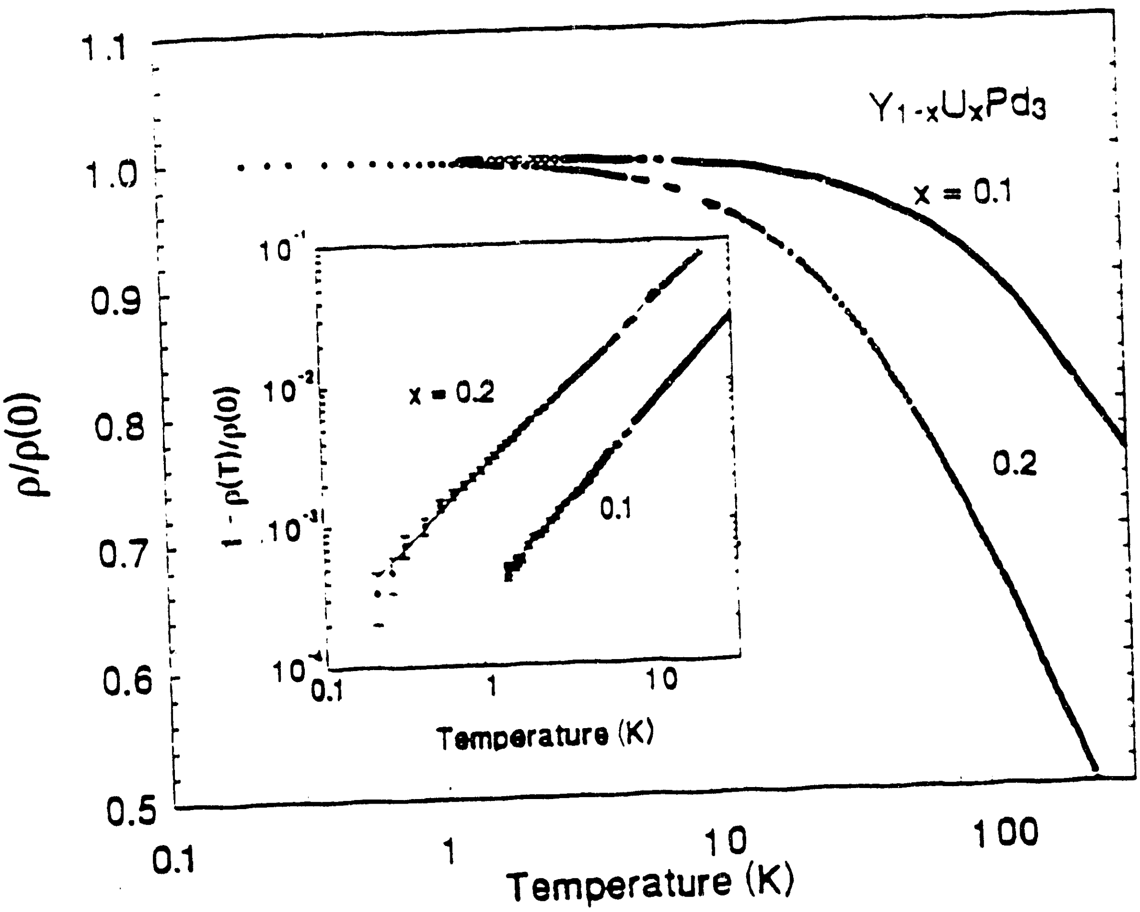

$T > T_K$: $\rho(T) \sim -\ln T \Rightarrow$ Kondo effect

$T << T_K$: $\rho(T)/\rho(0) = 1 - (T/T_0)^n$ $\{\ln[1-\rho(T)/\rho(0)] = n\ln T - n\ln T_0\}$

x	n	T_0	T_K [from C(T)]
0.1	1.30 ± 0.05	1.8 T_K	220 K
0.2	1.13 ± 0.04	4.3 T_K	42 K

Theory: Single-channel Kondo $n = 2$ (Fermi liquid)

Two-channel Kondo $n = 1/2$

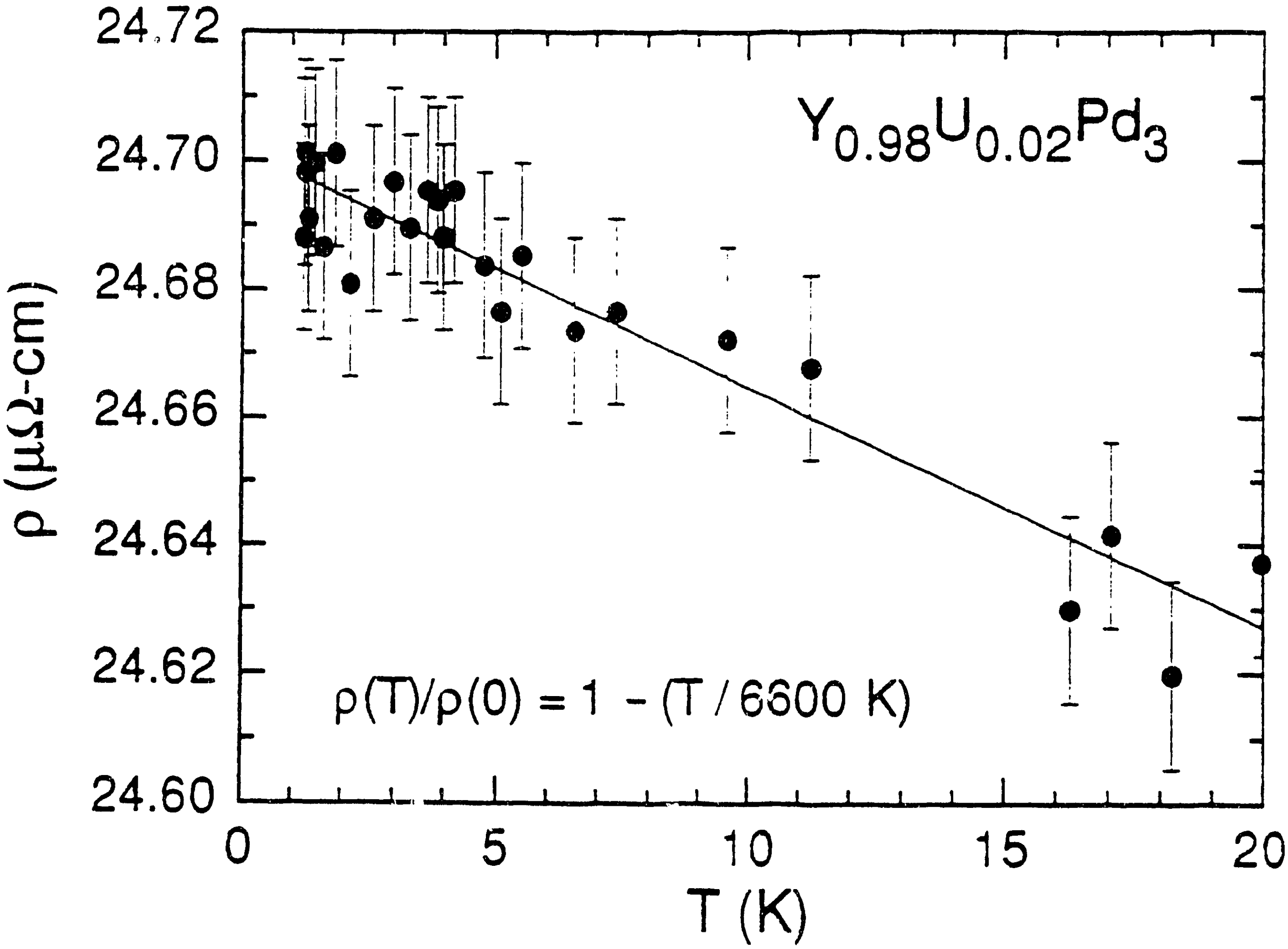

24.72
24.70
24.68
24.66
24.64
24.62
24.60
ρ (μΩ-cm)
0
5
10
15
20
T (K)
$Y_{0.98}U_{0.02}Pd_3$
$\rho(T)/\rho(0) = 1 - (T / 6600\ K)$

Electronic Specific Heat $\Delta C(T)$

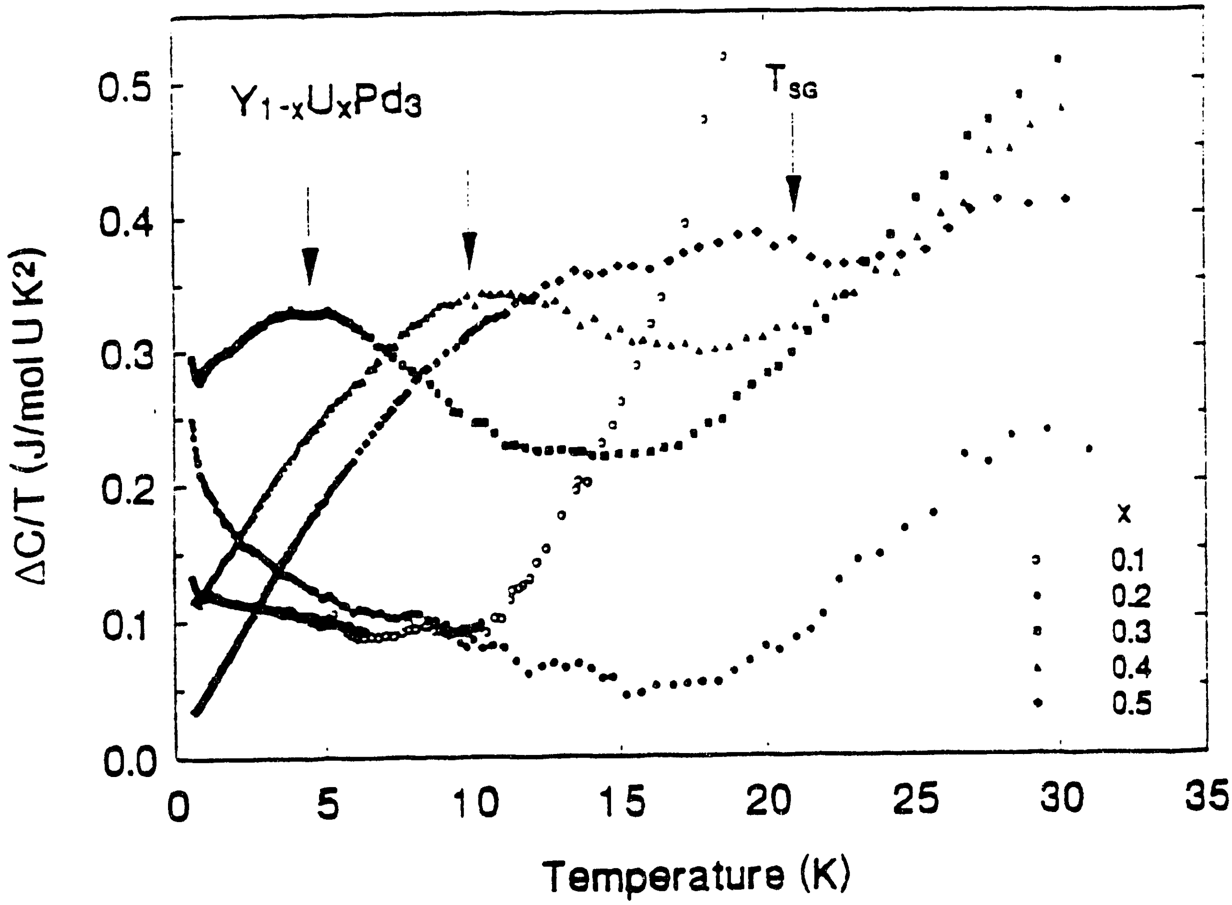

- x = 0.3, 0.4, 0.5 Broad anomalies (SG)
- Schottky anomaly (excited level ~ 10 meV)

  INS – UPd_4:
  Γ_5 ~ 5 meV above ground state Γ_3 (Furrer et al.,'77)

- x = 0.1, 0.2

  No peak (not SG)

  No saturation (not usual Kondo effect)

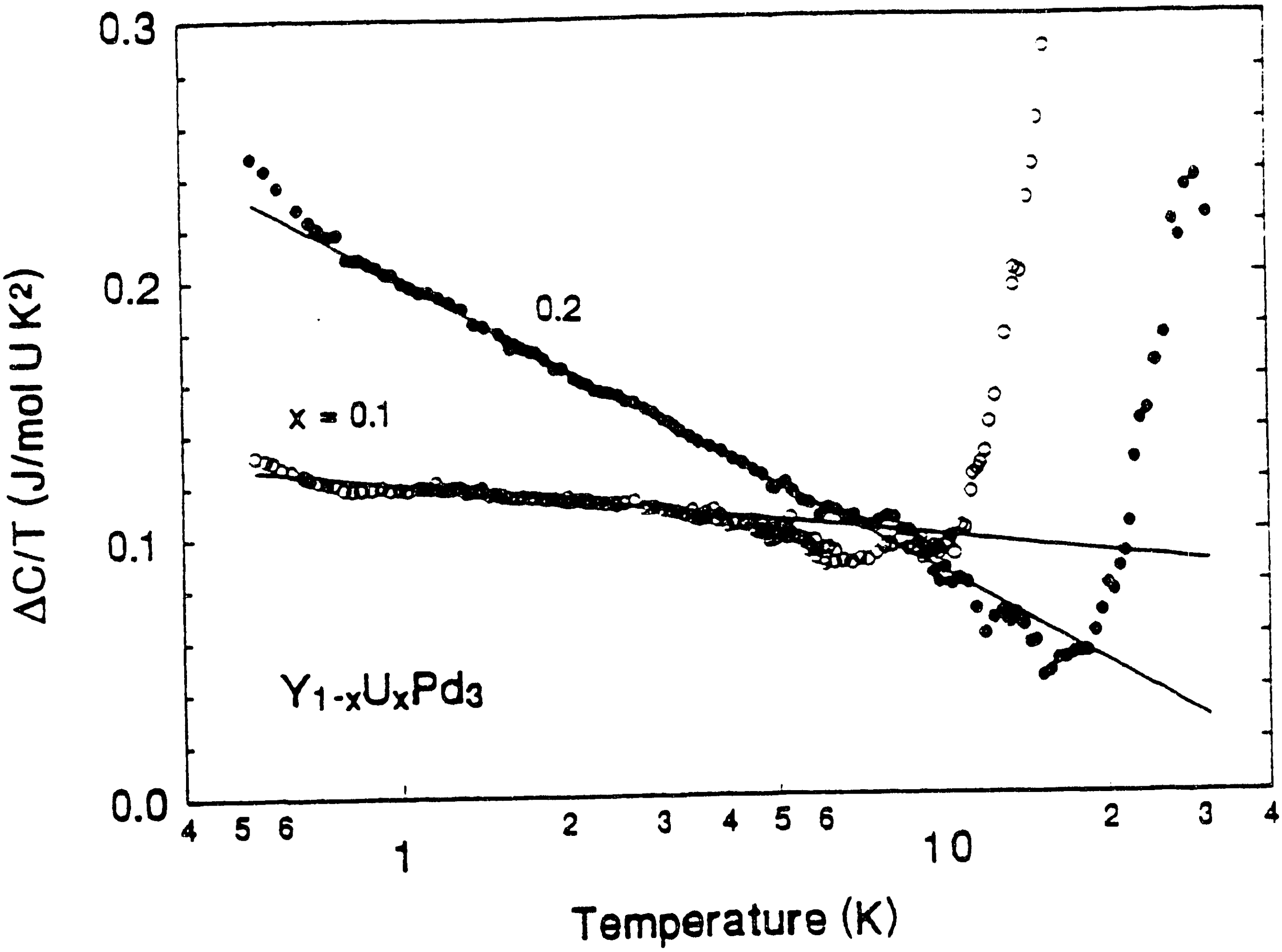

* Two-channel Kondo: $\frac{\Delta C(T)}{T} = \frac{-0.251}{T_K} \ln \frac{T}{0.41 T_K} + b$

(Tsvelik,'85)

(Sacramento & Schlottmann,'89)

x	T_K (K)	b (mJ/mol U K^2)
0.1	220	115
0.2	42	61

* $S(0) = (R/2)\ln(2)$

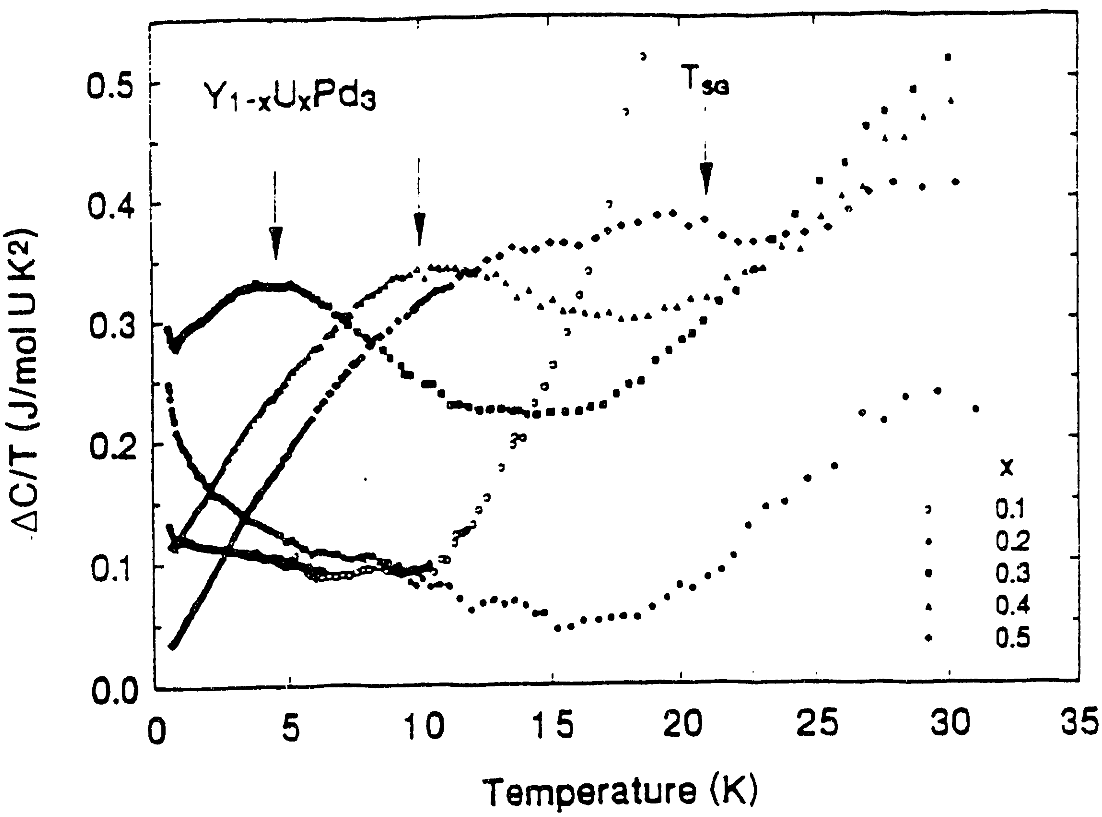

Y1-xUxPd3
TSG
ΔC/T (J/mol U K2)
Temperature (K)
x
0.1
0.2
0.3
0.4
0.5
0.0
0.1
0.2
0.3
0.4
0.5
0
5
10
15
20
25
30
35

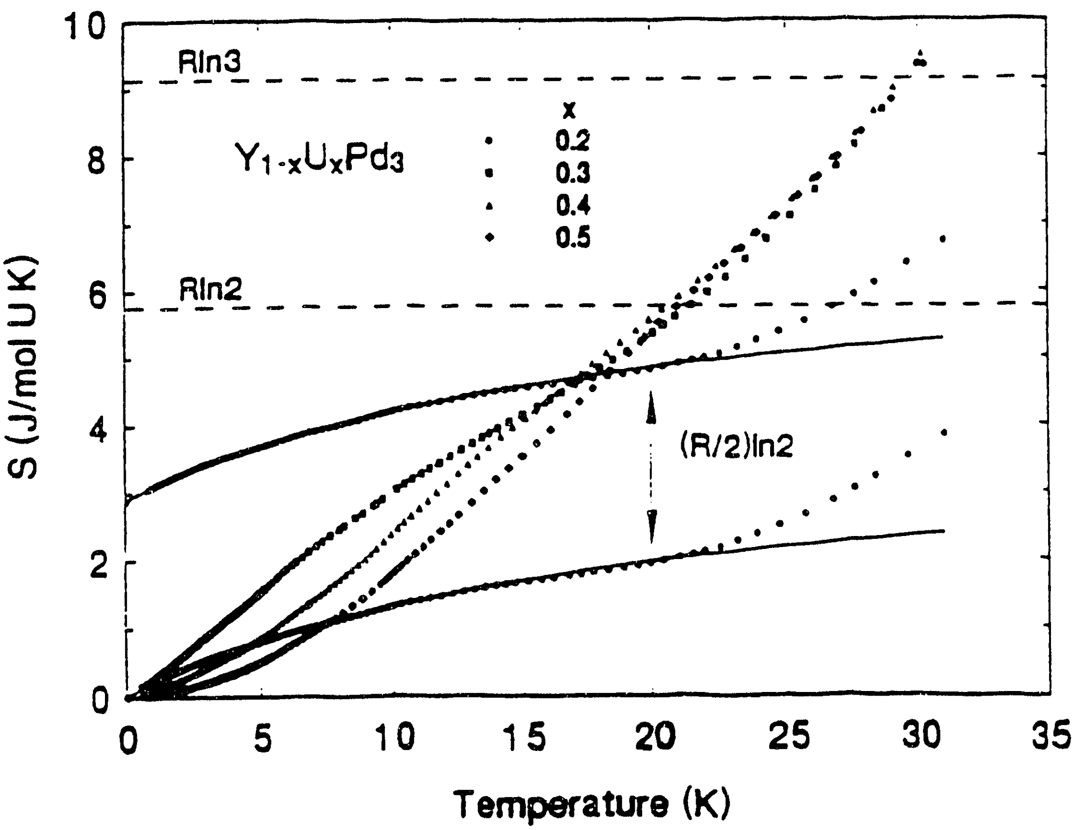

Rln3
Rln2
Y1-xUxPd3
x
0.2
0.3
0.4
0.5
(R/2)ln2
S (J/mol U K)
Temperature (K)
0
2
4
6
8
10
0
5
10
15
20
25
30
35

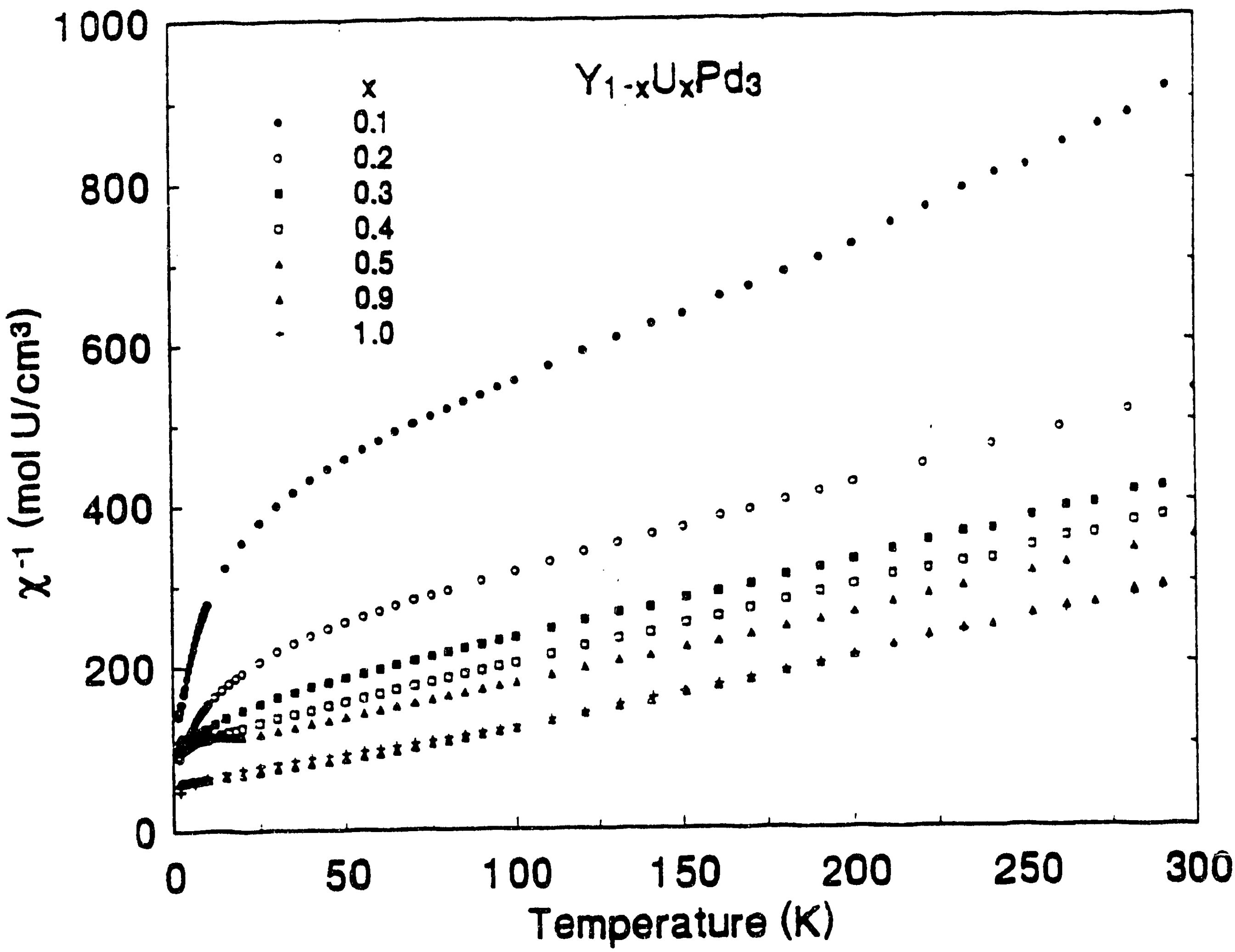

1000
800
600
400
200
0
χ^{-1} (mol U/cm^3)
$Y_{1-x}U_xPd_3$
x
0.1
0.2
0.3
0.4
0.5
0.9
1.0
0
50
100
150
200
250
300
Temperature (K)

Magnetic Susceptibility $\chi(T)$

High T: $\chi(T) = \chi_o + C/(T - \Theta_{CW})$

- $\mu_{eff} \approx 3.4\ \mu_B$ $\quad$ $\mu_{eff}(U^{4+}) = 3.58\ \mu_B$
  $\mu_{eff}(U^{3+}) = 3.62\ \mu_B$
- $\chi_o < 0 \Rightarrow$ Low $\chi_{Pauli} \propto N(E_F)$
- $\Theta_{CW} < 0 \Rightarrow$ AFM correlations

  Trend opposite to that for cooperative behavior

  Kondo systems: $|\Theta_{CW}| \approx 3 - 4\ T_K$

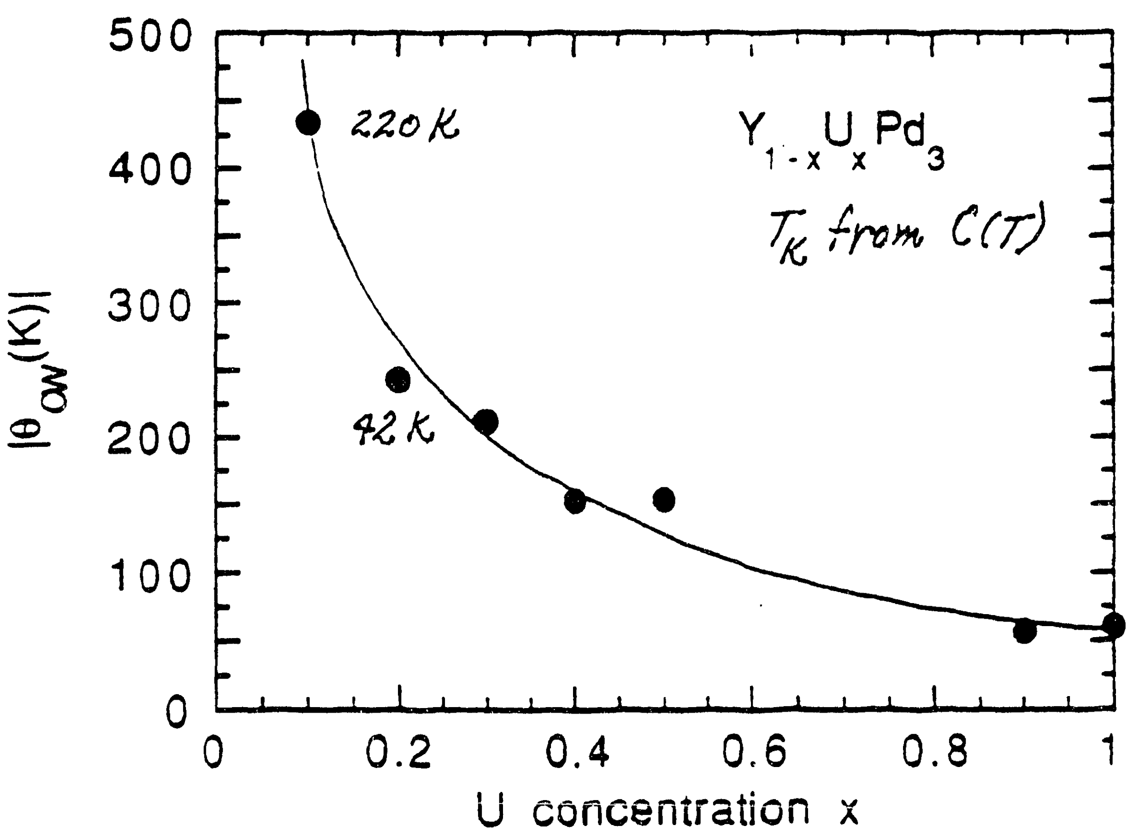

Low Temperature Magnetic Susceptibility

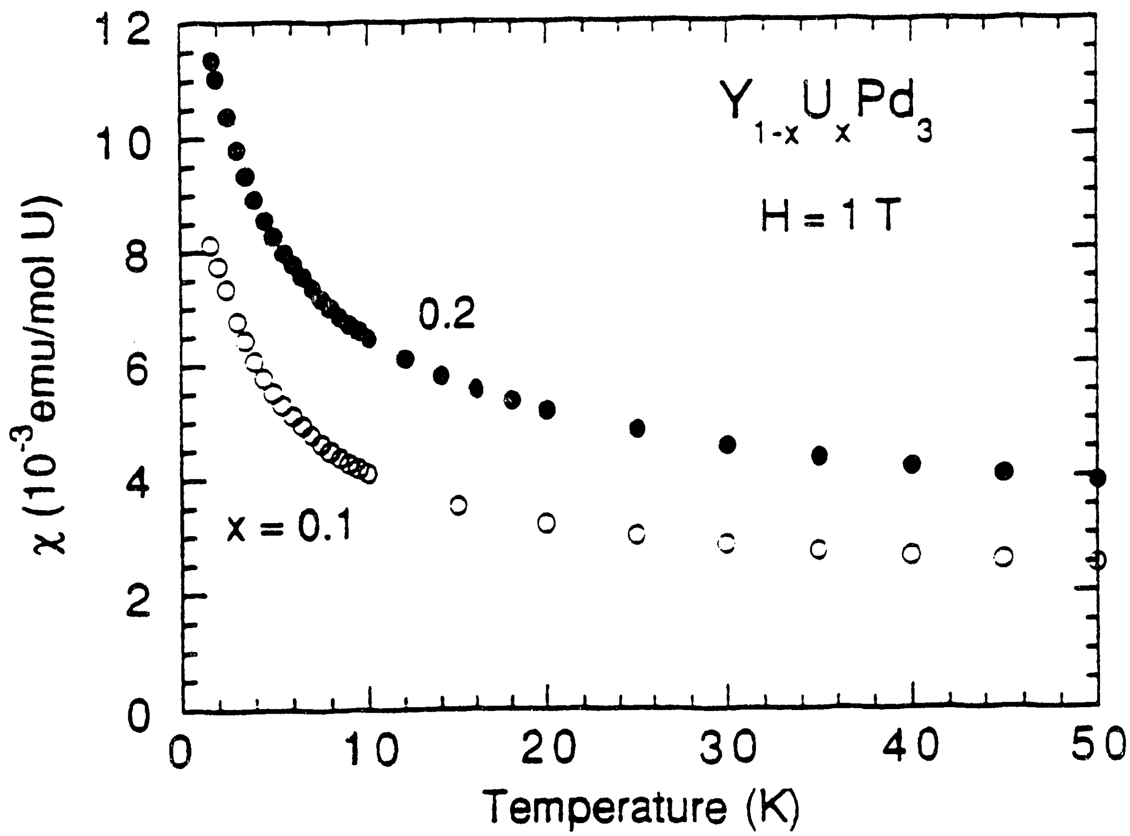

$\chi(T)$ does not saturate at low T

Fits to $\chi(T) = \chi(0)[1-\alpha(T/T_K)^{1/2}]$ (1.6 K $\leq$ T $\leq$ 5 K) (Cox,'91)

χ	$\chi(0)(10^{-3}$ emu/mol U)	α	T_K [from C(T)]
0.1	11.7	3.5	220 K
0.2	15.7	1.4	42 K

$\chi_{vV} \approx 16 \times 10^{-3}$ emu/mol U for Γ_5 10 meV above Γ_3

INS - 9K

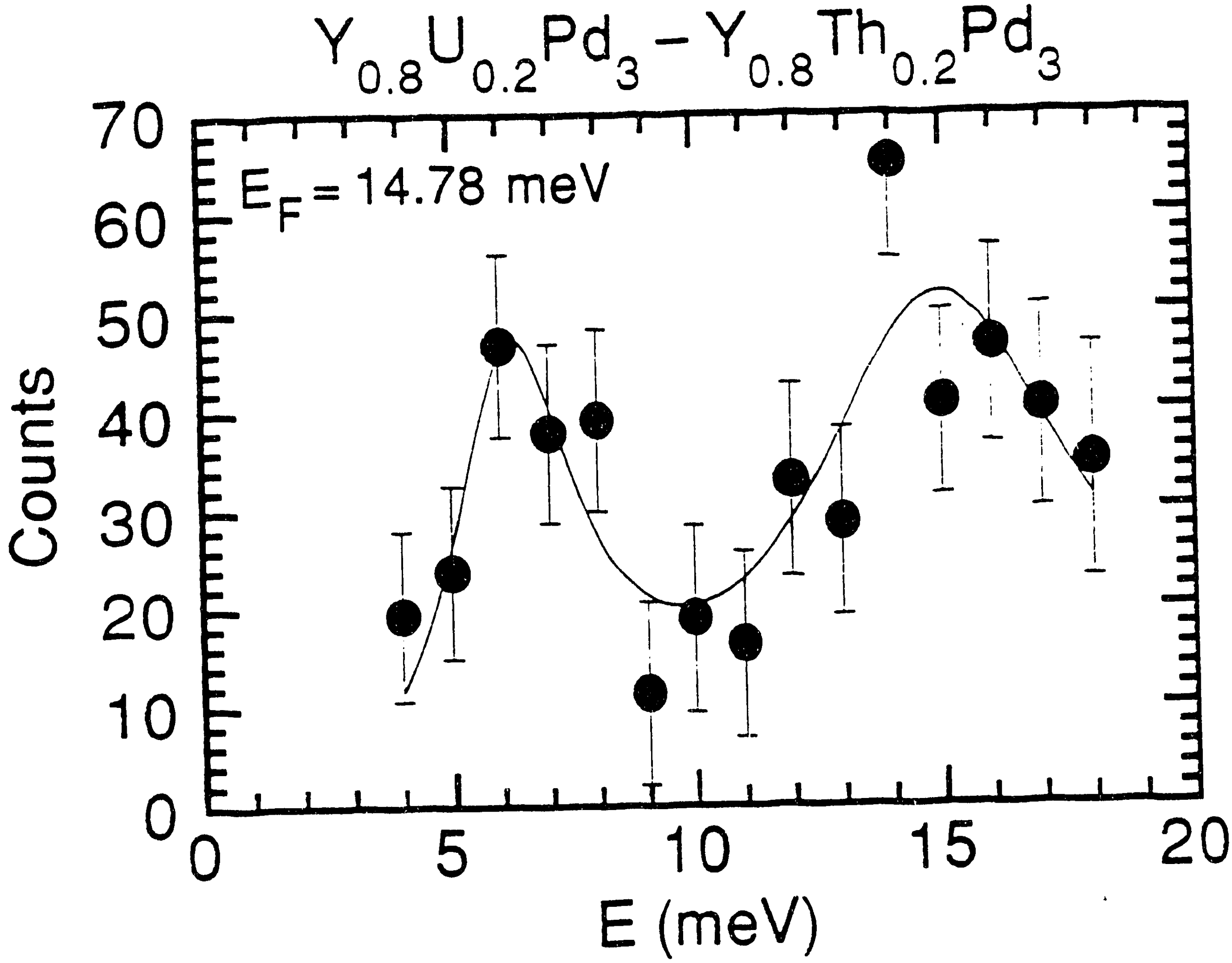

CEF peaks -

1) $\Gamma_3 \rightarrow \Gamma_5$ at ~6 meV, $\Gamma/2 \sim 1.5$ meV

2) $\Gamma_3 \rightarrow \Gamma_4$ at ~15 meV, $\Gamma/2 \sim 3$ meV

H. A. Mook et al, '92.

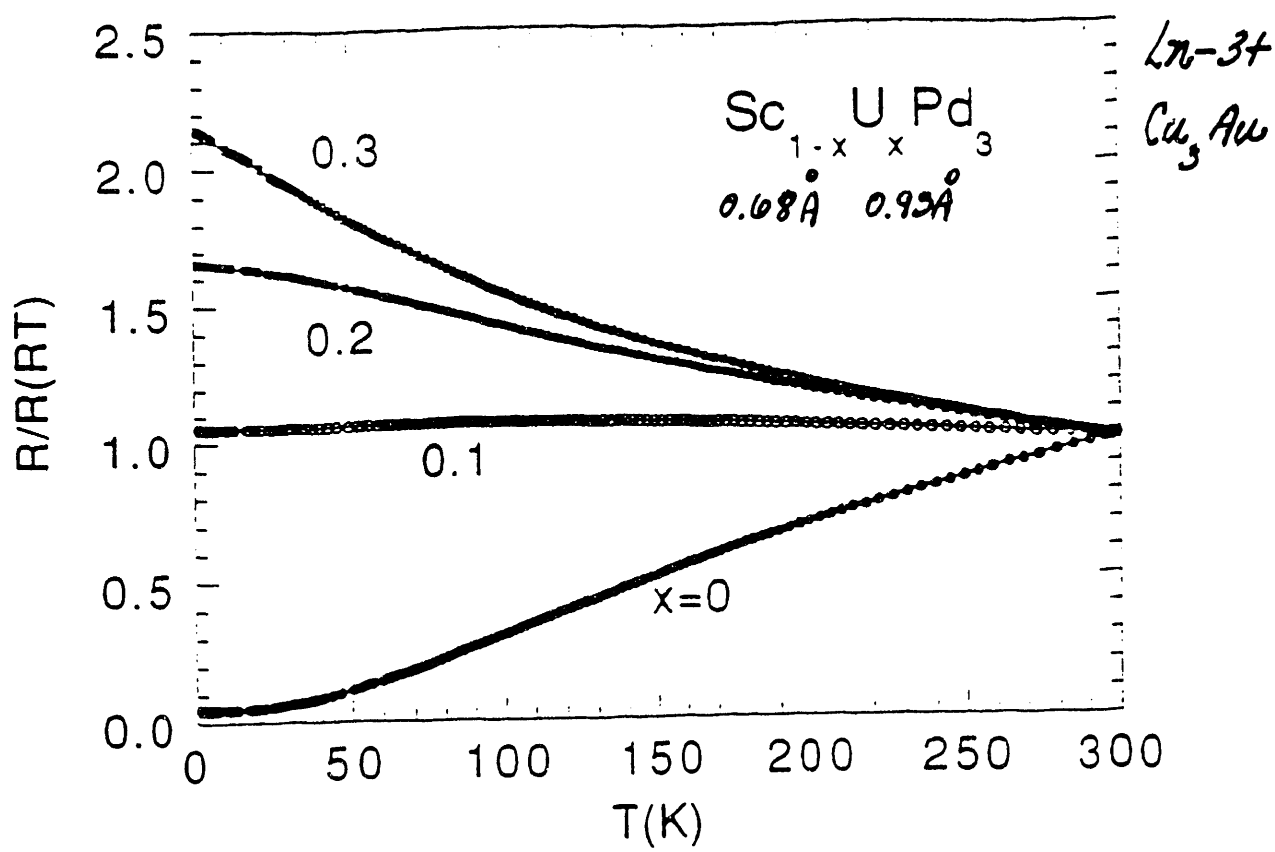
Ln-3+
Cu3 Au
Sc1-x Ux Pd3
0.68Å 0.93Å
0.3
0.2
0.1
x=0
R/R(RT)
T(K)

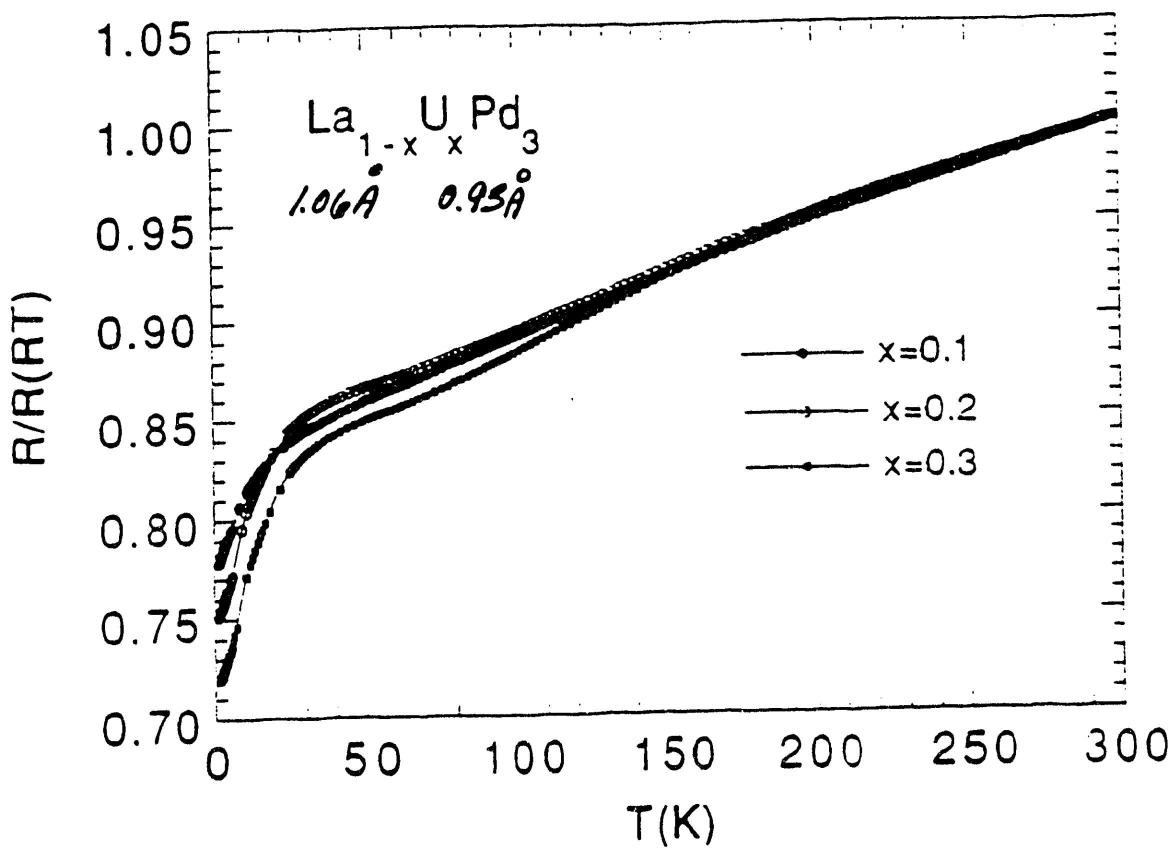
La1-x Ux Pd3
1.06Å 0.93Å
x=0.1
x=0.2
x=0.3
R/R(RT)
T(K)

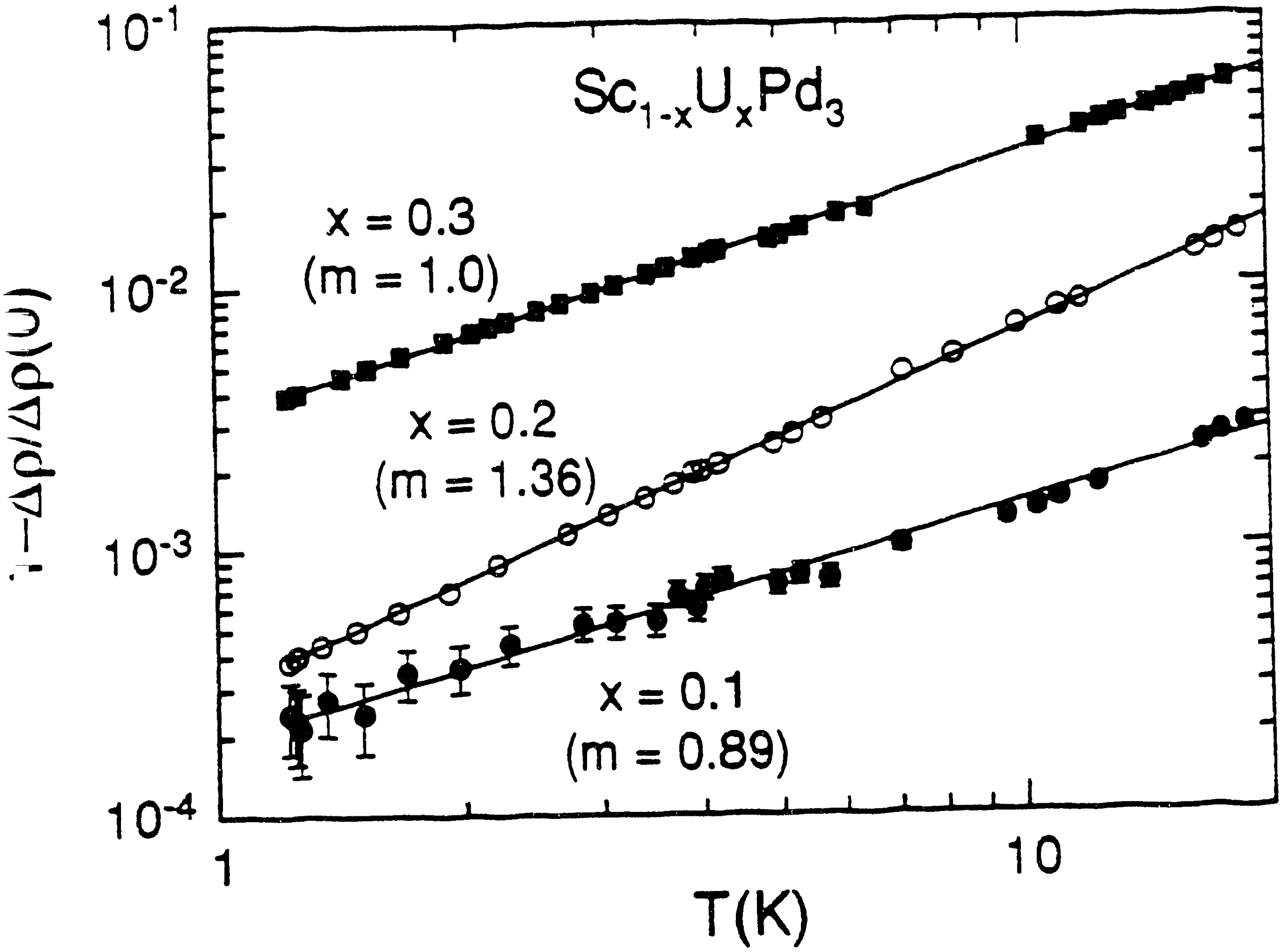

$$\Delta\rho(T)/\Delta\rho(0) = 1 - (T/T_0)^m$$

x	$\Delta\rho(0)$ ($\mu\Omega$-cm)	m	T_0(K)
0.1	63.92	0.89	15,000
0.2	176.62	1.36	386
0.3	417.3	1.00	311

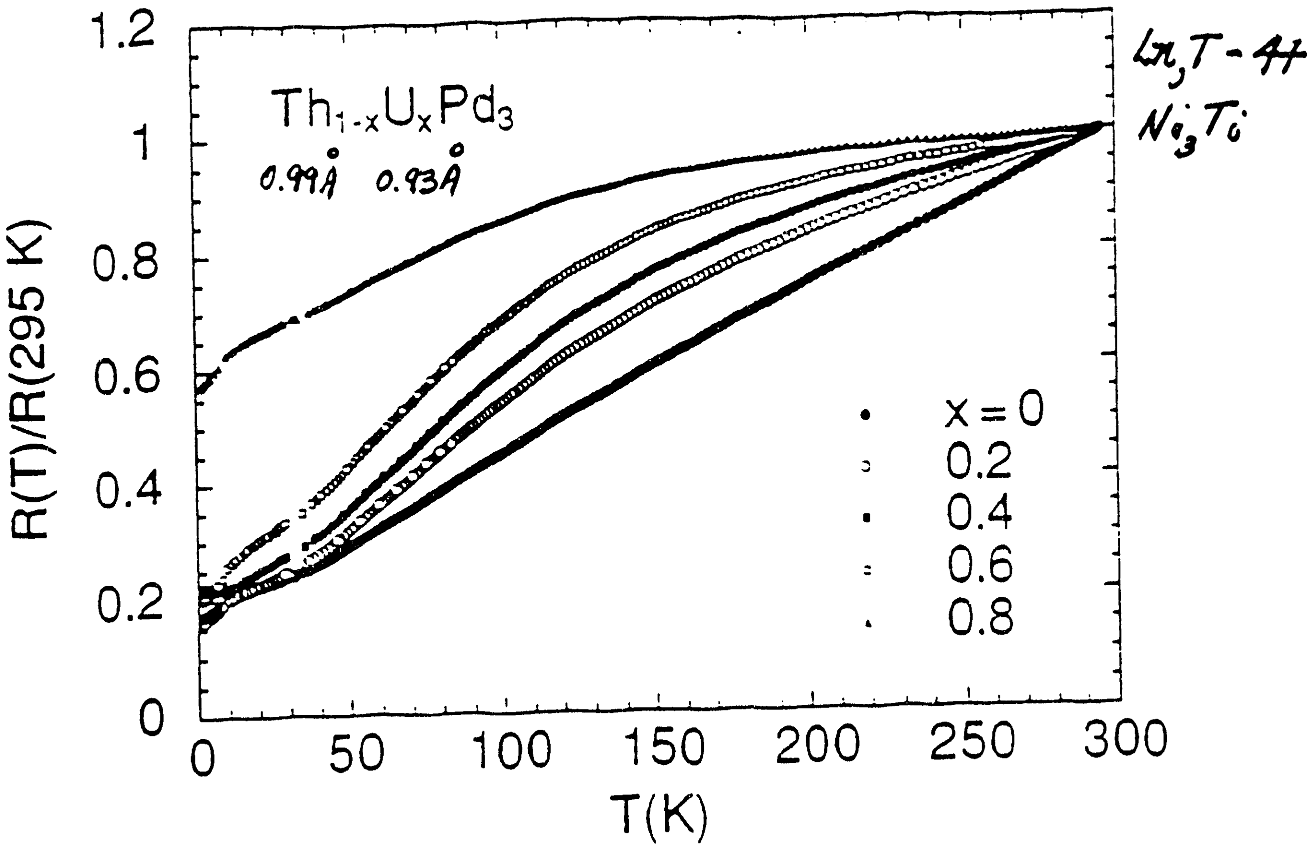

Th$_{1-x}$U$_x$Pd$_3$
0.99Å 0.93Å
R(T)/R(295 K)
T(K)
x = 0
0.2
0.4
0.6
0.8
Ln$_3$T-44
Ni$_3$Ti

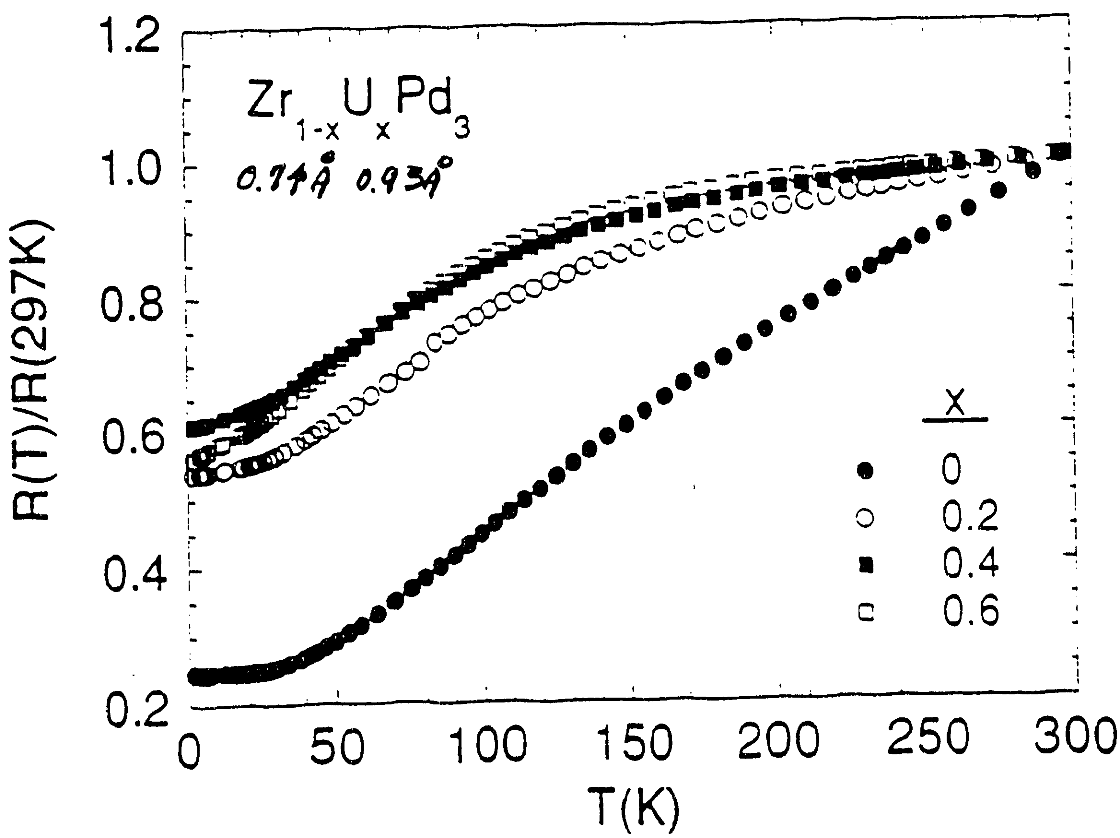

Zr$_{1-x}$U$_x$Pd$_3$
0.74Å 0.93Å
R(T)/R(297K)
T(K)
x
0
0.2
0.4
0.6

Conclusions

Fermi-level tuning: Observe decrease in T_K with x

Consistent with PES/BIS

Unprecedented for U system

Single-ion/cooperative effects compete for ground state

SG-like freezing $(0.3 \leq x \leq 0.5)$

Kondo effect $(x \leq 0.2)$

Unconventional (non-Fermi liquid) Kondo behavior $(T < T_K)$

$\rho(T) \sim 1 - T$

$\chi(T) \sim 1 - T^{1/2}$

$C(T)/T \sim -\ln T$

$S(0) \sim (R/2)\ln(2)$

Consistent with two-channel Kondo effect

Quadrupolar Kondo effect $\Rightarrow$ origin of two-channel behavior:

U^{4+} in cubic CEF $\Rightarrow \Gamma_3$ doublet ground state

$\chi(T) \sim 1 - T^{1/2}$

C(H): Crossover to single-channel Kondo

(Andraka & Tsvelik,'91)

INS: No strong, narrow quasielastic peak (Γ_4, Γ_5)

Heavy fermion superconductivity and magnetism

- Heavy fermion superconductors

  $CeCu_2Si_2$, UBe_{13}, UPt_3, UNi_2Al_3, UPd_2Al_3
  $\gamma \sim 1$ J/mole K^2 ($m^* \sim 10^2$-10^3 m_e, $T_0 \sim 1$-10 K), $T_c \sim 1$ K

- Anisotropic superconductivity

  $\Delta(\mathbf{k})$ vanishes at points or lines on Fermi surface
  $\Delta(\mathbf{k}) = 0$ — poles $\Rightarrow$ axial state, equator $\Rightarrow$ polar state

  Electron pairing mediated by AFM spin fluctuations

- SC coexists with weak AFM ($\mu \sim 10^{-2}\ \mu_B$)

- Multiple superconducting phases $\Rightarrow$
  Coupling of multicomponent superconducting order parameter and AFM order parameter

  Complex superconducting phase diagrams
  UPt_3 and, possibly, URu_2Si_2 — H-T plane
  $U_{1-x}Th_xBe_{13}$ — H-T and T-P planes

- Chemical substitution $\Rightarrow$
  Suppresses SC and weak AFM
  Induces local moment AFM or FM ($\mu \sim 1\ \mu_B$)
  UPt_3 — Th for U; Pd,Au for Pt $\Rightarrow$ local moment AFM
  URu_2Si_2 — Rh for Ru $\Rightarrow$ local moment AFM
  Re,Tc for Ru $\Rightarrow$ local moment FM

- Kondo effect — origin of heavy fermion state

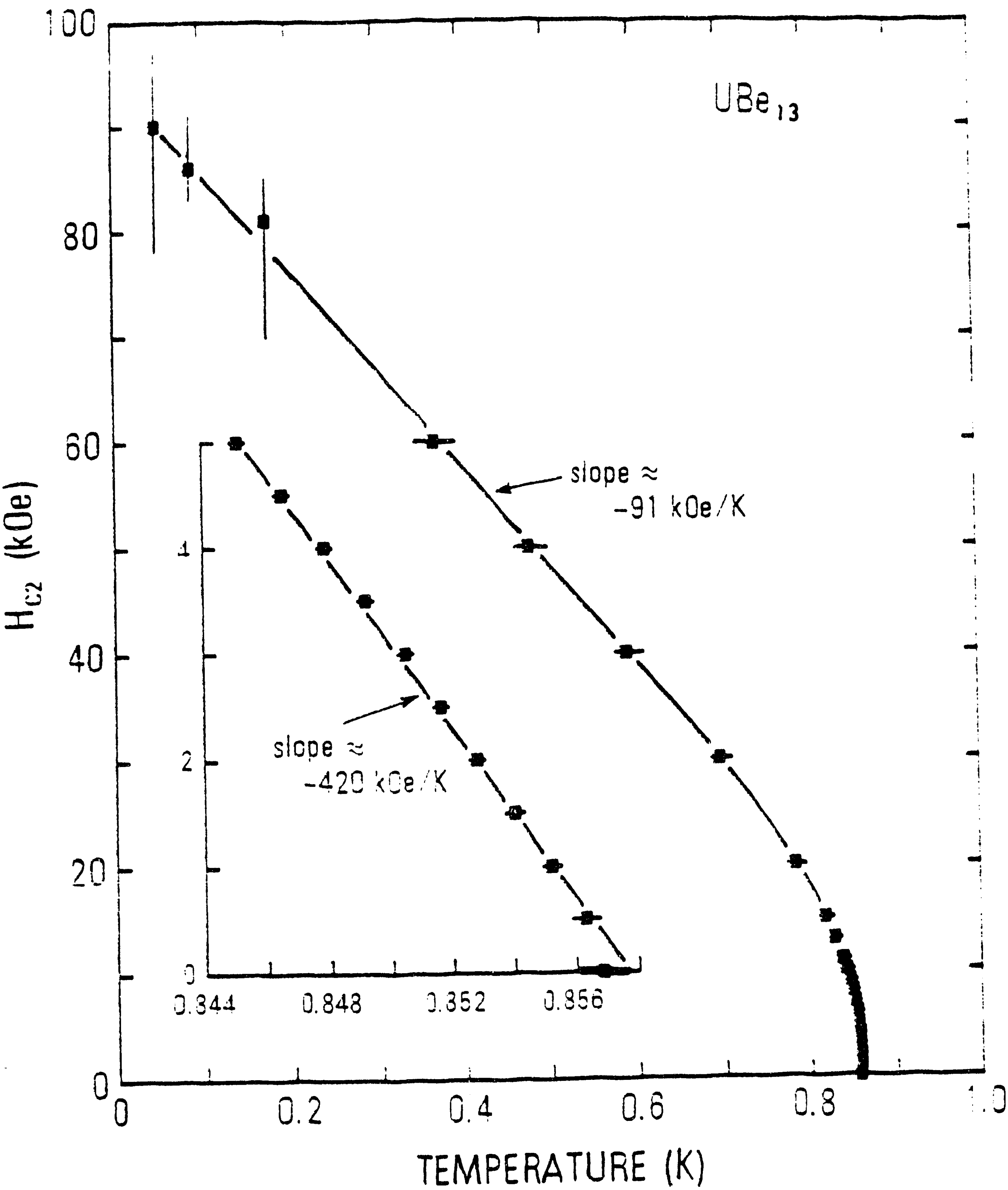

M.B. Maple et al., '84

$T_c(P)$ measurements on $(U_{1-x}Th_x)Be_{13}$

$\underline{P=0}$: $T_c(x)$ – Smith, Fisk, Willis, Roof, Ott, Rudigier & Felder, '85

$C(T)$ – Ott, Rudigier; Fisk & Smith, '85

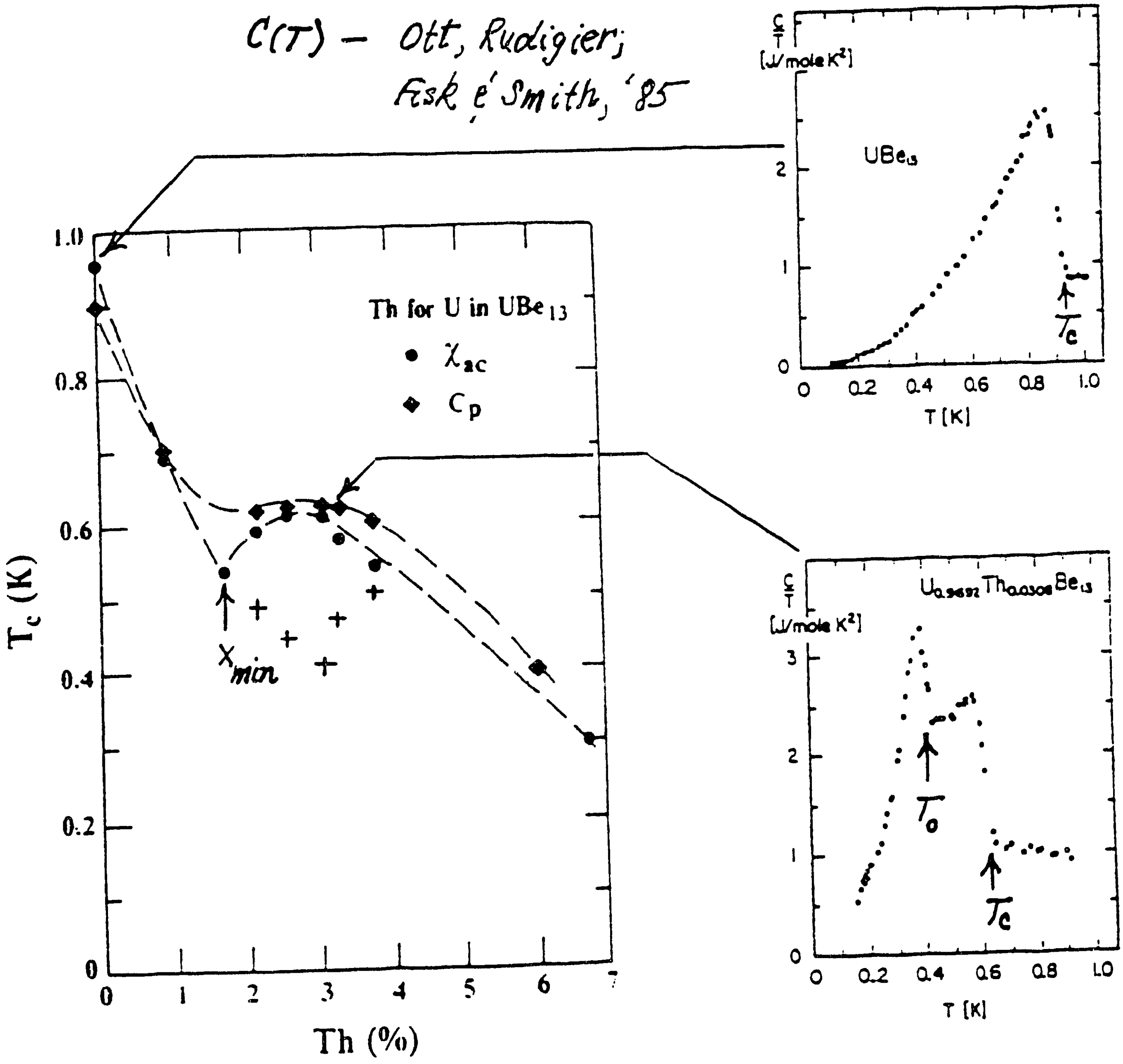

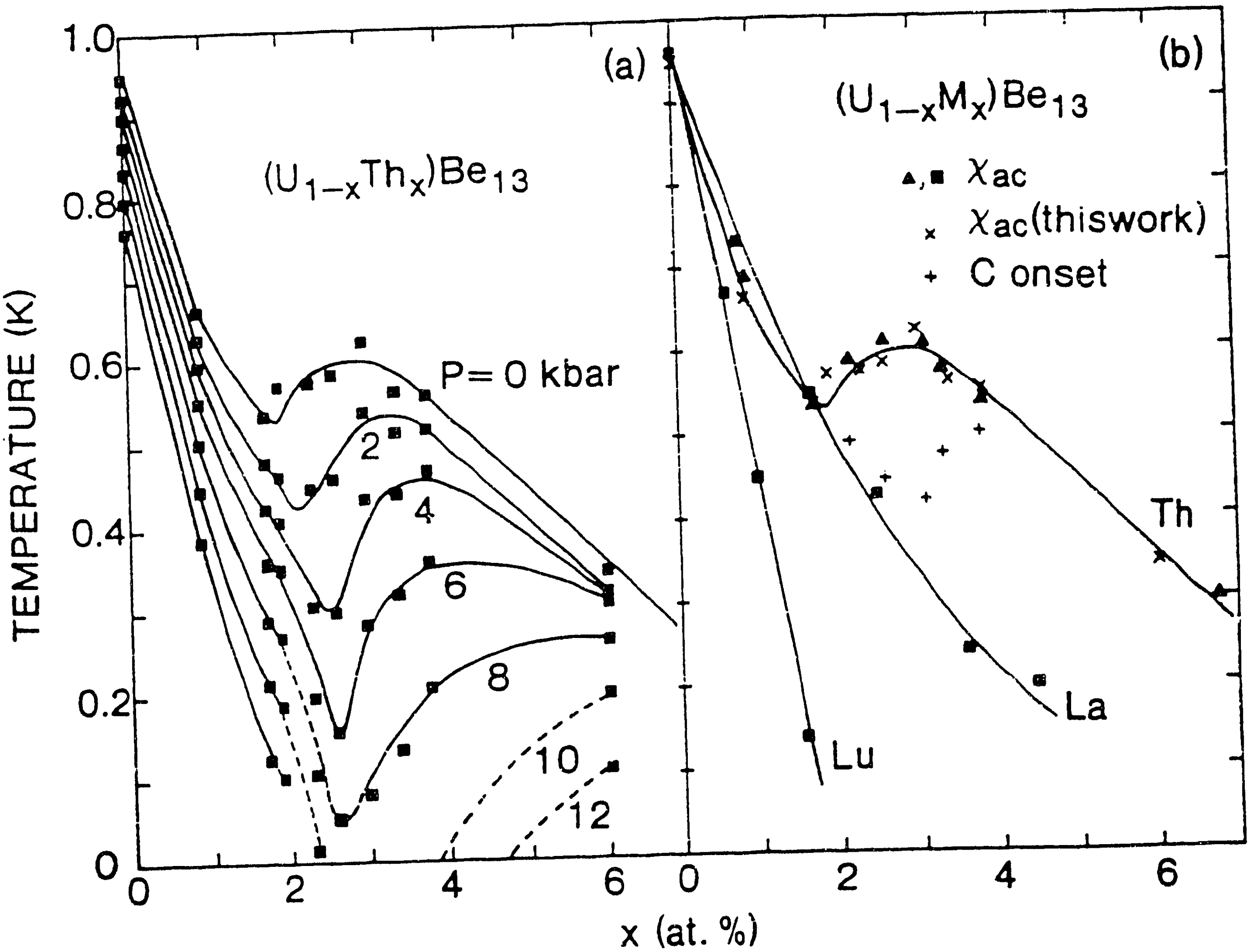

S.E. Lambert, Y. Dalichaouch, M.B. Maple, J.L. Smith & Z. Fisk (1986)

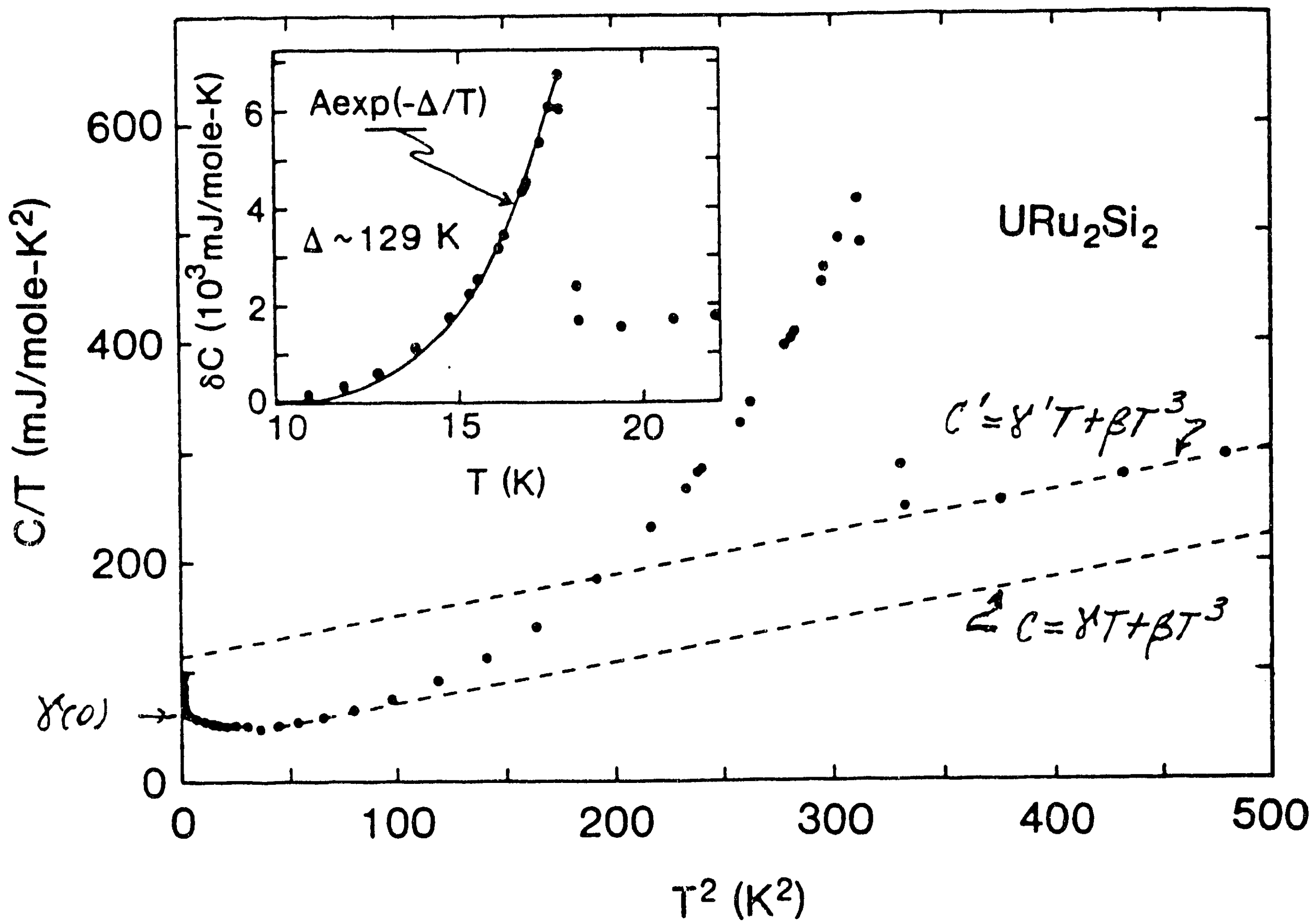

$\gamma' = 112$ mJ/mole U-K^2; $\theta_D = 294$ K

$\gamma(0) = 65.5$ mJ/mole U-K^2 ($m^* \sim 25 m_e$)

$\gamma(0)/\gamma' \simeq 0.6 \Rightarrow \sim 40\%$ Fermi surface removed by CDW or SDW

BCS-type mean field transition at $T_0 \sim 17.5$ K

$\delta C = A \exp(-\Delta/T)$; $\Delta \sim 10^2$ K ~ 10 meV

M. B. Maple, Y. Dalichaouch, T. Kohara, C. Rossel, M. S. Torikachvili, M. W. McElfresh & J. D. Thompson, '86

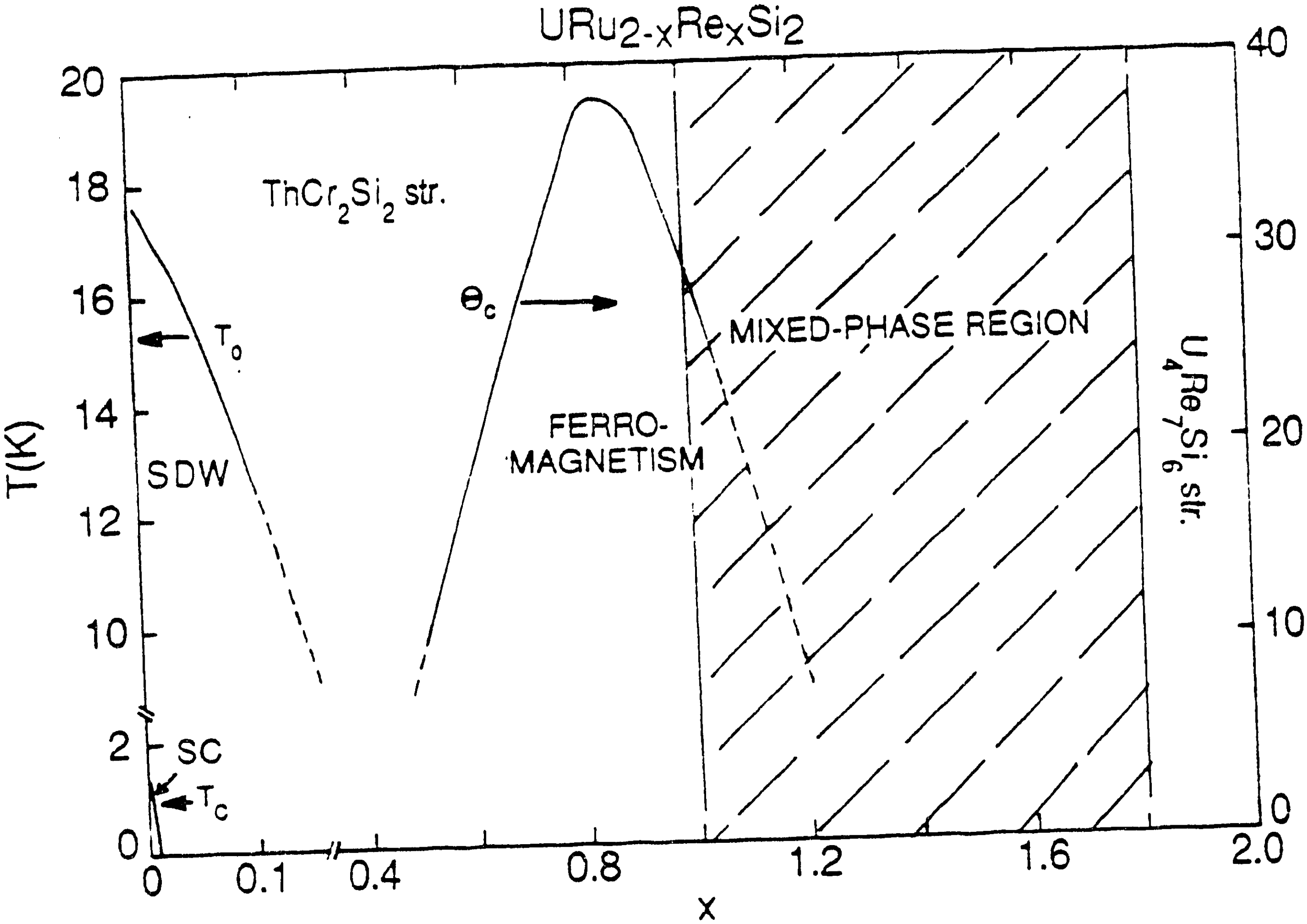

Y. Dalichaouch, M. B. Maple, M. S. Torikachvili, & A. L. Giorgi, '89

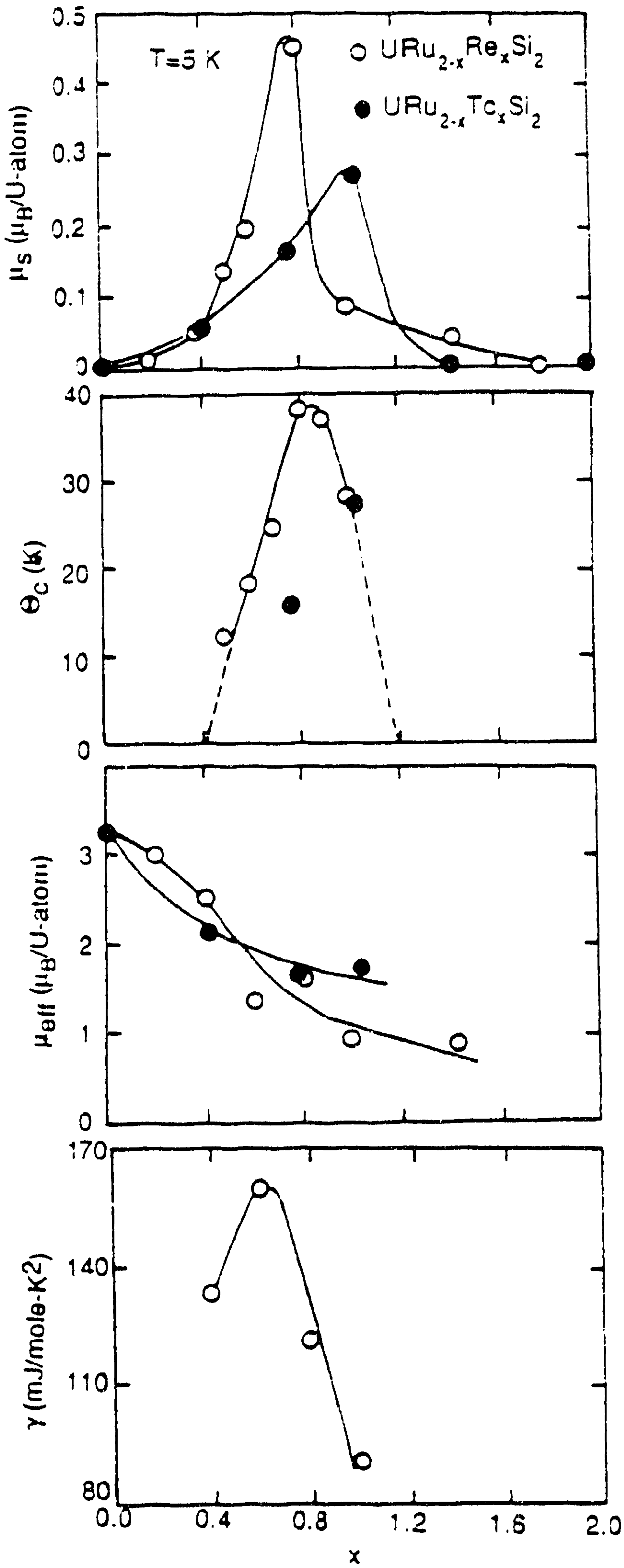

Y. Dalichaouch, M.B. Maple, M.S. Torikachvili, & A.L. Giorgi, '89

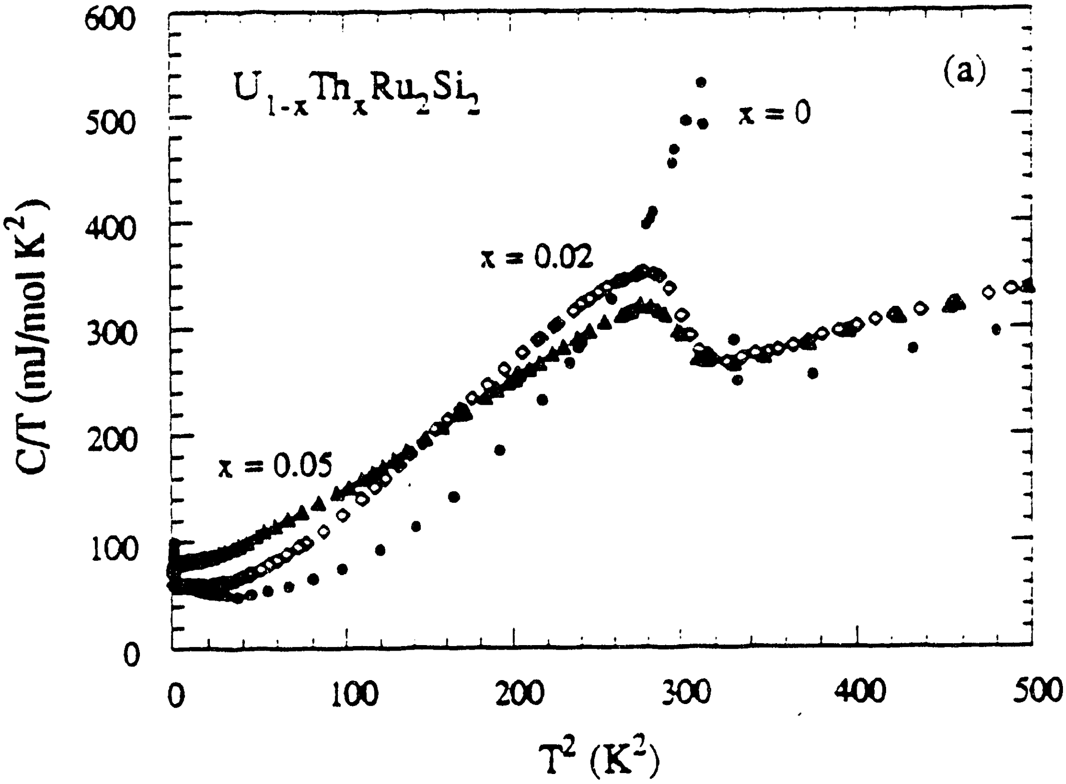

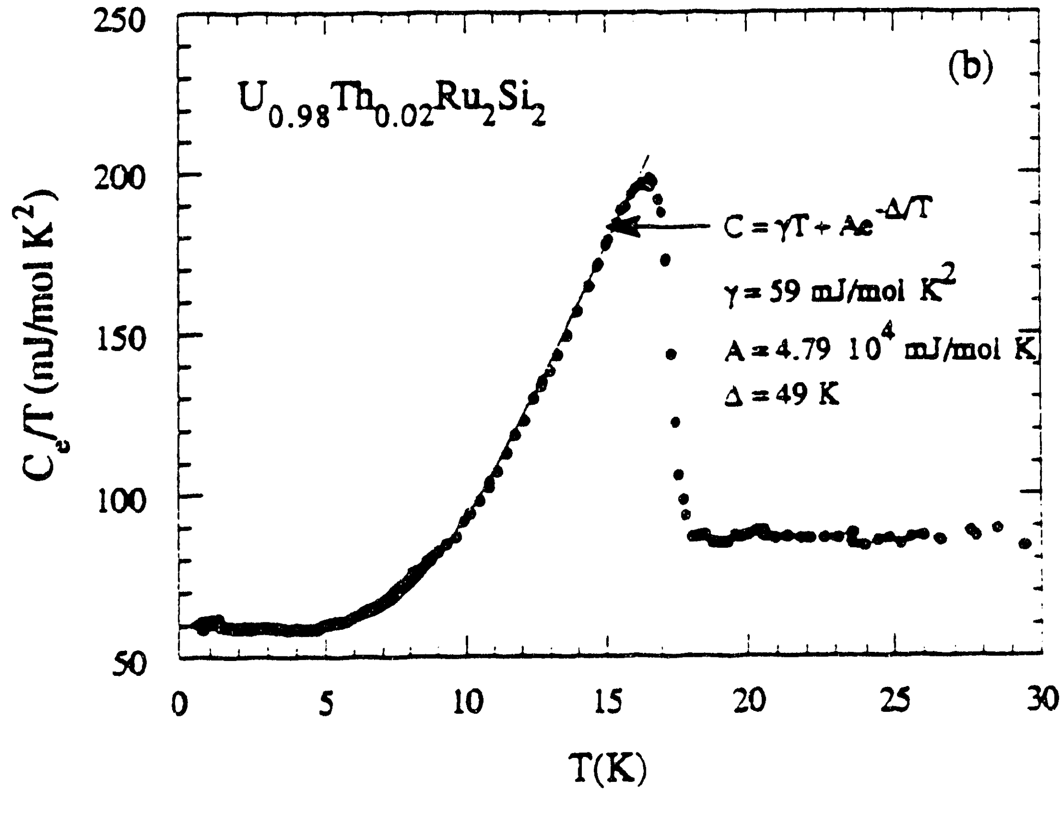

M. A. Lopez de la Torre et al, UCSD, '92

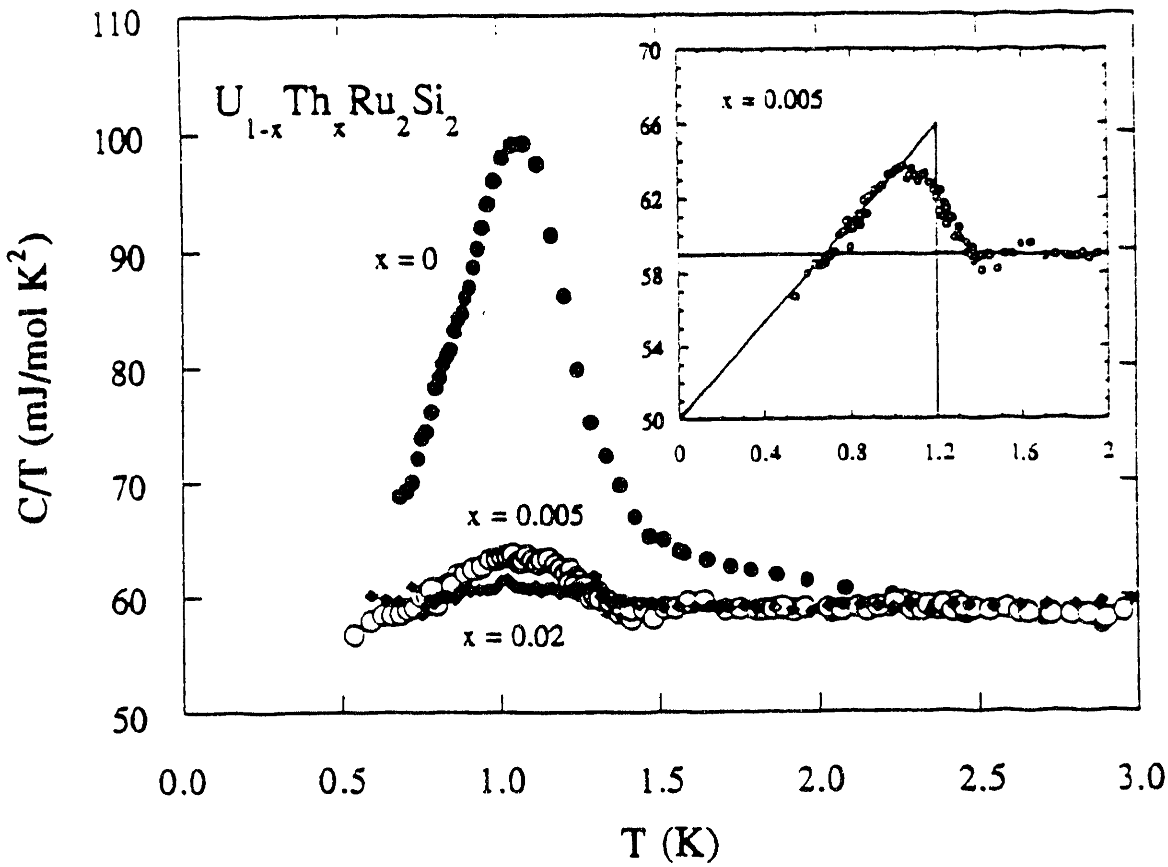

M.A. Lopez de la Torre et al., UCSD, '92

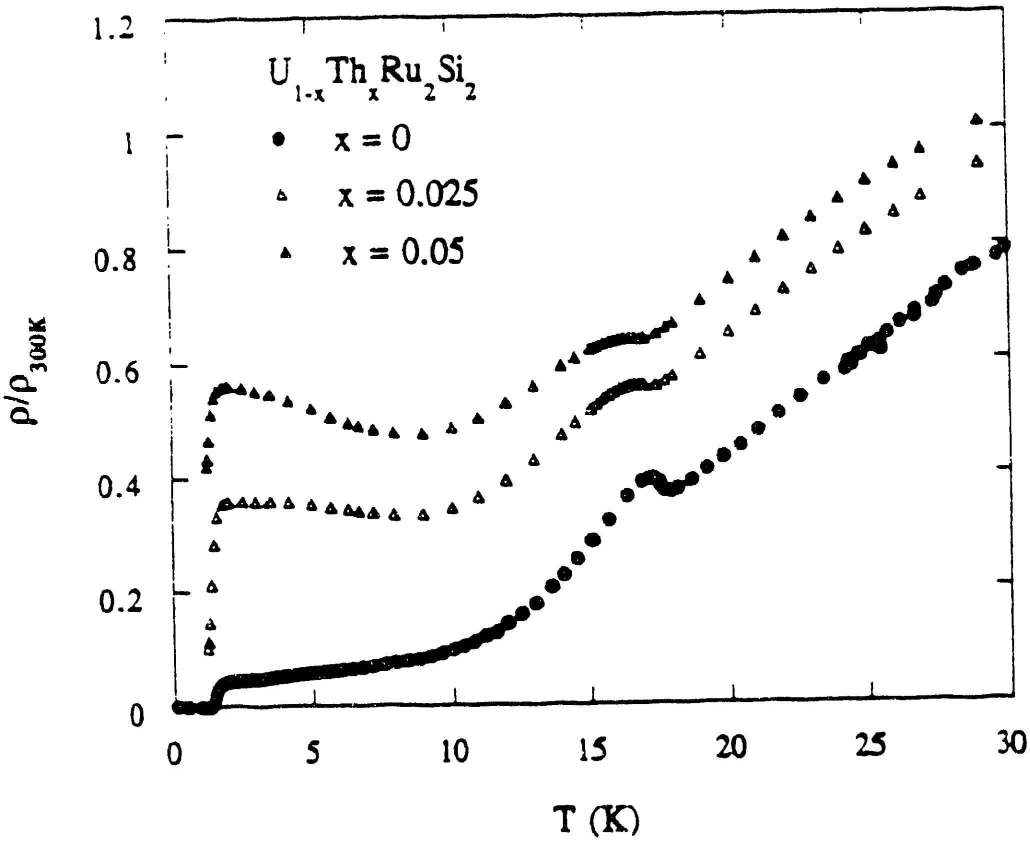

M.A. Lopez de la Torre et al., UCSD, '92

Hybridization gap semiconductors (Kondo insulators)

$CeFe_4P_{12}$, CeNiSn, $Ce_3Bi_4Pt_3$
SmB_6, "gold" SmS
TmSe, TmTe
YbB_{12}
UFe_4P_{12}, UPtSn, $U_3Sb_4Pd_3$

- Hybridization of flat f-band and broad conduction band with exactly two electrons per unit cell

- Two electrons fill lower hybridized band $\Rightarrow$ insulator

- $\Delta \sim 10\text{-}10^2$ meV
  low T $\Rightarrow$ semiconductor
  high T $\Rightarrow$ metal

Example: MFe_4P_{12}

bcc — derived from binary skutterudite structure ($CoAs_3$)
M cations — bcc sublattice
Fe cations — sc sublattice
P anions — distorted corner sharing octahedra centered by Fe cation

Metals: M = La, Pr, Nd, Sm, Eu
Semimetal: M = Th
Semiconductors: M = Ce, U

$LaFe_4P_{12}$ structure (W. Jeitschko & D. Braun, 1977)

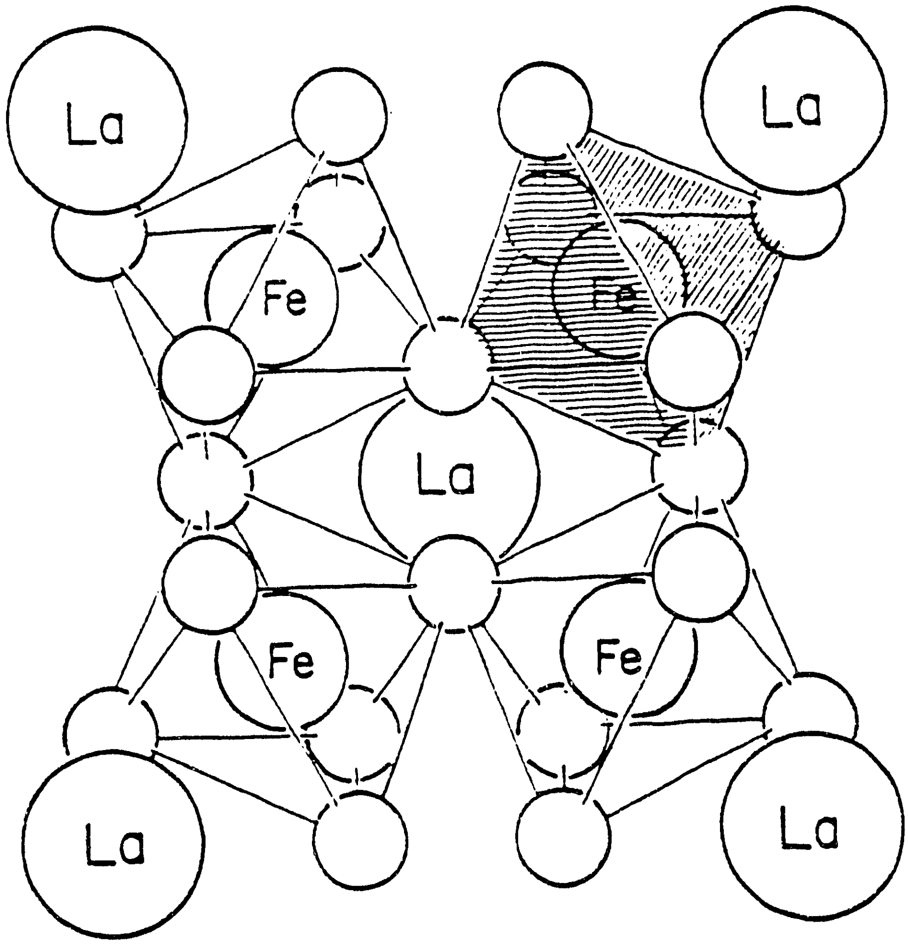

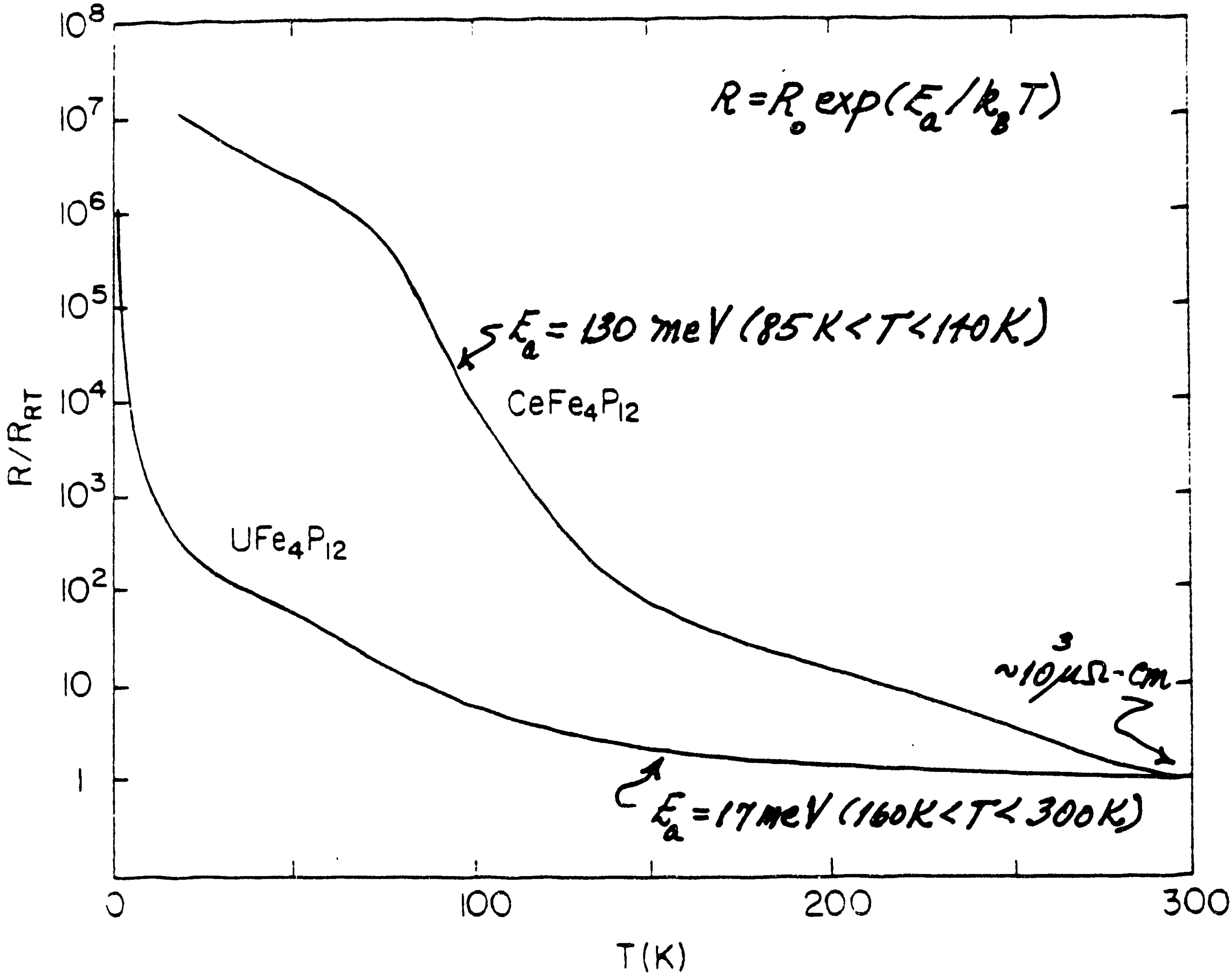

$CeFe_4P_{12}$ – paramagnetic semiconductor $d_{Ce} \sim 6.7 \mathring{A}$
$\Rightarrow$ intermeddate valence Ce

UFe_4P_{12} – ferromagnetic semiconductor $d_U \sim 6.7 \mathring{A}$
magnetic moment $5f^{\sim 2}$

G.P. Meisner et al., '85

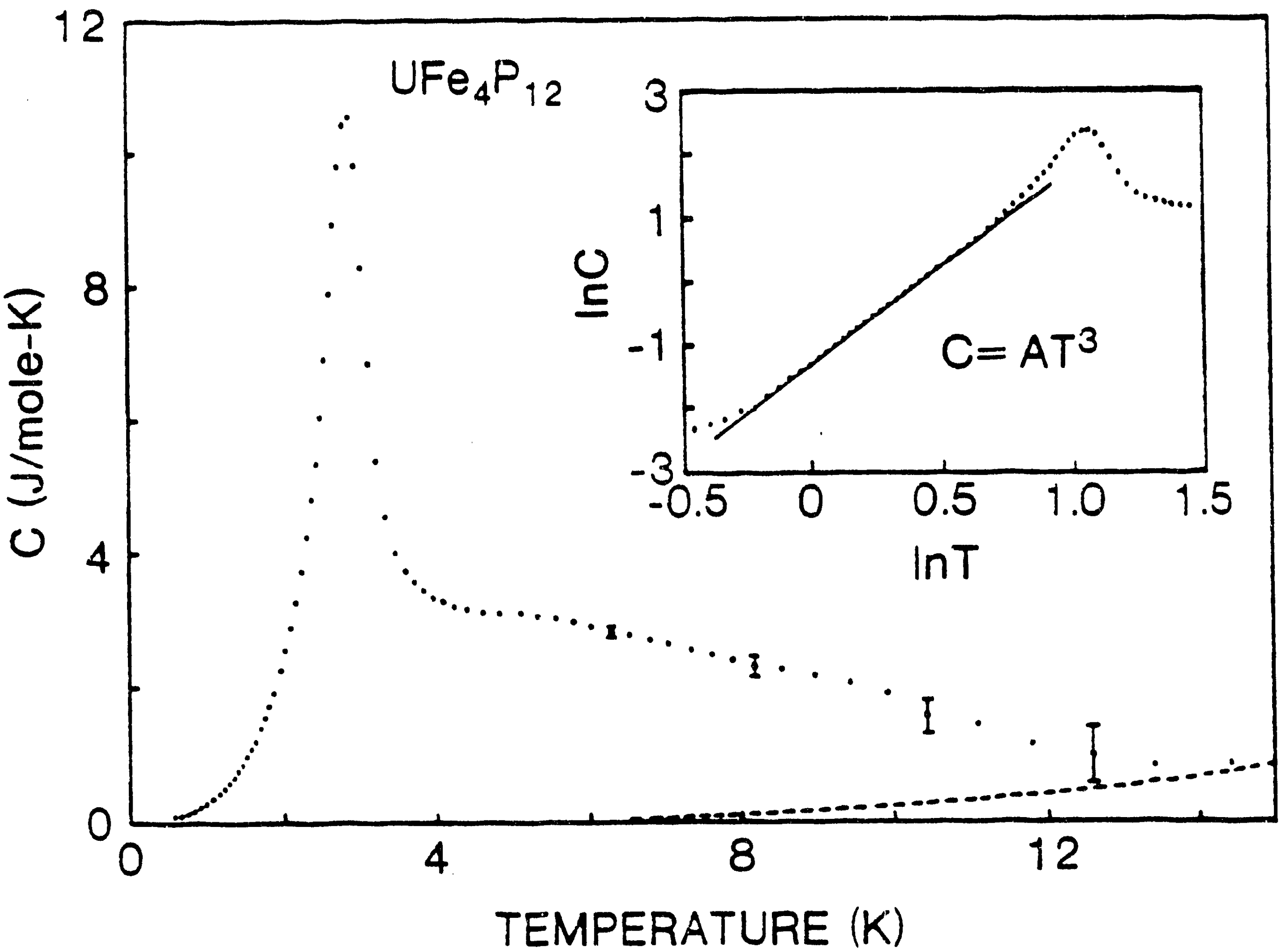

M.S. Torikachvili et al., '86

DATE FILMED

8/24/93

END